Oklahoma Geological Survey
Nicholas W. Hayman, *Director*

Circular 113
ISSN 0078-4397

Evaporite Karst in the Greater Permian Evaporite Basin (GPEB) of Texas, New Mexico, Oklahoma, Kansas, and Colorado

Kenneth S. Johnson, Lewis Land, and David D. Decker; *Editors*

2021

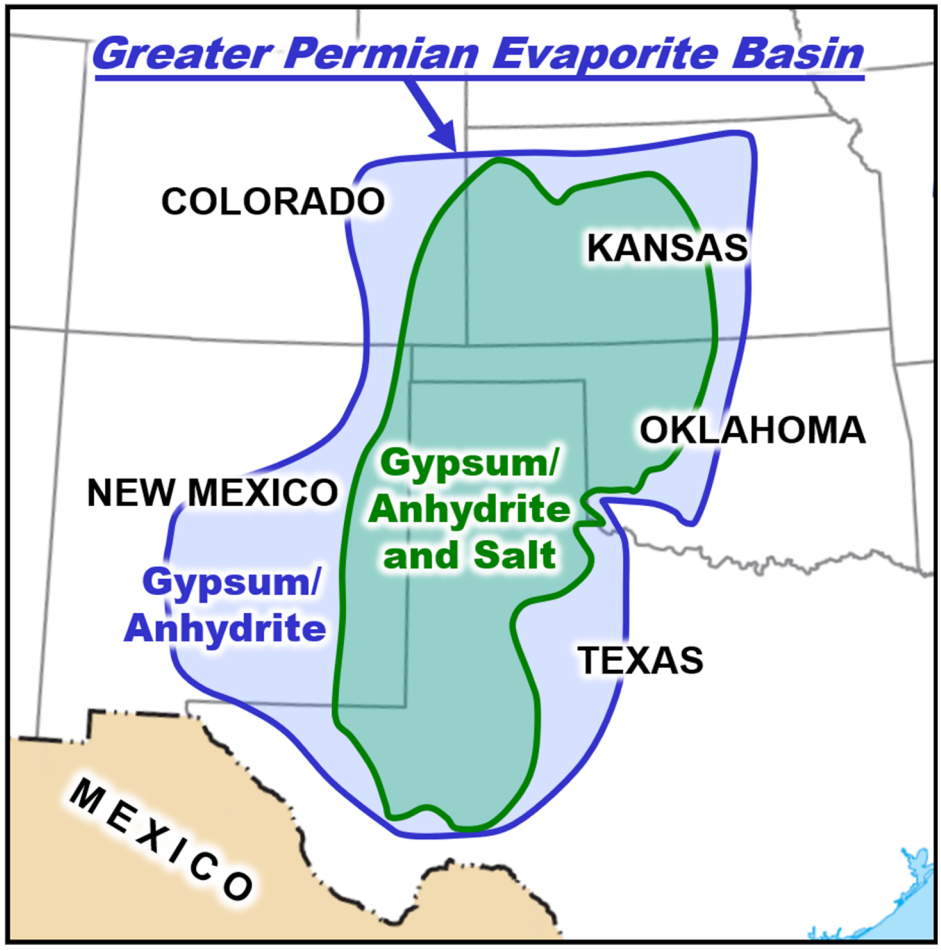

The University of Oklahoma
Norman, Oklahoma

PREFACE

Evaporite rocks, mainly gypsum (or anhydrite) and salt (halite), are the most soluble of common rocks. Their dissolution produces caves, sinkholes, disappearing streams, collapse structures, breccia pipes, and other karst features that are also commonly associated with carbonate rocks (limestones and dolomites). Evaporites underlie a vast region of southwestern United States that is herein named the Greater Permian Evaporite Basin (GPEB), and both natural and human-induced evaporite karst (EK) features are present in much of the region. Eight major evaporite sequences are present in Permian rocks in the GPEB, including: 1) Wellington/Hutchinson, 2) Lower Cimarron/Lower Clear Fork, 3) Upper Cimarron/Upper Clear Fork, 4) San Andres/Flowerpot/Blaine/Yelton, 5) Artesia, 6) Castile, 7) Salado, and 8) Rustler Formations or Groups. These evaporites and the GPEB occupy an area of about 650,000 km^2 in parts of five states, including Texas, New Mexico, Oklahoma, Kansas, and Colorado.

EK results from both natural processes and human activities. Natural EK occurs when precipitation or ground water circulates through, and dissolves, part or all of an evaporite deposit. Human activities that can produce EK include (1) construction upon, or directing water into or above, outcropping or shallow evaporites and (2) drilling boreholes, opening mines, or other excavations into subsurface evaporites, mainly salt deposits, followed by unsaturated water coming in contact with, and dissolving, the evaporite. The principal difference between karst in evaporite rocks and in carbonates is that EK features can form rapidly, in a matter of days, weeks, or years, whereas carbonate-karst features typically take years, decades, or centuries to form. Rapid development of EK can lead to engineering or environmental problems, including damage to, and/or collapse of, homes, buildings, civil projects (such as dams, bridges, and highways), and farmlands, and it can also result in injury or loss of life.

Being released in 2021, this publication is part of the celebration of the "International Year of Caves and Karst" (IYCK), which acknowledges the importance of karst in those parts of the world where carbonate and evaporite rocks are being dissolved at or near the Earth's surface. The IYCK is organized by the International Union of Speleology, the worldwide organization of cave and karst explorers, scientists, managers, and educators: the IYCK is being co-sponsored by about 150 national and international partner organizations.

This symposium volume results from a half-day theme session on EK in the GPEB that was held on September 24, 2019, as part of the annual meeting of the Geological Society of America (GSA) in Phoenix, Arizona. The session was organized by us, and was co-sponsored by three divisions of GSA: the Karst Division, Hydrogeology Division, and Environmental and Engineering Geology Division. We thank GSA and the three Divisions for their support in sponsoring the theme session. A total of 14 talks and posters presented at the GSA meeting are included in this volume, and we invited another 9 papers to be prepared especially for this volume. The 23 papers are grouped into *Introductory and General Papers*, and then into a series of geographic areas, based upon states.

The current volume is a companion to an earlier GSA-symposium volume published by the Oklahoma Geological Survey as: Johnson, K.S., and Neal, J.T., eds., 2003, Evaporite karst and engineering/environmental problems in the United States: Oklahoma Geological Survey, Circular 109, 353 p. http://ogs.ou.edu/docs/circulars/C109.pdf

KENNETH S. JOHNSON
Retired Geologist
Oklahoma Geological Survey
1321 Greenbriar Dr.
Norman, OK 73072
Phone: 405/329-4150
E-mail: ksjohnson@ou.edu

DAVID D. DECKER
Southwest Geophysical Consulting, LLC
5117 Fairfax Dr. NW
Albuquerque, NM 87114
Phone: 505/585-2550
E-mail: dave@swgeophys.com

LEWIS LAND
National Cave and Karst Research Institute
400-1 Cascades Ave.
Carlsbad, NM 88220
Phone: 575/932-9912
Email: lland@nckri.org

CONTENTS

Preface

INTRODUCTORY AND GENERAL PAPERS

1 **Overview of Evaporite Karst in the Greater Permian Evaporite Basin (GPEB) of Texas, New Mexico, Oklahoma, Kansas, and Colorado, USA**
Kenneth S. Johnson

39 **Evaporite Karst in the Greater Permian Evaporite Basin of Texas, New Mexico, Oklahoma, Kansas, and Colorado as Delineated by USGS Karst Mapping**
David J. Weary and Daniel H. Doctor

51 **Identification of Gypsum, Anhydrite, and Salt on Geophysical Logs in the Greater Permian Evaporite Basin**
Kenneth S. Johnson

WEST TEXAS AND SOUTHEASTERN NEW MEXICO

63 **Evaporite Karst as a Transportation and Infrastructure Geohazard in the Lower Pecos Region, Southeastern New Mexico and West Texas**
Lewis Land

79 **Geophysical Characterization of Playa Lakes in the Gypsum Karst of Southeastern New Mexico, USA**
David D. Decker, Lewis Land, and Barbara Luke

93 **Determining Annual to Decadal Subsidence Areas and Rates Using Airborne Lidar, GPS Surveys, and Topographic Maps at the Wink Sinkholes, West Texas**
Jeffrey G. Paine, Lucie Costard, John Andrews, Aaron Averett, Kutalmis Saylam, and John Hupp

105 **Sinkholes in Wink, Texas Observed by Satellite Radar Imagery**
Jin Woo Kim and Zhong Lu

111 **Assessing Collapse Risk in Evaporite Sinkhole-Prone Areas Using Commonly Available Oil Field Data in the Area of the Wink Sinks, Winkler County, Texas**
Robert C. Trentham and Miles A. Henderson

125 **Evaporite Dissolution and the Waste Isolation Pilot Plant (WIPP) in the Northern Delaware Basin, Southeastern New Mexico**
Dennis W. Powers and Robert M. Holt

151 **Speleogenetic Evolution of Castile Karst Manifestations of the Delaware Basin, West Texas and Southeastern New Mexico**
Kevin W. Stafford and Jessica Shields

165 Physical and Chemical Controls on Suffosion Development in Gypsic Soil, West Texas
Jonah Morris, Kevin Stafford, and Kenneth Farrish

177 Geophysical Delineation of Megaporosity and Fluid Migration Pathways for Geohazard Characterization within the Delaware Basin, Culberson County, Texas
Jonathan Woodard, Wesley Brown, and Kevin Stafford

189 Speleogenetic Model of Evaporite-Karst Occurrences of the Gypsum Plain Using Karst Mapping and LiDAR Analyses in Culberson County, Texas, USA
Jon T. Ehrhart and Kevin W. Stafford

201 A Novel Approach to Delineating Lithologic Variability of a Karsted Landscape Using CIR Imagery and GIS Analyses, Eddy County, New Mexico
Jessica Shields and Kevin W. Stafford

213 Evaporite Karst in the Permian Rustler, Salado, and Castile Formations at Red Bluff Dam on the Pecos River, Loving and Reeves Counties, Texas
Kenneth S. Johnson, Richard A. Shoemaker, John Charlton, and Cris Parker

233 Design and Implementation of a Grout Program in an Evaporite-Karst Foundation, Red Bluff Dam, Loving and Reeves Counties, Texas
John Charlton, Jenn Ostrowsky, Richard A. Shoemaker, and Kenneth S. Johnson

OKLAHOMA AND TEXAS PANHANDLE

247 Permian Blaine and San Andres Formations of Western Oklahoma and Palo Duro Basin of Texas: Their Correlation and Evaporite Karst
Kenneth S. Johnson

279 Delhi Sinkhole and Watonga Sinkhole Caused by Gypsum Karst in the Permian Blaine Formation of Western Oklahoma
Kenneth S. Johnson

KANSAS AND COLORADO

285 This Time it's Natural: Sinkhole Under Interstate 135 in McPherson County, Kansas
Neil M. Croxton

295 Karst Feature Predictability Models Within Barber County, Kansas
G.M. Kelner, K.L. Gauvey, and J.B. Sumrall

305 Gypsum Karst in South-Central Kansas
Kaitlyn L. Gauvey and Jonathan B. Sumrall

319 Salt Dissolution and the Wallace Sinkhole in the Sharon Springs–Wallace area, Wallace County, Western Kansas
Kenneth S. Johnson

337 Dissolution of the Permian Flowerpot Salt Beneath the Great Plains Reservoirs, Queens State Wildlife Area, in Kiowa, Prowers, and Bent Counties, Southeast Colorado
Kenneth S. Johnson

Overview of Evaporite Karst in the Greater Permian Evaporite Basin (GPEB) of Texas, New Mexico, Oklahoma, Kansas, and Colorado, USA

Kenneth S. Johnson
Retired Geologist, Oklahoma Geological Survey,
Norman, Oklahoma

ABSTRACT.—One of the major evaporite regions in the world is herein named the Greater Permian Evaporite Basin (GPEB). This evaporite region extends far beyond the traditional Permian Basin of west Texas and southeast New Mexico, and embraces about 650,000 km^2 in parts of Texas, New Mexico, Oklahoma, Kansas, and Colorado. The eight main Permian evaporite sequences, each containing salt (halite) and gypsum and/or anhydrite, have a combined thickness generally ranging from 500 to 1500 m in various parts of the GPEB, and the evaporites extend from west Texas to northern Kansas and northeast Colorado. The GPEB embraces several structural and/or sedimentary basins, including the Delaware, Midland, Palo Duro, Hardeman–Hollis, Dalhart, Anadarko, Denver (south), Hugoton, and Salina Basins, each of which contains one or more thick sequences of Permian evaporites. Gypsum and/or anhydrite deposits are more widespread than salt deposits in the GPEB: anhydrite is the common form of calcium sulfate at depths below about 15 to 30 m, whereas gypsum is almost always the calcium sulfate at shallower depths and in outcrops.

Evaporites are the most soluble of the common rocks. Salt (halite, NaCl) and gypsum ($CaSO_4 \bullet 2H_2O$) can be dissolved naturally, or by human activities, to form the same kinds of karst features present in limestone and dolomite, such as caves, sinkholes, breccia pipes, disappearing streams, springs, and even catastrophic collapses (sinks or sinkholes). Anhydrite ($CaSO_4$), in contact with water, transforms to gypsum and then is susceptible to dissolution. Water in contact with salt or gypsum will dissolve some of the rock, if the water is unsaturated with respect to NaCl or $CaSO_4$, respectively, and will continue to dissolve the rock if it is contacted by additional unsaturated water. Evaporite karst is present in most parts of the GPEB.

Salt sequences underlie about 380,000 km^2 of the GPEB, and salt karst occurs naturally where the deep-seated salt beds rise to shallow depths of about 150 to 300 m. Each of the eight evaporite sequences in the GPEB has areas where natural salt dissolution occurs at least somewhere in the region. Two major examples of natural salt karst are (1) large subsidence troughs in the Delaware Basin that are now filled with Cenozoic sediments and (2) extensive dissolution of San Andres and Flowerpot/Blaine/Yelton salts in the Texas Panhandle, western Oklahoma and Kansas, and southeast Colorado. Salt karst can also occur when human activity, such as solution mining or some petroleum-related activities, enables unsaturated water to intentionally, or accidentally, dissolve the salt and create a water-filled cavity large enough to allow failure of its roof, and eventual collapse that can reach the land surface as a huge sinkhole. Examples of human-induced salt karst because of solution mining are the Cargill, Denver City, Borger, JWS, and Loco Hills Sinks. Salt-karst sinks related to petroleum or water supply activities include the Wink, McCamey, Jal, Panning, Berscheit, Hilton, Witt, and Crawford Sinks; other fea-tures related to petroleum activities are the Hutchinson gas explosion, the Freedom gas blowout, and Pecos County subsidence.

Johnson, Kenneth S., 2021, Overview of Evaporite Karst in the Greater Permian Evaporite Basin (GPEB) of Texas, New Mexico, Oklahoma, Kansas, and Colorado, USA, *in* Johnson, K. S.; Land, Lewis; and Decker, D. D. (eds.), Evaporite Karst in the Greater Permian Evaporite Basin (GPEB) of Texas, New Mexico, Oklahoma, Kansas, and Colorado: Oklahoma Geological Survey, Circular 113, p. 1–37.

Gypsum deposits underlie the entire 650,000 km^2 of the GPEB, and natural gypsum karst is common and widespread in areas of gypsum outcrops on the east and west sides of the region. Gypsum caves and sinkholes are abundant in the Delaware Basin of west Texas and southeast New Mexico, and include the Parks Ranch Cave which, with a total length of 6596 m, is the second longest gypsum cave in the western hemisphere. And on the east flank of the GPEB, the other major gypsum-karst area in the GPEB, major caves in Oklahoma include: (1) D.C. Jester Cave, which, with a total length of 10,065 m, is the longest gypsum cave in the western hemisphere; (2) Alabaster Cavern, developed as a major tourist cave; and (3) Selman Cave, which is now an outdoor living laboratory and field station dedicated to research and teaching. Natural gypsum karst has caused the abandonment of proposed and actual damsites in Oklahoma, Texas, and New Mexico. Gypsum karst can, however, be an advantage: the freshwater Blaine aquifer provides irrigation water in southwest Oklahoma and north-central Texas. Although gypsum karst can also be accelerated by human activities, the only examples in the GPEB are: (1) reservoirs that are now losing water through gypsum-karst features and (2) reservoirs that had been proposed or built (and are now abandoned) in areas of gypsum karst.

THE GREATER PERMIAN EVAPORITE BASIN (GPEB)

The traditional Permian Basin of west Texas and southeast New Mexico is a complex system of basins, platforms, and shelf areas that contain sedimentary rocks and sediments of Cambrian through Quaternary age and covers an area of nearly 200,000 km^2 (Figure 1). Permian-age rocks in the Permian Basin are mostly dominated by evaporites—mainly salt (halite) and gypsum or anhydrite. However, these evaporites are not restricted to what is regarded as the traditional Permian Basin area: they extend a great distance to the north, and lesser distances to the east and west. This vast region, herein named the GPEB, embraces about 650,000 km^2 in parts of Texas, New Mexico, Oklahoma, Kansas, and Colorado, where Permian gypsum/anhydrite beds can be continuously traced (Figure 2): Permian salt sequences underlie about 380,000 km^2 of this region. The thickness of these Permian evaporites in the GPEB generally ranges from about 500 to 1500 m, and this is one of the thickest and most extensive accumulations of evaporites in the world. Typically, the evaporites are interbedded with redbed clastics and thinner carbonates; however, redbeds and/or carbonates locally make up a large, or even a greater, portion of the evaporite sequence.

The GPEB has been an area of major petroleum exploration and production since the early 1900s. With the development of hydraulic fracturing, horizontal drilling, and advancements in well completion technology over the past two decades, exploration and petroleum production in many parts of the GPEB have increased sharply. In addition to potential environmental and engineering problems related to living in, or construction on, areas of evaporite karst, virtually all exploration boreholes drilled for petroleum or other purposes in the region entail drilling through one or several Permian-age evaporite units. This may result either in encountering natural

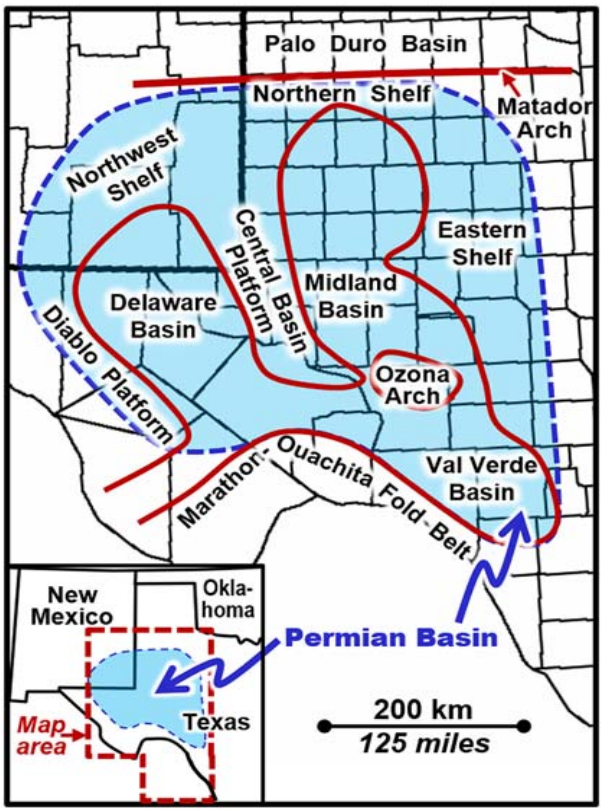

Figure 1. Map of the traditional Permian Basin of west Texas and southeast New Mexico showing major structural and tectonic features, including basins, platforms, and shelf areas.

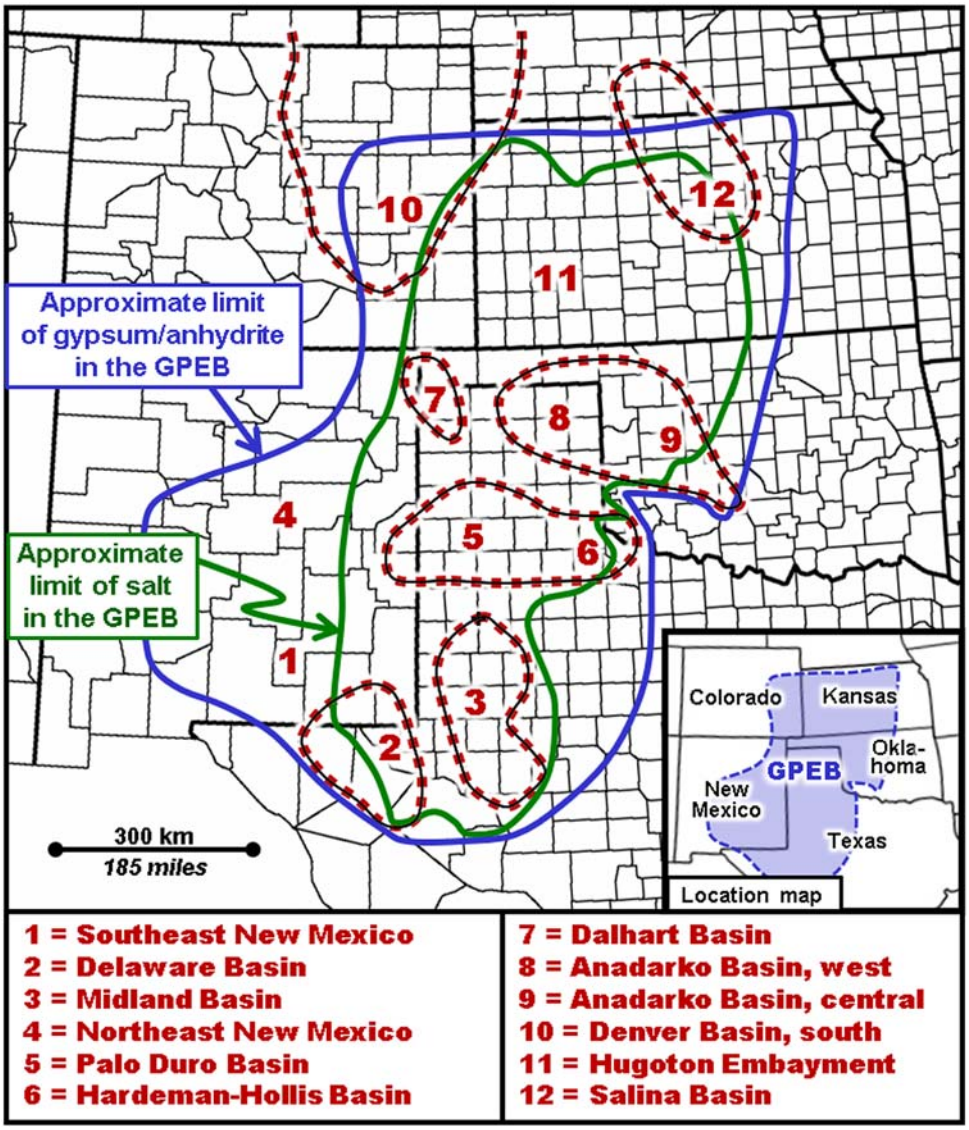

Figure 2. Map showing: (1) approximate limits of Permian salt and gypsum/anhydrite in the Greater Permian Evaporite Basin (GPEB); (2) outlines of major structural/sedimentary basins (dotted red lines) in GPEB; and (3) stratigraphic columns 1–12 (red numbers and names) that are shown in Figure 3.

evaporite-karst features that complicate drilling operations, or the boreholes may create man-made karst problems where inadvertent dissolution of evaporites and formation of water-filled cavities can result in subsidence, collapse, or sinkholes at the land surface.

The GPEB is somewhat similar to the earlier concept of the "Permian salt basin," as used by Bachman and Johnson (1973, p. 2) when they referred to the region that "includes a series of discontinuous sedimentary basins in which halite and associated salts accumulated during Permian time." The difference is that their "Permian salt basin" embraces just the area underlain by salt, whereas the GPEB includes the 650,000 km^2 underlain by salt *and* intimately associated gypsum/anhydrite.

Boundaries of the GPEB on the east and west are erosional limits, where the evaporite units crop out, and on the south, it is the Marathon–Ouachita Fold Belt. The north limit of the basin is where the Wellington evaporites grade into clastics in north-central Kansas, and where the Blaine Formation is less than 6 m thick in northwest Kansas and the Denver Basin of northeast Colorado. A number of Permian evaporites (mainly salt) are present farther north in the Denver Basin, and beyond, but they are not traced continuously into evaporites at the north end of the GPEB.

Within the GPEB are a number of major structural and/or sedimentary basins, including (from the south) the Delaware, Midland, Palo Duro, Hardeman–Hollis, Dalhart, Anadarko, Denver (south), Hugoton, and Salina Basins (Figure 2). Each of these basins has been the site for the accumulation of thick sequences of Permian rocks, and evaporites make up a significant (or major) part of the Permian in each area. Figure 3 shows the

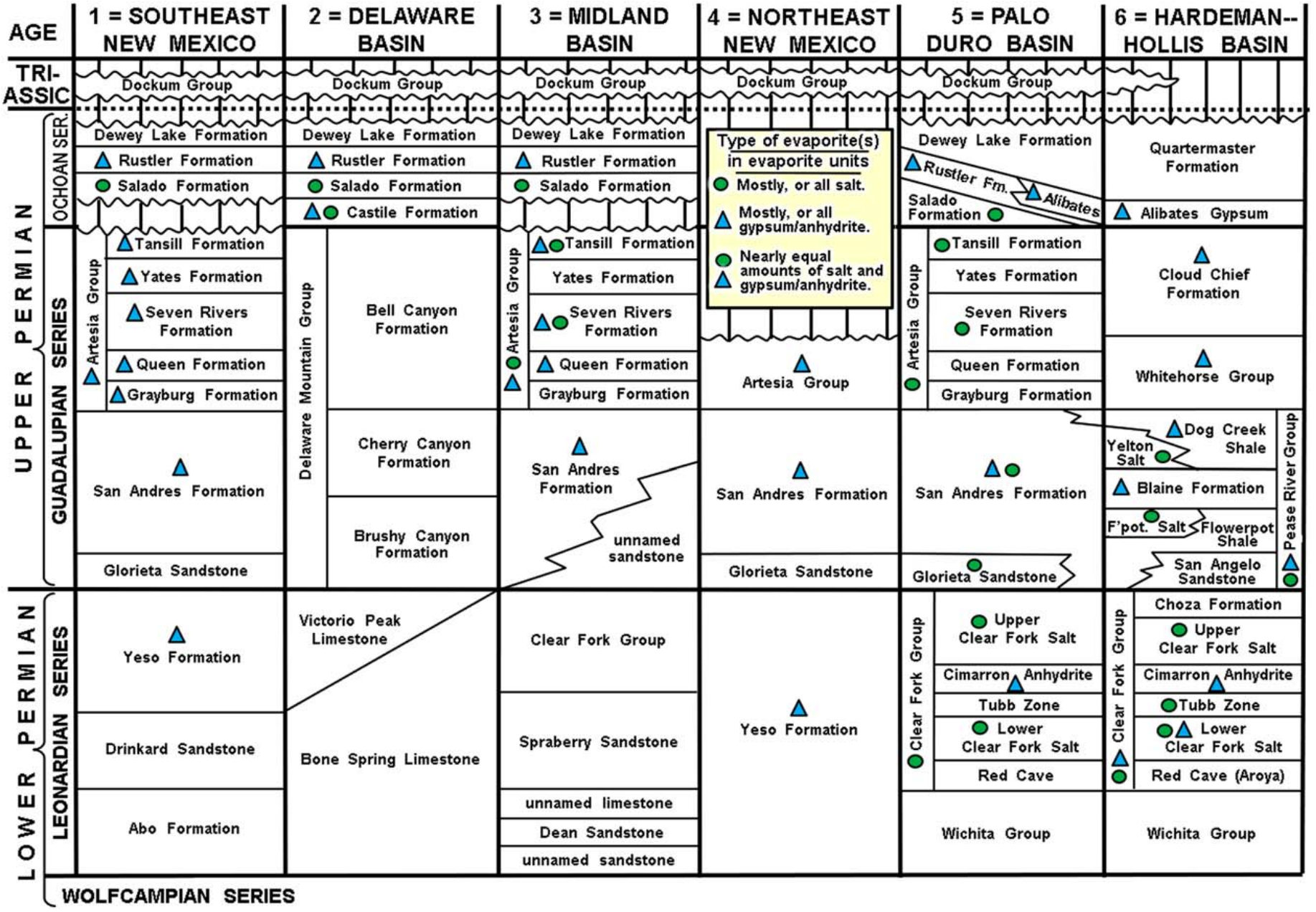

Figure 3. Stratigraphic nomenclature of Permian strata in GPEB showing rock units containing significant amounts of salt and/or gypsum/anhydrite. Location of columns 1–12 is shown in Figure 2.

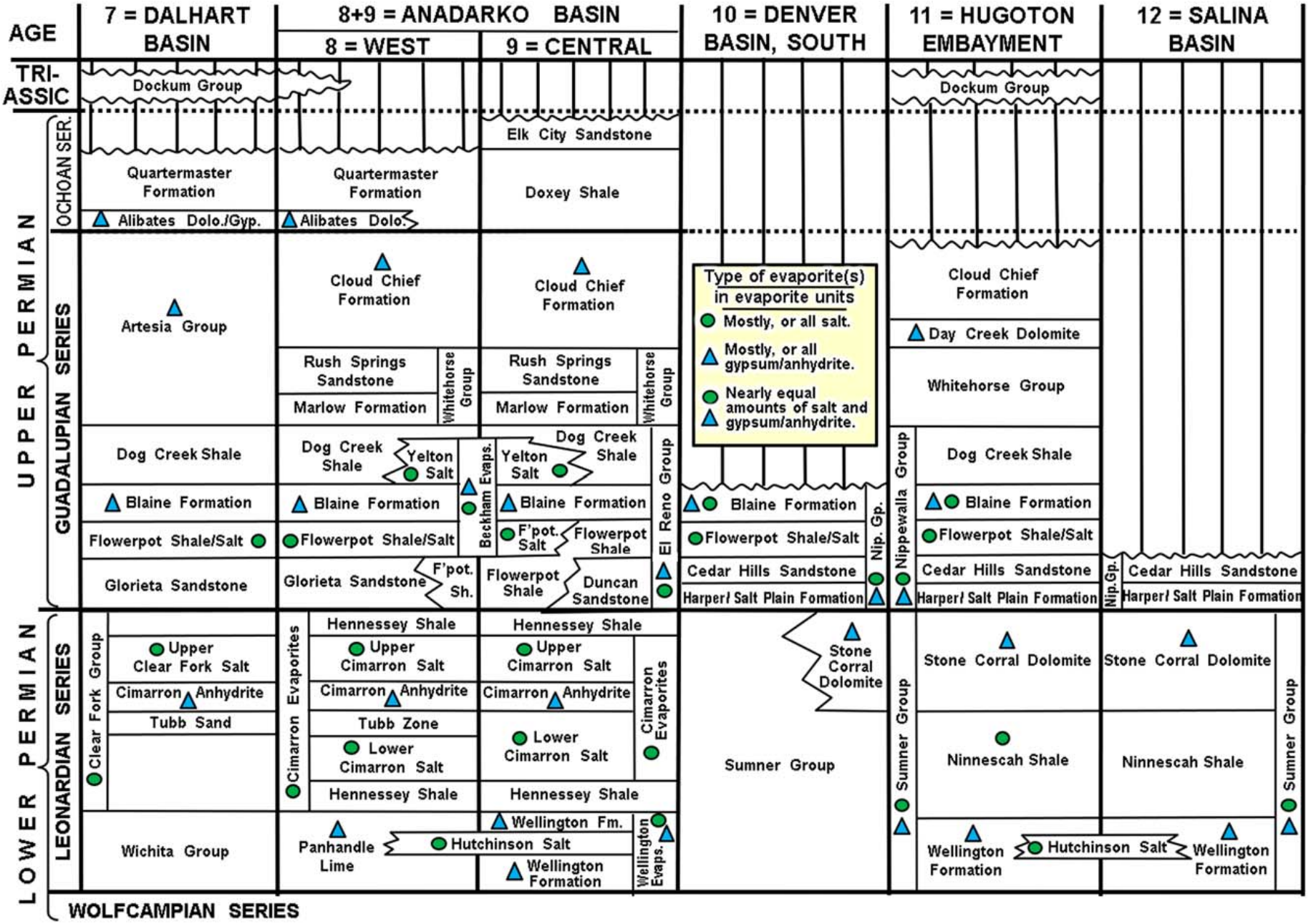

Figure 3 (continued). Stratigraphic nomenclature of Permian strata in GPEB showing rock units containing significant amounts of salt and/or gypsum/anhydrite. Location of columns 1–12 is shown in Figure 2.

Permian stratigraphic units in each of the 12 basins or shelf areas identified in the GPEB as shown in Figure 2, and indicates those units that contain significant amounts of evaporites (salt and/or gypsum/anhydrite). This two-part chart (Figure 3) is modified slightly from four charts published by the American Association of Petroleum Geologists in 1983–1988 as "Correlation of Stratigraphic Units of North America (COSUNA) Project." The four COSUNA charts are "Texas–Oklahoma Tectonic Region," "Mid-Continent Region," "Southwest/Southwest Mid-Continent Region," and "Central and Southern Rockies Region." Note that, in Figure 3, where the type of evaporite in a rock unit is mostly salt or gypsum/anhydrite, it does not mean that the evaporite(s) is/are necessarily the major rock type: the unit may be mostly limestone, sandstone, or shale, but if evaporites are a significant part of the rock unit, then I want to show which of the evaporites is more abundant. Note also, in Figure 3, that some workers place the Glorieta/San Angelo/Duncan Sandstone in the Leonardian Series, along with part or all of the Nippewalla Group.

Figure 4 is a schematic cross section summarizing the distribution, principal evaporite(s), and nomenclature of each of the principal evaporite units in the GPEB. It summarizes data from Figure 3, and graphically shows that evaporite deposition was a dominant aspect of Permian history throughout the region. Furthermore, it demonstrates the continuity of evaporite deposition from its earliest phase of Wellington/Hutchinson evaporites in the north, to the final stages of Rustler evaporite deposition in the Delaware Basin area of west Texas and southeast New Mexico in the south. Clearly, it shows that the evaporite depocenter moved progressively to the south (or south-southwest) during approximately 25 million years of the Leonardian, Guadalupian, and Ochoan Epochs. The close relationships and continuity of these evaporite units throughout the region shows why we can group them into a nearly continuous sequence of evaporite deposition in the "Greater Permian Evaporite Basin."

The eight major evaporite units in the GPEB are, starting with the oldest: (1) Wellington/Hutchinson; (2) Lower Clear Fork/Lower Cimarron; (3) Upper Clear Fork/Upper Cimarron; 4) San Andres/Flowerpot/Blaine/Yelton; (5) Artesia; (6) Castile; (7) Salado; and (8) Rustler (Figure 4). Five lesser units that consist only, or predominantly, of gypsum/anhydrite as the evaporite are, from

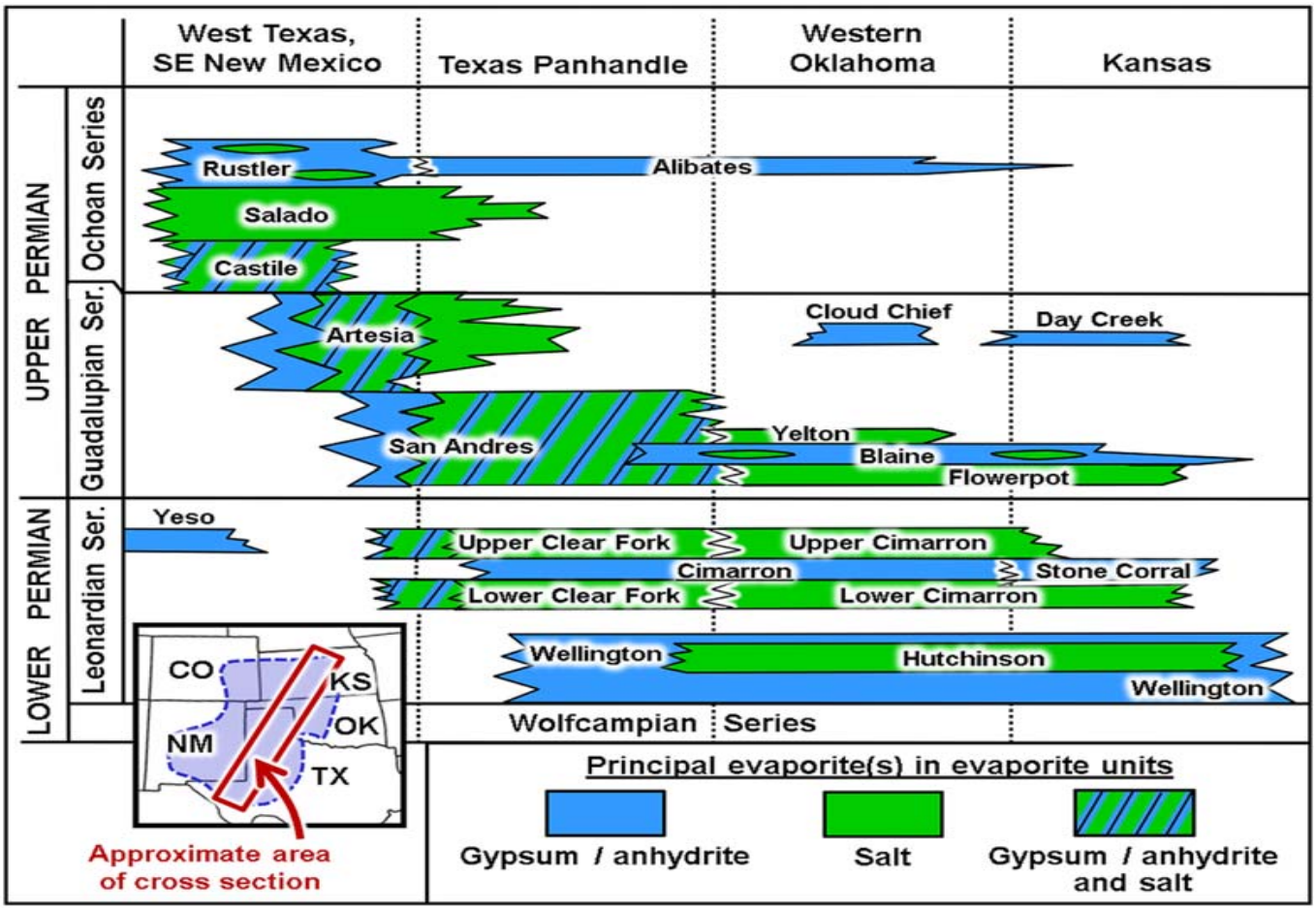

Figure 4. Schematic cross section showing nomenclature of each of the principal evaporite units in the GPEB. There is a progressive shift to the south of the depocenter for evaporite deposition from Leonardian through Ochoan time. This cross section shows the evaporite units identified in Figure 3.

the oldest: (1) Cimarron/Stone Coral; (2) Yeso; (3) Cloud Chief; (4) Day Creek; and (5) Alibates. Gypsum/anhydrite beds in these five lesser units typically are 3 to 30 m thick.

Maps of seven major Permian salt units in the GPEB (Figure 5) show the approximate distribution of these salt units, and also indicate areas where natural dissolution of each of the salt units is occurring, or has occurred in the past. Although the Rustler Formation is one of the eight major evaporite units in the GPEB, it has relatively minor amounts of salt that have escaped dissolution (Powers and Holt, 2000) and it is not here considered a major salt-bearing unit. Numerous reports have been done on individual salt deposits in the various parts of the GPEB, and the reader is referred to the five State Geological Surveys as prime sources of this information. Comprehensive overviews covering all the salt units throughout the entire region are provided by Pierce and Rich (1962), Lefond (1969), Johnson and Gonzales (1978), and Ege (1985). The oldest salt unit, the Hutchinson Salt (Figure 5A), is in the far north of the GPEB, and, in general, younger salt units are in progressively more southerly positions.

Permian gypsum and/or anhydrite deposits are more widespread than the salt in the GPEB (Figure 2), and gypsum crops out in many parts of the region. Anhydrite ($CaSO_4$) is the common form of sulfate rock in the moderate-to-deep subsurface (at depths of more than about 15 to 30 m below land surface), whereas gypsum ($CaSO_4 \cdot 2H_2O$), which results from hydration of anhydrite, is almost always the sulfate rock at shallow depths, and certainly in most outcrops. In this report, I will commonly use the term gypsum to refer to either gypsum or anhydrite when referring to sulfate rock in outcrops or shallow subsurface. There are many reports on individual gypsum units in various parts of the GPEB, and again the reader is referred to the five State Geological Surveys as prime sources of this information. Comprehensive bibliographies or discussions of principal gypsums throughout the region are provided by Withington and Jaster (1960), Withington (1962), Smith and others (1973), and Johnson and others (1989).

NATURAL EVAPORITE KARST IN THE GPEB

Evaporites, including salt (halite, NaCl) and gypsum ($CaSO_4 \cdot 2H_2O$), are the most soluble of the common rocks. They are dissolved readily to form the same type of karst features normally found in limestone and dolomite, such as caves, sinkholes, breccia pipes, disappearing streams, springs, and (occasionally) dramatic or catastrophic subsidence features. The process for dissolution of evaporites was discussed by Johnson (1981, 2005b) with reference to salt dissolution, but the principles also apply to gypsum dissolution: groundwater in contact with salt or gypsum will dissolve some of the rock, providing that the water is not already saturated with NaCl or $CaSO_4$, respectively. For extensive dissolution to occur, the resulting brine must be removed from the evaporite rock, or else the brine becomes saturated and the dissolution process stops. The basic requirements for evaporite dissolution to occur are (1) a deposit of salt or gypsum against which, or through which, water can flow; (2) a supply of water unsaturated with NaCl or $CaSO_4$, respectively; (3) an outlet whereby the resulting brine can escape; and (4) energy, such as a hydrostatic head or density gradient, to cause water to flow through the system. Examples of natural evaporite karst are present in most parts of the GPEB, and the following discussion will highlight only some of them. Once again, the reader is referred to the five State Geological Surveys as prime sources of information about areas and examples of evaporite karst in their state.

Natural Salt Karst

Salt deposits underlie most parts of the GPEB (Figures 2, 5), and natural dissolution is, or has been, going on along some part of the periphery of all seven of the major salt units (Figure 5). Whereas dissolution fronts are widespread in most of these salt units, the Lower and Upper Cimarron salts (Figure 5B and 5C) are being dissolved at relatively shallow depths only in small portions of northwest Oklahoma (the dissolution front of the Lower Cimarron salt may also extend into southwest Kansas). Dissolution has been going on in the Texas Panhandle (Figure 5D) at least since Miocene–Pliocene time (Gustavson and Finley, 1985), and it's likely that it has persisted in some areas even longer than that, perhaps even as early as Late Cretaceous time. Figure 6A shows the areas or sites of natural salt karst in the GPEB. Evidence that natural dissolution of salt is still going on is clearly shown by virtue of the many salt plains and salt springs that are present in the Arkansas, Red, Brazos, and Pecos River drainage areas.

Examples of Natural Salt Karst

Delaware Basin Subsidence Troughs. One of the areas of significant paleodissolution of salt is in the Delaware Basin, which contains a great thickness of Castile and Salado salts (Figures 5, 6A, 7, 8). An excellent summary of the geologic setting, the evaporites, and karst features in the Delaware Basin is provided by Hill (1996), and further discussion of a variety of karst features in southeast New Mexico is given by Hill (2003). Salt beds in the Castile Formation have been dissolved on the west side of the Delaware Basin, and those in the Salado Formation are dissolved on the west and east sides of the basin: most of the dissolution occurred during the Cenozoic Era and was accompanied by subsidence of overlying strata and infilling of the subsidence

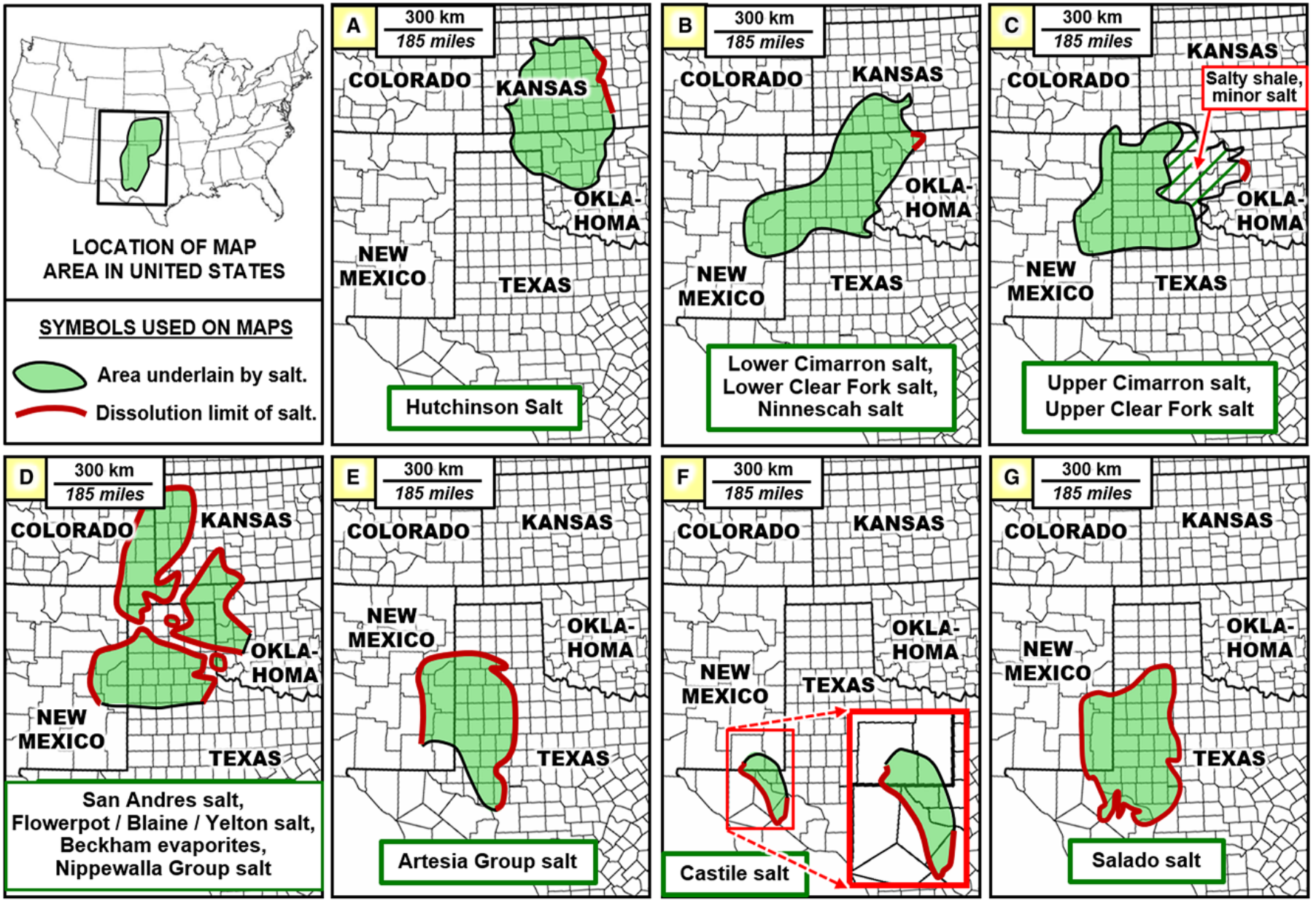

Figure 5. Maps showing approximate distribution and dissolution limits of seven major Permian salt units in the GPEB of southwestern United States. Based primarily on Pierce and Rich (1962), Johnson and Gonzales (1978), and Ege (1985).

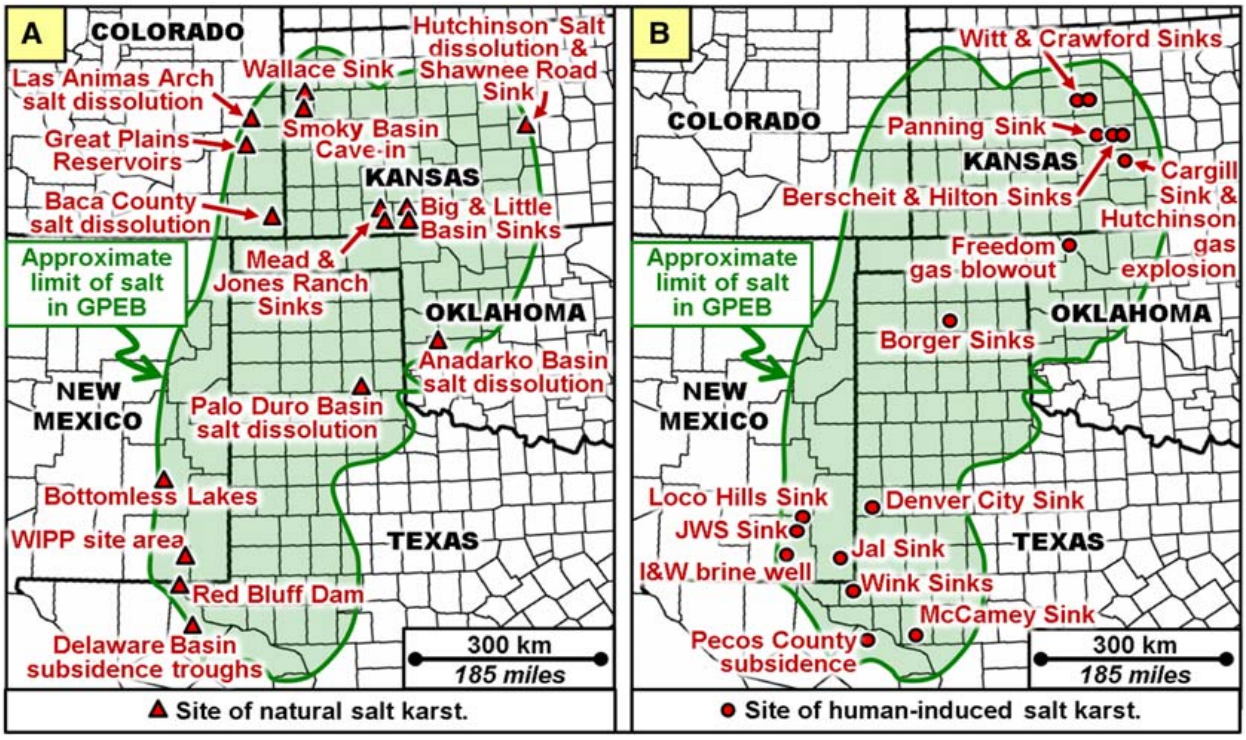

Figure 6. Sites of natural or human-induced salt karst in the GPEB discussed in this report. (A) Natural salt karst and (B) Human-induced salt karst.

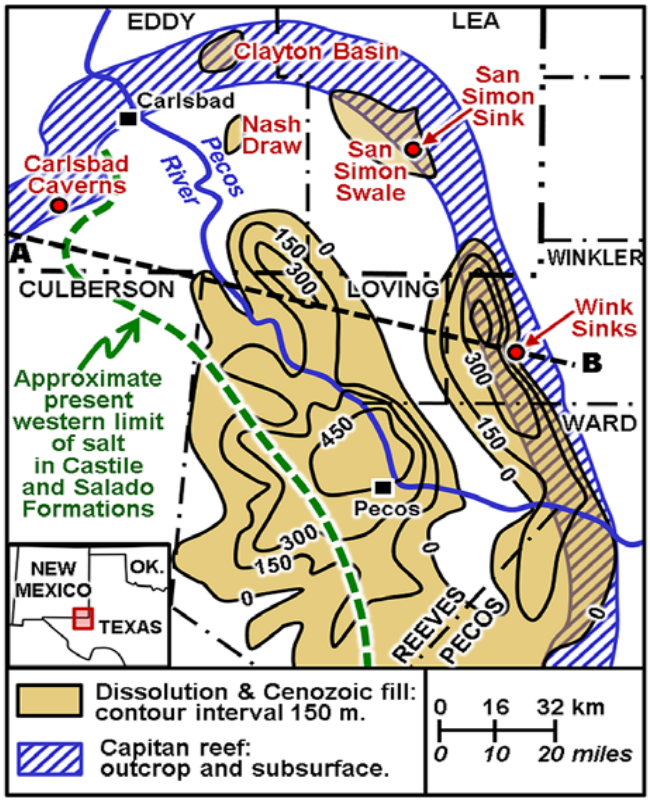

Figure 7. Map of Delaware Basin showing dissolution/collapse features that resulted in subsidence basins with Cenozoic fill. Modified from Maley and Huffington (1953) and Baumgardner and others (1981). Cross section A—B is shown in Figure 8.

troughs with more than 450 m of Cenozoic fill (Maley and Huffington, 1953; Lambert, 1983; Bachman, 1984) (Figures 7, 8). The stratigraphic positions of the dissolved Castile salt beds on the west side of the basin are now marked by zones of brecciated anhydrite that result from collapse and lowering of overlying units (Anderson and others, 1972, 1978; Anderson, 1981).

Red Bluff Dam. Red Bluff Reservoir, located adjacent to the small community of Red Bluff on the Pecos River in Loving and Reeves Counties, Texas (Figure 6A), has experienced a loss of water through collapse features and karst zones in the outcropping Rustler Formation that underlies the dam foundation. Rocks in the Rustler are largely broken up and chaotic, mainly because of natural dissolution of salt and gypsum in the Rustler and the underlying Salado and Castile Formations (Johnson and others, 2021). The Rustler consists mainly of interbedded dolomite, gypsum, and shale, and originally it also contained some salt interbeds. Dissolution of the salt and gypsum has caused extensive collapse structures and breccia pipes, and as water flows in and around the brecciated rock it further dissolves the gypsum and dolomite to produce additional karst features beneath the dam. The dam was completed in 1936, and soon afterward extensive seepage was noted at several places along the toe and downstream slope of the dam. Initial programs for grouting the dam's foundation were carried out in 1973 and 1978, and details of the latest grouting program are discussed by Charlton and others (2021).

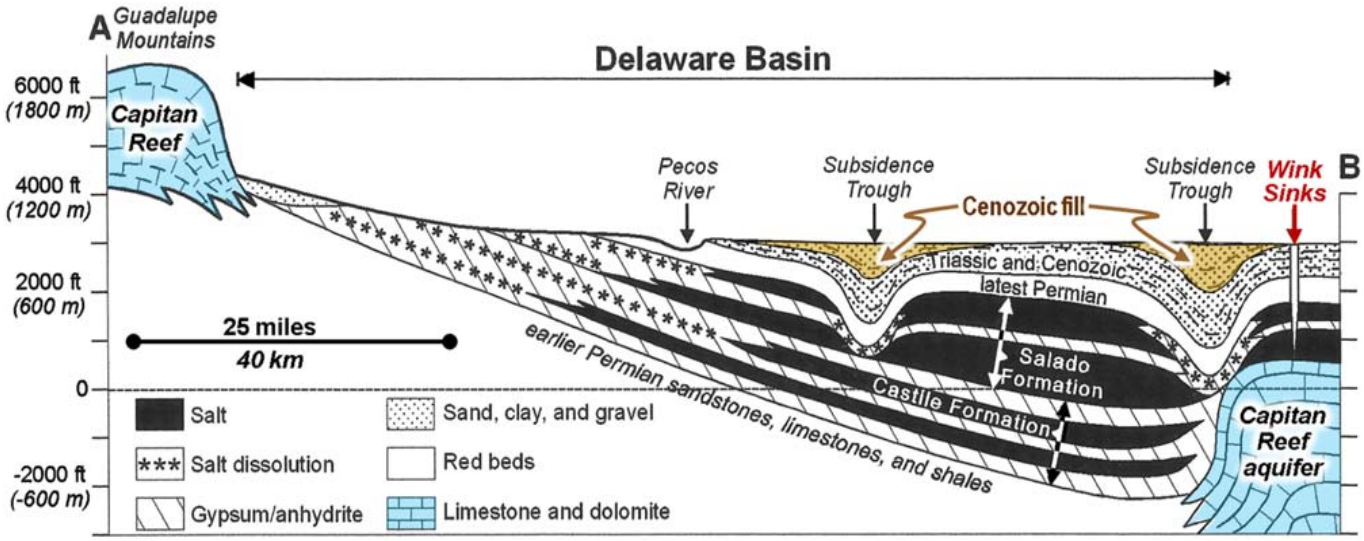

Figure 8. Cross section through Delaware Basin showing sediment-filled subsidence troughs resulting from the natural dissolution of salt and collapse of overlying strata (modified from Martinez and others, 1998). Wink Sinks are shown at east end of cross section. Location of cross section is shown in Figure 7.

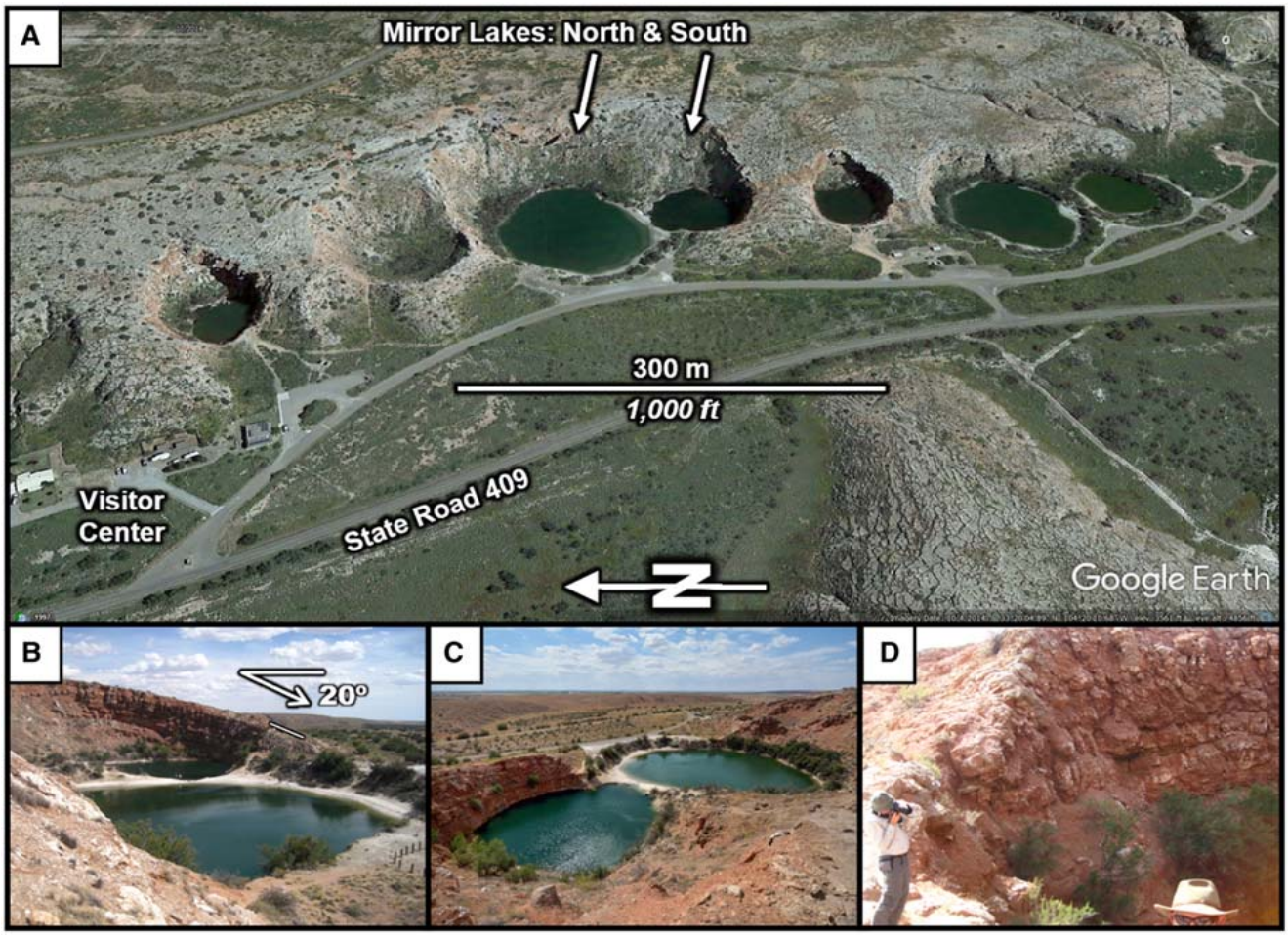

Figure 9. Views of Bottomless Lakes State Park. (A) Oblique aerial view of sinkholes; Google Earth, dated October 4, 2014. (B) View of Mirror Lakes, looking to south; gypsum beds dip sharply (20°) to southwest, because of dissolution of underlying salt and gypsum. (C) View of Mirror Lakes, looking to northwest; photo courtesy Anthony H. Cooper. (D) View of red-stained gypsum (white on fresh surfaces) and redbeds of Artesia Group in wall of sinkhole.

Waste Isolation Pilot Plant (WIPP) Site Area. The WIPP has been intensively investigated for the possibility of salt karst that could adversely impact the safe, long-term storage of radioactive waste from US defense programs (investigations summarized in Powers and Holt, 2021). Since 1999, transuranic wastes have been placed in mined-out cavities in salt beds of the Salado Formation at a depth of about 650 m at the WIPP site, about 40 km east of Carlsbad, in Eddy County, New Mexico (Figure 6A). Although salt karst is known in the vicinity of the WIPP site, it has not been identified within the boundaries of the project area, except for evidence of minor salt dissolution in the middle part of the overlying Rustler Formation. Surface evidence of evaporite karst is present in Nash Draw, to the west of the WIPP site, and five "dome" or breccia-pipe structures located about 17 to 32 km northwest of WIPP—several of which result from the deep-seated dissolution of salt beds. Although the WIPP site has yielded only minor evidence of natural salt dissolution, it is included in this report because of the intensive evaporite-karst research that has been conducted in the surrounding areas and is documented by Powers and Holt (2021).

Bottomless Lakes. Major karst features along the lower Pecos River Valley are present in the Bottomless Lakes State Park (BLSP) area, about 18 km ESE of Roswell, in Chaves County, New Mexico (McLemore, 1999; Land, 2003; Rawling and McCraw, 2010) (Figures 6A, 9). Natural ground-water movement and dissolution of salt and gypsum in the underlying San Andres artesian aquifer and the lower part of the Artesia Group have caused the collapse of the outcropping upper Artesia Group (Seven Rivers Formation in BLSP) gypsum and redbeds, thus forming a series of cenotes, or sinkhole lakes (the "Bottomless Lakes"). Water in all the lakes comes entirely from groundwater seepage, and evidence of salt and gypsum dissolution is found in the brackish and saline quality of water in four of the lakes (Land 2003): total dissolved solids range from about 6000 to 38,000 ppm, and average about 21,000 (all figures are in ppm); chlorides range from about 2150 to 15,600, and average about 8600; and sulfates range from about 2100 to 8900, and average about 4800.

Sinkholes at BLSP are adjacent to the Pecos River floodplain, and the river is now located about 2 km to the west. Artesia Group strata normally dip about 1° to the east in the area, but at BLSP they dip sharply to the southwest at 20–40° (Land, 2003) because of dissolution of underlying salt and gypsum beds (Figure 9B). Most of the sinkholes and lakes are 50 to 100 m in diameter (Figure 9A), but Lea Lake (not shown in Figure 9A), formed by the coalescence of several sinkholes, measures about 250 m by 400 m. The steep-to-vertical walls of the sinkholes are generally 30 to 60 m high, and the depth of water in the lakes ranges from about 5 to 27 m. Although these sinkholes have been present since prehistoric times, the continued mass wasting and collapse of the cenote walls shows that dissolution is still going on in the area (Land, 2003).

Palo Duro Basin Salt Dissolution. Natural dissolution of salts in the San Andres Formation is widespread in the Texas Panhandle (Figures 6A, 10, 11), and has been going on since at least Miocene–Pliocene times (Gustavson, 1986). The Bureau of Economic Geology, at The University of Texas at Austin, has conducted extensive studies of salt deposits and salt karst in the Texas Panhandle: pertinent references and a brief summary of these studies are given by Johnson (2021a).

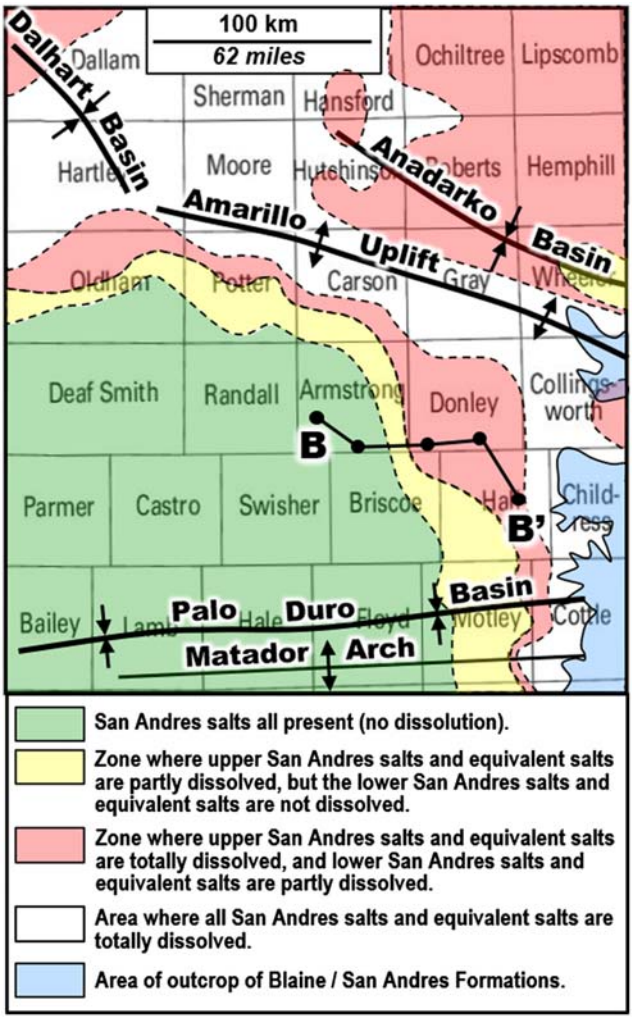

Figure 10. Map showing zones of salt dissolution in the lower and upper San Andres Formation and equivalent strata in the Palo Duro, Dalhart, and Anadarko Basins. Based on work by Presley (1981) in the Palo Duro Basin, and by Jordan and Vosburg (1963) and Johnson (1976) in the Dalhart and Anadarko Basins. Cross section B—B' is shown in Figure 11.

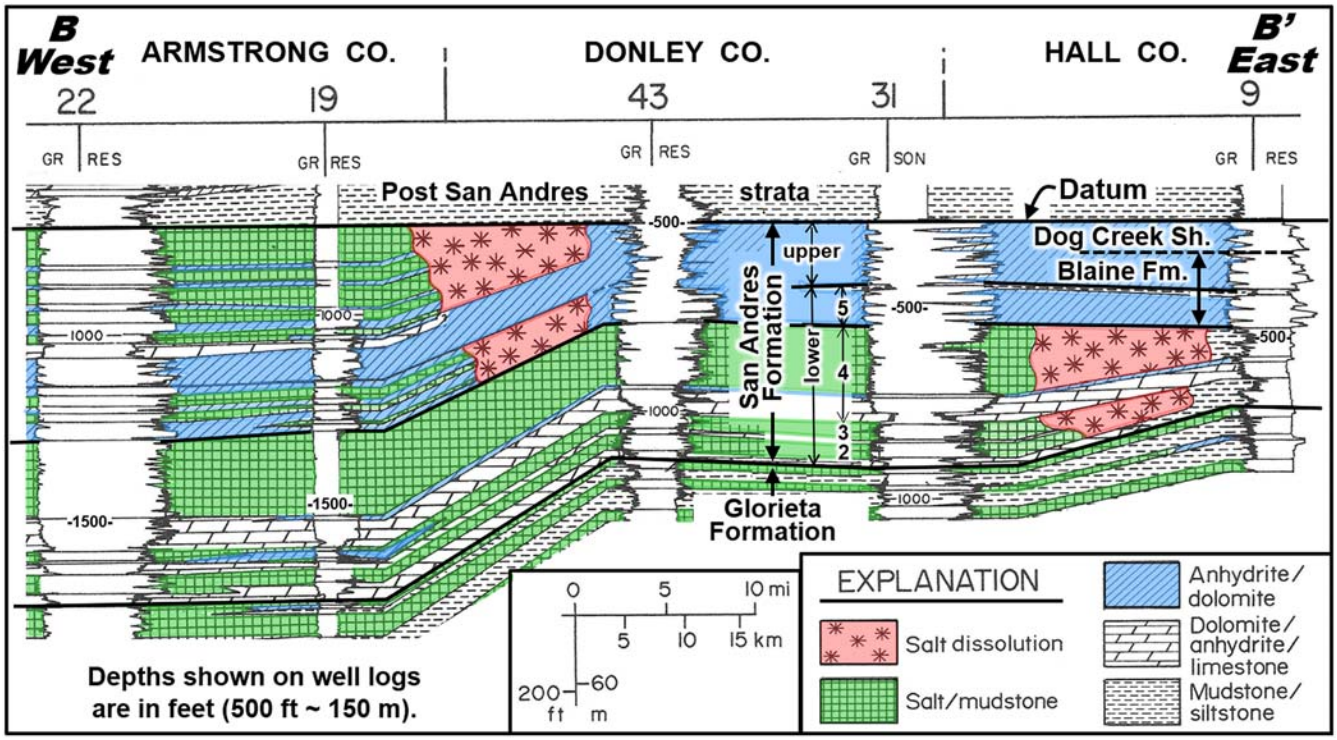

Figure 11. Regional stratigraphic cross section B—B' showing transition of part of the San Andres Formation to the Blaine Formation in the Palo Duro Basin (modified from Presley, 1981). Salt beds of the San Andres in the Palo Duro Basin are all dissolved where they approach the eastern outcrops in north-central Texas. Location of cross section is shown in Figure 10.

Net salt thicknesses of up to 120 m in the lower San Andres, and up to 90 m in the upper San Andres, are present in the deep Palo Duro Basin: these salt beds are partially or totally dissolved where they rise to depths of 150 to 300 m below the current land surface. At these relatively shallow depths, dissolution and removal of the salt has caused overlying strata to be fractured, disrupted, and chaotically dropped, resulting in sinkholes, complex folds, faults, breccias, and breccia pipes. A cross section in the east part of the Palo Duro Basin (Figure 11) shows that the upper San Andres salts are dissolved at a depth of about 150 m in Well #43, and the remaining lower San Andres salts are also dissolved where they would be at a depth of about 150 m in Well #9.

Anadarko Basin Salt Dissolution. Examples of natural dissolution of Permian salts in the Anadarko Basin of Oklahoma are given by Ward (1961) and Johnson (1976, 2003a, 2013, 2017, 2021a) (Figures 6A, 12). Salts in the Blaine Formation and associated strata (the Beckham evaporites) are up to 250 m thick along the axis of the Anadarko Basin in eastern Beckham County, and they tend to be dissolved on the flanks of the basin where they rise to depths of less than 150 to 300 m (Figure 12). Outcropping strata in this part of the Anadarko Basin normally dip at angles of less than one degree (less than 10 m/km) toward the axis of the basin, but dissolution of these salts has resulted in a number of collapse structures at the land surface. Where salt has been dissolved (primarily the Yelton salt), overlying strata have subsided, settled, or collapsed into underground water-filled cavities, producing outcrops of collapse blocks that dip erratically at angles of 5 to 30°, as well as breccia pipes in which blocks of Cretaceous limestone and sandstone have been dropped some 50 m, or more, and are juxtaposed against various Permian formations (Suneson, 2012; Johnson, 2013, 2017, 2021a).

Western Kansas. In Kansas, Merriam and Mann (1957) describe a large number of natural sinkholes and depressions that result from dissolution of salts in the Blaine and/or Flowerpot Formations, and in the Hutchinson Salt Member of the Wellington Formation. Sinks such as the **Mead**, **Jones Ranch**, **Big Basin**, **and Little Basin Sinks** in southwest Kansas are undoubtedly related to dissolution of Blaine and/or Flowerpot salts (note: these sinks are bold and underlined here because they are shown in Figure 6A). Evidence of ongoing dissolution is the **Wallace Sinkhole**, which formed in July 2013 about 14 km north of the town of Wallace, in Wallace County (Figure 6A). The sink reached about 60 m across and 27 m deep, as a result

of dissolution of the Flowerpot and Blaine salts (Johnson, 2021b). A nearby petroleum test, drilled about 3 km south of the sink, encountered 12 m of middle Blaine Formation salt at a depth of 704 m (2310 feet), and 67 m of Flowerpot salt at a depth of 727 m (2385 feet): these are the shallowest salts in the area. It is likely that natural dissolution of the Blaine and Flowerpot salts created a water-filled cavity that migrated upward and finally breached the surface as the Wallace Sinkhole in 2013.

Also in Wallace County, western Kansas, the **Smoky Basin Cave-in** formed just 8 km east of Sharon Springs in 1926 (Merriam and Mann, 1957; Johnson, 2021b) (Figure 6A). In little more than 1 month, the sink was about 75 by 105 m wide, and, in its center, the sink was filled with about 50 m of water. Although the early common view was that the Smoky Basin Cave-in resulted from dissolution of carbonate rocks (the Cretaceous Niobrara Chalk) (Merriam and Mann, 1957), the sink undoubtedly formed because of natural dissolution of the Blaine and Flowerpot salts, in the same manner as the Wallace Sinkhole was formed (Johnson, 2021b). Several other sinkholes in the Sharon Springs–Wallace area that formed at earlier or unknown times are Sinks 1, 2, and 3, in Bradshaw Draw, and Old Maid's Pool (Johnson, 2021b).

Hutchinson Salt Dissolution. The Hutchinson Salt shows a prime example of salt dissolution along part of its eastern margin in central Kansas (Figures 5A, 6A, 13). The Hutchinson Salt is typically 60 to 120 m thick in the area, where it has not been affected by

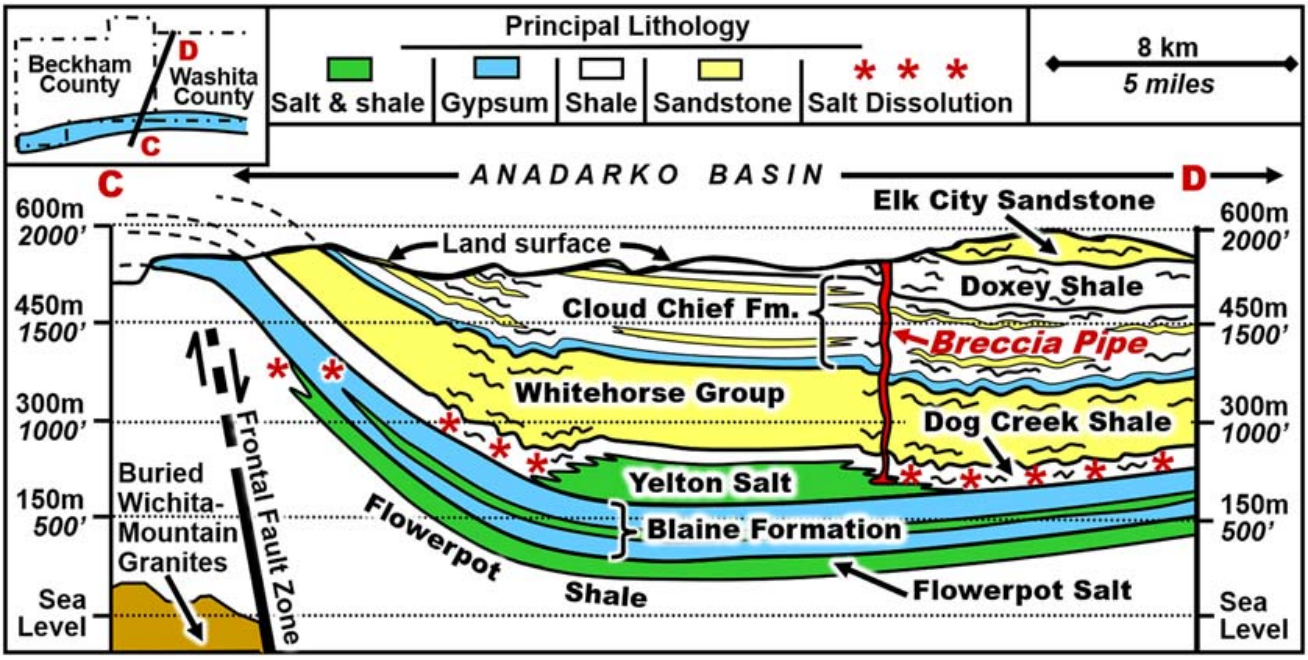

Figure 12. Cross section showing the dissolution of Permian salt units in eastern Beckham and western Washita Counties, Oklahoma (from Johnson, 2013). The Flowerpot salt, Blaine Formation, and Yelton salt are collectively referred to as the Beckham evaporites by Jordan and Vosburg (1963).

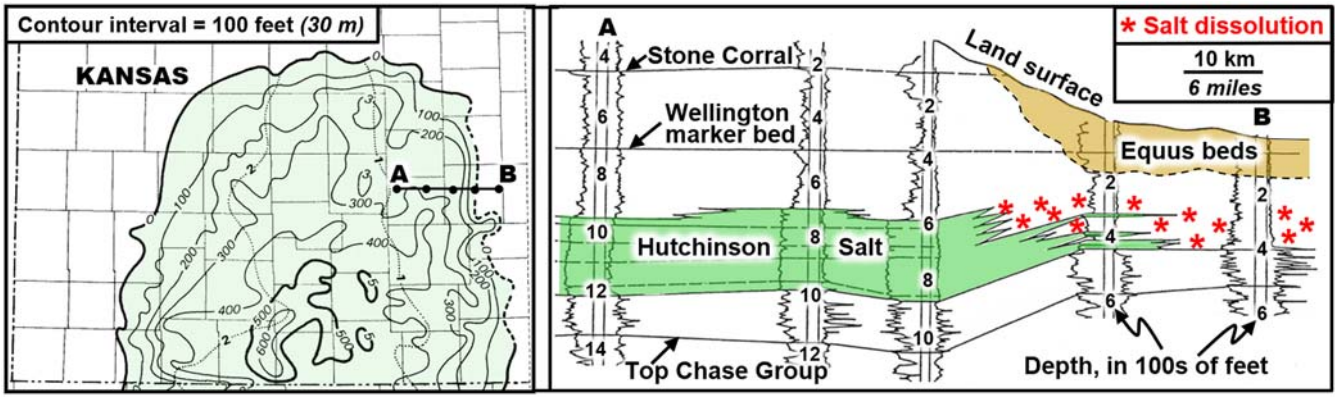

Figure 13. Map and cross section showing natural dissolution of Hutchinson Salt across Rice and McPherson Counties, Kansas. Equus beds were deposited in subsidence basins formed by salt dissolution. Map from Johnson and Gonzales (1978); cross section modified from Anderson and others (1995b).

dissolution, but within an easterly distance of only 10 to 15 km, most of the salt has been dissolved along much of its east margin. The salt has been removed in this area because unsaturated groundwater has circulated down to, and around, the salt beds, and dissolved them from Tertiary time through to the present (Walters, 1978; Watney and Paul, 1980; Watney and others, 1988; Anderson and others, 1995a, 1995b). Cavernous conditions in the dissolution zone have created a "lost circulation zone," wherein boreholes drilled through the zone cannot recirculate drilling fluids that are lost into the cavities. Gogel (1981) discusses the emission of brines derived from dissolution of the Hutchinson Salt in central Kansas, and provides a number of cross sections showing the salt dissolution front (Gogel, 1981, Plate 2). Dissolution of this salt has caused overlying strata to subside, and a series of subsidence basins were filled by Tertiary through Recent sediments deposited over the dissolution zone (Figure 13). The presence of bones and teeth of Quaternary horses in these unconsolidated layers of silt, sand, and gravel led to them being referred to as the "Equus beds," which locally reach a thickness of about 85 m (Walters, 1978). This dissolution front, accompanied by subsidence and subsequent infilling, is similar to the salt dissolution and Cenozoic fill in the Delaware Basin (see above).

A recent example of Hutchinson Salt dissolution and resultant subsidence is reported in this volume by Croxton (2021) at a site about 7 km SE of Lindsborg, in northern McPherson County, Kansas. Bedrock beneath the northbound lanes of Interstate 135 here has subsided about 1.5 m since 1967, when the interstate was constructed, and the subsidence is centered near a pier of an overpass bridge carrying a county road named Shawnee Road; the subsidence feature is referred to as the **Shawnee Road Sink** (Figure 6A). This has caused a noticeable depression in northbound lanes, and eventually, they will need to be built up to preserve visibility and prevent ponding during heavy rains. Because the bridge itself is being affected (it shows noticeable dips), and because clearance beneath the bridge could be compromised by bringing the interstate back up to grade, it was decided to remove the bridge and close the county road at the site. Croxton (2021) reports that the Hutchinson Salt is about 45 to 60 m below the land surface here, and that natural dissolution of the salt has resulted in numerous shallow depressions and sinkholes in McPherson County and adjacent areas.

Baca County Salt Dissolution. Natural salt dissolution occurs in Baca County, southeast Colorado, where dissolution of salt in the middle of the Blaine Formation is affirmed at several places along a profile that is about 50 km long (Figures 6A, 14). Askew (2013) shows that this middle Blaine salt unit, typically 18 to 22 m thick in most of his 2000 km^2 study area, abruptly thins to about 3 m (all salt is probably gone, and only clastics remain) in a number of elongated "zones" that are 2 to 8 km wide and 5 to 20 km long. These zones, where the salt has been removed, are elongated with a north-northeast orientation, which is consistent with a series of deep-seated, en-echelon-type faults mapped in Ordovician rocks beneath the area. Strata above the salt, including overlying Permian and Triassic (Dockum Formation) units, remain a constant thickness over all parts of the study area (including over the patches of thin salt), thus indicating that local dissolution of the salt occurred after Dockum deposition. Askew (2013) postulates that recurrent movement along the deep-seated faults during the Laramide Orogeny (Late Cretaceous through Early Eocene), and later tectonic activity, might have allowed migration of freshwater from the overlying Cretaceous Dakota Sandstone and Tertiary Ogallala Formation down to the middle Blaine salt, and bring about its partial dissolution along these preferred fault/fracture zones.

Great Plains Reservoirs. Natural dissolution of the Flowerpot salt beneath the Great Plains Reservoirs area has resulted in ten large, natural depressions being formed in prehistoric times: these contiguous depressions are now being used to store water in four major reservoirs in Kiowa County, Colorado (Johnson, 2021c) (Figure 6A). The Flowerpot salt is generally 60 to 75 m thick in the northeast part of the study area, but it thins sharply and is mostly dissolved to the southwest across a major salt dissolution front. Some residual masses of salt up to 54 m thick are present in the southwest, showing that dissolution is not complete. Individual natural depressions range from 1.6 to 13.0 km^2, and are probably some of the largest salt dissolution/collapse features in southeast Colorado. The timing of salt dissolution here is unknown, but, because the large depressions are still present in the current landscape, it has probably persisted until at least the late Pleistocene or Holocene Epochs.

Las Animas Arch Salt Dissolution. Another example of natural salt dissolution in Colorado is reported by Berry (2018). Using a 3D seismic survey and petroleum-test geophysical logs, he examined dissolution phenomena over the Las Animas Arch in parts of Cheyenne and Kiowa Counties (Figure 6A). The Flowerpot salt, referred to by Berry as the "lower Blaine halite," is about 55 to 60 m thick in the east half of his study area, but is totally dissolved in the west half. The middle Blaine salt, referred to by Berry as the "upper Blaine halite," is dissolved at most places in his study area, but is about 12 m thick where not dissolved. Berry (2018) concluded that dissolution of the middle Blaine salt occurred mainly before Taloga deposition (Late Permian), and dissolution

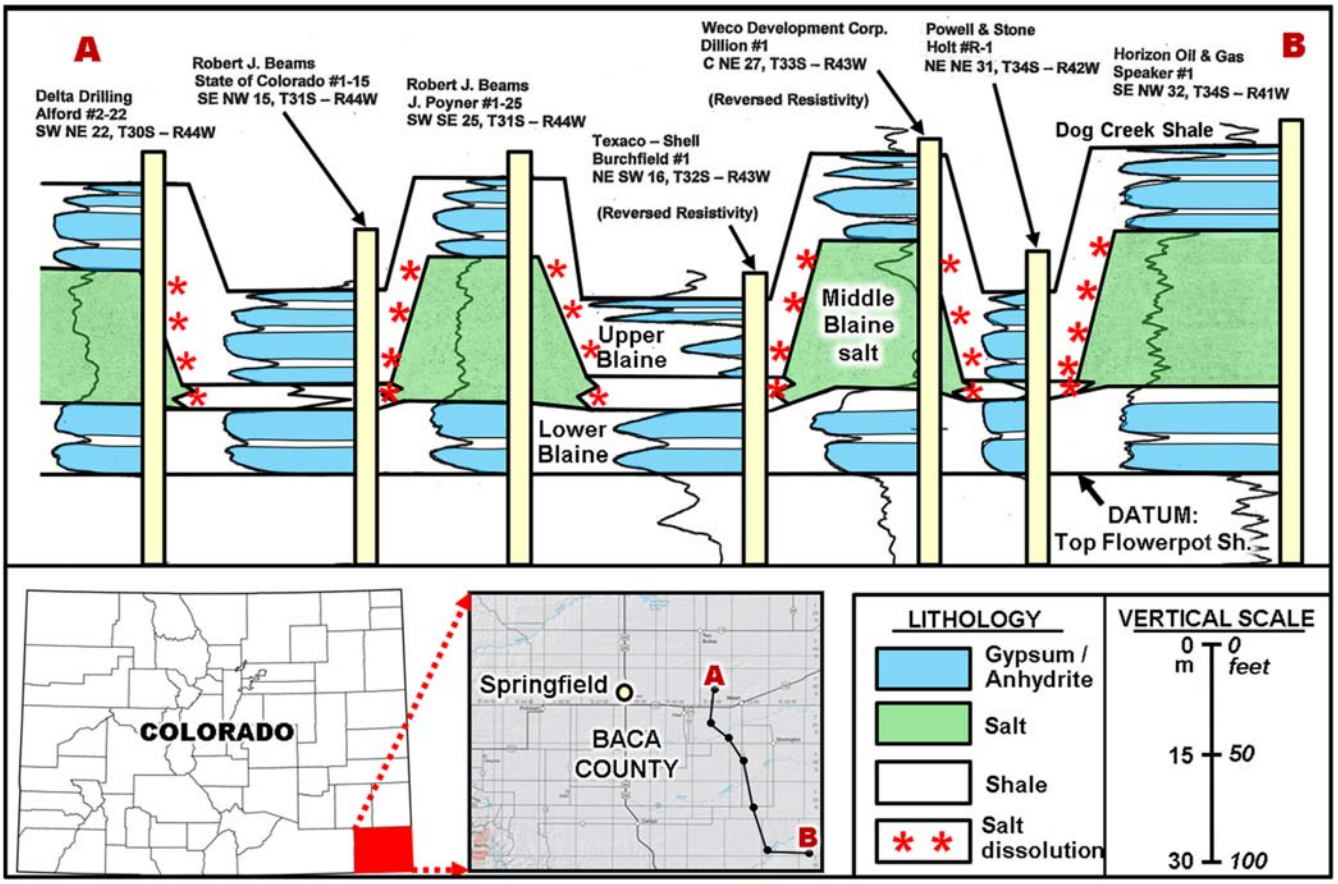

Figure 14. Cross section showing the natural dissolution of salt in middle part of Blaine Formation in eastern Baca County, Colorado (modified from Askew, 2013). Depth to the top of salt ranges from about 365 m in north (A) to about 200 m in the south (B). Most well logs here are gamma-ray logs; however, two resistivity log curves have been flipped, or reversed ("Reversed Resistivity"), horizontally to mimic the deflections of the gamma-ray logs.

of the deeper Flowerpot salt occurred in post-Taloga time, but before deposition of the Dakota Formation (Late Cretaceous).

Natural Gypsum Karst

Although gypsum is more widespread than salt in the GPEB, the areas of gypsum karst are not as widespread: gypsum is much less soluble than salt, and natural gypsum karst typically is limited to areas where gypsum crops out, or is less than about 30 m below the land surface. One or more formations containing gypsum (or anhydrite) are present in the subsurface beneath all parts of the GPEB (Figure 3); however, outcrops of gypsum are chiefly along the western and eastern sides of the GPEB (Figure 15). In these areas, typical gypsum-karst features abound (Figure 16): gypsum karst on the western side is described by Sares and Wells (1987), Belski (1992), Hill (1996), Forbes and Nance (1997), Stafford and others (2008a, 2008b, 2017), Stafford and Nance (2009, 2018), Stafford (2013), and Land (2021); gypsum karst on the eastern side is described by McGregor and others (1963), Reddell and Russell (1963), Myers and others (1969), Bozeman (1987, 2003), Johnson (1989, 1990, 1996, 2003a, 2003b, 2018, 2021d), Bozeman and Bozeman (2002), Johnson and Wilkerson (2013), and Johnson and others (2013). Individual gypsum beds typically are 3 to 10 m thick in most GPEB formations, but are up to 30 m thick in the Cloud Chief Formation of the Anadarko Basin and 20 to 200 m thick in the Castile Formation of the Delaware Basin (Johnson and others, 1989). Quinlan and others (1987) report that there are more than 500 gypsum caves in the United States, and that most of them are in the Permian Basin.

Examples of Natural Gypsum Karst

Delaware Basin. The Delaware Basin of west Texas and southeast New Mexico contains one of the greatest accumulations of evaporites in the United States (Johnson and others, 1989). Evaporites (gypsum/anhydrite and salt) of the Castile, Salado, and Rustler Formations typically are 500 to 1500 m thick within the Delaware Basin and are more than 450 m thick where these

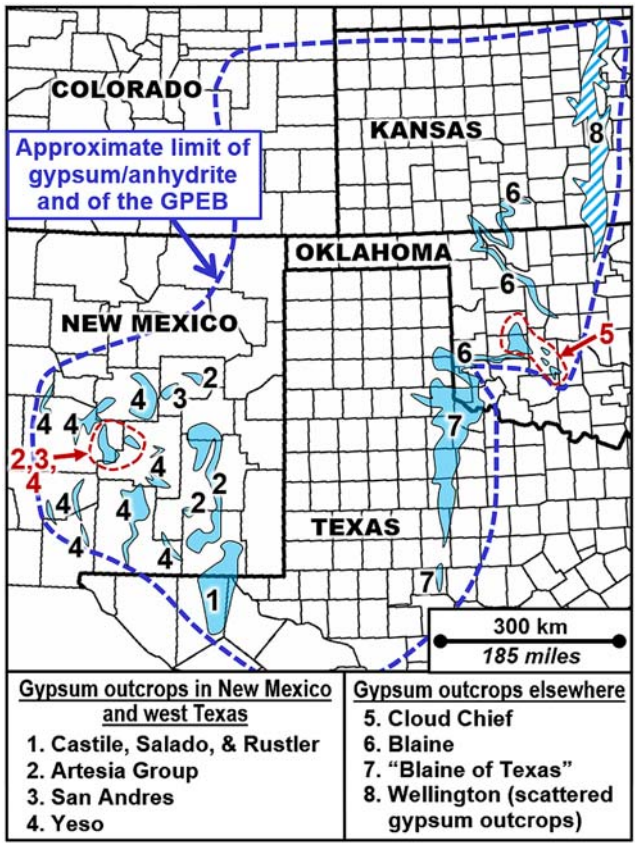

Figure 15. Outcrops of post-Wolfcampian Permian gypsum formations in GPEB. Gypsum karst may be present in any part of these outcrops. Sources: New Mexico (Weber and Kottlowski, 1959), Texas (Garner and others, 1979), Oklahoma (Johnson, 1969), and Kansas (Kulstad and others, 1956).

deposits extend to the north and east. Outcrops of these three formations constitute the most extensive examples of gypsum karst and subsidence in the nation. The area referred to as the Gypsum Plain comprises about 2600 km^2 of outcropping gypsum of the Castile and Salado Formations (Kirkland and Evans, 1980), and additional gypsum outcrops are present just to the east, in the Rustler Hills and into Reeves County, Texas.

Outcrops of gypsum in the Delaware Basin contain abundant sinkholes, caves, closed depressions, collapse sinks, and underground drainage (Figure 16C); excellent summaries are provided by Hill (1996), Stafford and others (2008a, 2008b), Stafford and Nance (2009, 2018), Land and others (2018b), and Land (2021). Four principal areas of gypsum karst in the Delaware Basin are the Gypsum Plain, Nash Draw, Burton Flat, and the Pecos River Valley (Hill, 1996). All four areas contain sinkholes ranging from a few meters to 100 m across; there are active collapse features in all four areas, and generally they extend down to shallow, underground caverns less than 100 m deep. One sinkhole, formed during a storm in 1918, collapsed suddenly to form a gaping hole about 25 m across and 20 m deep (Hill, 1996).

Caves are prominent and abundant on the Gypsum Plain and Burton Flat (Sares and Wells, 1987; Belski, 1992; Stafford and others, 2017; Stafford and Nance, 2018). The Parks Ranch Cave, with a total length of 6596 m, is the second longest gypsum cave system in the western hemisphere (after the D.C. Jester Cave, described below) (Stafford and others, 2008a). The Parks Ranch Cave is developed in the Castile Formation in Chosa Draw, Eddy County, New Mexico. A specialized study of karst geohazards in the Rustler Formation was conducted along the route of US Highway 285 in the area from Loving, New Mexico, south to the Texas state line (Land and others, 2018b). Surface mapping and near-surface electrical resistivity (ER) surveys along US 285 indicate that most sinkholes in the Rustler are less than about 3 m below the surface (Land and others, 2018a).

Pecos River Valley. Along the west flank of the GPEB, in eastern New Mexico, gypsum crops out extensively along parts of the Pecos River Valley (Figures 9, 15). Various gypsum and carbonate units are present in the Permian Artesia Group and San Andres Formation, and they contain a large number of sinkholes, caves, and subsidence features in the Vaughn–Roswell area (Fischer and Hackman, 1964; Kelley, 1971; Forbes and Nance, 1997). Several of the caves in this area are more than 3.2 km long, and the deepest has a vertical extent of more than 120 m (Forbes and Nance, 1997). Gypsum beds of the upper Artesia Group crop out extensively in the walls of the large sinkholes or cenotes formed by dissolution of salt and gypsum at Bottomless Lakes State Park (described above).

East flank GPEB. Another major gypsum-karst area of the GPEB is along its east flank, in north-central Texas, western Oklahoma, and southwest Kansas (Figures 15, 16) (McGregor and others, 1963; Reddell and Russell, 1963; Myers and others, 1969; and Johnson, 2018). Principal gypsum units are the Blaine Formation, with gypsum beds generally 3 to 9 m thick, and the Cloud Chief Formation, with a single massive gypsum bed up to 30 m thick. The number of known gypsum caves in north Texas and western Oklahoma is 122 and 248, respectively (Johnson, 2018). Several of the more important gypsum-karst studies on the east flank of the GPEB are described below and focus on (1) three well-known gypsum caves in Oklahoma, (2) two gypsum sinkholes in Oklahoma, (3) the major freshwater Blaine aquifer, (4) abandonment of two proposed karstic damsites, (5) the Wellington Formation in Kansas, and (6) caves in southwest Kansas.

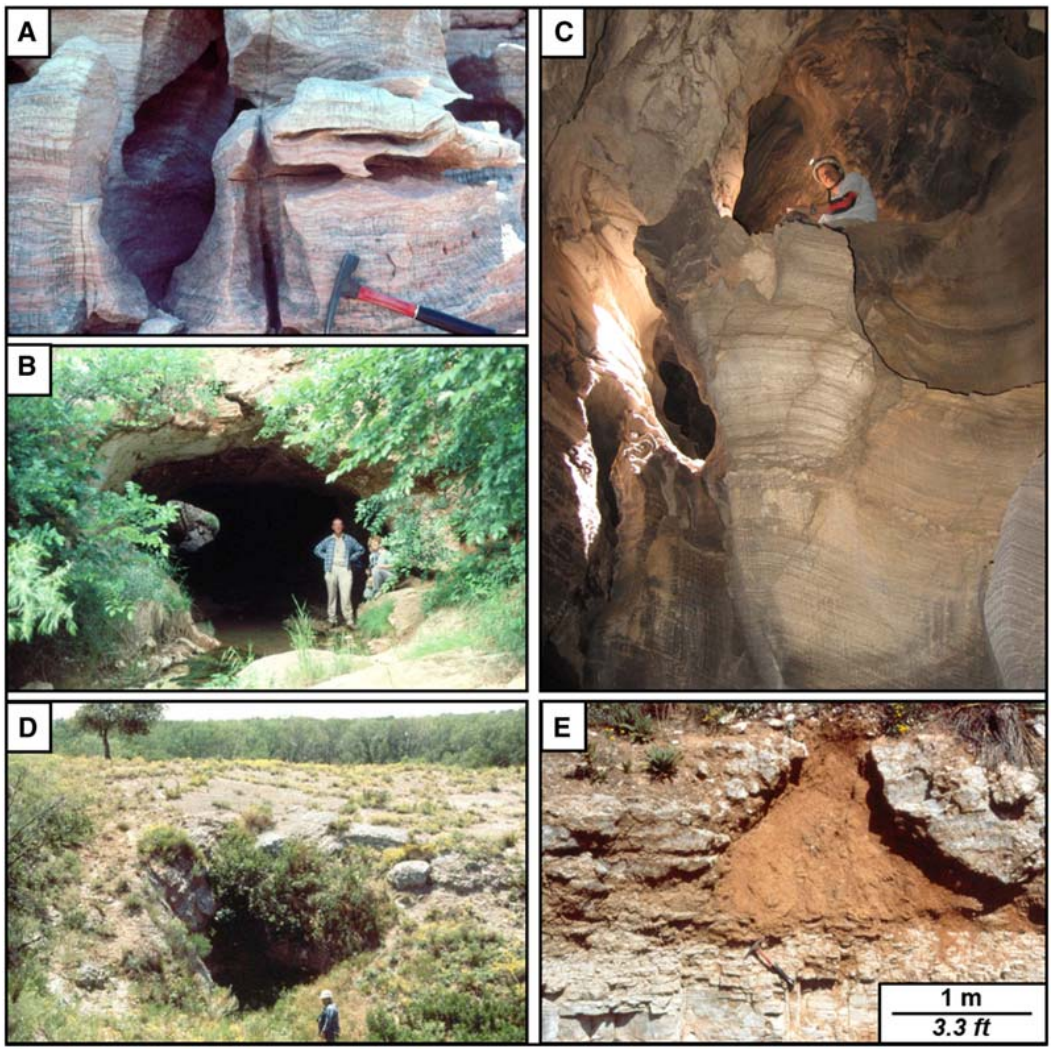

Figure 16. Examples of gypsum karst, sinkholes, and caves in the GPEB. (A) Karst in Cloud Chief Gypsum in Oklahoma, with dissolution most pronounced along joints and bedding planes. (B) Entrance to Jester Cave in Blaine Formation, Greer County, Oklahoma. (C) Interior of Gazelle Cave in thick gypsum of Castile Formation, Culberson County, Texas (photo courtesy of Kevin Stafford). (D) Large gypsum sinkhole in Blaine Formation, Greer County, Oklahoma. (E) Dissolution channel in Blaine Formation, Oklahoma, which is now filled with Quaternary sediment deposited from through-flowing water.

Three gypsum caves in Oklahoma. There are 248 known gypsum caves in western Oklahoma (Johnson, 2018). One well-known cave, the D.C. Jester Cave (Figure 16B), located in Greer County, southwestern Oklahoma, has a main passage that is 2413 m long, but, along with the side passages, the total length is 10,065 m (Bozeman, 1987); it is, therefore, the longest reported gypsum cave system in the western hemisphere. The cave, developed in the Blaine Formation, has passageways that typically are 1 to 5 m in diameter, and locally are up to 20 m wide (Bozeman, 1987; Johnson, 1989b, 1990, 2003a, 2018, 2021a). The second well-known cave, Alabaster Caverns in Woodward County, northwestern Oklahoma, is now developed as a tourist cave. It has a main passage about 700 m long in the Blaine Formation; it has a maximum width of 18 m and a maximum height of 15 m (Myers and others, 1969; Johnson, 2011, 2018, 2021a). And the third well-known cave is Selman Cave, developed in the Blaine Formation gypsums in Woodward County, northwestern Oklahoma (Bozeman, 2002; Johnson, 2018). Selman Cave is unique among caves in the region, inasmuch as it has been established as an outdoor living laboratory and field station run by the University of Central Oklahoma (UCO). The UCO Selman Living Laboratory is being used for classes and research on a host of disciplines. Selman Cave has a total length of 4794 m, and is the third longest gypsum cave system reported in the western hemisphere (after D.C. Jester Cave and Parks Ranch Cave).

Delhi Sinkhole and Watonga Sinkhole. Two sinkholes formed as a result of natural gypsum karst in the Blaine Formation in western Oklahoma (Johnson 2021d). The Delhi Sinkhole developed in 2011 in Beckham County, southwest Oklahoma; at first it was 12 m wide and 12 m deep, but eventually, it reached a diameter of 18 m. The Watonga Sinkhole formed in 1957 in Blaine County, northwest Oklahoma: it reached a diameter of 14 m and a depth of 5.2 m. Both sinks formed in open fields where about 15 to 30 m of Quaternary terrace deposits and dune sands overlie the bedrock, and there was no damage to infrastructure. The depth to the shallowest gypsum at both sites is about 20 to 30 m.

Blaine aquifer. A major freshwater aquifer is developed in the Blaine Formation of southwestern Oklahoma and north-central Texas (Steele and Barclay, 1965; Johnson, 1990, 2003a, 2019; Runkle and others, 1997; Hopkins and Muller, 2011). Water is produced from the karstic and cavernous gypsum and dolomite beds of the Blaine aquifer in Harmon, Jackson, and Greer Counties, Oklahoma, and mainly in Childress and Collingsworth Counties in north-central Texas. The aquifer is 50 to 65 m thick and consists of nine thick gypsum beds (each 3 to 8 m thick), interbedded with thinner dolomite beds (0.1 to 1.5 m thick) and shale beds (0.3 to 8.0 m thick). Because of the high total dissolved solids in the water (average about 3100 mg/L), it is unacceptable as drinking water, but is extensively used for irrigation. A recharge demonstration project was carried out to show that the aquifer can be recharged with surface runoff that is channeled by gravity flow down wells or sinkholes into cavities in the karst aquifer (Osborn and Eckenstein, 1997).

Abandonment of proposed and actual damsites. Problems associated with constructing dams on areas of gypsum karst were described by Johnson (2008). Two proposed damsites in the GPEB had to be abandoned because of gypsum karst: the original Upper Mangum and Cedar Ridge Damsites. Also, McMillan Dam, which was built on an area of gypsum karst, was abandoned after nearly 100 yr of use.

The original Upper Mangum Damsite, about 14 km west of Mangum on Salt Fork of Red River in Greer County, Oklahoma, was proposed for siting on gypsum beds in the Blaine Formation. At this site, the Blaine Formation is about 60 m thick and consists of nine major gypsum beds, each 3 to 9 m thick, interbedded with shales and dolomites (Johnson, 2003b). Favorable topography made the Upper Mangum site seem attractive since 1937, but extensive gypsum karst at the proposed damsite and in the reservoir area (Figure 16D) always required additional study. The final study of the Upper Mangum site found many open cavities, clay-filled cavities, and other karst features in and near the proposed abutments, and water losses during pressure tests ranged from 60 to 250 L/min in most tests, and were 1600 to 5300 L/min in one borehole (Johnson, 2003b). A final assessment in 1999 reaffirmed the unsatisfactory, karstic conditions, and recommended abandonment of the site in favor of another location, about 11 km farther downstream in the Flowerpot Shale, where gypsum karst would not be a problem (Johnson, 2003b, 2003c).

Cedar Ridge Dam was originally proposed at a site on the Clear Fork Brazos River, about 27 km SW of Throckmorton, in southwest Throckmorton County, Texas (Johnson and Wilkerson, 2013). However, initial coring of the damsite encountered unsuspected gypsum beds in the Permian Jager Bend/Valera Formation. The gypsum-bearing sequence here is 30 to 45 m thick, and consists of eight gypsum beds, mostly 1 to 3 m thick, interbedded with shale and limestone units 1 to 10 m thick. Gypsum beds comprise 25 to 30% of the gypsum sequence. Gypsum was not known to crop out in the area, and previous studies of the area made no mention of gypsum in the Jager Bend/Valera Formation. So, it was surprising to core karstic gypsum at the damsite, and to know that this gypsum would also be in the reservoir-impoundment area: these conditions could allow water to escape the reservoir by passing under or around the dam. In addition, a blowout of natural gas occurred in a borehole at a depth of 20 m below the proposed damsite (it is an area of oil and gas production). After re-evaluation of the area, a new damsite was proposed on the same river, about 8 km to the southwest, where the gypsum beds would be about 23 m below the newly proposed site and are expected to be too deep to be karstic or pose any problems (Johnson and Wilkerson, 2013).

Lake McMillan was created in 1893 by damming the Pecos River at a site about 22 km NNW of Carlsbad, New Mexico (Land, 2021). Unfortunately, McMillan Dam and the reservoir-impoundment area were located on gypsum beds of the Permian Seven Rivers Formation. As a result, lake water immediately started leaking through gypsum-karst features and reappeared in the Pecos River about 6 km farther downstream. Leakage from the lake was considerable at various times, although water-borne sediment did cover and plug some of the karst features. Sediment on the lake bottom decreased the storage capacity of the reservoir, but the idea of dredging this sediment was abandoned because that would re-expose karst features under the lake (Land, 2021). Storage capacity of the original reservoir was reduced to less than 50% by the 1940s. A new dam, Brantley Dam, was constructed in 1987 about 6 km downstream from McMillan Dam, which was then breached to allow its water to flow into Brantley Lake. Based on recommendations by Cox (1967), Brantley

Dam and its reservoir are located mostly over the less-soluble dolomitic part of the Seven Rivers Formation.

Wellington Formation in Kansas. In Kansas, Kulstad and others (1956) describe widespread subsidence and surface slump structures in the outcrop area of the Wellington Formation, which, they say, "shows that some material, probably gypsum, has been removed by subsurface solution." Although gypsum outcrops are rare in the Wellington Formation, 30 to 45 m of anhydrite interbeds are present in the subsurface just west of the outcrops, showing that the Wellington should contain gypsum at and just below the surface in its outcrop area. This is supported by locally abundant gypsum outcrops in Saline and Dickenson Counties (Kulstad and others, 1956, plate 3), and the assumption that gypsum is probably also present just below the surface elsewhere in the Wellington Formation outcrop area. Young and Beard (1993) briefly state that the only caves known to them in the Wellington Formation are "one cave in Dickinson County and a now-filled cave in Sedgwick County:" no other data are given.

Gypsum caves in southwest Kansas. In an overview of gypsum caves in the Blaine Formation of Comanche and Barber Counties, southwest Kansas, Young and Beard (1993) reported that there are more than 235 known caves in Comanche County, and more than 205 in Barber County: these caves range from small, 6-m-deep shelter caves to an 860-m-long cave system. Typical gypsum caves in Kansas are only 30 to 90 m long, and have two or more entrances, including one or more sinkhole entrances: although most of the passages are crawlways, some passages have rooms 12 m high. Young and Beard (1993) describe the D.E.S. Cave, which is 611 m long, and provide general information on the breakdown of caves, slumping of caves, and natural bridges in the area. Subsequent studies of gypsum karst in the Blaine Formation in Barber County have been carried out by Gauvey and Sumrall (2021) and Kelner and others (2021). Their studies describe typical gypsum-karst features, such as caves, sinkholes, springs, and losing streams. They are looking at processes that lead to local karst development, and their studies are the first stage of a karst study intending to develop predictive karst models that will help landowners reduce the risk of collapses that can cause structural damage and/or aquifer contamination.

HUMAN-INDUCED EVAPORITE KARST IN THE GPEB

Evaporite karst can result from human activities. Impounding water in contact with, or above, an evaporite deposit can cause unsaturated water to come in contact with salt or gypsum, resulting in some dissolution and possible settlement or collapse. Generally of greater concern is the drilling of boreholes into or through subsurface salt deposits: this may allow unsaturated water to flow through or against a salt deposit, and allow the development of small or large dissolution cavities. Although a water-filled cavity may be formed either intentionally (solution mining or development of a storage cavity in salt) or unintentionally (fugitive water escaping from a borehole and dissolving the salt), if the cavity is large enough and shallow enough it is possible that successive roof failures above the cavity can cause land subsidence or catastrophic collapse.

Human-Induced Salt Karst

Human activities that are most likely to induce karst in salt deposits are: (1) solution mining of salt that intentionally creates cavities in the salt; or (2) petroleum or other activities that involve drilling boreholes into or through subsurface salt deposits, and then inadvertently allowing unsaturated water to enter the borehole, dissolve the salt, and create a water-filled cavity. In either case, if uncontrolled dissolution of the salt occurs, the cavity may increase in width to the point where the roof can no longer be supported. Collapse of the roof, followed by a series of successive roof failures, can then cause the water-filled cavity to migrate upward. If the original cavity is large enough and shallow enough, the successive roof failures can reach the land surface, resulting either in land subsidence or in sudden, catastrophic collapse (a sinkhole). In general, most sinkholes resulting from salt dissolution are about 50 to 100 m in diameter when they first form, but some can enlarge considerably as time passes. Reports describing general subsidence and/or collapse of salt cavities caused by human activities are given by Walters (1978), Ege (1979), Dunrud and Nevins (1981), Coates and others (1985), Johnson and others (2003), Johnson (2005a, b), and Cooper (2020a). The location of human-induced salt karst in the GPEB discussed in this report is shown in Figure 6B.

It is also possible for sinkholes and subsidence features to form above dry (room-and-pillar) salt mines, if a large amount of water enters the mine and dissolves the salt: three examples are the Jefferson and Weeks Island salt dome mines in Louisiana, and the Retsof salt mine in New York (Martinez and others, 1998; Johnson, 2005a, b). However, the only three room-and-pillar operations in salt or potash in the GPEB have had no such problems: two of them, salt mining at Hutchinson, Kansas, and potash mining near Carlsbad, New Mexico, are only mentioned here, but excavation of salt for storage of transuranic radioactive waste at the WIPP, also near Carlsbad, is described elsewhere in this paper.

Impacts from Solution Mining

Solution mining involves dissolving and extracting soluble minerals, such as salt or potash, or creating an underground cavity in salt for storage of liquids or gases, such as oil, propane, or natural gas. Solution mining involves the following: (1) drilling a borehole into a salt formation; (2) introducing unsaturated water into the soluble rock in the subsurface; (3) dissolving the minerals and forming a brine; (4) recovering the brine; and (5) either extracting the mineral from the brine (salt or potash production), or storing another liquid or gas in the water-filled cavity. Solution mining therefore typically entails creation of one or several large, underground, brine-filled cavities (Marsden and Lucas, 1973). When used for the underground storage of liquids and gases, the liquids and gases are injected into the storage cavity to displace the brine, and they can be recovered later by reinjecting the brine.

Solution-mining cavities created in bedded salts typically are 10 to 100 m in diameter, and their height is usually controlled by the thickness of the salt. Cavities may become larger or shallower than planned as a result of: (1) uncontrolled dissolution; (2) unanticipated geologic conditions; or (3) engineering/construction problems. This has resulted in subsidence of the land surface, or even of collapse structures (sinkholes) at a number of solution mines. Dunrud and Nevins (1981) reported ten areas of solution mining and collapse existed at that time within the United States alone, and additional sites are known from many other parts of the world. Most of the unanticipated solution-mining collapses result from cavities formed 60 to more than 100 yr ago, before modern-day engineering safeguards were developed: proper, modern design has virtually eliminated this problem in new facilities.

Cargill Sink. The Cargill Sink, located in the southeast part of the town of Hutchinson, in Reno County, Kansas, is one example of solution mining and resultant sinkhole development in the GPEB (Walters, 1978; Dyni, 1986; Johnson, 2005a, b) (Figures 6B, 17). The collapse occurred in 1974, on the property of Cargill, Inc., and the crater stabilized with a diameter of about 90 m and a maximum depth of about 15 m. The volume of the crater was calculated to be about 70,000 m^3. Salt has been solution-mined on these properties since 1888 (Walters, 1978). The Hutchinson Salt here is about 105 m thick and occurs at a depth of about 130 m below the ground surface (Figure 17). Locations of many of the earlier brine wells are not known, and early day dissolution methods were often uncontrolled; therefore, the location and extent of many of the solution cavities on this property are not well known. The sink developed within an active brine field that included both operating and abandoned wells. Embraced within the sinkhole was a brine well that was drilled in 1908 and was finally plugged and abandoned in 1929.

Post-subsidence drilling at the Cargill Sink showed that a northeast-trending cavern had developed in the Hutchinson Salt beneath the sink (Walters, 1978). Elongation of the cavern parallels a line of brine-producing wells that were hydraulically connected. The span of the cavern roof is more than 400 m in its long dimension, and less than 90 m in its short dimension. The roof span apparently exceeded the capacity of overlying shales to support the overburden. Failure of the roof caused the collapse of successive overlying rock units until the uppermost rock layer finally collapsed into the water-filled void. At this point, water-saturated Quaternary sands dropped into the cavity, creating the surface sink (Figure 17). The sand flowed down and now fills a subsurface chimney that is about 30 m in diameter and located below the center of the sinkhole.

The report by Dyni (1986) also describes several other sinkholes that formed around brine field wells drilled into the Hutchinson Salt in the Hutchinson area. These include one sink that formed in 1952, and two sinks that formed in 1978. The 1952 sink (referred to as the Barton Sinkhole), located about 350 m NNW of the Cargill Sink, was about 75 m in diameter and 10 m deep; the sink was adjacent to the salt plant and was filled in. The top of the Hutchinson Salt at this site is 129 m below the surface in borehole V-5, drilled just outside the dissolution cavity. The two sinks formed in 1978 (referred to as the Carey Sinkholes) are about 2.25 km ENE of the Cargill Sink, in the east part of Hutchinson: these sinks are water filled, and are about 45 and 60 m across (based on Google Earth photography, June 2019).

Denver City Sink. In 2009, a sinkhole opened up about 2 km ENE of Denver City, in Yoakum County, Texas (Figure 6B): the sink is about 65 m wide and 15 m deep. Scant data are published on this sink (Land, 2013), but correspondence by the New Mexico Oil Conservation Division (no date) provides the following information. In 1984, Salty Brine Inc. acquired, from Vulcan Chemicals, a brine-producing well (Well no. 3) that began production in 1974. Brine was produced in the well by dissolving the Salado salt, which here is about 640 to 853 m below the surface: the cavern was developed at a depth of about 655 m. In 1997, Well no. 3 suffered the collapse of its casing at a depth of about 213 m: the well was then "plugged up to 300' [91.4 m] subsurface at that time," and then in the year 2000 it was "plugged from a depth of 295' [89.9 m] to surface with all three casing strings remaining in the ground." When the sink formed in 2009, the casing of Well no. 3 was clearly visible, nearly at the center of the sinkhole, making it most likely that the roof of the deep-seated cavern at Well no. 3 collapsed, ultimately leading to the formation of the surface sinkhole.

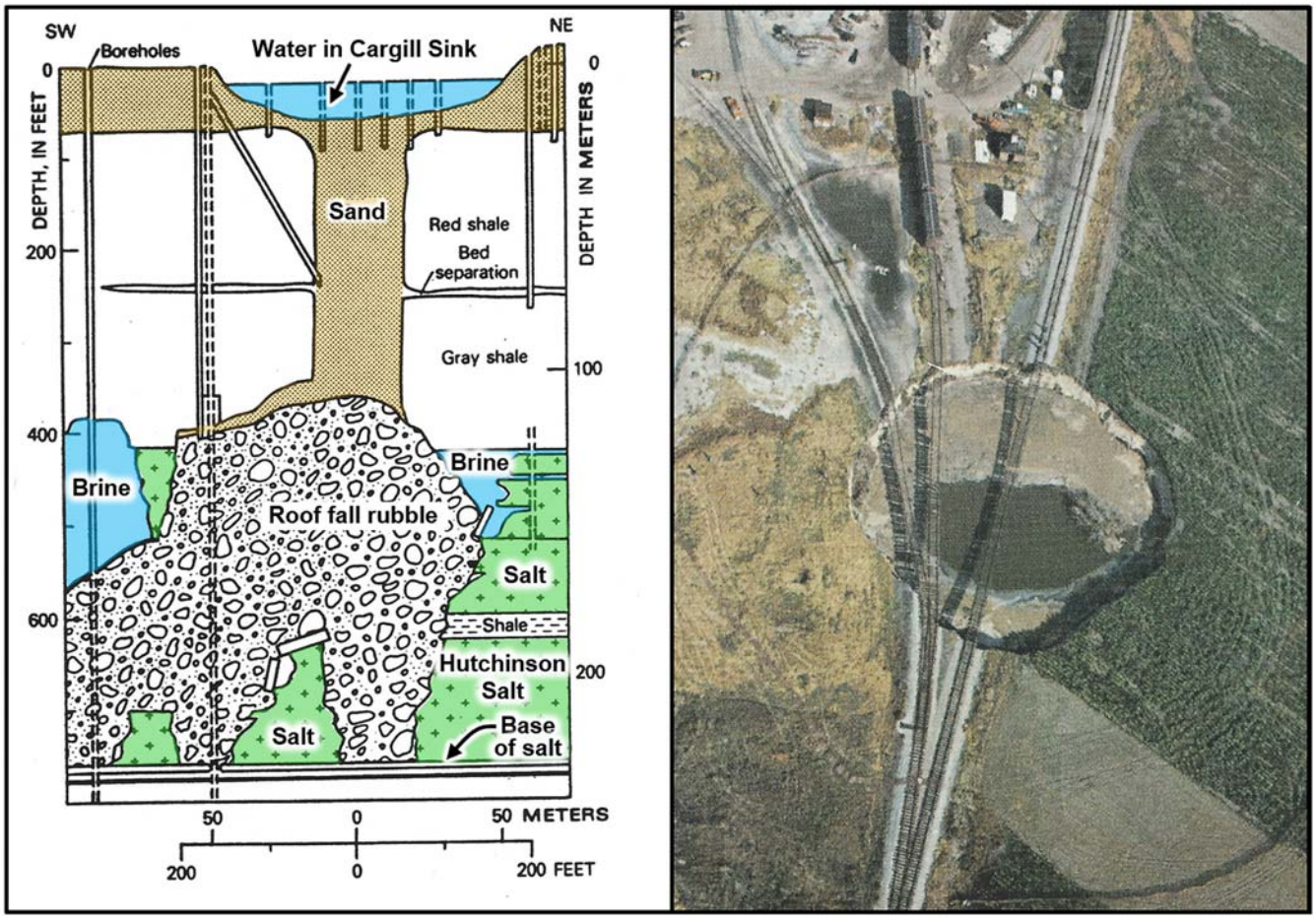

Figure 17. Cargill Sink, developed in Hutchinson Salt at Hutchinson, Kansas. On left is cross section through sink (modified from Walters, 1978); cavity shape is hypothetical, and investigative boreholes were drilled after the sink was formed. On right is an air photo of the sink, formed in 1974 as a result of solution mining of salt (photograph courtesy of Deming Studio): formation of this 90-m-diameter sinkhole left the Missouri Pacific Railroad tracks suspended 6 m in the air.

A response by the Railroad Commission of Texas (RRC), appended to the New Mexico Oil Conservation Division (no date) data, stated: "Although [RRC] staff do not dispute that the operation of Well no. 3 ultimately led to the development of the sinkhole, unfortunately—the information necessary to diagnose exactly what those operations were, and how they ultimately led to sinkhole development, does not exist because those operations occurred so long ago." RRC staff believed it was most plausible that the cavern that developed during Vulcan's operation was much larger than typical Salado salt caverns in Texas. However, definitive data are lacking, because all of Vulcan's operations occurred prior to RRC assuming primacy over Class III brine mining in Texas.

Borger Sinks. Phillips Petroleum drilled five brine-producing wells from 1959 to 1961 near the town of Borger, in Hutchinson County, Texas (Figure 6B); they were drilled into the Flowerpot salt at a depth of about 200 m, and then interconnected by hydraulic fracturing to create a single cavity (Johnson and others, 2003). Brine was produced from the wells until 1964 when surface subsidence near the brine wells indicated that the cavern was unstable. At that time, when production ceased, the brine-filled cavern was about 380 m long and about 120 m wide. The first sinkhole, with a diameter of about 45 m, developed above the cavern in 1969; the second sinkhole, with a diameter of about 60 m, formed over the cavern in 1978. The first sinkhole contained about 20 million liters of brine, with a chloride content of 26,000 to 31,000 mg/L, whereas the second sinkhole was filled and leveled (Johnson and others, 2003).

A second cavern, developed by Phillips in the Flowerpot salt about 150 to 200 m from the collapsed cavern, was operated from 1964 to 1966. This second cavern, which had a roof span of about one-half of the first caverns and about one-third the volume, had no history of

surface subsidence of collapse. In comparing the two caverns (same depth, same salt unit), it is likely that the large volume, excessive roof span, and shallow depth all contributed to the collapse of the first cavern and formation of the Borger Sinks (Johnson and others, 2003).

JWS Sink. In 2008, a driver of a water service company noticed a rumbling noise while at a brine well site in northern Eddy County, New Mexico (Figure 6B); he quickly vacated the site, and minutes later a large sinkhole engulfed the brine well and associated surface structures (Land and Aster, 2009; Land, 2013, 2021). The site is just north of State Road 217 (Hagerman Road), about 3.5 km SW of its intersection with State Highway 360, and is about 17 km WSW of the small community of Loco Hills. Brine was being produced by pumping freshwater into the 86-m-thick Salado Formation at a depth of about 120 m, and recovering it to be sold as oil-field drilling fluid (Figure 18). The JWS sink (previously referred to as "Loco Hills Sinkhole #1," but now referred to by the initials of the well operator) was originally tens of meters across and filled with water up to about 12 m below the land surface. Within 12 days, the sink had: (1) expanded to a diameter of about 111 m; (2) reached a depth of about 45 m; (3) developed a series of concentric radial fractures around the sink; and (4) and the water originally present apparently had subsided into the subsurface (Land and Aster, 2009; Land, 2013, 2021).

Loco Hills Sink. A second sinkhole formed in 2008 at the site of another brine-well collapse in northern Eddy County, New Mexico, about 1.1 km north of US Highway 82 where it goes through the community of Loco Hills (Land and Aster, 2009; Land, 2013, 2021) (Figure 6B). Brine was produced by dissolving salt in the Salado Formation at a depth of about 100 m, and downhole surveys conducted in 2001 showed there were three stacked solution cavities, with the shallowest being about 150 m below the surface. This brine well had been shut in 3 months earlier, after it failed a mechanical integrity test that was part of a statewide review of brine wells. Surface structures and a water-storage tank fell into the sink, which reached a diameter of at least 80 m (Land and Aster, 2009). The Loco Hills Sink was subsequently filled in (Land, 2013).

I&W Brine Well. The I&W brine well facility, located within the city limits of Carlsbad, in Eddy County, New Mexico, started operation in 1979 and recovered brine by pumping freshwater into the Salado salt at a depth of 139 to 181 m (Land and Veni, 2012; Land, 2021) (Figure 6B). Because the I&W cavity is at about the same depth as collapsed cavities at the JWS and Loco Hills Sinks (described above), the I&W brine well facility was shut down. Surface facilities and infrastructure near, or above, the I&W cavity are (1) BN&SF rail line; (2) intersection of two major

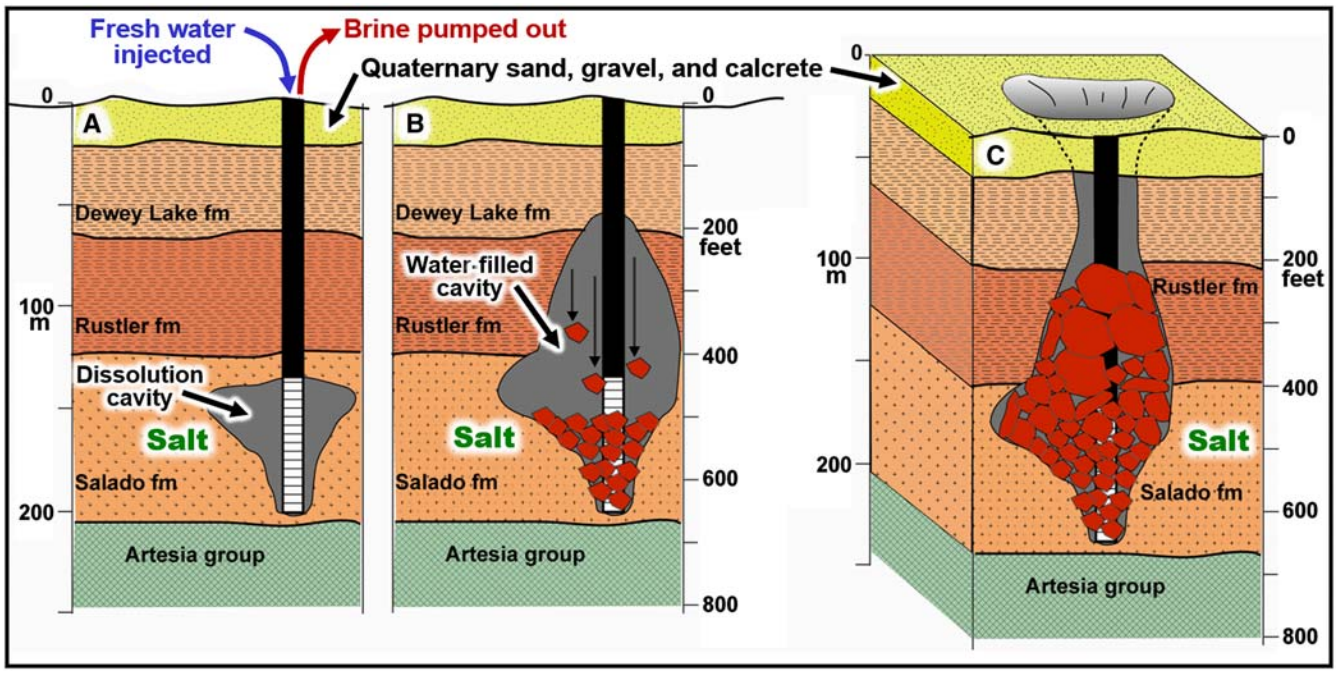

Figure 18. Sequence of events that led to JWS sinkhole: (A) freshwater is injected, and resultant brine is extracted from cavity; (B) mechanical strength of mudstone and gypsum in overlying formations is insufficient to prevent upward stoping of cavity; and (C) cavity reaches land surface, forming sinkhole. Modified from Land and Aster (2009) and Land (2013).

highways, known as the "South Y;" (3) The Carlsbad Irrigation District South Canal; and 4) several businesses, such as a feed store, a truck stop, a mobile home park, and a church. A sinkhole developed at this site would cause great damage to private property and infrastructure, and possibly cause fatalities. Geotechnical studies of the site indicate that "upward stoping and roof fall are occurring at a rate of about 30 cm per year, and, in the absence of any remediation, failure will occur in 10 to 25 years" (Land, 2021). Remediation at this site consists of 26 wells drilled around the perimeter of the cavity in 2018 for injection of sand and grout, and this remediation process is projected to be completed by Fall, 2020 (Land, 2021).

Impacts from Petroleum and Water-Supply Activities

Petroleum-industry activities that may lead to adverse impacts from salt karst include the drilling of exploration, production, or salt water disposal (SWD) boreholes into, or through, subsurface salt units (Johnson and others, 2003; Johnson, 2005a, b). Unintentional dissolution of the salt can create a cavity that is as large and shallow as those created by solution-mining activities. And if the cavity becomes too large for the roof to be self-supporting, successive roof failures may cause the collapse to migrate upward and perhaps reach the land surface. Most collapses related to petroleum activity involve boreholes drilled long ago, before the development of proper engineering safeguards pertaining to drilling mud design (use of salt-based drilling fluids), casing placement (sealing salt beds from circulating fluids), and salt-tolerant cements (to prevent the breakdown of cement in the borehole). Wells drilled through salt deposits in search of freshwater that is beneath the salt can also produce unintentional collapse features.

With the increase in rotary drilling during the 1920s, 1930s, and 1940s, boreholes drilled by petroleum companies typically used water-based drilling muds that circulated against the walls of the holes. In most areas, these muds were probably unsaturated with respect to salt (NaCl). Under these conditions, it was common for salt units in a borehole to be at least slightly enlarged, or perhaps even greatly enlarged. In areas underlain by shallow salt deposits, companies now use a drilling fluid that is saturated with respect to salt, and that also provides desirable drilling-mud characteristics. And to ensure that salt units encountered in a borehole are properly sealed off, longer strings of surface casing and intermediate protective casing are commonly used (with improved cements), and the annulus (the interval between the casing and surrounding rock) typically is filled with cement all the way to the surface upon completion of the drilling.

Sources of unsaturated waters that can reach salt units in poorly cemented or poorly cased old wells, or in wells with corroded tubing or casing, include: (1) fresh groundwater that can seep down from shallower aquifers; (2) unsaturated formation brine that enters the borehole from above or below the salt; (3) unsaturated brine that is coproduced with the oil and/or gas; and (4) unsaturated brine pumped down an injection well, either for brine disposal or for enhancing petroleum production (secondary recovery). With all the early drilling and petroleum production throughout the GPEB region, it is not surprising that there are places where salt has been dissolved inadvertently and has created solution cavities that collapsed—and there is a possibility that similar sinks may develop in the future.

Wink Sinks. Several large sinkholes and subsidence features formed in the Hendrick oil field near the town of Wink, in Winkler County, Texas (Figures 6B, 8, 19). The first sinkhole was described in detail by Baumgardner and others (1982) and Johnson (1986, 1989a). Descriptions of the first and second sinkhole, and nearby subsidence features, were then made by Johnson and others (2003) and Johnson (2005a, b). Later work involving InSAR, LIDAR, gravimetry, and/or GPS monitoring of ongoing deformation of subsidence features at Wink has been carried out by Paine and others (2009, 2021), Kim and Lu (2018, 2021), Kim and others (2019), Shi and others (2019), and Trentham and Henderson (2021).

The Hendrick oil field, which embraces the collapse and subsidence features near Wink, is one of the giant oil fields of Texas, with more than 1400 wells drilled since the discovery of the field in 1926. Wink Sink #1 formed about 3 km NNE of the town of Wink in 1980: within 2 days, the sinkhole was about 110 m wide and 33 m deep, and its volume was estimated at about 160,000 m^3 (Johnson and others, 2003). One abandoned oil well (the Hendrick well 10–A), drilled in 1928, was incorporated within the sink itself. The sink resulted from an underground cavity in the Salado salt migrating upward by successive roof failures, thus producing a collapsed chimney filled with brecciated rock (Baumgardner and others, 1982; Johnson, 1986, 1989a, 2005a, b; Johnson and others, 2003) (Figure 20). Eventually, the collapsed chimney reached the land surface and created Wink Sink #1 (Figure 21A). In this area, the Salado salt is about 260 m thick and is about 400 to 660 m beneath Wink Sink #1.

Dissolution and collapse associated with Wink Sink #1 apparently resulted from, or at least was accelerated by, the Hendrick 10–A well, which may have been a pathway for unsaturated water to come in contact with the Salado salt (Johnson, 1986, 1989a, 2005a, b; Johnson and others, 2003). Reasons for assuming this are (1) the well was probably drilled with freshwater drilling fluid that enlarged the borehole in the salt sequence; (2) because of probable borehole enlargement during

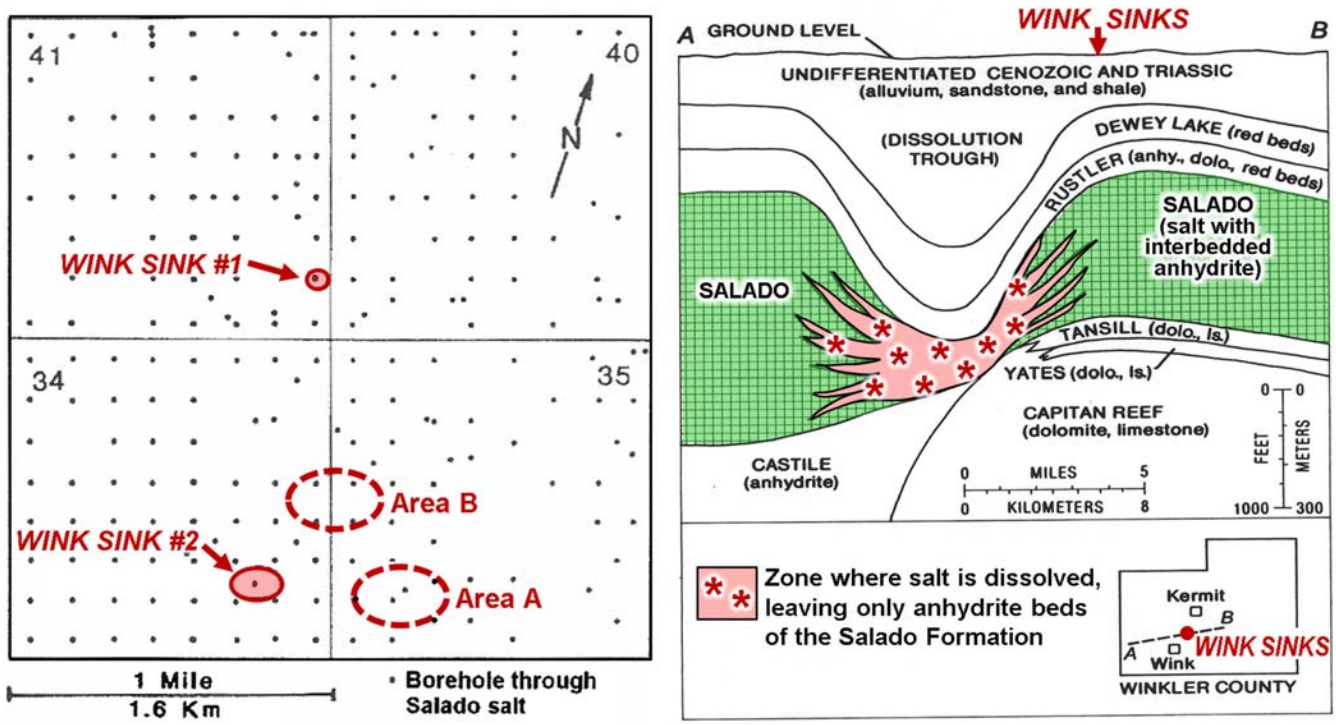

Figure 19. Map and cross section of Wink Sinks area in Winkler County, Texas. Map on left shows the location of Wink Sinks no. 1 and no. 2, and two broad subsidence areas, A and B (modified from Johnson, 2005a). Cross section on right shows the natural dissolution of Salado salts on east side of Delaware Basin and the location of Wink Sinks (modified from Johnson and others, 2003).

drilling through the salt, the small amount of cement reportedly used to set casing in the hole was probably enough to cement only the lower part of the hole, thus leaving most of the salt section uncemented behind the casing; (3) casing in the well was probably perforated by corrosion because of subsequent production of great quantities of oil-field brine along with the oil; (4) explosives used to realign well 10–A while drilling in the underlying Tansill Formation not only fractured the Tansill, but also may have fractured the cement lining farther up the borehole; and (5) casing was removed from the well in 1964, leaving an unlined borehole from the base of the Santa Rosa aquifer to the top of the Rustler Formation for a period of 16 yr, until the formation of Wink Sink #1. All these activities, although consistent with standard industry practices during the life of Hendrick well 10–A, could have aided in conducting freshwater from shallow aquifers down the borehole to the salt beds (Johnson, 1986, 1989a, 2005a, b; Johnson and others, 2003).

It is also possible that salt-dissolving waters ascended to the Salado Formation from the Capitan Reef below. Baumgardner and others (1982) noted that the hydraulic head in the Capitan is above the Salado here, and that a brine-density flow cycle could bring unsaturated water up the borehole to the Salado salt under artesian pressure. The dense brine thus formed could then go back down the borehole under gravity flow, and then be replaced by additional unsaturated water rising from the Capitan Reef. In general, in abandoned boreholes where the salt section is unprotected, it is possible for such a borehole to be a conduit that allows deep fluids to rise and cause dissolution of the salt.

Subsequent studies (Collins, 2000; Johnson and others, 2003; Kim and Lu, 2021; Paine and others, 2021; Trentham and Henderson, 2021) showed that subsidence has continued adjacent to Wink Sink #1: the area just east of the sinkhole apparently has subsided about 8.5 m since 1980, and a series of concentric tension fractures are now present within about 100 m of the sink (Figure 21A). In addition, two broad areas of ground subsidence were observed about 1 to 1.5 km SSE of Wink Sink #1 in 1999 (areas A and B on the map in Figure 19). Earth fissures, sagging power lines, tilted poles, and dip on a once-level well pad caused Collins (2000) to do a field study that documented significant ground subsidence in areas A and B. Between 1970 and 1999, the ground in area A subsided as much as 7 m, and the ground in area B subsided as much as 8.5 m. Later studies (Paine and others, 2021) indicate that parts of area A (also called the "Wink Sag" by Trentham and Henderson, 2021) had subsided up to 8.8 m between 1968 and 2013, an average annual subsidence rate of about 20 cm/yr. Most oil wells in

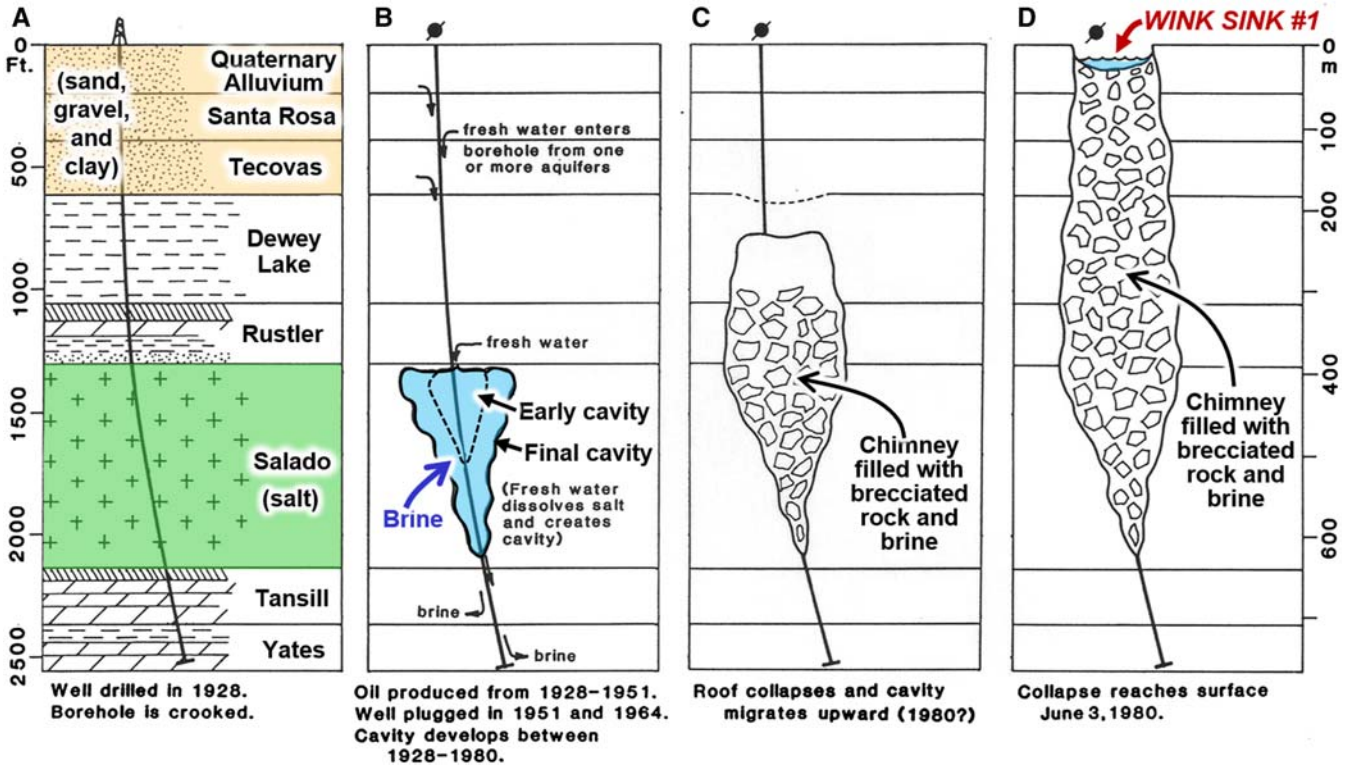

Figure 20. Schematic cross section through the Hendrick well 10–A, showing possible relationship of this oil well to the development of Wink Sink no. 1. (A) Geologic setting. (B) Freshwater may have circulated down the borehole to dissolve the salt and create a cavity. (C) By successive roof failures, the cavity migrated upward toward the land surface. (D) Collapse reaches the land surface and creates Wink Sink no. 1. Modified from Johnson (1989a).

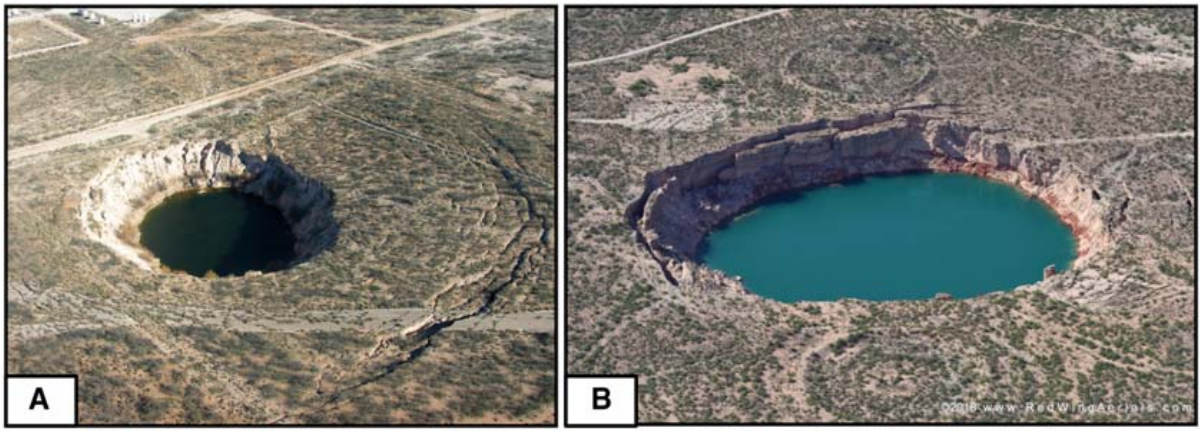

Figure 21. Aerial views of Wink Sinks just northeast of Wink in Winkler County, Texas. (A) Wink Sink no. 1: diameter now about 115 m across, and note concentric tension fractures extending about 100 m out from the sink. (B) Wink Sink no. 2: initially about 140 m wide, but, as seen here, this sink is now about 250 m wide and the walls are about 30 m high (photo B, courtesy of Ryan Short, RedWingAerials.com).

areas A and B were drilled in the late 1920s, and drilling and completion methods were probably similar to those used in drilling Hendrick well 10–A. It is likely that subsidence in areas A and B results from subsurface dissolution of the Salado salt, and may be partly related to petroleum activity (Collins, 2000; Johnson and others, 2003). If deep-seated cavities do exist under areas A and/or B, it (or they) has (have) not yet breached the surface as sinkholes.

Wink Sink #2 formed in 2002 at a site 1.5 km south of Wink Sink #1 and about 400 m nsouth and west of areas A and B (Johnson and others, 2003) (Figure 19, map; Figure 21B). By the end of the first day, Wink Sink #2 was about 140 m long and 100 m wide and water level

in the sink was about 30 m below land surface. The sink grew larger by undercutting its vertical walls and sloughing unconsolidated material into the water-filled hole. The volume of the sinkhole was estimated earlier at 1.33 million m^3 (Johnson and others, 2003), and its current width is estimated to be about 250 m (Figure 21B). Wink Sink #2 embraced a former water-supply well (Gulf WS–8) that was drilled in 1960 into the Capitan Reef, at a total depth of 1092 m (Johnson and others, 2003): the top and base of the Salado salt here are at depths of 412 and 686 m, respectively, so the formation is 274 m thick. It is possible that the Gulf WS–8 well may have been a pathway for unsaturated water to come in contact with Salado salts, and that created a solution cavity that migrated upward and caused the collapse of the land surface as Wink Sink #2 (Johnson and others, 2003).

McCamey Sink. The McCamey Sink formed in 1977 about 15 km east of McCamey, in Upton County, Texas, at the site of a SWD well: the RR Kennedy Production Well No. 17, in the Rodman–Noel field (Johnson and others, 2003) (Figure 6B). The well was permitted in 1967 to inject salt water co-produced with oil into the Permian Grayburg Formation at a depth of about 550 to 610 m. At this site, about 189 m of Salado salt was penetrated at a depth interval of 259 to 448 m. It is likely that injected (unsaturated) salt water was not confined to the Grayburg Formation, and that some of the brine came in contact with, and dissolved, some of the Salado salt. Uncontrolled dissolution of salt in the borehole may have led to the formation of a large cavity, and, with the failure of its roof, the cavity could have migrated upward and eventually reached the surface to form the sinkhole (Johnson and others, 2003). Initially, the sinkhole was about 21 m across and 21 m deep, and later reports indicate the sinkhole enlarged to about 90 m across, and up to 30 m deep (Johnson and others, 2003).

Pecos County Subsidence. Several sites in Pecos County, Texas, have experienced subsidence of the land surface that probably is related to the subsurface dissolution of the Salado salt (Kim and Lu, 2018) (Figure 6B). The sites include (1) three separate sites that are 7–11 km southwest of the town of Imperial and (2) Santa Rosa Spring, located about 13 km southwest of Grandforth, or about 25 km west of Imperial. At all four of these sites, the land surface has subsided at rates of 0.7–8.9 cm/yr, based on InSAR data from late 2014 to April 2017, but there has been no collapse or sinkhole formation. The three subsidence sites just southwest of Imperial embrace, or are near, abandoned or active petroleum boreholes, and are underlain by the Salado salt at depths of 300 to 500 m. The maximum rate of land subsidence at these sites, including Boehmer Lake (which did not exist prior to 2003), is from 1.5 to 3.9 cm/yr (Kim and Lu, 2018). Kim and Lu (2018, p. 6–7) state: "Through unplugged abandoned wells, corroded pipes, or cracks in the casing, freshwater flows down and/or artesian water rises to the Salado Formation, accelerating the dissolution of the evaporite, creating voids in the beds, and causing rapid subsidence on the surface."

Although there has been drilling of oil wells in the vicinity of Santa Rosa Spring, it is believed that here the Salado salt, at a depth of 300 to 450 m, is probably being dissolved naturally by groundwater (Kim and Lu, 2018). The subsiding area is about 1.4 by 1.0 km, and the maximum subsidence shown by InSAR data are about 8.9 cm/yr. Studies in Pecos County show that the highest salinity of groundwater in the region is at Santa Rosa Spring (7224 mg/L), and that the salinity of water in Santa Rosa Spring increased by 4894 mg/L from the 1940s to 1987 (Kim and Lu, 2018).

Jal Sink. In 1998, a sinkhole formed at a site about 15 km NNW of Jal, in southern Lea County, New Mexico (Powers, 2003; Johnson and others, 2003) (Figure 6B). The Jal Sink (also known as the Whitten Ranch Sinkhole) formed close to the Skelly No. 2 Jal Water System well (Jal WS-2) that was drilled into the Capitan Reef in 1967 to provide a source of freshwater. The well was drilled to a depth of 1372 m, was cased from the surface to a depth of 1186 m, and the hole was left open (no casing) from 1186 m to total depth. Salt was encountered in both the Rustler and Salado Formations in the well, and Powers (2003) estimates the uppermost Rustler salt was at a depth of about 518 m, and the Salado salt was penetrated from 610 to 1006 m deep.

In 1979, casing in the well collapsed at 501 m, and the well was plugged and abandoned. After plugging portions of the well, Powers (2003) estimated that about 91 m of the upper Salado salt and all of the Rustler salts remained open (unplugged) behind the casing. The various plugs may have done nothing to prevent freshwater in the Capitan aquifer from circulating up through the production casing and collapsed casing into the Rustler salt, and possibly the Salado salt. Jal Sink eventually reached about 50 m in diameter, about 18 m deep, and has been dry (no water in the surface depression); the edge of the sinkhole is about 20 m from Jal WS-2. Although a natural origin cannot be ruled out for the development of the Jal Sink, it is likely that the nearby Jal WS-2 well allowed freshwater to circulate into the salt beds, and the collapsing chimney worked its way up to the land surface (Powers, 2003).

Panning Sink. Panning Sink formed in 1959 by subsidence and collapse around a SWD well on the Panning lease in Barton County, Kansas (Fader, 1975; Walters,

1978; Anderson and others, 1995a; Johnson, 2005a, b) (Figures 6B, 22). The sink is about 7 km ESE of Ellinwood, and 1.5 km south of US Highway 56. The well was originally an oil-producing well, and was drilled through 91 m of Hutchinson Salt starting at a depth of 298 m. When originally drilled in 1938, freshwater drilling fluids dissolved the salt to an excessive diameter (1.4 m), and only about half of this washed-out zone was then cemented behind the casing (Walters, 1978). From 1949 to 1958, the well was converted to the disposal of salt water that was co-produced with petroleum from other oil wells in the area. A large quantity of unsat-urated oil-field brine (containing about 28,000 ppm NaCl) was then pumped into the well and, because of corrosion in the casing, the brine inadvertently encountered, and further dissolved, the salt. A large cavern was formed, and with successive roof falls, the water-filled void migrated upward causing surface subsidence, tilting of an oil-field derrick, and eventual collapse (Figure 22). Initially, the sinkhole had a diameter of 90 m and was at least 18 m deep; later data (Google Earth, June 2015) shows that the sink has reached dimensions of 150 m

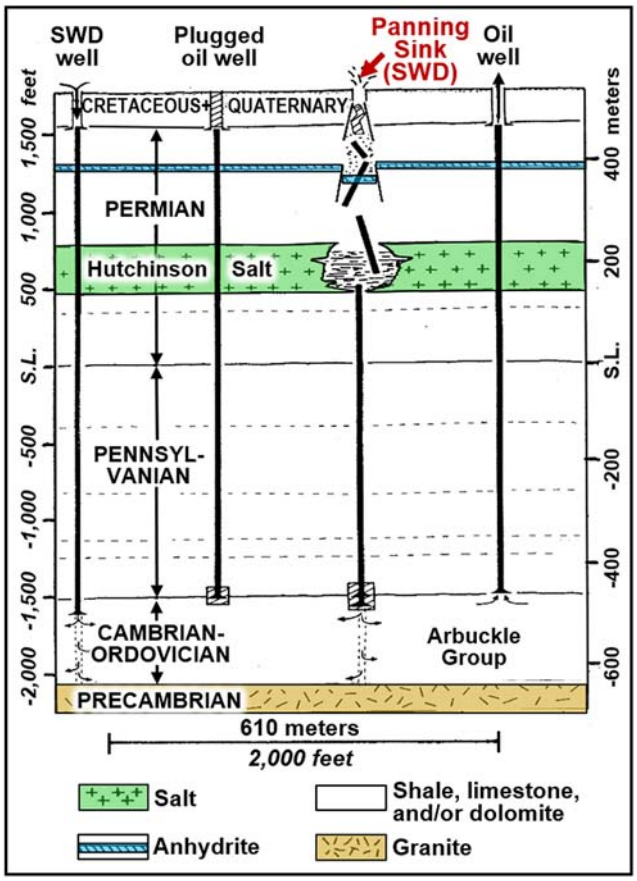

Figure 22. Cross-section through the Panning salt water disposal (SWD) well showing the result of unplanned dissolution of the Hutchinson Salt and development of the Panning Sink in Kansas (modified from Walters, 1978).

by 180 m, and still later data (Google Earth, June 2019) show water filling a depression (the sink, plus adjacent land that slopes down toward the sink) that is about 230 m by 255 m.

Berscheit and Hilton Sinks. Two sites of Hutchinson Salt dissolution and subsidence are present in western Rice County, Kansas (Fader, 1975; Walters 1978) (Figure 6B). Here the Hutchinson Salt is about 90 m thick and the top of the salt is about 290 m below land surface. These two subsidence features are the Berscheit and Hilton Sinks: Berscheit Sink is 9 km east of Ellinwood and 600 m south of US Highway 56; Hilton Sink is 2 km SW of the small community of Chase. Both sinks enveloped SWD wells that were drilled specifically to dispose of oil-field brines into the Arbuckle Group, and the general geology and history are similar to that of the Panning Sink (above), once the Panning well was converted to SWD (Figure 22). The principal difference is that the land surface at both the Berscheit and Hilton Sinks did not collapse, but instead underwent slow subsidence. The Berscheit well was drilled in 1936, and was abandoned in 1972. By 1975, the pond filling the depression was 157 m by 114 m, and the subsidence was estimated to be about 5 m (Walters, 1978); later data (Google Earth, June 2015) indicated that the pond (assumed to be the sink/depression area) is about 150 m across. On the Hilton lease, two wells were drilled 60 m apart: one well was drilled in 1948 and plugged in 1951, and the other well was drilled in 1951 and plugged in 1965. Subsidence was first noted at this site starting in 1964, and Fader (1975) estimated that by 1968 the land surface had subsided 6 m. Aerial photos (Google Earth, June 2015) show that the pond in the sink/depression is 160 m by 190 m.

Witt and Crawford Sinks. Slow subsidence is occurring at two sites along Interstate 70 in the Gorham oil field, in Russell County, Kansas, because of dissolution of the Hutchinson Salt (Fader, 1975; Walters, 1978, 1991; Croxton, 2002, 2003; Johnson, 2005a, b) (Figure 6B). Oil wells drilled in the field from the 1920s through the 1940s penetrated 75 m of salt at a depth of 390 m. Many of the wells are now plugged and abandoned, but the corroded casing was left in some of the boreholes at depths above, within, and below the salt unit; this probably has allowed unsaturated water to flow down some of the abandoned boreholes and dissolve large volumes of salt. Subsidence was not evident prior to highway construction in 1966, but by 1971, two sites of pronounced subsidence were obvious. The Witt Sink and the Crawford Sink are located adjacent to the east-bound lanes (south side) of I-70: they are about 800 m apart, and about 4.5 and 5.3 km, respectively, ESE of the town of Gorham.

Early subsidence at the sinks occurred at rates of about 10 to 15 cm/yr, and by 1971 the east-bound lanes had dropped so much that they had to be regraded: paving was raised about 1.5 m at both sinks, at a cost of US $220,000 (Croxton, 2002, 2003). By 1984, the lanes at the Witt Sink had again subsided nearly 2.5 m, and a line-of-sight problem arose because cars down in the sink could not be seen by oncoming traffic. Witt Sink was again regraded and repaved in 1986, at a cost of nearly US $500,000. A borehole was drilled adjacent to the abandoned oil well believed to be the cause of the Witt Sink, and cement was injected to plug the old well at the base of the salt. This appeared to stop the settling for about 6 months, but then subsidence resumed at a rate of 12 to 15 cm/yr. Plans call for continuing to regrade 1–70, as needed, because a more economical solution to the subsidence problem has not been found (Croxton, 2002, 2003).

Hutchinson Gas Explosion. This is an example of natural salt karst affecting a petroleum-related problem. A series of natural-gas explosions and geysers occurred within the city of Hutchinson, Kansas, in 2001, resulting in the death of two people (Watney and others, 2003) (Figure 6B). The loss of an estimated 4,049,000 m^3 (143 million ft^3) of gas was reported from an underground, high-pressure, natural-gas-storage facility, the Yaggy facility, about 11 km northwest of Hutchinson. Gas explosions began 2½ days after a major gas leak in a natural-gas-storage well at the facility where the gas is stored in dissolution caverns formed in the Hutchinson Salt. The gas presumably traveled underground through a series of shallow fracture systems that had been partly produced by dissolution of the deeper, upper salt beds of the Hutchinson Salt that underly the entire area: the top of the salt rises from a depth of about 180 m at the Yaggy facility to depths of about 120 to 140 m beneath the city of Hutchinson (Watney, 2003, see his Figure 6). Dissolution of the uppermost salt beds formed an elongated northwest-trending trough that extends beneath the gas-storage facility and Hutchinson. This northwest trend of fracturing and dissolution probably reflects the location of a deep-seated tectonic fracture system. Therefore, it appears that the tectonic fracture system aided in the development of fractures in the Hutchinson Salt and overlying strata, and these fractures apparently acted as conduits for unsaturated groundwater to reach and partly dissolve the uppermost Hutchinson Salt beds. This led to development of the elongated northwest-trending fracture system that conducted natural gas from the storage facility to the city of Hutchinson.

Freedom Gas Blowout. This is another example of natural salt karst helping to bring about a petroleum-related problem. In 1980, natural gas erupted at a number of places in the flood plain of Cimarron River, about 6 km WNW of the town of Freedom, along the Woods–Woodward County line in northwest Oklahoma (Figure 6B). This event was described by Preston (1980a, 1980b) and summarized by Johnson (2003a). Alluvium in the Cimarron River floodplain overlies the Flowerpot Shale, which, in the shallow subsurface, contains salt beds of the Flowerpot salt. The top of the karstic Flowerpot salt here is about 60 m below the surface, and the top of the Cimarron salts is about 150 m deep: however, just 3 km to the west (beneath Big Salt Plain) the top of the salt is actively being dissolved at a depth of only 10 m (Johnson, 1981). At first, venting of the gas created a crater 6 m wide, from which viscous mud was ejected to a height of more than 15 m (Preston, 1980b), and other craters in the area were up to 9 m wide and 3.7 m deep. More than 50 separate vents were mapped in an area about 1.5 km by 2.5 km. Preston (1980a, 1980b) estimated that the total gas emitted from the larger vents alone was about 566,000 m^3/day (20 million ft^3/day), and that much more was emitted from smaller vents and by general effusion of gas through the sandy soils.

Nearby gas-producing wells were checked to see if there was a mechanical failure that produced the gas, but all of them were intact. Analyses of the escaping gas showed that it was probably coming from the Mississippian Chester/Oswego interval, at depths of about 1700 m in the area. Although origin of the gas was not proven, the Oklahoma Corporation Commission (OCC) concluded that it probably came from a well about 16 km southwest of the blowout. The suspect well was drilled to a depth of 2449 m, and, following a drillstem test, high-pressure natural gas in the well caused a blowout just 4 days prior to the gas eruptions near Freedom. The Oklahoma Corporation Committee officials concluded (Vanderwater, 1980) "that the same pressure that caused the blowout at the . . . well fractured the underground rock. That let natural gas below the well's casing [set at 305 m] enter caverns which honeycomb the area, building up pressure there and eventually erupting through weak surface points like cracks and under ponds [in the Cimarron River floodplain]." If that analysis is correct, then gas escaping from the well may have done the following: (1) entered the intrastratal karst system in the Cimarron and/or Flowerpot salt; (2) migrated laterally up-dip for 16 km to the northeast through natural, salt-dissolution cavities; and (3) then (within 4 days) reached the land surface through the fractured Flowerpot Shale which overlies the karstic salts. So, it appears that natural salt karst in the area allowed fugitive, high-pressure natural gas to travel a long distance (16 km) in a short time, thus creating a potentially hazardous condition at a site far removed from the site of the initial well blowout (Johnson, 2003a).

Human-Induced Gypsum Karst

Gypsum karst and subsidence can be accelerated by human activity, including the same activities that may cause problems in carbonate terranes, such as: (1) building structures that induce differential compaction of soils above an irregular gypsum bedrock surface; (2) building structures directly upon gypsum-collapse features; and (3) impounding water above, or directing water into, a gypsum unit where soil piping can divert water (and soil) into underground gypsum cavities (Johnson, 2005b; Cooper, 2020b). These human activities can cause land subsidence, or can cause new or concealed sinkholes and cave systems to open up; this can result in settling or catastrophic collapse of the ground.

Human activities have caused problems in gypsum-karst areas in various parts of the United States, especially in the Black Hills area of South Dakota and Wyoming (Rahn and Davis, 1996; Davis and Rahn, 1997; Epstein, 2003), and in the failure of the Quail Creek Dike near St. George in southwest Utah (Gourley, 1992; Payton, 1992; Payton and Hansen, 2003). However, such examples are rare in the GPEB. The main examples I am aware of in the GPEB are where dams have been proposed in areas of gypsum karst. Red Bluff Dam (described above under "Natural Salt Karst") is now losing water through gypsum-karst features that are largely collapsed because of dissolution of underlying salt and gypsum beds. Other dams originally proposed in areas of gypsum karst, but that were abandoned as a result of detailed evaluation and alternate sites were recommended, include the original Upper Mangum, Cedar Ridge, and McMillan Damsites (described above under "Natural Gypsum Karst").

CONCLUSIONS

The newly identified GPEB is one of the major accumulations of evaporites in the world, covering about 650,000 km^2 in parts of Texas, New Mexico, Oklahoma, Kansas, and Colorado. Eight major Permian evaporite sequences that contain salt (halite) and gypsum/anhydrite have a combined thickness of 500 to 1500 m in various parts of the GPEB. These evaporites extend across a series of structural and sedimentary basins in the region, with the evaporite depocenter shifting progressively to the south (or southwest) during about 25 million years of the Leonardian, Guadalupian, and Ochoan Epochs. The earliest evaporites are the Wellington/Hutchinson evaporites, centered in Kansas on the north, and the final stage of evaporite deposition was the Rustler Formation in west Texas and southeast New Mexico. Whereas Permian gypsum/anhydrite units extend throughout the full 650,000 km^2 of the GPEB, the salt-bearing units are restricted to about 380,000 km^2 of the region.

Evaporite karst is widespread in the GPEB, and results from both natural processes and human activities. Typical karst features here include caves, sinkholes, breccia pipes, disappearing streams, springs, and even catastrophic collapses. Each of the eight evaporite sequences in the GPEB has areas of natural karst features somewhere in the region.

Natural salt karst has resulted in major subsidence troughs in the Delaware Basin that are now filled with Cenozoic sediments, as well as smaller-scale subsidence/collapse features in all five states of the GPEB. Salt karst is also generated by human activities: solution mining of underground salt deposits can inadvertently create a large cavity in the salt, and if the cavity becomes too large it can result in failure of its roof that can then reach the land surface as a huge sinkhole; petroleum or water-supply wells can also accidentally create large cavities in salt deposits that result in failure of the roof and upward stoping of the cavity until it reaches the land surface as a giant sinkhole.

Natural gypsum karst is common on both the west and east sides of the GPEB. Gypsum caves and sinkholes are common in the Delaware Basin of west Texas and New Mexico, as well as on the east side of the GPEB in north-central Texas, western Oklahoma, and southwest Kansas. A number of the longest and most significant gypsum caves are present on both sides of the region, and solution cavities in gypsum have created significant aquifers in some areas. Natural gypsum karst has caused loss of water around or beneath some existing dams, and has also caused the abandonment of several proposed or functioning dams.

It is hoped that this report on evaporite karst in the GPEB provides an overview of the scope and significance of actual and potential evaporite-karst problems in the region, and also provides an impetus for further research on various aspects of evaporite studies.

Appreciation is expressed to Dr. Lewis Land, geologist with the National Cave and Karst Research Institute, for his review and constructive comments on an early draft of this report.

REFERENCES

Anderson, N.L., Knapp, R.W., Steeples, D.W., and Miller, R.D., 1995a, Plastic deformation and dissolution of the Hutchinson Salt Member in Kansas: Kansas Geological Survey, Bulletin 237, p. 66-70. http://www.kgs.ku.edu/Publications/Bulletins/237/Anderson3/hutchinson2.pdf

Anderson, N.L., Watney, W.L, Macfarlane, P.A., and Knapp, R.W., 1995b, Seismic signature of the Hutchinson Salt and associated dissolution features: Kansas Geological Survey, Bulletin 237, p. 57-63. http://www.kgs.ku.edu/Publications/Bulletins/237/Anderson2/hutchinson.pdf

Anderson, R.Y., 1981, Deep-seated salt dissolution in the Delaware Basin, Texas and New Mexico: New Mexico Geological Society, Special Publication No. 10, p. 133–145. https://wipp.energy.gov/library/cca/CCA_1996_References/Chapter%202/CREL4992.PDF

Anderson, R.Y., Dean, W.E., Jr., Kirkland, D.W., and Snider, H.I., 1972, Permian Castile varved evaporite sequence, west Texas and New Mexico: Geological Society of America, Bulletin, Vol. 83, No. 1, p. 59-86.

Anderson, R.Y., Kietzke, K.K., and Rhodes, D.J., 1978, Development of dissolution breccias, northern Delaware Basin, New Mexico and Texas, *in* Austin, G.S., compiler, Geology and mineral deposits of Ochoan rocks in Delaware Basin and adjacent areas: New Mexico Bureau of Mines and Mineral Resources, Circular 159, p. 47-52. https://geoinfo.nmt.edu/publications/monographs/circulars/downloads/159/Circular-159.pdf

Askew, R.L., 2013, Distribution of the Permian Blaine Formation salt in the subsurface of the Hugoton Embayment area of Baca County, southeast Colorado: Rocky Mountain Association of Geologists, The Mountain Geologist, Vol. 50, No. 2, p. 65-75.

Bachman, G.O., 1984, Regional geology of Ochoan evaporites, northern part of Delaware Basin: New Mexico Bureau of Mines and Mineral Resources, Circular 184, 23 p. https://geoinfo.nmt.edu/publications/monographs/circulars/downloads/184/Circular-184.pdf

Bachman, G.O., and Johnson, R.B., 1973, Stability of salt in the Permian salt basin of Kansas, Oklahoma, Texas, and New Mexico: U.S. Geological Survey, Open-file Report 73-14, 62 p. https://pubs.usgs.gov/of/1973/0014/report.pdf

Baumgardner, R.W., Jr., Hoadley, A.D., and Gustavson, T.C., 1981, Salt dissolution and formation of the Wink Sink, Winkler County, Texas, *in* Gustavson, T.C., and others, Geology and geohydrology of the Palo Duro Basin, Texas Panhandle: The University of Texas at Austin, Bureau of Economic Geology, Geological Circular 81–83, p. 152-155.

Baumgardner, R.W., Jr., Hoadley, A.D., Goldstein, A.G., 1982, Formation of the Wink Sink, a salt dissolution and collapse feature, Winkler County, Texas: The University of Texas at Austin, Bureau of Economic Geology, Report of Investigations No. 114, 38 p.

Belski, D.S., ed., 1992, GYPKAP report, no. 2, 1988–1991: National Speleological Society, Southwest Region, 56 p.

Berry, H.D., 2018, Dissolution of Permian salt, Las Animas Arch, Colorado: Unpublished M.S. thesis, University of Louisiana at Lafayette, 96 p.

Bozeman, J., 2003, Exploration of western Oklahoma gypsum caves, *in* Johnson, K.S., and Neal, J.T., eds., Evaporite karst and engineering/environmental problems in the United States: Oklahoma Geological Survey, Circular 109, p. 57-64. http://ogs.ou.edu/docs/circulars/C109.pdf

Bozeman, J., and Bozeman, S., 2002, Speleology of gypsum caves in Oklahoma: Carbonates and Evaporites, Vol. 17, No. 2, p. 107-113.

Bozeman, S., ed., 1987, The D.C. Jester Cave system: Central Oklahoma Grotto, Oklahoma Underground, Vol. 14, 56 p.

Bozeman, S., ed., 2002, The Selman Cave System, Woodward County, Oklahoma: Central Oklahoma Grotto, Oklahoma City, Oklahoma Underground, Vol. 20, 44 p.

Charlton, J, Boehm, R., and Johnson, K.S., 2021, Design and implementation of a grout program in an evaporite-karst foundation, Red Bluff Dam, Orla, Texas: *in* Johnson, K.S., Land, L., and Decker, D.D., eds., Evaporite karst in the Greater Permian Evaporite Basin (GPEB) of Texas, New Mexico, Oklahoma, Kansas, and Colorado: Oklahoma Geological Survey, Circular 113.

Coates, G.K, Lee, C.A., McClain, W.C., and Senseny, P.E., 1985, Closure and collapse of man-made cavities in salt, in Schreiber, B.C., and Harner, H.L., eds., Sixth international symposium on salt: The Salt Institute, Alexandria, Virginia, Vol. 2, p. 139-157.

Collins, E.W., 2000, Reconnaissance investigation of active subsidence and recent formation of earth fissures near the 1980 Wink Sink in the Hendrick oil field, Winkler County, Texas: Geological Society of America, Abstracts with Programs, Vol. 32, No. 3, p. A-6.

Cooper, 2020a, Geologic hazards from salt mining, brine extraction and natural salt dissolution in the UK, *in* Giles, D.P., and Griffiths, J.S., eds., Geologic hazards in the UK: their occurrence, monitoring and mitigation—Engineering Group Working Party Report: Geological Society, London, Engineering Geology Special Publications 20, Chapter 14, p. 369-387.

Cooper, 2020b, Geohazards caused by gypsum and anhydrite in the UK: including dissolution, subsidence, sinkholes and heave, *in* Giles, D.P., and Griffiths, J.S., eds., Geologic hazards in the UK: their occurrence, monitoring and mitigation—Engineering Group Working Party Report: Geological Society, London, Engineering Geology Special Publications 20, Chapter 16, p. 403-423.

Cox, E.R., 1967, Geology and hydrology between Lake McMillan and Carlsbad Springs, Eddy Co., New Mexico: U.S. Geological Survey, Water-Supply Paper 1828, 48 p. https://pubs.er.usgs.gov/search?q=water-supply+paper+1828

Croxton, N.M., 2002, Subsidence of I–70 in Russell County, Kansas, related to salt dissolution—A history: The Professional Geologist, Vol. 39, No. 8, p. 2-7.

Croxton, N.M., 2003, Subsidence on Interstate 70 in Russell County, Kansas, related to salt dissolution—A history, *in* Johnson, K.S., and Neal, J.T., eds., Evaporite karst and engineering/environmental problems in the United States: Oklahoma Geological Survey, Circular 109, p. 149-155. http://ogs.ou.edu/docs/circulars/C109.pdf

Croxton, N.M, 2021, Sinkhole under Interstate 135 in McPherson County, Kansas, *in* Johnson, K.S., Land, L., and Decker, D.D., eds., Evaporite karst in the Greater Permian Evaporite Basin (GPEB) of Texas, New Mexico, Oklahoma, Kansas, and Colorado: Oklahoma Geological Survey, Circular 113.

Davis, A.D., and Rahn, P.H., 1997, Karstic gypsum problems at wastewater stabilization sites in the Black Hills of South Dakota: Carbonates and Evaporites, Vol. 12, p. 73-80.

Dunrud, C.R., and Nevins, B.B., 1981, Solution mining and subsidence in evaporite rocks in the United States: U.S. Geological Survey, Miscellaneous Investigations Series, I–1298, 2 plates, scale 1:5,000,000. https://pubs.er.usgs.gov/publication/i1298

Dyni, R.C., 1986, Subsidence investigations over salt-solution mines, Hutchinson, KS: U.S. Bureau of Mines, Information Circular 9083, 23 p. https://ia800300.us.archive.org/30/items/subsidenceinvest00dyni/subsidenceinvest00dyni.pdf

Ege, J.R., 1979, Subsurface subsidence and collapse in relation to extraction of salt and other soluble evaporites: U.S. Geological Survey, Open-File Report 79–1666, 34 p. https://pubs.usgs.gov/of/1979/1666/report.pdf

Ege, J.R., 1985, Maps showing distribution, thickness and depth of salt deposits of the United States: U.S. Geological Survey, Open-File Report 85–28, 11 p. 4 plates. https://pubs.er.usgs.gov/publication/ofr8528

Epstein, J.B., 2003, Gypsum karst in the Black Hills, South Dakota–Wyoming: geomorphic development, hazards, and hydrology, *in* Johnson, K.S., and Neal, J.T., eds., Evaporite karst and engineering/environmental problems in the United States: Oklahoma Geological Survey, Circular 109, p. 241-254. http://ogs.ou.edu/docs/circulars/C109.pdf

Fader, S.W., 1975, Land subsidence caused by dissolution of salt near four oil and gas wells in central Kansas: U.S. Geological Survey, Water-Resources Investigations 27-75, 28 p. https://pubs.usgs.gov/wri/1975/0027/report.pdf

Fischer, W.A., and Hackman, R.J., 1964, Geologic map and sections of the Torrance Station 4 NE quadrangle, Lincoln County, New Mexico: U.S. Geological Survey, Miscellaneous Geological Investigations Map 1-400. https://pubs.usgs.gov/imap/0400/report.pdf and https://ngmdb.usgs.gov/Prodesc/proddesc_1283.htm

Forbes, J., and Nance, R., 1997, Stratigraphy, sedimentology, and structural geology of gypsum caves in southeast New Mexico: Carbonates and Evaporites, Vol. 12, p. 64-72.

Garner, L.E., St. Clair, A.E., and Evans, T.J., 1979, Mineral resources of Texas map: The University of Texas at Austin, Bureau of Economic Geology, Energy and Mineral Resource Maps, ER0002, scale 1:1,000,000.

Gauvey, K., and Sumrall, J.B., 2021, Gypsum karst in south-central Kansas, *in* Johnson, K.S., Land, L., and Decker, D.D., eds., Evaporite karst in the Greater Permian Evaporite Basin (GPEB) of Texas, New Mexico, Oklahoma, Kansas, and Colorado: Oklahoma Geological Survey, Circular 113.

Gogel, T., 1981, Discharge of saltwater from Permian rocks to major stream-aquifer systems in central Kansas: Kansas Geological Survey, Chemical Quality Series 9, 60 p. http://www.kgs.ku.edu/Publications/Bulletins/CQS9/index.html

Gourley, C., 1992, Geological aspects of the Quail Creek Dike failure, *in* Harty, K.M., ed., Engineering and environmental geology of southwestern Utah: Utah Geological Association, Publication 21, p. 17-38.

Gustavson, T.C., 1986, Geomorphic development of the Canadian River Valley, Texas Panhandle: an example of regional salt dissolution and subsidence: Geological Society of America, Bulletin, Vol. 97, p. 459-472.

Gustavson, T.C., and Finley, R.J., 1985, Late Cenozoic geomorphic evolution of the Texas Panhandle and northeast New Mexico—Case studies of structural controls on regional drainage development: The University of Texas at Austin, Bureau of Economic Geology, Report of Investigations No. 148, 42 p.

Hill, C.A., 1996, Geology of the Delaware basin – Guadalupe, Apache, and Glass Mountains, southeastern New Mexico and west Texas: SEPM Permian Basin Section, Publication 96-39, 480 p.

Hill, C.A., 2003, Intrastratal karst at the Waste Isolation Pilot Plant site, southeastern New Mexico, *in* Johnson, K.S., and Neal, J.T., eds., Evaporite karst and engineering/environmental problems in the United States: Oklahoma Geological Survey, Circular 109, p. 197-209. http://ogs.ou.edu/docs/circulars/C109.pdf

Hopkins, J., and Muller, C., 2011, Water quality in the Blaine aquifer: Texas Water Development Board, Report 376, 40 p. http://www.twdb.texas.gov/publications/reports/numbered_reports/doc/R376_Blaine.pdf

Johnson, K.S., 1969, Mineral map of Oklahoma (exclusive of oil and gas fields): Oklahoma Geological

Survey, Map GM–15, scale 1:750,000. http://ogs.ou.edu/docs/geologicmaps/GM15.pdf

Johnson, K.S., 1976, Evaluation of Permian salt deposits in the Texas Panhandle and western Oklahoma for underground storage of radioactive wastes: unpublished report submitted to Union Carbide Corporation, Oak Ridge National Laboratories, Office of Waste Isolation, Y/OWI/Sub–4494/1, 73 p. Also available from: Oklahoma Geological Survey, Open-File Report 19–2018. http://www.ou.edu/content/dam/ogs/documents/data/OF19-2018.pdf

Johnson, K.S., 1981, Dissolution of salt on the east flank of the Permian Basin in the southwestern U.S.A.: Journal of Hydrology, Vol. 54, p. 75-93. https://www.researchgate.net/publication/245098253

Johnson, K.S., 1986, Salt dissolution and collapse at the Wink Sink in west Texas: unpublished report submitted to Office of Nuclear Waste Isolation, Battelle Memorial Institute, BMI/ONWI–598, 83 p. Also available from: Oklahoma Geological Survey, Open-File Report 19–2018. http://www.ou.edu/content/dam/ogs/documents/data/OF19-2018.pdf

Johnson, K.S., 1989a, Development of the Wink Sink in west Texas, U.S.A., due to salt dissolution and collapse: Environmental Geology and Water Sciences, Vol. 14, No. 2, p. 81-92. https://www.researchgate.net/publication/226582541

Johnson, K.S., 1989b, Geology of Jester Cave: NSS News, National Speleological Society, Huntsville, AL, Vol. 47, No. 1, p. 11-17. https://www.researchgate.net/publication/307970029

Johnson, K.S., 1990, Hydrogeology and karst of the Blaine gypsum–dolomite aquifer, southwestern Oklahoma: Oklahoma Geological Survey, Special Publication 90–5, 31 p. http://ogs.ou.edu/docs/specialpublications/SP90-5.pdf

Johnson, K.S., 1996, Gypsum karst in the United States, *in* Klimchouk, A., and others, eds., Gypsum karst of the world: International Journal of Speleology, Vol. 25, Nos. 3–4, p. 183-193. https://scholarcommons.usf.edu/ijs/vol25/iss3/13/

Johnson, K.S., 2003a, Evaporite karst in the Permian Blaine Formation and associated strata of western Oklahoma, *in* Johnson, K.S., and Neal, J.T., eds., Evaporite karst and engineering/environmental problems in the United States: Oklahoma Geological Survey, Circular 109, p. 41–55. http://ogs.ou.edu/docs/circulars/C109.pdf

Johnson, K.S., 2003b, Gypsum karst and abandonment of the Upper Mangum Damsite in southwestern Oklahoma, *in* Johnson, K.S., and Neal, J.T., eds., Evaporite karst and engineering/environmental problems in the United States: Oklahoma Geological Survey, Circular 109, p. 85-94. http://ogs.ou.edu/docs/circulars/C109.pdf

Johnson, K.S., 2003c, Gypsum karst as a major factor in the design of the proposed Lower Mangum Dam in southwestern Oklahoma, *in* Johnson, K.S., and Neal, J.T., eds., Evaporite karst and engineering/environmental problems in the United States: Oklahoma Geological Survey, Circular 109, p. 95-111. http://ogs.ou.edu/docs/circulars/C109.pdf

Johnson, K.S., 2005a, Salt dissolution and subsidence or collapse caused by human activities, *in* Ehlen, J., Haneberg, W.C., and Larson, R.A., eds., Humans as geologic agents: Geological Society of America, Reviews in Engineering Geology, Vol. XVI, p. 101-110. https://www.researchgate.net/publication/273125732

Johnson, K.S., 2005b, Subsidence hazards due to evaporite dissolution in the United States: Environmental Geology, Vol. 48, No. 3, p. 395-409. https://www.researchgate.net/publication/227194203

Johnson, K.S., 2008, Gypsum-karst problems in constructing dams in the USA: Environmental Geology, Vol. 53, No. 5, p. 945-950. https://www.researchgate.net/publication/226513928

Johnson, K.S., 2011, Alabaster Caverns State Park: Oklahoma City Geological Society, Shale Shaker, Vol. 62, No. 2, p. 108-112. https://www.researchgate.net/publication/306373810

Johnson, K.S., 2013, Salt karst and collapse structures in the Anadarko Basin of Oklahoma and Texas, *in* Land, L., Doctor, D.H., and Stephenson, J.B., eds., Sinkholes and the engineering and environmental impacts of karst–Proceedings of the thirteenth multidisciplinary conference, Carlsbad, NM, May 6 through 10, 2013: National Cave and Karst Research Institute, Carlsbad, NM, p. 103-112. http://scholarcommons.usf.edu/cgi/viewcontent.cgi?article=1118&context=sinkhole_2013

Johnson, K.S., 2017, Evaporite karst and collapse breccia in Permian strata, Canton Lake Dam, Blaine County, Oklahoma: Oklahoma Geological Survey, Oklahoma Geology Notes, Vol. 76, No. 3, p. 5-18. http://ogs.ou.edu/docs/geologynotes/GN-V76N3.pdf

Johnson, K.S., 2018, Gypsum caves of north Texas and western Oklahoma, *in* Stafford, K.W., and Veni, G., eds., Hypogene karst of Texas: Texas Speleological Survey, Monograph 3, p. 111-122. https://www.texasspeleologicalsurvey.org/PDF/Hypogene_Karst_of_Texas.pdf

Johnson, K.S., 2019, Blaine aquifer in the Hollis Basin of southwest Oklahoma: structure-contour map and stratigraphic/hydrologic data: Oklahoma Geological Survey, Geologic Map GM–45, scale 1:125,000.

http://ou.edu/content/dam/ogs/documents/GMs/GM-45%20map.pdf

Johnson, K.S., 2021a, Permian Blaine and San Andres Formations of western Oklahoma and Palo Duro Basin of Texas: their correlation and evaporite karst, *in* Johnson, K.S., Land, L., and Decker, D.D., eds., Evaporite karst in the Greater Permian Evaporite Basin (GPEB) of Texas, New Mexico, Oklahoma, Kansas, and Colorado: Oklahoma Geological Survey, Circular 113.

Johnson, K.S., 2021b, Salt dissolution and the Wallace Sinkhole in the Sharon Springs–Wallace area, Wallace County, Kansas, *in* Johnson, K.S., Land, L., and Decker, D.D., eds., Evaporite karst in the Greater Permian Evaporite Basin (GPEB) of Texas, New Mexico, Oklahoma, Kansas, and Colorado: Oklahoma Geological Survey, Circular 113.

Johnson, K.S., 2021c, Dissolution of Permian Flowerpot salt beneath the Great Plains Reservoirs, Queens State Wildlife Area, in Kiowa, Prowers, and Bent Counties, southeast Colorado, *in* Johnson, K.S., Land, L., and Decker, D.D., eds., Evaporite karst in the Greater Permian Evaporite Basin (GPEB) of Texas, New Mexico, Oklahoma, Kansas, and Colorado: Oklahoma Geological Survey, Circular 113.

Johnson, K.S., 2021d, Delhi Sinkhole and Watonga Sinkhole due to gypsum karst in the Permian Blaine Formation of western Oklahoma, *in* Johnson, K.S., Land, L., and Decker, D.D., eds., Evaporite karst in the Greater Permian Evaporite Basin (GPEB) of Texas, New Mexico, Oklahoma, Kansas, and Colorado: Oklahoma Geological Survey, Circular 113.

Johnson, K.S., and Gonzales, S., 1978, Salt deposits in the United States and regional characteristics important for storage of radioactive waste: prepared for Union Carbide Corp., Nuclear Division, Oak Ridge National Laboratory, Office of Waste Isolation, Y/OWI/SUB-7414/1, 188 p. Also available from: Oklahoma Geological Survey, Open-File Report 18–2018. http://www.ou.edu/content/dam/ogs/documents/data/OF18-2018.pdf

Johnson, K.S., and Wilkerson, J.M., 2013, Gypsum karst causes relocation of proposed Cedar Ridge Dam, Throckmorton County, Texas *in* Land, L., Doctor, D.H., and Stephenson, J.B., eds., Sinkholes and the engineering and environmental impacts of karst–Proceedings of the thirteenth multidisciplinary conference, Carlsbad, NM, May 6 through 10, 2013: National Cave and Karst Research Institute, Carlsbad, NM, p. 133-139. https://scholarcommons.usf.edu/cgi/viewcontent.cgi?article=1121&context=sinkhole_2013

Johnson, K.S., Gonzales, S., and Dean, W.E., 1989, Distribution and geologic characteristics of anhydrite deposits in the United States, *in* Dean, W.E., and Johnson, K.S., eds., Anhydrite deposits of the United States and characteristics of anhydrite important for storage of radioactive wastes: U.S. Geological Survey, Bulletin 1794, p. 9-90. https://pubs.usgs.gov/bul/1794/report.pdf

Johnson, K.S., Collins, E.W., and Seni, S.J., 2003, Sinkholes and land subsidence owing to salt dissolution near Wink, west Texas, and other sites in western Texas and New Mexico, *in* Johnson, K.S., and Neal, J.T., eds., Evaporite karst and engineering/environmental problems in the United States: Oklahoma Geological Survey, Circular 109, p. 183-195. http://ogs.ou.edu/docs/circulars/C109.pdf

Johnson, K.S., Bangsund, W.J., and Hines, N.A., 2013, Gypsum karst and potential risk in siting wind turbines in Blaine County, Oklahoma, *in* Land, L., Doctor, D.H., and Stephenson, J.B., eds., Sinkholes and the engineering and environmental impacts of karst–Proceedings of the thirteenth multidisciplinary conference, Carlsbad, NM, May 6 through 10, 2013: National Cave and Karst Research Institute, Carlsbad, NM, p. 151-159. http://scholarcommons.usf.edu/cgi/viewcontent.cgi?article=1123&context=sinkhole_2013

Johnson, K.S., Shoemaker, R.A., Charlton, J., and Parker, C., 2021, Evaporite karst in the Permian Rustler, Salado, and Castile Formations at Red Bluff Dam on the Pecos River, Loving and Reeves Counties, Texas, *in* Johnson, K.S., Land, L., and Decker, D.D., eds., Evaporite karst in the Greater Permian Evaporite Basin (GPEB) of Texas, New Mexico, Oklahoma, Kansas, and Colorado: Oklahoma Geological Survey, Circular 113.

Jordan, L., and Vosburg, D.L., 1963, Permian salt and associated evaporites in the Anadarko Basin of the western Oklahoma–Texas Panhandle region: Oklahoma Geological Survey, Bulletin 102, 76 p. http://ogs.ou.edu/docs/bulletins/B102.pdf

Kelley, V.C., 1971, Geology of the Pecos country, southeastern New Mexico: New Mexico Bureau of Mines and Mineral Resources, Memoir 24, 78 p. https://geoinfo.nmt.edu/publications/monographs/memoirs/downloads/24/Memoir-24.pdf

Kelner, G.M., Gauvey, K, and Sumrall, J.B., 2021, A karst feature predictability model within Barber County, Kansas, *in* Johnson, K.S., Land, L., and Decker, D.D., eds., Evaporite karst in the Greater Permian Evaporite Basin (GPEB) of Texas, New Mexico, Oklahoma, Kansas, and Colorado: Oklahoma Geological Survey, Circular 113.

Kim, J-W., and Lu, Z., 2018, Association between localized geohazards in west Texas and human activities, recognized by Sentinel-1A/B satellite radar imagery: Scientific Reports 8, 4727. https://doi.org/10.1038/s41598-018-23143-6

Kim, J-W., and Lu, Z., 2021, Sinkholes in Wink, Texas, observed by satellite radar imagery, *in* Johnson, K.S., Land, L., and Decker, D.D., eds., Evaporite karst in the Greater Permian Evaporite Basin (GPEB) of Texas, New Mexico, Oklahoma, Kansas, and Colorado: Oklahoma Geological Survey, Circular 113.

Kim, J-W., Lu, Z., and Kaufmann, J., 2019, Evolution of sinkholes over Wink, Texas, observed by high-resolution optical and SAR imagery: Remote Sensing of Environment, No. 222, p. 119-132. https://www.smu.edu/-/media/Site/Dedman/Academics/Departments/EarthSciences/PDF/Lu/176_Kim_TSX_Sinkhole_Wink_RSE_2019.pdf?la=en

Kirkland, D.W., and Evans, R., 1980, Origin of castiles on Gypsum Plain of Texas and New Mexico, *in* Dickerson, P.W., and Hoffer, J.M., eds., Trans-Pecos region, southeastern New Mexico and west Texas: New Mexico Geological Society, 31st Field Conference, p. 173-178. https://nmgs.nmt.edu/publications/guidebooks/downloads/31/31_p0173_p0178.pdf

Kulstad, R.O., Fairchild, P., and McGregor, D., 1956, Gypsum in Kansas: Kansas Geological Survey, Bulletin 113, 110 p. http://www.kgs.ku.edu/Publications/Bulletins/133/index.html

Lambert, S.J., 1983, Dissolution of evaporites in and around the Delaware Basin, southeastern New Mexico: Sandia National Labs, Albuquerque, New Mexico, SAND86–0461, 96 p. https://www.wipp.energy.gov/library/CRA/2009_CRA/references/Others/Lambert_1983_Dissolution_of_Evaporites_in_Delaware_Basin_SAND82_0461.pdf

Land, L., 2003, Evaporite karst and regional groundwater circulation in the lower Pecos River Valley of southeastern New Mexico, *in* Johnson, K.S., and Neal, J.T., eds., Evaporite karst and engineering/environmental problems in the United States: Oklahoma Geological Survey, Circular 109, p. 227-232. http://ogs.ou.edu/docs/circulars/C109.pdf

Land, L., 2013, Evaporite karst in the Permian Basin region of west Texas and southeastern New Mexico: the human impact, *in* Land, L., Doctor, D.H., and Stephenson, J.B., eds., Sinkholes and the engineering and environmental impacts of karst–Proceedings of the thirteenth multidisciplinary conference, Carlsbad, NM, May 6 through 10, 2013: National Cave and Karst Research Institute, Carlsbad, NM, p. 113-121. http://scholarcommons.usf.edu/cgi/viewcontent.cgi?article=1119&context=sinkhole_2013

Land, L, 2021, Evaporite karst as a transportation and infrastructure geohazard in the lower Pecos Region, southeastern New Mexico and west Texas, *in* Johnson, K.S., Land, L., and Decker, D.D., eds., Evaporite karst in the Greater Permian Evaporite Basin (GPEB) of Texas, New Mexico, Oklahoma, Kansas, and Colorado: Oklahoma Geological Survey, Circular 113.

Land, L., and Aster, R., 2009, Seismic recordings of an anthropogenic sinkhole collapse, *in* Proceedings of the Symposium on the Application of Geophysics to Engineering and Environmental Problems: Environmental and Engineering Geophysical Society, 2009 Annual Meeting, Fort Worth, Texas, p. 511-519. http://www.nckri.org/research/applied_science/Sinkhole_Collapse.pdf

Land, L., Cikoski, C.K., and Veni, G., 2018a, Sinkholes as transportation and infrastructure geohazards in mixed evaporite-siliciclastic bedrock, southeastern New Mexico, *in* Sasowsky, I.D., Byle, M.J., Land, L., eds., Proceedings of the Fifteenth Multidisciplinary Conference on Sinkholes and the Engineering and Environmental Impact of Karst, Shepherdstown, WV. National Cave and Karst Research Institute Symposium 7. Carlsbad (NM): National Cave and Karst Research Institute. p. 367-377.

Land, L., Cikoski, C., McCraw, D., and Veni, G., 2018b, Karst geohazards and geophysical surveys: US 285, Eddy County, New Mexico: National Cave and Karst Research Institute, Report of Investigations 7, 89 p. http://www.nckri.org/about_nckri/investigations/NCKRI_RI-7%20screen%20quality.pdf

Land, L., and Veni, G., 2012, Electrical resistivity surveys of anthropogenic karst phenomena, southeastern New Mexico: New Mexico Geology, Vol. 34, No. 4, p. 117-125. https://geoinfo.nmt.edu/publications/periodicals/nmg/34/n4/nmg_v34_n4_p117.pdf

Lefond, S.J., 1969, Handbook of world salt resources: Plenum Press, New York, 384 p.

Maley, V.L., and Huffington, R.M., 1953, Cenozoic fill and evaporite solution in the Delaware Basin, Texas and New Mexico: Geological Society of America, Bulletin, Vol. 64, p. 539-546.

Marsden, R.W, and Lucas, J.R., 1973, Specialized underground extraction systems, *in* Cummins, A.B., and Given, I.A., eds., SME mining engineering handbook: Society of Mining Engineers of American Institute of Mining, Metallurgical, and Petroleum Engineers, Vol. 2, sec. 21, p. 1-118.

Martinez, J.D., Johnson, K.S., and Neal, J.T., 1998, Sinkholes in evaporite rocks: American Scientist, Vol. 86, No. 1 (January–February), p. 38-51. https://www.researchgate.net/publication/250968543

McGregor, D.R., Pendery, E.C., and McGregor, D.L., 1963, Solution caves in gypsum, north central Texas: Journal of Geology, Vol. 71, p. 108-115.

McLemore, V.T., 1999, Bottomless Lakes: New Mexico Geology, Vol. 21, No. 2, p. 51-55. https://geoinfo.nmt

.edu/publications/periodicals/nmg/21/n2/nmg_v21_n2_p51.pdf

Merriam, D.F., and Mann, C.J., 1957, Sinkholes and related geologic features in Kansas: Kansas Academy of Science, Transactions, Vol. 60, No. 3, p. 207-243. https://digital.lib.usf.edu/SFS0054165/00001

Myers, A.J., Gibson, A.M., Glass, B.P., and Patrick, C.R., 1969, Guide to Alabaster Cavern and Woodward County, Oklahoma: Oklahoma Geological Survey, Guidebook 15, 38 p. http://ogs.ou.edu/docs/guidebooks/GB15.pdf

New Mexico Oil Conservation Division, no date, General correspondence, Brine Well Work Group. http://ocdimage.emnrd.state.nm.us/Imaging/FileStore/santafeadmin/ao/73512/pcjc0906359521_1_ao.pdf

Osborn, N.I., and Eckenstein, E., 1997, Blaine gypsum groundwater recharge demonstration project data report: Oklahoma Water Resources Board, Technical Report 97–4, 308 p. https://www.owrb.ok.gov/studies/reports/reports_pdf/tr97_4_blaine_gypsum.pdf

Paine, J.G., Buckley, S., Collins, E.W., Wilson, C.R., and Kress, W., 2009, Assessing sinkhole potential at Wink and Daisetta, Texas, using gravimetry and radar interferometry in Proceedings, 22nd Symposium on the Application of Geophysics to Engineering and Environmental Problems, Fort Worth, Texas, March 29–April 2, p. 480–488. https://pdfs.semanticscholar.org/e0bd/01cdae36f445dc27f4e4e95e6cf6ac6e9ac1.pdf?_ga=2.11563440.58905847.1566680052-1121615753.1564344073

Paine, J.G., Costard, L., Andrews, J., Averett, A., Saylam, K., and Hupp, J., 2021, Determining annual to decadal subsidence areas and rates using airborne Lidar, GPS surveys, and topographic maps at the Wink Sinkholes, west Texas, *in* Johnson, K.S., Land, L., and Decker, D.D., eds., Evaporite karst in the Greater Permian Evaporite Basin (GPEB) of Texas, New Mexico, Oklahoma, Kansas, and Colorado: Oklahoma Geological Survey, Circular 113.

Powers, D.W., and Holt, R.M., 2021, Evaporite dissolution and the Waste Isolation Pilot Plant (WIPP) in the northern Delaware Basin, southeastern New Mexico, *in* Johnson, K.S., Land, L., and Decker, D.D., eds., Evaporite karst in the Greater Permian Evaporite Basin (GPEB) of Texas, New Mexico, Oklahoma, Kansas, and Colorado: Oklahoma Geological Survey, Circular 113.

Payton, C.C., 1992, Geotechnical investigation and foundation design for the reconstruction of Quail Creek Dike, *in* Harty, K.M., ed., Engineering and environmental geology of southwestern Utah: Utah Geological Association, Publication 21, p. 39-51.

Payton, C.C., and Hansen, M.N., 2003, Gypsum karst in southwestern Utah: failure and reconstruction of Quail Creek Dike, *in* Johnson, K.S., and Neal, J.T., eds., Evaporite karst and engineering/environmental problems in the United States: Oklahoma Geological Survey, Circular 109, p. 293-303. http://ogs.ou.edu/docs/circulars/C109.pdf

Pierce, W.G., and Rich, E.I., 1962, Summary of rock salt deposits in the United States as possible storage sites for radioactive waste materials: U.S. Geological Survey, Bulletin 1148, 91 p., 6 plates. https://pubs.er.usgs.gov/publication/b1148

Powers, D.W., 2003, Jal sinkhole in southeastern New Mexico: evaporite dissolution, drill holes, and the potential for sinkhole development, *in* Johnson, K.S., and Neal, J.T., eds., Evaporite karst and engineering/environmental problems in the United States: Oklahoma Geological Survey, Circular 109, p. 219-226. http://ogs.ou.edu/docs/circulars/C109.pdf

Powers, D.W., and Holt, R. M., 2000, The salt that wasn't there: mudflat facies equivalents to halite of the Permian Rustler Formation, southeastern New Mexico: Journal Sedimentary Research, Vol. 70, No. 1, p. 29-36. https://www.researchgate.net/publication/240778734

Presley, M.W., 1981, Middle and Upper Permian salt-bearing strata of the Texas Panhandle: lithologic and facies cross sections: The University of Texas at Austin, Bureau of Economic Geology, Cross Sections CS0003, 10 p. 7 cross sections.

Preston, D.A., 1980a, Bursting natural-gas bubble, Woods County, Oklahoma: Oklahoma Geology Notes, Vol. 40, No. 1, p. 1-2. http://ogs.ou.edu/docs/geologynotes/GN-V40N1.pdf

Preston, D.A., 1980b, Gas eruptions taper off: Geotimes, Vol. 25, No. 10, p. 18-20.

Quinlan, J.F., Smith, R.A., Johnson, K.S., 1987, Gypsum karst and salt karst of the United States of America, in Atti symposio internationale sul carsismo nelle evaporiti (Proceedings, international symposium on karst in evaporites), Palermo, Italy, October 27–30, 1985: Le Grotte d'Italia, Series 4, Vol. 13, p. 73-92.

Rahn, P.H., and Davis, A.D., 1996, Gypsum foundation problems in the Black Hills area, South Dakota: Environmental and Engineering Geoscience, Vol. II, No. 2, p. 213-223.

Rawling, and McCraw, 2010, Geologic map of the Bottomless Lakes quadrangle, Chaves County, New Mexico: New Mexico Bureau of Mines and Mineral Resources, Open-file Geologic Map 126, scale 1:24,000. https://geoinfo.nmt.edu/publications/maps/geologic/ofgm/downloads/126/BottomlessLakes_v2p-00.pdf

Reddell, J.R., and Russell, W.H., 1963, The caves of northwest Texas: Texas Speleological Survey, Vol. 1, No. 8, 56 p. https://www.texasspeleologicalsurvey.org/PDF/TSS_Volume1/TSS%201(8)%20compressed.pdf

Runkle, D.L., Bergman, D.L., and Fabian, R.S., 1997, Hydrologic data for the Blaine aquifer and associated units in southwestern Oklahoma and northwestern Texas: U.S. Geological Survey, Open-File Report 97–50, 213 p. https://pubs.usgs.gov/of/1997/0050/report.pdf

Sares, S.W., Wells, S.G., 1987, Geomorphic and hydrogeologic development of the Gypsum Plain karst, Delaware Basin, New Mexico, in Powers, D.W., and James, W.C., eds., Geology of the western Delaware Basin, West Texas and Southeastern New Mexico: El Paso Geological Society, Guidebook 18, p. 98-117.

Shi, Y., Tang, Y., Lu, Z., Kim, J-W., and Peng, J., 2019, Subsidence of sinkholes in Wink, Texas, from 2007 to 2011 detected by time-series InSAR analysis: Geomatics, Natural Hazards and Risk, Vol. 10, No. 1, p.1125-1138. https://www.researchgate.net/publication/331174035

Smith, G.I., Jones, C.L., Cubertson, W.C, Ericksen, G.E., and Dyni, J.R., 1973, Evaporites and brines, *in* Brobst, D.A., and Pratt, W.D., eds., United States mineral resources: U.S. Geological Survey, Professional Paper 820, p. 197-216. https://pubs.usgs.gov/pp/0820/report.pdf

Stafford, K.W., 2013, Evaporite karst and hydrogeology of the Castile Formation: Culberson County, Texas, and Eddy County, New Mexico, *in* Land, L., Doctor, D.H., and Stephenson, J.B., eds., Sinkholes and the engineering and environmental impacts of karst–Proceedings of the thirteenth multidisciplinary conference, Carlsbad, NM, May 6 through 10, 2013: National Cave and Karst Research Institute, Carlsbad, NM, p. 123-131. https://pdfs.semanticscholar.org/fa26/e653bc2c3ae95007f83dde9a1d4eab38211d.pdf

Stafford, K.W., and Nance, R., 2009, The Gypsum Plain of southeastern New Mexico and far west Texas: *in* Palmer, A., and Palmer, M., eds., Caves and karst of the USA: Huntsville, Alabama, National Speleological Society, p. 267-272.

Stafford, K.W., and Nance, R.G., 2018, Evaporite karst of west Texas: Delaware Basin, *in* Stafford, K.W., and Veni, G., eds., Hypogene karst of Texas: Texas Speleological Survey, Monograph 3, p. 36-50. https://www.texasspeleologicalsurvey.org/PDF/Hypogene_Karst_of_Texas.pdf

Stafford, K.W., Nance, R., Rosales-Lagarde, L., and Boston, P.J., 2008a, Epigene and hypogene gypsum karst manifestations of the Castile Formation: Eddy County, New Mexico and Culberson County, Texas: International Journal of Speleology, Vol. 37, No. 2, p. 83-98. https://www.researchgate.net/publication/26500041

Stafford, K.W., Rosales-Lagarde, L., and Boston, P.J., 2008b, Castile evaporite karst potential map of the Gypsum Plain, Eddy County, New Mexico and Culberson County, Texas: A GIS methodological comparison: Journal of Cave and Karst Studies, Vol. 70, No. 1, p. 35-46. https://scholarworks.sfasu.edu/cgi/viewcontent.cgi?article=1013&context=geology

Stafford, K.W., Brown, W.A., Ehrhart, J.T., Majzoub, A.F., and Woodard, J.D., 2017, Evaporite karst geohazards in the Delaware Basin, Texas: review of traditional karst studies coupled with geophysical and remote sensing characterization: International Journal of Speleology, Vol. 46, No. 2, p. 169-180. https://doi.org/10.5038/1827-806X.46.2.2089

Steele C.E., and Barclay, J.E., 1965, Ground-water resources of Harmon County and adjacent parts of Greer and Jackson Counties, Oklahoma: Oklahoma Water Resources Board, Bulletin 29, 96 p.

Suneson, N.H., 2012, Custer County oysters: Oklahoma City Geological Society, Shale Shaker, Vol. 62, No. 6, p. 422-429. http://www.ogs.ou.edu/pdf/ShaleShakerOYSTERS2012.pdf

Trentham, R.C., and Henderson, M.A., 2021, Assessing collapse risk in evaporite sinkhole-prone areas using commonly available oil field data in the area of the Wink Sinks, Winkler County, Texas, *in* Johnson, K.S., Land, L., and Decker, D.D., eds., Evaporite karst in the Greater Permian Evaporite Basin (GPEB) of Texas, New Mexico, Oklahoma, Kansas, and Colorado: Oklahoma Geological Survey, Circular 113.

Vanderwater, B., 1980, Re-entry slated in suspect well: The Daily Oklahoman [newspaper], August 27, p. 23.

Walters, R.F., 1978, Land subsidence in central Kansas related to salt dissolution: Kansas Geological Survey, Bulletin 214, 82 p. http://www.kgs.ku.edu/Publications/Bulletins/214/index.html

Walters, R.F., 1991, Gorham oil field, Russell County, Kansas: Kansas Geological Survey Bulletin 228, 111 p. http://www.kgs.ku.edu/Publications/Bulletins/228/Bull228.pdf

Ward, P.E., 1961, Geology and ground-water features of salt springs, seeps, and plains in the Arkansas and Red River basins of western Oklahoma and adjacent parts of Kansas and Texas: U.S. Geological Survey, Open-File Report 63–132, 94 p. https://pubs.er.usgs.gov/publication/ofr63132

Watney, W.L., and Paul, S.E., 1980, Maps and cross sections of the Lower Permian Hutchinson Salt Member

in Kansas: Kansas Geological Survey, Open-File Report 80–7, 11 p., 9 maps, 3 cross sections.

Watney, W.L., Berg, J.A., and Paul, S.E., 1988, Origin and distribution of the Hutchinson Salt Member (lower Leonardian) in Kansas, *in* Morgan, W.A., and Babcock, J.A., eds, Permian rocks of the Mid-Continent: Society of Economic Paleontologists and Mineralogists, Midcontinent Section, Special Publication 1, p. 113-135.

Watney, W.L., Nissen, S.E., Bhattacharya, S., and Young, D., 2003, Evaluation of the role of evaporite karst in the Hutchinson, Kansas, gas explosions, January 17 and 18, 2001, *in* Johnson, K.S., and Neal, J.T., eds., Evaporite karst and engineering/environmental problems in the United States: Oklahoma Geological Survey, Circular 109, p. 119-147. http://ogs.ou.edu/docs/circulars/C109.pdf

Weber, R.H., and Kottlowski, F.E., 1959, Gypsum resources of New Mexico: New Mexico Bureau of Mines and Mineral Resources, Bulletin 68, 68 p. https://geoinfo.nmt.edu/publications/monographs/bulletins/68/

Withington, C.F., 1962, Gypsum and anhydrite in the United States, exclusive of Alaska and Hawaii: U.S. Geological Survey, Mineral Investigations Resource Map MR–33.

Withington, C.F., and Jaster, M.C., 1960, Selected annotated bibliography of gypsum and anhydrite in the United States and Puerto Rico: U.S. Geological Survey, Bulletin 1105, 126 p. https://pubs.usgs.gov/bul/1105/report.pdf

Young, J., and Beard, J., 1993, Caves in Kansas: Kansas Geological Survey, Educational Series 9, 48 p.

Evaporite Karst in the Greater Permian Evaporite Basin of Texas, New Mexico, Oklahoma, Kansas, and Colorado as Delineated by USGS Karst Mapping

David J. Weary and Daniel H. Doctor
Florence Bascom Geoscience Center, U.S. Geological Survey, Reston, Virginia

ABSTRACT.—The Greater Permian Evaporite Basin (GPEB) (Johnson, 2021) is a composite of the Anadarko, Dalhart, Delaware, Denver, Estancia, Las Vegas, Midland, Palo Duro, Raton, Salina, Tatum, Tucumcari, and Val Verde sedimentary basins and the Hugoton Embayment; it underlies an area of about 278,000 mi^2 (720,000 km^2) in Texas, New Mexico, Oklahoma, Kansas, and Colorado.

Evaporite-rich formations within the basin typically occur at depths of 30 to 1300 ft (10 to 400 m). This area is important for the exploration and development of energy and other natural resources. Knowledge of the extent of both surface and subsurface evaporite rocks is critical to mitigating collapse hazards for many human activities including siting of hydrocarbon exploration and distribution equipment, the location of wind turbine tower sites, pipelines, and transportation corridors. Evaporite mineral-bearing rocks with potential for karst development in the Permian Basin include the Blaine, Briggs, Castile, Gatuna, Malone, Quartermaster, Rustler, Salado, and San Angelo Formations, the Dewey Lake Redbeds, and the Clear Fork and Whitehorse Groups in Texas; the Castile, Grayburg, Queen, Salado, Seven Rivers, Yates, Tansill, and Yeso Formations, and the Artesia, Chinle, and San Rafael Groups in New Mexico; the Blaine, Cloud Chief, Marlow, and Rush Springs Formations, Dog Creek and Flowerpot Shales, and the El Reno and Whitehorse Groups in Oklahoma; the Lykins, Morrison, and Ralston Creek Formations in Colorado; and the Big Basin Formation, and Nippewalla and Sumner Groups in Kansas.

The U.S. Geological Survey (USGS) produced a report and digital database on the nationwide extent of rocks at the earth's surface with the potential for the development of karst features as USGS Open-File Report 2014-1156 (Weary and Doctor, 2014). The delineation of rock units with potential evaporites is based on analysis and compilation of State geologic map data at various resolutions. The database contains information on lithostratigraphic unit names, gross lithology, age, wet versus dry climate setting, and ecoregions. This report also includes a rough delineation of areas potentially underlain by evaporite rocks and the main evaporite basins.

INTRODUCTION

The Greater Permian Evaporite Basin (GPEB) comprises one of the largest volumes of evaporite rocks in the contiguous United States (Figure 1). The basin, a composite of the Anadarko, Dalhart, Delaware, Denver, Estancia, Las Vegas, Midland, Palo Duro, Raton, Salina, Tatum, Tucumcari, and Val Verde sedimentary basins and the Hugoton Embayment underlies an area of about 278,000 mi^2 (721,000 km^2) in Texas, New Mexico, Oklahoma, Kansas, and Colorado (Figure 2). Evaporite-rich formations within the basin typically occur at depths of 30 to 1300 ft (10 to 400 m) and crop out locally, in up-dip basin margin areas.

Karst features in the GPEB, both at the surface and in the subsurface, affect human activities including housing development, transportation and energy transmission corridors, pipelines, energy resource extraction, and mineral commodity mining (Figure 3).

This region is one of the most productive in the United States for both hydrocarbon extraction and wind energy generation. Widespread subsurface drainage of meteoric

Weary, D. J.; and Doctor, D. H., 2021, Evaporite Karst in the Greater Permian Evaporite Basin of Texas, New Mexico, Oklahoma, Kansas, and Colorado as Delineated by USGS Karst Mapping, *in* Johnson, K. S.; Land, Lewis; and Decker, D. D. (eds.), Evaporite Karst in the Greater Permian Evaporite Basin (GPEB) of Texas, New Mexico, Oklahoma, Kansas, and Colorado: Oklahoma Geological Survey, Circular 113, p. 39-49.

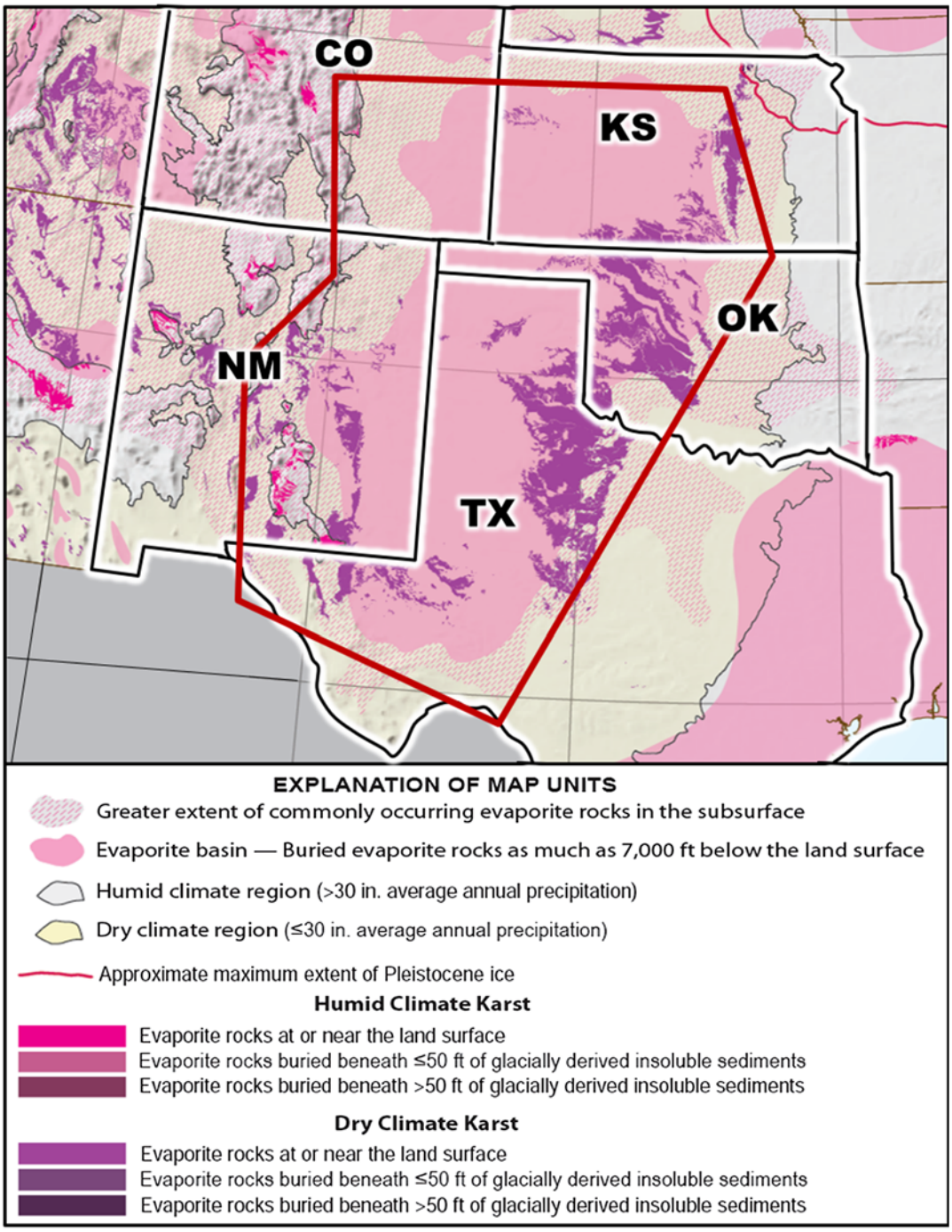

Figure 1. Map showing areas underlain by evaporite rocks at various depths up to 7000 ft below the land surface (Weary and Doctor, 2014). Red-outlined polygon delineates the approximate outline of the Greater Permian Evaporite Basin used for this report.

water in karst systems exacerbates a general lack of surface water availability in this relatively arid region.

The U.S. Geological Survey (USGS) karst report, maps, and database (Weary and Doctor, 2014) include documentation of evaporite-rich stratigraphic units at or near the earth's surface. Most of the spatial data compiled for that project originated as lithologic map units on geologic maps produced by State geological surveys. Versions of the original source maps are available for purchase or download from the respective State geological surveys. Much of the digital map data were compiled from a series of integrated geologic map databases for the United States produced by the USGS Mineral Resources Program (see http://mrdata.usgs.gov/geology/state/, accessed December 12, 2019). The state compilations used in Weary and Doctor (2014) were

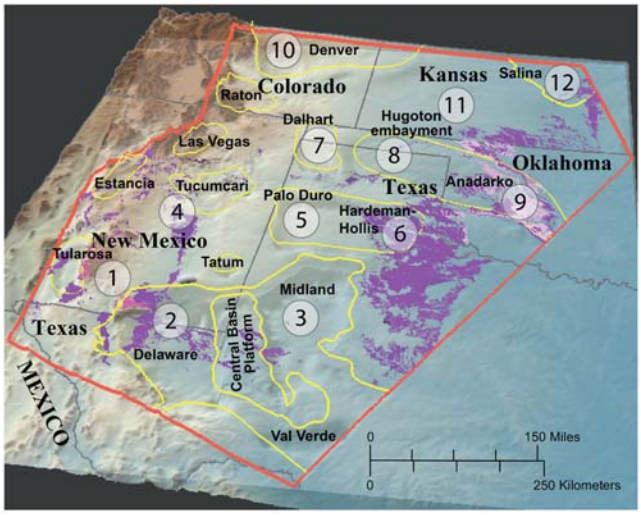

Figure 2. Map showing areas underlain by evaporite rocks (magenta, pink, and purple colors) at or near the land surface (Weary and Doctor, 2014), and the major constituent basins in the Greater Permian Evaporite Basin (GPEB). Red-outlined polygon delineates the arbitrary boundary of the GPEB for this report. Exaggerated surface topography (blueish and brown tones) is generated from the USGS National Elevation Dataset (NED). Exaggerated subsurface basin topography (gray-shaded depressions) generated from unpublished estimates is compiled from multiple publicly available sources.



Figure 3. Early stages of remediation of collapse into the Hutchinson Salt Member of the Wellington Formation, near Hutchinson, Kansas. The Wellington Formation occurs only in the subsurface in the Greater Permian Evaporite Basin, and is not represented among the map units in Weary and Doctor (2014). This collapse affected major railroad and highway corridors. 2005 photograph (D. Weary, USGS).

data from the 2013 Mineral Resources Program publication and have since been revised and superseded (Horton and others, 2017).

POTENTIALLY KARSTIC EVAPORITE-BEARING LITHOSTRATIGRAPHIC UNITS OF THE GREATER PERMIAN EVAPORITE BASIN

In the classification of potentially karstic rocks defined by Weary and Doctor (2014), lithostratigraphic map units were designated as either carbonate or evaporite-bearing based on their component lithologies as described in the various State geologic map compilations (U.S. Geological Survey, 2013). Because some of these units contain both carbonate and evaporite rocks, some units that contain significant amounts of evaporite rocks were included in the carbonate classification. These units are noted in the discussion to follow. Many of the map units in either the evaporite or carbonate groups are comprised of mixed lithologies and significant portions of them may be clastic, non-karstic rocks.

As a result of varying degrees of solutional porosity within units of mixed lithologies, our designation of evaporite-bearing karstic units may differ slightly from those of other workers in the GPEB region; for example, see the paper by Johnson (2021).

The Southern Part of the Greater Permian Evaporite Basin

Lithostratigraphic units bearing evaporite rocks with the potential for the development of karst features in the southern part of the GPEB (Figure 2) range in age from Pennsylvanian to Holocene (Table 1). Most of these units are Permian in age; however, there are some younger evaporite-bearing deposits including the Upper Jurassic Malone Formation and Pleistocene to Holocene alkali flats, bolson, and caliche deposits.

In southeastern New Mexico (Figure 2, areas 1 and 2; Table 1), map units classified as chiefly carbonates rather than evaporites (Weary and Doctor, 2014) include the Pennsylvanian Panther Seep Formation; the Permian Rustler, and San Andres Formations, undivided; the San Andres Limestone and Glorieta Sandstone, undivided; and the Yeso Formation, Glorieta Sandstone, and San Andres Limestone, undivided. The Panther Seep Formation is described in the New Mexico State geologic map compilation as fine-grained mixed clastic, limestone, and evaporite. The Rustler Formation and the San Andres Formation are both described as carbonate, fine-grained mixed clastic, and evaporite. The Yeso Formation is described as sandstone, carbonate, fine-grained mixed clastic, and evaporite.

Northeastern New Mexico and the Palo Duro and Hardeman–Hollis Basins

In northeastern New Mexico and the Palo Duro and Hardeman–Hollis Basins in northern Texas and Oklahoma (Figure 2, areas 4–6), map units containing evaporite rocks range in age from Permian to Triassic

TABLE 1.—Lithostratigraphic map units bearing evaporite rocks in southeastern New Mexico and the Delaware and Midland Basins of New Mexico and west Texas (Figure 2, areas 1–3). The Unit-Link item in these tables ties each map unit to the State geological map compilation (U.S. Geological Survey, 2013) and the karst report of Weary and Doctor (2014).

Southeastern New Mexico (1), Delaware Basin (2), Midland Basin (3)							
	Unit Name	**State**	**Unit-Link**	**Age**	**Lith1**	**Lith2**	**Lith3**
Evaporites	Alkali flat deposits	Texas	TXQaf;0	Holocene	Playa	Evaporite	Clay or mud; sand; dolostone (dolomite)
	Artesia Group	New Mexico	NMPat;0	Permian	Fine-grained mixed clastic	Dolostone (dolomite)	Evaporite
	Blaine Formation	Texas	TXPb;0	Permian	Mudstone	Evaporite	Dolostone (dolomite); sandstone
	bolson deposits	Texas	TXQb;0	Pleistocene and Holocene	Clay or mud	Silt	Sand; evaporite
	Briggs Formation	Texas	TXPbg;0	Permian	Evaporite	Dolostone (dolomite)	N/A
	caliche deposits	Texas	TXQc;0	Pleistocene and Holocene	Evaporite	N/A	N/A
	Castile Formation	New Mexico	NMPc;0	Permian	Evaporite	Limestone	N/A
	Chinle Group	New Mexico	NMTRc;0	Triassic	Medium-grained mixed clastic	Fine-grained mixed clastic	Limestone; chert; evaporite
	Clear Fork Group	Texas	TXPcf;0	Permian	Mudstone	Sandstone	Dolostone (dolomite); siltstone; evaporite
	Dewey Lake Redbeds	Texas	TXPd;0	Permian	Fine-grained mixed clastic	Evaporite	N/A
	Gatuna Formation	Texas	TXQg;0	Middle (?) Pleistocene	Sand	Conglomerate	Evaporite; limestone; siltstone; shale
	Grayburg and Queen Formations, undivided	New Mexico	NMPgq;0	Permian	Carbonate	Sandstone	Evaporite; shale; bentonite; mudstone

(continued on next page)

TABLE 1.—Lithostratigraphic map units bearing evaporite rocks in southeastern New Mexico and the Delaware and Midland Basins of New Mexico and west Texas (Figure 2, areas 1–3). The Unit-Link item in these tables ties each map unit to the State geological map compilation (U.S. Geological Survey, 2013) and the karst report of Weary and Doctor (2014) (continued)

	gypsiferous eolian deposits	New Mexico	NMQeg;0	Quaternary	Eolian	Evaporite	N/A
	gypsite deposits	Texas	TXQgy;0	Pleistocene and Holocene	Evaporite	N/A	N/A
	gypsum of Rustler, Salado, and Castile Formations, undivided	Texas	TXPrc;0	Permian;	Evaporite	N/A	N/A
	Malone Formation	Texas	TXJm;0	Late Jurassic	Limestone	Shale	Siltstone; evaporite; sandstone; conglomerate
	Permian rocks, undivided	Texas	TXP;0	Permian	Shale	Sandstone	Evaporite; dolostone (dolomite); siltstone
	Quartermaster Formation	Texas	TXPq;0	Permian	Shale	Sandstone	Evaporite; dolostone (dolomite)
	Salado and Castile Formations, undivided	Texas	TXPsc;0	Permian	Evaporite	Evaporite	Limestone
	Salado Formation	New Mexico	NMPsl;0	Permian	Evaporite	Sandstone	N/A
	San Angelo Formation	Texas	TXPsa;0	Permian	Mudstone	Siltstone	Evaporite
	Seven Rivers Formation	New Mexico	NMPsr;0	Permian	Evaporite	Fine-grained mixed clastic	Dolostone (dolomite)
	Whitehorse Group and Blaine Formation, undivided	Texas	TXPwb;0	Permian	Sandstone	Shale	Evaporite; conglomerate
	Whitehorse Group	Texas	TXPwh;0	Permian	Sandstone	Shale	Evaporite
	Yates and Tansill Formations, undivided	New Mexico	NMPty;0	Permian	Fine-grained mixed clastic	Carbonate	Evaporite
	Yesa Formation	New Mexico	NMPy;0	Permian	Sandstone	Limestone	Mudstone; evaporite
Carbonates	Panther Seep Formation	New Mexico	NMPAps;0	Pennsylvanian	Fine-grained	Limestone	Evaporite

(continued on next page)

TABLE 1.—Lithostratigraphic map units bearing evaporite rocks in southeastern New Mexico and the Delaware and Midland Basins of New Mexico and west Texas (Figure 2, areas 1–3). The Unit-Link item in these tables ties each map unit to the State geological map compilation (U.S. Geological Survey, 2013) and the karst report of Weary and Doctor (2014) (continued)

					mixed clastic		
	Rustler Formation	New Mexico	NMPr;0	Permian	Carbonate	Fine-grained mixed clastic	Evaporite
	San Andres Formation	New Mexico	NMPsa;0	Permian	Carbonate	Fine-grained mixed clastic	Evaporite
	San Andres Limestone and Glorieta Sandstone, undivided	New Mexico	NMPsg;0	Permian	Fine-grained mixed clastic	Carbonate	Evaporite
	Yeso, Glorieta, and San Andres Formations, undivided	New Mexico	NMPys;0	Permian	Sandstone	Carbonate	Fine-grained mixed clastic; evaporite

(Table 2). The Triassic Chinle Group and the Jurassic San Rafael Group in New Mexico are chiefly clastic rocks, but also contain minor amounts of evaporites and may be locally, marginally karstic.

All karst map units in this region (Figure 2, areas 4–6), except for the San Andres Formation and the San Andres Formation and Glorieta Sandstone, undivided, in New Mexico were classified as evaporite karst (Weary and Doctor, 2014). These two map units were classified as a chiefly carbonate based on their lithologic description in the State geologic map compilation (U.S. Geological Survey, 2013) listing carbonate constituent in predominance before evaporite.

Dalhart and Anadarko Basins

In the Dalhart and Anadarko Basins in New Mexico, Texas, Oklahoma, and Kansas (Figure 2, areas 7–9), map units containing evaporite rocks range in age from Permian to Holocene (Table 3). Most of these units are Permian in age; however, there are some younger evaporite-bearing deposits including the Triassic Chinle Group in New Mexico, and Pleistocene to Holocene caliche deposits in Texas. The potentially karstic units in this region were classified as evaporite-bearing rather than carbonate by Weary and Doctor (2014).

South Denver Basin, Hugoton Embayment, and the Salina Basin

In the Denver Basin, Hugoton Embayment, and Salina Basin of New Mexico, Colorado, Oklahoma, and Kansas (Figure 2, areas 10–12), map units containing evaporite rocks range in age from possibly Pennsylvanian to Jurassic (Table 4). Most of these units are Permian in age; however, there are some younger evaporite-bearing deposits including the Triassic Chinle Group in New Mexico; Mesozoic and Paleozoic rocks, undifferentiated, the Permian–Triassic Lykins Formation, and the Jurassic Morrison and Ralston Creek Formations, undivided in Colorado. The potentially karstic units in this region were classified as evaporite-bearing rather than carbonate by Weary and Doctor (2014).

U.S. GEOLOGICAL SURVEY KARST MAP UPDATES

Future update and revision of the open-file report on potentially karstic rocks in the United States (Weary and Doctor, 2014) is planned. It will include refinement in the classification of karst areas to reflect known occurrences of caves (e.g., Weary and Doctor, 2018) and the relative density of closed depressions at the land surface (Doctor and others, 2020, in press). Expansion of geographic

TABLE 2.—Lithostratigraphic map units bearing evaporite rocks in northeastern New Mexico, the Palo Duro and Hardeman–Hollis Basins in New Mexico, Texas, and Oklahoma (Figure 2, areas 4–6). The Unit-Link item in these tables ties each map unit to the State geological map compilation (U.S. Geological Survey, 2013) and the karst report of Weary and Doctor (2014).

Northeast New Mexico (4), Palo Duro Basin (5), Hardeman-Hollis Basin (6)							
	Unit Name	**State**	**Unit-Link**	**Age**	**Lith1**	**Lith2**	**Lith3**
Evaporites	Artesia Group	New Mexico	NMPat;0	Permian	Fine-grained mixed clastic	Dolostone (dolomite)	Evaporite
	Blaine Formation	Oklahoma	OKPb;0	Early Permian	Evaporite	Dolostone (dolomite)	Shale
	Blaine Formation	Texas	TXPb;0	Permian	Mudstone	Evaporite	Dolostone (dolomite); sandstone
	caliche deposits	Texas	TXQc;0	Pleistocene and Holocene	Evaporite	N/A	N/A
	Chinle Group	New Mexico	NMTRc;0	Triassic	Medium-grained mixed clastic	Fine-grained mixed clastic	Limestone; chert; evaporite
	Clear Fork Group	Texas	TXPcf;0	Permian	Mudstone	Sandstone	Dolostone (dolomite); siltstone; evaporite
	Dog Creek Shale	Oklahoma	OKPdc;0	Early Permian	Shale	Sandstone	Siltstone; dolostone (dolomite); evaporite
	Elm Fork Member of Blaine Formation	Oklahoma	OKPbe;0	Early Permian	Dolostone (dolomite)	Evaporite	N/A
	Flowerpot Shale	Oklahoma	OKPf;0	Early Permian	Shale	Siltstone	Dolostone (dolomite); evaporite; sandstone; conglomerate
	Grayburg and Queen Formations, undivided	New Mexico	NMPgq;0	Permian	Carbonate	Sandstone	Evaporite; shale; bentonite; mudstone
	Quartermaster Formation	Texas	TXPq;0	Permian	Shale	Sandstone	Evaporite; dolostone (dolomite)
	Quartermaster Formation and Whitehorse	Texas	TXPqw;0	Permian	Mixed clastic/carbonate	Evaporite	N/A

(continued on next page)

TABLE 2.—Lithostratigraphic map units bearing evaporite rocks in northeastern New Mexico, the Palo Duro and Hardeman–Hollis Basins in New Mexico, Texas, and Oklahoma (Figure 2, areas 4–6). The Unit-Link item in these tables ties each map unit to the State geological map compilation (U.S. Geological Survey, 2013) and the karst report of Weary and Doctor (2014) (continued)

	Group, undivided						
	San Angelo Formation	Texas	TXPsa;0	Permian	Mudstone	Siltstone	Evaporite
	San Rafael Group	New Mexico	NMJsr;0	Jurassic	Medium-grained mixed clastic	Fine-grained mixed clastic	Evaporite; limestone
	Seven Rivers Formation	New Mexico	NMPsr;0	Permian	Evaporite	Fine-grained mixed clastic	Dolostone (dolomite)
	Van Vacter Member of Blaine Formation	Oklahoma	OKPbv;0	Early Permian	Dolostone (dolomite)	Evaporite	Shale
	Whitehorse Group	Oklahoma	OKPwh;0	Early Permian	Sandstone	Siltstone	Dolostone (dolomite); evaporite; shale
	Whitehorse Group	Texas	TXPwh;0	Permian	Sandstone	Shale	Evaporite
	Yates and Tansill Formations, undivided	New Mexico	NMPty;0	Permian	Fine-grained mixed clastic	Carbonate	Evaporite
	Yeso Formation	New Mexico	NMPy;0	Permian	Sandstone	Limestone	Mudstone; evaporite
Carbonates	San Andres Formation	New Mexico	NMPsa;0	Permian	Carbonate	Fine-grained mixed clastic	Evaporite
	San Andres Limestone and Glorieta Sandstone, undivided	New Mexico	NMPsg;0	Permian	Fine-grained mixed clastic	Carbonate	Evaporite

coverage to include Guam and the islands of Rota and Saipan in the Commonwealth of Northern Mariana Islands is also planned.

Numerous comments and suggestions from representatives of State geological surveys and academic karst experts following the publication of the first report and database (Weary and Doctor, 2014) were addressed. For example, modifications to the coverage for Oklahoma and adjacent areas have been made based on dialogue with Kenneth Johnson (Oklahoma Geological Survey). Map unit polygons based on earlier State geologic map compilations (USGS, 2013) will be updated to comply with the revised 2017 data (Horton and others, 2017). We thank all of those who have provided their feedback and suggestions for the improvement of the database.

TABLE 3.—Lithostratigraphic map units bearing evaporite rocks in the Dalhart and Anadarko Basins in New Mexico, Texas, and Oklahoma (Figure 2, areas 7–9). The Unit-Link item in these tables ties each map unit to the State geological map compilation (U.S. Geological Survey, 2013) and the karst report of Weary and Doctor (2014).

Dalhart Basin (7), Anadarko Basin West (8), Anadarko Basin East (9)							
	Unit Name	**State**	**Unit-**	**Age**	**Lith1**	**Lith2**	**Lith3**
Evaporites	Big Basin Formation	Kansas	KSPbd;0	Permian	Sandstone	Shale	Siltstone; dolostone (dolomite)
	Blaine Formation	Oklahoma	OKPb;0	Early Permian	Evaporite	Dolostone (dolomite)	Shale
	Blaine Formation	Texas	TXPb;0	Permian	Mudstone	Evaporite	Dolostone (dolomite); sandstone
	caliche deposits	Texas	TXQc;0	Pleistocene and Holocene	Evaporite	N/A	N/A
	Chinle Group	New Mexico	NMTRc;0	Triassic	Medium-grained mixed clastic	Fine-grained mixed clastic	Limestone; chert; evaporite
	Cloud Chief Formation	Texas	TXPcl;0	Permian	Evaporite	Shale	Sandstone
	Cloud Chief Formation	Oklahoma	OKPcc;0	Late Permian	Shale	Siltstone	Sandstone; dolostone (dolomite); evaporite
	Dog Creek Shale	Oklahoma	OKPdc;0	Early Permian	Shale	Sandstone	Siltstone; dolostone (dolomite); evaporite
	El Reno Group	Oklahoma	OKPer;0	Early Permian	Shale	Evaporite	Dolostone (dolomite); sandstone; siltstone; conglomerate
	Flowerpot Shale	Oklahoma	OKPf;0	Early Permian	Sandstone	Siltstone	Shale; evaporite; dolostone (dolomite)
	Marlow Formation	Oklahoma	OKPm;0	Early Permian	Sandstone	Siltstone	Shale; evaporite; dolostone (dolomite)
	Nippewalla Group	Kansas	KSPwn;0	Late Permian	Siltstone	Sandstone	Shale; evaporite
	Permian rocks, undifferentiated	Oklahoma	OKPu;0	Late Permian to Early Permian	Shale	Sandstone	Siltstone; limestone; dolostone (dolomite); evaporite
	Quartermaster Formation and Whitehorse Group, undivided	Texas	TXPqw;0	Permian	Mixed clastic/carbonate	Evaporite	N/A

(continued on next page)

TABLE 3.—Lithostratigraphic map units bearing evaporite rocks in the Dalhart and Anadarko Basins in New Mexico, Texas, and Oklahoma (Figure 2, areas 7–9). The Unit-Link item in these tables ties each map unit to the State geological map compilation (U.S. Geological Survey, 2013) and the karst report of Weary and Doctor (2014) (continued)

	Rush Springs Formation	Oklahoma	OKPr;0	Early Permian	Sandstone	Evaporite	Dolostone (dolomite); shale
	Weatherford Gypsum Bed of Rush Springs Formation	Oklahoma	OKPrw;0	Early Permian	Evaporite	Dolostone (dolomite)	N/A
	Whitehorse Group	Oklahoma	OKPwh;0	Early Permian	Sandstone	Siltstone	Dolostone (dolomite); evaporite; shale
Carbonates	N/A						

TABLE 4.—Lithostratigraphic map units bearing evaporite rocks in the Denver Basin, Hugoton Embayment, and Salina Basin in New Mexico, Colorado, Oklahoma, and Kansas (Figure 2, areas 10–12). The Unit-Link item in these tables ties each map unit to the State geological map compilation (U.S. Geological Survey, 2013) and the karst report of Weary and Doctor (2014).

Denver Basin South (10), Hugoton Embayment (11), Salina Basin (12)							
	Unit Name	**State**	**Unit-Link**	**Age**	**Lith1**	**Lith2**	**Lith3**
Evaporites	Chinle Group	New Mexico	NMTRc;0	Triassic	Medium-grained mixed clastic	Fine-grained mixed clastic	Limestone; chert; evaporite
	Flowerpot Shale	Oklahoma	OKPf;0	Early Permian	Shale	Siltstone	Dolostone (dolomite); evaporite; sandstone; conglomerate
	Lykins Formation	Colorado	COTRPl;0	Triassic-Permian	Siltstone	Shale	Limestone
	Lykins Formation and Lyons Sandstone, undivided	Colorado	COTRPll;0	Triassic-Permian	Sandstone	Mudstone	Limestone
	Mesozoic and Paleozoic rocks, undifferentiated	Colorado	COMZPZ;0	Mesozoic-Pennsylvanian	Clastic	Evaporite	N/A
	Morrison and Ralston Creek Formations, undivided	Colorado	COJmr;0	Jurassic	Mudstone	Sandstone	Limestone; evaporite
	Nippewalla Group	Kansas	KSPwn;0	Late Permian	Shale; evaporite	Sandstone	Shale; evaporite
	Sumner Group	Kansas	KSPs;0	Late Permian	Shale	Limestone	Siltstone; dolostone (dolomite); evaporite
Carbonates	N/A						

REFERENCES

Doctor, D.H., Jones, J., Wood, N., Falgout, J., and Rapstine, N.I., 2020, Progress toward a preliminary karst depression density map for the conterminous United States, *in* Land. L., Byle, M., and Kromhout, C., eds., Proceedings of the 16th Multidisciplinary Conference on Sinkholes and the Engineering and Environmental Impacts of Karst, April 20-24, 2020, San Juan, Puerto Rico, National Cave and Karst Research Institute, in press.

Horton, J.D., San Juan, C.A., and Stoeser, D.B., 2017, The State Geologic Map Compilation (SGMC) geodatabase of the conterminous United States (ver. 1.1, August 2017): U.S. Geological Survey, Data Series 1052, 46 p. https://doi.org/10.3133/ds1052.

Johnson, K.S., 2021, Overview of evaporite karst in the Greater Permian Evaporite Basin (GPEB) of TX, NM, OK, KS, and CO, *in* Johnson, K.S., Land, L., and Decker, D.D., eds., Evaporite karst in the Greater Permian Evaporite Basin of Texas, New Mexico, Oklahoma, Kansas, and Colorado: Oklahoma Geological Survey, Circular 113.

U.S. Geological Survey, 2013, Geologic maps of U.S. States: U.S. Geological Survey, Mineral Resources Program, Mineral Resources Online Spatial Data, accessed August 8, 2013, at http://mrdata.usgs.gov/geology/state/.

Weary, D.J., and Doctor, D.H., 2014, Karst in the United States: A digital map compilation and database: U.S. Geological Survey, Open-File Report 2014–1156, 23 p. http://dx.doi.org/10.3133/ofr20141156

Weary, D.J. and Doctor, D.J., 2018, A Preliminary Map Showing the Distribution of Solution Caves in Carbonate and Evaporite-Bearing Geologic Units in The United States: Geological Society of America, Abstracts with Programs, Vol. 50, No. 6. http://dx.doi.org/10.1130/abs/2018AM-320651

Oklahoma Geological Survey Circular 113, 2021

Identification of Gypsum, Anhydrite, and Salt on Geophysical Logs in the Greater Permian Evaporite Basin

Kenneth S. Johnson
Retired Geologist, Oklahoma Geological Survey,
Norman, Oklahoma

ABSTRACT.—The Greater Permian Evaporite Basin contains several major evaporite units consisting of salt (halite), gypsum, and/or anhydrite. They are interbedded mainly with red-bed shales, siltstones, and sandstones, as well as dolomites and limestones. These rocks are readily identified in outcrops, but it can be a challenge to recognize some of them in boreholes, unless they have been cored. However, data about these evaporites can be gleaned from the many petroleum tests drilled in the region, providing geophysical logs have been run through the evaporite formations encountered in the wells. The current report describes common logs made in petroleum tests, and their usefulness in identifying evaporite beds in the subsurface, because identifying the evaporite beds in subsurface can be critical to establishing karstic areas where they have been partly or totally dissolved.

INTRODUCTION

Geophysical logs, also known as electric logs or wireline logs, record characteristics of the rocks and fluids encountered in drilling of a borehole. Over the years, logging tools have been developed to measure electrical, acoustic, natural gamma ray, and stimulated radioactive response of rocks and fluids, and these data help geologists and engineers understand the lithology, porosity, and fluid content of rocks in the subsurface. Most wells drilled in the Greater Permian Evaporite Basin (GPEB) (Johnson, 2021) not only seek information about the presence of oil and gas, but they can also provide information on the presence and character of evaporite units. Unfortunately, in some parts of the GPEB, logs only provide information on rocks in the deeper subsurface (where oil and gas typically occur), because some operators do not log shallower Permian strata that contain the evaporites.

Where evaporite units are logged, information can be obtained as to their lithology, distribution, and thickness. Geologists can then determine if subsurface evaporite units contain dissolution/collapse features, or if they may be a present or future problem for drilling operations. Drilling problems include the unexpected drop of drill bits and loss of drilling fluids in dissolution cavities, as well as the potential for excessive borehole enlargement caused by unexpected dissolution of salt beds; hole enlargement can affect proper casing placement and/or cementing of casing, and if the dissolution cavity becomes too large, it could lead to a collapse of overlying strata and formation of a sinkhole.

The following discussion of interpreting geophysical logs in evaporite units is based on the literature, as well as the author's experience in studying evaporites in the subsurface in various parts of the GPEB and other evaporite basins of the United States. I appreciate very much the review and excellent suggestions of Philip Schenewerk and Bruce Heath to an early draft of this report. Their comments and suggestions have been incorporated, and they greatly improve the accuracy and clarity of the final text.

The example logs shown here represent most of the major evaporite units in the GPEB (Figure 1): some of the lithologies shown with the logs are based upon cores, and some are interpretations based upon general knowledge of the lithology from nearby cores, outcrops, or descriptions in the literature. Many books and articles have been released on the interpretation of geophysical logs, but this brief article is presented here in the hope that geologists not familiar with using such logs in the GPEB will see that their use can be understood and can greatly enhance the subsurface study of evaporites, as well as the recognition and delineation of karst features.

Johnson, K. S., 2021, Identification of Gypsum, Anhydrite, and Salt on Geophysical Logs in the Greater Permian Evaporite Basin, *in* Johnson, K. S.; Land, Lewis; and Decker, D. D. (eds.), Evaporite Karst in the Greater Permian Evaporite Basin (GPEB) of Texas, New Mexico, Oklahoma, Kansas, and Colorado: Oklahoma Geological Survey, Circular 113, p. 51–61.

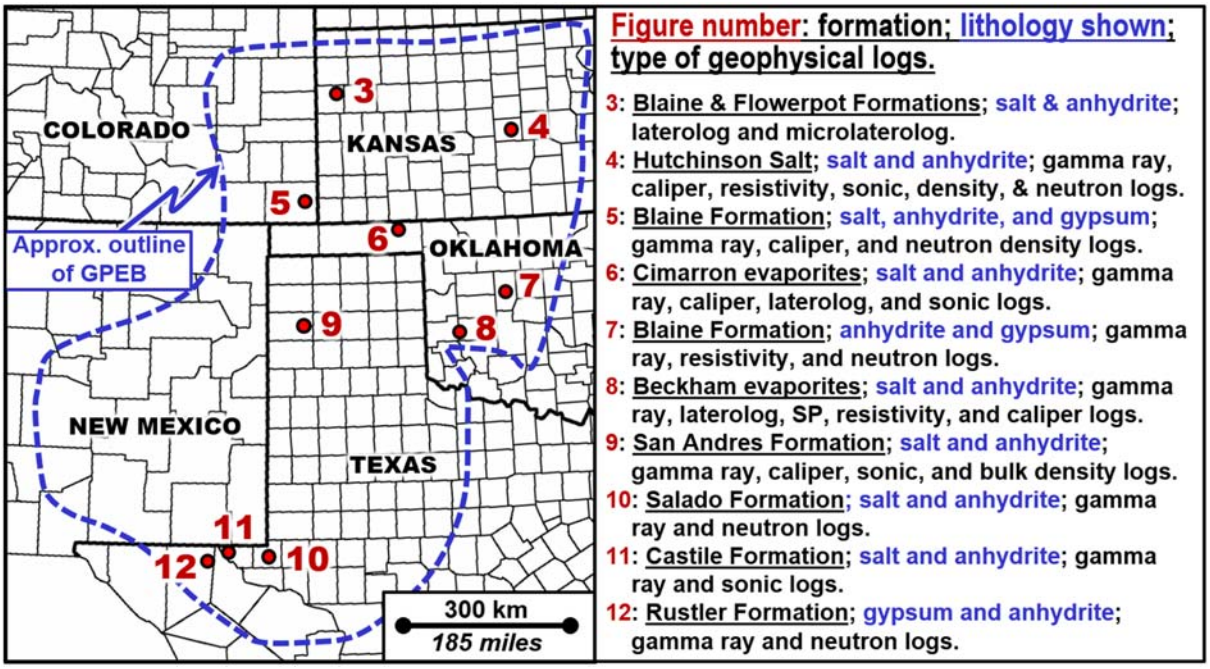

Figure 1. Location and figure numbers for geophysical logs shown in this report, and the approximate outline of Greater Permian Evaporite Basin (GPEB).

GEOPHYSICAL-LOG PROPERTIES OF COMMON EVAPORITES

Geophysical logs and their properties have been discussed by several authors, including Ellis (1987), Rider (2002), and Asquith and Krygowski (2004), and there are many Web sites where these subjects are described. Several authors have specifically discussed the interpretation of geophysical logs in evaporite units, including Alger and Crain (1966) and Nurmi (1978), and a Web site for recognizing a wide variety of evaporite minerals on geophysical logs is prepared by John K. Warren, of Saltworks Consultants: https://saltworkconsultants.com/wireline-skills-evaporite/. The following discussion of interpreting geophysical logs in evaporite units is based mainly on the data in Alger and Crain (1966) and Nurmi (1978), and on the current author's experience studying evaporites in various parts of the GPEB and elsewhere in the United States.

Table 1 shows the typical log responses on geophysical logs for principal evaporites and associated rocks: the upper table shows the general responses for various log types, as summarized from Alger and Crain (1966) and Nurmi (1978), and the lower table shows specific values for various log types, as presented in Alger and Crain (1966). Figure 2 graphically shows the general responses on the different geophysical logs to principal evaporites and other rocks commonly encountered in the GPEB. However, as noted by Presley and Ramondetta (1981, Table 1), "The reader should be aware that many factors in addition to lithology, such as borehole diameter, type and density of drilling mud, and type and position of measuring tool, can affect absolute log values."

Geophysical logs provide the best records when the rock layers are at least 1–1.5 m thick, or more, and the evaporite beds are of high purity. Rock layers that are less than 0.6–1 m thick may make only a small blip on the curve of most logs to suggest their presence, although micrologs do provide a finer resolution and show beds that are as thin as about 0.3 m thick. If an evaporite bed contains other materials (such as salt with shale inclusions, or thin interbeds of shale in any evaporite), then the log values will not be the same as those in high-purity beds.

Geophysical logs are commonly made or run several times during drilling of a well. As each segment of the well is drilled (through hundreds or thousands of meters), logging tools are lowered into the hole to measure rock/fluid properties before the steel casing is inserted to prevent caving of the just-drilled segment. Once this steel casing is inserted in the well, few of the usual formation-logging tools can be used because they are unable to make measurements through the steel and cement. Cased-hole versions of the standard gamma-ray and neutron logs, along with more specialized pulsed neutron tools, can provide rock-property information after the well is cased, but these logs may not always be available.

Gamma-Ray Logs

Gamma-ray logs record a measurement of the natural gamma-ray emissions from rock units, expressed in API

TABLE 1.—Two tables showing responses on geophysical logs for principal evaporites and associated rocks: data from Alger and Crain (1966), lower table, and Nurmi (1978), upper table. These rock properties and log responses appear to be applicable to the evaporite sequences encountered in all parts of the GPEB. Upper table shows general responses for various log types; lower table shows specific values for various log types.

Lithology	Gamma Ray (natural radiation in API units)	Caliper (borehole enlargement in inches)	Resistivity (resistance to electrical current in OHM m^2/m)	Microlog (resistance to electrical current in OHM m^2/m)	Sonic (transmission of sound waves in microseconds per foot, Δt)	Neutron (number of irradiated neutrons that pass through rock)	Density (specific gravity in gm/cc)
Anhydrite	0	very small	very high	very high	50	very high	2.96
Gypsum	0	very small	very high	very high	52	low	2.32
Halite (Salt)	0	very large	very high	very high	67	very high	2.16
Limestone*	5-10	very small	moderate	moderate	62	moderate	2.54
Dolomite*	10-20	very small	moderate	moderate	58	moderate	2.68
Sandstone*	10-30	small	moderate	moderate	65	moderate	2.49
Shale	80-140	large	very low	very low	70-150	low	2.2-2.75

Name	Sp. Gr.	Log ρ_B (gm/cc)	Average Δt	(GNT) Neutron ϕN	Deflection γ-ray (API) (d = 8")
Anhydrite	2.960	2.977	50	0	0
Gypsum	2.320	2.351	52.5	49	0
Halite (Salt)	2.165	2.032	67	0	0
Limestone*	2.540	2.540	62	10	5-10
Dolomite*	2.680	2.683	58	13.5	10-20
Sandstone*	2.489	2.485	65.3	3	10-30
Shale		2.2-2.75	70-150	25-60	80-140

* Values for limestone, dolomite, and sandstone assume a porosity of 10%.

(American Petroleum Institute) units. Gamma rays are emitted by rocks containing radioactive elements such as uranium, thorium, and potassium-40 (^{40}K, or K-40). All of these elements may be present in shales, and generally to a lesser extent in sandstones. Shales typically generate moderate to high gamma-ray emissions, chiefly because of the presence of K-40, whereas clean sandstone or carbonate formations have much lower gamma-ray emissions. Both radioactive and non-radioactive potassium commonly occur in sedimentary rocks, in minerals such as K-feldspars, biotite, muscovite, and illite.

K-40 is the main radioactive element associated with evaporite beds: 1) it is virtually absent from gypsum and anhydrite, which show very low gamma-ray emissions; 2) it may be present in small to moderate amounts in salt (salt can contain some potassium from evaporating Permian sea water), and thus most salt beds show some gamma-ray emissions—particularly if there are K-40-bearing shale inclusions in the salt; and 3) it is abundant in potash salts, such as sylvite and carnallite, which show very high gamma-ray emissions. Logs showing potash salts are not included in this report; within the GPEB, potash salts are limited only to the Carlsbad potash district in Eddy and Lea Counties, southeast New Mexico. Gamma-ray logs are the only logs commonly run that record data through casing; therefore, many geophysical well logs will record several types of data below surface or intermediate casing in a well, but only the gamma-ray curve will show data where the upper part of the hole is cased—***if*** the operator records natural gamma radiation while raising the tool through the cased part of the hole.

Caliper Logs

Caliper logs are a measure of the diameter of the borehole. Permian rock units that are typically competent and

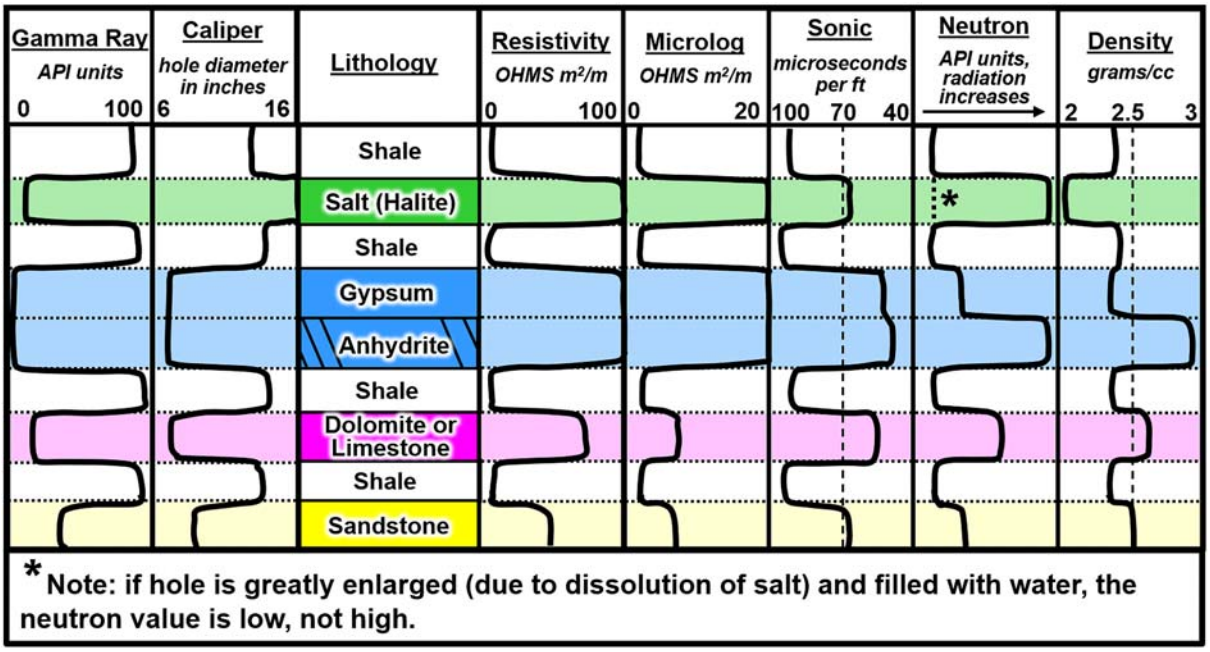

Figure 2. Examples of general responses on geophysical logs to principal evaporites and associated rocks.

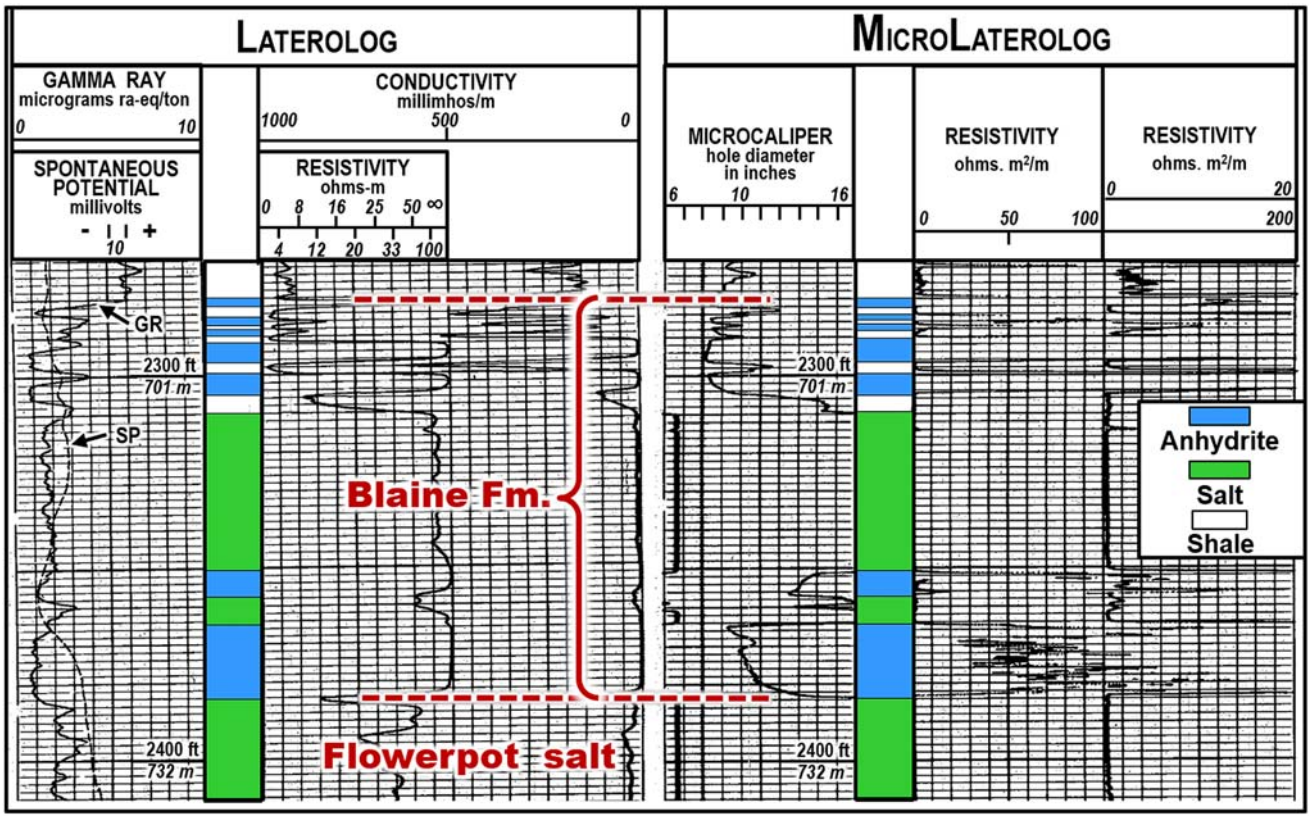

Figure 3. Geophysical logs and lithologic interpretation of the Blaine and upper Flowerpot Formations in the General Crude Oil Co., Delia F. Adams No. 1, sec. 15, T. 12 S., R. 39 W., Wallace County, Kansas. On the laterolog, the gamma-ray curve shows a slightly higher radioactivity in salt than in anhydrite, and the resistivity curve shows a slightly lower resistivity in salt than in anhydrite. The microlaterolog provides a sharp definition of the top and base of anhydrite beds on both the caliper and resistivity curves. On the microcaliper log, the hole has been enlarged considerably in the salt units.

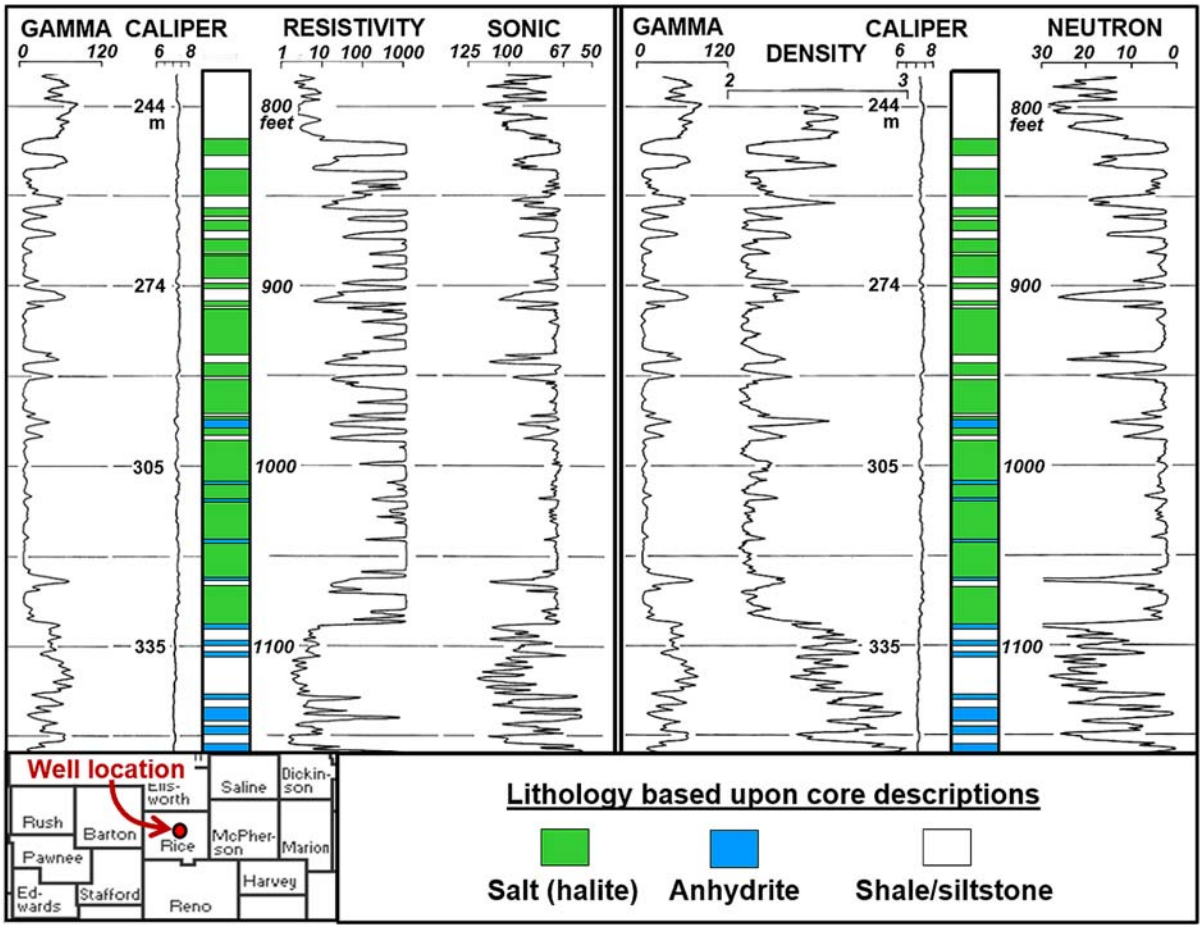

Figure 4. Geophysical logs and core descriptions of the Hutchinson Salt in the AEC Test Hole No. 1, drilled by the Atomic Energy Commission in sec. 26, T. 19 S., R. 8 W., about 5 km NNE of the city of Lyons, in Rice County, Kansas (modified from Walters, 1978). The large suite of logs includes gamma ray, caliper, resistivity, sonic, density, and neutron logs. Caliper log shows no hole enlargement in salt because of the use of salt-based drilling fluid (AEC wanted full recovery of salt cores). Sonic log shows faster transit time in anhydrite (Δt ±50) than in salt (Δt ±67). Density log shows lower specific gravity of salt (±2.1-2.2), compared to anhydrite (±2.9-3.0).

well lithified, such as gypsum, anhydrite, and carbonates, usually show only a small (if any) enlargement of the borehole. However, if rocks are soluble (such as salt), or if they cave into the wellbore (such as slightly lithified shale or friable sandstone), then the hole can be enlarged considerably beyond the diameter of the drill bit. At times, the hole enlargement is so great that the curve goes off-scale. It is possible that drilling mud can accumulate on the side of the wellbore. This "mud cake" results when a permeable formation (i.e., sandstone), acting as a filter, allows liquids to be squeezed out of the drilling mud and into the formation, leaving behind a layer of mud solids plastered on the wall of the borehole. A layer of "mud cake" decreases the size of the borehole.

Resistivity Logs

Resistivity logs measure the degree to which a rock layer (and any contained fluids) resists the flow of an electrical current. Gypsum, anhydrite, and salt all offer a very high resistance to an electric current, and therefore, the curve is deflected more significantly than for other rocks in the GPEB. In most units in the GPEB, gypsum and anhydrite provide the greatest resistance to an electric current, whereas salt units, if they contain shale inclusions or thin shale interbeds, can offer somewhat less resistance. Shales have low resistance to an electric current, and thus show little or no deflection of the curve. Lateral resistivity logs (laterologs) increase the resolution and definition of a rock layer and decrease the effect of adjacent beds; thus, they are very useful in the study of evaporites.

Micrologs

Micrologs are pad-mounted resistivity logs, as described above, except that they measure the rock/fluid properties of a very small volume of material (only a few

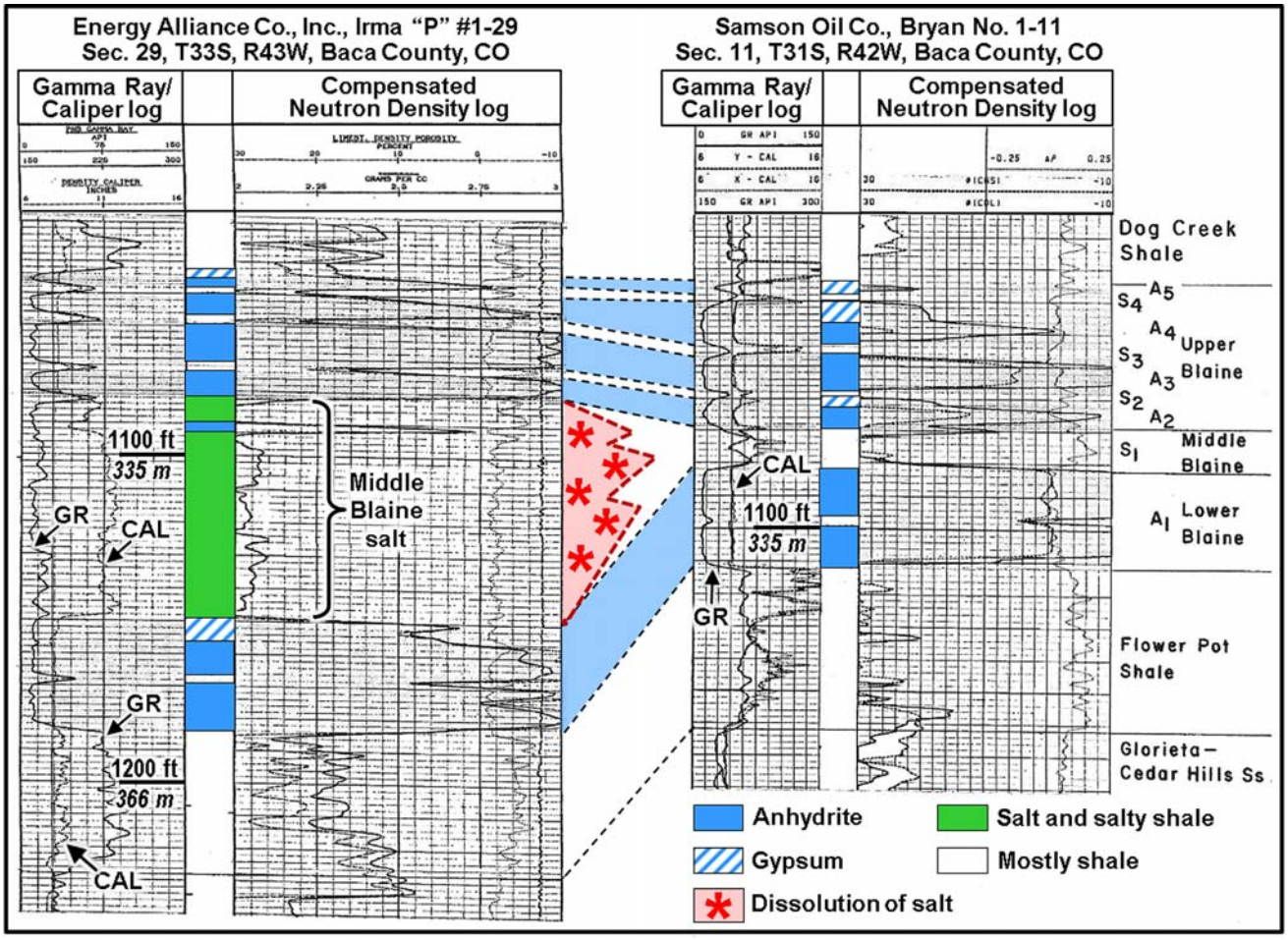

Figure 5. Geophysical logs and lithologic interpretation in two wells about 29 km apart in Baca County, Colorado, showing salt and gypsum/anhydrite beds in the Blaine Formation (modified from Askew, 2013). The neutron density log in both wells shows lower-density, neutron-absorbing gypsum at top of several anhydrite beds. Also, hole on the left is enlarged (on caliper log) to about 11 inches in salt, but is about 8 inches in the anhydrites.

cubic inches) adjacent to the borehole wall, and thus are much more accurate and detailed for showing contacts between various rock layers and for showing rock layers that are as thin as about 0.3 m. The design of the tool measurements may also yield a possible indication of the rock layer's ability to transmit fluids. As above, gypsum and anhydrite have the greatest resistance to an electric current, whereas salt beds, if they contain shale inclusions or shale interbeds, show somewhat less resistance, and shales have low resistance.

Sonic Logs

Sonic logs record a measure of the time that it takes, in microseconds (μs), for a sonic compressional wave to travel 1 foot (0.305 m) in the rock unit. The more compact the rock is, the higher the velocity of the sound wave traveling through the rock, and therefore, the shorter the time (Δt) it takes to travel 1 foot. Sonic logs, if available, are very good for differentiating between salt and gypsum or anhydrite; the Δt for salt is 67 μs/ft, whereas for anhydrite, it is 50 μs/ft, and for gypsum, it is 52 μs/ft. Dolomites, limestones, and sandstones have Δt values in the same range as salt and gypsum or anhydrite, but shales typically have very high Δt values.

Neutron Logs

Neutron logs, or neutron porosity index logs, record the response of the rock unit to bombardment by high-energy neutrons and primarily indicate the presence or absence of hydrogen atoms in the rock and its fluids. As these high-energy neutrons collide with atoms in the formation, they are slowed down, and eventually may be captured, by elements in the formation or its fluids. Depending on the tool design, the measurement is either a count of the slowed neutrons that make it back to the detector or the gamma rays that result from the capture of these neutrons. Older tools recorded neutron counts in API units, but in more modern tools, these counts are

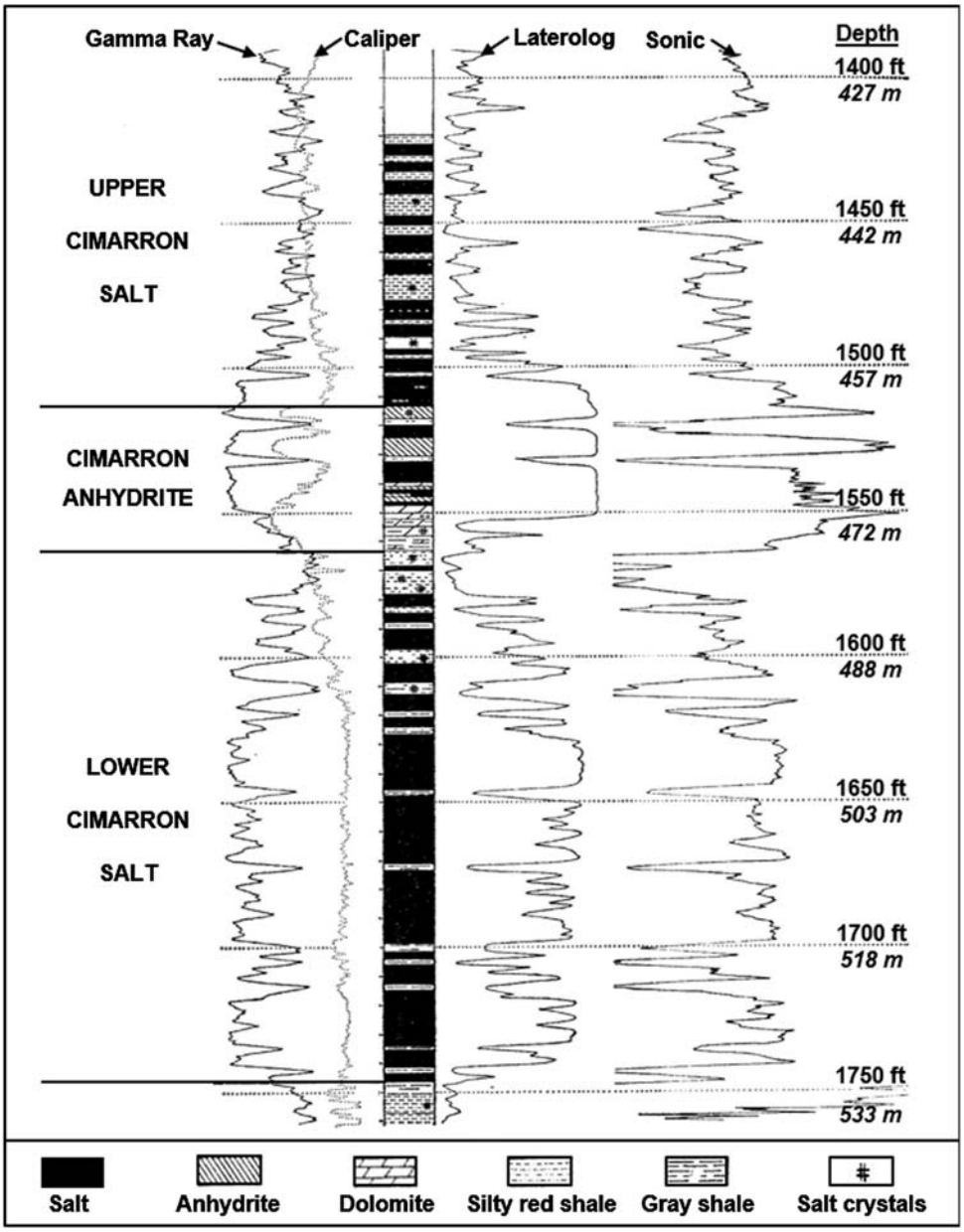

Figure 6. Geophysical logs and core descriptions of Cimarron evaporites in the Gulf-Warren Petroleum, SWD-1 well at the Warren Petroleum Corp., Mocane LPG-storage plant, sec. 18, T. 5 N., R. 25 ECM, Beaver County, Oklahoma. Modified from Jordan (1962) and Jordan and Vosburg (1963). Caliper log shows only moderate hole enlargement in salt because the hole was drilled with salt-based mud. Core description notes that salt contains shale inclusions and is thinly interbedded with moderate amounts of shale, and logs show that the salt is impure. Laterolog shows slightly higher resistivity of anhydrite than salt. Sonic log curve shows faster travel time (Δt) in anhydrite and dolomite than in salt.

converted into a measurement of the rock's porosity. This porosity is dependent on the assumption of a particular matrix type and can be corrected to a different matrix assumption using service-company charts.

In rocks containing a large amount of hydrogen, chiefly as water (H_2O), these neutrons are absorbed quickly, and so the count of neutrons that pass through the rock is very small. These logs are useful to differentiate between gypsum ($CaSO_4 \cdot 2H_2O$) and anhydrite ($CaSO_4$—"anhydrous" means "no water"). Note, however, if the borehole is greatly enlarged in a salt unit (caused by dissolution), then the neutron absorption can be high (and the neutron curve would be low) because of the large amount of hydrogen (H_2O) in that part of the hole.

Density Logs

Density logs record a measure of the density of rock units in gm/cc. The logging tool uses a gamma-ray

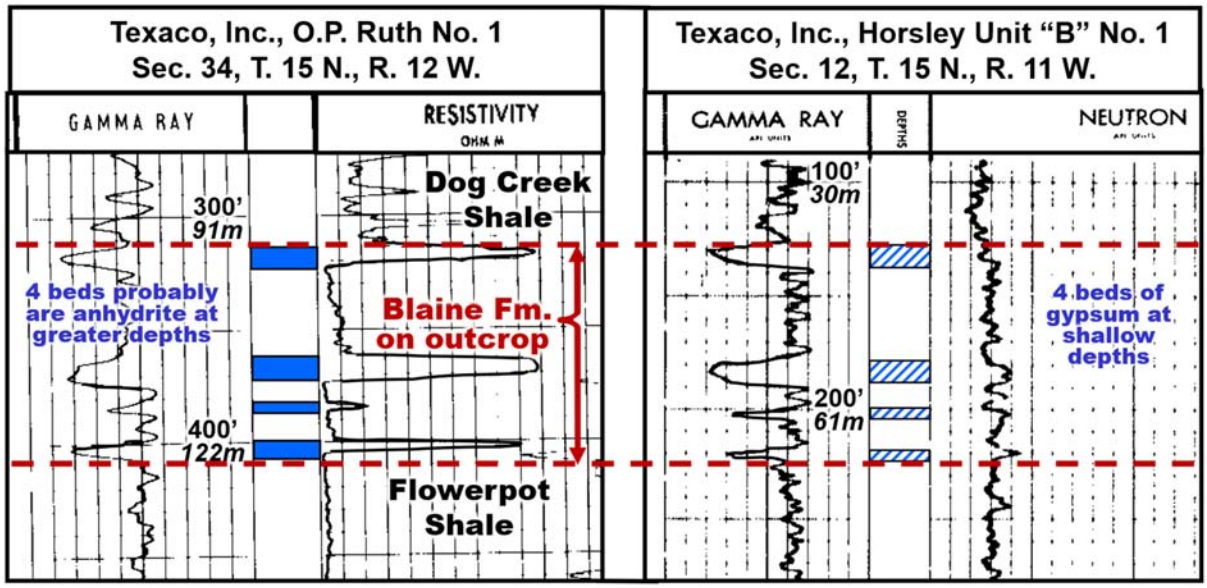

Figure 7. Geophysical logs and lithologic interpretation of two wells about 13 km apart showing gypsum beds (log on right) of the Blaine Formation in the shallow subsurface of Blaine County, northwest Oklahoma (from Johnson and others, 2013). Gamma-ray and resistivity logs readily differentiate the gypsum or anhydrite beds from shale. Gypsum beds, because they contain hydrogen, do not show log deflections on the neutron log on right; well on left does not have neutron log, but sulfate beds here are deeper and probably are anhydrite.

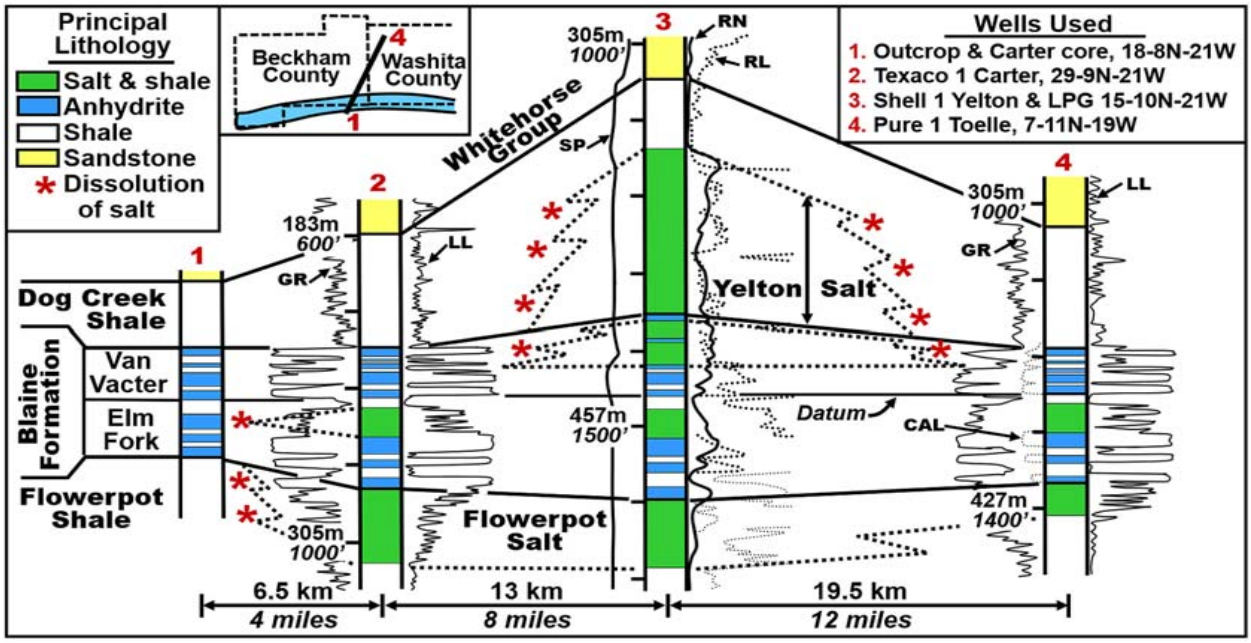

Figure 8. Geophysical logs and lithologic interpretation of three wells showing salt and gypsum/anhydrite beds in the Blaine Formation and associated strata (Beckham evaporites) in the subsurface of Beckham and Washita Counties, southwest Oklahoma (from Johnson, 2013). Types of logs, from left: GR (gamma ray), LL (laterolog = resistivity), SP (spontaneous potential), RN (resistivity, normal), RL (resistivity, lateral), and CAL (caliper). These types of logs do not differentiate between gypsum and anhydrite, but, at these depths, the sulfate beds are probably mostly, or all, anhydrite. Laterologs and resistivity logs show higher values (deflections to right) in anhydrite beds than in salt beds, which probably contain shale inclusions and shale interbeds. Gamma-ray logs show higher radioactivity (deflections to right) in salt than in anhydrite, probably because of radioactive isotopes of potassium in the salt and/or inter-mixed clays. Caliper log in well no. 4 shows hole enlargement in salt and shale, and small hole diameter in anhydrite beds.

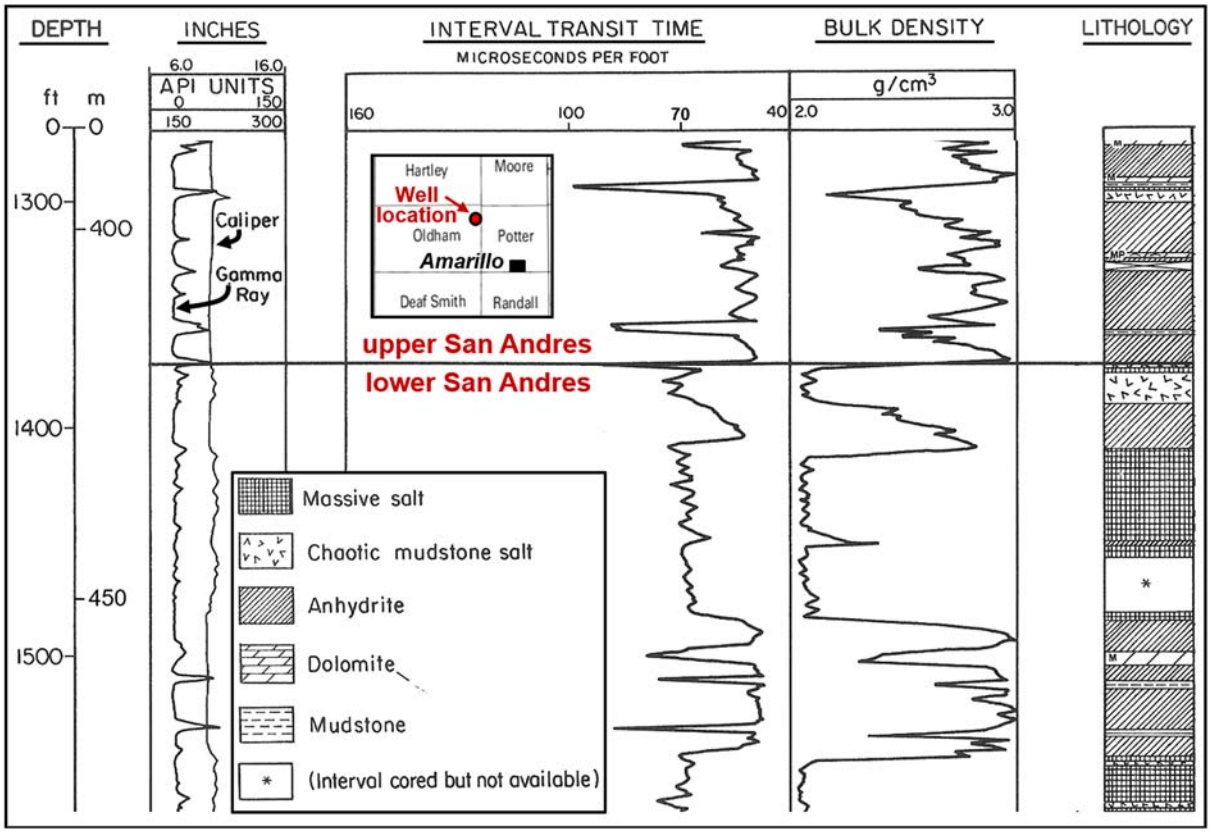

Figure 9. Geophysical logs and core descriptions of part of the San Andres Formation in the DOE-Stone & Webster, No. 1 Mansfield well drilled in northeastern Oldham County, Texas. Modified from Ruppel and Hovorka (1983). Caliper log shows no hole enlargement in salt because of the use of salt-based drilling fluid. Sonic log (interval transit time) distinguishes between salt ($\Delta t = 67$) and anhydrite ($\Delta t = 50$). Bulk density log differentiates salt (±2.1) from anhydrite (±2.9-3.0).

source pressed against the side of the borehole. The tool emits gamma rays with a known energy level and records the number of lower energy gamma rays returned to the tool because of collisions with electrons in the atoms within the formation and its fluids. This count is a measure of the electron density of the formation and is easily converted to a more useful standard bulk density in gm/cc. This bulk density can be used as is or can be converted into an estimation of the formation's porosity. Common evaporites in the GPEB are readily differentiated on density logs. Anhydrite (sp.gr. 2.96), the most common form of sulfate rock at depths below 30 m or so, contrasts greatly from salt (sp.gr. 2.165) and from gypsum (sp.gr. 2.32). The density of most of the nonevaporite rocks in the GPEB is about midway between anhydrite and salt.

SAMPLE GEOPHYSICAL LOGS SHOWING COMMON EVAPORITES

This part of the report shows a selection of ten sets of geophysical logs covering major evaporite units in different parts of the GPEB (Figure 1), and how the logs are interpreted for the evaporites they show. Most of the logs (Figures 3–12) were presented previously in the literature, and only two (Figures 3, 11) were not. Four of the logs are accompanied by core descriptions, whereas the other six are accompanied by lithologic interpretations that are based upon general knowledge of the lithology from nearby cores, outcrops, or descriptions in the literature.

REFERENCES CITED

Alger, R.P., and Crain, E.R., 1966, Defining evaporite deposits with electrical well logs, *in* Rau, J.L., ed., Second symposium on salt: Cleveland, Ohio, The Northern Ohio Geological Society, Inc., Vol. 2, p. 116-130. http://www.ross-crain.com/freepubs/1966-2%20Defining%20Evaporite%20Deposites%20With%20Electrical%20Well%20Logs%20%20NOGS-SALT%20Alger-Crain.pdf

Askew, R.L., 2013, Distribution of the Permian Blaine Formation salt in the subsurface of the Hugoton Embayment area of Baca County, southeast Colorado:

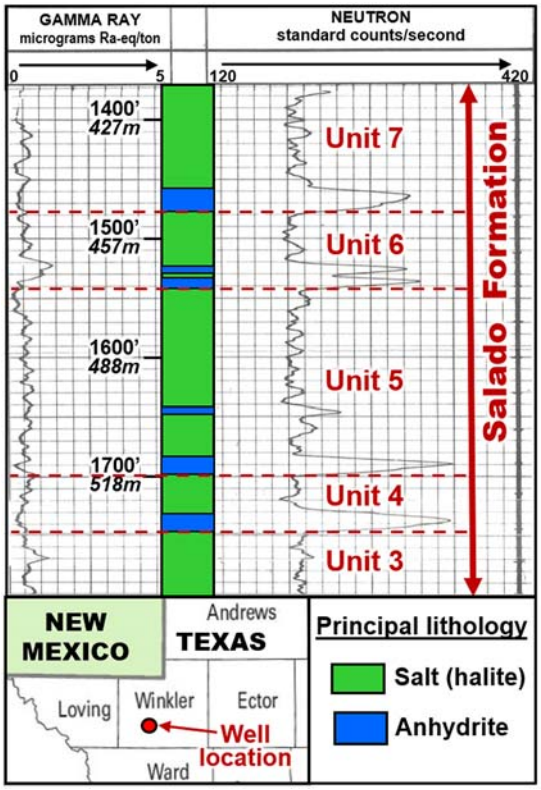

Figure 10. Geophysical logs and lithologic interpretation of the J.W. Starr, Pan Am Hendrick B#2, sec. 35, Block B-5, PSL Survey, Winkler County, Texas, showing salt and anhydrite beds in the Salado Formation (modified from Johnson, 1993). This well is about 730 m southeast of Wink Sink no. 1. Neutron log here readily differentiates anhydrite (high values) from salt (lower values); normally, anhydrite and salt both have high neutron values, but because borehole probably is enlarged in salt units (caused by salt dissolution), the large amount of water in these parts of the hole causes high neutron absorption (lower neutron values).

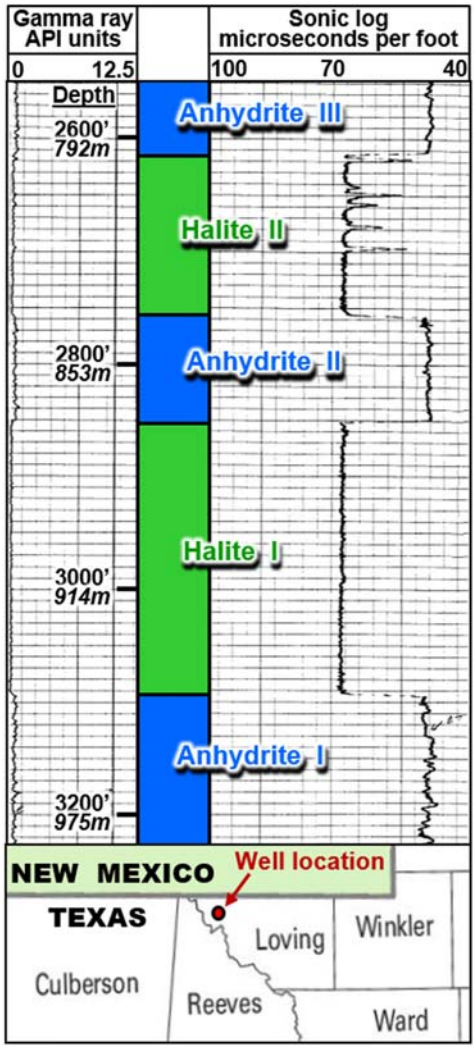

Figure 11. Geophysical logs and lithologic interpretation of part of the Castile Formation in the Texaco Inc., Lago Unit No. 1, Loving County, Texas. Surprisingly, the gamma-ray log shows very slightly higher gamma radiation for anhydrite than for salt; this suggests that the salt is of high purity, with no clay minerals or potash salts (thus no radioactive isotopes of potassium). Sonic log readily differentiates anhydrite ($\Delta t = 50$) from salt ($\Delta t = 67$); also, it shows the presence of several thin layers of anhydrite in the upper half of Halite II.

Rocky Mountain Association of Geologists, The Mountain Geologist, Vol. 50, No. 2, P. 65-75.

Asquith, G., and Krygowski, D, 2004, Basic well log analysis (second edition): American Association of Petroleum Geologists, AAPG Methods in Exploration Series 16, 244 p. https://www.academia.edu/35430322/Basic_Well_Log_Analysis_Second_Edition_with_sections_by_Steven_Henderson_and_Neil_Hurley_AAPG_Methods_in_Exploration_Series_16

Eager, G.P., 1983, Core from the lower Dewey Lake, Rustler, and upper Salado Formations, Culberson County, Texas, *in* Shaw, R.L., and Pollan, B.J., eds., Permian Basin cores—a workshop: Permian Basin Section, S.E.P.M. Core Workshop #2, p. 273-283.

Ellis, D.V., 1987, Well logging for earth scientists: New York, Elsevier Science Publishing Co., Inc., 532 p.

Johnson, K.S., 1993, Dissolution of Permian Salado salt during Salado time in the Wink area, Winkler County, Texas, *in* D. W. Love and others, eds., Carlsbad region, New Mexico and west Texas: New Mexico Geological Society Guidebook, 44th Annual Field Conference (October 6–9, 1993), p. 211-218. https://www.researchgate.net/publication/268385405

Johnson, K.S., 2021, Overview of evaporite karst in the Greater Permian Evaporite Basin (GPEB) of TX, NM, OK, KS, and CO, *in* Johnson, K.S., Land, L.A., and

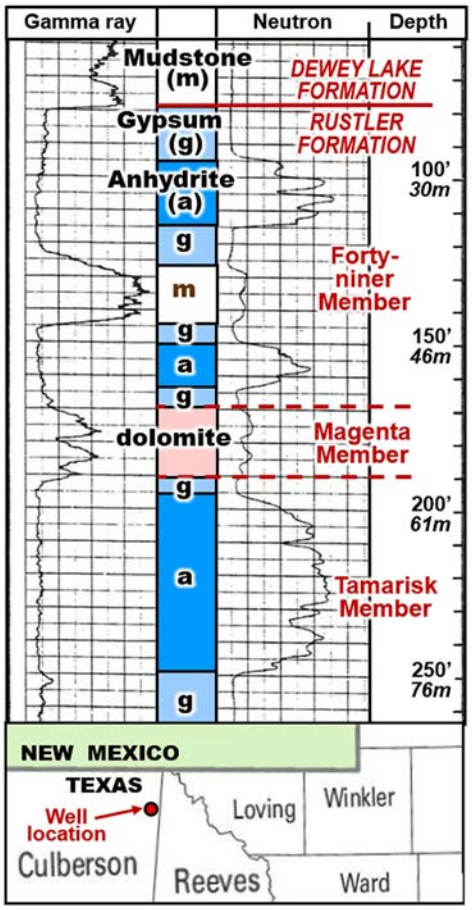

Figure 12. Geophysical logs and core descriptions of the Texasgulf, Inc., sulphur-exploration core, sec. 5, PSL Survey, Block 45, Culberson County, Texas (20 km southwest of Orla), showing parts of the Dewey Lake and Rustler Formations (modified from Eager, 1983). Gamma-ray log shows higher radioactivity in mudstones, probably because of radioactive isotopes of potassium in the clays, and in dolomite. Neutron log readily differentiates hydrogen-bearing gypsum from anhydrite.

Decker, D.D., eds., Evaporite karst in the Greater Permian Evaporite Basin (GPEB) of Texas, New Mexico, Oklahoma, Kansas, and Colorado: Oklahoma Geological Survey, Circular 113.

Johnson, K.S., Bangsund, W.J., and Hines, N.A., 2013, Gypsum karst and potential risk in siting wind turbines in Blaine County, Oklahoma, *in* Land, L., Doctor, D.H., and Stephenson, J.B., eds., Sinkholes and the engineering and environmental impacts of karst–Proceedings of the thirteenth multidisciplinary conference, Carlsbad, NM, May 6 through 10, 2013: National Cave and Karst Research Institute, Carlsbad, NM, p. 151-159. http://scholarcommons.usf.edu/cgi/viewcontent.cgi?article=1123&context=sinkhole_2013

Jordan, L., 1962, LPG storage in Cimarron salt, Beaver County, Oklahoma: Oklahoma Geological Survey, Oklahoma Geology Notes, Vol. 22, No. 2, p. 23-26. http://ogs.ou.edu/docs/geologynotes/GN-V22N2.pdf

Jordan, L., and Vosburg, D.L., 1963, Permian salt and associated evaporites in the Anadarko Basin of the western Oklahoma–Texas Panhandle region: Oklahoma Geological Survey, Bulletin 102, 76 p. http://ogs.ou.edu/docs/bulletins/B102.pdf

Nurmi, R.D., 1978, Use of well logs in evaporite sequences, *in* Dean, W.E., and Schreiber, B.C., eds, Marine evaporites: Society of Economic Paleontologists and Mineralogists, SEPM Short Course No. 4 held in Oklahoma City, p. 144-176.

Presley, M.W., and Ramondetta, P.J., 1981, Hydrocarbon potential of San Andres carbonates in the Palo Duro Basin—stratigraphic and facies analysis: *in* Gustavson, T.C., and others, Geology and geohydrology of the Palo Duro Basin, Texas Panhandle: The University of Texas at Austin, Bureau of Economic Geology, Geological Circular 83–4, p. 59-63.

Rider, M., 2002, The geological interpretation of well logs: Sutherland, Scotland, Rider-French Consulting, Ltd., 2nd edition, 280 p.

Rupple, S.C., and Hovorka, S.D., 1983, Stratigraphic section along the northwestern margin of the Palo Duro Basin: core analysis of DOE–Stone and Webster No. 1 Mansfield test well, Oldham County, Texas, *in* Gustavson, T.C., and others, Geology and geohydrology of the Palo Duro Basin, Texas Panhandle: The University of Texas at Austin, Bureau of Economic Geology, Geological Circular 83–4, p. 47-48 and plate II.

Walters, R.F., 1978, Land subsidence in central Kansas related to salt dissolution: Kansas Geological Survey, Bulletin 214, 82 p. http://www.kgs.ku.edu/Publications/Bulletins/214/index.html

Evaporite Karst as a Transportation and Infrastructure Geohazard in the Lower Pecos Region, Southeastern New Mexico and West Texas

Lewis Land
National Cave and Karst Research Institute, Carlsbad, New Mexico

ABSTRACT.—Sinkholes and other surface karst features are naturally occurring phenomena in regions underlain by soluble bedrock such as limestone or gypsum. The lower Pecos region of southeastern New Mexico and west Texas is particularly susceptible to karst geohazards because of the widespread occurrence of Permian evaporites at or near the land surface. Sinkholes in this region occur over a broad spectrum of scales, ranging from less than one to several hundred meters in diameter, and are often associated with human activity such as solution mining or oil and gas operations. Depending on thickness and mechanical properties of the overburden, sinkholes may develop slowly as broad subsidence basins or rapidly by catastrophic collapse. Sinkholes receive widespread news coverage when they form in densely populated parts of the country, such as Florida or Kentucky. When these features form in more sparsely populated regions, such as the desert southwest, they may go unreported for long periods of time. Sinkholes and other evaporite-karst processes nevertheless pose a geohazard for the transportation and pipeline network in southeastern New Mexico; their occurrence is sometimes difficult to predict, and remediation is often challenging and expensive.

INTRODUCTION

Evaporite-karst phenomena in the lower Pecos region of southeastern New Mexico span over three degrees of latitude, extending for more than 400 km from Santa Rosa in the north to the state line south of Carlsbad, and beyond into west Texas (Figure 1). The presence of soluble gypsum and halite bedrock in outcrop or in the subsurface throughout the Permian section (Figure 2) has resulted in manifestations of karst processes at a variety of scales, from small sinkholes and caves to regional subsidence basins, and has significantly influenced the topography along the margins of the Pecos River valley (Bachman, 1984; 1987; Land, 2003). Anthropogenic processes, such as solution mining, road construction, and improperly cased or plugged oil and water wells, have also accelerated and modified the ongoing natural evolution of the evaporite-karst landscape (e.g., Johnson and others, 2003; Powers, 2003; Land and Aster, 2009; Land and Veni, 2012; Land, 2013).

The Guadalupe Mountains region of southeastern New Mexico and west Texas is world famous for its caves formed in carbonate bedrock (e.g., Hill, 1987; Love and others, 1993; Palmer and Palmer, 2000; Hose and Pisarowicz, 2000; Land and others, 2006, among a great many others), the most obvious example being Carlsbad Cavern, one of three world heritage sites in New Mexico (UNESCO, 2020). However, with a few exceptions (Land and Burger, 2008), most limestone caves in the Guadalupe Mountains are located above the regional water table and have little direct impact on societal infrastructure. Apart from tourism, the greatest human impact of carbonate karst phenomena in southeastern New Mexico lies in the regional karstic aquifers formed in Permian limestones of the Capitan Reef and Roswell Artesian Basin (Hiss, 1973; Welder, 1983; Land and Newton, 2008; Land, 2016). Evaporite-karst features and processes, by contrast, have had a profound influence on the geomorphology, hydrology, economy, and infrastructure of the lower Pecos region.

SANTA ROSA AREA

The northernmost occurrences of karst phenomena in the Pecos Valley are found in northern Guadalupe County, ~25 km upstream from the town of Santa Rosa, where the Pecos River flows across outcrops of

Land, L., 2021, Evaporite Karst as a Transportation and Infrastructure Geohazard in the Lower Pecos Region, Southeastern New Mexico and West Texas, *in* Johnson, K. S.; Land, Lewis; and Decker, D. D. (eds.), Evaporite Karst in the Greater Permian Evaporite Basin (GPEB) of Texas, New Mexico, Oklahoma, Kansas, and Colorado: Oklahoma Geological Survey, Circular 113, p. 63–77.

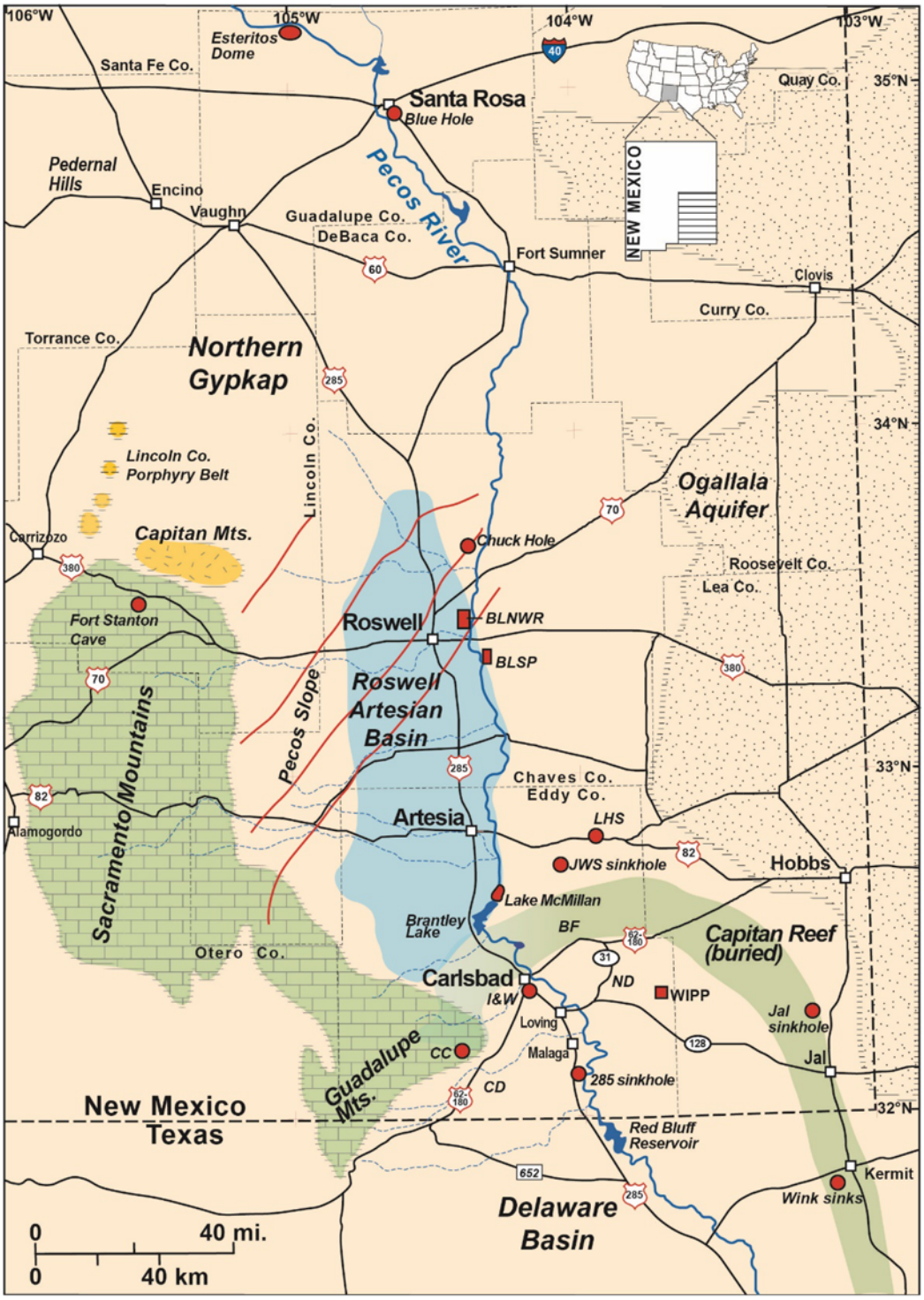

Figure 1. Regional map of southeastern New Mexico and west Texas. Red filled circles show relevant gypsum sinkholes, other evaporite-karst features, and other locations mentioned in this report. BF=Burton Flats; BLNWR=Bitter Lake National Wildlife Refuge; BLSP=Bottomless Lakes State Park; CC=Carlsbad Cavern; CD=Chosa Draw; I&W=I&W brine well; LHS=Loco Hills Sinkhole; ND=Nash Draw; WIPP=Waste Isolation Pilot Plant. Red lines show the Pecos Buckles, wrench faults extending SW-NE across the Pecos Slope.

the San Andres Formation and Artesia Group along the north flank of Esteritos Dome (Figure 1; Trauger, 1972). Along this reach of the river, the Pecos loses water that is undersaturated with respect to calcium carbonate through fractured and cavernous San Andres limestones. Groundwater flows southeast through these highly

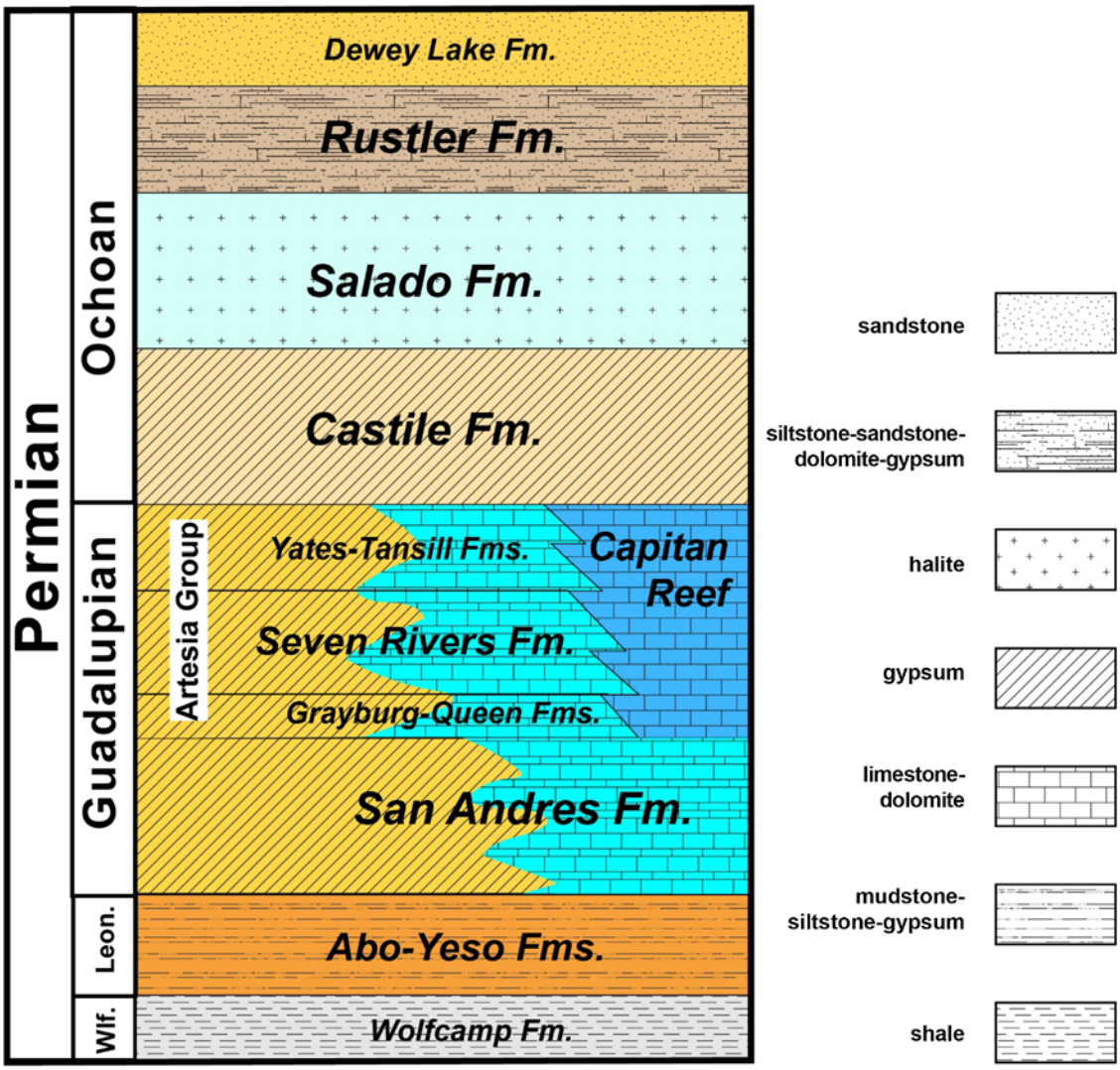

Figure 2. Permian stratigraphy of southeastern New Mexico and west Texas. Leon.=Leonardian; Wlf.=Wolfcampian.

transmissive carbonates and discharges from springs along the river, and by upward artesian flow into sinkhole lakes (Dinwiddie and Clebsch, 1973; Land, 2009).

The San Andres Formation grades from a predominantly carbonate facies in western Guadalupe Co. to an anhydrite–gypsum–halite facies as it dips eastward into the Tucumcari Basin (Trauger, 1972). Although the precise nature and location of this subsurface facies change are not well-constrained, the change is clearly reflected in changes in water chemistry in the Pecos River. Near Santa Rosa, an increase in chloride content in the river reflects the presence of salt beds in the subsurface (Sweeting, 1972; Dinwiddie and Clebsch, 1973).

The community of Santa Rosa is located on the northeast margin of a broad, solution-subsidence depression about 10 km in diameter and 120 m deep, displayed on the state geologic map as a circular fault (Scholle, 2003). The physiography of the depression is clearly visible when entering Santa Rosa from the east or west on Interstate 40. The Pecos River enters the depression through a narrow gorge north of town and flows southward across the eastern floor, exiting through the southern drape wall of the sink. The location of the Santa Rosa subsidence depression is very likely controlled by subsurface dissolution of evaporites in the vicinity of the carbonate–evaporite facies change. Kelley (1972) reported that the subsidence results from dissolution of gypsum and halite in the San Andres Formation, which is ~180 m deep beneath the floor of the basin.

The Santa Rosa depression has been filled with several tens of meters of Tertiary and Quaternary sand and gravel deposited by the Pecos River and is rimmed by inward-sloping sandstone beds of the Triassic Santa Rosa Formation. In addition to the larger solution-subsidence depression, a great many smaller sinkholes occur in the Santa Rosa area, primarily along the

northern and western margin of the basin. Where soluble rocks in the San Andres are overlain by relatively thin sandstone beds of the Triassic Santa Rosa Formation, upward stoping and collapse have produced vertical-walled sinkholes of typical cenote morphology, such as Blue Hole (Figure 1), although formed in siliciclastic rocks (Kelley, 1972; Land, 2009).

NORTHERN GYPKAP/ROSWELL BASIN

The Northern Gypkap (Gypsum Karst Project) refers to a vast and sparsely populated area in east-central New Mexico covering more than 20,000 km^2, encompassing parts of Chaves, Lincoln, Guadalupe, DeBaca, and Torrance Counties (Figure 1). The region is bounded to the south by the Capitan Mountains batholith, and to the north by the Pedernal Hills, a late Paleozoic landmass composed of Precambrian granite, granite gneiss, and metaquartzite that was later partially buried by younger sedimentary strata (Gonzalez and Woodward, 1972; Kottlowski, 1985). The Lincoln County Porphyry Belt lies to the west (Kelly, 1971), and the eastern margin is approximately defined by the Pecos River valley. Most of the region is underlain in outcrop or in the shallow subsurface by evaporitic facies of the San Andres Formation and Artesia Group, and by the Yeso Formation, which also contains evaporitic lithologies (Figures 1 and 2; Weber and Kottlowski, 1959; Kelly, 1971; Kelly and Kelly, 1972; Scholle, 2003).

The Northern Gypkap designation derives from an effort by members of the Southwest Region of the National Speleological Society to explore and map the gypsum karst of southeastern New Mexico (Eaton, 1987). Gypsum bedrock in the region is host to dozens of caves, some with a surveyed length of more than 3 km and a vertical extent exceeding 130 m (Figure 3; Forbes and Nance, 1997). Surface mapping and air photo interpretation indicate the presence of many thousands of sinkholes in the area (Eaton, 1987; Belski, 1992; Lee, 1996).

The city of Roswell, the largest population center in southeastern New Mexico, is located at the northern end of the Roswell Artesian Basin, one of the most intensively farmed areas in the state outside the Rio Grande Valley (Figure 1; Land and Newton, 2008; Land, 2009).

Communities in the Roswell Basin derive virtually all of their irrigation, industrial, and municipal drinking water from groundwater in a shallow alluvial aquifer and a karstic artesian aquifer formed in middle Permian limestone of the San Andres Formation and overlying carbonates of the Artesia Group (Figure 2; Welder, 1983; Land and Newton, 2008). Recharge to the artesian aquifer originates in the southern Sacramento Mountains



Figure 3. Sinkhole entrance to Torgac Cave, formed in gypsum bedrock of the San Andres Formation, Lincoln Co., NM.

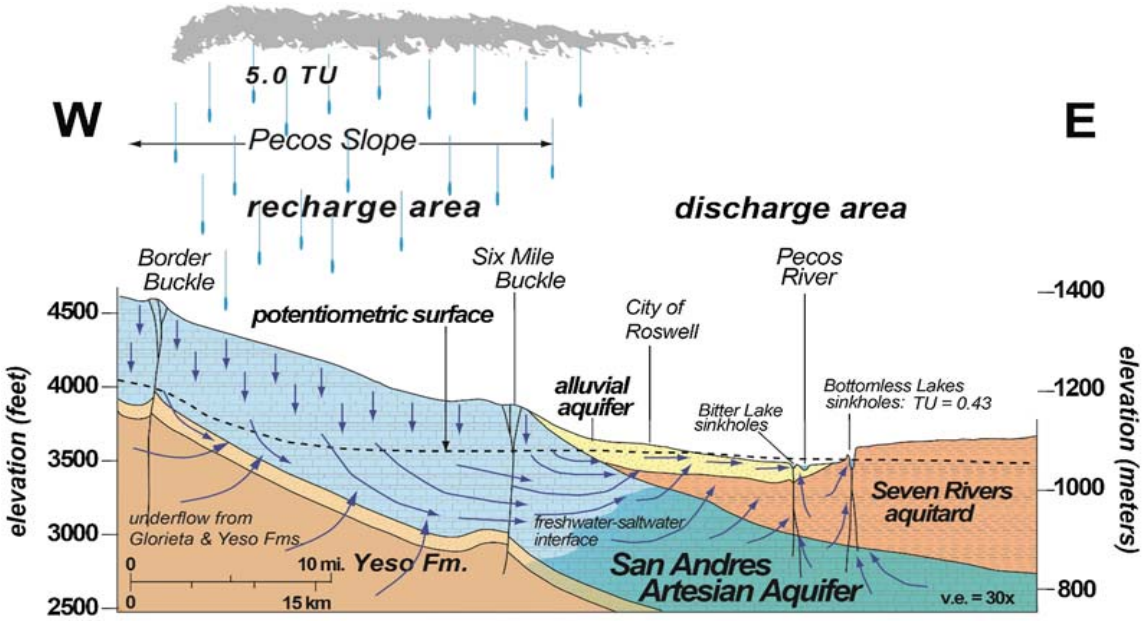

Figure 4. West-east hydrostratigraphic profile of artesian aquifer in Roswell Artesian Basin. TU = tritium units. Groundwater at Bitter Lake NWR and Bottomless Lakes SP is depleted in tritium, a result of mixing of recent recharge with premodern groundwater originating from the underlying Glorieta and Yeso Formations (Land and Huff, 2010).

to the west, and through solution-enlarged fissures on the Pecos Slope. In predevelopment times, groundwater discharged at the downgradient end of the regional aquifer system from karst springs and gypsum cenotes at Bitter Lake National Wildlife Refuge and Bottomless Lakes State Park. Since the inception of irrigated agriculture in the early 20th century, most of the downgradient flow is now intercepted by hundreds of irrigation wells in the Artesian Basin (Figures 1 and 4; Land, 2003; Land and Huff, 2010).

Human activity in the Gypkap region to the north, by contrast, is represented only by isolated ranches and almost uninhabited villages, such as Encino and Duran. Both this demographic disparity and the abundance of gypsum-karst features in the Northern Gypkap are a function of south to north facies changes that occur within the San Andres Formation and Artesia Group.

Regional stratigraphic models of the San Andres show deposition of mixed carbonates and evaporites occurring over an extremely broad shelf of very low relief in east-central and southeastern New Mexico and west Texas. The formation is comprised mostly of carbonates in southern New Mexico, where it is bounded to the southeast by a low-relief shelf margin on the northern flank of the Delaware Basin (Silver and Todd, 1969; Elliott and Warren, 1989). The San Andres Formation becomes increasingly evaporitic to the north and east (Kelley, 1971; Ward and others, 1986) and is correlative with gypsum of the Blaine Formation in western Oklahoma. Similar facies changes occur in the overlying Artesia Group (Land, 2003).

In the subsurface of the Roswell Artesian Basin carbonate lithologies predominate, and the evaporitic component of the San Andres is represented primarily by intraformational solution-collapse breccias, known as "rubble zones," created by dissolution of interbedded evaporites by circulating groundwater. These breccia zones provide much of the groundwater storage capacity for the artesian aquifer system (Motts and Cushman, 1964; Welder, 1983). The Artesian Basin also includes a shallow alluvial aquifer formed from sediment deposited by the ancestral Pecos River. These deposits attain their greatest saturated thickness (~75 m) in subsidence basins developed by dissolution of evaporites in the underlying Permian bedrock (Lyford, 1973; Welder, 1983). Evaporite-karst processes may thus be said to have contributed directly to the civic water supply infrastructure, and by extension the prosperity of agricultural communities in the Roswell Artesian Basin.

North of Roswell, shelfward facies change results in a San Andres and Grayburg section that consists mostly of gypsum, with relatively thin interbeds of dolomite or limestone (Eaton, 1987; Forbes and Nance, 1997). Common features in the Northern Gypkap area are thus sinkholes and gypsum caves with dolomite ceilings or floors, rather than the extensive solution-collapse breccias found farther south in the Artesian Basin. These caves are located above the regional water table, which is several hundred meters deep in much of the Northern Gypkap area, and do not provide significant potential for storage of groundwater, other than as highly localized perched aquifers. The limited water resources in this

region, attributable in part to regional facies changes that occur within these middle Permian units, account for the sparse population and lack of economic development in the Northern Gypkap (Land, 2009).

Despite the lack of agricultural potential, in the past two decades the Northern Gypkap region has become an attractive area for the development of wind farms. Wind-farm projects may involve construction and installation of more than a hundred individual wind turbines and may occupy several tens to hundreds of square kilometers (Johnson and others, 2013). Wind farms also have a significant visual impact on their surroundings, and for these reasons are often sited in remote, sparsely populated, and undeveloped areas (Bangsund and Johnson, 2013). The Northern Gypkap, with its limited population, subdued topography, nearly treeless plains, and frequent strong winds, provides an attractive setting for wind-farm projects.

Evaporite-karst processes pose the most significant geohazard for wind-farm development in the Northern Gypkap region. Spread footings are the most common type of foundation for an individual turbine, with a foundation width of 15–22 m. Turbines have relatively low dead loads but high overturning moments. Differential settlement of even a few centimeters across a 15-m wide turbine foundation can cause the turbine to be out of tolerance, leading to tilting or toppling. This risk is significant, because an individual wind turbine can cost two to five million dollars (Bangsund and Johnson, 2013). The absence of surface karst features does not necessarily ensure the stability of a site, since many areas in the Northern Gypkap are covered with a thin veneer of alluvium, masking potential cavities in the shallow subsurface. Johnson and others (2013) report that the hazard diminishes with increasing thickness (>25 m) of insoluble overburden.

DAM FOUNDATIONS

Lake McMillan, located ~35 km north of the city of Carlsbad, was one of the earliest impoundments on the Pecos River (Figure 1). McMillan dam was constructed in 1893 to provide storage of irrigation water for farmers in the Carlsbad area at a time when geologic assessments of dam sites were rarely conducted (US Bureau of Reclamation, 1957). Construction of dams and reservoirs on karst terrain is historically known to include a high element of risk. Despite highly detailed geological and geophysical site investigations, the possibility for dam failure cannot be entirely eliminated because of the highly random and unpredictable distribution of solution conduits in a karst environment (Milanović, 2002; 2011). In addition to the risk of subsidence or collapse, leakage from artificial impoundments in karst regions is globally widespread (e.g., Mohammadi, 2007).

Gypsum karst presents particular problems for dam foundations because of the highly soluble nature of that mineral. Once groundwater flow beneath a dam is established, solution conduits can enlarge quickly, undermining the dam and diminishing storage capacity of the reservoir (Johnson, 2008; Johnson and others, 2021). In addition to the risk of catastrophic failure, remediation of dam sites in gypsum karst terrain can be very expensive and require years or decades of effort (e.g., Jarvis, 2003; Johnson and Wilkerson, 2013).

Lake McMillan is located within the evaporite facies belt of the middle Permian Seven Rivers Formation (Figure 2). Because of the soluble nature of the underlying gypsum bedrock, McMillan reservoir almost immediately began experiencing leakage problems through sinkholes and solution channels formed in the lake bed, particularly along the eastern margin of the lake. Water flowed through karstic conduits in the Seven Rivers gypsum and returned to the Pecos River through discharge from Major Johnson Springs, ~5.6 km downstream (Theis, 1938). East and southeast of the facies change, the less soluble dolomite facies of the Seven Rivers retard any significant formation of solution channels. In 1908–1909, a dike was constructed along the southeast shore of the lake, near the base of the McMillan Escarpment, in an attempt to isolate the areas of worst sinkhole formation, with limited success. The dike was extended in 1953–1954 along most of the eastern shore to prevent water from reaching exposed sinkholes during periods of high lake level. Occasionally, breaks would occur in the dikes causing lake water to inundate the sinkholes. At these times, whirlpools were reported in the lake, indicating that sediment cover over sinkholes in the lake bed had been disturbed. High rates of leakage would occur for short periods of time, until the dikes were repaired and sediment cover on the floor of the lake restored (Cox, 1967; Land and Love, 2006).

Storage capacity of Lake McMillan steadily decreased after the dam was constructed because of deposition of suspended sediment, and by the early 1940s less than half of its original storage capacity remained. The possibility of dredging was considered, but soon discarded when it was realized that removal of the accumulated sediment would considerably increase leakage through karst fissures in the gypsum bedrock underlying the lake. Fortunately, loss of storage capacity decreased by the mid-1940s because a stand of salt cedar became established in bottom lands upstream from Lake McMillan, acting as a baffle for much of the suspended sediment carried by the Pecos River (Cox, 1967; Land and Love, 2006).

Consideration for construction of a new dam began as early as 1905. The U.S. Bureau of Reclamation began construction of Brantley Dam in 1984, and in 1991 McMillan Dam was breached and Lake McMillan

allowed to drain into Brantley Lake. Based on recommendations by Cox (1967), the new reservoir is located mostly within the less soluble dolomitic facies belt of the Seven Rivers Formation.

ANTHROPOGENIC KARST

A small but significant number of sinkholes in the lower Pecos region are of human origin, including the Wink Sinks in Winkler Co., Texas (Figure 1). The first Wink Sink formed in 1980 outside the small community of Wink, Texas, within the giant Hendrick oil field, destroying crude-oil pipelines and oil-field infrastructure. That sinkhole ultimately expanded to a diameter of 110 m and a depth of 34 m. In 2002, a new sinkhole formed ~1.6 km south of the original Wink Sink. Wink Sink no. 2 is significantly larger than its predecessor, with a maximum width of ~250 m and an estimated total volume of more than 1.3 million m^3. Both sinkholes are assumed to have formed by dissolution of salt beds in the upper Permian Salado Formation, in association with improperly cased abandoned oil- and water-supply wells (Baumgardner and others, 1982; Johnson and others, 2003). The potential for continued subsidence or collapse still exists, based on InSAR and microgravity surveys conducted by investigators with the University of Texas-Austin and Southern Methodist University (Payne and others, 2012; Kim and others, 2019).

Solution mining of salt can also cause sinkhole formation. A dramatic example of this process occurred in July, 2008, when a truck driver for Jim's Water Service, a local water-hauling company, was parked at the site of a brine well in northern Eddy County, New Mexico. The operator had taken over an abandoned oil well and converted it to an injection well, pumping fresh water into salt beds of the Salado Formation, ~150 m below ground level (bgl). The dissolution of salt creates a brine that was pumped to the surface to sell as drilling fluid in nearby oil fields. This process, which also creates a sizeable cave in the salt beds, is common in many parts of the world where bedded salt is present in the shallow subsurface. Various geotechnical and engineering methods are employed to prevent collapse of the cavity, but these methods are not always successful (Land and Aster, 2009).

While on location, the driver noticed a rumbling noise and quickly vacated the site. Minutes later, a large sinkhole abruptly formed, engulfing the brine well and associated structures. This sinkhole (now referred to as the JWS sinkhole after the brine well's operator) eventually grew to a diameter of more than 100 m and a depth of about 50 m. Large concentric fractures developed around the perimeter of the sink, threatening the integrity of a nearby county road (Figure 5). Less than four months later, another brine well collapse occurred 16 km to the northeast near the small community of Loco Hills (Figure 1), forming a sinkhole of similar dimensions. Then in July, 2009, another sinkhole abruptly formed near Denver City, Texas, ~115 km east of Loco Hills. The Denver City collapse was also the product of a failed solution-mining operation (Land, 2013a; 2013b).

Both of the Eddy County sinkholes formed in the middle of a giant oil field where the population of pump jacks far outnumbers the human population; thus, the impact on infrastructure was minimal. In the aftermath of these events, the New Mexico Oil Conservation Division (NM OCD) conducted an inventory of brine well operations in the state of New Mexico. Most of the brine wells identified by OCD were completed at greater depths, farther to the east in the Delaware Basin. However, one well, the I&W brine well, was identified within the city limits of Carlsbad (Figure 1) and had a geologic setting, depth, and pumping history very similar to the two brine wells that had collapsed in northern Eddy Co. Unlike the northern Eddy Co. sinks, this potential sinkhole is sited beneath the intersection of two major highways, an irrigation canal, a feed store, a mobile home park, and a Jehovah's Witnesses church. Needless to say, a catastrophic collapse would inflict extensive damage to individual property and civic infrastructure, and possibly cause fatalities (Land and Veni, 2012).

Electrical resistivity surveys of the I&W brine well site indicate that the area is underlain by multiple low resistivity zones that represent either open cavities filled with brine in the Rustler and Salado Formations or brine-saturated rubble resulting from roof fall into underlying cavities (Figure 6; Land and Veni, 2012). These low resistivity zones extend to the north beneath the highway intersection and south beneath residential areas and the Carlsbad Irrigation District South Canal (Figure 7). The resistivity profiles also indicate that solution mining of the Salado Formation has caused significant upward stoping into overlying Rustler strata.

Following the collapse of the JWS sinkhole, the state ordered closure of the I&W brine well and the operator declared bankruptcy. Geotechnical investigations indicated that upward stoping and roof fall are occurring at a rate of about 30 cm per year, and in the absence of any remediation, failure will occur in 10 to 25 yr. In 2018, the state dedicated funds for remediation of the I&W brine well, and 26 injection wells were drilled around the perimeter of the cavity for injection of sand and grout.

KARST IN OCHOAN EVAPORITES

Upper Permian (Ochoan) evaporites crop out in southeastern Eddy Co., New Mexico and northern Culberson Co., Texas, and dip down to the east into the northern Delaware Basin (Bachman, 1980; 1984). This region, which is dominated by outcrops of the Ochoan Castile and Rustler Formations across an area encompassing



Figure 5. JWS sinkhole, about one month after initial collapse. County Road 117 is visible in the upper right corner. Two-track dirt roads converging on the sinkhole originally led to the brine well facility prior to the collapse.

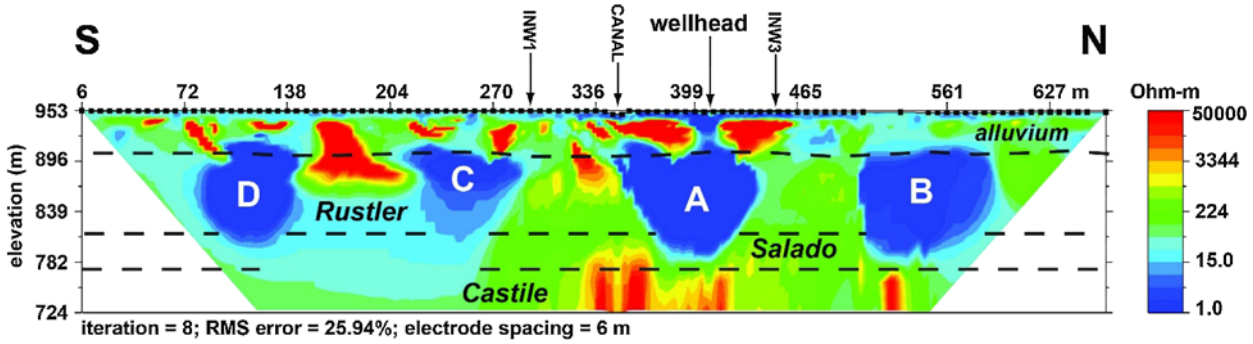

Figure 6. Electrical resistivity profile across I&W brine well site. Low resistivity zones, shown in blue, indicate brine-filled cavities or brine-saturated rubble. This line passes within 2 m of the wellhead (Figure 7), crossing directly over the subsurface cavity (A) excavated during solution-mining operations. Zones B, C, and D are interpreted to be additional cavities or rubble zones that may be associated with solution-mining activity, but not connected to the main void space (from Land and Veni, 2012, Figure 6D).

~2800 km^2, is commonly known as the gypsum plain (Hill, 1996; Stafford, 2017).

Extensive exposures of the Rustler Formation, one of the uppermost members of the Ochoan Series (Figure 2), occur east and west of US 285 south of the village of Malaga, NM, where the unit is disrupted by numerous small diapirs and related sinks associated with dissolution and/or flow of the underlying Salado Formation (Kelley, 1971). The Rustler also crops out in Nash Draw (Figure 1), a well-documented karst basin ~30 km east of Carlsbad containing abundant sinkholes, small caves, and karst valleys, developed by dissolution and erosion of soluble lithologies in the Rustler and underlying Salado Formations (e.g., Lee, 1925; Robinson and Lang, 1938; Vine, 1963; Bachman, 1981; Powers and others, 2006; Goodbar and others, 2020).

The Rustler Formation is a heterogeneous unit consisting of interbedded gypsum, mudstone, dolomite,

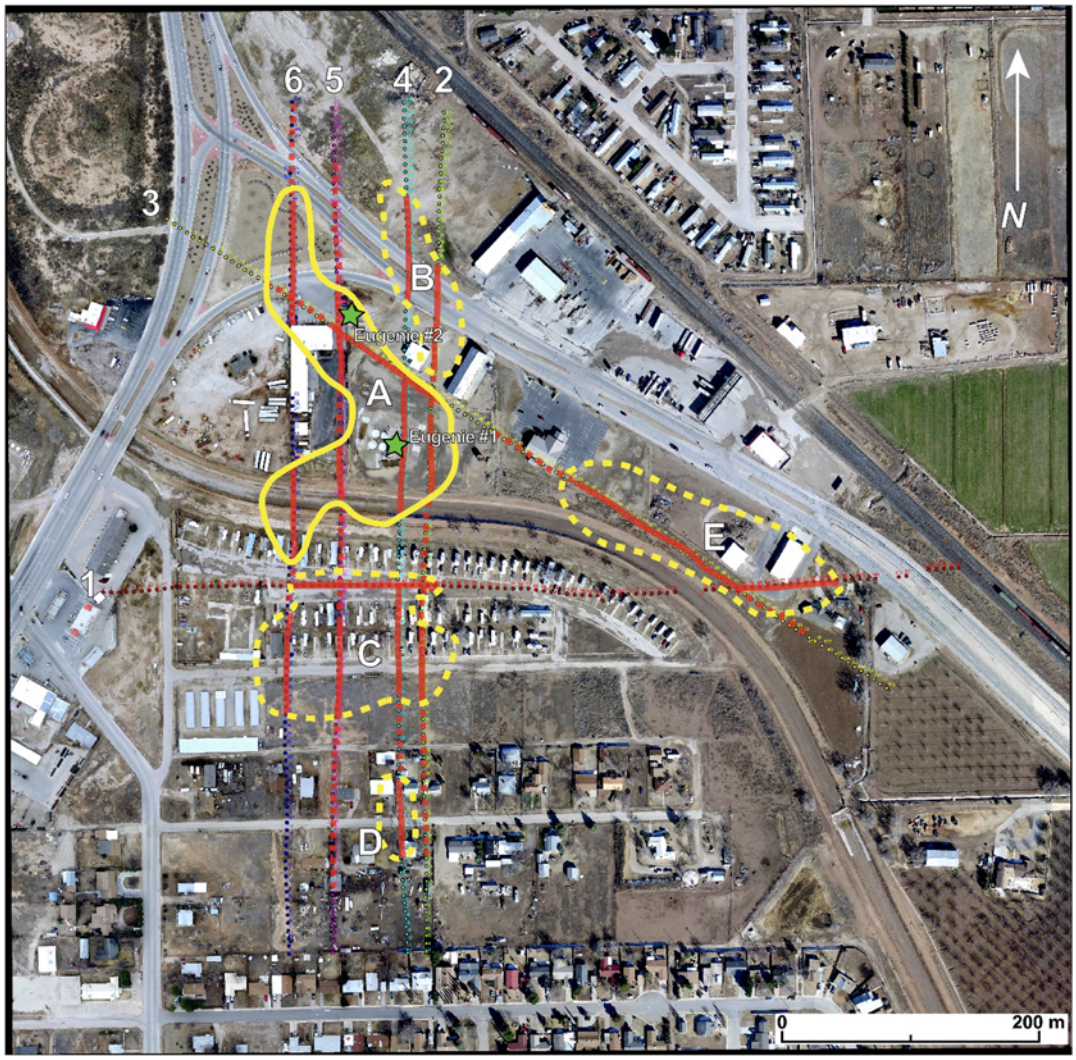

Figure 7. Map showing locations of possible subsurface cavities in the Rustler and Salado Formations. Numbered lines show locations of resistivity surveys one through six. Line four passes within 2 m of the wellhead. Much of the area outlined in solid yellow is probably underlain by a significant cavity. Areas delimited by dashed yellow lines are interpreted to represent additional cavities or rubble zones not connected to the main void space (from Land and Veni, 2012, Figure 9).

and fine sandstone (Bachman, 1984). The diversity of lithologies influences the types of karst features formed in the Rustler. Land and others (2018) observed that many small sinkholes formed in the lowermost Los Medaños Member along US 285 were relatively shallow (<3 m deep), without deep roots, and attributed this phenomenon to layers of insoluble mudstone underlying more soluble gypsum beds. However, Decker and others (2020) identified larger caves and sinkholes in the Burton Flats area east of Carlsbad, formed in gypsum and dolomite beds of the upper Rustler Formation.

Sinkholes and caves in the Rustler are a geohazard for the transportation and pipeline network in the oil fields of the region (Land and others, 2018). Portions of NM highways 31 and 128 extend across karst terrain in Nash Draw, and much of US 285 between the village of Loving and the state line is underlain by gypsum beds of the lower Rustler Formation (Figure 1). Road improvements have been proposed, but as of this writing that portion of the US 285 corridor consists of a two-lane highway with narrow shoulders and abundant small sinkholes along the highway right of way (Land and others, 2018). During periods when drilling activity in the region is high, oil field traffic along US 285 is extremely heavy, earning it the nickname, "the deadliest highway in America" (Wolaver, 2019, personal communication).

The Salado Formation, the middle unit of the Ochoan Series, is very poorly exposed in outcrop because of its soluble lithology, which is ~90% halite (Kelley, 1971; Holt and others, 2006). Surface exposures of the Salado

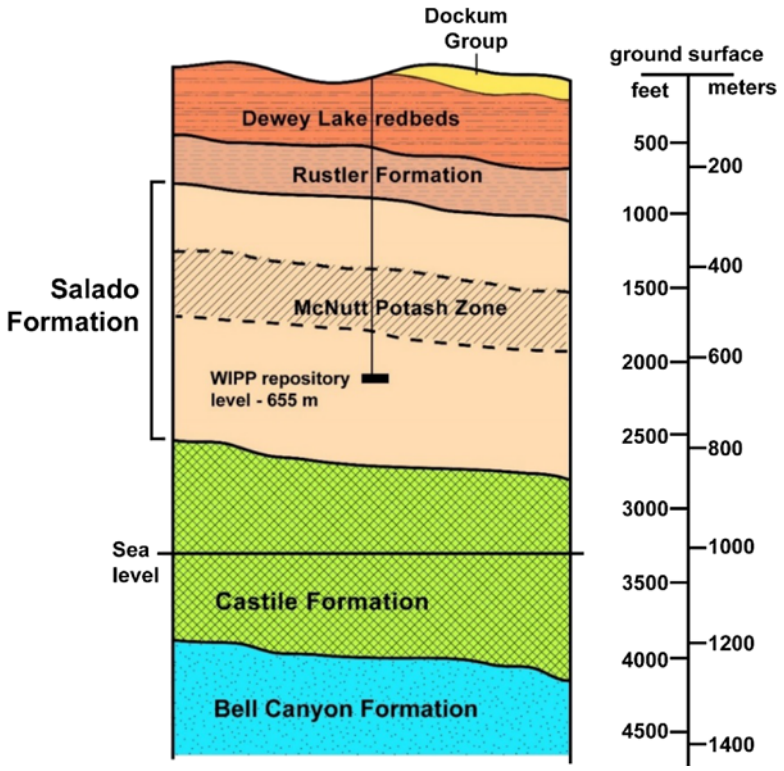

Figure 8. Upper Permian stratigraphy at the Waste Isolation Pilot Plant, Eddy Co., New Mexico. Modified from Weart and others (1998).

consist primarily of brecciated gypsum and insoluble residue (Bachman, 1984), and its type locality is in a drill hole in Loving Co., TX (Lang, 1935). However, the presence of the Salado in the subsurface of the Delaware Basin has had a profound influence on surface and near-surface karst phenomena, including formation of the Wink Sinks in Winkler Co., TX (Baumgardner and others, 1982; Johnson and others, 2003; Payne and others, 2012; Kim and others, 2019); anthropogenic sinkholes in Eddy and Lea Cos., NM (Powers, 2003; Land and Veni, 2012; Land, 2013a; 2013b); and leakage and disruption of the dam foundation at Red Bluff Reservoir on the Pecos River between Reeves and Loving Cos., TX (Figure 1; Johnson and others, 2021).

The Castile Formation crops out on the gypsum plain in southern Eddy Co., NM and northern Culberson Co., TX. The Castile is the host rock for Parks Ranch Cave, the second longest gypsum cave in the United States, located in Chosa Draw, ~35 km southwest of Carlsbad (Figure 1; Gulden, 2019). The Castile consists of laminated couplets of anhydrite and calcite/organic material interbedded with poorly laminated halite (Anderson, 1972) and has been identified as a classic example of a marine, deepwater evaporite deposit. Where exposed at the surface, the Castile anhydrite has mostly altered to gypsum. Unlike the overlying Rustler and Salado Formations, the Castile is confined to the Delaware Basin and does not extend onto the Northwest Shelf of the basin (Scholle and others, 2004).

The Castile gypsum underlies significant portions of US 62-180 (National Parks Highway) southwest of Carlsbad, and Texas Farm to Market Road 652 in northern Culberson Co., TX (Figure 1). FM 652 is the main corridor linking highways 285 and 62-180 and is subject to high levels of oil field traffic. Karst geohazards are commonly encountered in this region, including subsurface instability and intersection of voids during drilling operations and pipeline construction, and road failure in areas where sinkholes and caves occur (Stafford and others, 2017). Stafford (2008) suggested that ~10,000 gypsum karst features are present within the gypsum plain. More recent works by Stafford and his team (e.g., Ehrhart, 2016; Ehrhart and Stafford, 2020; Stafford and Shields, 2020) indicate that this figure may be an underestimate by at least an order of magnitude, in part because that estimate does not consider deeper-seated hypogene karst features farther east and downdip that have not yet been breached by surface erosion.

WASTE ISOLATION PILOT PLANT

This review of the impact of evaporite karst on human infrastructure in southeastern New Mexico would not be complete without noting the potential significance of evaporite-karst processes in the development of the Waste Isolation Pilot Plant (WIPP). The WIPP site is located in eastern Eddy Co., NM (Figure 1) and is designed for permanent sequestration of transuranic radioactive waste in massive salt beds of the Salado Formation 655 m below ground level (Figure 8). Transuranic waste (the term "transuranic" refers to elements with atomic numbers greater than uranium in the periodic table) is legacy waste produced during the manufacture of nuclear weapons at production facilities such as Rocky Flats and Los Alamos National Lab. The waste at WIPP is stored in steel drums sequestered in horizontal drifts excavated in the Salado Formation. Because halite behaves in a ductile manner at great depths and high confining pressures, the assumption is that, once the drifts are sealed, the salt will eventually flow and crush the drums, and the impermeable nature of the salt will permanently entomb the waste in the subsurface (Chaturvedi, 1993; Weart and others, 1998).

The geology and hydrology of the WIPP site have been exhaustively investigated by Sandia National Labs, among other entities (e.g., Anderson, 1978;

Powers and others, 1978; Weart, 1983; Bachman, 1985; Powers, 1996 among a great many others). Nevertheless, as with all proposed radioactive waste disposal facilities, the WIPP site is controversial (e.g., Chaturvedi, 1993; Hill, 2003). Local residents in Carlsbad for the most part welcomed the facility, because construction and maintenance of WIPP are compatible with skills required for work in the potash mines east of Carlsbad, an important component of the local economy (Weart and others, 1998). However, as the site was developed it attracted many protestors. Because WIPP is located ~13 km east of Nash Draw, some workers have proposed that karstic conduits developed in the Rustler Formation and other soluble surface rocks might provide avenues for leakage of radioactive waste to the surface, ultimately contaminating water resources in the Pecos River (Phillips, 1987; Hill, 2003). A complete discussion of the WIPP site is beyond the scope of this paper. However, it is one of the few instances this author is aware of when the subject of karst became a volatile political topic.

CONCLUSIONS

Karst features formed in carbonate bedrock in southeastern New Mexico have a global reputation. However, evaporite-karst processes and phenomena have had a far greater human impact. Manifestations of evaporite karst are ubiquitous in the lower Pecos region and have had a profound influence on the geology, hydrology, economy, and human infrastructure of southeastern New Mexico and far west Texas.

REFERENCES CITED

Anderson, R.Y., Dean, W.E Jr., Kirkland, D.W., Snider, H.I., 1972, Permian varved Castile evaporite sequence, west Texas and New Mexico: Geological Society of America, Bulletin, Vol. 83, p. 59-86.

Anderson, R.Y., 1978, Report to Sandia Laboratories on deep dissolution of salt, northern Delaware Basin, New Mexico: Copy on file in the Sandia WIPP Central Files, Sandia National Laboratories, Albuquerque, NM as WPO29527-WPO29530.

Bachman, G.O., 1980, Regional geology and Cenozoic history of the Pecos Region, southeastern New Mexico: US Geological Survey, Open File Report 80-1099, 117 p.

Bachman, G.O., 1981, Geology of Nash Draw, Eddy County, NM: US Geological Survey, Open-File Report 81-31, 10 p.

Bachman, G.O., 1984, Regional geology of Ochoan evaporites, northern part of Delaware Basin: New Mexico Bureau of Mines and Mineral Resources, Circular 184, 22 p.

Bachman, G.O., 1985, Assessment of near-surface dissolution at and near the Waste Isolation Pilot Plant (WIPP), southeastern New Mexico: Albuquerque (NM), Sandia National Laboratories, Contractor Report SAND84-7178, 33 p.

Bachman, G.O., 1987, Karst in evaporites in southeastern New Mexico: Albuquerque (NM), Sandia National Laboratories, Contractor Report SAND86-7078, 82 p.

Bangsund, W.J., Johnson, K.S., 2013, Evaluating karst risk at proposed windpower projects, *in:* Land, L., Doctor, D.H., and Stephenson, J.B., eds., Proceedings of the Thirteenth Multidisciplinary Conference on Sinkholes and the Engineering and Environmental Impact of Karst, Carlsbad, New Mexico: National Cave and Karst Research Institute, Symposium 2, p. 27-36.

Baumgardner, R.W., Jr., Hoadley, A.D., Goldstein, A.G., 1982, Formation of the Wink Sink, a salt dissolution and collapse feature, Winkler County, Texas: The University of Texas at Austin, Bureau of Economic Geology, Report of Investigations 114, 38 p.

Belski, D., ed., 1992, GYPKAP Report volume #2: Southwestern Region of the National Speleological Society, Albuquerque (NM), 56 p.

Chaturvedi, L., 2003, WIPP-related geological issues, *in:* Love, D.W., Hawley, J.W., Kues, B.S., Adams, J.W., Austin, G.S., Barker, J.M., 1993, eds.: New Mexico Geological Society Guidebook 44, Carlsbad region, New Mexico and west Texas, p. 331-338.

Cox, E.R., 1967, Geology and hydrology between Lake McMillan and Carlsbad Springs, Eddy Co., New Mexico: US Geological Survey, Water-Supply Paper 1828, 48 p.

Decker, D., Land, L., and Luke, B., 2021, Geophysical characterization of playa lakes in the gypsum karst of southeastern New Mexico and West Texas, USA, *in:* Johnson, K.S., Land, L., and Decker, D.D., eds., Evaporite karst in the Greater Permian Evaporite Basin (GPEB) of Texas, New Mexico, Oklahoma, Kansas, and Colorado: Oklahoma Geological Survey, Circular 113.

Dinwiddie, G.A., and Clebsch, A., Jr., 1973, Water resources of Guadalupe County, New Mexico: New Mexico Bureau of Mines and Mineral Resources, Hydrologic Report 3, 43 p.

Eaton, J., ed., 1987, GYPKAP 1987 Annual Report: Southwestern Region of the National Speleological Society, Alamogordo (NM), 35 p.

Elliott, L.A., Warren, J.K., 1989, Stratigraphy and depositional environment of lower San Andres Formation in subsurface and equivalent outcrops: Chaves, Lincoln, and Roosevelt Counties, New Mexico: American Association of Petroleum Geologists, Bulletin 73, p. 1307-1325.

Ehrhart, J., 2016, Speleogenesis and delineation of megaporosity and karst geohazards through geologic cave mapping and LiDAR analyses associated with infrastructure in Culberson County, Texas: unpublished MS thesis, Stephen F. Austin State University, Nacogdoches (TX), 159 p.

Ehrhart, J., and Stafford, K.W., 2021, Speleogenetic model of evaporite occurrences of the Gypsum Plain utilizing karst mapping and LiDAR analyses in Culberson County, Texas, USA, *in* Johnson, K.S., Land, L., and Decker, D.D., eds., Evaporite karst in the greater Permian Evaporite Basin (GPEB) of Texas, New Mexico, Oklahoma, Kansas, and Colorado: Oklahoma Geological Survey, Circular 113.

Forbes, J., Nance, R., 1997, Stratigraphy, sedimentology, and structural geology of gypsum caves in east central New Mexico: Carbonates and Evaporites, Vol. 12, p. 64-72.

Goodbar, A.K., Powers, D.W., Goodbar, J.R., and Holt, R.M., 2020, Karst and sinkholes at Nash Draw, southeastern New Mexico (USA), *in* Land, L., Kromhout, C., and Byle, M., eds, Proceedings of the Sixteenth Multidisciplinary Conference on Sinkholes and the Engineering and Environmental Impact of Karst (first edition): National Cave and Karst Research Institute, Symposium 8, Carlsbad (NM), p. 287-298.

Gulden, B., 2019, World's longest gypsum caves [Internet]: National Speleological Society, Long & Deep Caves [updated 2019 July 1; cited 2020 June 26]. Available from: http://www.caverbob.com/gypcave.htm.

Hill, C.A., 1987, Geology of Carlsbad Cavern and other caves in the Guadalupe Mountains, New Mexico and Texas: New Mexico Bureau of Mines and Mineral Resources, Bulletin 117, 150 p.

Hill, C.A., 1996, Geology of the Delaware Basin, Guadalupe, Apache and Glass Mountains: New Mexico and West Texas: Permian Basin Section-SEPM, Publication 96-39, 480 p.

Hill, C.A., 2003. Intrastratal karst at the WIPP Site, southeastern New Mexico, *in* Johnson, K.S., and Neal, J.T., eds., Evaporite Karst and Engineering/Environmental Problems in the United States: Oklahoma Geological Survey, Circular 109, p. 197-209.

Hiss, W.L., 1973, Capitan aquifer observation well network, Carlsbad to Jal, New Mexico: New Mexico State Engineer, Technical Report 38, 76 p.

Holt, R.M., Powers, D.W., and Lowenstein, T.K., 2006, Halite depositional cycles in the upper Permian Salado Formation, *in* Land, L., Lueth, V., Raatz, B., Boston, P., and Love, D., eds., Caves and Karst of Southeastern New Mexico: New Mexico Geological Society, Guidebook 57, 78-80 p.

Hose, L.D., and Pisarowicz, J.A., eds., 2000. The caves of the Guadalupe Mountains Research Symposium: Journal of Cave and Karst Studies, Vol. 2 (2), 157 p.

Jarvis, T., 2003, The money pit: Karst failure of Anchor Dam, Wyoming, *in* Johnson, K.S., Neal, J.T., eds., Evaporite karst and engineering/environmental problems in the United States: Oklahoma Geological Survey, Circular 109, p. 271-278.

Johnson, K.S., 2008, Gypsum karst problems in constructing dams in the USA: Environmental Geology, Vol. 53, No. 5, p. 945-950.

Johnson, K.S., Collins, E.W., and Seni, S.J., 2003, Sinkholes and land subsidence owing to salt dissolution near Wink, Texas, and other sites in western Texas and New Mexico, *in* Johnson, K.S., and Neal, J.T., eds., Evaporite karst and engineering/environmental problems in the United States: Oklahoma Geological Survey, Circular 109, p. 183-195.

Johnson, K.S., and Wilkerson, J.M., 2013, Gypsum karst causes relocation of proposed Cedar Ridge dam, Throckmorton County, Texas, *in* Land, L., Doctor, D.H., and Stephenson, J.B., eds., Proceedings of the Thirteenth Multidisciplinary Conference on Sinkholes and the Engineering and Environmental Impact of Karst, Carlsbad, New Mexico: National Cave and Karst Research Institute, Carlsbad (NM), Symposium 2, p. 133-139.

Johnson, K.S., Bangsund, W.J., and Hines, N.A., 2013, Gypsum karst and potential risk in siting wind turbines in Blaine County, Oklahoma, *in* Land, L., Doctor, D.H., and Stephenson, J.B., eds., Proceedings of the Thirteenth Multidisciplinary Conference on Sinkholes and the Engineering and Environmental Impact of Karst, Carlsbad, New Mexico: National Cave and Karst Research Institute, Carlsbad (NM), Symposium 2, p. 151-159.

Johnson, K.S., Shoemaker, R.A., Charlton, J., and Parker, C., 2021, Evaporite karst in the Permian Rustler, Salado, and Castile Formations at Red Bluff Dam on the Pecos River, Loving and Reeves Counties, Texas, *in* Johnson, K.S., Land, L., and Decker, D.D., eds., Evaporite karst in the Greater Permian Evaporite Basin (GPEB) of Texas, New Mexico, Oklahoma, Kansas, and Colorado: Oklahoma Geological Survey, Circular 113.

Kelley, V.C., 1971, Geology of the Pecos country, Southeastern New Mexico: New Mexico Bureau of Mines and Mineral Resources, Memoir 24. 78 p.

Kelley, V.C., 1972, Geology of the Santa Rosa area, *in* Kelley, V.C., and Trauger, F.D., eds., East Central New Mexico: New Mexico Geological Society, Guidebook 23, p. 218-220.

Kelley, V.C., Kelley, R.W., 1972, Road log of Santa Rosa, Clines Corners, Encino, Duran, and Vaughn country, *in* Kelley, V.C., and Trauger, F.D., eds., East Central New Mexico: New Mexico Geological Society, Guidebook 23, p. 56-64.

Kim, J.W., Lu, Z., and Kaufman, J., 2019, Evolution of sinkholes over Wink, Texas, observed by high-resolution optical and SAR imagery: Remote Sensing of Environment, 222, p. 119-232.

Kottlowski, F.E., 1985, Shoreline facies of the Yeso Formation in the northern Pedernal Hills, *in* Lucas, S.G., and Zidek, J., eds., Santa Rosa area-Tucumcari region: New Mexico Geological Society, Guidebook 36, p. 167-169.

Gonzalez, R.A., and Woodward, L.A., 1972, Petrology and structure of Precambrian rocks of the Pedernal Hills, New Mexico, *in* Kelley, V.C., and Trauger, F.D., eds., East Central New Mexico: New Mexico Geological Society, Guidebook 23, p. 144-147.

Lang, W.B., 1935, Upper Permian formations of Delaware Basin of Texas and New Mexico. American Association of Petroleum Geologists, Bulletin 19, p. 262-270.

Land, L., 2003, Evaporite karst and regional ground water circulation in the lower Pecos Valley *in* Johnson, K.S., and Neal, J.T., eds, Evaporite karst and engineering/environmental problems in the United States: Oklahoma Geological Survey, Circular 109, p. 227-232.

Land, L., 2009, The impact of hypogenic processes on water resources in the arid southwest: Examples from the lower Pecos region of New Mexico, USA, *in* Stafford, K.W., Land, L., Veni, G., eds., Advances in hypogene karst studies: National Cave and Karst Research Institute, Symposium 1, p. 149-156.

Land, L., 2013a, Geophysical records of anthropogenic sinkhole formation in the Delaware Basin region, southeast New Mexico and west Texas, USA: Carbonates and Evaporites, Vol. 28 (1-2), p. 183-190.

Land, L., 2013b, Evaporite karst in the Permian Basin region of west Texas and southeastern New Mexico: The human impact, *in* Land, L., Doctor, D.H., and Stephenson, J.B., eds., Proceedings of the Thirteenth Multidisciplinary Conference on Sinkholes and the Engineering and Environmental Impact of Karst, Carlsbad, New Mexico: National Cave and Karst Research Institute, Carlsbad (NM), Symposium 2, p. 113-121.

Land, L., 2016, Overview of fresh and brackish water quality in New Mexico: New Mexico Bureau of Geology and Mineral Resources, Open-File Report 583: http://geoinfo.nmt.edu/publications/openfile/downloads/500-599/583/OFR-583_NM_BrackishHR.pdf

Land, L., Lueth, V., Raatz, B., Boston, P., and Love, D., eds, 2006, Caves and Karst of Southeastern New Mexico: New Mexico Geological Society, Guidebook 57, 344 p.

Land, L., and Love, D., 2006, Third Day Road Log, *in* Land, L., Lueth, V., Raatz, B., Boston, P., and Love, D., eds., 2006, Caves and Karst of Southeastern New Mexico: New Mexico Geological Society, Guidebook 57, p. 85-96.

Land, L., and Burger, P., 2008, Rapid recharge events in a karstic aquifer: An example from Lake of the White Roses, Lechuguilla Cave, NM, *in* Yuhr, L., Alexander, E.C. Jr., and Beck, B., eds., Proceedings of the Eleventh Multidisciplinary Conference on Sinkholes and the Engineering and Environmental Impacts of Karst, Tallahassee, Florida: ASCE Geotechnical Special Publication 183, p. 396-403.

Land, L., and Aster, R., 2009, Seismic recordings of an anthropogenic sinkhole collapse, *in* Proceedings of the Symposium on the Application of Geophysics to Engineering and Environmental Problems: Environmental and Engineering Geophysical Society. 2009 Annual Meeting, Fort Worth, Texas, p. 511-519.

Land, L., and Newton, B.T., 2008, Seasonal and long-term variations in hydraulic head in a karstic aquifer: Roswell Artesian Basin, New Mexico: Journal of the American Water Resources Association, Vol. 44, p. 175-191.

Land, L., and Huff, G.F., 2010, Multi-tracer investigation of groundwater residence time in a karstic aquifer: Bitter Lake National Wildlife Refuge, New Mexico, USA: Hydrogeology Journal, Vol. 18, p. 455-472.

Land, L., and Veni, G., 2012, Electrical resistivity surveys of anthropogenic karst phenomena, southeastern New Mexico: New Mexico Geology, Vol. 34 (4), p. 117-125.

Land, L., Cikoski, C.K., and Veni, G., 2018, Sinkholes as transportation and infrastructure geohazards in mixed evaporite-siliciclastic bedrock, southeastern New Mexico, *in* Sasowsky, I.D., Byle, M.J., and Land, L., eds., Proceedings of the Fifteenth Multidisciplinary Conference on Sinkholes and the Engineering and Environmental Impact of Karst, Shepherdstown, WV: National Cave and Karst Research Institute, Carlsbad (NM), Symposium 7, p. 367-377.

Lee, W.T., 1925, Erosion by solution and fill, *in* Contributions to the geology of the United States, 1923-24: US Geological Survey, Bulletin 760C, p. 107-121.

Lee, J., ed., 1996, GYPKAP report volume 3, January 1992-April 1996: Southwestern Region of the National Speleological Society, Alamogordo (NM), 68 p.

Lorenz, J.C., 2006, Assessment of the geological evidence for karst in the Rustler Formation at the WIPP site, *in* Land, L., Lueth, V., Raatz, B., Boston, P., and Love, D., eds., Caves and Karst of Southeastern New Mexico: New Mexico Geological Society, Guidebook 57, p. 243-252.

Love, D.W., Hawley, J.W., Kues, B.S., Adams, J.W., Austin, G.S., and Barker, J.M., 1993, eds., Carlsbad region, New Mexico and West Texas: New Mexico Geological Society, Guidebook 44, 357 p.

Lyford, F.P., 1973, Valley fill in the Roswell-Artesia area, New Mexico: US Geological Survey, Open-File Report 73-163, 26 p.

Milanović, P., 2002, Subsidence hazards as a consequence of dam, reservoir and tunnel construction: International Journal of Speleology, Vol. 31 (1/4), p. 169-180.

Milanović, P., 2011, Dams and reservoirs in karst, *in* van Beynen, P., ed., Karst Management: Springer, Dordrecht, p. 47-73.

Mohammadi, Z., 2007, Hydrogeological uncertainties in delineation of leakage at karst dam sites, Zagros region, Iran: Journal of Cave and Karst Studies, Vol. 69 (3), p. 305-317.

Motts, W.S., and Cushman, R.L., 1964, An appraisal of the possibilities of artificial recharge to ground-water supplies in part of the Roswell Basin, New Mexico: US Geological Survey, Water-Supply Paper 1785, 86 p.

Paine, J.G., Buckley, S.M., Collins, E.W., and Wilson, C.R., 2012, Assessing collapse risk in evaporite sinkhole-prone areas using microgravimetry and radar interferometry: Journal of Environmental and Engineering Geophysics, Vol. 17 (2), p. 75-87.

Palmer, A.N., and Palmer, M.V., 2000, Hydrochemical interpretation of cave patterns in the Guadalupe Mountains, New Mexico: Journal of Cave and Karst Studies, Vol. 62 (2), p. 91-108.

Phillips, R.H., 1987, The prospects for regional groundwater contamination due to karst landforms in Mescalero Caliche at the WIPP site near Carlsbad, New Mexico: unpublished PhD dissertation, University of Oregon, Eugene (OR), 341 p.

Powers, D.W., 1996, Tracing early breccia pipe studies, Waste Isolation Pilot Plant, southeastern New Mexico: A study of the documentation available and decision-making during the early years of WIPP: Sandia National Laboratories, Report SAND94-0991, 53 p.

Powers, D.W., 2003, Jal sinkhole in southeastern New Mexico: Evaporite dissolution, drill holes, and the potential for sinkhole development, *in* Johnson, K.S., and Neal JT, eds., Evaporite Karst and Engineering/Environmental Problems in the United States: Oklahoma Geological Survey, Circular 109, p. 219-226.

Powers, D.W., Lambert, S.J., Shaffer, S.E., Hill, L.R., and Weart, W.D., eds, 1978, Geological characterization report, Waste Isolation Pilot Plant (WIPP) Site, Southeastern New Mexico: Sandia National Laboratories, Report SAND78-1596, Vol. 1-2.

Powers, D.W., and Owsley, D., 2003, Field survey of evaporite karst along New Mexico Highway 128 realignment routes, *in* Johnson, K.S., and Neal, J.T., eds., Evaporite Karst and Engineering/Environmental Problems in the United States: Oklahoma Geological Survey: Circular 109, p. 233-240.

Powers, D.W., Beauheim, R.L., Holt, R.M., and Hughes, D.L., 2006, Evaporite karst features and processes at Nash Draw, Eddy County, New Mexico, *in* Land, L., Lueth, V., Raatz, B., Boston, P., and Love, D., eds., Caves and Karst of Southeastern New Mexico: New Mexico Geological Society, Guidebook 57, p. 253-266.

Robinson, T.W., and Lang, W.B., 1938, Geology and ground-water conditions of the Pecos River valley in the vicinity of Laguna Grande de la Sal, New Mexico: New Mexico State Engineer, 12th and 13th Biennial Reports, p. 79-100.

Robison, D.M., 2015, Successful Foundation Preparations in Karst Bedrock of the Masonry Section of Wolf Creek Dam, *in* Doctor, D.H., Land, L., and Stephenson, J.B., eds., Proceedings of the Fourteenth Multidisciplinary Conference on Sinkholes and the Engineering and Environmental Impact of Karst, Rochester, Minnesota: National Cave and Karst Research Institute, Carlsbad (NM), Symposium 5, p. 595-604.

Rogers, J.D., 2015, Hales Bar and the pitfalls of constructing dams on karst, *in* Doctor, D.H., Land, L., and Stephenson, J.B., eds., Proceedings of the Fourteenth Multidisciplinary Conference on Sinkholes and the Engineering and Environmental Impact of Karst, Rochester, Minnesota: National Cave and Karst Research Institute, Carlsbad (NM), Symposium 5, XIV.

Scholle, P.A., 2003, Geologic map of New Mexico: New Mexico Bureau of Geology and Mineral Resources, scale 1:500,000.

Scholle, P.A., Goldstein, R.H., and Ulmer-Scholle, D.S., 2004, Classic upper Paleozoic reefs and bioherms of west Texas and New Mexico: New Mexico Institute of Mining and Technology, 166 p.

Silver, B.A., Todd, R.G., 1969, Permian cyclic strata, northern Midland and Delaware Basins, west Texas and southeastern New Mexico. American Association of Petroleum Geologists, Bulletin, Vol. 53, p. 2223-2251.

Stafford, K.W., 2006, Gypsum karst of the Chosa Draw area, *in* Land, L., Lueth, V., Raatz, B., Boston, P., and Love, D., eds., Caves and Karst of Southeastern New Mexico: New Mexico Geological Society, Guidebook 57. p. 82-83.

Stafford, K.W., Rosales-Lagarde, L., and Boston, P.J., 2008, Castile evaporite karst potential map of the Gypsum Plain, Eddy County, New Mexico and Culberson County, Texas: A GIS methodological comparison: Journal of Cave and Karst Studies, Vol. 70 (1), p. 35-46.

Stafford, K.W., Brown, W.A., Ehrhart, J.T., Majzoub, A.F., and Woodard, J.D., 2017, Evaporite karst geohazards in the Delaware Basin, Texas: Review of traditional karst studies coupled with geophysical and remote sensing characterization: International Journal of Speleology, Vol. 46 (2), p. 169-180.

Stafford, K.W., and Shields, J., 2021, Speleogenetic evolution of Castile karst manifestations of the Delaware Basin, west Texas and southeastern New Mexico, *in* Johnson, K.S., Land, L., and Decker, D.D., eds., Evaporite karst in the greater Permian Evaporite Basin (GPEB) of Texas, New Mexico, Oklahoma, Kansas, and Colorado: Oklahoma Geological Survey, Circular 113.

Sweeting, M.M., 1972, Karst and solution phenomena in the Santa Rosa area, New Mexico, *in* Kelley, V.C., and Trauger, F.D., eds., East Central New Mexico: New Mexico Geological Society, Guidebook 23, p. 168-170.

Theis, C.V., 1938, Origin of water at Major Johnson Springs near Carlsbad, New Mexico: New Mexico State Engineer, 12th-13th Biennial Reports, 1934-1938, p. 251-252.

Trauger, FD., 1972, Ground water in east-central New Mexico, *in* Kelley, V.C., and Trauger, F.D., eds., East Central New Mexico: New Mexico Geological Society, Guidebook 23, p. 201-207.

UNESCO. 2020, World heritage list [internet]. Paris (FR): United Nations Educational, Scientific and Cultural Organization [UNESCO]. [cited 2020-07-22]. Available from: https://whc.unesco.org/en/list/

US Bureau of Reclamation, 1957, Summary of geological material, terminal storage for the Carlsbad project: US Bureau of Reclamation, Project Development Division, Albuquerque Project Office, open-file report, May 1957, 55 p.

Vine, J.D., 1963, Surface geology of the Nash Draw quadrangle, Eddy Co., New Mexico: US Geological Survey, Bulletin 1141-B, 46 p.

Ward, R.F., Kendall, C.G., and Harris, P.M., 1986, Upper Permian (Guadalupian) facies and their association with hydrocarbons – Permian Basin, west Texas and New Mexico: American Association of petroleum Geologists, Bulletin, Vol. 70, p. 239-262.

Weart, W.D., 1983, Summary evaluation of the Waste Isolation Pilot Plant (WIPP) site suitability: Sandia National Laboratories, Report SAND83-0450, 31 p.

Weart, W.D., Rempe, N.T., and Powers, D.W., 1998, The Waste Isolation Pilot Plant: Geotimes, October, 1998.

Weber, R.H., and Kottlowski, F.E., 1959, Gypsum resources of New Mexico: New Mexico Bureau of Mines and Mineral Resources, Bulletin 68, 68 p.

Welder, G.E., 1983, Geohydrologic framework of the Roswell Ground-Water Basin, Chaves and Eddy Counties, New Mexico: New Mexico State Engineer, Technical Report 42, 28 p.

Geophysical Characterization of Playa Lakes in the Gypsum Karst of Southeastern New Mexico, USA

David D. Decker
Southwest Geophysical Consulting, LLC, Albuquerque, New Mexico

Lewis Land
National Cave and Karst Research Institute, Carlsbad, New Mexico

Barbara Luke
University of Nevada, Las Vegas, Las Vegas, Nevada

ABSTRACT.—Southeastern New Mexico is host to many karst features, including caves, swallets, sinkholes, solution tubes, and springs, which are at risk of compromise by ongoing petroleum extraction. Playa lakes are shallow depressions found on gypsum bedrock in southeastern New Mexico and west Texas, and on Quaternary alluvial gravels in eastern New Mexico. These depressions are curious in that some of them are obviously linked to underground conduits via surface openings, whereas others have no such connections. These features could be cover-collapse sinkholes that have filled in with Quaternary windblown alluvium and soil, or they could be solutionally formed via pooling of rainwater, dissolution of the gypsum and re-precipitation as the water evaporates, and subsequent deflation of the unconsolidated gypsum by wind. In this study, we use field observations and three complimentary geophysical methods (ground penetrating radar, electrical resistivity imaging, and surface-wave seismic) to make inferences about the subsurface structure of these depressions and their relationship to the karst features located in and around them. The speleogenetic model that we develop from the data indicates that these playa lakes could well be karst features, as opposed to surface hydrologic features, and therefore should be treated the same way as other karst features in the region when determining the routing of linear infrastructure and the placement of resource-extraction-related pads and ponds.

INTRODUCTION

Background

Playa lakes are shallow, usually dry depressions found in soils above gypsum bedrock in the Delaware Basin in southeastern New Mexico and west Texas (Rustler and Castile Formations), the back-reef facies of the Guadalupe Reef as far north as Vaughn and Santa Rosa, New Mexico (Seven Rivers Formation), and even on Quaternary alluvial gravels in eastern New Mexico (Ogallala Formation). Many of these shallow depressions are only visible because they either host an abundance of salt-tolerant plant life or, in some cases, no plant life at all. These depressions are curious in that some of them are obviously linked to underground conduits (caves) via surface openings (swallets), whereas others have no such features (Figure 1).

The Delaware Basin and back-reef facies of the Capitan Reef escarpment are currently undergoing rapid infrastructure build-up as petroleum exploration, discovery, and exploitation escalate. It is necessary to determine if these features provide pathways from the surface to the aquifer, and if so, to make a case for avoiding them, if possible, during pipeline and well-pad construction, road building, power-line installation, and other infrastructure development (Bureau of Land Management, 2015). Many karst features are already known in the region, including caves, swallets, cover-collapse sinkholes, caprock-collapse sinkholes, solution tubes, and springs. Currently, the recommended buffer for these

Decker, D. D.; Land, L.; and Luke, B., 2021, Geophysical Characterization of Playa Lakes in the Gypsum Karst of Southeastern New Mexico, USA, *in* Johnson, K. S.; Land, Lewis; and Decker, D. D. (eds.), Evaporite Karst in the Greater Permian Evaporite Basin (GPEB) of Texas, New Mexico, Oklahoma, Kansas, and Colorado: Oklahoma Geological Survey, Circular 113, p. 79-92.

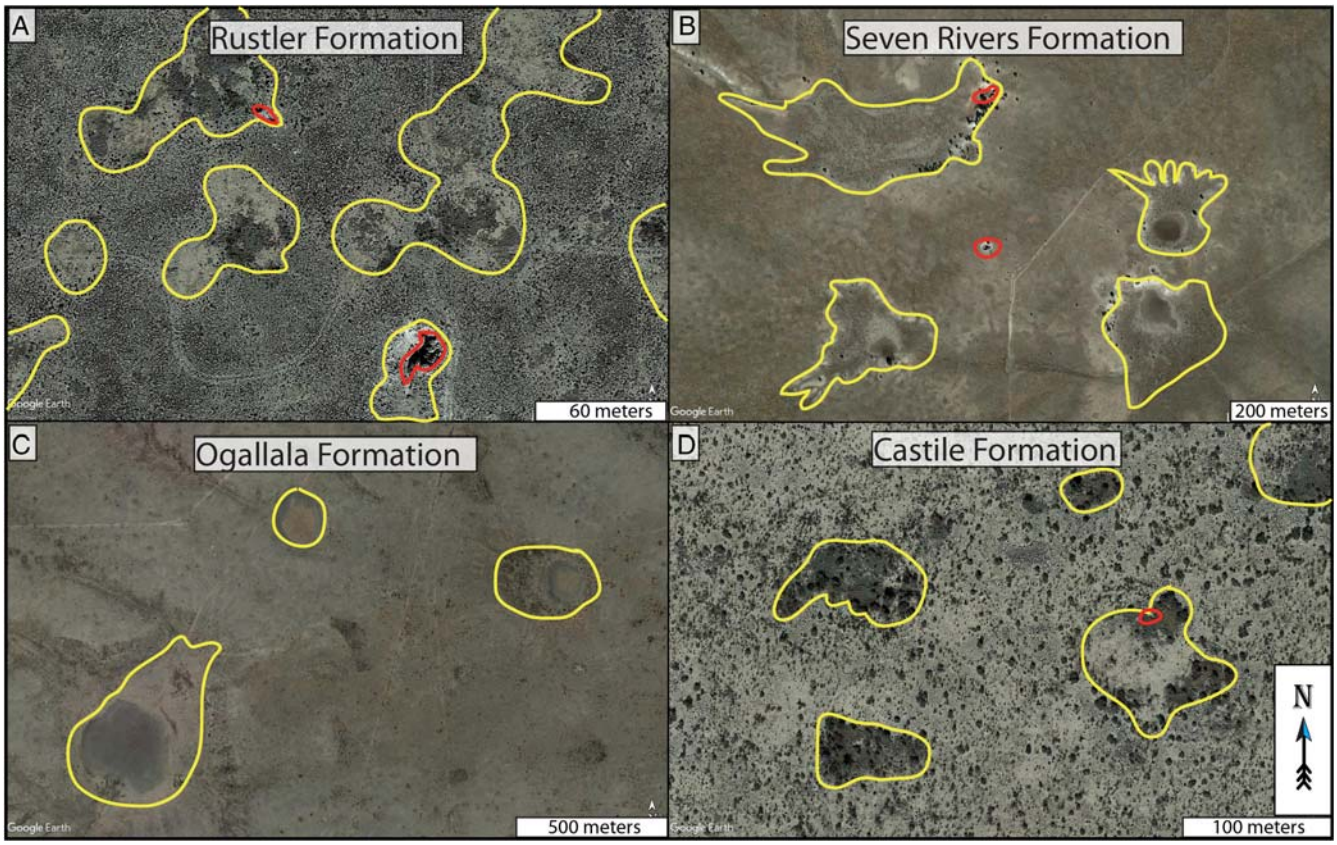

Figure 1. A. Playa lakes in the Rustler Formation (yellow outline). Several have no obvious outlet. The one on the upper left has a 2-m-diameter swallet on the eastern edge (red outline). The one in the lower right has a 4-m-diameter cave opening. B. Four playa lakes in the Seven Rivers Formation. Three of the six have no obvious outlet, whereas the fourth has a 2.5-m-diameter swallet on the eastern edge. Additionally, a 3-m-diameter sinkhole is located centrally to all four depressions. C. Three playa lakes in the Ogallala formation. None of the playa lakes in the Ogallala Formation are known to have karst features associated with them. D. Five playa lakes in the Castile Formation. Four have no karst features associated with them, the fifth has a 1-m-wide swallet in the northern edge. Notice that all of the karst features associated with a playa lake are on the perimeter.

features is determined by the likelihood of a spill or other contamination making its way to the aquifer. This buffer is currently set at 50 m for smaller karst features, or those with clogged conduit, and 200 m for larger karst features or those with open conduit (Rybacki, 2017—personal communication). What is not known is how, or even if, the playa lakes are linked to these karst features and why they are so closely associated spatially. If we find that these playa lakes should be considered karst features, rather than surface hydrologic or aeolian deflation features as some suggest, then they should be given the same buffer as other karst features in the region when determining the routing of linear infrastructure and the placement of infrastructure pads and ponds.

For this study, we chose two playa lakes with no visible outlets and a known cave that are located in the Burton Flats area (Figure 2), approximately 26 km northeast of Carlsbad, New Mexico, to conduct ground penetrating radar (GPR), electrical resistivity imaging (ERI), and multichannel analysis of surface waves (MASW) seismic surveys. We used the known cave as a baseline (the control) for all three geophysical methods, and then we ran identical surveys over nearby playa lakes with no associated surface features to see if there was an identifiable relationship between the playa lakes and other karst features. A secondary goal, to determine the depth to which the playa lakes extend beneath the surface, was not realized but is anticipated in a future study.

Study Area

Location and Land Ownership

The study area is a 65-hectare region selected for its numerous swallets, caves, sinkholes, and playa lakes. This area is in the Burton Flats, 26 km northeast of Carlsbad, New Mexico (Figure 2), specifically in the SE SW and SW SW quarter of section 28 and the NE NW and NW NW quarter of section 33 of T19S, R29E.

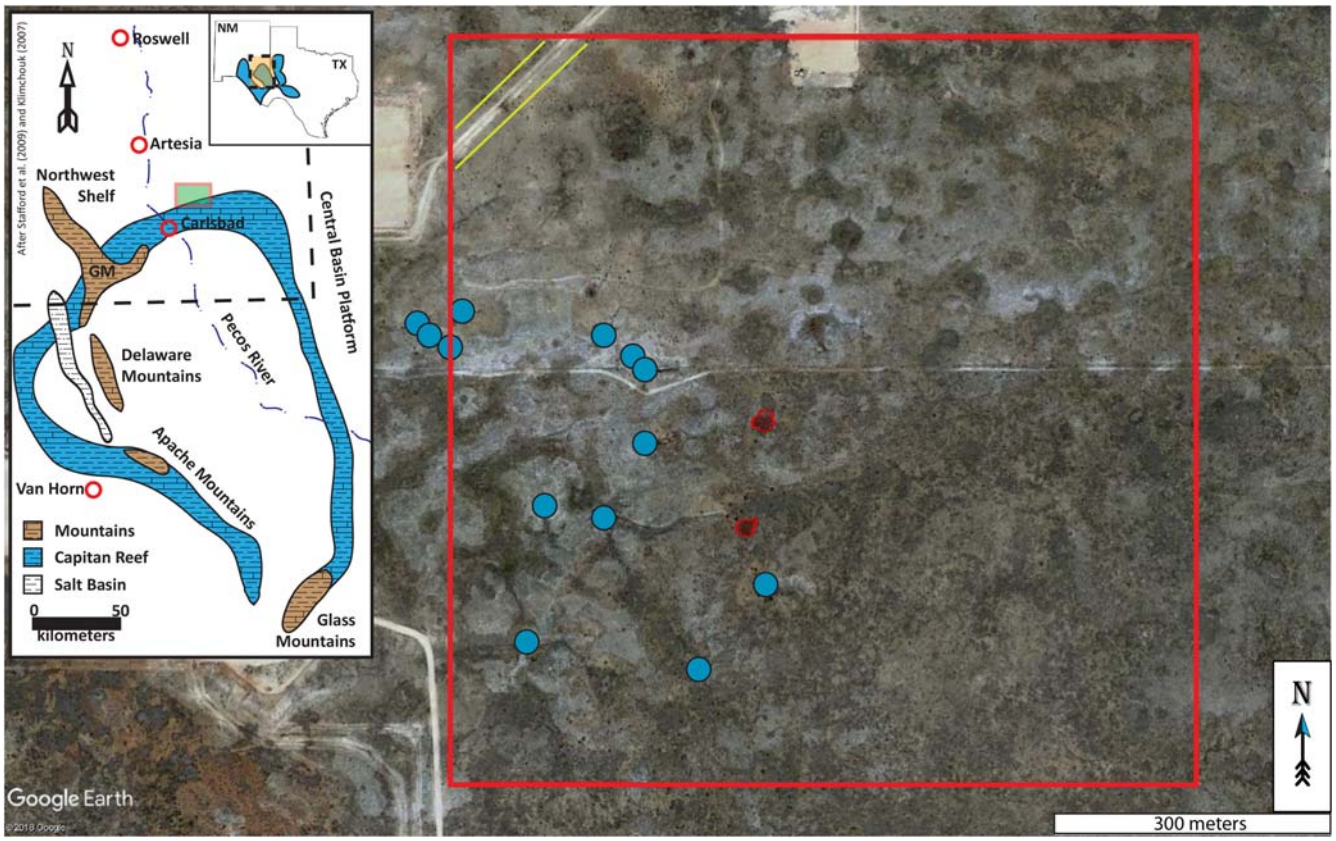

Figure 2. Study area (red square). The relationship of the study area to Carlsbad, New Mexico is shown on the regional map as a green square outlined in red. Numerous cave entrances and swallets (blue dots) and playa lakes exist in this region (playa lakes chosen for the study are highlighted in transparent red polygons). Parallel yellow lines in the northwest of the image highlight the pipeline mentioned in the text.

The land ownership of the area under study is Bureau of Land Management—Carlsbad Field Office (BLM-CFO) managed lands (36.5 hectares, southern 56%) and New Mexico State Land Office managed lands (28.5 hectares, northern 44%), with the demarcation line being the east-west two-track road near the center of Figure 2.

Land Use

The Burton Flats are presently used for cattle grazing by local ranchers, petroleum production by several large oil companies, and potash mining, predominantly by the Intrepid Potash Corporation. There are several abandoned ranch homes in the area, suggesting that historically the area was more heavily used for cattle grazing prior to the proliferation of fossil fuel extraction. There are currently only two occupied residences in the Burton Flats, neither of which are within the study area. There are numerous active well pads nearby, as well as buried pipelines that traverse the area in the far northwest corner (Figure 2). This specific area was selected for the study to minimize interference and the introduction of artifacts from radio frequency noise, pipelines, and previously disturbed soils. In the 1940s and 1950s, Burton Flats were used by the Army Airforce as a bombing range. There are two documented sites within the Burton Flats that contain practice target ranges and a third, undocumented site (Decker, 2019) that appears to have been a live-ammunition dump. Prehistoric artifacts have been found within the Burton Flats and there are several archaeological sites within the region suggesting use by Native Americans for hunting and gathering.

Terrain and Geology

The terrain of the Burton Flats area consists of gently rolling hills, flatlands, and occasional cliffs. The area has numerous caves, sinkholes, swallets, and other minor karst features (currently over 1000 documented features [Decker, 2019; Atkinson, 2018; Belski, 2018 (personal communication)]), all aligned from southwest to northeast along the dominant lineament trend in the region; this includes the playa lakes (Figure 3). The major rock types in the area are the gypsum, dolomite, and minor sandstones of the upper Permian Rustler Formation, an evaporite facies that was deposited during the Lopingian Epoch (Ochoan Series, 259–251 Ma) (Powers and others, 1999; Sewards and others, 1991).

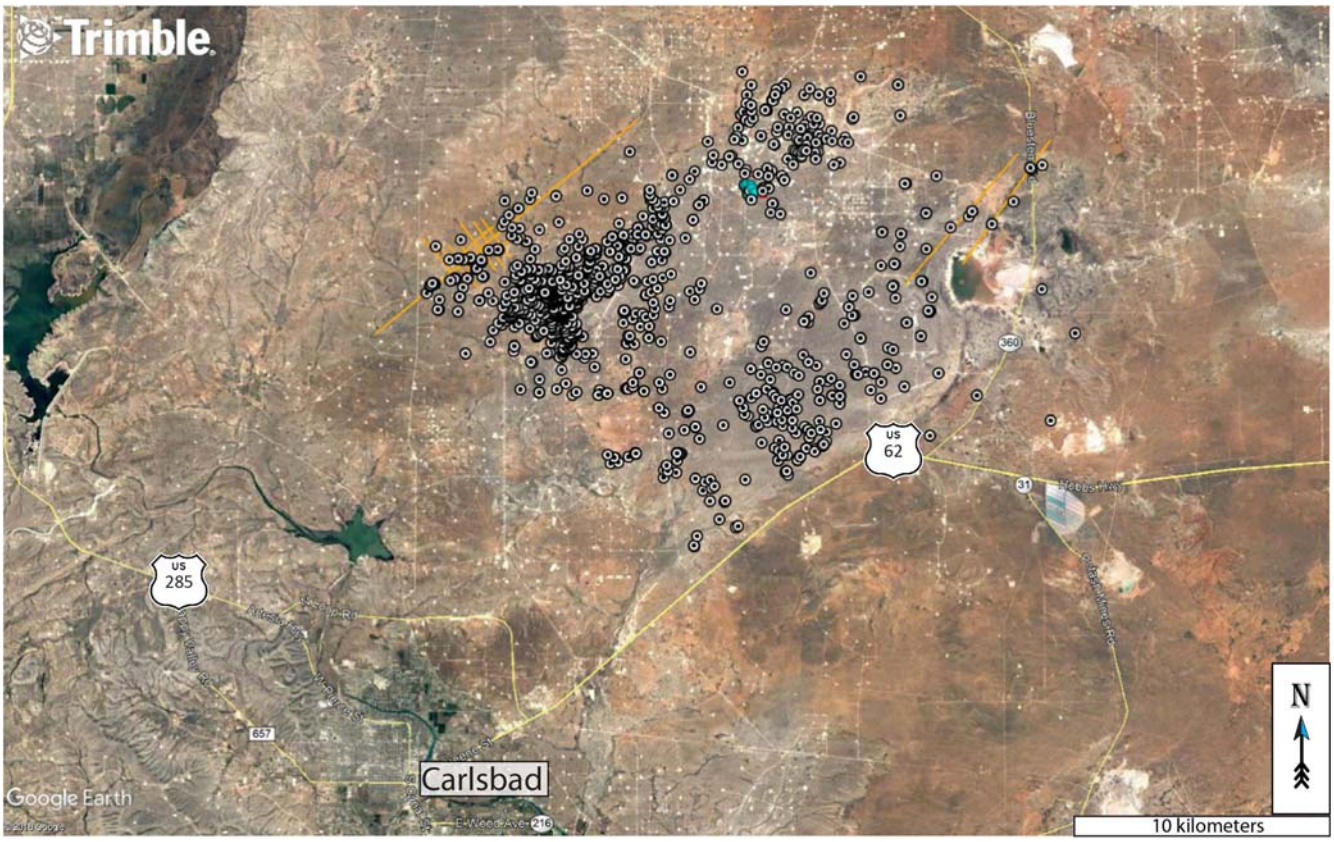

Figure 3. Karst feature distribution. Black and white dots are known or suspected karst features including caves, sinkholes, and swallets. Orange lines are tectonic lineaments. Field area is the blue triangle in the upper-central portion of the image. Note the tremendous number of white squares throughout the background image. These are all well pads, central tank batteries, or other fossil fuel extraction-related infrastructure. Background image: Google Earth. Image date: December 30, 2016. Image datum: WGS-84.

The Rustler Formation consists, in descending order, of the Forty-Niner member (gypsum), the Magenta Dolomite, the Tamarisk member (gypsum), the Culebra Dolomite, and the Los Medaños member (halitic, gypsiferous siliciclastics) (Goodbar, 2013; Powers and others, 1999). Both the Magenta Dolomite and the Culebra Dolomite host shallow aquifers (Holt, 1997). In the study area, the local dip is to the southwest.

Caves in the Burton Flats are generally formed in the Magenta Dolomite with horizontal entrances in blind arroyos. Occasionally, a caprock-collapse sinkhole opens directly into cave passage. These sinkholes are generally not associated with the playa lakes, whereas the blind arroyos, horizontal cave entrances, and swallets are nearly always on the edges of these playa lakes (Figures 1, 4). Some playa lakes in the region also exhibit small (usually less than 1 m diameter and 50 cm deep) closed swallets at or near the center of the playa lake in soil. A nearby area that has had the surface soils removed for installation of an impoundment pond exposed solutionally enlarged fractures, small conduits, and other epikarst features (Figure 4E). The Rustler Formation is underlain by the Permian Salado Formation, which is predominantly halite and is mined in this area by the Intrepid Potash Corporation. Numerous abandoned "wildcatter" drill holes are found throughout the Burton Flats which may intercept the Salado Formation, allowing fresh meteoric water to infiltrate and dissolve the halite.

METHODS

Ground Penetrating Radar

Ground penetrating radar reflection profiles are created by the reflection of radar energy from interfaces that are created by differences in the dielectric constant between two types of material (e.g., rock and air), or differences in water saturation levels within similar materials (Conyers, 2014). These reflection profiles are interpreted based on knowledge of the local geology, amount of recent rainfall in the area of interest, and other factors specific to the study. Depth of investigation and resolution are determined by several factors including, but not limited to, the center frequency of the antenna, soil moisture, and rock type.



Figure 4. Karst features (Decker, 2019). A and B—Caprock-collapse sinkholes. C and D—Horizontal cave entrances on the edges of playa lakes. E—Solution tube exposed by bulldozer (pole is 1.3 m in length for scale).

A Geological Survey Systems Incorporated, D400HS 350 MHz, hyperstacking antenna, and SIR-4000 control unit were used to image the top 2 m of the subsurface. A Juniper Systems Geode submeter global positioning system was used to georeference the radar profiles collected. Radar controller settings for the GPR were: 95 scans per second, 512 samples per scan, and 32 bits per sample. A dielectric constant (Ɛ) of 14 was chosen based on the soil type (moist gypsite) at the survey location, and a scan window of 55.4 nanoseconds was used, giving a survey depth of 2.2 m. A 10-m-long odometer calibration and a site-specific initialization were performed prior to collecting the radar reflection profiles. A boxcar background removal filter set at 513 scans was used to remove horizontal radar reflections because our target was void space and irregular subsurface reflections. The software used for post data processing was RADAN-7 version 7.5.18.02270. During processing, a high-pass filter of 175 MHz and a low-pass filter of 740 MHz were used to filter out low and high frequency background noise, respectively. A logarithmic 8-point range gain was used to enhance signal strength at depth.

Electrical Resistivity Imaging

Electrical resistivity (ER) surveys are a common and effective geophysical method for detection of subsurface voids (e.g., Land and Veni, 2012; Land, 2013; Land and Asanidze, 2015; Land and others, 2018). The basic operating guideline for an ER survey involves generating a direct current between two metal electrodes implanted in the ground, while measuring the ground voltage between two other implanted electrodes. Given the current flow and voltage drop between the electrodes, differences in subsurface electrical resistivity can be determined and mapped. Modern resistivity surveys employ an array of multiple electrodes connected with electrical cable. Over the course of a survey, pairs of electrodes are activated by means of a switchbox and resistivity meter. The depth of investigation for a typical ER survey is approximately one-fifth the length of the array of electrodes.

Resistivity profiles illustrate vertical and lateral variations in subsurface resistivity. The presence of water or water-saturated ground will strongly affect the results of a resistivity survey by indicating a low resistivity zone. Air-filled caves or air-filled pore space provide a

distinctive high resistivity signature, since air has near-infinite resistivity, in contrast with the 10–15 orders of magnitude more conductive surrounding bedrock.

An Advanced Geosciences, Inc. SuperSting R8/IP electrical resistivity system provided by the National Cave and Karst Research Institute was used to collect resistivity data, employing a dipole–dipole array configuration. All of the ER surveys conducted at Burton Flats for this project used a 56-electrode array at 2-m electrode spacing, for a target depth of investigation of approximately 23 m.

A Topcon GR3 GPS instrument package was used to collect survey-grade GPS coordinates for each electrode. Elevation data collected during these surveys were used to correct the resistivity data for variations in topography. Electrical resistivity data were processed and inverted using EarthImager2D™ software. The EarthImager software chooses a resistivity scale unique to each inversion, designed to highlight natural conditions in the subsurface; thus, resistivity profiles from a given survey area may not have the same resistivity scale.

Multichannel Analysis of Surface Waves

The seismic testing followed the MASW method (Miller and others 1999; Park and others 1999; Xia and others 1999). A surface-coupled linear array of geophones recorded ground vibrations generated in line with the sensors by a vertical impact source. The response is dominated by Rayleigh-type surface waves, whose amplitudes are greatest at the ground surface near the source and decay with depth and with distance from the source. The wave transmission and decay pattern from each source impact are analyzed in the frequency domain using processes of forward modeling and inversion to infer a vertical layered profile of shear-wave velocity in the subsurface. This one-dimensional profile is assigned spatially to the center point of the geophone group analyzed. The measurement is duplicated, shifting source and sensor sets incrementally along the array so that the individual layered velocity profiles can be merged to create a two-dimensional vertical slice depicting shear-wave velocity beneath the array. Time-history data were collected using a system provided by the University of Nevada, Las Vegas that included a Geometrics Geode-based seismograph with 72 4.5-Hz vertical geophones coupled to the ground with spikes. The geophones were spaced 1.5 m apart to create a 106.5-m-long array. A source consisting of a rubber-band assisted weight-drop type, trailer-mounted piston. Analysis was in roll-along mode, using 24-trace gathers and 6-m offset of source to nearest sensor. The source was advanced in 3-m increments. All processing of the time histories, to include frequency-domain conversion, dispersion curve selection, inversion, and interpolation to develop the final shear-wave velocity image, was completed using commercial software SurfSeis v.6 (Kansas Geological Survey).

Only one seismic array could be completed in the time available because of the time- and labor-intensive nature of the data gathering, inclement weather (high winds and heavy rain), and equipment issues both related and unrelated to the weather.

RESULTS

The control for this study was Owl Cave, which is located on the west side of a small playa lake at the end of a 36-m-long blind arroyo. The entrance room of the cave is 5 m wide, 12 m deep, and 6 m tall (Figure 5). A 0.5-m-diameter hole in the floor drops into a lower level which, according to the map (Figure 6), corkscrews down to a mud-floored room before pinching out. The roof of the entrance room is only 1.5–2 m beneath the surface at a point 1 m from the dripline. This location was chosen to maximize the returns from the GPR since it was not expected to see more than 2–2.5 m deep. At this location, the soil was less than 5 cm in depth; gypsum bedrock composed the remainder.

Two playa lakes were chosen for the study, both in close proximity to Owl Cave. The first (PL-01) was located 130 m east-northeast of Owl Cave. PL-01 is 1 m deep and 23 m across at the location of the survey. The second (PL-02) was located 140 m southeast of Owl Cave. Topographically, this playa lake was barely visible at approximately 5–10 cm deep and was discernable more by change in vegetation than its depth. PL-02 was 25 m across at the location of the measurements.

Ground Penetrating Radar

This study was conducted at the beginning of the local monsoon season; therefore, the ground was wet but not saturated. This condition provided the opportunity for a larger than normal difference in dielectric constant between wet soils ($14 < \varepsilon < 30$) and cave passage ($\varepsilon = 1$, that of air). The processed GPR data for Owl Cave show negative amplitude reflections directly above the cave as well as 20 m to the east, and another negative amplitude reflection 60 m to the west (Figure 7). These negative amplitude reflections indicate a change in dielectric constant from high to low, and in this case are consistent with changes in radar wave velocity from moist gypsum to air. However, since the noise floor is between 1 and 1.5 m in depth, we are likely only seeing the very top of the cave or just the air-filled fractures directly above the cave roof rather than the cave itself. Further to the east, the radar energy is highly attenuated by moist soil and clay in the bed of the small playa lake that feeds Owl Cave.

At PL-02, there were high amplitude, negative radar reflections just outside of and along the edges of the



Figure 5. Owl Cave entrance room. Dr. Lewis Land (left panel) and field assistants Michael Jones and David Brumbaugh (both panels) for scale. Left panel view is to the southwest. Right panel view is to the north.

playa lake (black and white reflections) that might indicate fractured rock. Lower amplitude returns (yellow) indicate a change in dielectric and most likely are where the moisture from the recent rains has infiltrated into the subsurface. This same moisture response is seen within the playa lake, along with minor attenuation of the signal because of clay and soil.

Ground penetrating radar survey was not conducted over PL-01 because of the amount of vegetation and the local topographic relief.

Electrical Resistivity

High resistivity anomalies may represent either air-filled void space in the subsurface (caves or potential sinkholes) or brecciated/leached zones in gypsum bedrock with air-filled pore space (Land and Asanidze, 2015). Laterally continuous layers of high or low resistivity may reflect near-surface stratigraphy, such as gypsum or dolomite beds (generally higher resistivity), or mudstone/shale layers (lower resistivity). Very near-surface low resistivity layers may indicate water-saturated fine-grained sediment accumulated in surface depressions. In the case of Owl Cave, both of the void spaces that underlie the array show up unequivocally, along with another possible cave to the west. The low resistivity clays of the Owl Cave playa lake are visible just to the east at ground level (BF-1, Figure 8, upper panel).

PL-02 (BF-2 in Figure 8, lower panel) also shows the low resistivity clay-rich playa floor along with what we interpret as a possible fluid flow channel along the edges and fractured or brecciated rock beneath, based on resistivity values that are high (22,000 Ohm-m), but not as high as Owl Cave (100,000 Ohm-m). We see a similar pattern, less pronounced, and with lower overall resistivity contrasts at PL-01 (Figure 9, upper panel). Results show a possible fluid flow conduit along the western edge as well as the very low resistivity clays of the playa

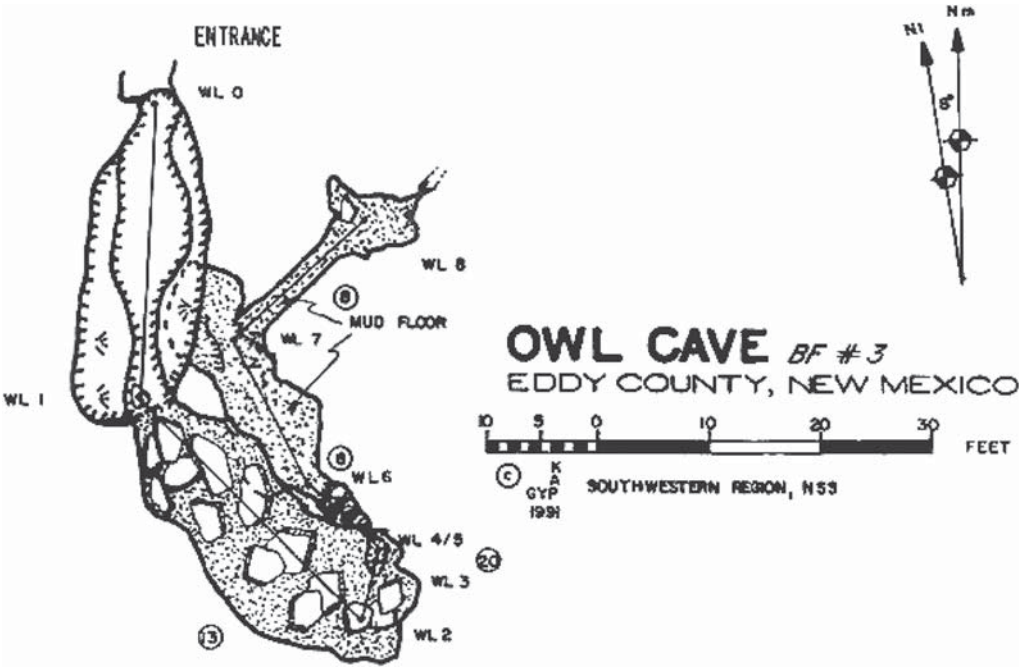

Figure 6. Owl Cave (Knapp, 1991). When overlain on the satellite imagery (see Fig. 13) the upper-level passage wraps around the outer edge of the playa lake, whereas the lower passage trends linearly along the dominant regional tectonic fractures.

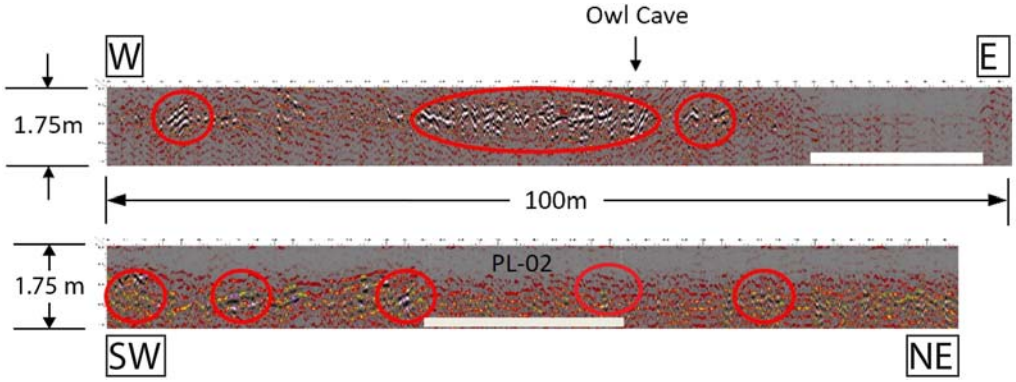

Figure 7. Radar reflection profiles. Upper panel is over Owl Cave. Lower panel is over PL-02. Red ellipses indicate high-amplitude, negative reflections. White bar on the bottom of each panel indicates the extent of the playa lake associated with that radar transect.

lake. We also ran a resistivity line along the surface in an area that had no known karst features or playa lakes (Figure 9, lower panel). Here we saw the locally southwest dipping gypsum beds and no evidence for voids or for fluid flow paths.

Multichannel Analysis of Surface Waves

Results from the seismic testing over PL-02 are shown in Figure 10. Twenty-five vertical shear-wave velocity profiles developed at 3-m spacing were interpolated to generate the single image which represents 72 m laterally and ~30 m vertically. The top surface was adjusted before interpolation to reflect topography. Velocities range from about 200 to 800 m per second, with higher values appearing in isolated patches at depth.

Shear-wave velocities are representative of material stiffness and density. Layered soil and rock strata associated with undisturbed sedimentary deposition and subsequent weathering would present a similarly layered shear-wave velocity image, following the dip of the strata. The image beneath the playa lake does not follow this pattern. Instead, it shows distinctly lower velocity directly beneath the surface depression, extending to ~3–6 m deep. Velocities increase to about 700 m per second at about 10 m depth. Beneath that depth are seen

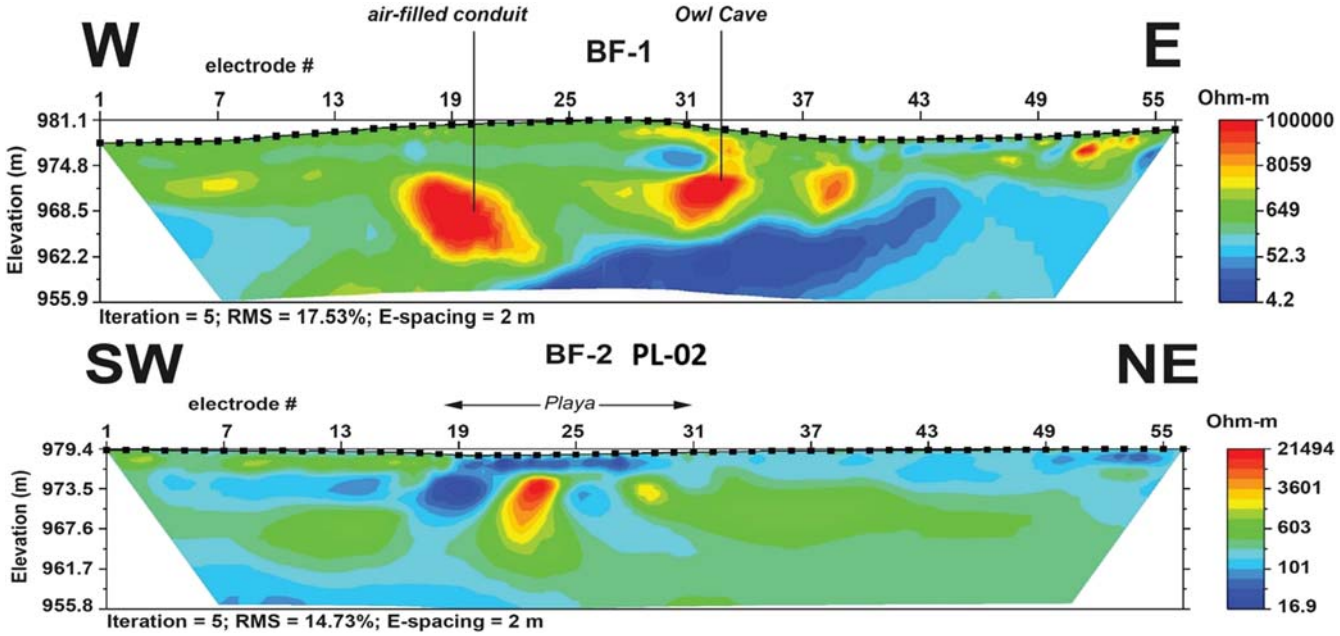

Figure 8. Upper panel: resistivity line BF-1 over Owl Cave. Lower panel: resistivity line BF-2 over PL-02. Notice that the color scales are different.

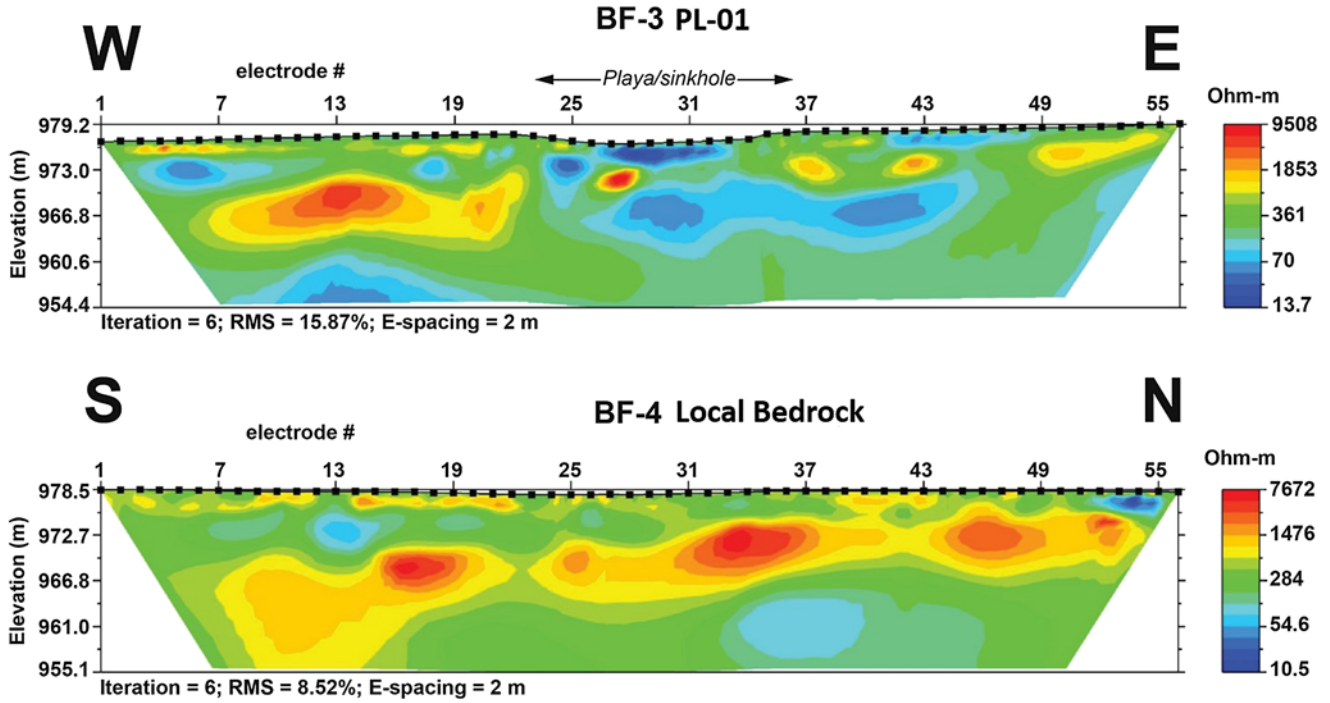

Figure 9. Upper panel: resistivity line BF-3 over PL-01. Lower panel: resistivity line BF-4 over local bedrock with no karst features. Notice that the color scales are similar, but not the same. The panels show the strata dipping gently toward the southwest.

lateral velocity fluctuations consistent with disturbed ground, possibly broken rock and uncemented matrix associated with rock stoping/brecciation. The highest velocities in the image appear beyond the edges of the playa, perhaps beyond the zone of disturbance from a breccia pipe. However, the velocity fluctuations are not limited to the zone directly adjacent to the playa.

When interpreting the results of a surface-wave survey, one should bear in mind that confidence is highest at shallow depths, where the wave energy concentrates,

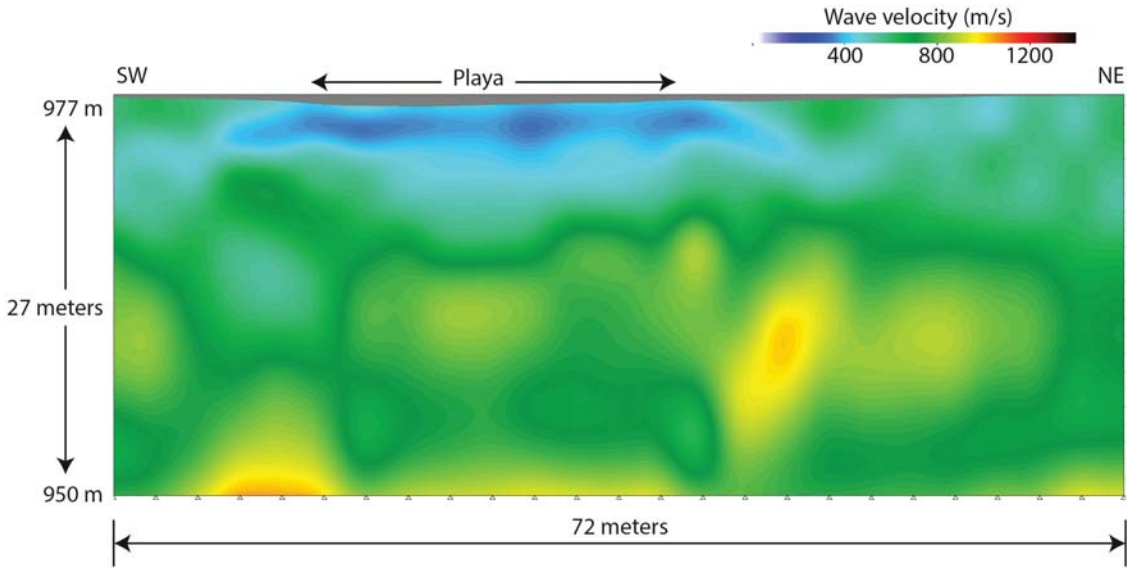

Figure 10. MASW results over PL-02.

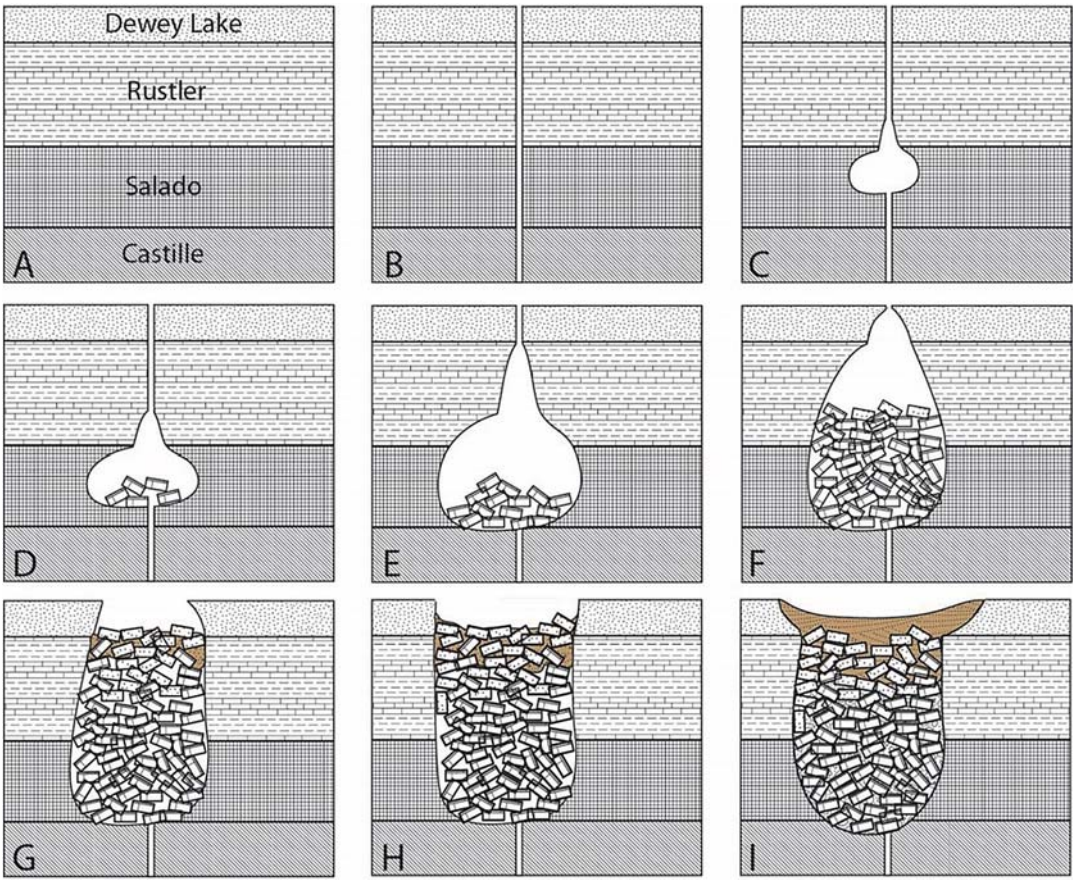

Figure 11. Hypothesis 1. Progression of sinkhole development. A: Prekarst formation. B: Fracture or drill hole allows fresh meteoric water to penetrate to the Salado Formation. C: Dissolution of halite begins. D–F: Stoping occurs. G: Void breaches surface forming sinkhole. H: Windblown deposits begin to fill brecciated sinkhole. I: Playa lake forms. Not shown: secondary voids begin to form along and within the brecciated edge of the playa lake.

and away from the ends of the array, where data density declines.

DISCUSSION

We consider two hypotheses for the formation of these playa lakes. In the first (Figure 11), playa lakes are formed by dissolution at depth, possibly as deep as the Salado Formation. Voids are formed by this dissolution and stope to the surface, where the newly created breccia pipes are slowly infilled by aeolian and biological processes. Fractures formed by the collapse of the surface allow water infiltration, which dissolves conduits and voids in the gypsum bedrock along the edges of the playa lakes forming the caves and swallets during a secondary speleogenetic episode. In this case, we would expect the geophysical data to show a demarcation between the edge of the breccia pipe and the surrounding strata.

In the second hypothesis (Figure 12), playa lakes are solutionally formed via pooling of rainwater in terrain-induced topographic low areas. Dissolution of gypsum at the surface within these areas begins when meteoric water undersaturated in gypsum pools in these low spots and is re-precipitated as a gypsite powder as the water evaporates. Subsequent deflation of the unconsolidated gypsum by wind occurs, thereby preferentially making the area available for more rainwater collection, enhancing the process. As dissolution at the surface progresses, voids and conduits already present in the subsurface are truncated by the edges of the playa lake as it grows deeper. In this case, we would expect to see no boundary between the playa lake proper and the surrounding strata, nor any brecciated material directly underneath.

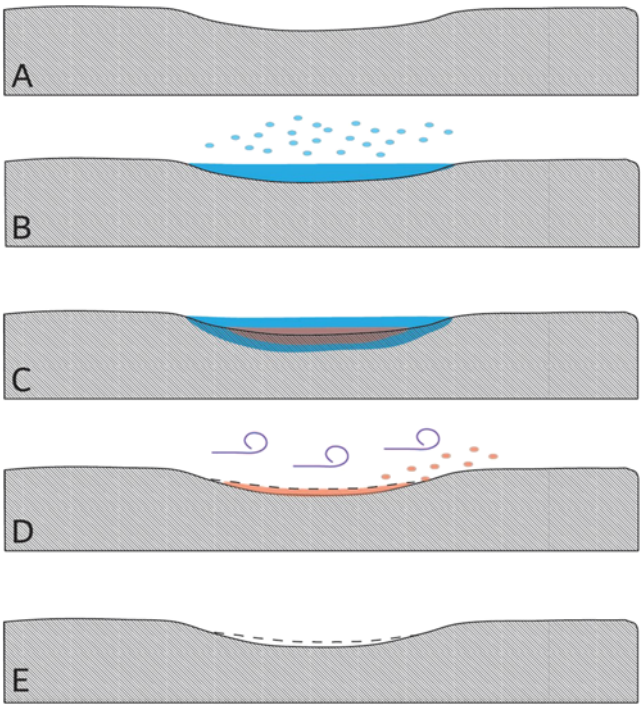

Figure 12. Hypothesis 2. A: Slight topographic depression in gypsum bedrock. B: Meteoric water fills the depression. C: Dissolution of gypsum (orange) occurs. D: As water evaporates or drains, gypsum is deposited as crust or dust and is deflated by wind. E: The depression becomes deeper (original surface denoted by dashed line). Not shown: voids already present in the subsurface are truncated by the growing depression. Note: Unlike in hypothesis 1, there is no boundary beneath the playa lake.

When the results of the ERI and GPR data over Owl Cave are studied, the void spaces (and fractures above them) stand out prominently, as do the clay-filled portions of the associated playa lake. Alignment of the resistivity and radar profiles with the satellite imagery and superimposed cave map (Figure 13) clearly demonstrates that mapped voids in the subsurface coincide with resistivity and radar anomalies. The playa lake at the east end of both profiles displays as low resistivity and attenuated radar energy, as expected. We conducted postprocessing of the ERI and GPR data before the cave map became available to us; thus, the passage to the east of the main conduit was unknown when the postprocessing was done. This serendipitous sequence of events provided excellent ground truth for the study area.

When the results of all three methods are compared for PL-02 (Figure 14), consistent features are evident throughout all three profiles. In the resistivity profile, high resistivity areas that are interpreted as fractures exist near the edges of the playa lake (orange bars in Figure 14). Low resistivity areas near the surface are verified clay-rich soil, whereas those that trend downward from the surface of the playa lake are interpreted to be hydrologic conduits that funnel water into the subsurface. This same set of features can be seen in the PL-01 resistivity profile (Figure 9, upper panel). In the radar reflection profile, the tops of these same features can be seen as negative amplitude radar returns. This is most likely caused by air- or soil-filled fractures. At the surface of the playa lake, mild attenuation is occurring, consistent with the clay-rich soil. In the seismic shear-wave velocity profile, areas of low wave speed (blue) are consistent with the shallow fine-grained soils at the surface depression of the playa, and areas of high velocity (yellow) are consistent with undisturbed bedrock outside of the playa and discrete breakdown blocks beneath the playa (Figure 14).

Based on these results, we propose the following model for the formation of a playa lake: Dominant southwest to northeast tectonic trends in the region provide pathways for meteoric water to percolate through the subsurface to the Salado Formation, where it dissolves the soluble bedrock forming a void. This void then stopes upward forming a breccia pipe through the Rustler

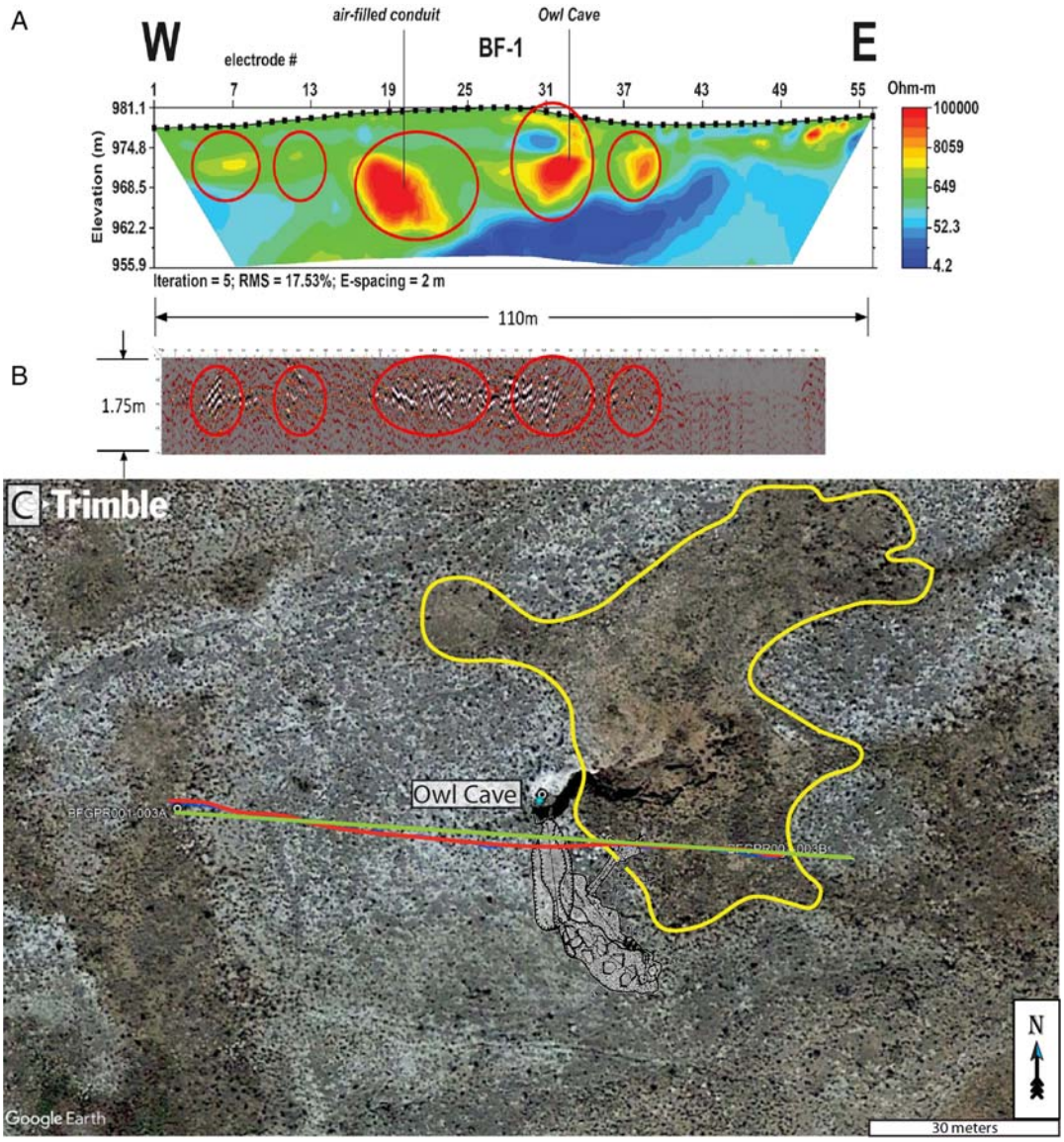

Figure 13. Resistivity versus radar versus Owl Cave map. The ERI profile (green line) is 110 m in length (vertical scale exaggerated 2.2:1) and the GPR profile (red line) is 100 m in length. The vertical scale on the GPR image is highly exaggerated (63:1). The presence of the lower passage was unknown to the authors prior to conducting the geophysical surveys. Cave map overlays from Knapp (1991).

Formation which, if it reaches the surface, creates a caprock-collapse sinkhole. This sinkhole fills in through time with aeolian sediment and locally derived soils forming the playa lake. Concurrently, the fracture rim and breccia beneath the surface of the playa lake act as highly permeable pathways, rapidly diverting water that collects in the playa lake to the subsurface along preferential flow paths, creating a secondary speleogenetic event. Since gypsum is easily dissolved in fresh water [$K_{sp} = 4.93 \times 10^{-5}$ versus limestone $K_{sp} = 3.36 \times 10^{-9}$; Lide (2000)], these preferential flow routes enlarge along the outside edges of the playa lake relatively quickly from the surface downward. Eventually the conduit breaks through to the tectonic fractures and allows the meteoric water to begin to dissolve the gypsum along these trends. Our review of maps of nine out of ten of the known caves within the study area (Figure 2) supports this model.

Our results do not support the second hypothesis involving surface deflation, in that there are clearly subsurface structural anomalies evident in the results of all three methods. This is not consistent with a model in which there has been no disturbance of the bedrock below the playa lakes.

Our findings indicate that these playa lakes should be considered as part of the karst feature catalog and treated as such when planning for future development in the

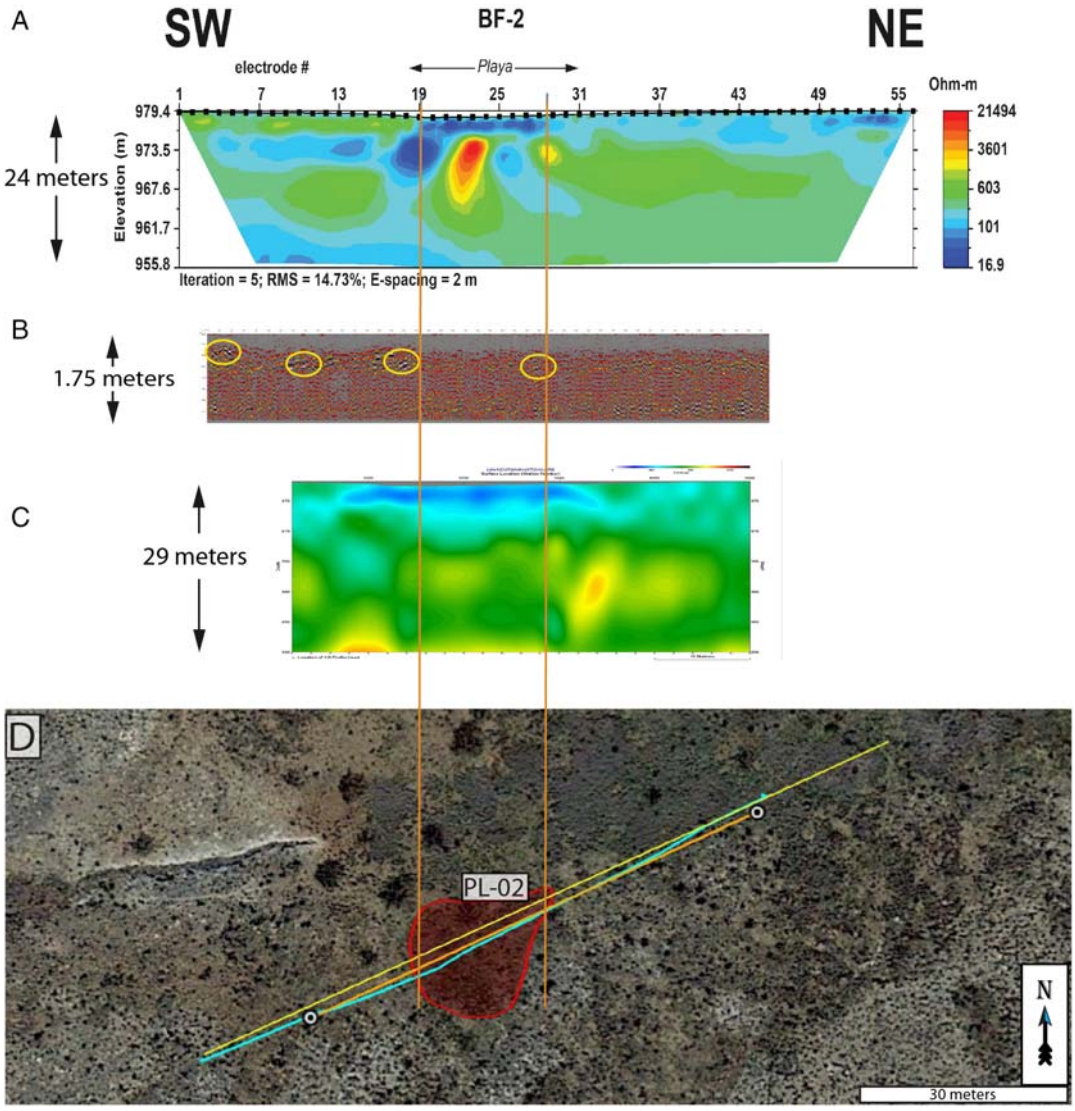

Figure 14. PL-02 resistivity, radar, and seismic comparison. The ERI profile (yellow line) is 110 m in length (no vertical exaggeration), the GPR profile (blue line) is 90 m in length (vertical scale exaggerated 63:1), and the MASW profile (orange line) is 72 m in length (no vertical exaggeration). The red transparent area on the satellite image shows the location of the playa lake.

Burton Flats and other areas of gypsum bedrock that support these features. Future planned research includes at least one of the authors visiting the interior of the caves within the study area to verify the maps and gain further insight into the formation of these karst features. Additionally, six pseudo three-dimensional resistivity surveys are planned south of the original study area where the BLM-CFO is considering implementing an Area of Critical Environmental Concern (ACEC). This ACEC contains numerous small caves, swallets, and playa lakes. Each survey area will cover approximately 3.6 hectares and extend to between 30 and 50 m in depth. Ground truth of these results will include drilling selected high resistivity areas to test for the existence of voids.

SUMMARY

Three complimentary geophysical methods were used in this study. Results indicate distinct boundaries around, and the possibility of fractured rock beneath, the two playa lakes studied.

We interpret our results to indicate the soft soils of the playa lake, disturbed bedrock, and possible minor void spaces (fractures). High resistivity areas in the ERI image for PL-02 correspond to highly reflective (negative amplitude) areas in the GPR image and low shear-wave velocity regions in the seismic image (all of which are consistent with geologic disturbance below the playa lake). Low resistivities and low velocities along the outside edge of the playa lake may indicate hydrologic

conduits. These interpretations are consistent with the fractured perimeter and collapse rubble described in the caprock-collapse sinkhole hypothesis which would indicate that the playa lakes in this study are karst related and should be protected accordingly.

ACKNOWLEDGEMENTS

We wish to thank the organizations that provided monetary support, including the Robertson Association, the National Speleological Society, and the Cave Conservancy Foundation. Additionally, we wish to thank the organizations that provided material and personnel support, including the National Cave and Karst Research Institute, the University of Nevada, Las Vegas, the Sandia Grotto of the National Speleological Society, and Southwest Geophysical Consulting, LLC.

REFERENCES CITED

Atkinson, G., 2018, unpublished data, New Mexico Cave Survey Database.

Bureau of Land Management, 2015, Cave and karst resources management: BLM Manual H-8380-1, Denver, CO, 59 p.

Conyers, L.B., 2014, Interpreting ground penetrating radar for archaeology: Routledge Press, 220 pp.

Decker, D.D., 2019, unpublished data, Southwest Geophysical Consulting, LLC, Cave and Karst Survey Database.

Goodbar, J.R., 2013, Solution mining and the protection of karst groundwater supplies in Burton Flats, southeast New Mexico, USA, *in* Land, L., and Joop, M., eds., 20th National Cave and Karst Management Symposium: National Cave and Karst Research Institute, Carlsbad (NM), p. 13-18.

Holt, R.M., 1997, Conceptual model for transport processes in the Culebra Dolomite Member, Rustler Formation: Sandia National Laboratories, SAND97-0194, p. 162.

Knapp, R., 1991, Burton Flats – Area #1, *in* Belski, D., ed., Gypsum Karst Project, Vol. 2, p. 37-39.

Land, L., 2013, Geophysical records of anthropogenic sinkhole formation in the Delaware Basin region, southeast New Mexico and west Texas, USA: Carbonates and Evaporites, Vol. 28 (1-2), p. 183-190.

Land, L., and Asanidze, L., 2015, Roll-along resistivity surveys reveal karstic paleotopography developed on near-surface gypsum bedrock, *in* Doctor, D.H., Land, L., and Stephenson, J.B., eds., Proceedings of the Fourteenth Multidisciplinary Conference on Sinkholes and the Engineering and Environmental Impact of Karst, Rochester, Minnesota: National Cave and Karst Research Institute, Carlsbad (NM), Symposium 5, p. 365-370.

Land, L., Cikoski, C.K., and Veni, G., 2018, Sinkholes as transportation and infrastructure geohazards in mixed evaporite-siliciclastic bedrock, southeastern New Mexico, *in* Sasowsky, I.D., Byle, M.J., and Land, L., eds., Proceedings of the Fifteenth Multidisciplinary Conference on Sinkholes and the Engineering and Environmental Impact of Karst, Shepherdstown, WV: National Cave and Karst Research Institute, Carlsbad (NM), Symposium 7, p. 367-377.

Land, L., and Veni, G., 2012, Electrical resistivity surveys of anthropogenic karst phenomena, southeastern New Mexico: New Mexico Geology, Vol. 34 (4), p. 117-125.

Lide, D.R., 2000, Handbook of chemistry and physics: CRC Press, Vol. 81, Ch. 8, p. 112.

Miller, R.D., Xia, J., Park, C.B., and Ivanov, J.M., 1999, Multichannel analysis of surface waves to map bedrock: The Leading Edge, Vol. 18 (12), p. 1392-1396.

Park, C., Miller, R.D., and Xia, J., 1999, Multi-channel analysis of surface waves: Geophysics, Vol. 64 (3), p. 800-808.

Powers, D.W., and Holt, R.M., 1999, The Los Medaños Member of the Permian (Ochoan) Rustler Formation: New Mexico Geology, Vol. 21, No. 4, p. 97-103.

Sewards, T., Glenn, R., and Keil, K., 1991, Mineralogy of the Rustler Formation in the WIPP-19 Core: Sandia National Laboratories, SAND87-7036, p. 98.

Xia, J., Miller, R.D., and Park, C.B., 1999, Estimation of near-surface shear-wave velocity by inversion of Rayleigh waves: Geophysics, Vol. 64 (3), p. 691-700.

Determining Annual to Decadal Subsidence Areas and Rates Using Airborne Lidar, GPS Surveys, and Topographic Maps at the Wink Sinkholes, West Texas

Jeffrey G. Paine, Lucie Costard, John Andrews, Aaron Averett, Kutalmis Saylam, and John Hupp
Bureau of Economic Geology, Jackson School of Geosciences,
The University of Texas at Austin, Austin, Texas

ABSTRACT.—Data from repeat airborne lidar topographic surveys, differential GPS surveys, satellite radar interferometry, and older topographic maps suggest that rapid land subsidence has been occurring for many years near two large (100- to 200-m diameter) sinkholes that formed in 1980 and 2002 in the Hendrick Oil Field near Wink, Texas. The sinkholes and surrounding subsiding area overlie Permian bedded evaporite strata on the Central Basin platform on the eastern margin of the Delaware Basin. Early investigations using interferograms constructed from synthetic aperture radar data acquired in 2007 and 2008 with the Advanced Land Observation Satellite PALSAR L-band satellite-borne instrument identified local areas that were subsiding at rates reaching 26 cm/yr. These results focused ground-based microgravity surveys on areas where subsidence was occurring to identify where shallow mass deficits exist that would increase the likelihood of future subsidence or collapse. We have quantified ongoing and longer term elevation change by comparing (1) digital elevation models (DEMs) constructed from a high-resolution airborne lidar survey flown in 2013 with lower resolution DEMs constructed from U.S. Geological Survey photogrammetry-derived elevations from 1968; (2) differential GPS measurements acquired during a 2015 microgravity survey with 2013 lidar-derived baseline elevations; and (3) elevations determined from a second airborne lidar survey in 2017 with those determined from the 2013 lidar survey. These comparisons reveal that total subsidence reaches 8.8 m over 45 years in some areas. Maximum net rates of subsidence measured on the decadal time scale are about 20 cm/yr. Differential GPS-derived elevations measured in 2015 were as much as 0.91 m lower than 2013 lidar-derived elevations, yielding maximum subsidence rates of 61 cm/yr. Elevation loss between the 2013 and 2017 airborne lidar surveys is as great as 2.8 m over nearly four years, yielding net rates as high as 73 cm/yr. These recent rates are similar to those determined from radar interferometry in other studies and are higher than the maximum decadal-scale rates, although the decadal rates could have been higher if subsidence began after 1968 or if rates have varied over time.

INTRODUCTION

Sinkholes are a common geologic hazard in many parts of the world (e.g., Beck, 1995; Johnson and Neal, 2003; Bell and others, 2005). In Texas, sinkholes are associated with dissolution of bedded Paleozoic salt beneath the High Plains of the Texas panhandle and within the Permian basins of western Texas, limestone in central Texas, and shallow salt domes of eastern Texas and the coastal plain (Fig. 1). Several geophysical and remote-sensing methods, including satellite radar interferometry (InSAR), microgravity surveying, airborne lidar topographic surveying, and differential GPS measurements, offer noninvasive approaches to assessing sinkhole collapse risk by determining areal extent and rates of ground subsidence, identifying shallow mass deficits that could cause continued gradual subsidence or sudden collapse, and characterizing surficial features

Paine, J. G.; Costard, Lucie; Andrews, John; Averett, Aaron; Saylam, Kutalmis; and Hupp, John, 2021, Determining Annual to Decadal Subsidence Areas and Rates Using Airborne Lidar, GPS Surveys, and Topographic Maps at the Wink Sinkholes, West Texas, *in* Johnson, K. S.; Land, Lewis; and Decker, D. D. (eds.), Evaporite Karst in the Greater Permian Evaporite Basin (GPEB) of Texas, New Mexico, Oklahoma, Kansas, and Colorado: Oklahoma Geological Survey, Circular 113, p. 93-103.

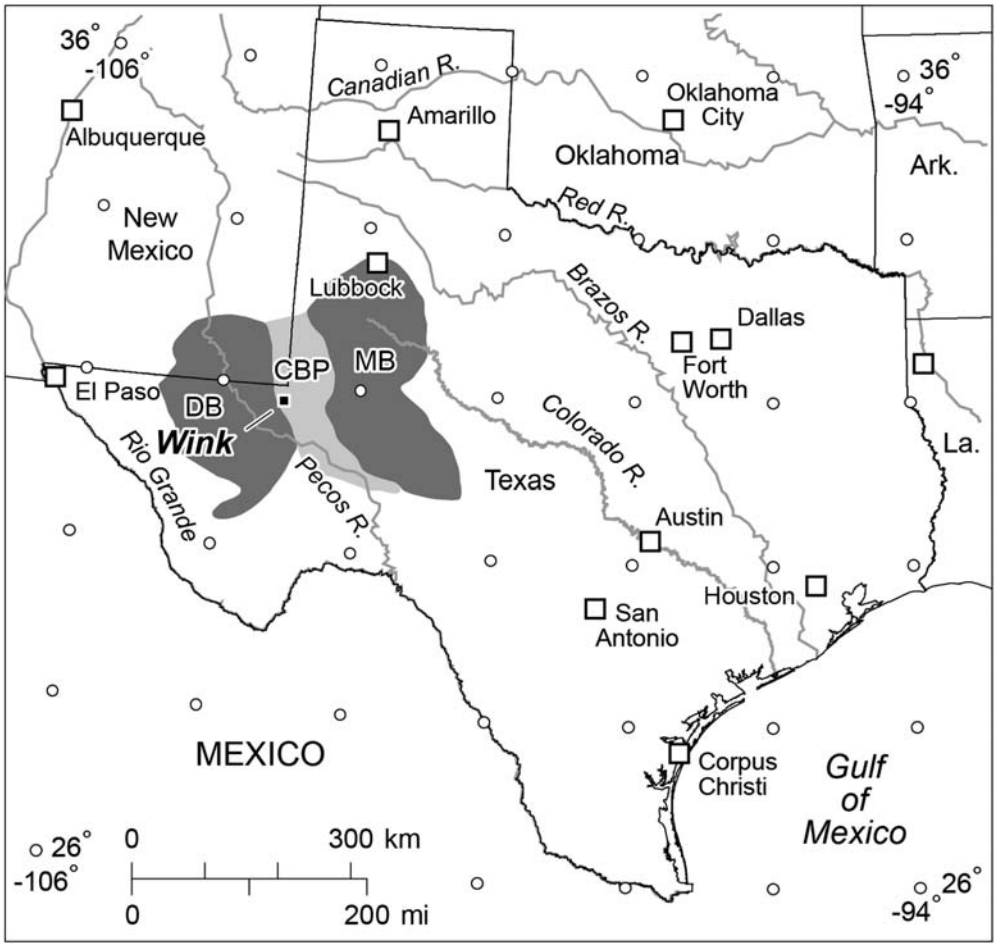

Figure 1. Map showing the location of the Wink sinkhole area, western Texas. Structural features in the Permian basin include the Central Basin platform (CBP), the Midland Basin (MB), and the Delaware Basin (DB).

related to sinkhole formation. In this study, we built upon earlier subsidence studies in the vicinity of Wink, Texas (Fig. 1), that relied upon radar interferometry to identify currently subsiding areas and microgravity surveys to identify areas underlain by shallow mass deficits (Paine and others, 2012). This study employs repeat airborne lidar surveys and GPS measurements to ascertain ground movement on the years scale and compares recent elevation models with 1968 topography to estimate decadal-scale topographic change.

WINK SINKHOLES, PERMIAN BASIN

Two large sinkholes formed in June 1980 (Wink Sink 1) and May 2002 (Wink Sink 2) near the community of Wink (Fig. 1) in the Permian basin of western Texas (Baumgardner and others, 1982; Johnson, 1989; Collins, 2000; Johnson and others, 2003; Paine and others, 2012). These sinkholes formed in the Hendrick Oil Field (discovered in 1926) at the western margin of the Central Basin platform above the Permian Capitan Reef complex, which underlies Permian interbedded salt and anhydrite at depths of 400 to 670 m. Wink Sink 1, formed on June 3, 1980, measured 110 m across and 34 m deep at the time of collapse. Over time, it has expanded to an approximately circular outline that is 94–117 m across (as of 2018) and is elongated to the northeast-southwest. The sinkhole outline encircles the Hendrick No. 10-A, a 780-m-deep well that was drilled in 1928, produced oil from the Tansill and Yates formations below the salt section, and was abandoned in 1964 (Baumgardner and others, 1982). Flow of unsaturated water from above or below the salt section, possibly through natural or induced fractures or the borehole itself, is cited as the most likely cause of salt dissolution and collapse at Wink Sink 1 (Baumgardner and others, 1982; Johnson and others, 2003). Wink Sink 2 formed 1.6 km south of Wink Sink 1 on May 21, 2002. This sinkhole has expanded from its original surface width of 137 m to an oval shape with widths ranging from 225 to 250 m (as of 2018) and also elongated in the northeast-southwest direction. Both Wink sinkholes have an elongation ratio of 1.1 to 1.2. Wink Sink 2 encircles the Gulf WS-8, a water-supply well that was drilled through the

salt section to 1092 m in 1960 and is estimated to have yielded 800 million bbl of water for waterflood operations in the Hendrick Field (Johnson and others, 2003). The cause of collapse at Wink Sink 2 has not been established with certainty, but is thought to be related to the WS-8 well (Johnson and others, 2003). Both sinkholes are partly filled with water. Lidar data acquired in 2013 indicate that the water level is about 26 m below the land surface at Wink Sink 1 and about 28 m below the land surface at Wink Sink 2. Recent work suggests that ongoing subsidence in the area is partly influenced by seasonal changes in groundwater levels (Kim and others, 2016) and freshwater migration downward through fissures (Kim and Lu, 2018; Kim and others, 2019).

METHODS

The repeat lidar surveys, GPS measurements, and historical elevation data acquired and analyzed in this study extend early work at Wink (Paine and others, 2012) using satellite-based InSAR to identify subsiding areas and microgravity surveys to identify shallow mass deficits. InSAR measures centimeter-scale surface motion toward or away from the radar instrument. The ability to obtain viable InSAR deformation measurements depends on how surface radar scattering properties vary over time. For the previous study, we processed Advanced Land Observation Satellite (ALOS, launched by the Japanese Space Agency in January 2006) PALSAR (polarimetric L-band) data to produce radar interferograms spanning the time period from January 2007 to November 2008 (22 months). The ALOS satellite ceased operating in April 2011. Its successor, ALOS II, launched in May 2014.

Historical topographic data were obtained from 1/3 arc-second digital elevation models (DEMs) produced by the U.S. Geological Survey (USGS) for the Wink area using photogrammetric methods from photographs acquired in 1968. The resulting DEM has 10 × 10 m grid cells.

Airborne lidar data were acquired in November 2013 and August 2017 using a Chiroptera airborne lidar instrument (Airborne Hydrography AB) to produce high-resolution DEMs. The November 2013 survey covered 30 km^2 at a flight height of 460 m, a laser pulse rate of 280 kHz, and an average ground-point density of 13 m^{-2}. The August 2017 survey covered 33 km^2 at a flight height of 500 m, a laser pulse rate of 200 kHz, and an average point density of 16 m^{-2}. For both surveys,

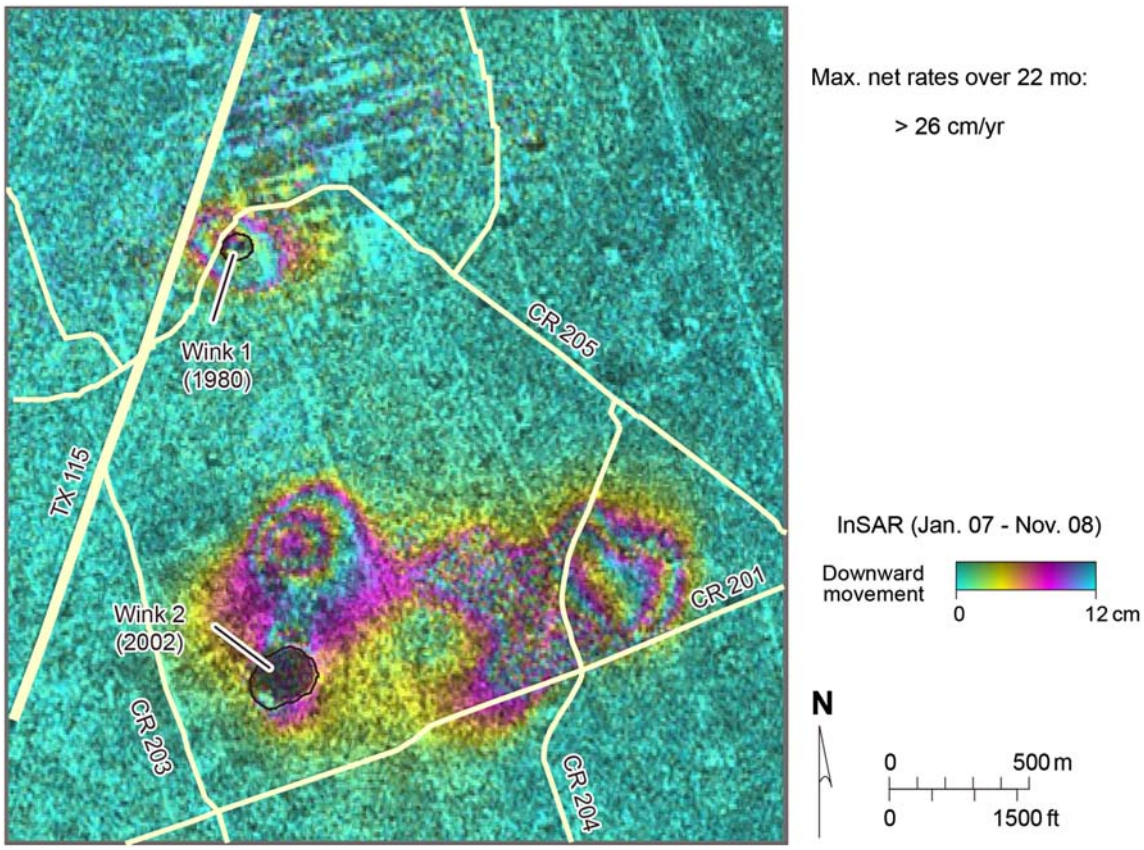

Figure 2. InSAR interferogram showing net ground movement and maximum rate of movement between January 2007 and November 2008 (22 months) constructed from ALOS L-band radar data (Paine and others, 2012).

GPS data from survey-area base stations and nearby Continuously Operating Reference Stations were combined with aircraft-based GPS and inertial navigation-system data to produce highly accurate instrument trajectories that, when combined with laser orientation and travel-time information, allowed determination of absolute surface reflection positions accurate to within a few cm. Laser returns were binned to produce high-resolution DEMs of the area using a 1 × 1 m cell size.

Differential GPS-derived elevations were acquired along microgravity survey lines in May 2015 using a Trimble NetR9 base station and a Trimble R8 rover. Data were collected at 40-m intervals along the microgravity lines.

SHORT-TERM (MONTHS) SUBSIDENCE RATES FROM RADAR INTERFEROMETRY

We used InSAR during early work at Wink to detect recent vertical movement over a large area surrounding the 1980 and 2002 sinkholes. InSAR results focused more intensive field, geophysical, and subsurface investigations on areas that showed evidence of recent subsidence. A representative radar interferogram of the Wink area, constructed from satellite-based radar data acquired on January 1, 2007 and November 23, 2008, depicts the net change in surface elevation between those two dates (Fig. 2). Areas of notable subsidence are evident on an enlarged part of the interferogram in the vicinity of Wink Sinks 1 and 2. Subsidence areas generally match those determined from previous leveling surveys conducted by industry representatives and from a 1999 reconnaissance topographic profile surveyed with an optical level before the collapse of Wink Sink 2 (Collins, 2000; Johnson and others, 2003). Maximum net subsidence rates for the 22-month period exceed 26 cm/yr. Recent intensive InSAR-based work using high repeat frequency C-band radar data from the Sentinel-1A (launched in April 2014) and Sentinel-1B (launched in April 2016) satellites, and higher frequency X-band radar data from the terraSAR-X satellite (launched June 2010) (Kim and others, 2016; Kim and Lu, 2018; Kim and others, 2019) have further clarified the areas and rates of recent subsidence (at maximum rates exceeding 50 cm/yr), established the dominantly vertical component of elevation change, and have postulated factors affecting subsidence including improperly plugged wells, cracks in cement well casings, downward migration of fresh water through fissures, and drought.

ANNUAL TO DECADAL RATES FROM LIDAR SURVEYS

Two airborne lidar surveys have been flown in the Wink area to examine longer term (years to decades) subsidence in the Wink area. Lidar surveys produce two main products: point clouds (with associated x-, y-, and z-coordinates) that represent the absolute location of laser reflection points on the ground surface (Fig. 3a), and DEMs constructed by binning all points within each grid cell to produce a high-resolution elevation model of the survey area (Fig. 3b). The first lidar survey was flown in November 2013 to examine morphology of the sinkholes and other subsiding areas, establish a topographic baseline for future monitoring, and provide an areally extensive elevation data set to support determining longer term subsidence through comparison with topographic data from the 1960s. The second lidar survey was flown in August 2017 to quantify ground movement over the nearly four years that had elapsed since the 2013 survey.

The DEM constructed from the 2013 lidar survey depicts a land surface that generally slopes from north to south, with a prominent topographic ridge that extends southward along the western edge of Wink Sinks 1 and 2 (Fig. 4). Local topographic lows are found at and near both sinkholes within two extensive subsiding areas identified from the 2007–2008 InSAR data. A third InSAR anomaly, located in the southern part of the survey area, has no associated topographic depression.

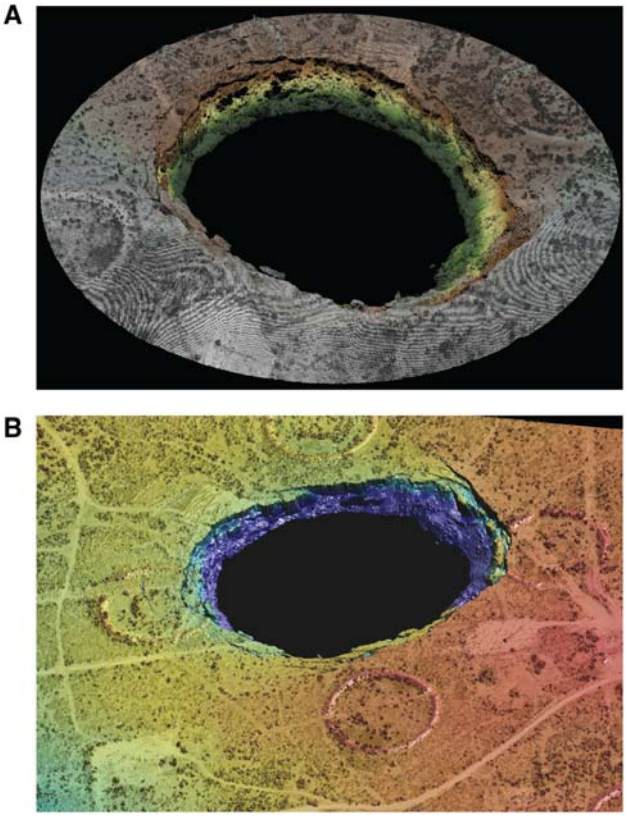

Figure 3. Perspective views of (a) point cloud and (b) high-resolution digital elevation model (DEM) constructed from lidar data acquired near Wink Sink 2 during the November 2013 airborne survey.

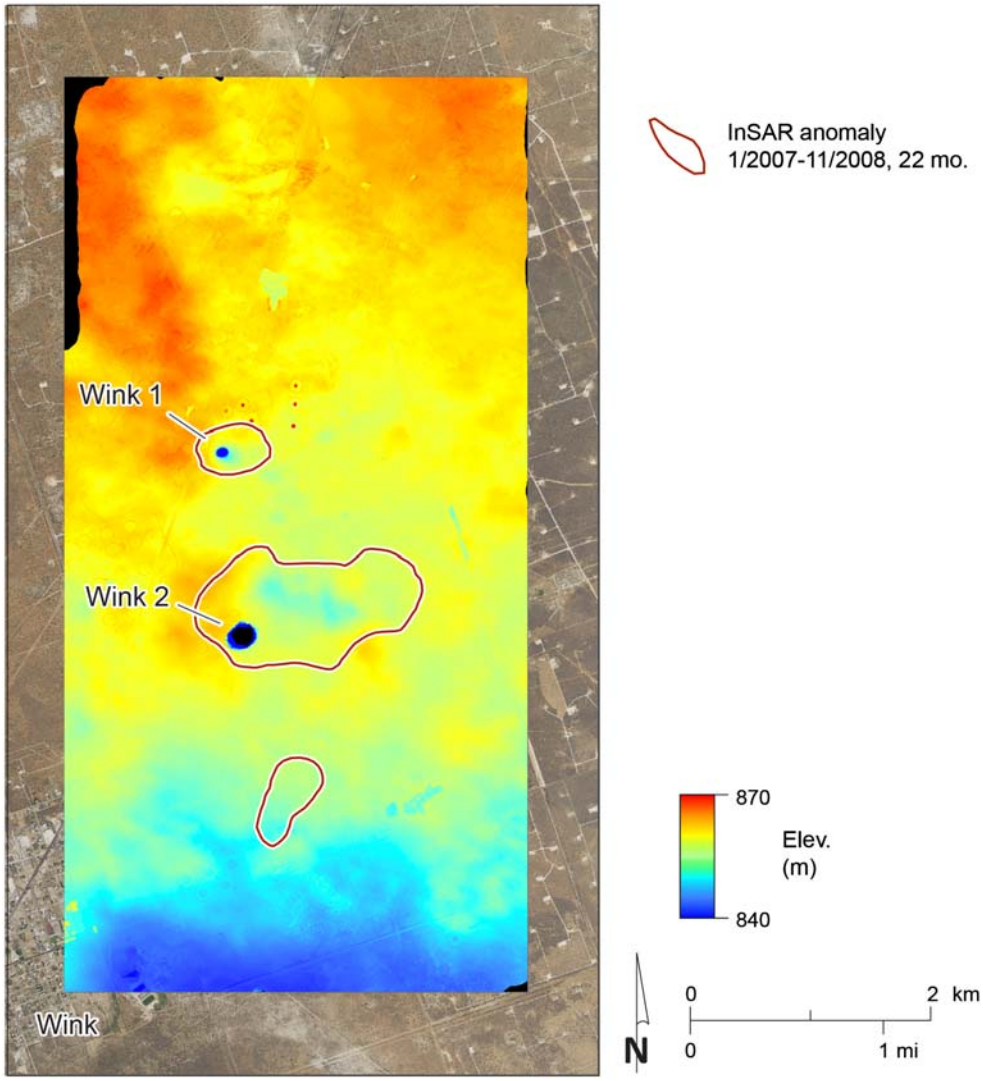

Figure 4. High-resolution (1-m grid cell) DEM of the Wink Sink area constructed from lidar data acquired in November 2013. Superimposed on the DEM are the outlines of InSAR anomalies identified from ALOS L-band radar data acquired in January 2007 and November 2008.

Microgravity profiles and GPS-based elevation measurements acquired in 2015 across this feature show no evidence of subsidence or presence of shallow mass deficits that might indicate potential for future subsidence or collapse.

The DEM constructed by the USGS from 1968 aerial photography (Fig. 5) has significantly lower resolution than the 2013 lidar-derived DEM, but depicts the same general southerly slope and main topographic features. Wink Sinks 1 and 2, which had yet to collapse in 1968, are absent from the older DEM, as are the larger topographic lows near them that are evident on the 2013 DEM.

By assigning the DEMs to a common vertical datum, jointly georeferencing them as accurately as possible, and making minor adjustments in the area-wide elevations to minimize apparent elevation change beyond the obvious subsiding areas, we attempted to estimate net elevation change from 1968 to 2013 across the survey area (Fig. 6). Net elevation change ranges from +13 to –28 m, but net change is near 0 m over the majority of the study area. Apparent increases in elevation are limited to artificial structures (towers, tanks, and buildings) that were excluded from the 1968 DEM, areas where land has been built up by fill, and perhaps some natural eolian features. Small areas of elevation gain or loss are likely artifacts caused by features not adequately captured at the lower resolution of the 1968 DEM. The greatest loss of elevation is associated with Wink Sink 1 (26 m from the 1968 ground surface to the 2013 water level) and Wink Sink 2 (28 m to water), where sudden collapse in 1980 and 2002 dropped the

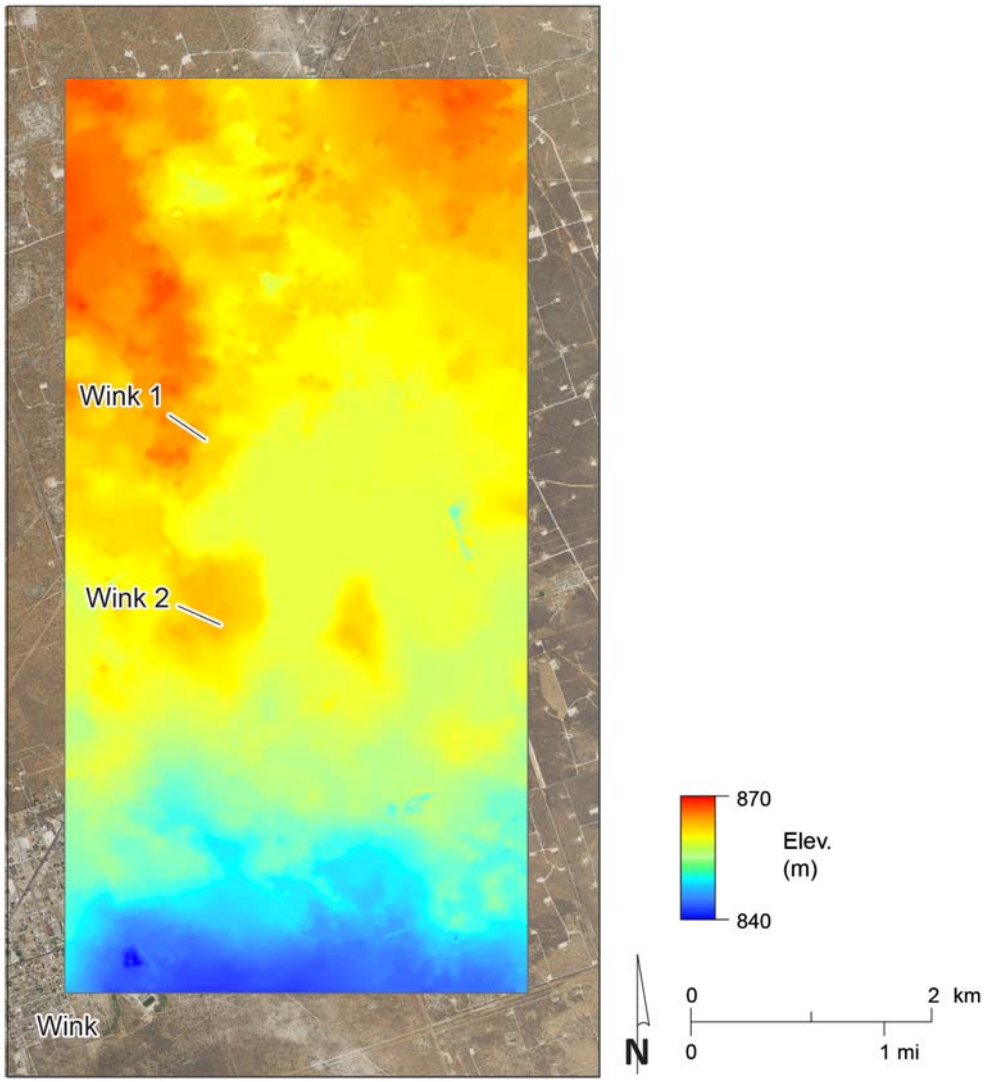

Figure 5. DEM of the Wink Sink area produced by the USGS using photogrammetric and land-surveying methods from aerial photographs acquired in 1968. Cell resolution is 10 m.

land surface more than 30 m. Numerous other areas of elevation loss are evident (features A through F, Fig. 6). Elevation loss between 1968 and 2013 across these features ranges from 1.6 m (feature F) to 8.8 m (feature E, the largest subsiding area east and northeast of Wink Sink 2). Field investigations in May 2014 suggested that features A and B are likely to be pits excavated after 1968. The remainder of the features appear to be caused by land subsidence. Maximum measured land-surface elevation loss is 8.8 m, representing an average annual subsidence rate of 20 cm/yr between 1968 and 2013. Actual rates within this period could have been higher if subsidence began after 1968 or rates varied over time.

Topographic profiles showing elevation change can be constructed by differencing the elevation surfaces (Fig. 7). Profile E (Fig. 8) crosses feature E, the most extensive subsidence feature identified in the area (Fig. 6), from west-northwest to south-southeast. Maximum land-surface elevation loss between 1968 and 2013 is about 6.8 m along this line. Average rates of subsidence over the 45 years elapsed between 1968 and 2013 are 15 cm/yr, but actual rates during the period could have been higher.

The second lidar survey of the Wink area, acquired in August 2017 while also surveying the Imperial and McCamey sinkholes in west Texas, shows the same general features as those identified in the 2013 survey. Subtracting the 2013 DEM from the 2017 DEM reveals broad areas of relatively little elevation loss surrounding Wink Sink 1 and Wink Sink 2 (Fig. 7). Greater elevation loss occurred in the southeastern part of the survey area, where two foci of rapid subsidence are located along profile DE oriented north-northwest to south-southeast near a closed segment of Winkler County Road 204 (Figs. 2, 7, and 9). Elevation loss between 2013 and 2017 reaches as much as 1.25 m in the northern depression and 2.75 m

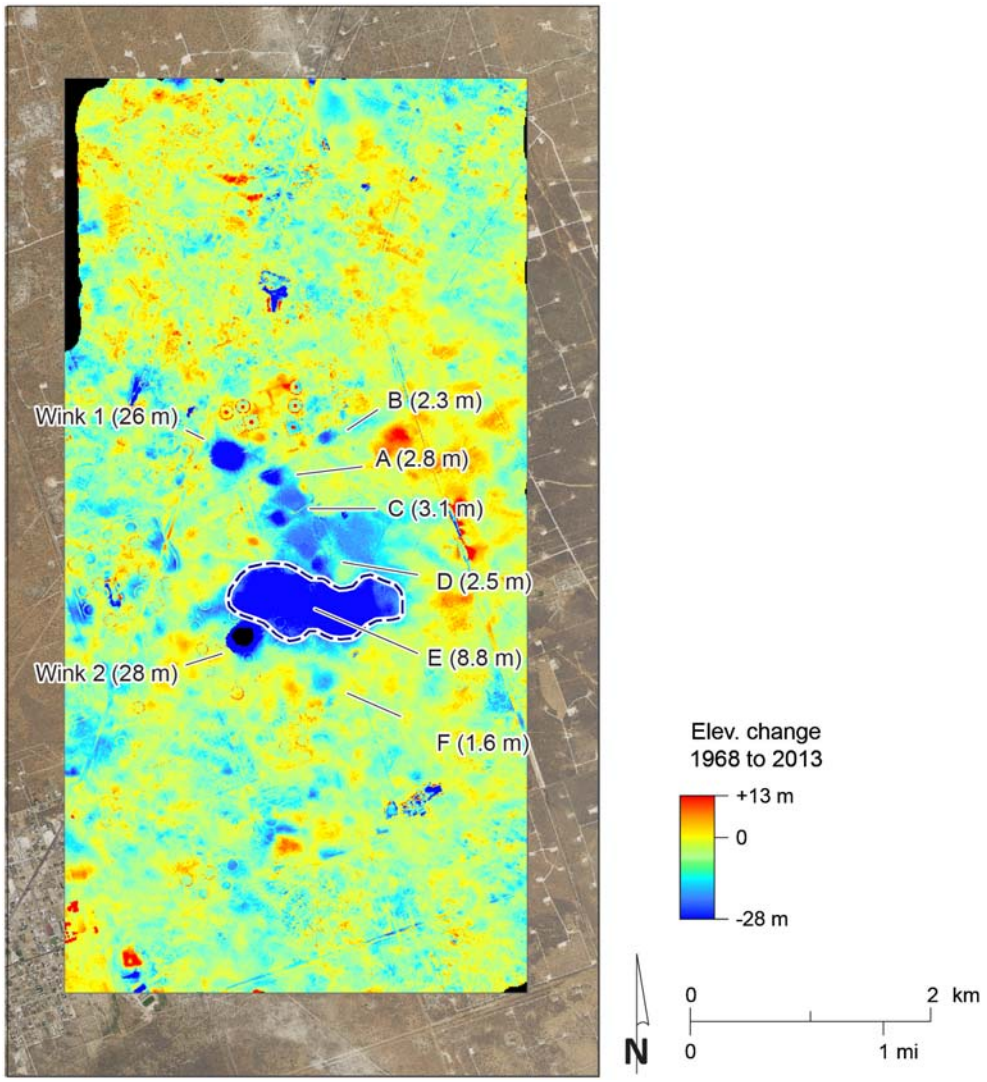

Figure 6. Elevation difference calculated by subtracting the 1968 photogrammetry-derived DEM from the 2013 lidar-derived DEM of the Wink Sink area. Wink Sink 1, Wink Sink 2, and features A through F identify laterally extensive areas where elevation losses are greater than 1.6 m.

in the southern depression. Average net subsidence rates over the nearly four years elapsed between surveys are 33 cm/yr in the northern depression and 73 cm/yr in the southern depression near the intersection of Winkler County Roads 201 and 204. Field investigations during lidar, GPS, and microgravity surveys reveal abundant evidence of rapid subsidence across the southern feature, including extensive fissures along the margins of the subsiding area and fault-bounded, progressively down-dropped blocks on the slopes of the depression along County Road 204.

ANNUAL RATES FROM GPS MEASUREMENTS

Differential GPS measurements were acquired at 91 sites at 40-m intervals along lines 6 and 7 (Fig. 10) during a May 2015 microgravity survey to enable accurate elevation-related corrections to be applied to gravity measurements. While the gravity measurements were unremarkable, the GPS-derived elevations, when compared to the elevations at the same locations determined from the 2013 lidar survey, also showed areas of significant elevation loss over the 18 months elapsed between the lidar and GPS surveys. Most measurement sites underwent less than 15 cm of elevation loss between 2013 and 2015, including all stations on line 7, which crossed an anomaly identified from 2007 to 2008 InSAR data (Fig. 10). The eastern and western parts of line 6 also underwent less than 15 cm of land loss between 2013 and 2015. GPS measurements along a segment of line 6 that intersects the southern subsidence area along profile DE (Fig. 7) revealed elevation loss as great as 91 cm,

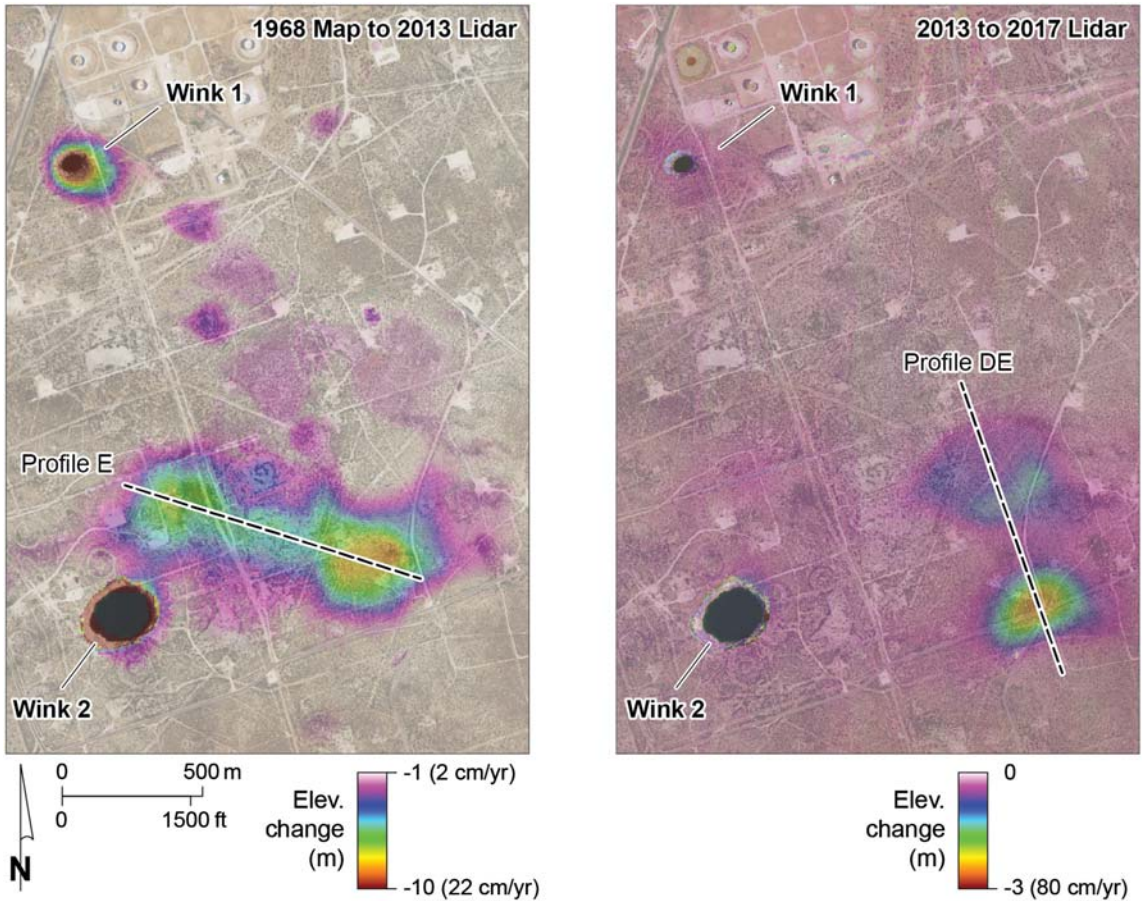

Figure 7. Elevation difference and rates of change calculated by (left panel) subtracting the 1968 photogrammetry-derived DEM from the 2013 lidar-derived DEM and by (right panel) subtracting the 2013 DEM from the 2017 lidar-derived DEM of the Wink Sink area.

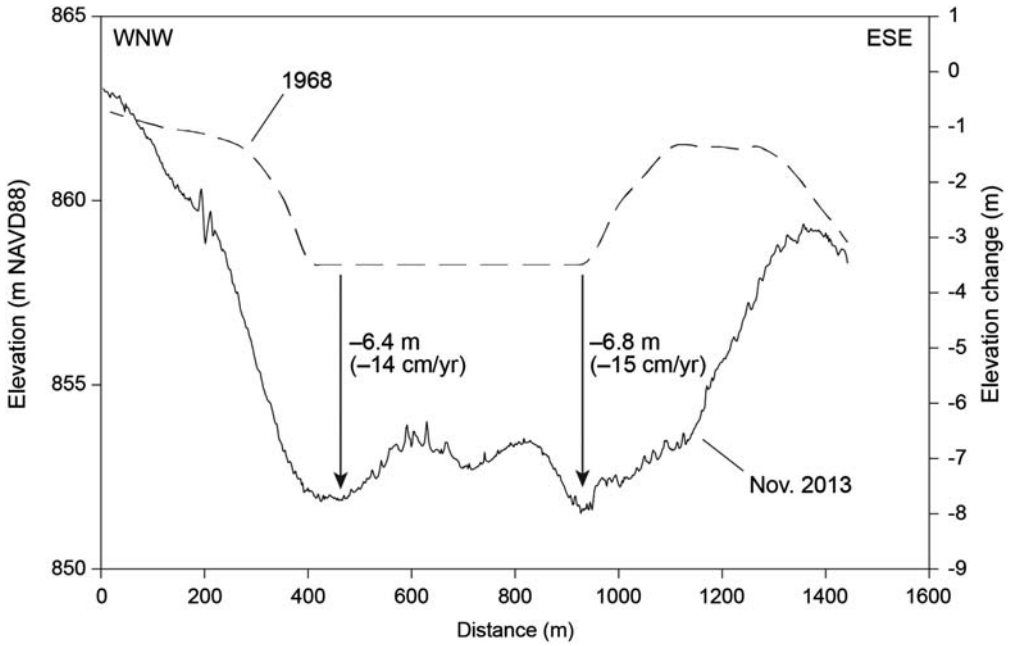

Figure 8. Elevation and elevation change between 1968 and 2013 along profile E (fig. 7).

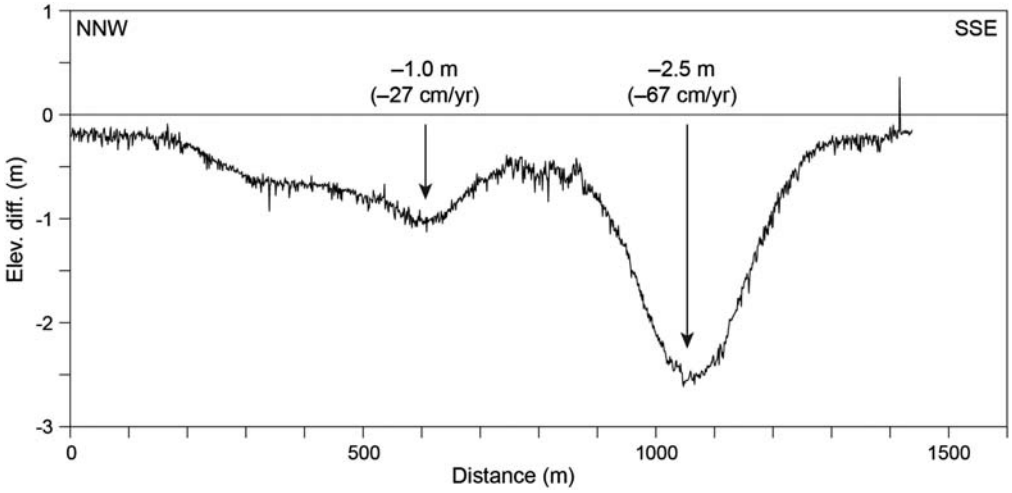

Figure 9. Elevation change and maximum rates of change along profile DE (fig. 7) calculated by subtracting the 2013 DEM from the 2017 lidar-derived DEM of the Wink Sink area. The profile crosses subsidence features D and E identified by comparing 1968 and 2013 elevations (fig. 6).

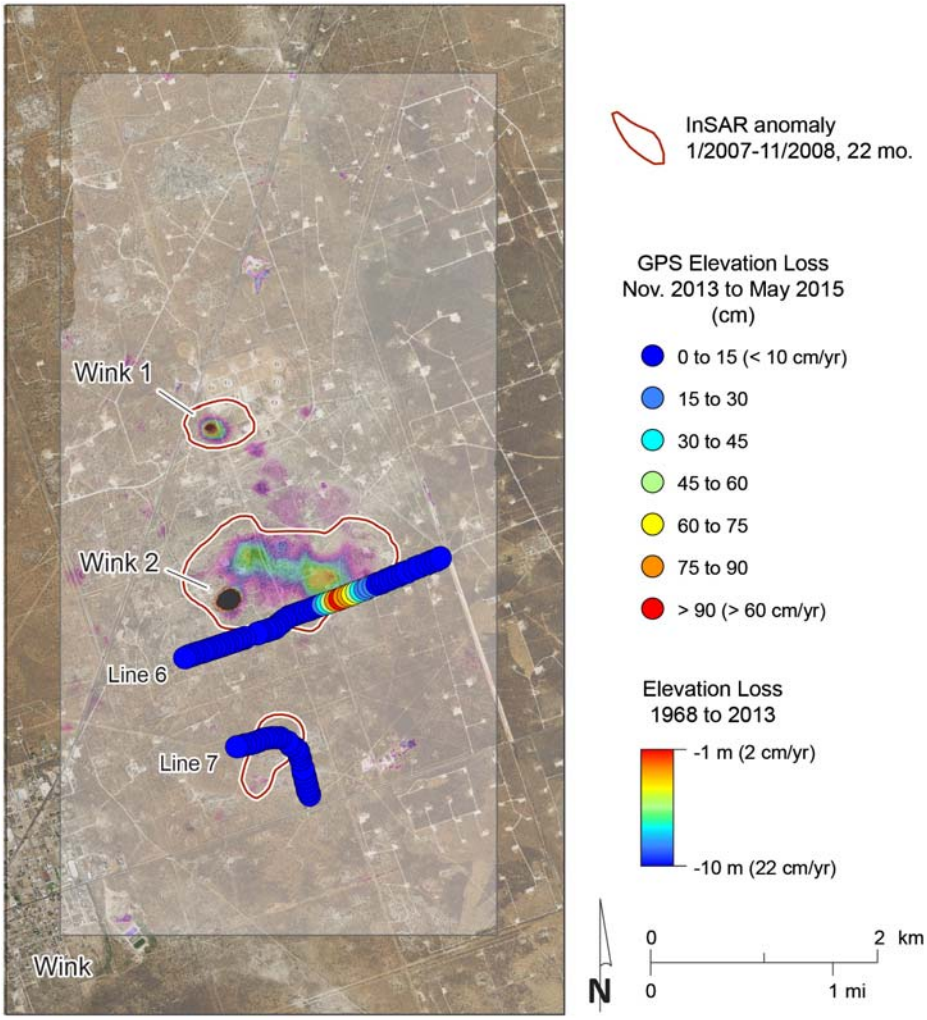

Figure 10. Elevation loss and average rates of elevation loss between the November 2013 lidar survey and the May 2015 microgravity survey (lines 6 and 7), superimposed on 1968–2013 elevation change. Also shown are the 2007–2008 InSAR anomalies.

translating to an average maximum rate of subsidence of 61 cm/yr. This value is similar to the maximum rate calculated between the 2013 and 2017 lidar surveys as well as the maximum subsidence rates reported from recent InSAR analysis (Kim and Lu, 2018; Kim and others, 2019).

CONCLUSIONS

No matter the method employed, whether examining elevation change over the short-term (months to a few years) using InSAR data, over the intermediate term (a few years) from InSAR, repeat lidar surveys, and GPS measurements, or over a longer term (a few decades) using elevations from historical topographic maps, subsidence in the Wink Sink area has been easily detectable and the subsidence rates are high. Historical rates determined by comparing 1968 elevations with 2013 elevations show net subsidence as great as 9 m over the 45-year period at an average rate of 20 cm/yr. That rate likely underestimates maximum subsidence rates over that period because subsidence might have begun after 1968 (and thus occurred over a shorter period) and rates likely varied over time. Comparisons of elevations determined from lidar surveys flown in 2013 and 2017 revealed as much as 2.75 m of subsidence over nearly four years, translating to maximum subsidence rates of 73 cm/yr during that period. Elevation comparisons from differential GPS measurements taken in 2015 with lidar-derived elevations determined in 2013 revealed elevation losses as great as 0.91 m at average rates of 61 cm/yr, largely confirming similar maximum rates determined from repeat lidar surveys and recent InSAR studies.

Given the high repeat frequency of current radar satellites, the InSAR method provides a valuable tool for monitoring ground subsidence and detecting when subsidence rates change, which could be a precursor to sudden collapse as occurred at Wink Sinks 1 and 2. Baseline elevations over relatively large areas at high lateral (1 m or less) and vertical (a few cm) resolution, a prerequisite for effective GPS and lidar-based elevation monitoring, are currently best accomplished through airborne lidar surveying. Differential GPS measurements are labor intensive and site specific, but are necessary for ground verification of lidar-derived elevations and can be extremely accurate. Continuous monitoring of critical sites could be accomplished through installation of permanent GPS monitoring sites, but cannot be achieved with satellite-based radar or airborne lidar surveying. Each approach has advantages and disadvantages; all can be helpful depending on the hazard, vulnerability, and lead time required for actions to mitigate the hazard to the public and to infrastructure.

ACKNOWLEDGMENTS

Wink investigations were supported by the State of Texas Advanced Resource Recovery (STARR) geologic hazards program at the Bureau of Economic Geology. J. Paine and L. Costard acquired GPS and microgravity data during the May 2015 survey. 2013 and 2017 lidar data were acquired and processed by Bureau of Economic Geology staff A. Averett, J. Andrews, J. Hupp, and K. Saylam. Publication authorized by the Director, Bureau of Economic Geology, Jackson School of Geosciences, The University of Texas at Austin.

REFERENCES CITED

Baumgardner, R.W., Jr., Hoadley, A.D., and Goldstein, A.G., 1982, Formation of the Wink Sink, a salt dissolution and collapse feature, Winkler County, Texas: The University of Texas at Austin, Bureau of Economic Geology, Report of Investigations 114, 38 p.

Beck, B.F., editor, 1995, Karst Geohazards: Engineering and environmental problems in karst terrane: Proceedings of the Fifth Multidisciplinary Conference on Sinkholes and the Engineering and Environmental Impact of Karst: Balkema, Rotterdam, 582 p.

Bell, F.G., Culshaw, M.G., and Waltham, T., 2005, Sinkholes and subsidence: karst and cavernous rocks in engineering and construction: Springer, Berlin, ISBN 3-540-20725-2, 383 p.

Collins, E.W., 2000, Reconnaissance investigation of active subsidence and recent formation of earth fissures near the 1980 Wink Sink in the Hendrick oil field, Winkler County, Texas (abstract): Geological Society of America, South-Central Section, Abstracts with Programs, v. 32, no. 3, p. A-6.

Johnson, K.S., 1989, Development of the Wink Sink in West Texas due to salt dissolution and collapse: Environmental Geology and Water Science, v. 14, p. 81-92.

Johnson, K.S., Collins, E.W., and Seni, S.J., 2003, Sinkholes and land subsidence owing to salt dissolution near Wink, West Texas, and other sites in western Texas and New Mexico, *in* Johnson, K.S., and Neal, J.T., eds., Evaporite karst and engineering/environmental problems in the United States: Oklahoma Geological Survey, Circular 109, p. 183-195.

Johnson, K.S., and Neal, J.T., eds., 2003, Evaporite karst and engineering/environmental problems in the United States: Oklahoma Geological Survey, Circular 109, 353 p.

Kim, J., Lu, Z., 2018, Association between localized geohazards in West Texas and human activities, recognized by Sentinel-1A/B satellite radar imagery: Scientific Reports, v. 8, 4727, 13 p.

Kim, J.-W., Lu, Z., and Degrandpre, K, 2016, Ongoing deformation of sinkholes in Wink, Texas, observed by time-series Sentinel-1A SAR interferometry (preliminary results): Remote Sensing, v. 8, no. 313, 11 p.

Kim, J.-W., Lu, Z., and Kaufmann, J., 2019, Evolution of sinkholes over Wink, Texas, observed by high-resolution optical and SAR imagery: Remote Sensing of Environment, v. 222, no. 1, p. 119-132.

Paine, J.G., Buckley, S.M., Collins, E.W., and Wilson, C.R., 2012, Assessing collapse risk in evaporite sinkhole-prone areas using microgravimetry and radar interferometry: Journal of Environmental and Engineering Geophysics, v. 17, no. 2, p. 73-87.

Sinkholes in Wink, Texas, Observed by Satellite Radar Imagery

Jin Woo Kim and Zhong Lu
Roy M. Huffington Department of Earth Sciences,
Southern Methodist University, Dallas, Texas

ABSTRACT.—Two sinkholes in Wink, Texas (Wink Sinks #1, #2), collapsed in 1980 and 2002, respectively. The area where the sinkholes are located in Winkler County, west Texas, is underlain by thick salt beds at depth of about ~400 m. Anthropogenic activities related to oil and water production have been considered as a primary cause of the sinkhole development and creation. Previous studies have suggested that poor wellbore management, which failed to prevent the intrusion of freshwater and/or unsaturated saltwater into soluble rocks, resulted in the cavity formation, roof failure, and successive upward cavity migration. Interferometric synthetic aperture radar (InSAR) measurements using Advanced Land Observation Satellite Phased Array type L-band Synthetic Aperture Radar and TerraSAR-X images during 2007–2011 and 2015–2016 revealed fine spatial details about the progression of the existing sinkholes and neighboring regions. The immediate vicinities of both existing sinkholes are still subsiding, albeit at a decreasing rate, from ~18 cm/yr in 2011 to about ~8 cm/yr in 2016, possibly because of the gradual deposit of the debris from overlying rock formation into the cavity. However, an alarming rate of subsidence can be found ~1 km east of Wink Sink #2. The peak subsidence rate of this area ranged from ~40 cm/yr during 2007–2011 to more than 60 cm/yr during 2015–2016. Although the initial trigger of the subsidence feature over the area 1 km east of Wink #2 might be similar to that of Wink Sinks #1 and #2 (i.e., poor borehole management, water-flooding operations in a karst environment), the recent expansion and accelerated subsidence may be attributed to the severe drought in 2011. Continuous monitoring of the subsidence in the broader vicinity of the Wink sinkholes is needed for preventing future catastrophic outcomes of long-term developing geohazards to the area's oil production facilities, infrastructure, and human safety.

INTRODUCTION

Sinkholes, depressions or holes caused by collapse of land surface, are a major geohazard in karst environments worldwide (Beck and Pearson, 1995; Johnson and Neal, 2003; Gutiérrez and others, 2014). Sinkholes are generally formed when evaporite, carbonate, or gypsum rocks in karst terrains dissolve because of chemical or other processes that result in the development of underground cavities, failures of overlying sediments/rocks, upward cavity migration, and surface depression and collapses.

Well-known sinkholes in the world can be found over the coasts of the Dead Sea, northeastern Spain, the Netherlands, and North America (e.g., Baer and others, 2002; Galve and others, 2009; Chang and Hanssen, 2014; Paine and others, 2012; Jones and Blom, 2014; Kim and others, 2016; Kim and Lu, 2018). In the United States, 48 out of 50 states have karst terrains with most of the damaging sinkholes located along the Gulf Coast states including Texas, Louisiana, and Florida, among others (Kuniansky and others, 2016).

Sinkholes can be induced by both natural processes and anthropogenic activities. Recent studies provided evidence that the vast majority of newly formed sinkholes are of anthropogenic origins, including aquifer exploitation and mining dewatering resulting in water level decline, water impoundment and injection, and vegetation removal among others (Waltham and others, 2005; Kim and others, 2019). Impacts caused by sinkhole activities include economic losses and damage to infrastructure (Kuniansky and others, 2016). Because of the increasing demand for water and energy resources,

Kim, Jin Woo; and Lu, Zhong, 2021, Sinkholes in Wink, Texas, Observed by Satellite Radar Imagery, *in* Johnson, K. S.; Land, Lewis; and Decker, D. D. (eds.), Evaporite Karst in the Greater Permian Evaporite Basin (GPEB) of Texas, New Mexico, Oklahoma, Kansas, and Colorado: Oklahoma Geological Survey, Circular 113, p. 105–110.

it is anticipated that negative effects of sinkhole hazards will grow in the future.

Two cover-collapse sinkholes, namely Wink Sinks #1 and #2, in west Texas, collapsed in 1980 and 2002, respectively (Figure 1). These two sinkholes are located in a region underlain by the Salado Formation on the eastern edge of the Delaware Basin. Wink Sink #1 was created on 3 June 1980 and enveloped an abandoned plugged oil well that produced oil from 1928 to 1951 and became inactive after 1964. Wink Sink #2, formed on 21 May 2002, centered on a water-supply well. Past investigations suggest these two sinkhole collapses were associated with intense hydrocarbon drilling and production activities in the Hendrick oilfield that caused the salt dissolution, cavity formation, roof failure, upward cavity migration, and surface collapse (Johnson and others, 2003; Johnson, 2005; Kim and others, 2019).

Here we report on the evolution of the ground surface deformation over the area including and surrounding both Wink sinkholes using radar remote sensing images acquired by satellites during 2007 to 2011 and 2015 to 2016. Our goal is to assess the state of the ground surface subsidence over this sinkhole-prone area using high-spatial-resolution satellite observations, which provides a scientific basis for the need to mitigate potential sinkhole hazards.

DATA AND ANALYSIS

SAR and InSAR data

Interferometric synthetic aperture radar (InSAR) combines two or more synthetic aperture radar (SAR) images of the same imaging geometry from the same area to produce an interferogram (a.k.a. InSAR image) (e.g., Massonnet and others, 1993; Zebker and others, 1994; Rosen and others, 2000; Hanssen, 2001; Lu and Dzurisin, 2014). The interferometric phase, after the correction of topographic effect with the aid of a digital

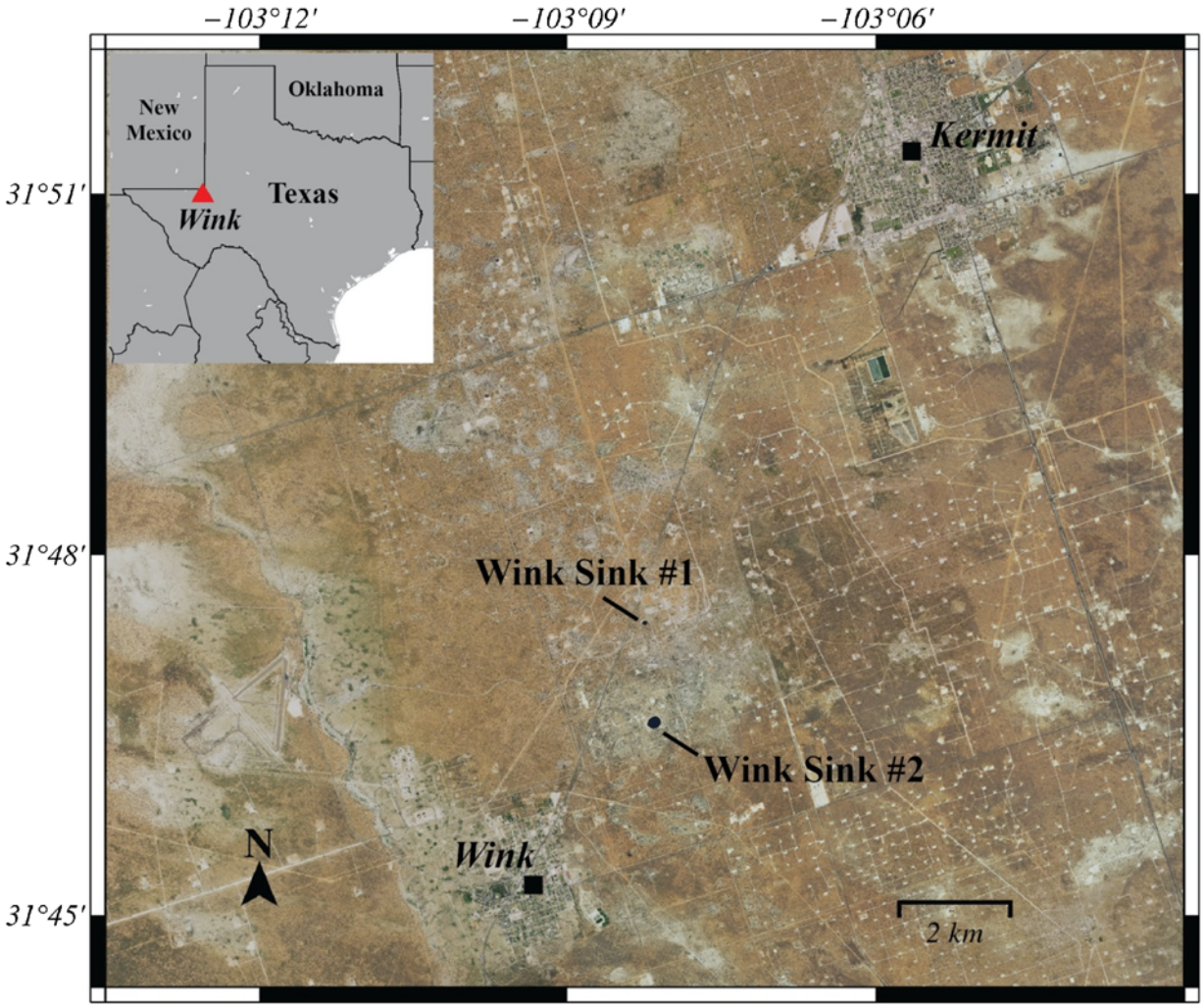

Figure 1. Location of Wink sinkholes near Wink in west Texas. Wink Sink #1, created in 1980, is located ~1.5 km north of Wink Sink #2, which formed in 2002. Wink Sinks #1 and #2 have a dimension of 80 m × 110 m and 200 m ×250 m, respectively.

elevation model, presents the range (the distance from the satellite to ground) change that includes subtle ground deformation and atmosphere artifacts and other noise. InSAR data, combined with geophysical modeling, have been used to characterize geohazards associated with volcanoes, landslides, earthquakes, and land subsidence among others (Lu and others, 2010). To improve the precision of InSAR measurements, multitemporal InSAR images are needed to obtain high temporal coherence and reduce atmospheric artifacts through time-series InSAR processing (e.g., Ferretti and others, 2001; 2011; Hooper and others, 2004; Lu and Zhang, 2014; Qu and others, 2015).

Two data sets are used in this report: L-band (wavelength of ~24 cm) Advanced Land Observation Satellite (ALOS) Phased Array type L-band Synthetic Aperture Radar images acquired from January 2007 to January 2011 by the Japan Aerospace Exploration Agency(JAXA) and X-band (wavelength 3.1 cm) high-resolution TerraSAR-X images acquired from October 2015 to March 2016 by the German Aerospace Center (DLR). The detailed characteristics of these SAR images can be found in Lu and Zhang (2014). The ALOS stripmap-mode SAR images have spatial resolutions of 10 to 20 m, whereas the TerraSAR-X spotlight-mode images used in this study have a spatial resolution of ~25 cm. The mean deformation rate from each satellite data set is obtained by stacking multiple coherent interferograms (Kwoun and others, 2006). As the observed ground deformation associated with sinkhole development is dominated by the vertical displacement (Kim and Lu, 2018), we convert the line-of-sight deformation into the vertical displacement to facilitate the evaluation of the evolution of the observed deformation.

Observed deformation

Based on the average subsidence rate map from ALOS data during 2007 to 2011, we can identify several subsidence cones (Figure 2). The first feature is the subsidence radiating about 600-m outward from Wink Sink #1. The subsidence peaks at a rate of ~12 cm/yr, located about ~100 m to the west of Wink Sink #1 (Figure 2). The second subsidence feature of an ellipsoid shape (500 m × 400 m in dimension) can be identified about ~500 m to the north of Wink Sink #2, with a peak subsidence of ~18 cm/yr (Figure 2). The third and the most prominent subsidence feature is located about 1 km east of Wink Sink #2. It resembles a tooth rotated sideway: the subsidence at the south peak, about 200 m northwest of the intersection of county roads 201 and

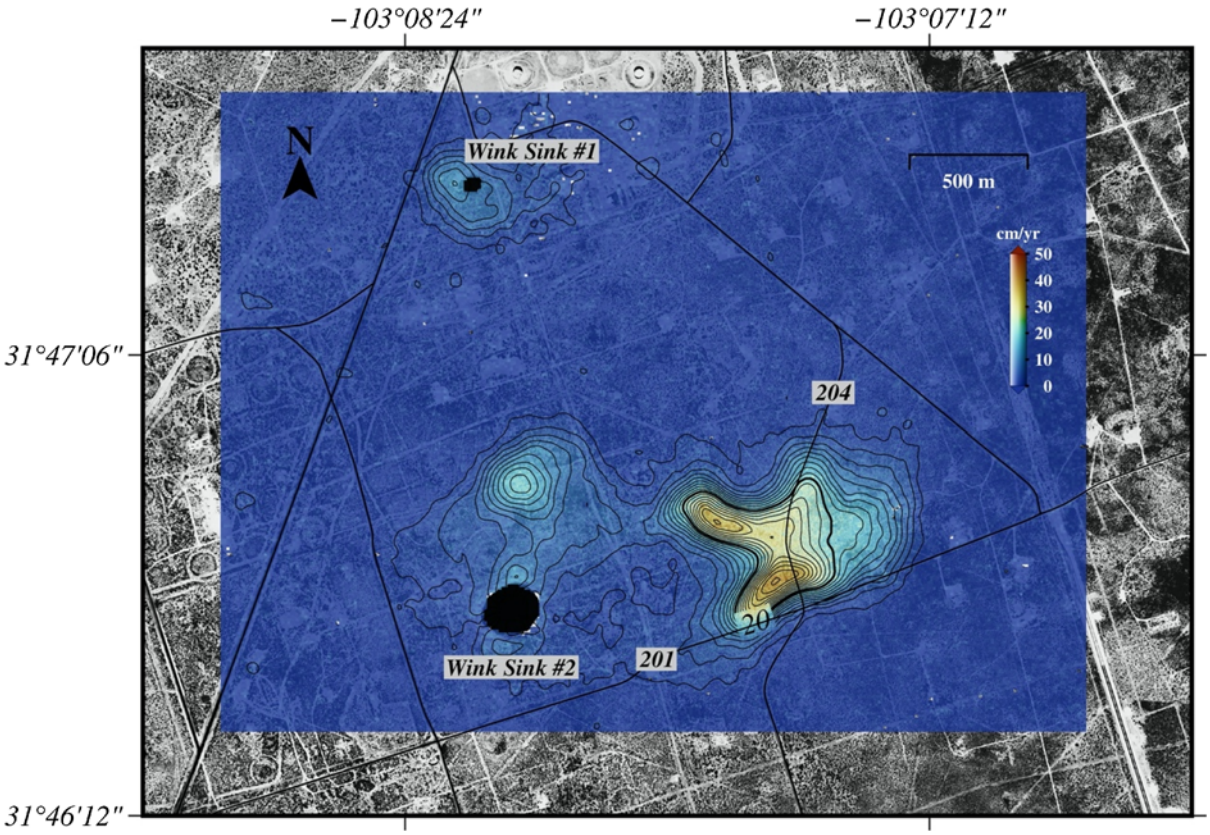

Figure 2. Average subsidence rate map from ALOS PALSAR images from January 2007 to January 2011. Contour lines are drawn at intervals of 2 cm/yr.

204, was about 40 cm/yr, whereas it was 35 cm/yr at the north peak (Figure 2).

The subsidence rate map for 2015 to 2016 from TerrraSAR-X images shows that the three subsidence features as seen during 2007 to 2011 changed over time to some degree (Figure 3). The subsidence rates at the first feature (i.e., near Wink Sink #1) and the second feature (north of Wink Sink #2) reduced to 4 and 4–8 cm/yr, respectively (Figure 3), and the extents of subsidence also shrank. However, the third and most prominent feature about 1 km east of Wink Sink #2 changed significantly. There were two distinct subsidence troughs in 2015 to 2016. The subsidence rate over the north peak reduced to about 26 cm/yr, whereas it increased to more than 60 cm/yr over the south peak located on county road 201, about 100 m west of the intersection of the county roads 201 and 204 (Figure 3). It is obvious the peak subsidence increased in magnitude from 2011 to 2015–2016 and that the location of the peak subsidence migrated southward.

DISCUSSION AND CONCLUSION

The subsidence observed near the existing Wink Sinks #1 and #2 suggests the underground cavity around each was continuously filled with debris from upper formations. This void filling process, called a suffusion, produced continuous surface subsidence over the newly formed sinkholes in the early stage of each sinkhole's collapse (Waltham and others, 2005; Kim and others, 2019). The subsidence rates and dimensions surrounding Wink Sinks #1 and #2 reduced over time, suggesting the two existing sinkholes stabilized as a consequence of nearly fully filled cavities (Waltham and others, 2005; Kim and others, 2019).

The double-peak subsidence feature about 1 km east of Wink Sink #2 manifests as alarming sinkholes under development, with the peak subsidence reaching more than 60 cm/yr during 2015 to 2016 near the intersection of county roads 201 and 204. The triggering mechanism for the observed subsidence has also been attributed to dissolution of the Salado Formation around ~400 m deep, similar to the cause of collapses at Wink Sinks #1 and #2 (Paine and others, 2012; Kim and others, 2016, 2019). There were numerous water wells and hydrocarbon-production wells, most of which have been inactive and abandoned. Inappropriate borehole management, as judged by current more stringent standards, could initiate the freshwater contact of the Salado layer through unplugged boreholes, corroded pipes, or leaked casing and other engineering issues (Paine and

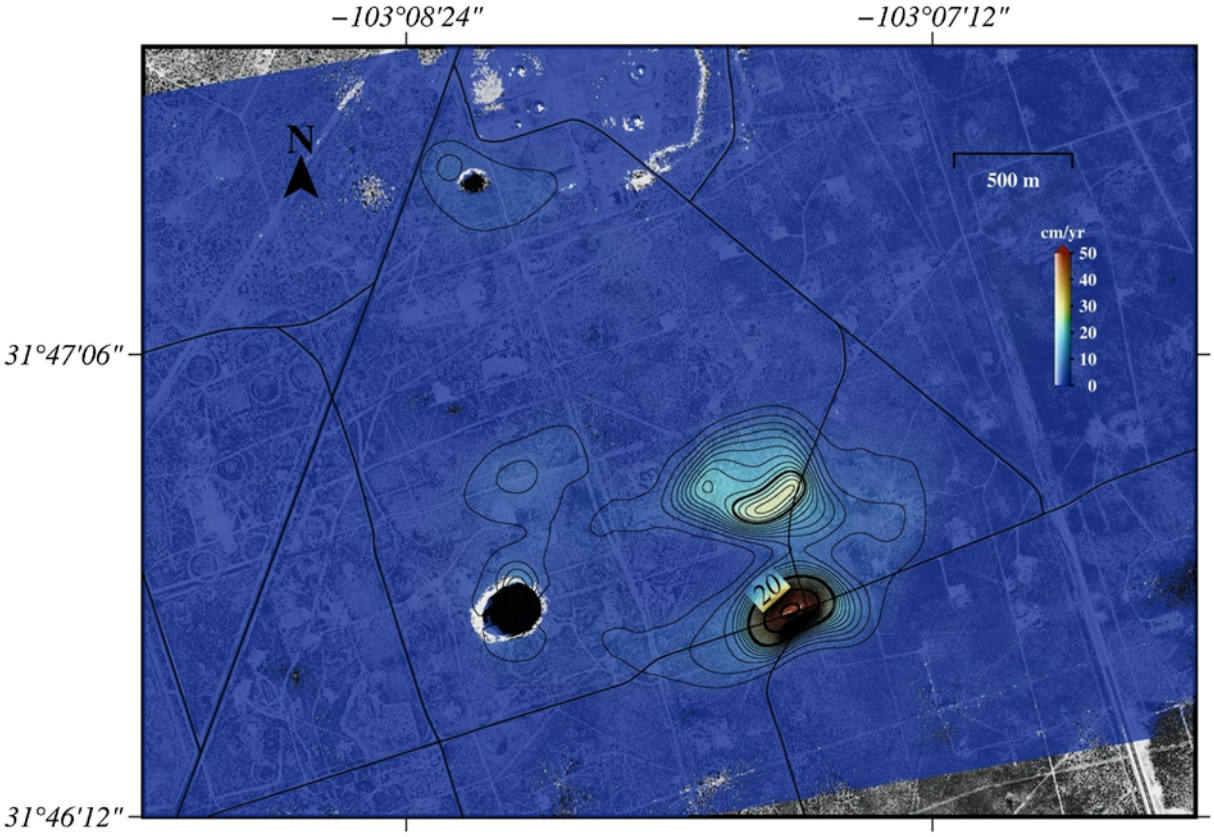

Figure 3. Average subsidence rate map from TerraSAR-X images from October 2015 to March 2016. Contour lines are drawn at intervals of 2 cm/yr.

others, 2012; Kim and others, 2016, 2019). In addition, intensive water-flooding operations were used in this area for several decades from the 1970s to the 2000s (Kim and others, 2019), which could act as an important contributor to the rapid subsidence. Fractures in the aquifer and formations surrounding the salt layer created by pressurized fluid injection and long-term hydrocarbon production could have allowed freshwater to intrude into the Salado Formation, initiating the dissolution process (Kim and others, 2019). The accelerated salt dissolution could cause cavity formation, upward migration, and the ground surface subsidence. Therefore, we believe the combined effects of improper borehole management and massive water production were responsible for the development of the subsidence feature east of Wink Sink #2.

Inspecting the deformation over the double-peak subsidence feature east of Wink Sink #2 suggests that not only did the rate of peak subsidence increase, but that the extent of the subsidence also expanded from 2007–2011 to 2015–2016 (Figures 2 and 3). For example, the peak subsiding area was contained to the north of county road 201 in 2007–2011, but expanded further south of county road 201 in 2015 to 2016. Kim and others (2019) attributed the accelerated subsidence at the developing sinkholes to a combination of human-induced (hydrocarbon and water flooding, etc.) and natural perturbations (droughts) in the subsurface surrounding the Salado layer. In fact, a severe drought hit the area in 2011, which was the worst in the past 30 yr in Texas (Kim and others, 2019). Because of decadal water-flooding operations that caused fractures in the formations surrounding the Salado Formation along with those formed during borehole drilling and realignment (Heithecker, 1932; Adams, 1944; Baumgardner and others, 1982; Johnson, 1989; Kim and others, 2019), the area already possessed a well-developed fracture system. The 2011 drought lowered groundwater levels, which in turn added overburden stress, and further compounded sinkhole development vulnerability. The increased effective stress and internal erosion in the overlying layers can result in more rapid downward percolation of freshwater in aquifer systems into the underlying salt beds, causing the acceleration of the salt dissolution and surface/subsurface subsidence (Linares and others, 2017; Kim and others, 2019). Although the double-peak subsidence feature has not yet resulted in a collapse as witnessed at Wink Sinks #1 and #2, the accelerated subsidence represents a significant potential geohazard in the area. Hence, continuous monitoring of the subsidence in the vicinity of the Wink sinkholes using satellite InSAR or other ground-based instruments is urgently needed to prevent future catastrophic outcomes that will endanger the area's oil production facilities, critical infrastructure, and human safety.

ACKNOWLEDGEMENTS

This work was supported in part by the NASA Earth Surface and Interior Program under Grants 80NSSC19K1491 and NNX16AL10G and in part by the Shuler-Foscue Endowment at Southern Methodist University.

REFERENCES CITED

Adams, J.E., 1944, Upper Permian Ochoan Series of Delaware Basin, west Texas and southeastern New Mexico: American Association of Petroleum Geologists, Bulletin, v. 28, p. 1596-1625.

Baer, G., Schattner, U., Wachs, D., Sandwell, D., Wdowinski, S., and Frydman, S., 2002, The lowest place on Earth is subsiding – an InSAR (interferometric synthetic aperture radar) perspective: Geological Society of America, Bulletin, v. 114, no. 1, p. 12-23.

Baumgardner, R.W., Hoadley, A.D., and Goldstein, A.G., 1982, The Wink Sinks; a case history of evaporite dissolution and catastrophic subsidence: Formation of the Wink Sink, a salt dissolution and collapse feature, Winkler County, Texas: Bureau of Economic Geology, The University of Texas at Austin, Report of Investigations No. 114, 38 p.

Beck, B.F., and Pearson, F.M., 1995, Karst Geohazards: Engineering and environmental problems in karst terrane, *in* Proceedings of the Fifth Multidisciplinary Conference on Sinkholes and the Engineering and Environmental Impact of Karst, Gatlinburg, Tennessee, 2–5 April 1995: Balkema, Rotterdam, 582 p.

Chang, L., and Hanssen, R.F., 2014, Detection of cavity migration and sinkhole risk using radar interferometric time series: Remote Sensing of Environment, v. 147, p. 56-64.

Ferretti, A., Prati, C., and Rocca, F., 2001, Permanent scatterers in SAR interferometry: IEEE Transactions on Geoscience and Remote Sensing, v. 39, p. 8-20.

Ferretti, A., Fumagalli, A., Novali, F., Prati, C., Rocca, F., and Rucci, A., 2011, A new algorithm for processing interferometric data-stacks: SqueeSAR: IEEE Transactions on Geoscience and Remote Sensing, v. 49, no. 9, p. 3460-3470.

Galve, J. P., Gutiérrez, F., Remondo, J., Bonachea, J., Lucha, P., and Cendrero, A., 2009, Evaluating and comparing methods of sinkhole susceptibility mapping in the Ebro Valley evaporite karst (NE Spain): Geomorphology, v. 111, no. 3/4, p. 160-172.

Gutiérrez, F., Parise, M., De Waele, J., and Jourde, H., 2014, A review on natural and human-induced geohazards and impacts in karst: Earth-Science Reviews, v. 138, p. 61-88.

Hanssen, R.F., 2001, Radar interferometry: data interpretation and error analysis: New York, Boston,

Dordrecht, London, Moscow, Kluwer Academic Publisher, 308 p.

Heithecker, R.E., 1932, Some methods of separating oil and water in west Texas fields, and the disposal of oil-field brines in the Hendrick Oil Field, Texas: US Bureau of Mines, Report of Investigations 3173, 16 p.

Hooper, A., Zebker, H., Segall, B., and Kampes, B., 2004, A new method for measuring deformation on volcanoes and other natural terrains using InSAR persistent scatterers: Geophysical Research Letters, v. 31, L23611, 5 p.

Johnson, K.S., 1989, Development of the Wink Sink in west Texas, U.S.A., due to salt dissolution and collapse: Environmental Geology and Water Sciences, v. 14, no. 2, p. 81-92.

Johnson, K.S., and Neal, J. T., 2003, Evaporite karst and engineering/environmental problems in the United States: Oklahoma Geological Survey, Circular 109, 353 p., ISSN 0078-4397.

Johnson, K.S., Collins, W.W., and Seni, S. J., 2003, Sinkholes and land subsidence due to salt dissolution near Wink, West Texas, and other sites in western Texas and New Mexico: Oklahoma Geological Survey, Circular 109, p.183–195.

Johnson, K.S., 2005, Subsidence hazards due to evaporite dissolution in the United States: Environmental Geology, v. 48, p. 395-409.

Jones, C.E., and Blom, R.G., 2014, Bayou Corne, Louisiana, sinkhole: Precursory deformation measured by radar interferometry: Geology, v. 42, no. 2, p. 111-114.

Kuniansky, E.L., Weary, D.J., and Kaufmann, J.E., 2016, The current status of mapping karst areas and availability of public sinkhole-risk resources in karst terrains of the United States: Hydrogeology Journal, v. 24, p. 613-624.

Kim, J.W., Lu, Z., and Degrandpre, K., 2016, Ongoing Deformation of Sinkholes in Wink, Texas, Observed by Time-Series Sentinel-1A SAR Interferometry (Preliminary Results): Remote Sensing, v. 8, no. 313, doi:https://doi.org/10.3390/rs8040313.

Kim, J.W., and Lu, Z., 2018, Association between localized geohazards in West Texas and human activities, recognized by Sentinel-1A/B satellite radar imagery: Scientific Reports, v. 8, no. 4727, doi:https://doi.org/10.1038/s41598-018-23143-6.

Kim, J.W., Lu, Z., and Kaufmann, J., 2019, Evolution of sinkholes over Wink, Texas, observed by high-resolution optical and SAR imagery: Remote Sensing of Environment, v. 222, p. 119-132.

Kwoun, O., Lu, Z., Neal, C., and Wicks, C., 2006, Quiescent deformation of the Aniakchak Caldera, Alaska, mapped by InSAR: Geology, v. 34, no. 1, p. 5-8.

Linares, R., Roqué, C., Gutiérrez, F., Zarroca, M., Carbonel, D., Bach, J., and Fabregat, I., 2017, The impact of droughts and climate change on sinkhole occurrence. A case study from the evaporite karst of the Fluvia Valley, NE Spain: Science of the Total Environment, v. 579, p. 345-358.

Lu, Z., Dzurisin, D., Jung, H.S., Zhang, J.X., and Zhang, Y.H., 2010, Radar Image and Data Fusion for Natural Hazards Characterization: International Journal of Image and Data Fusion, v. 1, p. 217-242.

Lu, Z., and Dzurisin, D., 2014, InSAR imaging of Aleutian volcanoes: monitoring a volcanic arc from space, Chichester, UK: Springer Praxis Books. Geophysical Sciences. ISBN 978-3-642-00347-9: 390 p.

Lu, Z., and Zhang, L., 2014, Frontiers of Radar Remote Sensing: Photogrammetric Engineering and Remote Sensing, v. 80, no. 1, p. 5-13.

Massonnet, D., Rossi, M., Carmona, C., Adragna, F., Peltzer, G., Feigl, K., and Rabaute, T., 1993, The displacement field of the Landers earthquake mapped by radar interferometry: Nature, v. 364, p. 138-142.

Paine, J.G., Buckley, S.M., Collins, E.W., and Wilson, C.R., 2012, Assessing collapse risk in evaporite sinkhole-prone areas using microgravimetry and radar interferometry: Journal of Environmental and Engineering Geophysics, v. 17, no. 2, p. 75-87.

Qu, F.F., Lu, Z., Zhang, Q., Bawden, G.W., Kim, J.W., Zhao, C.Y., and Qu, W., 2015, Mapping ground deformation over Houston-Galveston, Texas using Multi-temporal InSAR: Remote Sensing of Environment, v. 169, p. 290-306.

Rosen, P.A., Hensley, S., Joughin, I.R., Li, F.K., Madsen, S.N., Rodriguez, E., and Goldstein, R.M., 2000, Synthetic aperture radar interferometry: Proceedings of the IEEE, v. 88, no. 3, p. 333-382.

Shi, Y., Tang, Y.M., Lu, Z., Kim, J.W., and Peng, J.H., 2019, Subsidence of sinkholes in Wink, Texas from 2007 to 2011 detected by time-series InSAR analysis: Geomatics, Natural Hazards and Risk, v. 10, no. 1, p.1125-1138, DOI: https://doi.org/10.1080/19475705.2019.1566786.

Waltham, T., Bell, F., and Culshaw, M., 2005, Sinkholes and subsidence: karst and cavernous rocks in engineering and construction: Berlin, Springer, ISBN 3-540-20725-2, 383 p.

Zebker, H.A., Rosen, P.A., Goldstein, R.M., Gabriel, A., and Werner, C.L., 1994, On the derivation of coseismic displacement fields using differential radar interferometry—the Landers earthquake: Journal of Geophysical Research, 99:19617-19634.

Assessing Collapse Risk in Evaporite Sinkhole-Prone Areas Using Commonly Available Oil Field Data in the Area of the Winks Sinks, Winkler County, Texas

Robert C. Trentham and Miles A. Henderson
Department of Geosciences, University of Texas Permian Basin, Odessa, Texas

ABSTRACT.—The development of sinkholes above the bedded evaporite deposits of the Permian Basin of west Texas in the last 40 years has renewed interests in understanding these geologic hazards. Specifically, the development of two large sinkholes (90–300 m in diameter) near the town of Wink in June 1980 and May 2002, as well as other "sag" features have been identified in the area. Naturally occurring dissolution of subsurface salts near Wink, Texas, likely began as early as Laramide time and recurred through the Cenozoic, driven by meteoric flushing associated with regional uplift. However, the development of the sinkhole terrain and surface collapse features of the Wink Sinks have been exacerbated by oilfield-related drilling and pumping activities over the past 100 years. Additional areas of "sag", where the surface is deflated, have been identified by satellite-based radar interferometry and visual observations during field visits to the Wink Sinks. These sag areas show no surface collapse features and suggest that a simple brittle failure model is insufficient to wholly describe deflation in the area surrounding the Wink Sinks. Here, we summarize the historical, present, and the possible future conditions of the Wink Sinks with data commonly collected during oil- and gas-drilling operations. Specifically, we evaluate four (4) sets of data collected over a 70-km^2 (~27-mi^2) area surrounding the Wink Sinks, including oil well-plugging reports, water-supply well data, anecdotal reports of unusual production events, and produced-water sample analyses.

INTRODUCTION

Sinkholes are a common geologic hazard in many parts of the world (e.g., Beck, 1995; Johnson and Neal, 2003). In Texas, sinkholes are associated with bedded Paleozoic salt beneath the High Plains of northern Texas and the Permian Basin of west Texas, limestone karst in central Texas, and shallow salt domes of eastern Texas and the Coastal Plain (Fig. 1). The development of two large sinkholes over evaporitic deposits near the communities of Wink and Kermit in west Texas over the last 40 years highlights the need to determine the locations and likelihood of salt dissolution-induced subsidence and collapse in sinkhole-prone areas. The growth of the Wink Sinks is thought to be the result of salt breccia formation from freshwater circulation in the Salado Salt that was later exacerbated by water circulating around a borehole opening forming a dissolution cavity followed by successive roof collapse resulting in a breccia-filled pipe that eventually reached the surface (Baumgartner and others, 1982; Johnson, 1989). These areas of "brittle" surface failure are wholly or partially surrounded by areas of "sag" where the ground surface is deflated, but no open-cavity sinkhole has developed. Here, noninvasive oilfield-related methods are used to examine the potential for the development of the near-surface cavities that, as yet, have no expressed surface features. Using oilfield-related data, including plugging reports, water-supply well histories, produced water analyses, and anecdotal well/production data, they provide ample geologic data to supplement more technologically driven methods of interferometric synthetic aperture radar (InSAR) and microgravimetry measurements taken at the Wink Sinks. Together, these techniques can quantify the potential for vertical ground movement that may precede sinkhole collapse, and also quantify the extent and magnitude of shallow-subsurface deficits that would indicate areas with significant potential for sinkhole-related subsidence or collapse.

Trentham, Robert C.; and Henderson, Miles A., 2021, Assessing Collapse Risk in Evaporite Sinkhole-Prone Areas Using Commonly Available Oil Field Data in the Area of the Winks Sinks, Winkler County, Texas, *in* Johnson, K. S.; Land, Lewis; and Decker, D. D. (eds.), Evaporite Karst in the Greater Permian Evaporite Basin (GPEB) of Texas, New Mexico, Oklahoma, Kansas, and Colorado: Oklahoma Geological Survey, Circular 113, p. 111–124.

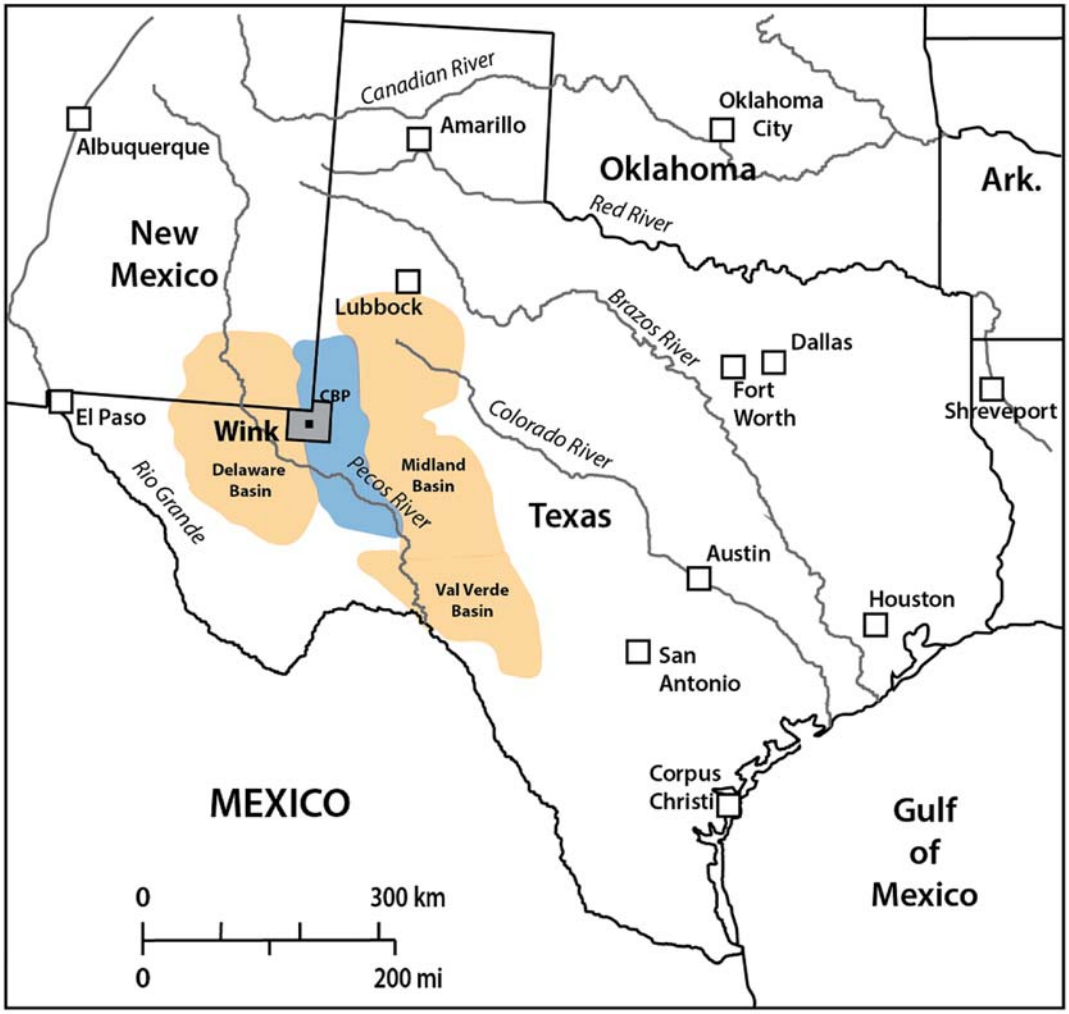

Figure 1. Regional map of Texas. The outlines of the Midland Basin, the Delaware Basin, and the Val Verde Basin, and Central Basin Platform (CBP) of the greater Permian Basin area are shown in orange and blue, respectively. The town of Wink is located on the edge of the Central Basin Platform in the sinkhole prone area above the Permian bedded salt deposits. Modified after Paine and others (2012).

GEOLOGY AND HISTORICAL BACKGROUND

Two large sinkholes have formed in the Permian Basin of west Texas. Wink Sink 1 (WS1) formed in June 1980 and Wink Sink 2 (WS2) formed in May 2002 near the communities of Wink and Kermit in Winkler County Texas (Baumgardner and others, 1982; Johnson, 1989; Collins, 2000; Johnson and others, 2003). These sinkholes formed above the Hendrick Field, originally discovered in 1926, along the western margin of the Central Basin Platform (Fig. 1) that produces from the upper Permian shelf sand reservoirs in the Yates and Tansill Formations, which lie immediately above the Permian Capitan Reef complex (Fig. 2). Approximately 200–300 m of interbedded salts with minor shale and anhydrite comprising the upper Permian Salado Formation overlies the producing horizons of the Tansill Formation at depths of ~400–670 m. Above the Salado Formation is the late Permian Rustler and Dewey Lake formations which are composed mostly of red beds and shales. Permian strata are then overlain by the Tecovas and Santa Rosa members of the Mesozoic Dockum Group composed of sands, silts, and shales. Near the surface is a variable section of Quaternary Alluvium with thicknesses related to salt dissolution associated with regional uplift and flushing of meteoric-derived fluids.

Wink Sink 1, which formed rapidly on June 3, 1980, measured 110-m across and 34-m deep soon after the time of collapse. Aerial photographs, taken in 2004, show that WS1 had an approximately circular outline 94–117-m across elongated to the northeast–southwest (Fig. 3). Water present in the bottom of WS1 is representative of the water table depth in the Quaternary Alluvium (Fig. 3C). The Hendrick No. 10-A, a 780-m-deep well drilled in 1928 and abandoned in 1964, which produced

System	Series	Delaware Basin	Central Basin Platform	
Quaternary		Alluvium	Alluvium	
Triassic		Dockum Group: Santa Rosa Tecovas	Dockum Group: Santa Rosa Tecovas	
Permian	Ochoan	Dewey Lake Rustler Salado Castile	Dewey Lake Rustler Salado	
	Guadalupian	Delware Mountain Group: Bell Canyon Cherry Canyon Brushy Canyon	Capitan Reef	Artesia Group: Tansill Yates Seven Rivers Queen Grayburg San Andres Glorieta

Figure 2. Generalized stratigraphy of the Permian Basin in the vicinity of the Wink Sinks. After Baumgartner and others (1982).

oil from the Tansill and Yates Formations below the salt section, was enveloped by the sinkhole (Baumgardner and others, 1982). Wink Sink 1 has continued to grow, initially thru collapse of the roof, and then rim that resulted in the eventual development of slopes with an angle of repose, which suggests that the cavern beneath the sink had been filled and any later collapsing rim material began to form the slope. Following the initial sink development, the area around the sink began to slowly sag without associated surface collapse, especially on the west side of the sink. The development of concentric horst and graben ring structures north, west, and south, and compression ridges perpendicular to the ring structures suggesting movement toward the center as the material is slowly tilting inward to the sink suggesting continued dissolution beneath the sink area. This response is different from that seen on the east side of the sink where there is a significant sag area that continues to develop and where the ring structures are absent. This long-term response suggests that the sag on the east side of WS1 is responding in a manner similar to that in the Wink Sag.

Since its opening, WS1 has not grown significantly in size; however, surface elevation changes are observed as a series of concentric horst and graben structures that have formed on the southwest, south, and southeast sides of WS1 (Fig. 3B and 3D). These graben structures suggest ductile deformation of the near surface around WS1, with the near-surface units stepping down and tilting inward toward the center of the sink. The outermost and largest of these horst and graben structures has a maximum offset of ~ 3 m from the outer horst into the graben center, and the inner horst is ~1.5 m below the outer horst (Fig. 3D). These features developed rapidly after WS1 formed and continued movement has been observed from the 1990s until the present day. Additional signs of surface movement surrounding WS1 are observed as a series of compression ridges noted on the caliche oil field road immediately west of the sinkhole. These compression features occur where the conical horst and graben structures are most pronounced, and the ground is shifting from all directions toward the sinkhole. The result of this movement is a space issue in the near surface, and the compression ridges result from the excess volume of material moving toward the sink (Fig. 3B). The sides of WS1 have stabilized over time with material sloughed off the flanks of the sink to create a stable, but steep, slope suggesting that the void space beneath the sink has been filled prohibiting further collapse. The area immediately east of the WS1 along the north–south lease road dropped significantly following the opening of the sinkhole and the resulting sag area continued to sink at a reduced rate. To the west, SH 115, ~180-m (600 ft) northwest of the sink has shown no evidence of elevation change; however, a 0.3-m (1ft) wide, 0.3-m (1ft) deep, and 30.5-m (100ft) long gap developed in the bar ditch of the road in 2005. The sag area to the east of WS1 is where a water supply well (Gulf Oil #11WS) is located southeast of the sink, and where the two oil storage tanks located ~300-m (1000 ft) east northeast of the sink had to be decommissioned when 0.3 m of tilt was identified on the roof of the larger tank. By 2005, the growth of the sag led to decommissioning and removal of two oil storage tanks located to the northeast of WS1 because of the 0.3-m tilt across the top of the larger of the two tanks (Fig. 4A and 4B). Within the past 20 years, the sag east–southeast of WS1 has grown to encompass the location of the plugged Gulf #10-WS well, a water supply wells immediately east of WS1 (Fig. 4C). Flow of unsaturated water from above or below the salt section, possibly through natural or induced fractures, or through holes in the local boreholes, is the most likely cause of salt dissolution and collapse at WS1 (Baumgardner and others, 1982; Johnson and others, 2003). Wink Sink 1 is monitored and has not grown further as noted during periodic field visits to confirm the surface geometry of WS1 and the surrounding area. The model for the development of WS1 is of an initial brittle failure with rapid development of the sink followed by ductile failure/sag of the eastern margin of the sink and a continual falling into the center point of the south, west, and north sides within ~ 182 m (600 ft) of the sink. This suggests that the area beneath the sink and the immediate area around it is continuing to

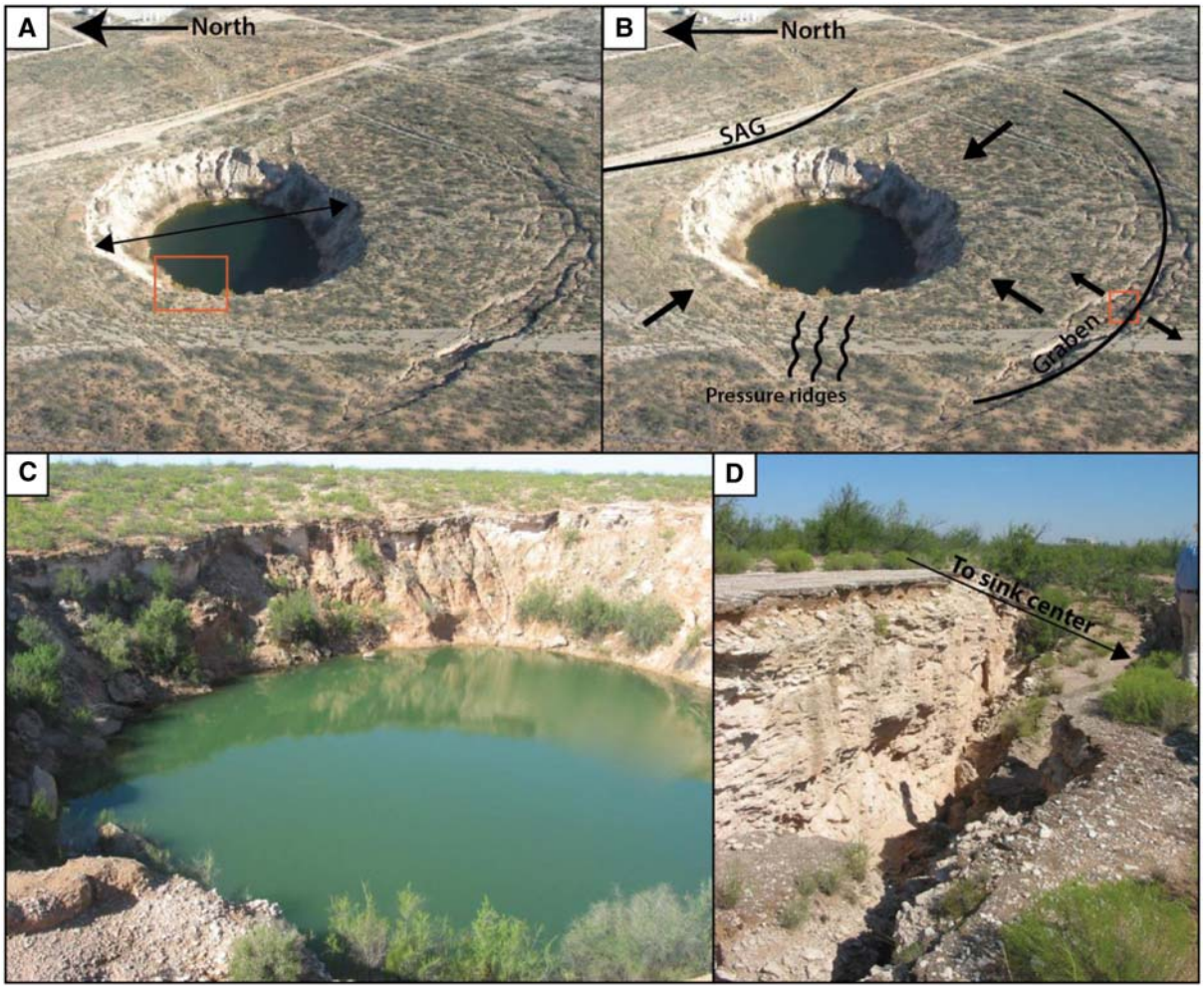

Figure 3. A) Oblique aerial view of Wink Sink 1. Arrow shows the axis of elongation. B) Same view as A, but with annotations showing the areas of movement outside of the sink. Arrows indicate the directions of surface movement that resulted in the development of a sag to the east of the sink and a graben structure to the west of the sink, and a pressure ridge to the west/northwest of the sink. C) View of Wink Sink 1 taken from the eastern side of the sink. The area is indicated as the orange box in A. D) Close up of the graben structure located to the west of the sink. The area is indicated in the orange box of B.

subside, but that the east is responding differently (ductile failure) from the north, west, and south which seem to have a combination of brittle and ductile failure. The surface geometry of the area around WS1 suggests that the areas > 180 m on the south west and north are stable at this time. Wink Sink 2 formed 1.6 km south of Wink Sink 1 on May 21, 2002 (Fig. 5). Wink Sink 2 has expanded from its original surface diameter of 137 m to an oval shape with widths ranging from 225 to 325 m with elongation in the northeast–southwest direction. Wink Sink 2 grew so rapidly that parts of almost vertical walls would fail and collapse into the sink (Fig. 5B and 5C). As the sink grew, there was little evidence of a 'bottom' to the sink as sections of the north and east walls would almost completely disappear below the water table, suggesting that WS2 had a much larger void space beneath it than WS1. Within the last few years, debris aprons have developed and stabilized along parts of the north and east walls, suggesting that the void space beneath the sink has begun to fill (Fig. 5D). It is not possible at this time to estimate the size of the initial cavern. In recent years, an area on the south side of WS2 has seen accelerated growth of a sag, or slump, with the development of an associated debris apron which bears continued observation. Wink Sink 2 encircles the location of the former Gulf #8-WS, a water-supply well that was drilled through the salt section to a depth of 1092 m in 1960 and is estimated to have yielded 800 million bbl of water for waterflood operations from the Capitan Reef in the Hendrick Field (Johnson 1982, 2003). The cause of collapse at WS2 has not been determined, but it is thought to be related to the WS-8 well (Johnson and others, 2003). Immediately after WS2 began to form, the Texas Railroad Commission, the petroleum industry

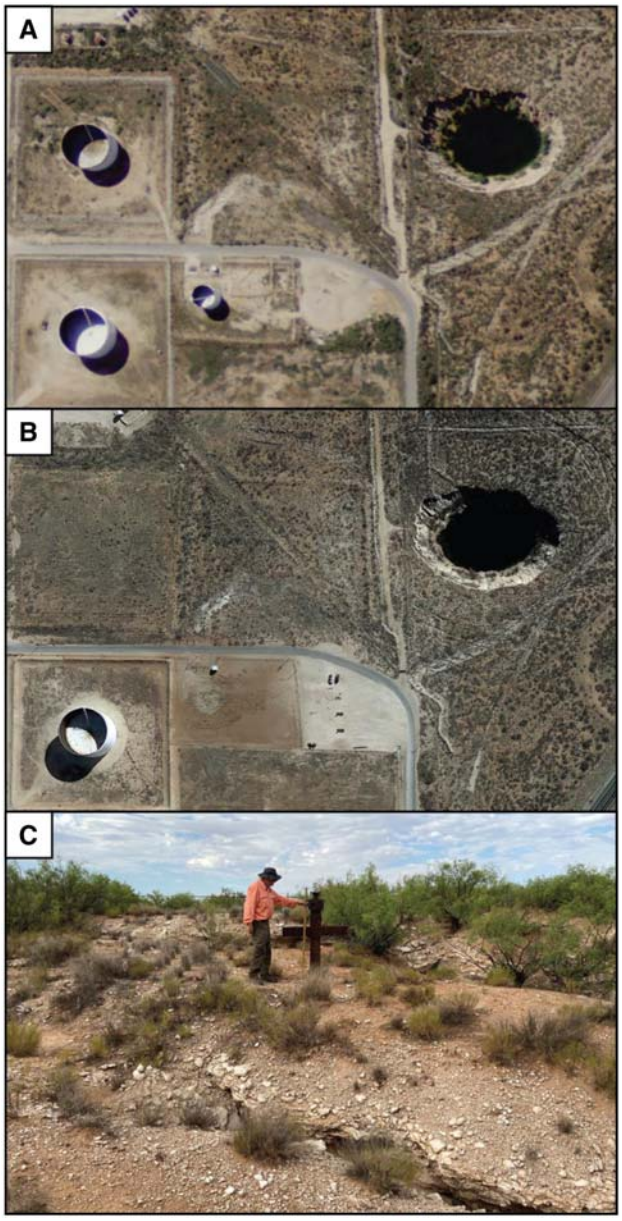

Figure 4. A) Satellite image of the tank area located north of WS1 from 2008. B) Satellite image of the tank area located to the north of WS1 from 2020. Notice two of the tanks have been removed. C) Plugged Gulf #10-WS well located on a horst structure to the south of WS1. The ground elevation has dropped approximately 1.5 m (5 ft) from the top of the well casing.

regulation agency in Texas, required that the operator begin plugging the producing wells within a quarter mile radius of the sinkhole and the surface owner placed a 2.5-m (~ 8 ft) fence around WS2. A few years later, the initial fence was engulfed by the sinkhole and a second fence was constructed around the sinkhole. As the sinkhole continued to grow, the second fence partially collapsed into the sinkhole and a third fence encompassing an area of 0.5 km^2 was constructed around WS2. Wink Sink 2, now almost 20 years old, continues to grow, and the west, north, and east sides continue to exhibit almost vertical walls with sections spalling off from these sides and collapsing into the sink (Fig. 5C). Within the past 2 years, this activity has diminished, and slopes have begun to form along the base of the steep cliffs, suggesting that the sink is entering a fill phase, as WS1 did. Discussions with local officials and field-workers indicate that they were convinced at the time that WS2 was going to form in the center of the Wink Sag area. As with WS1, the formation of WS2 was sudden and the growth was rapid in an area where there was no evidence of pre-existing surface features or sag. Over the past decade, the elevation on the north and west sides has remain stable; however, the south side has shown a significant drop in elevation, and the east side has shown a less severe drop.

About a decade after WS1 formed, local residents and oil field workers began to notice an area about 1.6-km (1 mile) east of the eventual location of WS2, and just northwest of the intersection of Winkler County Roads 201 and 204, had begun to sag or deflate (Fig. 6) eventually leading to the closure of CR 204, and relocation of many of the oil and gas pipelines in the area. This area is called the "Wink Sag" by local residents and Hendrick Field workers. A series of surface fissures forming incomplete concentric elliptical arcs encircle the depressed area centering on the area of the greatest elevation change (Fig. 6). The surface manifestations of these fractures typically are 0.3 m wide and 1–3 m deep with no apparent elevation changes across the fractures. A small study completed in 2004 to 2005 to evaluate the extent of the recently developed fractures associated with the Wink Sag (Burch & Trentham, 2007). A hand-held GPS unit was used to identify the location of the larger surface fractures identified around the Wink Sag. Two concentric elliptical "rings" were partially identified by tracking the surface fractures around the Wink Sag to the east, south, and west of the sag (Fig. 7). These surface features were not identified to the north of the sag area. The surface expression of these features was attributed to ductile failure in the subsurface salt that does not extend to the north. The area to the north of the sag has the potential brittlely fail in the future. Additional partial rings continue to slowly develop to the south of the Wink Sag. At the same time, several compression ridges began to form where the surface was more competent (caliche roads and drilling pads) and at four locations older abandoned buried oil field pipes (~20.3-cm diameter) buckled and rose above the ground surface up to the heights of 1.5 m. Similar deformed pipe features are seen around WS1 and WS2.

In 2006, the Apache #1 well on the eastern margin of the Sag failed and was plugged, and in 2010, the casing

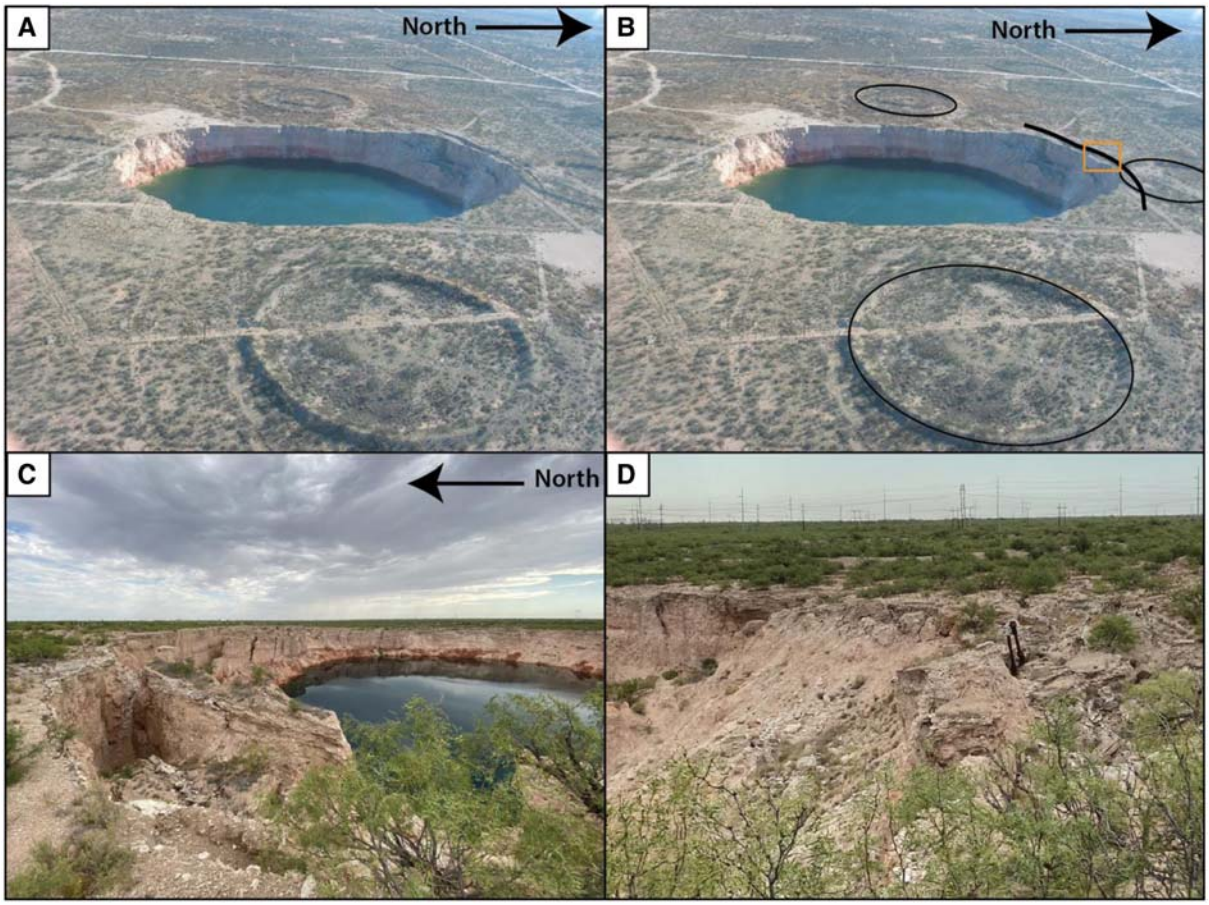

Figure 5. A) Oblique aerial view of Wink Sink 2. A scarp has developed to the North of sink that is likely to collapse into the sink in the near future. The circular features located around the sink are the surface earthen berm from the 1930s drilling activity in the area. B) Annotated view of A showing the outlines of the earthen berms surrounding WS2. C) Nearly vertical wall that is migrating toward the center of the sink. Photo shows the view of the sink from the western edge. The orange box in B shows the location of C. D) Stabilized debris aprons showing the nearly vertical walls of the sink have stabilized around a plugged well.

from the Apache #3 second well collapsed/sheared in the salt section suggesting possible collapse or shifting in the subsurface. These wells were subsequently plugged and abandoned. What concerned the residents initially about the Wink Sag was a fissure, estimated at ~28-cm deep in places, 0.6-m wide, and ~60-m long that began to form through a power substation and exposed a gas line, which provided natural gas to the local homes, businesses, and Wink Elementary School (Fig. 8). After the initial development of the fissure, it slowly ceased to grow; however, the power substation continues to be monitored and the pipeline to Wink has been rerouted away from the sinks. Additional concentric arcs began to develop and have continued to develop on the west and south of the center of the Sag. The rate of growth appears to be greatly reduced in the past 10 years to the point where many of the fissures appear to be stable, although their location relative to the county roads and power lines continues to be monitored.

Ackers and others (1930) presented evidence of natural dissolution and collapse in the subsurface of the Hendrick Field. Two examples of core recovered in 1928 from the Southern Crude #T-88-P-1 Hendrick show collapse in the "anhydrite section" (Fig. 9A), and from the Southern Crude #T-88-N-3, Sec 28, Blk 26, the well was 32° off vertical, showed 40° dip on beds at 716 m (2350 ft) near the base of the Salado Formation (Fig. 9B). Highly deviated wells were common in Hendrick Field and these cores were recovered to evaluate where and why the deviation was occurring in the salt section. These cores show that some of the dissolution and collapse features present in the salt section were present prior to any oil and gas activities in the area. This dissolution was likely associated with tectonic uplift that affected the western Permian Basin beginning with the Laramide Orogeny and continuing intermittently through Rio Grande Rifting and Basin and Range extension. These tectonic events had various effects on

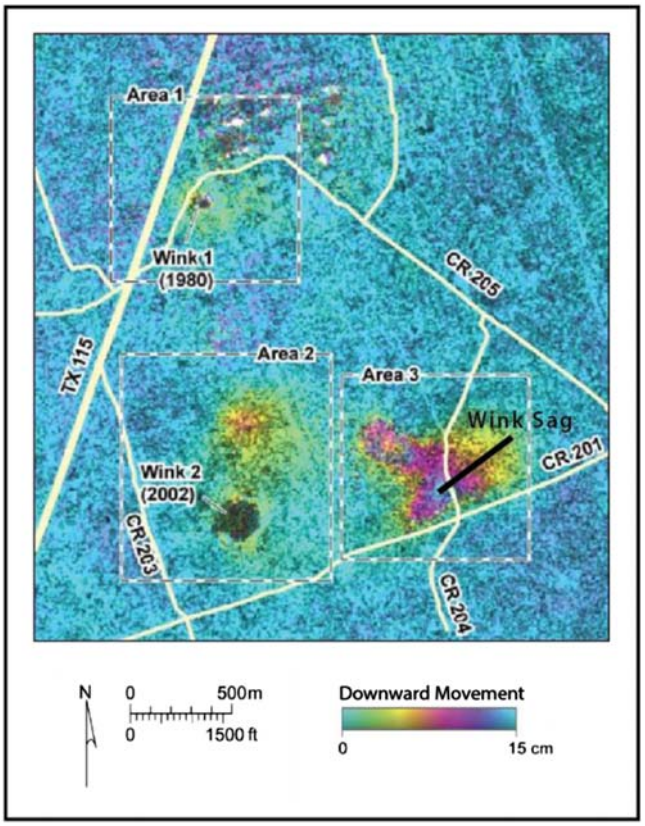

Figure 6. InSAR inferogram of the Wink Sinkhole area showing the downward movement that occurred between January and July 2007 modified from Paine and others (2012). Areas of subsidence are observed around WS1 and WS2. Additional areas of increased subsidence are noted to the east if WS1, north of WS2, and at the location of the Wink Sag east of WS2.

the western margin of the Central Basin Platform and across the Delaware Basin where meteoric derived flushing fluids resulted in significant dissolution in the Salado Salt. The eastern edge of dissolution coincides with the north–south trend of the Hendrick Field. Early total dissolved solid (TDS) analyses of produced waters from the Hendrick Field varied from 1000 ppm to 100,000 ppm TDS suggesting circulation of fresh waters between the Capitan Reef and the Yates/Tansill formations prior to oilfield operations in the area. The evidence of the collapse breccias from core reported by Ackers and others (1930) suggests that these pathways likely extended upward into the salt section.

Additional anecdotal evidence for subsurface changes is identified by unusual oilfield production activity in the Hendrick Field. Following the formation of WS1 on June 3, 1980, the Gulf #28 T. G. Hendricks, originally drilled in 1928, suddenly flowed 23,000 BO in 20 days in 1982. Operators in the field thought that this short-term multithousand-barrel increase in production was tied to recent salt dissolution opening pathways to isolated oil-charged caverns at virgin reservoir pressures in the salt section. The report was "every frac tank" in Winkler County which was lined up to store the oil. The well returned to "normal" production as rapidly as it surged and continued with normal production until plugging in 1986. During plugging, the crew reported "Bad Pipe" at 441 m (1450 ft) opposite the Salado. The Arrington #2-A Hendrick, also drilled in 1928, approximately 130 m from the SW edge of WS1 (Fig. 10), suddenly began flowing oil in 1997, and produced 10,000 BO in 30 days. This well was still "flowing on 9/64' choke" today, making as much as 40–50 BOPD as reported by a fieldworker during a July 2020 site visit. When attempts were made to increase the production by opening the choke, the well rapidly began to produce only water suggesting a thin oil column above a pressurized water leg near WS1. The behavior of the Arrington well to the southwest of WS1 suggests that there is a significant movement at greater depths that can be interpreted based on the near-surface behavior.

When WS2 formed rapidly in 2002, oilfield workers reported that there were "some" minor movements in the area during the 2-week period before the sink formed in a single day. However, the surface movements noted were not located where WS2 is located but in the area between WS1 and the eventual location of WS2. In 2005, Apache Corporation (Apache #12) was drilling a well 7.24-km (4.5 miles) northwest of WS1 (Fig. 10) where circulation was lost at ~548 m (~1800 ft) in Salado salt, the bit dropped ~5 m ~(16ft), and the well began to flow 100 BO per hour. After flowing for a number of days, the Apache #12 well ceased flowing oil, the "Salt Cavern" interval was cased, and drilling and completion continued. The Apache #12 well is a direct offset to other 20-acre spacing wells, suggesting that there was an isolated, oil-filled cavern no larger than 10 acres. It is possible that a cavern developed in the salt section and oil migrated into the cavern and then was sealed off, remaining at virgin reservoir conditions until it was penetrated by the drill bit. No attempt was made to evaluate the size of the cavern before casing was set in the well. The Apache #12 well was eventually plugged and abandoned in the Tansill and Yates without producing.

In 2006, Apache reported a relatively new well (Apache #1 T.G. Hendrick T-89-C) located on the southeast edge of the Wink Sag (Fig. 10) had to be Plugged and Abandoned in September 2007 because of sheared casing at shallow depth in the salt section. The deepest plug was set at ~342 m (~1124 ft), suggesting that attempts to reach the Yates and Tansill producing interval were unsuccessful. Approximately 160 sacks of cement were pumped into the Apache #1 without filling the well bore more than a few feet, suggesting that the Capitan, Yates/Tansill, and Salado Salt are likely still in communication unless there were plugs set earlier and not in the

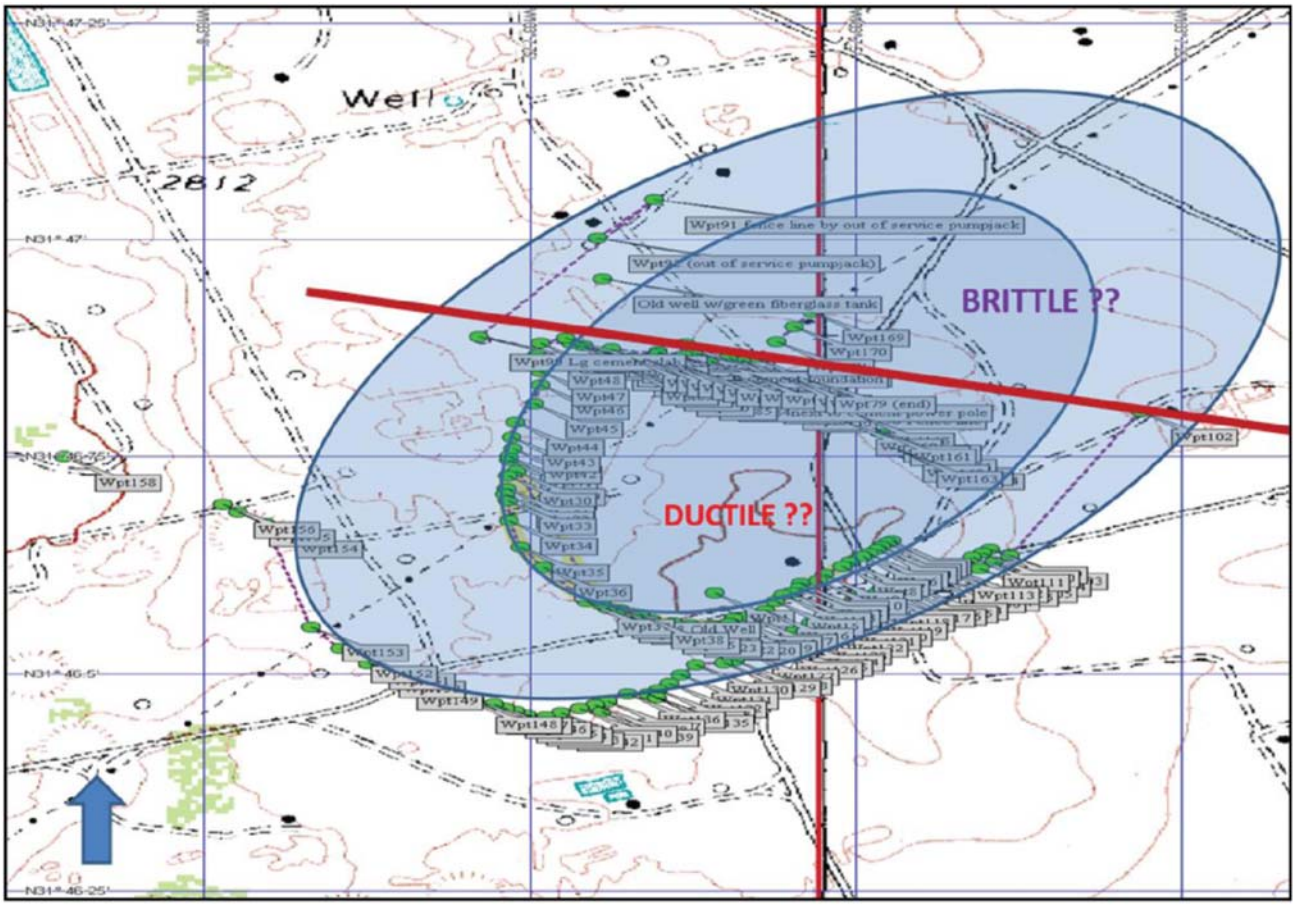

Figure 7. Ellipse features identified by GPS mapping of surface expression of large fractures surrounding the Wink Sag. The fractures are easily traced to the south, southeast, and southwest of the sag area. Burch and Trentham (2007) interpret this surface expression as ductile failure in the subsurface where the surface features are identified and possible brittle failure possible in the future to the north where they are not identified.

available plug and abandonment report. Apache reported another well (Apache #3 T.G. Hendrick T-89-C) also located on the southeast edge of the Wink Sag was plugged and abandoned in August 2010 because of sheared casing at a shallow depth of ~335 m (~1100 ft) in the Salt Section. The deepest plugs in the Apache #3 were set across the producing zone, and the shallower plugs in the Apache #3 were set across the fresh water-producing interval. Before the casing collapse, the well was making 16 BOPD.

WATER ANALYSES

Produced waters were collected for the analysis of Total Dissolved Solids (TDS), pH, percent (%) oil cut, and resistivity from Apache Corporation wells at the University of Texas Permian Basin. Locally, fresh water is produced from both Quaternary alluvial deposits and the Santa Rosa Member of the Dockum Group. The Occidental Petroleum-operated El Capitan Water Supply wells, producing from the Capitan Reef, have historically been capable of producing +/- 50,000 barrels of water a day from each well, which is indicative of the productive potential of the Capitan Reef. The Capitan Reef water in this area is brackish with 7000 to 12,000-ppm TDS and is used primarily for "make-up" water in San Andres and Grayburg waterfloods elsewhere in the basin. Two water supply wells, drilled in the 1950s, are aerially related to the Wink Sinks, and as a result, the location and history of all the water supply wells needed to be documented. Produced water analyses range in Total Dissolved Solids (TDS) from a few thousand part per million (PPM) to 100,000 PPM. Those wells with higher TDS suggest the potential for the development of holes in the casing opposite the salt section in some wells. Those wells with the lowest TDSs suggest artesian flow from the Capitan Reef below the productive Yates and into the salt section. Anecdotal evidence from unusual, multithousand barrels, short-term changes in production in isolated wells suggests that salt dissolution may be opening isolated oil-charged caverns at virgin reservoir pressures in the salt section that were formed preoil production. Produced water from

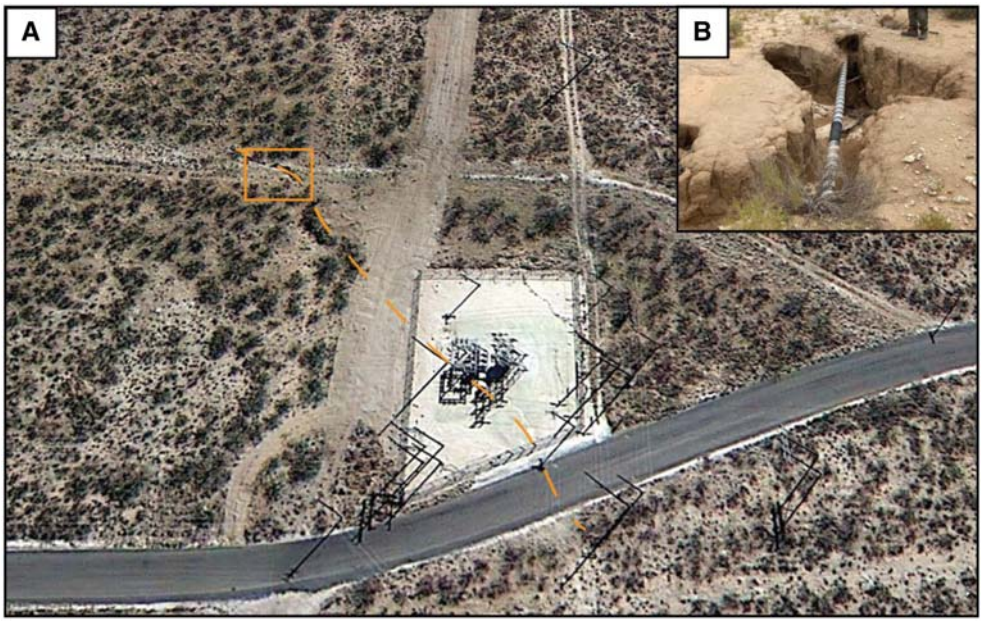

Figure 8. A) Location of 28-cm deep, 0.6-m wide, and approximately 60-m-long surface fissure going through the power substation. B) Exposed natural gas pipeline exposed by the surface fissure.

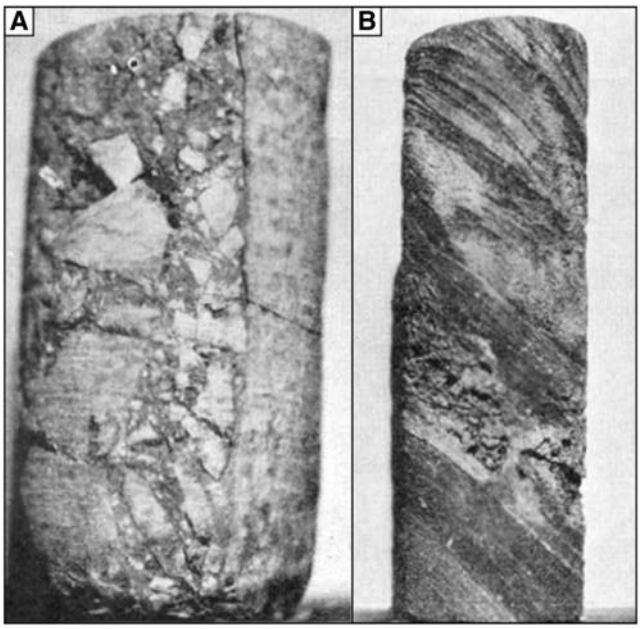

Figure 9. Example of well cores recovered from the Hendrick Field from Ackers and others (1930). A) Southern Crude #T-88-P-1 Hendrick showing collapse in the anhydrite section from 1928. This collapse breccia from salt dissolution was present prior to any oilfield activities in the area. B) Core from Southern Crude #T-88-N-3, Sec 28, Blk 26 showing 40˚ dip on beds at −2350 ft. The borehole was 32˚ off vertical

31 wells from Apache Corp wells in the Hendricks Field (Fig. 10) was sampled and analyzed for TDS PPM. Wells with TDS > 31,400 ppm are noted in red, and wells with TDS ≤ 31,400 ppm are noted in blue. Two clusters of high TDSs were identified. These wells with high TDS correspond to those with significant plugging issues, one associated with identification of the Wink Sinks, and one centered ~ 4.8 km (3 mi) north of Wink Sink 1. One well with TDS > 31,400 ppm is noted between these two clusters. Also, random high-risk wells are spread across the surveyed area. The proximity of 2 of the Gulf oil drilled water supply wells to the sinks and sags suggested that they may have been a contributing cause of dissolution of the Salado salt if holes developed in the casing opposite the salt section.

WELL-PLUGGING REPORTS

During the 90+ year history of the Hendrick Field, the field had gone from producing high oil cuts to producing large volumes of water that required the building of a large number of surface evaporation pits to dispose of produced water, to requiring large volumes of Capitan Reef water as part of a field wide waterflood, to the present when most of the original wells have been plugged and only a fraction of the field is still in production, and in many cases producing from relatively new wells (Fig. 11). Well-plugging reports were acquired from the publicly available Texas Railroad Commission (TRRC) electronic well file database, Gulf Oil water supply well data from files at the Midland Energy Library, and anecdotal evidence of unusual oil production events gathered from conversations with local oilfield workers and local government officials. The plugged oil wells were identified and scanned completion and plugging report

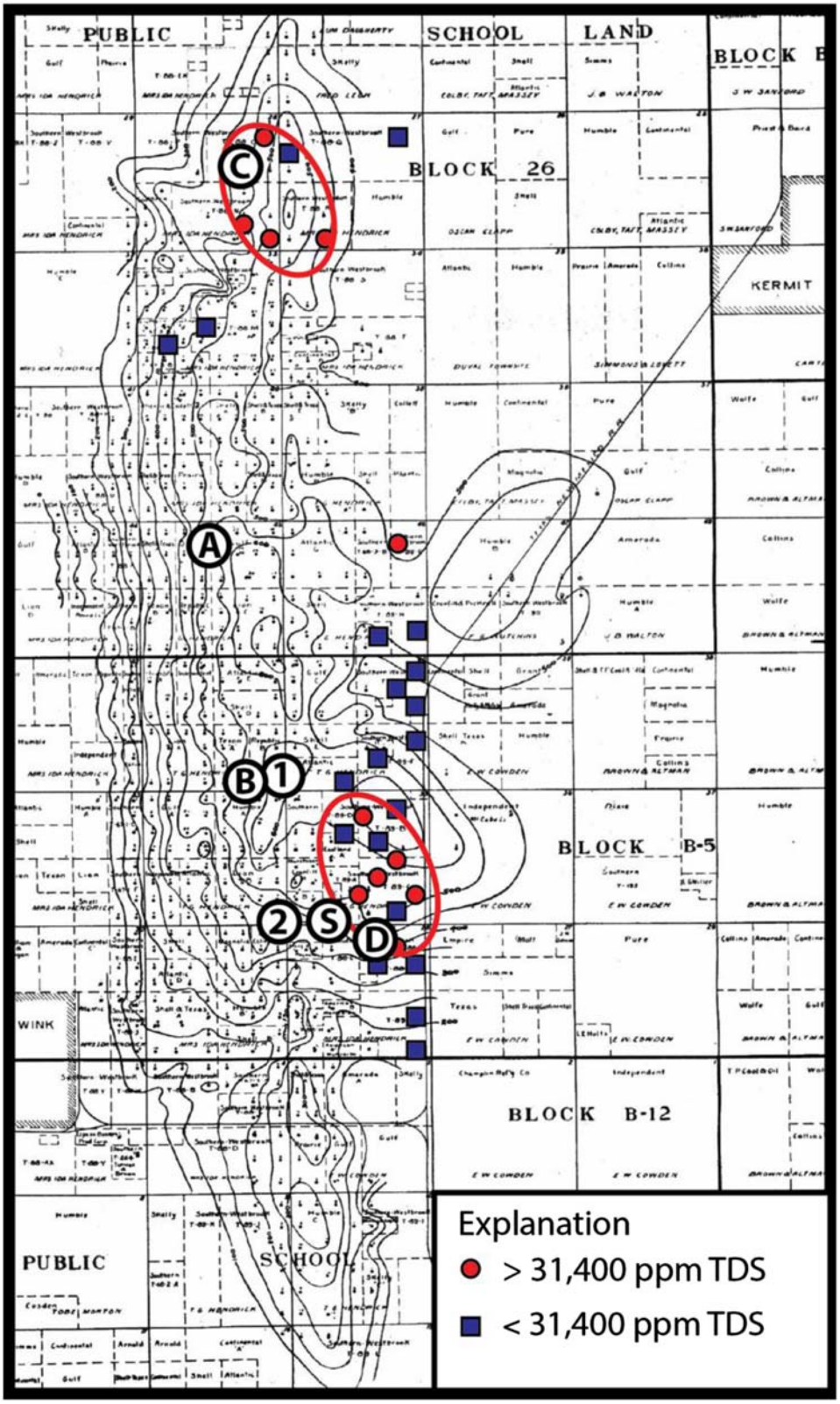

Figure 10. Location of produced water analyses from 33 Apache Corp. wells in the Hendricks Field analyzed for total dissolved solids (TDS). Five of the wells sampled fall off the map area (Hend Week #10, HEND T-88-GX #8, Hend T-88-GX #7, Hend T-88-F #1, and Hend T-88-D #7). Two clusters of wells with TDS > 31,400 ppm were identified. A single well with high TDS is located ~ 2-km northeast of WS1. 1=WS1, 2=W2, S=Sag, A=Gulf #28 well, B=Arrington #2-A well, C=Apache #12 well, D=Apache #1 and Apache #3 wells.

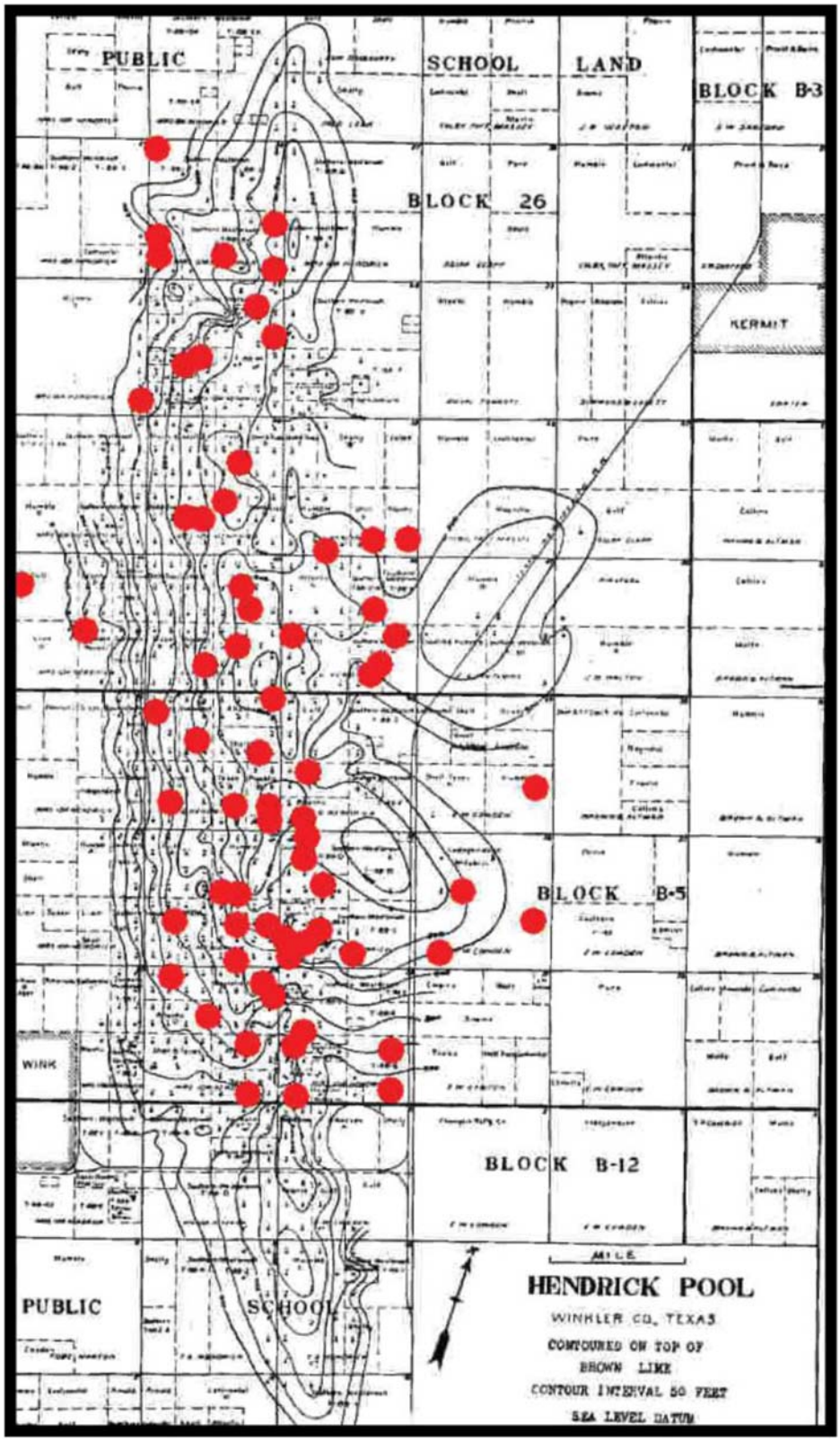

Figure 11. Approximate locations of wells in the Hendrick Field with bottom plugs set in or above the Salado Salt at depths between 240 m (800 ft) and 520 m (1700 ft). Base map contoured on the top of the Tansill Formation from Ackers and others (1930). Contour interval is 50 ft.

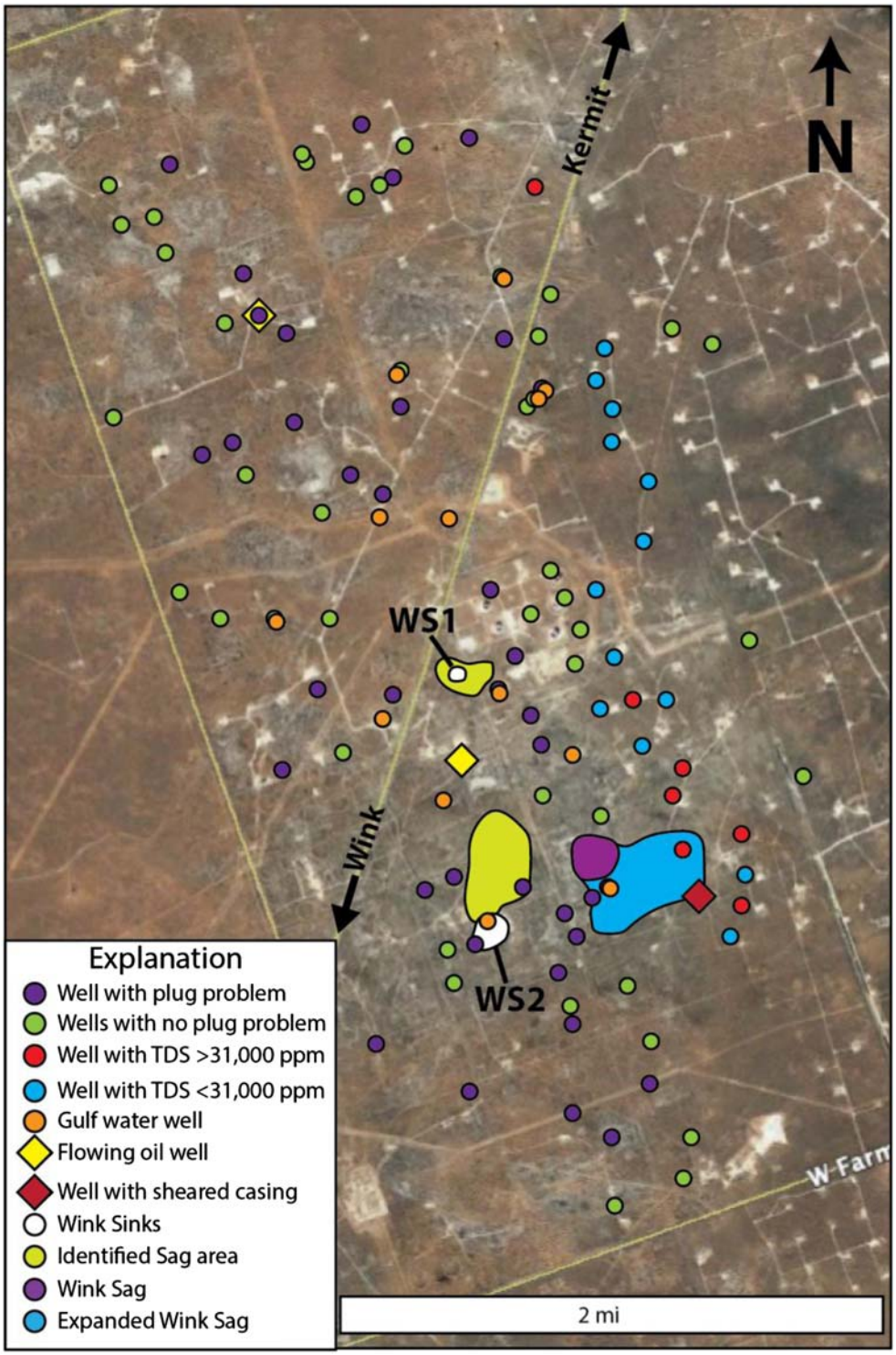

Figure 12. Locations of wells surrounding WS1, WS2, and the Wink Sag.

documents available for review were evaluated. As completion techniques have varied through time, the amount of cement used, whether the casing was cemented to surface or "tacked in" across the producing horizon was noted. In each case, as required by the former regulatory body, the Texas Board of Water Engineers (TBWE) and the current Texas Water Development Board (TWDB), the surface casing was cemented across the fresh-water zone to depths of approximately 182 m (600 ft). Today, the TWDB requires cement to be circulated to surface allowing for effective isolation of the salt section from the produced fluids. In wells where cement was not

circulated to surface, the volume of cement used was only sufficient enough to create a seal between the intermediate/deep well casing and penetrated the surrounding formation through the producing interval and the lower section of the Salado Formation.

Each plugging report includes data on the number of cement plugs, top/bottom of each plug, number of sacks of cement used in each plug, the casing and tubing left in the hole, and data on whether there were issues recovering tools, pumps, tubing, or other casing integrity issues. These data were collected and interpreted to evaluate the condition of the wellbore prior to plugging and that the well integrity was compromised if there was potential for production associated with salt dissolution. Problems identified during plugging operations include unusually large volumes of cement required, operations to cement the bottom of the well unable to reach the producing formation, or cementing operations unable to get below surface casing. Those wells with significant issues include large volumes of cement needed to set plugs, suggesting that there were significant holes in the well casing, inability to recover pumps and tools from below the salt section, collapsed casing or intervals where the casing is no longer intact within the salt section of the wells. A common practice when plugging a well is to attempt to isolate the Capitan Reef and the open hole or perforated Yates-Tansill section from the Salado salt section and to set shallow plugs to isolate the salt section from freshwater. Wells where cement plugs were not placed across the producing zone to separate it fully from the Salado Salt are considered high-risk wells. The TRRC required the operator to plug every well within a ¾ sq. mile area around the developing WS2. The three closest wells were the 2A, 13, and 15. The Arrington #3 Hendrick "A" well, 400' immediately south of WS 1, was plugged in 2000. A Cast Iron Bridge Plug was set above the producing perfs, and a series of 6 cement plugs were set in the well. The engineer who supervised the plugging of the well reported that the workover rig was in danger of sinking into the ground and that it appeared that the surface was "collapsing" beneath the rig, as they plugged the well. Of the 132 well-plugging reports reviewed, 32% (42 wells) had the bottom plug set in or above the Salado Salt (Fig. 11), with most wells noting casing issues between 240 m and 520 m (800–1700 ft). Clusters of problem wells associated with karst development near the Wink Sinks were identified along a north–south trend (Figs. 11 and 12). These well clusters do not appear to be associated with any surface features in the area. The plugging reports evaluated can be sorted into three risk categories: No Risk, Moderate Risk, and High Risk. No Risk wells are those where there were no issues encountered during plugging of the wells. Moderate Risk wells encountered minor issues during plugging. High risk wells encountered significant issues during plugging.

CONCLUSIONS

The development of the Sinks and Sag in the Hendrick Field area suggests that there are differing responses to subsurface dissolution and collapse. Oil-field personnel familiar with the development of both WS1 and WS2 and the Wink Sag generally agree that there was little warning of the formation of the Wink Sinks. They saw no significant changes at the surface that would have suggested the formation of the sinks. Conversely, the Wink Sag formed over a decade, and grew slowly to its current size and shape, as have areas peripheral to the sinks. As residents, government officials, and industry representatives wish to better understand the potential for sinkhole formation and growth in the area, further collection of water-chemistry data from other wells and access to additional well files is necessary to complete a more comprehensive study across the area. At Wink, as in similar settings worldwide, the issues that concern residents, government officials, and industry representatives are the same: how did the sinkholes form, will they continue to expand, and where might new sinkholes form that would threaten public safety and infrastructure? Although the specific cause of each sinkhole may never be known, for those in petroleum-producing provinces, well data can prove to be extremely useful in quantifying the risk. Incorporation of these data with remote sensing and geophysical methods, such as InSAR and Microgravimetry, can help understand critical issues, such as: subsurface groundwater movement, potential collapse areas not, as yet, identified by remote-sensing methodologies, the existence and location of precursor ground deformation, and the location of shallow collapses and caverns that indicate the potential for future gradual subsidence or collapse.

ACKNOWLEDGEMENTS

Funds to support Wink investigations were donated by several companies over the years including Chevron-Texaco, Devon, and Apache. Ron Truelove (Devon) facilitated access to sinkhole-area properties near Wink. We would also like to thank Judge Bonnie Leck (retired), Judge Charles Wolf, County Commissioner Robbie Wolf, and all the other Winkler County officials that have been so helpful in completing this work. Finally, thanks to Ken S. Johnson for the invitation to contribute to this volume on evaporative karst and for his valuable review of this contribution on the Wink Sinks.

REFERENCES CITED

Ackers, A.L., DeChicchis, R., and Smith, R.H., 1930, Hendrick Field, Winkler County, Texas: American Association of Petroleum Geology, Bulletin, Vol. 14, part 2, p. 923-944.

Baumgardner, R.W., Jr., Hoadley, A.D., and Goldstein, A.G., 1982, Formation of the Wink Sink, a salt dissolution and collapse feature, Winkler County, Texas: The University of Texas at Austin, Bureau of Economic Geology, Report of Investigations 114, 38 p.

Beck, B.F., editor, 1995, Karst Geohazards: Engineering and environmental problems in karst terrane: Proceedings of the Fifth Multidisciplinary Conference on Sinkholes and the Engineering and Environmental Impact of Karst, Balkema, Rotterdam, 582 pp.

Burch, M., and Trentham, R.C., 2007, Documentation of surface features associated with the continued development of the Wink Sag, Winkler County, Texas: West Texas Geological Society, Fall Symposium.

Collins, E.W., 2000, Reconnaissance investigation of active subsidence and recent formation of earth fissures near the 1980 Wink Sink in the Hendrick oil field, Winkler County, Texas (abstract): Geological Society of America, South-Central Section, Abstracts with Programs, Vol. 32 (3), A-6.

Johnson, K.S., 1989, Development of the Wink Sink in West Texas due to salt dissolution and collapse: Environmental Geology and Water Science, Vol. 14, p. 81-92.

Johnson, K.S., Collins, E.W., and Seni, S.J., 2003, Sinkholes and land subsidence owing to salt dissolution near Wink, West Texas, and other sites in western Texas and New Mexico, *in* Johnson, K.S., and Neal, J.T., eds., Evaporite karst and engineering/environmental problems in the United States, Oklahoma Geological Survey, Circular 109, p. 183-195.

Johnson, K.S., and Neal, J.T., eds., 2003, Evaporite karst and engineering/environmental problems in the United States: Oklahoma Geological Survey, Circular 109, 353 p.

Paine, J.G., Buckley, S.M., Collins, E.W., and Wilson, C.R., 2012, Assessing collapse risk in evaporite sinkhole-prone areas using microgravimetry and radar interferometry: Journal of Environmental and Engineering Geophysics, Vol. 17, no. 2, p. 73-87.

Evaporite Dissolution and the Waste Isolation Pilot Plant (WIPP) in the Northern Delaware Basin, Southeastern New Mexico

Dennis W. Powers and Robert M. Holt
Department of Geology and Geological Engineering, University of Mississippi, Oxford, Mississippi

ABSTRACT.—As a site in bedded salt for disposing transuranic waste from United States defense programs, Waste Isolation Pilot Plant (WIPP) has been intensively investigated for natural processes, including dissolution, that might affect long-term isolation of these wastes.

Downward dissolution of the evaporite sequence was considered from the beginning of locating the WIPP site. Dissolution investigations expanded and intensified with the discovery in late 1975 of a collapse chimney (aka breccia pipe) in a potash mine in the area of WIPP. Across the area, various surface depressions and subsurface features (structural changes, thickening, and thinning) of the evaporite sequence were identified. Lateral dissolution within the evaporite section and more localized dissolution from below were suggested as mechanisms for these features. From about 1977 to 1983, some of these features were investigated in detail by geophysical techniques, drilling and coring, and mapping to determine if they were induced by dissolution. Significant resources were devoted to these investigations; by 1983, most had been generally resolved, and the WIPP site was not found to include dissolution features or processes considered detrimental to long-term waste isolation.

Nash Draw is a major karst feature west of the WIPP site, and karst was proposed at WIPP in 1982 based on a micro-gravity survey. A significant gravity anomaly was detected across a surface depression outside of WIPP; an earlier drill hole in the depression had encountered cavernous porosity in Rustler units. Another such gravity anomaly in a surface depression outside of WIPP was drilled without encountering cavernous porosity or water inflow. Lack of geologic or hydrologic evidence for karst within the WIPP site is not considered by some to be significant evidence that karst does not exist at WIPP, and it is not clear that there is a reasonably falsifiable hypothesis of karst.

Prior to WIPP, Rustler Formation mudstones were believed to be dissolution residues. We now interpret these mudstones as largely facies changes based on detailed study of cores, interpretation of geophysical logs, and mapping in large-diameter shafts. The hydrogeological conceptual model of the Culebra Dolomite Member of the Rustler was revised using these data. The Culebra is the main hydrologic pathway for releases in failure scenarios for WIPP.

From early work for WIPP to more recent articles assessing dissolution, features have been assigned genetic terms or asserted to be dissolution features without direct evidence of dissolution. We provide evidence that contradicts a dissolution origin for two such features.

Early work was not measured against a well-defined performance standard and was commonly very conservative. The performance standard later established is the probability of release at the WIPP boundaries within 10,000 yr. This standard resulted in developing the means of evaluating processes; many early concerns about dissolution became insignificant under this standard. A performance standard is critical for evaluating any kind of facility where geological processes may be significant.

Powers, Dennis W.; and Holt, Robert M., 2021, Evaporite Dissolution and the Waste Isolation Pilot Plant (WIPP) in the Northern Delaware Basin, Southeastern New Mexico *in* Johnson, K. S.; Land, Lewis; and Decker, D. D.(eds.), Evaporite Karst in the Greater Permian Evaporite Basin (GPEB) of Texas, New Mexico, Oklahoma, Kansas, and Colorado: Oklahoma Geological Survey, Circular 113, p. 125–149.

INTRODUCTION AND BACKGROUND STUDIES

Objectives

Salt (halite) is highly soluble in water, and this property was and is of great interest for the disposal of radioactive waste in a mined location in salt. Stability of over geological time periods is expected. Although late Permian salt beds in northern Delaware Basin have survived over 250 Ma, there is also clear evidence that some to all salt has been removed, especially in the western part of the basin. Our objectives are to review the issues raised about dissolution at and near the location of Waste Isolation Pilot Plant (WIPP), extensive efforts to address those issues, and the general outcomes.

Concerns about, and perceptions and evaluations of, dissolution of evaporites affected locating, characterizing, and assessing the performance of the current site of the WIPP. Powers and Holt (2008) partially addressed some lessons learned about dissolution. We review in more detail the longer term and more extensive manner in which dissolution affected investigations of the WIPP site geology and hydrology. Through the course of locating the site in 1975 to the current operations of WIPP, our understanding of dissolution morphed into significantly different conclusions about the processes of dissolution, extent, timing, and effects. Standards for performance with respect to isolating the waste altered the approach to evaluating all factors related to WIPP performance. Dissolution is one process where our understanding and incorporation into performance assessment dramatically differ from early work.

We cannot address all assertions, suggestions, or rebuttals about processes, locations, stratigraphic intervals, timing, and consequence of dissolution. Nevertheless, we are interested in the directions and outcomes of WIPP activities as they developed in response to emerging issues or concerns. We also present specific counters (with evidence) to two long-standing assertions about dissolution as examples of how additional data should resolve issues or perhaps reduce speculation.

The two most thorough (and underappreciated) reviews to date of dissolution are by Lambert (1983) and Lorenz (2006a, b). Lambert undertook an extensive review of various dissolution proposals as they were understood at the time WIPP began to explore the underground through shafts and drifts. In response to a request by the US Environmental Protection Agency (EPA), Lorenz reviewed work related to karst and Rustler dissolution under general heading of "karst in the Rustler Formation."

Bachman (1987) presents a succinct, but extensive, review of karst and dissolution in the region that is built on his many years of research into the topic.

Rechard (2000) provides an excellent, detailed review of the history of the WIPP project with respect to regulations, laws governing WIPP, and performance assessment, combined with the geological and hydrological aspects that more directly affected performance. Weart and Chu (1997) review broadly scientific issues related to compliance with EPA standards; natural geological processes, including dissolution, were regarded as not affecting the performance during the 10,000-yr regulatory period.

Much of the study of dissolution occurred in the initial 15 yr of WIPP. Reports are less available as a consequence. A guide to the geotechnical literature of WIPP (~950 items) from 1972 to 1990 includes abstracts and some annotations (Powers and Martin, 1993). We provide URLs for certain documents that are available through various sources.

The Waste Isolation Pilot Plant (WIPP) and Dissolution Overview

WIPP is a geologic repository, located near Carlsbad in southeastern New Mexico (Fig. 1), for mixed transuranic waste from United States defense programs. The name reflects early history when it was proposed as a "pilot" plant to demonstrate safety for disposing radioactive waste in salt beds.

At the request of the Atomic Energy Agency (AEC), the National Academy of Sciences (NAS) reviewed options for the disposal of radioactive waste, recommending disposal in salt (NAS/NRC, 1957). A review of salt deposits in the United States (Pierce and Rich, 1962) led to selecting an existing salt mine near Lyons, Kansas, for experiments and, presumably, disposal of radioactive waste (e.g., Weart, 1979; Walker, 2006–2007). A significant technical problem was that some drill holes through the evaporites and into deeper aquifers created sinkholes. These drill holes were mainly saltwater disposal wells where injection of brines with H_2S corroded casings, allowing the undersaturated (with respect to halite) injected brine to dissolve salt to such an extent that the overlying rocks subsided or collapsed (e.g., Walters, 1975). Improperly plugged and abandoned oil wells similarly led to subsidence as freshwater traveled down through salt beds into underlying oil production zones (Croxton, 2003). Technical problems and growing public objections led to abandoning the Kansas site in 1972 (e.g., Walker, 2006–2007). Concern over effects from boreholes through the evaporites carried over and was incorporated into the task of locating the site now known as WIPP.

After further review at the national scale, the focus turned to southeastern New Mexico and the salt beds of the Delaware Basin (a part of the Permian Basin) (Fig. 1). Several early studies by the US Geological Survey (USGS) included information about dissolution of the salt beds in southeastern New Mexico (Bachman, 1973, 1976, 1980, 1981; Jones and others, 1973).

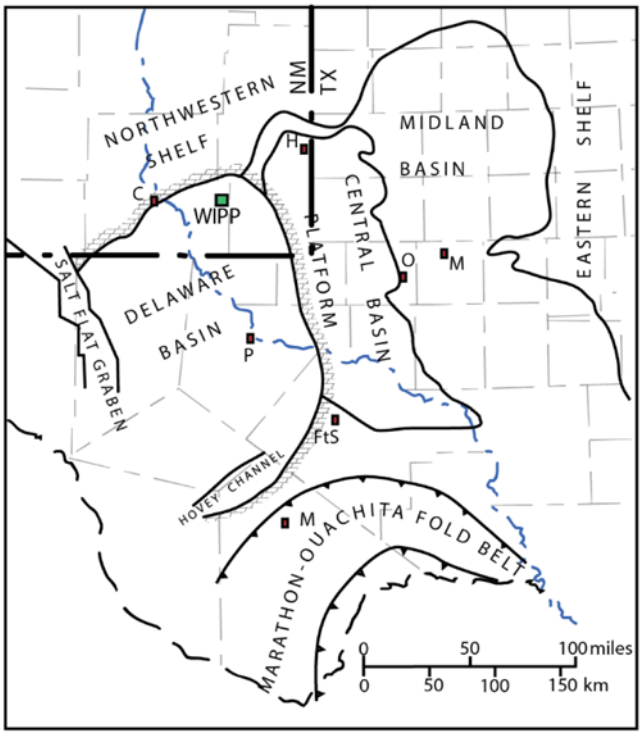

Figure 1. Structural setting in the Permian Basin region around WIPP at end of Permian (modified from Hills, 1984). WIPP is located in the northern Delaware Basin. C = Carlsbad, H = Hobbs, O = Odessa, M = Midland, FtS = Ft. Stockton, M = Marathon, and P = Pecos. The Pecos River is represented by the blue dashed line.

In 1974, Oak Ridge National Laboratories (ORNL) drilled two boreholes (AEC-7 and AEC-8) at an initial site in southeastern New Mexico (Fig. 2, "old site"). The project was transferred to Sandia National Laboratories (SNL) in Albuquerque, New Mexico, in 1975, under the administration of the Albuquerque office of the Energy Research and Development Administration (ERDA; later redesignated Department of Energy [DOE]). A third drill hole (ERDA-6), drilled in mid-1975 at that location, encountered highly deformed evaporites (Anderson and Powers, 1978; Jones, 1981; SNL and USGS, 1983) and pressurized brine with H_2S. The site did not meet one of the criteria—that the evaporites readily support mining along essentially horizontal beds—and was abandoned (Weart, 1979, 1983, 1999). The search for another location as a possible site in southeastern New Mexico culminated in early 1976 with the decision to investigate the current site of the WIPP (Figs. 1, 2).

Enough evidence of the geology and hydrology at WIPP had accumulated from surface investigations (e.g., Powers and others, 1978) that an exploratory shaft and a ventilation shaft were begun in 1981 and completed in 1982 (Black and others, 1983). A repository level was selected, and the shafts were connected. As the underground area was developed, site characterization continued with geologic and hydrologic investigations. The Land Withdrawal Act of 1992 transferred the WIPP area to the US Department of Energy. The Act was further revised in 1996, and WIPP was required to assess the performance of the site and its ability to meet the criteria for isolation of the waste (US EPA, 1996). US Environmental Protection Agency was designated as the regulating agency for radioactive waste under the Act. As the focus turned to performance assessment, hydrologic studies were emphasized because the main failure scenario was identified: borehole connection of a pressurized brine reservoir, the disposal layer, and the overlying Culebra Dolomite. Many of the features, events, and processes that were prominent issues in the early history of WIPP were found to be of little significance. The hydrology of the Culebra, number and anticipated state of boreholes through the repository in the future, and the probability of pressurized brine reservoirs at WIPP connected to the repository and/or Culebra became the impetus for most further investigations and analysis (US DOE, 1996).

Some legal issues were resolved in 1999, allowing for the first shipments of transuranic waste to be sent to WIPP and moved underground for disposal. Currently (August 2020), WIPP is disposing of defense-related mixed transuranic and waste. Construction has begun on a new shaft to provide additional ventilation. The renewal permit for continuing disposal of hazardous waste (https://wipp.energy.gov/2020-renewal-application.asp) is being reviewed by the New Mexico Environment Department. Re-certification applications were submitted in 5-yr increments beginning in 2004 (US DOE, 2004, 2009, 2014), and EPA is reviewing the most recent (2019) compliance recertification application (US DOE, 2019) to continue disposal of radioactive waste (https://wipp.energy.gov/library/CRA/CRA%202019/index.html).

WIPP Location and General Geology

WIPP is located near the northern edge of the Delaware Basin, a major structural element of the Permian Basin in west Texas and southeastern New Mexico (Fig. 1). The maximum thickness of Phanerozoic sediments is ~7,300 m (24,000 feet) (Hills, 1984); upper Permian evaporite rocks at the center of the WIPP site are about 1,100 m (~3,600 ft) thick in the interval from ~150 – 1,250 m (~500–4,100 feet) below ground level. The WIPP disposal layer is at a depth of ~650 m (2150 feet) below ground level in the Permian Salado Formation (Fig. 3).

There are three upper Permian evaporite-bearing formations (Fig. 3) at WIPP; all have been subjected to dissolution in parts of the Delaware Basin. The *Castile*

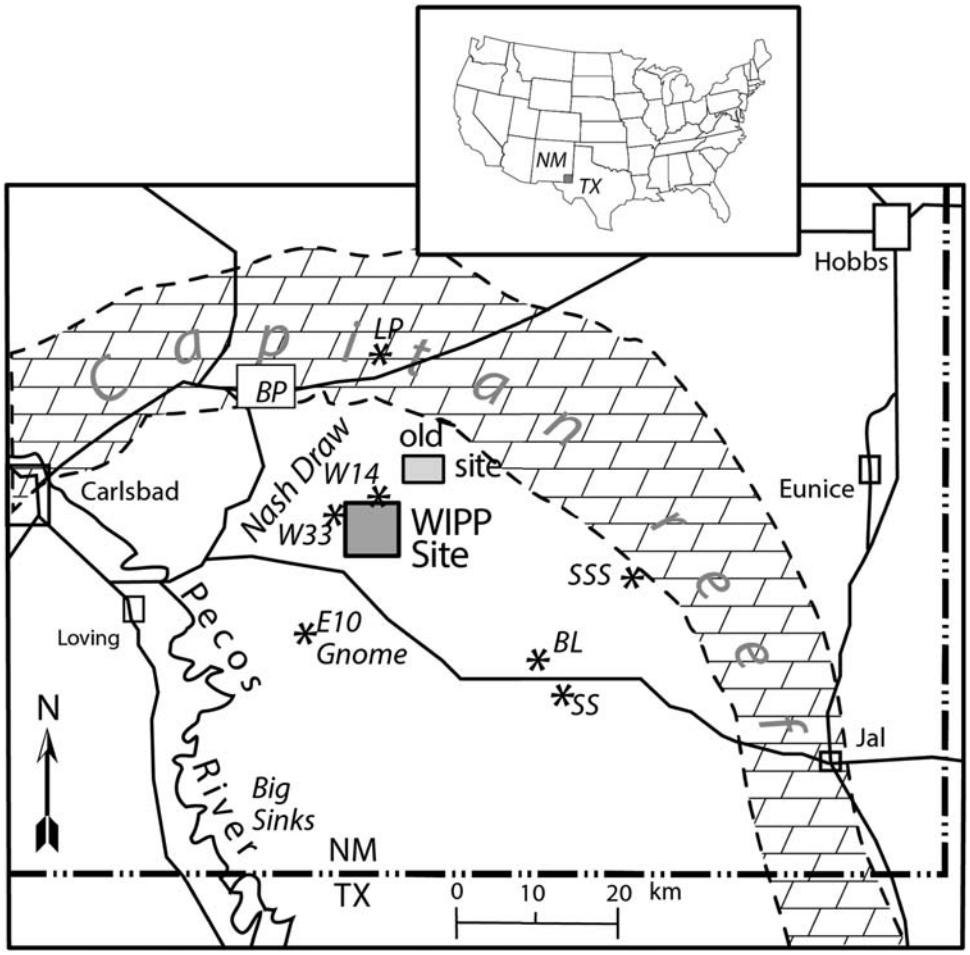

Figure 2. WIPP site relative to features noted with respect to dissolution. "old site" refers to the location initially examined by USGS and ORNL; it was rejected after encountering deformed evaporites and pressurized brine with H2S. SSS = San Simon sink, BL = Bell Lake, SS = Slick "sink," E10 = drillhole ERDA-10, Gnome = the site of Project Gnome, W33 = WIPP-33, W14 = WIPP-14, BP = general location of known collapse chimneys, LP = Laguna Plata.

Formation at the base of this sequence consists of beds of mainly halite and beds of mainly laminated anhydrite and carbonate. Informal nomenclature adapted from Anderson and others (1972) at the WIPP site has three main beds of laminated anhydrite/carbonate (A) and two beds of mainly halite (H) (Fig. 3). These interbeds are more complicated east and southeast of WIPP; to the west, halite beds thin or disappear (e.g., Bachman, 1984), with the processes (dissolution or nondeposition) for thinning in some dispute (e.g., Anderson, 1978; Anderson and others, 1978; Lambert, 1983; Bachman, 1984; Madsen and Raup, 1988). The Castile at the WIPP site center is ~400 m (~1,300 feet) thick. The *Salado Formation* near the center of WIPP is ~600 m (1970 feet) thick. The Salado is dominated by halite (~85%, Jones, 1972) with thinner sulfate interbeds (anhydrite, polyhalite). Some sulfate beds are really extensive and have been enumerated as marker beds (e.g., MB 103; Jones and others, 1960). The middle part of the Salado (McNutt potash zone) is noted for its potash minerals, mainly sylvite (KCl) with lesser langbeinite ($K_2Mg_2(SO_4)_3$). The disposal layer at WIPP is ~90 m (~300 ft) below the potash zone. The *Rustler Formation* is the upper evaporite-bearing unit. It is ~100 m (~330 ft) thick at WIPP and thickens eastward to more than 150 m (~500 feet) in the Delaware Basin at the depocenter. Five members have been named (Fig. 3). Each of the three members that is not dolomite includes halite eastward (e.g., Jones and others, 1973; Holt and Powers, 1988; Powers and Holt, 2000). Permian to Triassic clastics (*Dewey Lake Formation* [aka Quartermaster Formation] and *Dockum Group* [aka Chinle Group]) and thin, late Tertiary to Quaternary clastics (*Gatuña Formation*), pedogenic calcrete, a paleosol, and surficial dune sand overlie the Rustler.

The northern Delaware Basin has been tilted ~1° to the east, most recently mid-to-late Tertiary. From Triassic to late Tertiary, the area was mainly above sea level and subject to nondeposition, erosion, and undetermined dissolution (e.g., Bachman, 1973, 1976, 1980). Some of

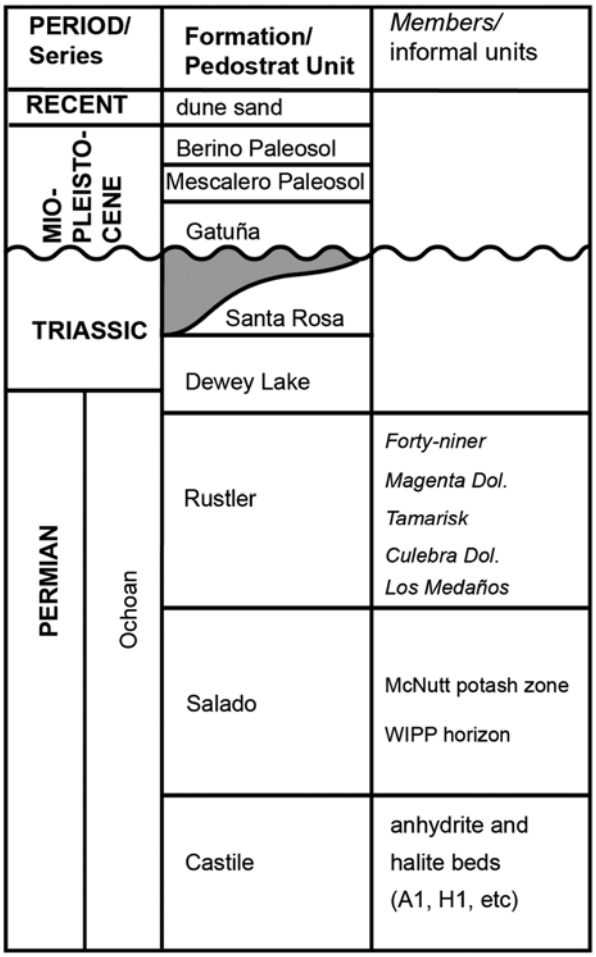

Figure 3. General stratigraphic column of evaporites and overlying units at WIPP. Not to vertical scale.

the evaporite interval was deformed (e.g., Anderson, 1978; Anderson and Powers, 1978; Jones, 1981; Barrows and others, 1983; Borns and others, 1983; Powers and others, 1996), partly in response to tilting.

Overall, the geology of the WIPP site is relatively predictable and natural processes, by themselves, pose little to no concern for isolating waste over the regulatory period of 10,000 yr (e.g., Chu and Weart, 2000).

Knowledge that evaporites in southeastern New Mexico have been partially dissolved, with surface and subsurface manifestations, is not new. W.T. Lee (1925) visited northern Nash Draw and proposed a process of "erosion by solution and fill" for the development of the draw. Robinson and Lang (1938) explored the geology and hydrology of southern Nash Draw in support of the burgeoning potash industry and defined the extent of the brine body at and above the top of Salado halite. J.E. Adams (1944) developed the stratigraphic framework of the Ochoan evaporites and interpreted intervals of dissolution. These and other early investigators deserve credit for understanding and interpreting much of the geologic history prior to more recent investigations.

We begin with a focus on background and details of evaporite dissolution related to site selection for the WIPP. Some of the interrelationships between different aspects of dissolution have been simplified or separated. Thus, deep dissolution could apply to collapse structures ("breccia pipes") as well as the concept of deep lateral (intrastratal) dissolution and localized dissolution from below. Shallow dissolution can apply to karst as well as the downward removal of halite from shallow formations and the brine aquifer. They are separated here because they were separated and emphasized at some point in time.

Each topic follows an approximate format: broad history of the topic as it developed with respect to WIPP, revisiting critical details of investigations or analysis, and the effects or conclusion of the topic. Because some topics developed concurrently, this is not described and discussed chronologically.

EVAPORITE DISSOLUTION AND WIPP

Site Selection and Dissolution

Griswold (1977) summarized the initial criteria used by the USGS and ORNL in 1972 to select an initial site (Fig. 2) in southeastern New Mexico for investigation. In brief, these criteria were

- A 3.24-km (2-mile) offset from any borehole through the evaporites and into underlying formations.
- High-purity salt < 914 m (<3000 feet) deep.
- Minimum depth to salt of 305 m (1000 feet).
- Avoid obvious mineral resources.

At that time (1972–1974), dissolution was of little concern; Jones and others (1973) had estimated it would be tens of millions of years before dissolution would affect proposed disposal levels.

After abandoning the initial site in 1975 because drill hole ERDA-6 encountered deformed strata and pressurized brine with H_2S, criteria for selecting a new location in southeastern New Mexico were modified as well as expanded. The location was expected to provide an area of nearly 8 km^2 (~3 $miles^2$) that would include surface facilities and the area considered for radioactive waste disposal. The main criteria (Griswold, 1977, p. 12) relevant to dissolution were

- Establishing a distance of 1 mi[le] [1.6 km] or more from suberosion [dissolution; aka subrosion in some documents] of the top of the Salado Formation.
- Avoid deep (through the evaporite beds) boreholes within 1 mile [1.6 km] of the area considered for disposal.

Avoiding through-going boreholes was very restrictive; Griswold (1977) summarized the factors that led

to reducing the borehole offset from 3.2 km (2 miles) to 1.6 km (1 mile). The shape of the site was initially an irregular octagon with boundaries on the southeast and northeast sides determined by existing through-going boreholes (Fig. 4). Subrosion at the top of the Salado (as interpreted at the time) slightly impinged on the boundary to the west (Fig. 4). The total area under study at the site location was ~79 km^2 (~30 miles^2).

The concern about dissolution (subrosion) at the top of the Salado in 1976 was that "regional and/or local dissolution must not breach the repository while the wastes represent a significant hazard to man" (Weart, 1979, p. 3). At that time, no performance criteria had been established, and an isolation period of 250,000 yr (~10 half-lives of Pu-239) was "adopted as a conservative value in evaluating WIPP sites" (Weart, 1979, p. 3). The period covered by performance assessment was established in 1985 in Appendix C to Part 191 of 40 CFR as 10,000 yr.

Why was the initial focus on dissolution at the top of the Salado? The "brine aquifer" discovered in Nash Draw (Robinson and Lang, 1938) was an important factor.

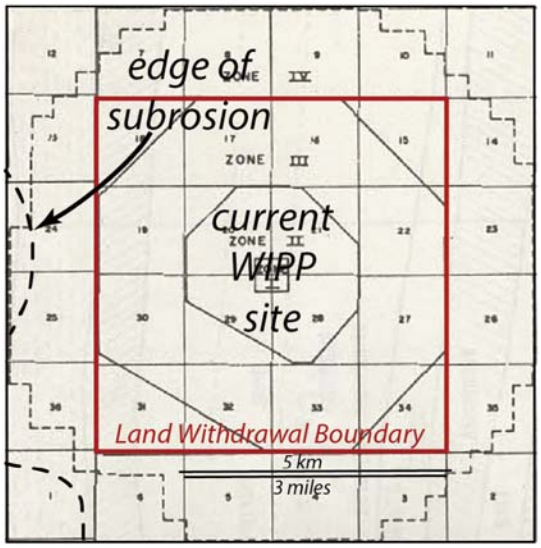

Figure 4. Slight impingement of the edge of subrosion (dissolution at top of Salado) on the western side of the outer zone originally established as this current site was located in 1975–1976. The subrosion front was noted (Griswold, 1977, figure 2) as "From U.S.G.S., as known in 1974." The crude octagonal zones of that time developed from exclusion distances from boreholes as well as other criteria. The red land withdrawal boundary was later established by legislation, and the previous zonation became moot. (Adapted from Griswold, 1977, figure 2).

The Brine Aquifer and Dissolution of Upper Salado

Robinson and Lang (1938, p. 86) noted that some potash test wells in the northern end of Nash Draw (Fig. 1) encountered "a strong sodium chloride brine just above the salt of the Salado halite." In their investigation of geology and groundwater in the southern end of Nash Draw near Laguna Grande de la Sal, Robinson and Lang (op. cit., plate 3) outlined an expanded area of these encounters. The brine aquifer extended slightly north of the north end of Nash Draw, southwest across the Pecos River, but it did not extend to the east and west sides of Nash Draw (Fig. 5). Robinson and Lang interpreted the brine to be because of dissolution of upper Salado halite and inferred that at least part of the formation of Nash Draw was because of this dissolution.

To support Project Gnome, a 3-kiloton nuclear device detonated (1961) in the Salado southeast of Nash Draw (Figs. 2, 5), Vine (1963) mapped the geology of Nash Draw. With the stratigraphy of the Rustler well established in a drill hole at the Gnome site, Vine mapped and discussed the relationships of the formations in Nash Draw while recognizing that both Rustler and upper Salado salt were significantly disturbed by dissolution. Vine did not discuss the brine aquifer or hydrology of Nash Draw. Vine mapped few sinkholes, but they can be related to sinkholes that are still evident. Vine did not identify any features at the current WIPP site as evidence of solution and/or collapse.

The USGS conducted several studies of salt beds in New Mexico prior to ORNL site investigations in

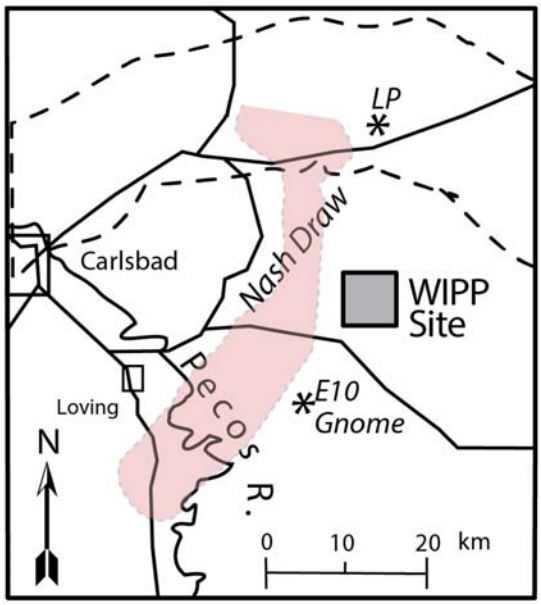

Figure 5. Approximate known extent of the brine aquifer (shaded light red) above Salado salt (Robinson and Lang, 1938). The extent shown on this map is somewhat generalized from Mercer (1983).

1974. Jones and others (1973) prepared a summary report on the "Los Medaños" area that focused on the initial ORNL site, but the study also covered the current WIPP location.

Jones and others observed that variable Salado thickness was because of deposition as well as dissolution, noting that in the western part of the area "percolating ground water has dissolved and removed some of it" (op. cit., p. 11). Jones and others (op. cit., figure 12) placed the edge of subrosion of the top of Salado halite west of the current site and well removed from the initial ORNL site. The hydrologic analysis noted that no wells were completed in the [Rustler] basal dissolution breccia zone, and the brine aquifer was not included in the analysis.

Jones and others (op. cit., p. 21) discounted the import of subrosion with respect to the initial site, explaining that "the whole situation appears to be highly stabilized and of long duration, with very little or practically no subrosion since the Pleistocene or, perhaps, even earlier." Using a rate of salt removal of 15 cm (0.5 foot) per 1,000 yr (Bachman and Johnson, 1973), Jones and others (1973) inferred that at least 1 million yr would be required to reduce the upper Salado to residue. Because the preferred disposal intervals were in the lower Salado, Jones and others (op. cit., figure 12) estimated that 25-30 Ma would be required to dissolve the Salado at the ORNL site down to the preferred disposal intervals. Most of the current WIPP site also fell into the same estimated time period to dissolve down to preferred disposal intervals.

Early in the exploration of the current WIPP site, several monitor wells were completed to observe inflow from the Rustler-Salado contact, i.e., "brine aquifer" (Mercer and Orr, 1977; Mercer, 1983). Inflow was very limited, and the permeability of the zone was clearly very low. The top of the "brine aquifer" near the Pecos River was generally above an elevation of ~808 m amsl (~2650 feet) (Robinson and Lang, 1938). The elevation of the disposal layer at WIPP has an elevation of ~381 m amsl (~1250 feet). Without hundreds of meters relative drop in the brine discharge point, there is no threat to the disposal layer from top-down dissolution of the Salado.

Bachman (1980) concluded also that estimates of the age of Nash Draw were too young and that it was "impractical" to estimate rates of upper Salado dissolution. Lambert (1983, p. 79) provides further discussion of arguments made about timing of dissolution and the inferred rates, pointing out the impossibility of determining the dissolution front at differing times to obtain a reasonable way to estimate a rate, either vertical or horizontal.

The last monitor well (H-10) completed across the Rustler-Salado contact was drilled in 1979. Two other boreholes were later tested across the interval (DOE-2: 1984; H-16: 1987), but the intervals were not completed for monitoring. The contact (i.e., brine aquifer) was not considered significant at the WIPP site as a hydrologic unit by 1983 (e.g., Weart, 1983).

Collapse Chimneys ("Breccia Pipes")

In late 1975, as the search for a new location for WIPP began, a report reached WIPP that Mississippi Chemical Corporation (now Intrepid Potash) had mined into a collapse feature under a surface domal structure (Hill C; Fig. 6) in northwestern Nash Draw. The history of the investigations into this and related features for WIPP are detailed by Powers (1996).

There are two surficial domes (Hills C and D) in northeastern Nash Draw and two more (Hills A and B) nearby in Clayton Basin. Hills A and C were drilled and cored by WIPP to confirm collapse and obtain details. Hill B shows some brecciation at the surface. Hill D has no known collapse and has been partially mined under. A third known collapse breccia (Wills-Weaver) was drilled

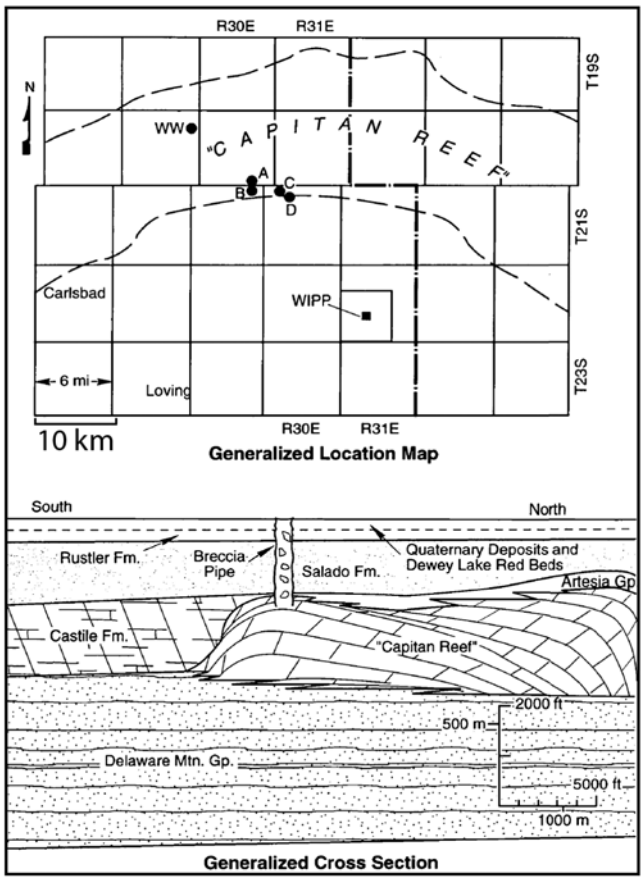

Figure 6. Locations of surface domes and collapse chimneys relative to WIPP. Hills A, B, C, and D are labeled by letter only. WW indicates the approximate location of the Wills-Weaver pipe. Modified from Powers (1996).

for potash resource evaluation (Snyder and Gard, 1982); it is more distant from WIPP. The collapse chimneys (aka breccia pipes) have a generally cylindrical or columnar vertical form. At depth, adjacent beds are tilted downward toward the collapse (Snyder and Gard, 1982). They are plugged with breccias of sulfate and halite at the mine level. At the surface, Hills A and C show a center subsidence/collapse (Vine, 1960; Snyder and Gard, 1982) with outward dips around the rim. Vine (1960) thought they might have formed because of dissolution of Rustler anhydrite. The theory of dissolution from below by brine density flow-through fractures and upward collapse was initially proposed by Anderson (1978). Bachman (1980) and Snyder and Gard (1982) modified the explanation, involving collapse in the underlying Capitan reef because of pressure reduction when the Pecos River incised the top of Capitan near Carlsbad. All recognized that the surficial domal structure was created by solution of upper Salado salt more broadly, with the collapse breccia resistant to dissolution.

As a feature, collapse chimneys were initially treated like a possible "fatal flaw" should one be found where the repository was to be located (see Powers and Holt, 2008). The investigations that followed over the next ~4 yr were extensive.

Several geophysical techniques were applied to a known collapse chimney to determine which had the best likelihood of identifying such a feature. Resistivity surveys were found most suitable and were subsequently applied to the entire site area and beyond (see review in Powers, 1996). Several anomalies were detected and classified. The most significant anomaly was in the northwest part of the WIPP site, and WIPP 13 was drilled in 1978 to ~53 m (175 feet) into the Salado (SNL and USGS, 1979) at the site of the anomaly. The drill hole encountered no evidence of brecciation or collapse. Other anomalies at the WIPP site that were drilled were not collapse features (Powers, 1996).

Early in 1980, the collapse at Hill C was drilled and cored (WIPP-16; Snyder and Gard, 1982) to the approximate depth of the mine encounter to obtain vertical information and to determine if fluids or gasses might be present. Horizontal drilling and coring were then carried out into and through the breccia from the mine level intercept. Hill A was drilled and cored later in 1980 to a depth equivalent to the upper Capitan reef (WIPP 31; Snyder and Gard, 1982). One of three drill stem tests in this collapse breccia yielded enough fluid for an interpretation that permeability was 0.90 mD (Mercer, 1982). These studies provided the direct evidence of origins and properties regarding these collapse chimneys.

By 1982–1983, there was little sense that collapse chimneys existed at, or were a threat to, WIPP. Drill stem tests and the general hydrologic system indicate that a feature such Hills A or C would not have been a significant threat to isolation, but treating them more or less as a fatal flaw in the beginning might have made such a defense difficult.

Later, however, Hill (2003, 2006) asserted that "Closer to WIPP are breccia pipes that extend to the surface, an example of which is Bell Lake Sink . . . ". This is covered more specifically in Localized Dissolution (below); Bell Lake "sink" is neither a breccia pipe, nor is it closer to WIPP than Hill C, a real collapse chimney.

Deep Dissolution—Lateral or Stratabound

"Deep dissolution" entered the lexicon for WIPP with a consultant report by Anderson (1978). Anderson was contracted by SNL in 1977 to evaluate dissolution rather broadly. Anderson prepared extensive maps of stratigraphic intervals from the lower Castile upward to try to identify specific locations or layers where dissolution might have occurred or could be occurring.

Anderson and Kirkland (1966) and Anderson and others (1972) had proposed that mm-cm carbonate-sulfate laminae of the Castile were annual (varve) deposits that could be correlated across long distances within the Delaware Basin. This was the initial basis for assuming or inferring that Castile salt beds were also deposited relatively uniformly across the basin. Thick Castile halite beds in the eastern part of the basin were correlated to "blanket breccia" in the western part of the basin (Anderson and others, 1972, 1978). These breccias consist of clasts mainly of carbonate-anhydrite laminae, commonly cemented by sulfate. The volume of halite remaining in the basin is about 50% of the volume estimated to have been deposited, assuming halite was deposited across the entire basin. Some halite beds deeper in the sequence yielded larger percentages removed than for some higher halite intervals and some higher (stratigraphically) halite beds apparently extend laterally across the margin of the lower halite, leading to the inference that dissolution could penetrate laterally into the evaporite sequence. Near the border with Texas south of WIPP, the "Big Sinks" area was considered an example of such lateral dissolution and collapse (Figs. 1, 2).

Anderson (1978) envisioned lateral deep dissolution occurring within the evaporite sequence (possibly along the Castile-Salado contact) and reaching the WIPP site before surface-down dissolution could breach the disposal layer. Anderson (op cit., p. i) postulated that this lateral dissolution "will reach the site locality within the next few million years."

ERDA-10 was drilled in 1977 at the location of Project Gnome as an early investigation of an area where the effects of lateral dissolution along the Castile-Salado contact (and elsewhere in the stratigraphic section) might be observable (SNL and D'Appolonia Consulting Engineers, 1983). The lower Salado as well as Castile was

cored; none of the cores were reported to show brecciation or residues after dissolution. A series of drill stem tests in Salado and Castile, including the reported contact, did not show enough fluid inflow to determine hydraulic conductivities. This was the main test of the hypothesis, although cores and logs from borehole DOE-2 (Mercer and others, 1987), which is adjacent to the WIPP site boundary, were later reviewed to evaluate whether "deep dissolution" had any part in evaporite deformation at that location.

Anderson and others (1972, p. 70) also noted that "Beds of laminated anhydrite as thin as one foot [30 cm] thick within halite beds more than 50 ft (15.2 m) thick are also present as unbrecciated layers within correlative breccia units, involve approximately the same number of laminae, and maintain their identity and remain undisturbed within overlying and underlying breccia beds despite the removal of salt." Anderson and others (1972, p. 81) interpreted these thin undisturbed laminated beds within brecciated beds as evidence that "... withdrawal of halite was a very gentle process." This explanation is difficult to support. Significant *halite* intervals were allegedly dissolved, creating breccias of *laminated anhydrite* above and below an undisturbed, unbrecciated thin *laminated anhydrite*. An undisturbed bed over breccia can be taken as evidence of a synsedimentary event (see review in Holt and Powers, 1988, chapter 8). It seems much more likely that the undisturbed bed indicates, at least, a synsedimentary origin to the lower breccia. Robinson (1989) and Robinson and Powers (1987) interpreted Castile breccias within a localized area of the western Delaware Basin as a fan deposit adjacent to an area that was likely subaerially exposed. Significant changes in the elevations of the base of Castile and top of lower Castile anhydrite (Robinson, 1989, figures 29 and 30) at that location are along the trend of the Huapache Monocline (Hayes, 1964) that may have reactivated approximately the time of deposition of the lower Castile halite. Relative uplift of the southwestern side of the monocline could have been the cause of subaerial exposure. More generally, the "deep water" depositional environment of the entire Castile has been challenged (Hovorka, 1989; Kendall and Harwood, 1989; Anderson, 1993; Leslie and others, 1993, 1996; Anderson and Kirkland, 1995; Hovorka and others, 2007), and the suggestion that subaerial exposure created breccias along basin margins (e.g., Robinson and Powers, 1987) is consistent with these later re-evaluations of Castile deposition.

Much later, Salado pore pressures in the far field (away from mining disturbance at WIPP) were determined to be at or very close to lithostatic pressure with little fluid movement (Beauheim and Roberts, 2002; Roberts and others, 1999; Holt and Powers, 2011). Drill stem tests in the Salado (Mercer, 1987) showed pressures indicating that the fluid would rise above ground level (given enough time). Monitor wells in the Rustler in a dolomite sandwiched by halite and with halite-filled fractures show pressure buildups that are slow (little inflow) but that exceed the normal hydrostatic levels and are still rising after ~15 yr. Creep deformation and plastic behavior of salt transmit lithostatic or near-lithostatic pressures to the fluids, little as they are, within the salt. It is unlikely that lateral deep dissolution within the evaporite section is a viable mechanism without the following: a stiff permeable unit, a driving force greater than the fluid (hydrostatic) pressure within the evaporites, and a means of circulation (e.g., Johnson, 1981; Holt and Powers, 2010).

Deep Dissolution—Localized or Point Dissolution

Anderson (1978) also considered localized dissolution at the base of the evaporite section (base of Castile/top of Delaware Mountain Group). Breccia pipes and San Simon sink around the northern margin of the Delaware Basin and mineralized collapses ("castiles") in the southern Delaware Basin provided examples, although castiles are not associated with the Capitan reef/aquifer. Anderson noted a variety of surface topographic depressions a well as structural depressions in the evaporite-bearing rocks within the Delaware Basin, using the term "sinks" and inferring that localized dissolution upward from the underlying Delaware Mountain Group (DMG) could be responsible.

The history of noting these surficial depressions and speculating about their origin(s) predates Anderson (1978). As part of their groundwater study of southern Lea County (NM), Nicholson and Clebsch (1961) noted surface features (e.g., playas, lagunas, depressions, sinks) and "structural" features (e.g., San Simon Swale and sink) that were variously attributed to subsidence or collapse. We focus on two examples: Bell Lake "sink" (T24S, R33E; Fig. 2) and Laguna Plata (T20S, R32E; Fig. 2), because data are available to contrast with assertions or speculation about origins as dissolution features.

Bell Lake "Sink"

Bell Lake is a somewhat circular depression ~2-3 km in diameter (Figs. 7a, b); a smaller depression ("Slick sink") ~6.3 km southeast of Bell Lake has been discussed in similar terms. Gypsum dunes on the east side of each depression "... can be taken to indicate two things: that the lakes are collapse depressions, the area of collapse providing the conduit for the upward movement of ground water; and that the head in the pre-Tertiary rocks at one time was much higher than now" (Nicholson and Clebsch, 1961, p. 47). They stated further that "there is no known source of gypsum near the surface in southern Lea County" other than in these dunes.

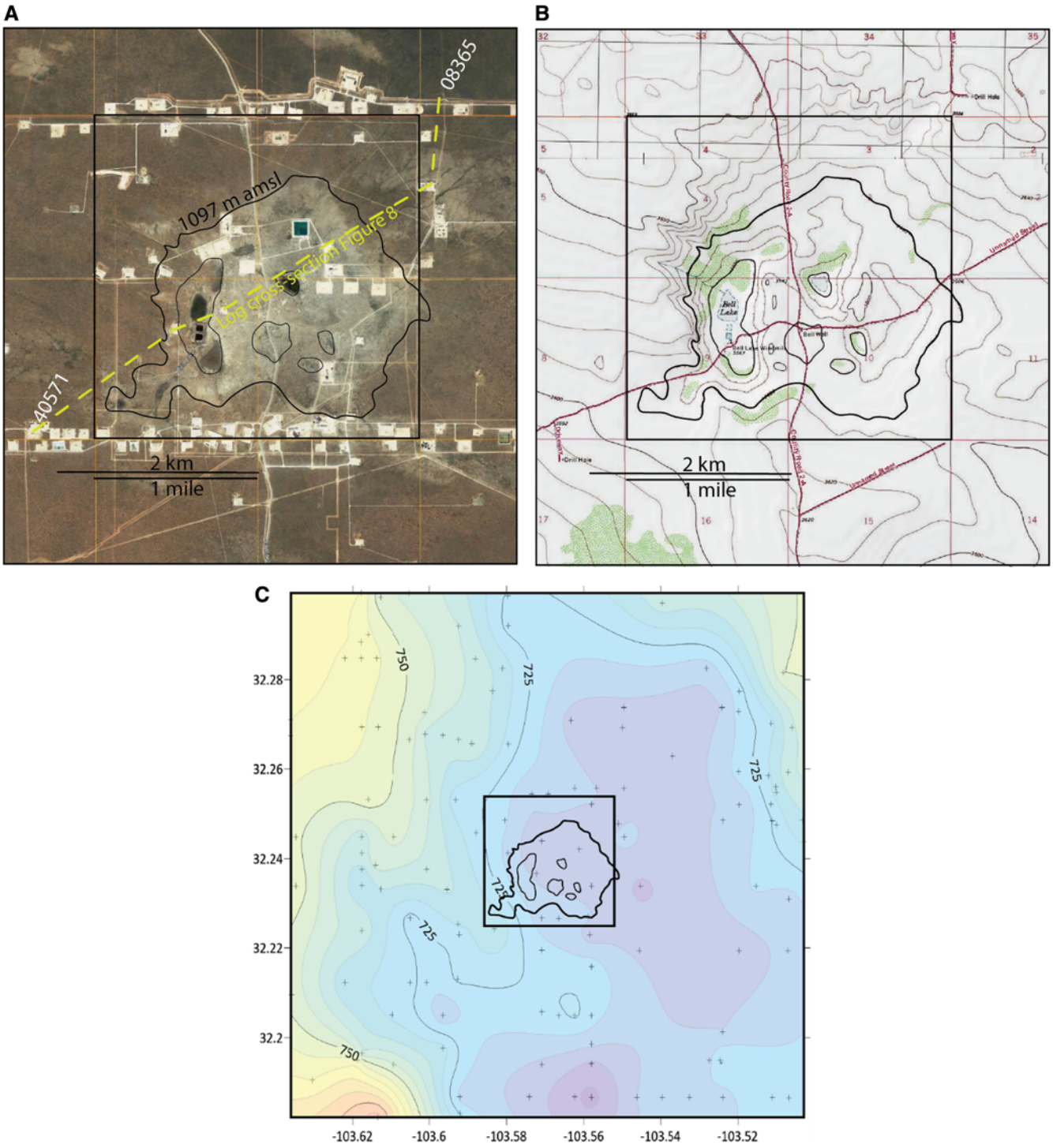

Figure 7. A. Aerial view of Bell Lake (from Google Earth, image date 11/2/2017). Approximate center point longitude -103.565 deg, latitude 32.235 deg. Outer irregular line approximates the position of the closed contour for 1097.28 m amsl (3600 ft amsl); the inner closed contours are ~1088 m amsl. The square provides a common reference area for figures 7B and 7C. The dashed line shows the connection between geophysical logs in figure 8. White squares, or rectangular patches, are pads for drill holes. B. Topography of Bell Lake depression (underlying image from TOPO!). C. Elevation (m amsl) of the top of Rustler Formation at Bell Lake and surrounding area. Contour interval is 5 m. The broad low of ~715 m amsl includes a large area without surface depressions and higher surface elevations. This area is a general depocenter with lower elevations and thicker intervals for the Rustler (e.g., Holt and Powers, 1988).

Anderson (1978) included Bell Lake and Slick "sink" as possible examples of breccia pipes or collapses because of deep dissolution. Anderson (1978, p. 46) suggested "that sulfate-rich waters rose up to the sink through fractures at least as deep as the Rustler Formation and perhaps deeper." On a field trip in 1980, Anderson remarked on finding barite and celestite nodules around the Bell Lake playa (Chaturvedi, 1980, p.32). Anderson (1980, p. 113) also cited maps of Bell Lake (Widdicombe, 1979) as evidence of faulted or downdropped Mescalero "caliche" and "Old Mescalero soil" and suggested "... that the sink is truly a collapse structure rather than a deflation feature."

Bell Lake was surveyed by gravity as a "... late-Wisconsin, solution-subsidence, collapse feature" (Barrows and others, 1983, p. 51), without the dissolved layer or interval being identified. Barrows and others (1983, p. 51) noted that "... topography is sufficient to make the shape of the gravity anomaly dependent on the density used to make the Bouguer slab correction." After noting some possible variations in near surface materials, Barrows and others (1983, p. 51) concluded that "... the gravity profiles still indicate complex subsurface density structure. These may be complex geologic structures, varying fill on an irregular collapse surface, or lateral density variations within relatively flat-lying strata." It was recommended that additional gravity surveys and multiple boreholes would be needed investigate further.

Hill (e.g., 1993, 1996, 2003, 2006) reported isotopic analyses ($\delta^{34}S$, $\delta^{13}C$, $\delta^{18}O$, and $^{87}Sr/^{86}Sr$ variously of barite, celestite, selenite, and calcite at Bell Lake. Hill (primarily 1996) considered that 1) the sulfur and carbon/oxygen isotopes were most representative of deeper anhydrites and/or pressurized brine reservoirs and 2) strontium isotopes were similar to surficial pedogenic calcretes. The Bell Canyon Formation (underlying the evaporites) was considered the most likely source for barium. Hill (2003, 2006) stated that the isotopic results "... supported Anderson's (1980a [1980 here]) model of deep-seated dissolution originating in the Bell Canyon Formation."

As with breccia pipes or collapse chimneys, by ~1983 there was no evidence of localized deep dissolution at the WIPP site. There have been no WIPP-directed activities for further investigations of localized dissolution and collapse. Borehole DOE-2, as previously noted, was drilled and cored in 1984 to evaluate deformation in the Castile and overlying units, and it was determined that the changes in thickness and structure of the Castile there were not produced by dissolution (Mercer and others, 1987).

There are enough boreholes (six) from Bell Lake to contradict assertions that it is a breccia pipe. The top of Rustler (Fig. 7c) does show some depression over a large area including Bell Lake, Slick "sink", and nearby areas with higher topography. The Rustler thickens across the same area, but the log cross section (Fig. 8) reveals that dolomite and sulfate beds remain near constant in thickness while the intervals with halite are thicker. This is within a larger depocenter for the Rustler (Holt, 1988; Holt and Powers, 1988; Powers and Holt, 1990) where Rustler halite beds thicken considerably.

Sulfate is available from sources not considered by Nicholson and Clebsch (1961) or later studies: Nash Draw gypsum/gypsite and dunes at ~40 km (~25 miles); Castile outcrops at ~60 km (~37 miles); salt flats of west Texas at ~140 km (~87 miles). White and others (2015) traced dust from White Sands gypsum more than 100 km (62 miles) downwind from White Sands, showing that surface sources are possible. Strontium is found in the Mescalero Paleosol (aka Mescalero caliche) (Brookins and Lambert, 1988). Smith and others (2013) report 223 mg/kg barium from the "A" layer from a sample 13.2 km (8.2 miles) east-southeast of Bell Lake. It is not known that these minerals observed by Anderson and analyzed by Hill are extensive enough to warrant an extraordinary source such as a breccia pipe and fluids circulating from great depth to the surface.

Nicholson and Clebsch (1961, plate 1) show modern Dockum potentiometric surface at ~ 76 m (~250 feet) below the base of fill/top of Dockum in Bell Lake. Long-published freshwater equivalent heads for the Delaware Mountain Group are well below surface levels at Bell Lake (Mercer, 1983), even without lower potentiometric surface because of high salinity (e.g., 140,000–160,000 mg/L chloride) known from nearby wells (Hiss, 1976). Dockum water has significant sulfate and minor barium (Ewing and others, 2008). Both may have had higher potentiometric surfaces during pluvials; neither is necessary as a source of barium and sulfate, and well data provide clear evidence that a collapse structure is not present.

Laguna Plata

Four shallow playas near the western boundary of Lea County were described by Nicholson and Clebsch (1961, p. 10) as having an irregular shape, flat bottom covered with halite and gypsum crystals, and a sand dune on the east side. Nicholson and Clebsch also suggest that these playas may have originated as subsidence/collapse features, similar to San Simon Swale. The top of the Dockum on the north side of Laguna Plata was noted as 6 m above the lake bed while potash drill holes in the lake bed encountered top of Dockum at ~6 and ~13 m (~20-43 feet) below the lake bed. This was thought to indicate collapse because of dissolution of underlying evaporites, similar to Bell Lake and Slick sink. Nicholson and Clebsch (1961, plate 1) neither mapped a fault along the northern part of Laguna Plata

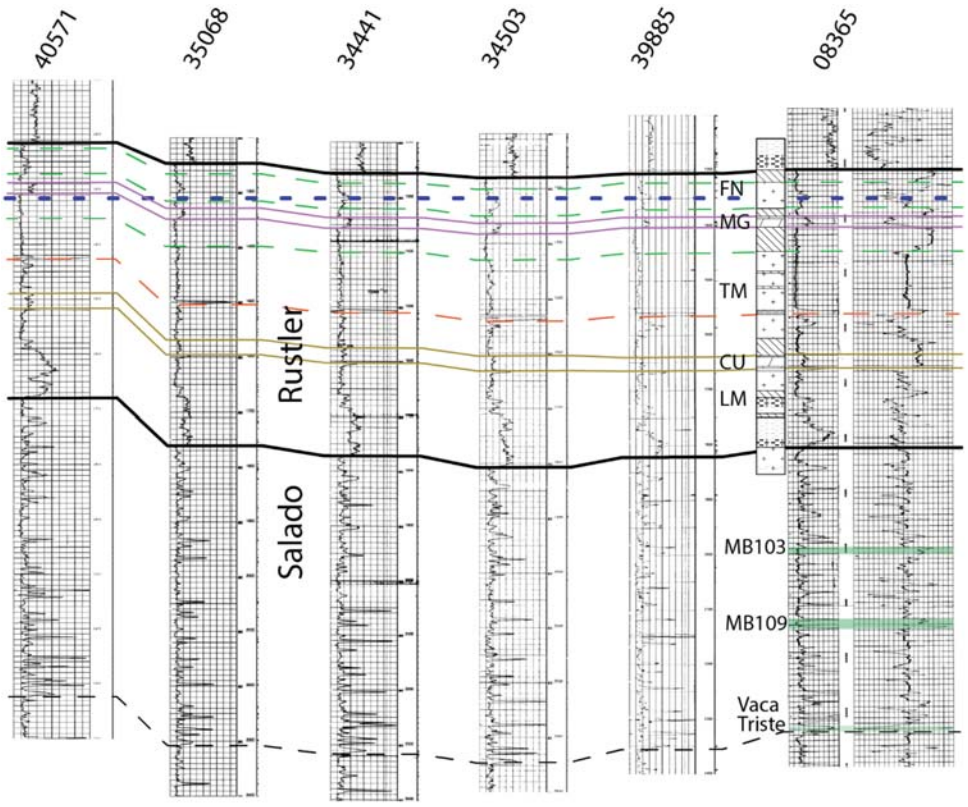

Figure 8. A short geophysical log cross section through Bell Lake shows continuity of Rustler and upper Salado beds (no collapse) and modest thickening of the noncarbonate intervals of the Rustler because of thicker halite. The number above the log is a shortened API #; the full API is 30-025-XXXXX. The log for 08365 has natural gamma on the left and acoustic travel time on the right. Other logs are gamma only. Horizontal dashed blue line is 700 m above sea level. Vertical scale for each log is the same. Horizontal distance between wells is not represented. See Figure 7a for cross section and identification of end point logs. Rustler members are abbreviated in a geological key: LM = Los Medaños, CU = Culebra Dolomite, TM = Tamarisk, MG = Magenta Dolomite, FN = Forty-niner.

nor extended contour lines (top of "red beds," aka Dockum or Chinle) south of Laguna Plata, presumably for lack of data. Their contours of the top of red beds in southern Lea County show significant relief that should be interpreted in light of the long period of predominantly subaerial exposure of these Triassic beds (e.g., Bachman, 1976).

Jones and others (1973, p. 64) suggested that these depressions "... are probably surface deflation structures resulting from erosion phenomena commonly found in arid regions." Their evaluation found little or no solution in the underlying Rustler. Bachman (1976) considered these playa depressions to be deflation features.

These depressions are mentioned in the geological characterization report for WIPP (Powers and others, 1978), and the implied origin is deflation. Lambert's (1983) review indicated mainly that mine workings under some of these depressions did not show stratigraphic effects of collapse. Lappin (1988) discusses dissolution at length without referring to either these depressions or the work of Reeves and Temple.

Reeves and Temple (1986) described top-of-Rustler elevation differences underlying Mound Lake (Lynn and Terry Counties, TX) and inferred that the formation had been thinned by ~9 m (~30 feet). They discussed processes at length, concluding that infiltration was likely the cause of salt removal to depress these units. Reeves and Temple (1986) listed 21 playas in the Texas panhandle and eastern New Mexico where "salt removed" ranged from 0 to 137 m (0–450 feet). Of the four lagunas in western Lea County, only Laguna Plata was listed as having salt removed (76 m; 250 feet). Reeves and Temple (1986) provided no evidence for these estimates of salt removed for any lake other than Mound Lake. Temple (1986) included specifics only for Mound Lake (TX), Yellowhouse Lake (TX), and Cedar Lake (NM).

Wood and Osterkamp (1987), Osterkamp and Wood (1987), and Wood (2002) concluded that such playas developed when a small surface depression was created by erosion, then enlarged through surficial solution of calcretes. The underlying High Plains Aquifer was recharged, carrying some solutes and fines. Dunes are common on the east/southeast side of playas. These

authors did not involve halite dissolution at depth in the process, nor did Holliday and others (1996).

Reeves and Temple (1986, p. 939) concluded that the "... evidence, combined with previous studies documenting salt-bed dissolution in areas surrounding a proposed high-level nuclear-waste repository site in Deaf Smith County, Texas, leads to serious questions about the rationale of using salt beds for nuclear-waste disposal."

Hill (1996, p. 295–296) suggested that these playas may represent surface expressions of breccia pipes and invoked the submarine channels or canyons through the underlying Capitan reef (Hiss, 1975) as a possible part of the process.

We question how major dissolution below Laguna Plata was claimed by Reeves and Temple without supporting evidence or reference. A possible source for the claim is a Salado isopach map (Brokaw and others, 1972, figure 9), where the Salado thins ~100 m (~330 feet) over Halfway oil field and *between* lagunas. Brokaw and others (1972, p. 46) note that "Within the shelf area, local reductions in thickness [of Salado] are sharp over pre-Salado knolls or 'highs' at the Getty, Barber, Halfway, and other small oilfields which appear as domal features ...". The reduced Salado thickness does not underlie Laguna Plata, and Brokaw and others (1972) did not invoke dissolution to explain these four depressions.

The lagunas are of no apparent significance to WIPP although they were peripherally mentioned during early regional studies and caused mention by Lambert (1983). We provide evidence to rebut speculation about their origins by Reeves and Temple (1986) and Hill (1999).

The area of Laguna Gatuna and Laguna Plata was examined in detail for stability with respect to halite dissolution (Powers, 2007) in support of a proposed site for surface storage facilities under the Global Nuclear Energy Partnership (GNEP) program. Rustler and upper Salado elevations under most of Laguna Plata are above trends with eastward regional dips along the east side of Laguna Plata and under Laguna Gatuna (Fig. 9).

Basin Dissolution Troughs

Maley and Huffington (1953) identified two troughs in the Delaware Basin by mapping the thickness of "fill." Many others have cited the same features, and salt dissolution is important in discussions of origins. The central trough (commonly referred to as the

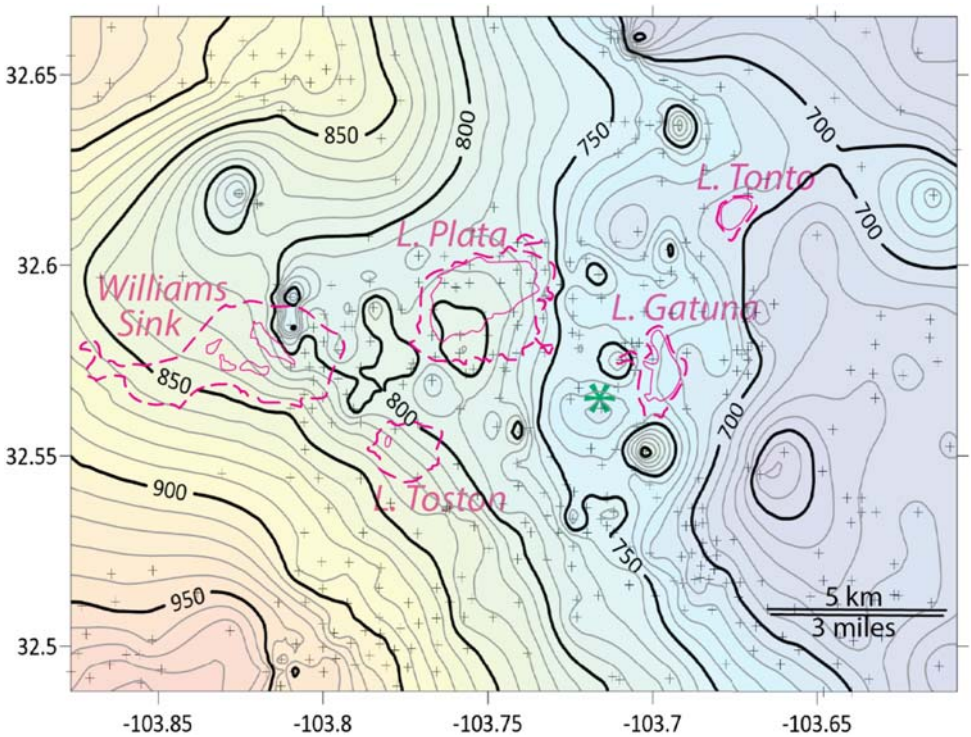

Figure 9. Elevation (m amsl) of the top of Rustler at Laguna Plata and nearby surface depressions. Contour interval 10 m. Outlines of the closed contours for each depression are shown. Most of Laguna Plata overlies an area at or above 800 m amsl, with contours deepening along the eastern area. There is no evidence consistent with removal of 76 m of halite under Laguna Plata. Note some single well departures from trends have not been resolved as original records reside at United States offices currently closed because of COVID 19. They do not detract from the conclusion. The green asterisk marks the approximate location for the GNEP investigation (Powers, 2007).

Balmorhea-Loving trough) was considered in evaluating deep dissolution (e.g., Anderson, 1978; Lambert, 1983). The trough referred to as the Belding-San Simon trough (Hiss, 1975) along the eastern Delaware Basin margin includes the San Simon Swale and sink and extends southward along the front of the Capitan reef into Texas and south of the Pecos River. Holt and Powers (1988) examined the changes in Rustler stratigraphy and structure in the northern Delaware Basin and onto the adjacent Central Basin Platform. They interpreted possible faults along this margin that may still have been active when the Dewey Lake was being deposited. Johnson (1993) separated out evidence of possible early dissolution of Salado halites in the Wink, TX, area from later dissolution and collapse in the trough along the reef margin.

Much more detail can be examined now with the large number of newer drill holes. Ewing and others (2012, figures 4.2.1, 4.2.2, 4.2.3, and 4.2.4) showed structure on the top and base of Rustler that provides more detail through these two areas, although the data were more limited in Texas by project restrictions. The elevation of the top of Rustler clearly reveals the presence of these troughs as well as other features (Fig. 10). These and other data are being developed for further detailed investigations of the stratigraphy, sedimentology, and postdepositional processes that have affected the evaporite formations in southeastern New Mexico and west Texas.

Rustler Formation Dissolution

During the early history of WIPP, mudstone equivalents to halite intervals of the Rustler were interpreted as dissolution residues of original halite beds (e.g., Jones and others, 1960; Vine, 1963; Griswold, 1977; Powers and others, 1978; Lambert, 1983; Bachman, 1984; Snyder, 1985). The underlying assumption (generally unstated) was that these beds were originally deposited continuously across the basin from east to west (or at least farther west than the WIPP site). In many early reports of the geology based on WIPP boreholes, these intervals were summarized as "dissolution residue" in the table of stratigraphic units (see discussion by Lorenz, 2006, p. 28). Little significance was attributed to the

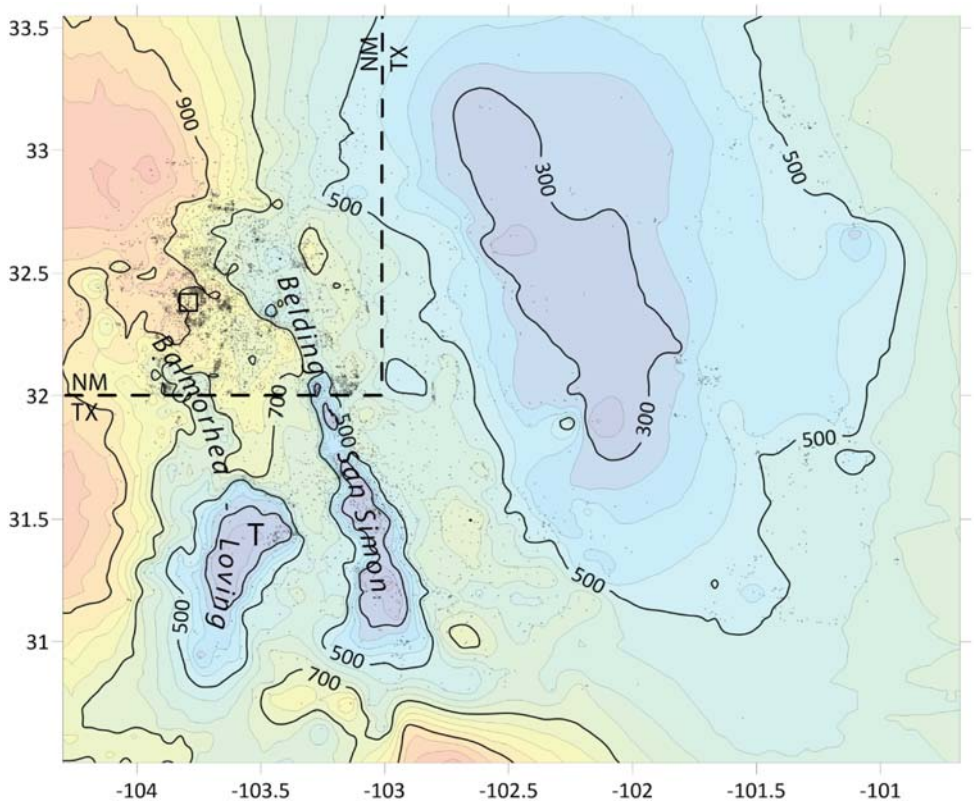

Figure 10. Regional view of the elevation (m amsl) of the top of Rustler. The small black square indicates the position of WIPP. This map was generated with 6212 data points. Contour interval is 50 m. The Belding–San Simon depression along the eastern side of the Delaware Basin is also shown in some detail in Ewing and others (2012), although with fewer data points. The Balmorhea–Loving trough of Maley and Huffington (1953) is less well indicated in New Mexico, but the depression near Toyah (T on map) is clear. The contrast with earlier maps is in the detail now practical with the vastly greater numbers of wells that have been drilled since WIPP work started (1975). Similar localized data sets will be examined for detailed study of Castile and Salado deposition, deformation, and dissolution.

history of these mudstones relative to the suitability of WIPP or WIPP performance until the early 2000s. Mercer (1983, p. 56) noted that Culebra Dolomite hydraulic properties "... vary considerably from place to place and appear to be related to the size and number of fractures and openings" and related these fractures and openings to Rustler and Salado dissolution. The hydrologic model for fluid flow for the Culebra Dolomite Member based on a geostatistical-based model of hydraulic properties determined at individual wells (e.g., LaVenue, 1992; LaVenue and others, 1988) was later revised to a model based on the relationship of hydraulic properties to geological information (Holt and others, 2005; Powers and others, 2003; Beauheim and others, 2007) that did not assume or infer major Rustler dissolution. The origin of the mudstones became a part of the discussion around this new hydrogeological conceptual model (e.g., Burgess and others, 2008).

In 1984, we mapped the WIPP waste handling shaft as it was being enlarged to its current diameter (~7 m) and configured for waste handling (Holt and Powers, 1984). During that mapping, mudstone intervals of the Rustler that had previously been designated "dissolution residues" were found to display sedimentary features highly unlikely to have survived any significant postdepositional removal of halite. That same year we mapped the exhaust shaft (Holt and Powers, 1986) with similar results.

These reports were met with considerable skepticism. A workshop was convened in 1985 by the New Mexico Environmental Evaluation Group (EEG) to discuss the geology and hydrology of the Rustler related to WIPP, in part because of the conclusions in Holt and Powers (1984) that the primary sedimentary structures were observed while mapping the waste shaft. The introduction to the report issued for this workshop (Chaturvedi, 1987, p. 5) included the following statement: "Also needed is an understanding of the recharge and discharge areas for the Rustler, the mechanics and time of removal of salt from the Rustler (or a convincing hypothesis of syn-depositional processes of selective deposition of salt) ...."

Our comprehensive study of Rustler cores, outcrops, and geophysical logs for the Rustler provided additional evidence of facies changes (Holt and Powers, 1988; Powers and Holt, 2000). This work had little effect on WIPP for some time. Precursors to performance assessment evaluated the difference: "The two differing interpretations [about the extent of deposition and dissolution of Rustler halite] have little impact on WIPP performance, because, as summarized by Lappin (1988), extrapolation of the maximum dissolution rates indicates no threat to the WIPP repository within 10,000 years" (Lappin and others, 1989).

In subsequent years, additional details were acquired through drilling, hydrologic testing, log analysis, and additional shaft mapping (e.g., Holt and Powers, 1990; Beauheim and Holt, 1990; Powers and Holt, 1999, 2000). By the mid-1990s, Holt had recognized the relationship between Culebra hydraulic parameters and geologic factors (e.g., depth/elevation and whether the upper Salado had been dissolved) that could be estimated reliably between boreholes (Holt, 1997; Holt and Yarborough, 2002; Holt and others, 2005; Beauheim and others, 2007; Powers and others, 2003). Those relationships led to a different approach to estimating transmissivity in the Culebra (a revised hydrogeology conceptual model). Hart and others (2008) added factors for fillings of Culebra vugs and for the areas where Culebra transmissivity was significantly lower because the Culebra was bracketed by units with halite and also displayed halite pore fillings (Powers and others, 2006b). Performance assessment was modified by this revised conceptual model.

A peer review panel conducted an intensive review in 2008 (Burgess and others, 2008) of the geology, hydrology, and geochemistry related to fluid flow in the Culebra. "The panel believes that the conclusions in the [Culebra conceptual model] from the integration of geology and hydrology are valid ..." (Burgess and others, 2008, p. 23), while noting areas that could be improved. The panel also suggested that there could be benefit from examining in more detail the relationship between the Rustler mudstone-halite facies distribution and both evaporite deformation and the development (geomorphology) of Nash Draw.

WIPP continues to utilize this conceptual model of Culebra hydrology, which has both empirical relationships and, at least some, acceptance of deposition as the main cause of halite distribution in the Rustler. The new shaft under construction at WIPP will provide another opportunity to examine this explanation.

Public comments to CRAs (2004, 2009, 2014) indicate that the discussion about Rustler dissolution has generally morphed from whether mudstone-halite intervals are dissolution residues to whether karst is present in the Rustler at WIPP and how karst would affect the performance assessment (search through https://www.epa.gov/radiation/certification-and-recertification-wipp).

Karst at WIPP

Vine (1963) is the first work set in the area of WIPP known to us to use the word "karst." Sinkholes, depressions, collapse features had all been recognized long before this (e.g., Lee, 1925), but "karst" was not associated specifically with WIPP until 1982 (Barrows, 1982; Barrows and others, 1983; Barrows and Fett, 1985). A gravity survey at WIPP and beyond in 1980 was unable to resolve anomalies expected because of evaporite deformation, but "It did indicate the degree and character

of karst development within the surveyed area" (Barrows and others, 1983, p. 3).

Borehole WIPP-33 (Fig. 2) was drilled in 1979 to explore a depression with thicker fill to determine if the location was a breccia pipe (SNL and USGS, 1981). The stratigraphic sequence was normal, although cavernous porosity was encountered at the top of Rustler as well as at the Magenta and Culebra. A detailed gravity survey over this location revealed a gravity low (e.g., Barrows and others, 1983). The gravity model and geologic interpretation included shallow alteration of the Dewey Lake, local gypsification of Rustler anhydrites, and a large density difference for small cavities in the Rustler (Barrows and others, 1983; Barrows and Fett, 1985).

Another closely spaced gravity survey provided more detail of a gravity anomaly along the northern boundary of the WIPP site (Barrows and others, 1983; Barrows and Fett, 1985). The gravity anomaly parallels a broadly defined valley with a topographic depression. A gravity anomaly and a depression were two factors in common with the WIPP-33 location. Borehole WIPP-14 was targeted at the depression and gravity anomaly (SNL and D'Appolonia Consulting Engineers, 1982). The stratigraphy at WIPP 14 was normal, no cavernous porosity was encountered, and no inflow of fluids was detected.

Barrows and others (1983) compared density logs for WIPP 14 and WIPP 34, a nearby borehole outside the gravity anomaly. Between ~120 and 140 m depth, the Dewey Lake (a siliciclastic unit) has an apparent density difference up to ~0.20 g/cc. Some density differences are indicated at Rustler sulfate beds. Barrows and others (1983) and Barrows and Fett (1985) presented only generalized horizontal cylinders of differing density and radius centered at a depth of 67 m to approximate the observed gravity profile at WIPP-14.

Bachman (1981) suggested the cavernous zones at WIPP-33 (outside WIPP boundaries) may be related to gypsite deposits in Nash Draw west of WIPP-33. Hill (1999, 2003, 2006) proposed theoretical arguments that karst must be present at the WIPP site and variously summarized the arguments of Barrows and others (1983) and Barrows and Fett (1985).

The Rustler was the locus of karsting in Barrows and others (1983). At that time, Rustler mudstone intervals were interpreted as dissolution residues created by post-depositional removal of mainly halite with variable hydration of anhydrite to gypsum and some sulfate solution. The Rustler-Salado contact, the mudstone below Culebra, and mudstone intervals of Tamarisk and Forty-niner Members were all considered zones of dissolution at the site. The previous section explains our data and later interpretation that these lateral changes are mainly depositional facies. Lowenstein (1987) presents some detailed observations about diagenetic changes in Rustler members.

Surficial depressions indicated by topographic contour closures ranked high in the expectations that they represented "sinks" or sinkholes caused by collapse. In an area of several sand dune fields of differing ages, filling topography on the underlying erosional surface causes thousands of such features. Relating surficial depressions to karst or collapse features is speculative, though asserted with confidence. Likewise, the assumption that a gravity anomaly is an indicator of karst (Barrows and others, 1983) is overstated. Lambert (foreword in Bachman, 1987, p. 5) was clear in stating "in view of the established geological observability of features associated with dissolution, this [a negative gravity anomaly indicating karst] may be an unwarranted assumption."

Karst was further discussed with respect to WIPP by Hill (1999, 2003, 2006) and was a topic of interest at New Mexico Environment Department hearings in early 1999 as part of permitting WIPP for hazardous waste disposal (e.g., Powers and Holt, 2008). Lorenz (2006a, b) extensively reviewed the data and analysis of karst, as proposed by various authors. Lorenz (2006b, p. 250) concluded that "... extrapolation of the known karst features in Nash Draw eastward to the WIPP site is unwarranted" and "... arguments offered for karst in the Rustler Formation at the WIPP site are speculative, and what evidence exists for karst is inconsistent and contradictory, and subject to other, more plausible interpretations."

Now there are additional data from WIPP and industry boreholes that might be used to re-evaluate the geology and gravity data for deformation and understanding the source(s) of gravity anomalies, including evaluating alternative gravity models. Where there are more recent data on the Gatuña north of WIPP, thicker deposits are consistent with Bachman's proposal. As we view the more recent geomorphic history of the WIPP site and surroundings, presand dune topography is broadly indicated by current topography. Generalized drainage patterns in the Nash Draw watershed based on current topography are generally consistent with thicker Gatuña that should be considered in evaluating gravity data as well. The elevation of the top of Rustler in the area around WIPP-14 also reveals significant deformation adjacent to WIPP-14 that is more severe with depth (Powers and others, 1996).

Despite extensive reviews and no direct evidence of karst (e.g., tool drops, cavernous porosity) in Rustler units within the WIPP site, this discussion is certain to continue. Waste Isolation Pilot Plant-14 is a clear example. Hill (1999, p. 38, 40) described concerns as follows:

"The fact that WIPP-14 did not intersect karst has sometimes been interpreted to mean that karst was not the cause of the 210 m-in-diameter topographic depression at this location. However, WIPP-14 was drilled to the side of the gravity anomaly (Figure14 [of Barrows and others,1983]), so an intersection of a small borehole

with the center of a sinkhole should not necessarily be expected. Instead, if WIPP-14 is a sinkhole involved with karst, it should be expected that the borehole would intersect a gypsiferous zone related to the conversion of anhydrite to gypsum along a seepage zone at the contact of the Magenta with the Forty-Niner Member . . . , since this contact should be a zone of water movement and hydration . . . .” Hill shows (p. 41, figure 17) an interpretation of why the borehole did not intersect karst. Hill makes it plain, however, that karst **was** intercepted, based on gypsification of a Rustler bed.

Despite Hill’s assertion to the contrary, Barrows and others (1983) showed that the borehole was drilled in the center of the anomaly trend and within the inner contours of the depression (Fig. 11) that has been designated an alluvial doline (Barrows, 1982, p. 8) and “. . . looked definitely like a sinkhole [from aerial photos] . . . in that it is perfectly round and has interior drainage” (Hill, 1999, p. 37).

The issue of karst has percolated at some level through discussions Rustler geology and WIPP hydrology since 1983. The review by Lorenz (2006a, b) of information, interpretations, and arguments with respect to karst is detailed, and his conclusions are straightforward. Chaturvedi (2009) reviews some relevant parts of the history of arguments made to regulatory bodies that karst exists at the WIPP site and is significant; there is considerable detail about the misuse of information. There is certainly a history of applying terminology rather indiscriminately without substantiation.

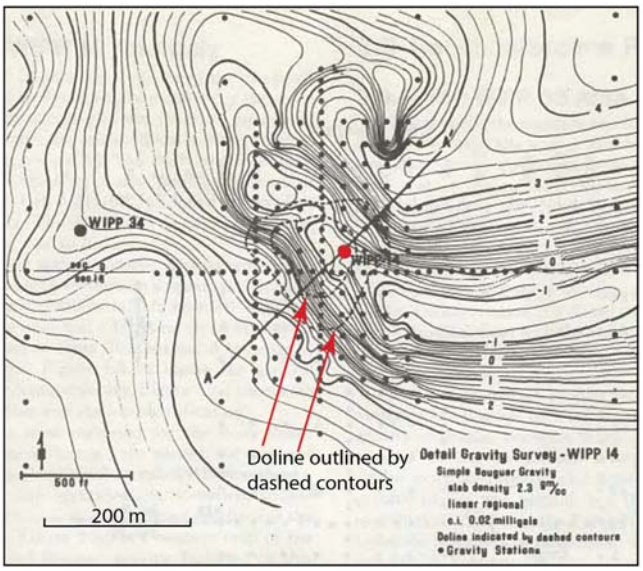

Figure 11. Relationship of WIPP 14 to gravity anomaly and surface depression (“doline”). WIPP-14 was clearly drilled in the middle of the anomaly and within the depression. Modified from Barrows and others (1983).

Untreated Dissolution Features

Two subjects related to dissolution are not detailed here: karst mounds and domes and collapse around boreholes.

Karst mounds and domes (Bachman, 1980) adjacent to the Pecos River and southwest of WIPP were initially identified by Vine (1960), Reddy (1961), and Gera (1974). Anderson (1978) thought they were likely because of regional dissolution of salt [rather than as localized deep dissolution]. One such feature in south-central Nash Draw was drilled and cored (WIPP-32) into the Salado in 1979 (SNL and USGS, 1980); the geology showed no brecciation or unusual stratigraphy at depth and shallow dissolution of upper Salado was consistent with that part of Nash Draw.

Borehole dissolution with collapse has become a regional issue because of the collapse of three boreholes involved in commercial brine production and three boreholes intersecting the Capitan aquifer (e.g., Baumgardner and others, 1982; Johnson, 1989; Johnson and others, 2003; Powers, 2003; Land, 2013). Brine production wells would be prohibited within the WIPP site during administrative control. Water to operate a brine well is not readily available in the area of the site. Unless a brine well was located at or below the repository level, there would be no connection.

DISCUSSION

The initial concern at WIPP was for dissolution from top of Salado salt down to disposal levels. This was generally assessed (~1972–1974) for the first (now abandoned) location and found not to be of concern for millions of years. Nevertheless, it factored into the selection of the current WIPP site (1975–1976) and delineation of areas for disposal as well as outer zones with restrictions. Early hydrologic tests and monitoring included the zone at the Rustler-Salado contact to determine the presence and significance of the brine aquifer known to occur above Salado salt at Nash Draw. The Rustler-Salado contact at the site yielded little brine and was found to be of little hydrologic significance. Salt in the Los Medaños Member above this interval across the site meant surface-down dissolution was not occurring, and that combination inspired the concept of a dissolution wedge for the Rustler-Salado contact at WIPP. Surface-down dissolution, however, generally became of less concern through early site characterization as it again was not apparent that it could affect a disposal layer over a relevant period. Although shaft mapping showed that this contact was not undergoing dissolution, having a regulatory period set for 10,000 yr and a specific criterion for failure in performance assessment made this concern irrelevant.

Discovery of a collapse chimney (“breccia pipe”) in a potash mine set in motion a large effort to understand

these features as well as to determine whether they might exist at the site. Anomalies at the site were investigated (e.g., WIPP-13, WIPP-33) and determined not to be breccia pipes. The known breccia pipes in the northern Delaware Basin were associated with the Capitan reef, which is not present at the site. With no evidence of breccia pipes at the site, concerns over their possible existence at the site were minimal by 1983.

Deep dissolution as a wedge to undercut the WIPP disposal area was directly tested by borehole ERDA-10. This testing did not find evidence of dissolution residues at Salado-Castile contact or in the Castile or evidence of fluid movement along the contact. The process was estimated to take millions of years to reach WIPP, and defining the regulatory period rendered the hypothesis (of a deep dissolution wedge reaching WIPP) moot. Some of the original background assumptions about rates and extent of deep dissolution have been questioned; the main proponent has also revised ideas about the depositional extent of Castile halites (Anderson, 1993; Anderson and Kirkland, 1995), which alters estimates of dissolution and rates.

Localized dissolution (deep) was mostly associated with specific features such as surficial depressions and changes in halite thickness or elevation (Anderson, 1978). None of these features were present in the current boundaries of WIPP. A change in elevation of Salado beds was found at a single potash drill hole within original outer zones on the northern side of WIPP. DOE-2 was drilled at this anomaly mainly to extract more information about expected evaporite deformation north of the WIPP site center. DOE-2 cores and logs provided evidence that the beds were deformed, not dissolved from below.

Surface depressions or lagunas or lakes outside of WIPP that were noted by Anderson (1978) have continued to be designated as "sinks" or breccia pipes or as evidence of dissolution without providing subsurface data. Subsurface evidence for two examples contradicts such assertions. It seems unlikely this will prevent such assertions where subsurface data are not available.

Basin troughs as dissolution features remain poorly constrained in timing and process because there are no cores to provide some critical evidence. The study by Johnson (1993) points the way to some differentiation of early removal of halite versus much more recent geological events. We provide a more detailed look at the structure of the top of Rustler here that compares with the interpreted elevation of top and base of Rustler (Ewing and others, 2012) and faults as an indicator of future enhancements of basin trough data.

Our ideas of depositional processes and dissolution of the Rustler have changed dramatically from early investigations. The new shaft at WIPP will provide yet another opportunity to check these ideas. Over time, these ideas have been extended well beyond WIPP, and we continue data analysis of the Rustler.

A surface gravity survey in the early 1980s across parts of northern WIPP, with detailed surveys of some specific surface depressions, led to one exploratory drill hole (WIPP-14). No clear evidence of karst was found at the location, but the drill hole data and location have been extensively discussed. Arguments have been made that karst exists at WIPP and is significant to the extent that WIPP should no longer be certified or continued. There seems to be no reasonably testable hypothesis of karst; any test without direct evidence is deemed unconvincing. It wasn't done at the right place or in the right way, or karst is inherently difficult to intercept in a borehole. A hypothesis that is extremely difficult to falsify leads us to believe that karst will continue to be raised as an issue for future EPA recertifications and NMED permits for the continued operation of WIPP.

The original Anderson (1978) study provided a framework, although strongly oriented toward dissolution as a potential explanation for many features, for investigating how dissolution might affect isolation of radioactive waste at WIPP. At the time, no regulatory period for isolation had been established, and the assumed limits of 250,000 yr (~10 half-lives of Pu^{239}) and an exposure point at Malaga Bend on the Pecos River allowed great latitude in suggesting how dissolution might be important. In addition, available borehole data were much more limited than they are today. It is highly likely that we or others will exploit the data now available to examine some of the ideas and their validity. Basic assumptions about evaporite deposition in the Delaware Basin, processes of dissolution, and whether the physical conditions required to enable such processes have already been modified through time.

We echo Lorenz (2006a, b) and Chaturvedi (2009) in being disturbed by how features such as sink, sinkhole, collapse, alluvial dolines, etc., are simply asserted to exist with only the slimmest of circumstantial evidence or how statements are taken out of context. We are mindful that karst does exist in the area and continue to examine its manifestations (e.g., Powers, 2003; Powers and Owsley, 2003; Powers and others, 2006a; Goodbar and others, 2020).

FINAL WORDS

Dissolution and the various perceptions, hypotheses, and assertions regarding its extent, timing, and significance to WIPP resulted in considerable expenditures of time and resources in investigations. The investigations have drawn significant analysis by regulatory and oversight organizations including the New Mexico Environmental Evaluation Group, National Academy of Sciences panels, New Mexico Environment Department,

and Environmental Protection Agency. Stakeholders have been active in reviewing and discussing dissolution.

By about the time WIPP was directly exploring the site through shafts (~1983), most of these original issues were reasonably settled. There was no evidence found of breccia pipes or localized deep dissolution at WIPP, and neither evidence of a dissolution wedge threatening WIPP at depth nor conditions for the process were obvious. The various reports and studies were numerous, culminating mainly with the report of Lambert (1983). Neill and others (1983), for example, considered these features/processes not to be a threat to the repository. Lappin and others (1989) summarized preperformance limits to the effects of these processes.

At this time, there is no specific concern expressed on the part of regulating parties that dissolution processes will affect continuing operations. The renewal application for the hazardous waste facility permit has been submitted to the New Mexico Environment Department for review. The compliance recertification application 2019 (CRA 2019) for continued disposal of defense-related transuranic waste is being reviewed for completeness by the US Environmental Protection Agency. We fully expect that some concerns, most likely mainly about karst, will continue to surface through stakeholder comments.

Some issues possibly could have been avoided or addressed easily with better and early understanding of conditions (e.g., extremely low permeability, high fluid pressures) within the evaporite sequence. Newer data, such as we present for Bell Lake "sink" and Laguna Plata, should help modify a few pieces of the record. Continuing to work on Nash Draw helps us maintain a sense of a differing hydrologic and geologic regime in the vicinity of WIPP.

ACKNOWLEDGMENTS

A significant part of our background work has been funded through WIPP, though not all. This publication, however, has not been funded by any WIPP agency or other source; it does not purport to represent any current opinion or position of WIPP or those organizations working at WIPP. We acknowledge helpful reviews by Kenneth S. Johnson and Anderson Ward; we absolve them of responsibility for content or any errors.

REFERENCES CITED

Adams, J.E., 1944, Upper Permian Ochoan Series of Delaware Basin, west Texas and southeast New Mexico: American Association of Petroleum Geologists, Bulletin, v. 28, p. 1596-1625.

Anderson, R.Y., 1978, Report to Sandia Laboratories on deep dissolution of salt, Northern Delaware Basin, New Mexico: Sandia National Laboratories, Albuquerque, NM. https://wipp.energy.gov/library/cca/CCA_1996_References/Chapter%202/CREL4311.PDF

Anderson, R.Y., 1980, Field trip notes for salt dissolution features in the Delaware Basin, *in* Chaturvedi (1980), p. 112-129.

Anderson, R.Y., 1993, The Castile as a "nonmarine" evaporite, *in* Love, D.W., Hawley, J.W., and others, eds., Carlsbad region, New Mexico and west Texas: New Mexico Geological Society, Forty-fourth Annual Field Conference, p. 12-13.

Anderson, R.Y., and Kirkland, D.W., 1966, Intrabasin varve correlation: Geological Society of America Bulletin, v. 77, p. 241-256.

Anderson, R.Y., and Powers, D.W., 1978, Salt anticlines in Castile-Salado evaporite sequence, northern Delaware Basin, *in* Austin, G.S., ed., Geology and mineral deposits of Ochoan rocks in Delaware Basin and adjacent areas: New Mexico Bureau of Mines and Mineral Resources, Circular 159, p. 79-84.

Anderson, R.Y, Kietzke, K.K., and Rhodes, D.J., 1978, Development of dissolution breccias, northern Delaware Basin, New Mexico and Texas, *in* Austin, G.S., ed., Geology and mineral deposits of Ochoan rocks in Delaware Basin and adjacent areas: New Mexico Bureau of Mines and Mineral Resources, Circular 159, p. 47-52.

Anderson, R.Y., Dean, W.E., Jr., Kirkland, D.W., and Snider, H.I., 1972, Permian Castile varved evaporite sequence, west Texas and New Mexico: Geological Society of America Bulletin, v. 83, p. 59-86.

Bachman, G.O., 1973, Surficial features and late Cenozoic history in southeastern New Mexico: US Geological Survey, Open-File Report USGS-4339-8, Denver, CO.

Bachman, G.O., 1976, Cenozoic deposits of southeastern New Mexico and an outline of the history of evaporite dissolution: Journal of Research of US Geological Survey, v. 4, p. 135-149.

Bachman, G.O., 1980, Regional geology and Cenozoic history of Pecos region, southeastern New Mexico: US Geological Survey, Open-file Report 80-1099, 116 p.

Bachman, G.O., 1981, Geology of Nash Draw, Eddy County, NM: US Geological Survey, Open-file Report 81-31, 10 p.

Bachman, G.O., 1984, Regional geology of Ochoan evaporites, northern part of Delaware Basin: New Mexico Bureau of Mines and Mineral Resources, Circular 184, 22 p.

Bachman, G.O., 1985, Assessment of near-surface dissolution at and near the Waste Isolation Pilot Plant (WIPP), southeastern New Mexico: Albuquerque,

NM, Sandia National Laboratories, SAND84-7178, 33 p.

Bachman, G.O., 1987, Karst in evaporites in southeastern New Mexico: Albuquerque, NM, Sandia National Laboratories, SAND86-7078, 82 p.

Bachman, G.O., and Johnson, R.B., 1973, Stability of salt in the Permian salt basin of Kansas, Oklahoma, Texas, and New Mexico: US Geological Survey, Open-file Report USGS-4339-4.

Barrows, L.J., 1982, WIPP geohydrology – the implications of karst, *in* Chaturvedi, L, and Channelll, 1985, The Rustler Formation as a Transport Medium for Contaminated Groundwater, Appendix A: EEG-32, Environmental Evaluation Group, Santa Fe, NM.

Barrows, L.J., and Fett, J.D., 1985, A high-precision gravity survey in the Delaware Basin of southeastern New Mexico: Geophysics, v. 50, no. 5, p. 825-833.

Barrows, L.J., Shaffer, S-E., Miller, W.B., and Fett, J.D., 1983, Waste Isolation Pilot Plant (WIPP) site gravity survey and interpretation: Sandia National Laboratories, Albuquerque, NM, SAND82-2922.

Baumgardner, R.W., Jr., Hoadley, A.D., and Goldstein, A.G., 1982, Formation of the Wink Sink, a salt dissolution and collapse feature, Winkler County, Texas: Bureau of Economic Geology, University of Texas at Austin, Report of Investigation 114.

Beauheim, R.L., and Holt, R.M., 1990, Hydrogeology of the WIPP site, *in* Powers, D.W., Holt, R.M., Beauheim, R.L., and Rempe, N., Geological and Hydrological Studies of Evaporites in the Northern Delaware Basin for the Waste Isolation Pilot Plant (WIPP), New Mexico: Dallas Geological Society, GSA Field Trip No. 14, p. 131-179.

Beauheim, R.L., and Roberts, R.M., 2002, Hydrology and hydraulic properties of a bedded evaporite formation: Journal of Hydrology, v. 259, p. 66-88.

Beauheim, R.L., Hassinger, B.W., and Klaiber, G.A., 1983, Basic data report for borehole Cabin Baby-deepening and hydrologic testing, Waste Isolation Pilot Plant (WIPP) project, southeastern New Mexico: WTSD-TME-020, US Department of Energy, Albuquerque, NM. Successes and experiences of the WIPP project.

Beauheim, R.L., McKenna, S.A., Powers, D.W., and Holt, R.M., 2007, Geoscientific data collection and integration for the Waste Isolation Pilot Plant: Linkage of Geoscientific Arguments and Evidence in Supporting the Safety Case, Second AMIGO Workshop Proceedings, Toronto, Canada, 20-22 September 2005, OECD NEA, p. 125-132 (ISBN 978-92-64-01966-9). https://www.researchgate.net/profile/Richard_Beauheim/publication/255277185_Geoscientific_data_collection_and_integration_for_the_Waste_Isolation_Pilot_Plant/links/0f317535fd05fb9460000000/Geoscientific-data-collection-and-integration-for-the-Waste-Isolation-Pilot-Plant.pdf

Black, S.R., Newton, R.S., and Shukla, D.K., eds., 1983, Results of site validation experiments, Waste Isolation Pilot Plant (WIPP) project, southeastern New Mexico: US Department of Energy, Albuquerque, NM, TME 3177, v. I and II.

Brookins, D.G., and Lambert, S.J., 1988, WIPP site studies: secondary selenite veins in the Rustler Formation and Dewey Lake Red Beds: Materials Research Society Symposium Proceedings, v. 112, p. 233-241 (doi: https://doi.org/10.1557/PROC-112-233)

Chaturvedi, L., 1980, WIPP site and vicinity geological field trip: Environmental Evaluation Group EEG-7. http://www.sric.org/nuclear/eeg/1980_10_EEG07.pdf

Chaturvedi, L., 1987, ed., The Rustler Formation at the WIPP site: EEG-34, Environmental Evaluation Group, Santa Fe, NM. http://www.sric.org/nuclear/eeg/1987_01_EEG-34.pdf

Chaturvedi, L., 2009, The karst and related issues at the Waste Isolation Pilot Plant: unpublished paper. (https://www.wipp.energy.gov/fctshts/Karst_Chaturvedi_062309.pdf)

Chu, M.S.Y., and Weart, W.D., 2000, Successes and experiences of the WIPP project: Sandia National Laboratories, Albuquerque, NM, SAND2000-2131C. https://www.osti.gov/servlets/purl/761878

Croxton, N.M., 2003, Subsidence on the Interstate 70 I Russell County, Kansas, related to salt dissolution –a history, *in* Johnson, K.S., and Neal, J.T., eds., Evaporite Karst and Engineering/Environmental Problems in the United States: Oklahoma Geological Survey, Circular 109, p. 149-155.

Ewing, J.E., Jones, T.L., Yan, T, Vreugdenhil, A.M., Fryar, D.G., Pickens, J.F., Gordon, K., Nicot, J-P., Scanlon, B.R., Ashworth, J.B., and Beach, J., 2008, Final report groundwater availability model for the Dockum aquifer: report for Texas Water Development Board. (find at https://www.twdb.texas.gov/groundwater/models/gam/dckm/dckm.asp)

Ewing, J.E., Kelley, V.A., Jones, T.L., Yan, T., Singh, A., Powers, D.W., Holt, R.M., and Sharp, J.M., 2012, Final groundwater availability model report for the Rustler aquifer: report for Texas Water Development Board. http://www.twdb.texas.gov/groundwater/models/gam/rslr/RSLR_GAM_Report.pdf

Gera, F., 1974, On the origin of the small hills in Nash Draw and Clayton Basin, southeastern New Mexico: Oak Ridge National Laboratory, Oak Ridge, TN, ORNL Central Files No. 74-2-29.

Goodbar, A.K., Powers, D.W., Goodbar, J.R., and Holt, R.M., 2020, Karst and sinkholes at Nash Draw,

southeastern New Mexico (USA), in Land, L., Kromhout, C., and Byle, M.J., eds., Proceedings of the Sixteenth Multidisciplinary Conference on Sinkholes and the Engineering and Environmental Impacts of Karst (first ed.): National Cave and Karst Research Institute, Carlsbad, NM, Symposium 8, p. 287-298.

Griswold, G.B., 1977, Site selection and evaluation studies of the Waste Isolation Pilot Plant (WIPP), Los Medaños, Eddy County, New Mexico: Sandia National Laboratories, Albuquerque, NM, SAND 77-0946.

Hill, C.A., 1993, Barite/celestite/selenite/calcite mineralization at Bell Lake sink, Lea County, New Mexico, in Love, D.W., Hawley, J.W., and others, eds., Carlsbad region, New Mexico and West Texas: New Mexico Geological Society, Forty-fourth Annual Field Conference, p. 317-320.

Hill, C.A., 1996, Geology of the Delaware Basin, Guadalupe, Apache, and Glass Mountains, New Mexico and west Texas: Permian Basin Section-SEPM Publication No. 96-39.

Hill, C.A., 1999, Letter Report: Intrastratal karst at the WIPP site: unpublished report to Sandia National Laboratories, 98 p.

Hill, C.A., 2003, Intrastratal karst at the Waste Isolation Pilot Plant site, southeastern New Mexico, *in* Johnson, K.S., and Neal, J.T., eds., Evaporite Karst and Engineering/Environmental Problems in the United States: Oklahoma Geological Survey, Circular 109, p. 197-209.

Hill, C.A., 2006, Intrastratal karst at the Waste Isolation Pilot Plant site, southeastern New Mexico, *in* Land, L., and others, eds., Caves & Karst of Southeastern New Mexico, NM: Geological Society Fifty-seventh Annual Field Conference Guidebook, p. 233-242. (reprint of Hill, 2003)

Hills, J.M., 1984, Sedimentation, tectonism, and hydrocarbon generation in Delaware basin, west Texas and southeastern New Mexico: American Association of Petroleum Geologists, Bulletin, v. 68, p. 260-267.

Hiss, W.L., 1975, Stratigraphy and ground-water hydrology of the Capitan aquifer, southeastern New Mexico and western Texas: unpublished Ph.D. Dissertation, University of Colorado, Boulder, 501 p.

Hiss, W.L., 1976, Chloride-ion concentration in ground water in Permian Guadalupian rocks, southeast New Mexico and west Texas: New Mexico Bureau of Mines & Mineral Resources, Socorro, NM, Resource Map 4.

Holliday, V.T., Hovorka, S.D., and Gustavson, T.C., 1996, Lithostratigraphy and geochronology of fills in small playa basins on the Southern High Plains, United States: Geological Society of America Bulletin, v. 108, p. 953-965.

Holt, R.M., 1988, The depositional environments of the late Permian Rustler Formation, in the vicinity of the Waste Isolation Pilot Plant (WIPP) site, southeastern New Mexico: unpublished M.S. thesis, University of Texas at El Paso.

Holt, R.M., 1997, Conceptual model for transport processes in the Culebra Dolomite Member, Rustler Formation: Sandia National Laboratories, Albuquerque, NM, SAND97-0194. https://www.osti.gov/servlets/purl/527459

Holt, R.M., and Powers, D.W., 1984, Geotechnical activities in the waste handling shaft, Waste Isolation Pilot Plant (WIPP) project, Southeastern New Mexico: Department of Energy, Carlsbad, NM, WTSD-TME 038.

Holt, R.M., and Powers, D.W., 1986, Geotechnical activities in the exhaust shaft, Waste Isolation Pilot Plant: Department of Energy, Carlsbad, NM, DOE-WIPP 86-008.

Holt, R.M., and Powers, D.W., 1988, Facies variability and post-depositional alteration within the Rustler Formation in the vicinity of the Waste Isolation Pilot Plant, Southeastern New Mexico: Department of Energy, Carlsbad, NM, WIPP-DOE-88-004. https://wipp.energy.gov/library/cca/CCA_1996_References/Chapter%202/CREL2063.PDF

Holt, R.M., and Powers, D.W., 1990, Geological mapping of the air intake shaft at the Waste Isolation Pilot Plant: DOE/WIPP 90-051, U.S. Department of Energy, Carlsbad, NM. http://www.ntis.gov/search/product.aspx?ABBR=DE91017780

Holt, R.M., and Powers, D.W., 2010, Evaluation of halite dissolution at a radioactive waste disposal site, Andrews County, TX: Geological Society of America Bulletin, v. 122, p. 1989-2004, DOI: https://doi.org/10.1130/B30052.1.

Holt, R.M., and Powers, D.W., 2011, Synsedimentary dissolution pipes and the isolation of ancient bacteria and cellulose: Geological Society of America Bulletin, v. 123, p. 1513-1523, DOI:https://doi.org/10.1130/B30197.1.

Holt, R.M., and Yarborough, L., 2002, Analysis report, Task 2 of AP-088, Estimating base transmissivity fields: ERMS# 523889, WIPP Records Center, Sandia National Laboratories, Carlsbad, NM.

Holt, R.M., Beauheim, R.L., and Powers, D.W., 2005, Predicting fractured zones in the Culebra Dolomite, *in* Faybishenko, B, Witherspoon, P.A., and Gale, J., eds., Dynamics of Fluids and Transport in Fractured Rock: AGU Geophysical Monograph Series, v. 162, p. 103-116.

Hovorka, S. D., 1989, Depth evolution of the Delaware Basin – Castile/Salado transition, *in* Harris, P.M, and

Grover, G.A., eds., Subsurface and Outcrop Examination of the Capitan shelf margin, Northern Delaware Basin: SEPM Core Workshop no. 13, p. 441-449.

Hovorka, S.D., Holt, R.M., and Powers, D.W., 2007, Depth indicators in Permian Basin evaporites, *in* Schreiber, B.C., Lugli, S., and Babel, M., Evaporites through space and time: Geological Society, London, Special Publication 285, p. 335-364.

Johnson, K.S., 1981, Dissolution of salt on the east flank of the Permian Basin in the southwestern USA: Journal of Hydrology, v. 54, p. 75-93.

Johnson, K.S., 1989, Development of the Wink sink in west Texas, USA, due to salt dissolution and collapse: Environmental Geology and Water Sciences, v. 14, p. 81-92.

Johnson, K.S., Collins, E.W., and Seni, S.J., 2003, Sinkholes and land subsidence owing to salt dissolution near Wink, west Texas, and other sites in western Texas and New Mexico, *in* Johnson, K.S., and Neal, J.T., eds., Evaporite Karst and Engineering/Environmental Problems in the United States: Oklahoma Geological Survey, Circular 109, p. 183-195.

Jones, C.L., 1972, Permian basin potash deposits, southwestern United States, *in* Richter-Bernburg, G., ed., Geology of saline deposits, UNESCO, p. 191-201.

Jones, C.L., 1981, Geologic data for borehole ERDA-6, Eddy County, New Mexico: US Geological Survey, Open-file Report 81-468.

Jones, C.L, Bowles, C.G., and Bell, K.G., 1960, Experimental drill hole logging in potash deposits of the Carlsbad District, New Mexico: US Geological Survey, Open-file Report 60-84.

Jones, C.L., Cooley, M.E., and Bachman, G.O., 1973, Salt deposits of Los Medaños area, Eddy and Lea Counties, New Mexico: USGS-4339-7, US Geological Survey, Denver, CO.

Lambert, S.J., 1983, Dissolution of evaporites in and around the Delaware Basin, southeastern New Mexico and west Texas: SAND82-0461, Sandia National Laboratories, Albuquerque, NM.

Land, L., 2013, Evaporite karst in the Permian Basin region of west Texas and southeastern New Mexico: The human impact, *in* Land, L., Doctor, D.H., and Stephenson, B., eds., Proceedings of the 13th Multidisciplinary Conference on Sinkholes and the Engineering and Environmental Impacts of Karst: National Cave and Karst Research Institute, Carlsbad, NM, p. 113-121.

Lappin, A.R., 1988, Summary of site-characterization studies conducted from 1983 through 1987 at the Waste Isolation Pilot Plant (WIPP) site, southeastern New Mexico: SAND88-0157, Sandia National Laboratories, Albuquerque, NM.

Lappin, A.R., Hunter, R.L, Garber, D.P., and Davies, P.B., eds., 1989, Systems analysis, long-term radionuclide transport, and dose assessments, Waste Isolation Pilot Plant (WIPP), southeastern New Mexico; March 1989: SAND89-0462, Sandia National Laboratories, Albuquerque, NM.

Lee, W.T., 1925, Erosion by solution and fill, *in* Contributions to geography in the United States: U.S. Geological Survey, Bulletin 760-C, p. 107-121.

Leslie, A., Kendall, A., and Harwood, G., 1993, The Castile Formation: a continuing paradox, *in* Love, D.W., Hawley, J.W., and others, eds., Carlsbad region, New Mexico and west Texas: New Mexico Geological Society, Forty-fourth Annual Field Conference, p. 13-14.

Leslie, A.B., Kendall, A.C., Harwood, G.M., and Powers, D.W., 1996, Conflicting indicators of palaeodepth during deposition of the Upper Permian Castile Formation, Texas and New Mexico, *in* Kemp, A.E.S., ed., Palaeoclimatology and Palaeoceanography from Laminated Sediments: Geological Society, London, Special Publication 116, p. 79-92.

Lorenz, J.C., 2006a, Assessment of the potential for karst in the Rustler Formation at the WIPP site: SAND2005-7303, Sandia National Laboratories, Albuquerque, NM, 102 p.

Lorenz, J.C., 2006b, Assessment of the geological evidence for karst in the Rustler Formation at the WIPP site, *in* Land, L., and others, eds., Caves and Karst of Southeastern New Mexico: New Mexico Geological Society, Fifty-seventh Annual Field Conference Guidebook, p. 243-251.

Lowenstein, T.K., 1987. Post Burial Alternation of the Permian Rustler Formation Evaporites, WIPP Site, New Mexico: Textural Stratigraphic and Chemical Evidence. EEG-36, New Mexico Health and Environment Department, Santa Fe, New Mexico. (https://wipp.energy.gov/library/cca/CCA_1996_References/Chapter%202/CREL4001.PDF)

Madsen, B.M., and Raup, O.B., 1988, Characteristics of the boundary between the Castile and Salado Formations near the western edge of the Delaware Basin, southeastern New Mexico: New Mexico Geology, v. 10, no. 1, p. 1-5, 9.

Mercer, J.W., 1982, Drill-stem tests, WIPP 31, *in* Snyder and Gard (1982), p. 67-69.

Mercer, J.W., 1983, Geohydrology of the proposed Waste Isolation Pilot Plant site, Los Medaños area, Southeastern New Mexico: US Geological Survey, Water-Resources Investigations Report 83-4016, Albuquerque, NM.

Mercer, J. W., 1987, Compilation of hydrologic data from drilling the Salado and Castile Formations near

the Waste Isolation Pilot Plant (WIPP) site in southeastern New Mexico: SAND86-0954, Sandia National Laboratories, Albuquerque, NM.

Mercer, J.W., and Orr, B.R., 1977, Review and analysis of hydrogeologic conditions near the site of a potential nuclear-waste repository, Eddy and Lea Counties, New Mexico: US Geological Survey, Open-file Report 77-123.

Mercer, J.W., Beauheim, R.I., Snyder, R.P., and Fairer, G.M., 1987, Basic data report for drilling and hydrologic testing of drillhole DOE-2 at the Waste Isolation Pilot Plant (WIPP) site: SAND86-0611, Sandia National Laboratories, Albuquerque, NM.

NAS/NRC, 1957, Disposal of radioactive wastes on land: National Academy of Sciences – National Research Council, Washington, D.C., Publication 519.

Neill, R.H., Channell, J.K., Chaturvedi, L., Little, M.S., Rehfeldt, K., and Spiegler, P., 1983, Evaluation of the suitability of the WIPP site: EEG-23, Environmental Evaluation Group, Sant Fe, NM. https://wipp.energy.gov/library/cca/CCA_1996_References/Chapter%202/CREL3987.PDF

Nicholson, A., Jr., and Clebsch, A., Jr., 1961, Geology and ground-water conditions in southern Lea County, New Mexico: State Bureau of Mines and Mineral Resources, Ground-Water Report 6, New Mexico Institute of Mining and Technology, Socorro, NM.

Osterkamp, W.R., and Wood, W.W., 1987, Playa-lake basins on the southern High Plains of Texas and New Mexico: Part I. Hydrologic, geomorphic, and geologic evidence for their development: Geological Society of America, Bulletin, v. 99, p. 215-223.

Pierce, W.G., and Rich, E.I, 1962, Summary of rock salt deposits in the United States as possible storage sites for radioactive waste materials: US Geological Survey, Bulletin 1148, Washington, D.C.

Powers, D. W., 1996, Tracing early breccia pipe studies, Waste Isolation Pilot Plant, southeastern New Mexico: A study of the documentation available and decision-making during the early years of WIPP: SAND94-0991, Sandia National Laboratories, Albuquerque, NM.

Powers, D.W., 2003, Jal Sinkhole in Southeastern New Mexico: Evaporite dissolution, drillholes, and the potential for sinkhole development, *in* Johnson, K.S., and Neal, J.T., eds., Evaporite Karst and Engineering/Environmental Problems in the United States: Oklahoma Geological Survey, Circular 109, p. 219-226.

Powers, D.W., and Holt, R.M., 1990, Sedimentology of the Rustler Formation near the Waste Isolation Pilot Plant (WIPP) site, *in* Powers, D.W., Holt, R.M., Beauheim, R.L., and Rempe, N., eds., 1990, Geological and Hydrological Studies of Evaporites in the Northern Delaware Basin for the Waste Isolation Pilot Plant (WIPP): Geological Society of America (Dallas Geological Society), Guidebook 14, p. 79-106.

Powers, D.W., and Holt, R.M., 1999, The Los Medaños Member of the Permian Rustler Formation: New Mexico Geology, v. 21, no. 4, p. 97-103.

Powers, D.W., and Holt, R.M., 2000, The salt that wasn't there: mudflat facies equivalents to halite of the Permian Rustler Formation, southeastern New Mexico: Journal of Sedimentary Research, v. 70, no. 1, p. 29-36.

Powers, D.W., and Holt, R.M., 2008, Lessons from early site investigations at the Waste Isolation Pilot Plant, *in* Rempe, N.T., ed., Deep Geologic Repositories: Geological Society of America, Reviews in Engineering Geology, v. XIX, p. 83-97, doi: https://doi.org/10.1130/2008.4019(09), March.

Powers, D.W., and Owsley, D., 2003, A field survey of evaporite karst along NM 128 realignment routes, *in* Johnson, K.S., and Neal, J.T., eds., Evaporite Karst and Engineering/Environmental Problems in the United States: Oklahoma Geological Survey, Circular 109, p. 233-240.

Powers, D.W., Beauheim, R.L., Holt, R.M., and Hughes, D.L., 2006a, Evaporite karst features and processes at Nash Draw, Eddy County, New Mexico, *in* Land, L., and others, eds., Caves & Karst of Southeastern New Mexico: New Mexico Geological Society, Fifty-seventh Annual Field Conference Guidebook, p. 253-266.

Powers, D.W., Holt, R.M., Beauheim, R.L., and McKenna, S.A., 2003, Geological factors related to the transmissivity of the Culebra Dolomite Member, Permian Rustler Formation, Delaware Basin, Southeastern New Mexico, *in* Johnson, K.S., and Neal, J.T., eds., Evaporite Karst and Engineering/Environmental Problems in the United States: Oklahoma Geological Survey, Circular 109, p. 211-218.

Powers, D.W., Holt, R.M., Beauheim, R.L., and Richardson, R.G., 2006b, Advances in depositional models of the Permian Rustler Formation, southeastern New Mexico, *in* Caves & Karst of Southeastern New Mexico, Land, L., and others, eds., New Mexico Geological Society, Fifty-seventh Annual Field Conference Guidebook, p. 267-276.

Powers, D.W., Lambert, S.J., Shaffer, S-E., Hill, L.R., and Weart, W.D., eds., 1978, Geological characterization report, Waste Isolation Pilot Plant (WIPP) site, southeastern New Mexico: SAND78-1596, v. I & II, about 1500 p., Sandia National Laboratories, Albuquerque, NM 87185.

Rechard, R.P., 2000, Historical background on performance assessment for the Waste Isolation Pilot Plant: Reliability Engineering and System Safety, v. 69, p. 5-46.

Reddy, G.R., 1961, Geology of the Queen Lake domes near Malaga, Eddy County, New Mexico: Unpublished M.S. thesis, University of New Mexico, Albuquerque, NM.

Reeves, C.C., Jr., and Temple, J.M., 1986, Permian salt dissolution, alkaline lake basins, and nuclear-waste storage, southern High Plains, Texas and New Mexico: Geology, v. 14, p. 939-942.

Roberts, R.M., Beauheim, R.L., and Domski, P.S., 1999, Hydraulic testing of Salado Formation evaporites at the Waste Isolation Pilot Plant site: final report: SAND98-2537, Sandia National Laboratories, Albuquerque, New Mexico.

Robinson, J.Q., 1989, A clastic evaporite deposit in the lower Castile Formation (Permian), Delaware Basin: Unpublished M.S. Thesis, University of Texas at El Paso.

Robinson, J.Q., and Powers, D.W., 1987, A clastic deposit within the lower Castile Formation, western Delaware Basin, New Mexico, *in* Powers, D.W., and James, W.C., eds., Geology of the western Delaware Basin, west Texas and southeastern New Mexico: El Paso Geological Society, Guidebook 18, p. 69-79.

Robinson, T.W., and Lang, W.B., 1938, Geology and ground-water conditions of the Pecos River valley in the vicinity of Laguna Grande de la Sal, New Mexico: New Mexico State Engineer, 12th and 13th Biennial Reports, p. 79-100. (scanned version at https://wipp.energy.gov/library/cca/CCA_1996_References/Chapter%202/CREL4706.PDF)

Smith, D.B., Cannon, W.F., Woodruff, L.G., Solano, Federico, Kilburn, J.E., and Fey, D.L., 2013, Geochemical and mineralogical data for soils of the conterminous United States: US Geological Survey, Data Series 801, 19 p., https://pubs.usgs.gov/ds/801/. Select Downloads, Appendix_3a_AHorizon_18 Sept2013.xls. Line # 2851, sample C-326121.

SNL (Sandia National Laboratories) and D'Appolonia Consulting Engineers, 1982, Basic data report for drillhole WIPP 14 (Waste Isolation Pilot Plant – WIPP): SAND82-1783, Sandia National Laboratories, Albuquerque, NM.

SNL (Sandia National Laboratories) and D'Appolonia Consulting Engineers, 1983, Basic data report for drillhole ERDA-10 (Waste Isolation Pilot Plant – WIPP): SAND79-0271, Sandia National Laboratories, Albuquerque, NM.

SNL (Sandia National Laboratories) and USGS (US Geological Survey), 1979, Basic data report for drillhole WIPP 13 (Waste Isolation Pilot Plant – WIPP): SAND79-0273, Sandia National Laboratories, Albuquerque, NM.

SNL (Sandia National Laboratories) and USGS (US Geological Survey), 1981, Basic data report for drillhole WIPP 33 (Waste Isolation Pilot Plant – WIPP): SAND80-2011, Sandia National Laboratories, Albuquerque, NM.

SNL (Sandia National Laboratories) and USGS (US Geological Survey), 1983, Basic data report for drillhole ERDA-6 (Waste Isolation Pilot Plant – WIPP): SAND79-0267, Sandia National Laboratories, Albuquerque, NM.

Snyder, R.P., and Gard, L.M., Jr., 1982, Evaluation of breccia pipes in southeastern New Mexico and their relation to the Waste Isolation Pilot Plant (WIPP) site, with section on Drill-stem tests: U.S. Geological Survey Open-file Report 82-968.

Temple, J.M., 1986, Permian salt dissolution related to alkaline lake basins, southern High Plains, Texas: Unpublished M.S. thesis, Texas Tech University, Lubbock TX, 87 p.

US DOE, 1996, Title 40 CFR Part 191 Compliance Certification Application: DOE/CAO 1996-2184, US Department of Energy, Carlsbad Field Office, Carlsbad, NM.

US DOE, 2004, Title 40 CFR Part 191 Compliance Recertification Application 2004 for the Waste Isolation Pilot Plant: DOE/WIPP 2004-3231, US Department of Energy, Carlsbad Field Office, Carlsbad, NM.

US DOE, 2009, Title 40 CFR Part 191 Compliance Recertification Application 2009 for the Waste Isolation Pilot Plant: DOE/WIPP 2009-342, US Department of Energy, Carlsbad Field Office, Carlsbad, NM.

US DOE, 2014, Title 40 CFR Part 191 Compliance Recertification Application 2014 for the Waste Isolation Pilot Plant: DOE/WIPP 2014-3503, US Department of Energy, Carlsbad Field Office, Carlsbad, NM.

US DOE, 2019, Title 40 CFR Part 191 Compliance Recertification Application 2019 for the Waste Isolation Pilot Plant: DOE/WIPP-19-3609, US Department of Energy, Carlsbad Field Office, Carlsbad, NM.

US EPA (Environmental Protection Agency), 1996, 40 CFR Part 194: Criteria for the Certification and Re-Certification of the Waste Isolation Pilot Plant's Compliance with the 40 CFR Part 191 Disposal Regulations; Final Rule. Federal Register, Vol. 61, No. 28, pp. 5224-5245, February 9, 1996. Office of Air and Radiation, Washington, D.C.

Vine, J.D., 1960, Recent domal structures in southeastern New Mexico: American Association of Petroleum Geologists, Bulletin, v. 44, p. 1903-1911.

Vine, J.D., 1963, Surface geology of the Nash Draw Quadrangle, Eddy county, New Mexico: U.S. Geological Survey, Bulletin 1141-B.

Walker, J.S., 2006-2007, An 'atomic garbage dump' for Kansas: The controversy over the Lyons radioactive waste repository, 1970-1972: Kansas History: A Journal of the Central Plains, v. 29, p. 266-285.

Weart, W.D., 1979, Evaluation of the proposed WIPP site in southeast New Mexico: SAND79-1113C, Sandia National Laboratories, Albuquerque, NM. https://inis.iaea.org/collection/NCLCollectionStore/_Public/11/500/11500464.pdf

Weart, W.D., 1983, Summary evaluation of the Waste Isolation Pilot Plant (WIPP) site suitability: SAND83-0450, Sandia National Laboratories, Albuquerque, NM. https://wipp.energy.gov/library/cca/CCA_1996_References/Chapter%202/CREL4255.PDF

Weart, W.D., 1999, Perspectives of the science advisor to the Waste Isolation Pilot Plant: SAND99-1600C, Sandia National Laboratories, Albuquerque, NM. https://www.osti.gov/servlets/purl/13070-vcPpRG/webviewable/

Weart, W.D., and Chu, M.S.Y., 1997, Critical scientific issues in the demonstration of WIPP compliance with EPA repository standards: SAND97-2851C, Sandia National Laboratories, Albuquerque, NM. https://www.osti.gov/servlets/purl/562597

White, W.H., Hyslop, N.P., Trzepla, K., Yatkin, S., Rarig, R.S., Jr., Gill, T.E., and Jin, L., 2015, Regional transport of a chemically distinctive dust: gypsum from White Sands, New Mexico (USA): Aeolian Research, v. 16, p. 1-10.

Widdicombe, R.E., 1979, Quaternary surficial features in the Delaware Basin, Eddy and Lea Counties, New Mexico: Unpublished M.S. thesis, University of New Mexico, Albuquerque, NM.

Wood, W.W., 2002, Role of ground water in geomorphology, geology, and paleoclimate of the Southern High Plains, USA: Ground Water, v. 40, p. 438-447.

Wood, W.W., and Osterkamp, W.R., 1987, Playa-lake basins on the southern High Plains of Texas and New Mexico: Part II. A hydrologic model and mass-balance arguments for their development: Geological Society of America, Bulletin, v. 99, p. 224-230.

Oklahoma Geological Survey Circular 113, 2021

Speleogenetic Evolution of Castile Karst Manifestations of the Delaware Basin, West Texas and Southeastern New Mexico

Kevin W. Stafford and Jessica Shields
Department of Geology, Stephen F. Austin State University, Nacogdoches, Texas

ABSTRACT.—The speleogenetic evolution of Castile evaporite karst within the Delaware Basin of west Texas and southeastern New Mexico attests to a complex diagenetic history of epigene and hypogene processes, commonly masked by variably thick gypsic soils. Epigene karst phenomena present within the basin include karren, sinkholes, vadose caves, phreatic caves, and solution–suffosion features. Hypogene karst phenomena include caves, intrastratal brecciation, evaporite calcitization, and clustered sites of native sulfur oxidation. Because of the significant geohazards, these karst phenomena create for infrastructure and petroleum development throughout the region, and this manuscript attempts to provide an initial conceptual evolutionary model for speleogenesis within Castile evaporites based on previous studies and spatial patterns of documented karst phenomena. Current research suggests that hypogene karst development initiated during the Late Paleogene with the occurrence of regional tilting and elevated geothermal gradients. Epigene karsting and the development of the Gypsum Plain likely did not begin until the Late Neogene when uplift surficially exposed Bell Canyon strata in the Delaware Mountains, as well as Castile evaporites for the first time since Ochoan deposition. Wet, temperate climates of the Pleistocene sculpted the Gypsum Plain, as it is observed today, with more intense periods of karsting/surface denudation occurring during glacial periods, with a reduction in solutional processes during interglacial periods. The Gypsum Plain continues to re-equilibrate from the climatic shift of the wet, temperate Pleistocene to the hot, arid conditions observed today. The eastward migration of the Pecos River throughout the Cenozoic has resulted in additional continued evolution and karst development across the Gypsum Plain, observed today at a slower rate than in the past.

INTRODUCTION

Evaporite karst development in the Permian Castile Formation of west Texas and southeastern New Mexico exhibits a complex speleogenetic history evidenced by the widespread, diverse karst features documented across the Gypsum Plain (Castile Formation outcrop region). The development of new and existing features continues today across the arid region, resulting in an ever-changing landscape of increasing complexity. Significant geohazard challenges associated with public infrastructure as well as industry operations within the area are posed by this karst development (e.g., Majzoub and others, 2017; Morris and others, 2021; Stafford and others, 2017; Woodard and others, 2021). Since approximately 2014, advances in nonconventional petroleum extraction have resulted in widespread oil and gas development throughout the interior of the Delaware Basin, including significant exploration and development that must contend with karst in Castile evaporites. This rapid increase in oilfield activity has led to the need to better understand the associated processes and relationships of karst within the Castile Formation, fueling recent research efforts to better understand the temporal and spatial development of local phenomena.

Karst manifestations include both extensive epigene (e.g., Stafford and others, 2008a) and hypogene (e.g., Stafford and others, 2018) components in Castile evaporites. Epigene karst phenomena include 1) surficial weathering producing complex karren; 2) development of gypsic soils and associated solution–suffusion caves; 3) epigene vadose caves and solution sinkholes;

Stafford, Kevin W.; and Shields, Jessica, 2021, Speleogenetic Evolution of Castile Karst Manifestations of the Delaware Basin, West Texas and Southeastern New Mexico, *in* Johnson, K. S.; Land, Lewis; and Decker, D. D. (eds.), Evaporite Karst in the Greater Permian Evaporite Basin (GPEB) of Texas, New Mexico, Oklahoma, Kansas, and Colorado: Oklahoma Geological Survey, Circular 113, p. 151–163.

4) solution-widened fractures; and 5) epigene phreatic caves and associated perched water resources. Hypogene karst phenomena include 1) isolated hypogene riser caves; 2) hypogene maze caves; 3) intrastratal brecciation and associated collapse structures; and 4) digenetic alteration through calcitization and subsequent oxidation processes. This manuscript provides a conceptual model for the temporal evolution of Castile karst development based on previous studies of karst occurrences throughout the Gypsum Plain. While this manuscript does not provide a guide to the complete spatial distribution of evaporite karst manifestations and phenomena types, this manuscript illustrates that the general spatial patterns of speleogenesis observed throughout the Gypsum Plain are the result of the continued evolution of a complex karst system that is migrating eastward across the Delaware Basin.

GEOMORPHIC SETTING

Castile evaporites crop out continuously within the western Delaware Basin over approximately 1800 km^2 (Fig. 1), but can be extended to over 2800 km^2 when shallow subcrop regions beneath surficial Rustler strata, regions of undifferentiated Castile and residual Salado strata are included (Hill, 1996). These outcrop/subcrop regions comprise the Gypsum Plain which extends throughout much of Culberson County, Texas, and Eddy County, New Mexico. Surficial strata are effectively bound within the western Delaware Basin by the Apache Mountains to the south, Guadalupe Mountains to the north, Delaware Mountains to the west, and descend into the subsurface to the east, filling the eastern portion of the Delaware Basin. The Gypsum Plain is located on the northern edge of the Chihuahua Desert where average annual precipitation is 267 mm, primarily occurring as late summer monsoonal storms (Sares, 1984). Anomalously high storm intensities exceeding 100 mm of precipitation within 48 hr do occur at decadal scales (Stafford and others, 2017). Annual average temperature is 17.3°C, with an average annual low and high of 9.2°C and 25.2°C, respectively (Sares, 1984).

Ochoan Castile evaporites are bound stratigraphically by Guadalupian Bell Canyon siliciclastics below and Ochoan Salado evaporites above (Fig. 2). Gypsum Plain Castile evaporites commonly exhibit an unconformable boundary with the Ochoan Rustler carbonates, originally deposited above the Salado Formation, because of intrastratal solutional removal of Salado units (Scholle and others, 2004). Castile strata were deposited within the interior of the Delaware Basin subsequent to Guadalupian deposition of the Capitan Reef, which is now exposed surficially in the Guadalupe and Apache mountains (Fig. 1). Castile evaporites represent deep-water, restricted marine deposits formed within the stratified,

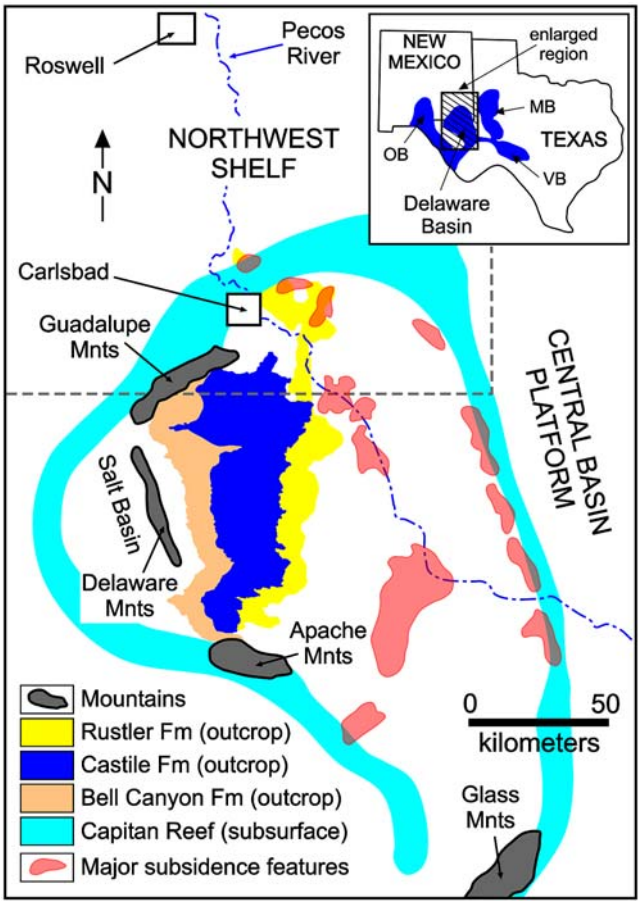

Figure 1. Regional map of the Delaware Basin including delineation of outcrop regions of the Bell Canyon, Castile and Rustler formations in relation to the buried extent of the Capitan Reef complex and major geomorphic features of the region (modified from Stafford and others, 2008a).

brine-filled Delaware Basin at the end of the Permian (Anderson and Kirkland, 1966). Castile strata consist of laminated calcite/gypsum (anhydrite in deeper subsurface) with interbedded halite. Calcite laminae represent periods of lower salinity deposition (wetter climate) coupled with gypsum laminae that represent periods of higher salinity deposition (drier climate) and interbedded halite during extended periods of elevated salinity (Anderson and others, 1972). Original Castile fabrics commonly show diagenetic alteration creating irregularly laminated, massive, nodular and selenitic textures in addition to regions of calcitization (Dean and others, 1975; Stafford and others, 2008b). Castile halite interbeds, as with the majority of the overlying Salado Formation, have also been removed from outcrop and shallow subcrop within the Gypsum Plain region through intrastratal dissolution.

The deposition of the Castile Formation largely filled the interior of the Delaware Basin during the late

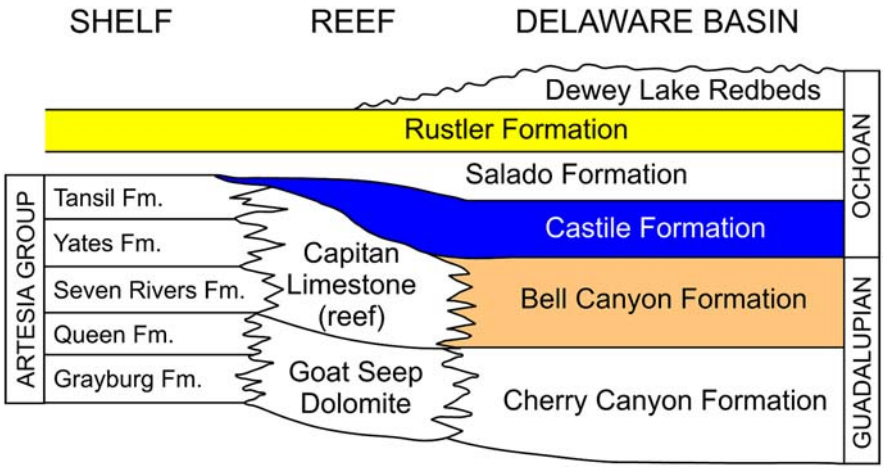

Figure 2. Simplified stratigraphic section from the Northwestern Shelf to the Delaware Basin showing the general relationship between Guadalupian and Ochoan units. Note that units of interest are color-coded to match outcrops shown in Figure 1 (modified from Scholle and others, 2004).

Permian—a total thickness of the Castile deposits ranged from 470 to 600 m (Hill, 1996). Subsequently, the late Ochoan deposition of the Salado and Rustler formations capped the region, including the surrounding shelf and platform environments—600–800 m of Salado and Rustler strata were deposited on top of Castile evaporites (Hill, 1996). This stratal capping provided regional low permeability seals that promoted isolation, development, and accumulation of petroleum resources in the region (Scholle and others, 2004). At the end of the Ochoan, the deposition of Dewey Lake Redbeds marked the final closure of the Delaware Basin at the transition from Permian to Triassic deposition. The Dewey Lake Formation records a transition from subaqueous to subaerial deposition and includes mixed siliciclastic deposits associated with the transition to fluvial, continental depositional regimes—this was coupled with the final assimilation of Pangea (Hill, 1996).

Throughout the Mesozoic and Cenozoic, the Permian Basin was largely subaerially exposed, thus, beginning ~250 million years in which the region was dominated by weathering, continental deposition/erosion, and diagenetic alteration of buried Permian strata. During the late Triassic, thick sequences of continental deposits (Chinle Group) were deposited unconformably on top of Dewey Lake Redbed deposits that had been eroded in the early to middle Triassic (Hill, 1996)—this deposition created a regional sag across the Permian Basin. The Jurassic marked an extended period of erosion following the breakup of Pangea and opening of the Gulf of Mexico, but a marine transgression introduced Cretaceous deposition (Cox Formation) to the region, marking the final stage of significant sedimentation within the Delaware Basin region (Hill, 1996).

Late Cretaceous-to-early Paleogene compression associated with the Laramide Orogeny induced stratal tilting of 3 to 5° to the east/northeast and uplifted the Delaware Basin region above sea level (Dickenson, 1980). Paleogene igneous activity, including dike emplacement, associated with the Trans-Pecos magmatic province elevated the regional geothermal gradient, but likely did not induce significant regional deformation (Hentz and Henry, 1989). Most regional brittle deformation is likely associated with Basin and Range extension in the early Neogene (Hentz and Henry, 1989), which manifests in the Gypsum Plain as conjugate joint/fault sets oriented at ~N75°E and ~N15°W (Nance, 1993). Since the Neogene, the region has remained tectonically stable. Throughout the Cenozoic, the Pecos River has moved from west to east, creating a slowly migrating potentiometric low that has continued to influence groundwater flow patterns within the Delaware Basin (Stafford and others, 2009).

In the Quaternary, weathering and surface denudation dominated the geomorphic evolution of the Gypsum Plain. Glacial/interglacial periods induced climate fluctuations that increased/decreased erosion rates, respectively (Hill, 1996). The results of climate shift from wet, temperate regimes of the Pleistocene to the dry, arid environment of today dominate the current landscape (Bachman, 1980). Modern rates of weathering, and surficial karst development, are considerably low today with reported average surface denudation rates of 30 cm/kyr for the Gypsum Plain (Stafford, 2013). Currently, the Castile Formation thins to a solutional margin on the western edge of the Gypsum Plain, but reaches a maximum thickness of 480 m in the subsurface of the eastern Delaware Basin (Kelley, 1971).

EVAPORITE KARST MANIFESTATIONS

Castile evaporite karst manifestations within the Gypsum Plain are diverse and widespread. Original estimates

by Stafford and others (2008c) suggested that approximately 10,000 gypsum karst features existed within the region. More recent studies indicate that this is likely a significant underestimate of total karst development (Ehrhart and Stafford, 2021), without consideration of deeper karst phenomena that occur within subsurface Castile evaporites east and downdip of the Gypsum Plain. Karst development can be subdivided into general classes of hypogene and epigene within the Gypsum Plain as detailed below; however, there is significant overprinting of multiple phases of speleogenesis that occurs within these systems. The Pecos River has provided a slowly migrating potentiometric low for the last 60 million years to fuel upward flow of confined to semiconfined fluids. It appears probable that much of the hypogene development is at least partially coupled to the eastern migration of the Pecos River across the Delaware Basin since the early Paleogene (Stafford and others, 2009).

Castile Hypogene Karst Manifestations

Hypogene karst development within the Castile Formation includes hypogene caves and solution-widened fractures, brecciation, and diagenetic alternation of host rock. Hypogene karst development has been documented most extensively along the western margin of the Gypsum Plain (Stafford and others, 2018) where surface denudation has significantly thinned the Castile Formation and placed the underlying contact with the Bell Canyon in close proximity with the land surface. However, Castile hypogene karst development has been documented throughout the entire Delaware Basin as evidenced by subsidence features (Fig. 1) and void interception proximal to the underlying Bell Canyon contact during drilling activities.

Intrastratal dissolution coupled with subsequent collapse is the most common and widespread evidence of hypogene karst within the Gypsum Plain. Fluids originating from the underlying Bell Canyon Formation have induced hypogene void development at the base of the Castile Formation. In many instances, these voids are sufficiently large that overlying strata cannot be supported and thus collapse occurs enabling ascending fluids to migrate through collapse zones vertically. The resulting breccia pipes are commonly hundreds of meters in diameter and vertical depth (Kirkland and Evans, 1976). While brecciated zones and breccia pipes are common in the Gypsum Plain, these features have also been documented throughout the Delaware Basin where they extend vertically through the overlying Salado and Rustler formations (Anderson and others, 1978). Many topographic highs within the Gypsum Plain are the result of differential weathering of breccia pipes (Fig. 3A). Commonly, these breccia pipes preserve remnants of Permian strata of the Rustler and Dewey Lake formations as well as Cretaceous Cox strata which were piped downward into upward stoping collapse structures (Shields, 2018). In addition, brecciated Castile strata (Fig. 3B) commonly form resistant highs, as secondary sulfate and calcite cements have reduced local permeability within these structures.

Similar to breccia pipes, blanket breccias and solution subsidence troughs within the Gypsum Plain attest to intrastratal dissolution along planar surfaces, most commonly associated with the solution of Castile halite interbeds (Anderson and Kirkland, 1980). Blanket breccias are commonly limited to a few decimeters in thickness, but may extend laterally over hundreds of meters, whereas solution subsidence troughs manifest as steep-walled valleys that geomorphically present as solution grabens. Blanket breccias commonly extend laterally to breccia pipes and attest to the lateral migration of ascending fluids along more soluble zones (Stafford and others, 2008b). All documented manifestations of intrastratal brecciation within the Gypsum Plain increase significantly in abundance westward across the Castile outcrop area, indicating that intrastratal dissolution is most intense proximal to the underlying Bell Canyon contact. However, evidence of intrastratal brecciation is found throughout the entire region indicating that the process is widespread and likely continues to occur today in the subsurface east of the Gypsum Plain.

Hypogene caves have been most abundantly documented throughout the western Gypsum Plain (Ehrhart and Stafford, 2021), with most caves formed as single or simple riser structures that exhibit variable degrees of epigene overprinting as a result of surface denudation induced breaching. Crystal Cave and the nearby Gazelle Cave (Fig. 3E) are typical examples of this single riser morphology: Crystal and Gazelle caves have surveyed depths of 93 m and 60 m, respectively, and consist largely of single passages with multiple dome pits that exhibit the classic suite of hypogene morphological features identified by Klimchouk (2007). Cave exploration terminates at the current water table in Crystal Cave and in breakdown in Gazelle Cave (Stafford and others, 2008a). Similar, single-riser caves have been documented throughout the Gypsum Plain including such features as Fissure Cave (Fig. 3F) and Wiggley Cave discussed elsewhere in this publication (Ehrhart and Stafford, 2021). Isolated, vuglike caves have been documented in rare instances within the Gypsum Plain that attest to localized hypogene dissolution in poorly fractured sulfates.

Locally, complex hypogene maze caves have also been documented within the Gypsum Plain, including features, such as Dead Bunny Hole (Stafford and others, 2008a) and Black Dog Cave (Shields, 2018). These do not generally manifest as the classic rectilinear, hypogene maze caves seen elsewhere in the world

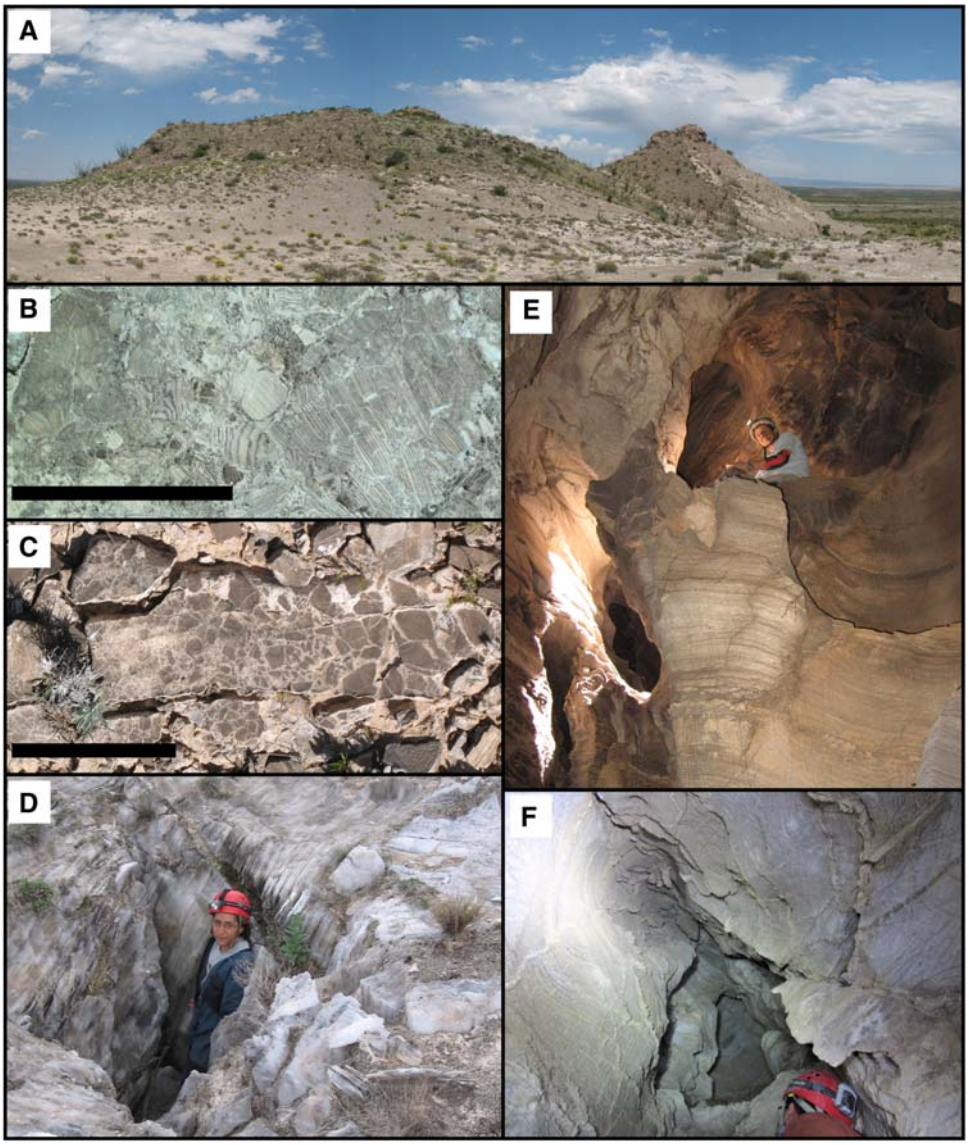

Figure 3. Hypogene karst phenomena: A) castile butte (~15 m tall) that forms resistant brecciated and calcitized mass; B) typical sulfate brecciation induced by intrastratal dissolution and collapse (black scale bar is ~20 cm long); C) calcitized blanket breccia (black scale bar is ~30 cm long); D) isolated, hypogene "vug" cave in secondary selenite; E) classic hypogene dome-pit riser morphologies in Gazelle Cave; and F) well-developed ceiling cupola in Fissure Cave.

(e.g., Klimchouk, 2007), but instead form as staggered, offset maze caves developed along small-scale anticlines and synclines, commonly exhibiting a crude, inverse dendritic pattern where cave passages diverge away from one another with depth. Further supporting hypogene origins, most hypogene caves documented within the Gypsum Plain are coupled to relatively small surface drainage basins (commonly only a few hectares) that could not support the volume of fluid needed to induce the dissolution of gypsum caves several hundreds of meters in surveyed length (Stafford and others, 2008a).

Castile strata commonly exhibit diagenetic alteration in the form of evaporite calcitization, sulfur mineralization, and selenitization. Features commonly referred to as Castile Buttes (Fig. 3A) are resistant topographic highs within the Gypsum Plain that can extend up to 30 m above the surrounding topography (Kirkland and Evans, 1976), with some features still actively degassing low concentrations of hydrogen sulfide that is oxidizing at the land surface (Stafford and others, 2008b). These features are largely composed of secondary calcite that resulted from sulfate reduction in the presence of ascending light hydrocarbons—some debate exists as to whether bacterial or thermal sulfate reduction can be attributed to these phenomena (e.g., Hill, 1996; Kirkland and Evans, 1976; Stafford and others, 2008b). Most

commonly, sulfate calcitization is observed proximal to the underlying Bell Canyon Formation contact where mineral alteration occurs with little disturbance to original depositional structure; however, calcitization is most commonly found associated with zones of brecciation where breccia pipes and blanket breccias (Fig. 3C) are partially to completely calcitized (Stafford and others, 2008b).

Outcrop and shallow subcrop occurrences of calcitization are commonly coupled with globular, lenticular, and/or linear occurrences of massive selenite (Stafford and others, 2008b). Subsurface calcitized masses are generally associated with sulfur ore deposits which have been economically mined in the past (Hentz and Henry, 1989). During evaporite calcitization, which was fueled by ascending light hydrocarbons from the underlying Bell Canyon Formation, anoxic conditions resulted in the emplacement of native sulfur in and proximal to the alteration zone. As subsequent surface denudation proceeded, oxic, meteoric water invaded the subsurface enabling oxidation of sulfur bodies into secondary selenite masses (Fig. 3D). It is probable that the process of selenitization is both a hypogene and epigene process where some meteoric water is delivered downward along preferential flow paths, whereas other oxic waters ascend from the underlying Bell Canyon Formation as a result of proximal groundwater recharge associated with the Delaware Mountains east of the Gypsum Plain. The oxidation of native sulfur to form selenite has been supported by isotope analyses and rare, isolated crystals of native sulfur preserved within selenite masses (Stafford and others, 2008b).

It has long been assumed that hypogene processes are still active in the Delaware Basin (e.g., Hill, 1996; Stafford and others, 2008a), but that the active sites of hypogene dissolution are occurring east of the Gypsum Plain where Castile strata are more deeply buried and isolated from surface processes. This has been supported by the development of large subsidence troughs (Fig. 1) filled with thick Quaternary sediments proximal to the current location of the Pecos River (Stafford and others, 2009) as well as the increased occurrence of native sulfur within calcitized masses beneath surficial exposures of Rustler Strata as compared to the dominance of selenite associated with calcitized masses within the Gypsum Plain (Hentz and Henry, 1989).

Recently, Stafford and others (2018) have identified that hypogene processes are still active as unconfined manifestations within the western portion of the Gypsum Plain as two general variants: solution-widened fissures and brecciated zones with dissolution enhanced by condensation corrosion and artesian discharge features. Fissures and high permeability zones within breccia pipes commonly exhibit localized ridges and domal structures (i.e., features reminiscent of tumuli but morphologically distinct) at the land surface that are composed of porous, secondary gypsite precipitates. These ridges prevent overland flow from actively migrating into these high permeability features. Instead, these features act as venting structures for moisture-laden convective flow toward the land surface, which induces solution widening and deposits secondary gypsum at the land surface because of high evaporation rates in the arid environment (Stafford and others, 2018).

Stafford and others (2018) also documented that during decadal-scale anomalous precipitation events, groundwater levels can rise to sufficient height to create artesian conditions in the western Gypsum Plain. Allogenic recharge from the Delaware Mountains into the underlying Bell Canyon siliciclastics results in the reactivation of relict hypogene karst features; thus, hypogene caves that had been breached by surface denudation and exhibit variable degrees of epigene overprinting act as ephemeral artesian springs. In addition, proximal to the Delaware River, the elevated hydraulic gradient continues to induce intrastratal dissolution by artesian waters during these anomalous periods of increased groundwater recharge. These regions exhibit differential settling and compaction after hydraulic gradients recede, attesting to buoyant lift and dissolution by artesian fluids (Stafford and others, 2018).

Castile Epigene Karst Manifestations

Epigene karst development within the Gypsum Plain occurs as surficial weathering, solutional cave development, and solution-enhanced suffosion features. In addition, most hypogene karst manifestations exhibit some degree of epigene overprinting, inevitable, because hypogene features that can be physically investigated must be exposed and/or breached by surface denudation. Gypsic soils ranging from less than a decimeter to more than 10-m-thick mantle the vast majority of the Gypsum Plain, with exposed Castile bedrock comprising less than 8% of the total surface area (Stafford, 2013). Much of this thick soil mantling obscures the extent of karst development and is the result of the climatic shift from humid, temperate conditions of the Pleistocene to the dry, arid climate of today (Hill, 1996).

The dominant geomorphic features of the Gypsum Plain are sinkholes (Fig. 4A), which manifest as: 1) deeply incised, arroyolike, solutional sinkholes; 2) near-vertical, collapse sinkholes; and 3) shallow, barely perceptible surface depressions. Stafford and others (2008c) noted that 55% of the sinkholes within the Gypsum Plain are the result of collapse into solutional voids (commonly hypogene caves) and 45% of the sinkholes are formed by solutional processes associated with overland flow. Therefore, it is probable that approximately half of the sinkhole manifestations documented within the Gypsum Plain are coupled with surficial

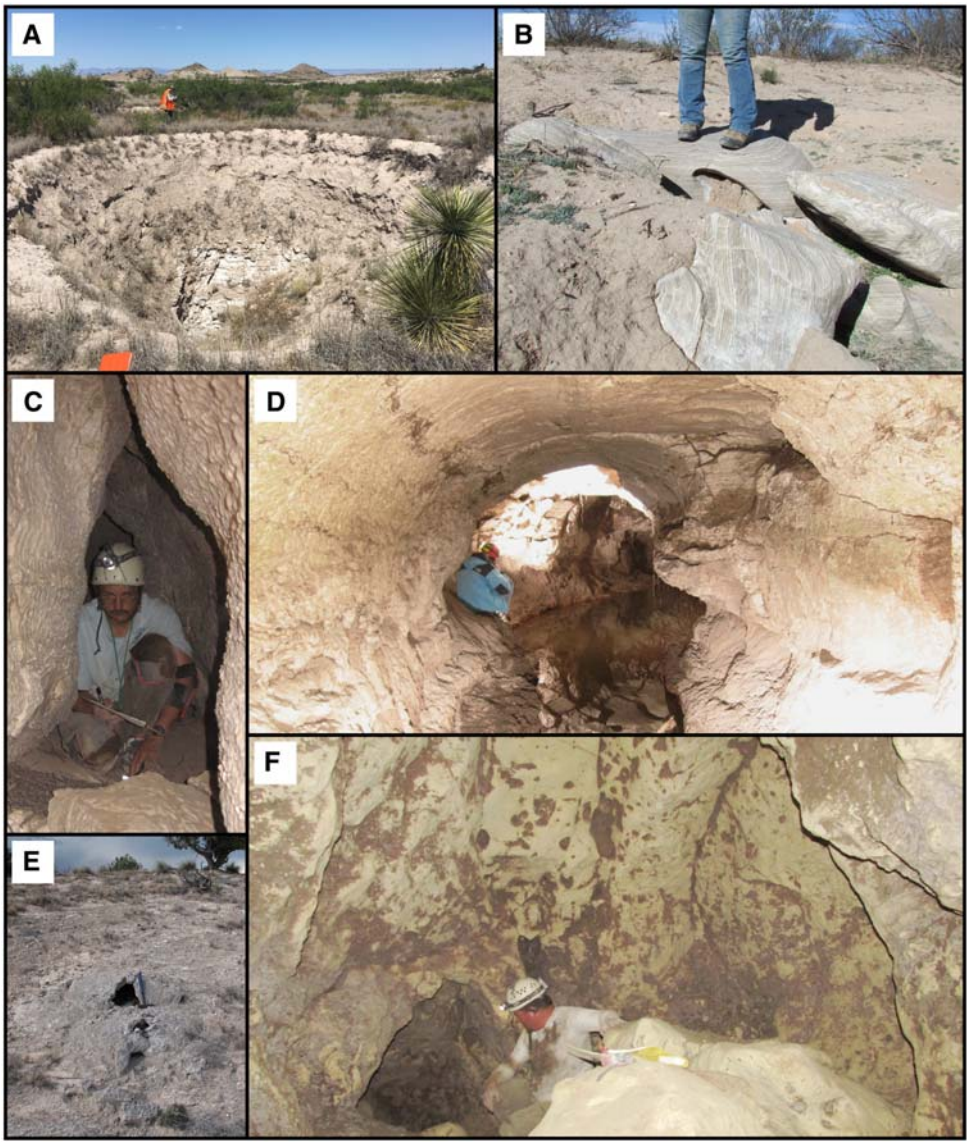

Figure 4. Epigene karst phenomena: A) elliptical sinkhole developing in thick gypsic soils (note person for scale on far side of sinkhole); B) irregular, hummocky surface between castile bedrock and variably thick gypsic soils; C) typical, epigene vadose cave passage; D) large-diameter, epigene phreatic cave passage; E) typical gypsum tumuli (note rock hammer for scale at center of picture); and F) large soil chamber within solution–suffosion cave.

breaching of hypogene caves, whereas the other half are associated with focused, meteoric recharge. Recent geophysical studies using resistivity analyses in the Gypsum Plain have indicated that far more sinkholes exist within the Gypsum Plain than previous recognized, but that many of these features have been completely infilled with gypsic soil and show no (or minimal) surface expression. These sinkholes are sites of increased groundwater infiltration and pose significant geohazard risk because of differential compaction (Stafford and others, 2017; Woodard and others, 2021).

At the interface between gypsic soils and underlying bedrock, hummocky solution surfaces are common with abundant macroconduits that rarely coalesce to produce organized flow. These soil/bedrock interfaces are similar to rundkarren in carbonate terrains, but are more subdued within the Gypsum Plain (Fig. 4B). In well-fractured bedrock, solutional-widening is common, which creates features reminiscent of grikes that extend from bedrock into overlying indurated soils, commonly creating vertical piping structures. On exposed bedrock, various karren morphologies are common, with spitzkarren, rillenkarren, and kaminitizas generally dominating—these karren forms also commonly develop on highly indurated gypsite. Locally, gypsum tumuli (Fig. 4E) occur in clusters of five-to-ten features within an area of several square meters—the largest tumuli documented are less than 150 cm in diameter and 40 cm tall (Stafford, 2013).

Purely epigene caves, not including hypogene caves modified by epigene processes, tend to be relatively small and linear. Most epigene caves are coupled with a relatively large solutional sinkhole and associated drainage area and exhibit vadose morphologies. These vadose epigene caves are generally less than a few tens of meters in length at widths large enough for human entry (Fig. 4C). They are generally developed along a single fracture plane to create a near-linear cave or they are developed along a series of conjugate fractures with sharp, angular passage junctions (Stafford and others, 2008a). Vadose epigene caves abruptly decrease in average height and width away from the insurgence and commonly contain abundant organic debris coating all wall surfaces with centimeter-scale scallops, suggesting that most of these features recharge large volumes of high velocity water during monsoonal storms. Epigene vadose caves tend to be widely spread across the Gypsum Plain and do not exhibit the clustering of features commonly observed with hypogene karst development in the region. Classic examples of vadose epigene caves within the Gypsum Plain include Dead East and Zombie caves as described by Stafford and others (2008a) and Nikad Cave and JC Gypsum Hole described by Ehrhart and Stafford (2021).

Epigene phreatic caves are much less common in the Gypsum Plain, but have been documented in close proximity to the Delaware River where it appears that shallow perched aquifer zones exist which are decoupled from deeper groundwater flow paths. These caves tend to form elliptical passages (Fig. 4D) that are commonly coated with thick mud deposits which likely armor bedrock from dissolution and enable meteoric waters to traverse greater distance before becoming saturated (Ehrhart and Stafford, 2021). Most phreatic caves are subhorizontal with gentle dips away from insurgences—all thus far documented eventually sump, but nearby springs (within a few hundred meters) in incised arroyos are likely connected to these localized shallow aquifer systems. Most of these phreatic caves contain troglobitic fauna, including observed but undocumented crayfish and amphipods, indicating that these are not ephemeral phreatic features but instead are persistent, water-filled conduits. Examples of phreatic gypsum caves include Brantley Stream Cave (Stafford and others, 2008a) and Death Tube Cave (Ehrhart and Stafford, 2021).

While originally considered relatively insignificant, suffusion caves within the indurated gypsum are now recognized as a significant component of the Gypsum Plain karst system and appear to be common and widespread. Unlike true suffusion caves, these "piping structures" in the Gypsum Plain are formed through a combination of dissolution and piping of insoluble residue within indurated gypsic soils (Morris and other, 2021). Suffosion caves are generally small, elliptical, subhorizontal caves that connect to epigene or hypogene caves where insoluble fractions that are mobilized can be transported—gypsic soils in the region commonly contain more than 70% soluble gypsum content. Commonly, these soil caves exhibit intermittent collapse and are commonly related to shallow catastrophic failures due to the inability of indurated soils to structurally support voids. Recent work in the Gypsum Plain (e.g., Ehrhart and Stafford, 2021; Morris and others, 2021; Stafford and others, 2017) has identified numerous examples of these solution–suffosion caves with some extending tens of meters in length that include isolated soil chambers several meters in diameter and height (Fig. 4F). Examples of these soil caves include the upper passages of Death Tube Cave (Ehrhart and Stafford, 2021), Quill Soil Cave (Shields, 2018), and Mousey Hole (Ehrhart, 2016).

SPELEOGENETIC EVOLUTION OF THE GYPSUM PLAIN

The speleogenetic evolution of the Castile Formation is a long and complex series of processes resulting from multiple phases of overprinting and the general eastward migration of processes as surface denudation erodes the updip margin of the Delaware Basin. After Permian deposition, there is no significant evidence to suggest that Castile strata were exposed to hypogene or epigene karst processes until the Cenozoic; however, postdepositional diagenetic alterations would have included, at a minimum, dehydration of gypsum to anhydrite. This dehydration would have induced localized buckling, endokinetic fissuring, and sulfate fabric alteration (Dean and others, 1975). Minor solutional porosity within the Castile Formation may have existed early in the diagenetic history because of dewatering during anhydrite conversion. Some researchers have suggested that during the Triassic, upper Ochoan strata were exposed to subaerial weathering as evidenced by the unconformable contact between the Dewy Lake Formation and overlying Triassic deposits (Hill, 1996), but there is no evidence that Castile strata were subjected to the near-surface processes at this time, but instead were isolated in a general sag across the entire Permian Basin (Hill, 1996). Throughout the Mesozoic, Castile and overlying Salado strata were likely stable and exhibited little alteration beyond localized phenomena associated with burial compaction and mineral dehydration.

In the late Cretaceous to early Paleogene, Laramide compression and crustal shortening elevated fluid pressures within the Delaware Basin and uplifted the region beyond the Stable Platform Phase that introduced minor Cretaceous deposition across the Permian Basin (Keith, 1982). By the late Paleogene (Fig. 5A), the region had been uplifted approximately 1600 m (Hill, 1996) and the ancestral Pecos River was beginning to migrate

eastward from the western margin of the buried Delaware Basin (Stafford and others, 2009; Thomas, 1972). Near the end of the Paleogene, Laramide compression shifted to Basin and Range extension, which induced gentle regional tilting of the Delaware Basin toward the east, accompanied by elevated geothermal gradients and igneous dyke emplacement in association with Trans-Pecos volcanism (Ernst, 2014; Hentz and Henry, 1989). Although published information is not available in regards to historical hydrocarbon maturation

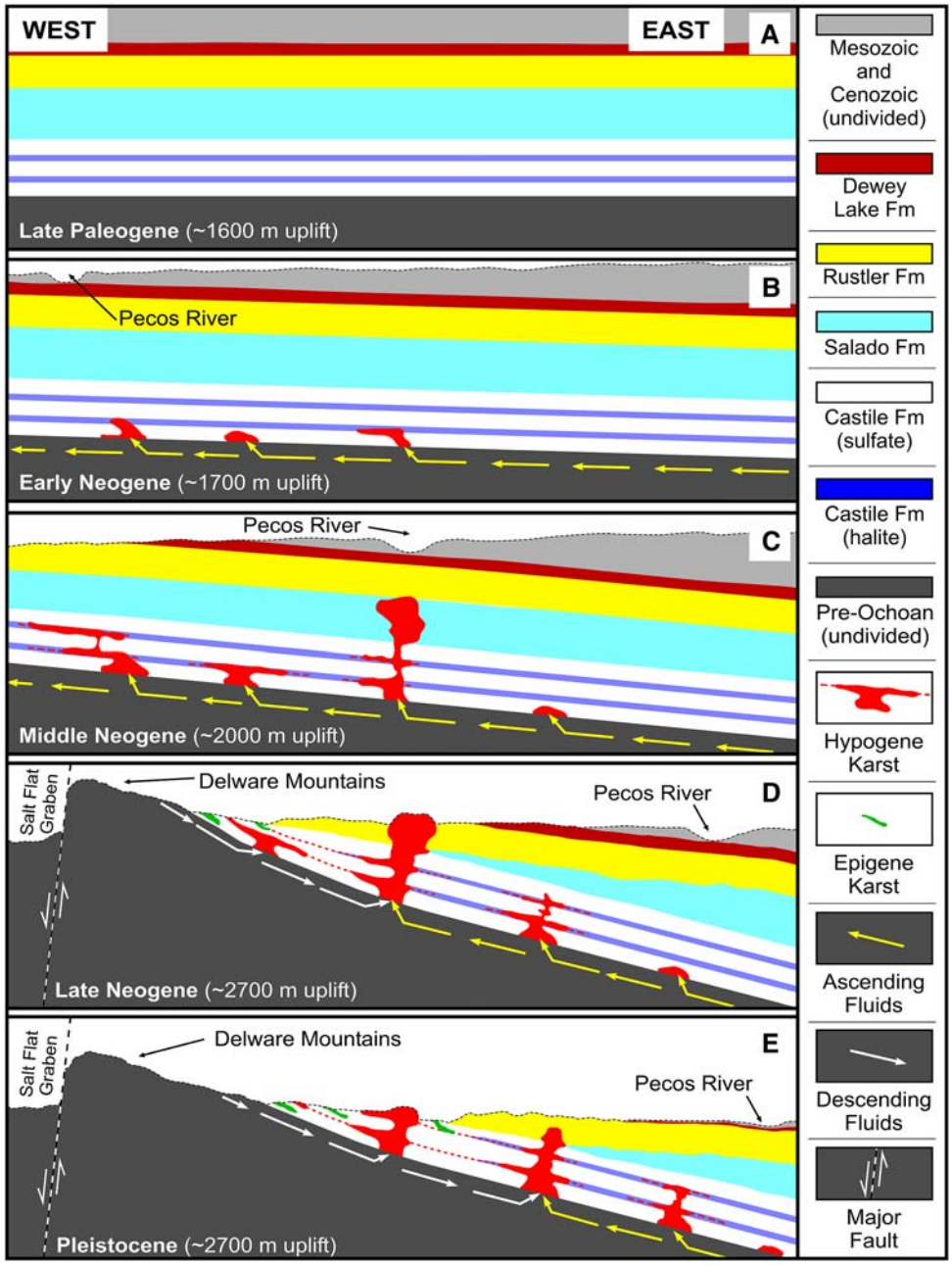

Figure 5. Conceptual model of speleogenetic evolution of Castile evaporite karst: A) Late Paleogene regional uplift prior to initiation of major karst development; B) Early Neogene initiation of hypogene karst associated with regional tilting, elevated thermal gradients and updip migration of basinal fluids; C) Middle Neogene significant uplift and exposure of updip margins of Ochoan strata with regional geothermal maxima accelerating hypogene karst development; D) Late Neogene development of the Salt Flat Graben exposes Bell Canyon strata, increasing groundwater recharge that promotes artesian hypogene karst, whereas the development of the Gypsum Plain introduces epigene karst processes to Castile strata; and E) Pleistocene glacial/interglacial periods promote eastward migration of Gypsum Plain and hypogene karst development.

and geothermal gradients, it is probable that this late Paleogene volcanic phase was the catalyst for initiating hydrocarbon maturation in pre-Ochoan strata of the Delaware Basin.

In the Early Neogene (Fig. 5B), hypogene dissolution likely initiated at the lower contact with the Bell Canyon Formation as Laramide-induced, elevated fluid pressures migrated updip along the actively uplifting western margin of the Delaware Basin (Hill, 1996). By the Middle Neogene (Fig. 5C), because of uplift (~2000 m at this time) and tilting as a result of Basin and Range deformation, updip portions of Ochoan sequences were exposed (DuChene and Cunningham, 2006). Exposure at this time would have reduced confinement pressures of Ochoan strata, whereas transient heating associated with Basin and Range extension likely reached its maximum (Kirkland, 2014). Therefore, it is probable that upward migration of light hydrocarbons into the Castile Formation began fueling evaporite calcitization and sulfur ore emplacement in the Middle Neogene (Hentz and Henry, 1989), primarily along advancing brecciated zones. By the Late Neogene (Fig. 5D), hypogene karst, including intrastratal dissolution of halite interbeds and development of breccia pipes, blanket breccias, and hypogene caves, was already well-developed in the western Delaware Basin, with brine density convection within brecciated zones accelerating hypogene dissolution (Anderson and Kirkland, 1980; Kirkland, 2014).

Evidence for significant regional hypogene karst development in the Late Neogene is supported by research conducted in the carbonate caves of the Guadalupe Mountains (Kirkland, 2014; Polyak and others, 1989). It is probable that hypogene development within the Castile Formation also accelerated at this time because of the same tectonic and geothermal regimes, the two regions, were exposed to. In the Guadalupe Mountains, researchers have shown that significant episodes of increased cave enlargement occurred during the late Miocene to early Pliocene, coupled with elevated geothermal gradients and Rio Grande rifting (Polyak and others, 1998; Polyak and Provencio, 2000).

By the end of the Late Neogene, the Salt Flat Graben formed as the most eastern extent of Basin and Range Deformation, which left pre-Ochoan siliciclastics exposed in the Delaware Mountains (Duchene and Cunningham, 2006). The Delaware Mountains subsequently became recharge loci for Delaware Mountain Group strata, including the Bell Canyon Formation, introducing the migration of oxic waters down-dip, beneath Castile strata (Kirkland and Evans, 1976; Lindsey, 1998). Recharge created artesian conditions to promote more intense hypogene karsting along the western margin of the developing Gypsum Plain and provided oxic waters to covert sulfur ore bodies into selenite in the updip regions of Castile strata (Stafford and others, 2008b). By the end of the Neogene, the Gypsum Plain had developed, although further west than its current position, and epigene karst development began in surficially exposed Castile evaporites. It is probable that at this time, some of the larger breccia pipes were becoming resistant topographic highs, having incorporated collapse material from upper Ochoan and Cretaceous material within the breccia pipe cores (Shields, 2018).

Throughout the Pleistocene (Fig. 5E), surface denudation dominated the evolving Gypsum Plain as it migrated eastward, whereas hypogene karst was continuously fed by a combination of ascending, anoxic basinal fluids and descending oxic meteoric fluids recharged through the updip exposure of the Bell Canyon Formation. Karst development through the Pleistocene was episodic, with increased solutional intensity during glacial periods and decreased solution intensity during interglacials (Harris, 1985; Bachman, 1984). The majority of epigene caves observed today were likely formed at this time. Similarly, breaching and epigene overprinting of documented hypogene caves likely occurred during the Pleistocene (Shields, 2018), with hypogene features becoming ephemeral artesian springs during wet glacial periods that promoted the development of many of the large arroyos in the region today.

The shift from wet, temperate climate of the Pleistocene to dry, arid climate of the Holocene marked the transition to the modern geomorphic system that we currently recognize as the Gypsum Plain (Hill, 1996). This shift resulted in widespread formation of gypsic soils and infilling of many sinkholes that would have been active karst interface features in the Pleistocene. While solution rates are likely much lower today than during the Pleistocene, karst processes are still active (Stafford, 2013). Active recharge during monsoonal events continues to modify epigene caves and surface karren. Light hydrocarbons still ascend and byproducts of calcitization which can be observed degassing from some calcitized regions (Stafford and others, 2008b). Hypogene caves are still forming in response to the potentiometric low of major fluvial bodies, primarily the Pecos River (Stafford and others, 2009). Other areas show continued hypogene development associated with anomalous episodes of high precipitation that induce ephemeral artesian conditions on the western margin of the Gypsum Plain (Stafford and others, 2018).

Currently, the Gypsum Plain appears to be in a state of mild disequilibrium where many karst features were plugged by heavy sedimentation and soil development during the Pleistocene–Holocene climate shift (Morris, 2018). Solution–suffosion features demonstrate well the current reactivation of karst features that have likely been inactive for many millennia. Effectively, current karst development within the Gypsum Plain reflects the perpetual eastward migration of the western

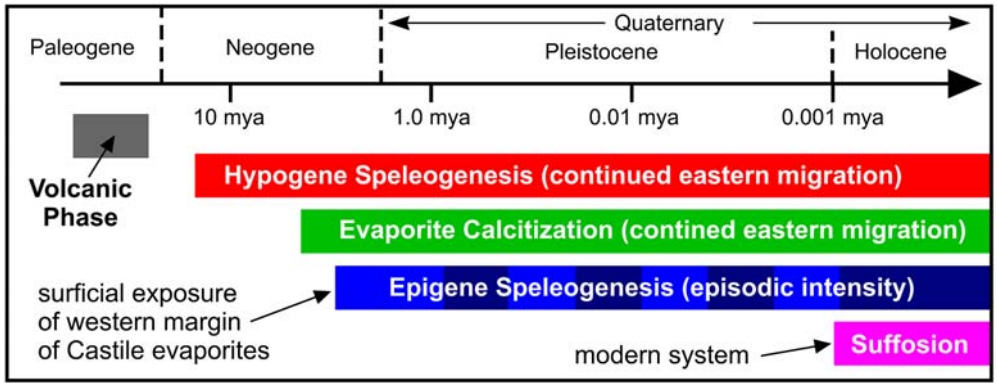

Figure 6. Simplified conceptual model of speleogenetic evolution of Castile evaporite karst. Note that karst processes are continuing to occur with a general eastward migration across the Delaware Basin.

solutional margin of the Castile Formation, where karst development is largely episodic in relation to seasonal weather patterns and longer term climate shifts.

The effects of intense anthropogenic activities within the Gypsum Plain are yet to be fully realized. However, recent increases in oilfield activity continuously encounter engineering problems associated with shallow epigene karst development, unstable solution–suffosion features, and deeper hypogene voids (Stafford and others, 2017). The effects of significant groundwater extraction for fracking operations are difficult to predict, but these activities will inevitably modify the aquifer hydraulics and associated evaporite karst processes of the Gypsum Plain.

CONCLUSIONS

Karst manifestations in Castile evaporites are diverse and extensive throughout the Gypsum Plain, including hypogene and epigene phenomena that have been evolving since the Late Neogene (Fig. 6). Castile speleogenesis exhibits an eastward migration across the Delaware Basin that began with hypogene karst development at the underlying contact with the Bell Canyon Formation. Cavernous porosity and brecciation, commonly coupled with sulfate reduction, likely initiated in the Late Paleogene. As surface denudation progresses, the surficial exposure of Castile strata is introduced to meteoric waters that promote epigene karst development and overprint breached hypogene phenomena. Aquifer waters recharged from the Delaware Mountains updip in Bell Canyon strata provide additional hypogene dissolution as ascending artesianlike waters through the Gypsum Plain, which, coupled with descending epigene waters, oxidize native-sulfur deposits into secondary selenite. Currently, the karst system of the Gypsum Plain appears to still be equilibrating from the climate shift of the wet, temperate Pleistocene to the dry, arid conditions of today.

This manuscript provides a conceptual model for the speleogenetic evolution of Castile karst; however, ever-increasing research of these evaporite-karst manifestations adds greater complexity to the system. This is not meant to be a definitive model for the speleogenetic evolution, but it is a first attempt to place karst processes within an evolutionary context for basin-filling evaporites of the Castile Formation. Future work will continue to refine this model to account for new karst phenomena that are being revealed in the area almost daily as rapid growth in petroleum exploration and development continues within the Delaware Basin. The need for continued improvements in delineating the evolution and spatial distribution of karst phenomena are ever increasing across the Gypsum Plain and the entire Delaware Basin.

ACKNOWLEDGEMENTS

This research was partially funded by the Texas Department of Transportation with support from the Department of Geology at Stephen F. Austin State University. The authors are indebted to the following field assistants that made this work possible: Wesley Brown, Aaron Eaves, Jon Ehrhart, Ashley Landers, Adam Majzoub, Raymond Nance, Laura Rosales-Lagarde, Jonah Morris, Lillian O'Shay, and Jonathan Woodard. Appreciation is expressed to Wesley Brown for his review of this manuscript and helpful contributions to its improvement.

REFERENCES CITED

Anderson, R.Y., Dean, W.E., Kirkland, D.W., and Snider, H.I., 1972, Permian Castile varved evaporite sequence, West Texas and New Mexico: Geological Society of America, Bulletin, v. 83, p. 59–85.

Anderson, R.Y., Kietzke, K.K., and Rhodes, D.J., 1978, Development of dissolution breccias, northern Delaware Basin and adjacent areas: New Mexico Bureau

of Mines and Mineral Resources, Bulletin 159, Socorro, NM, p. 47–52.

Anderson, R.Y., and Kirkland, D W., 1966, Intrabasin varve correlation: Geological Society of America, Bulletin, v. 77, p. 241–256.

Anderson, R.Y., and Kirkland, D.W., 1980, Dissolution of salt deposits by brine density flow: Geology, v. 8, p. 66–69.

Bachman, G.O., 1980, Regional geology and Cenozoic history of the Pecos Region, southeastern New Mexico: US Geological Survey, Open File Report 80-1099, 117 p.

Dean, W.E., Davies, G.R., and Anderson, R.Y., 1975, Sedimentological significance of nodular and laminated anhydrite: Geology, v. 3, p. 367–372.

Dickenson, W.R., 1981, Plate tectonic evolution of the southern Cordillera: Arizona Geological Society, Digest, v. 14, p. 113–135.

DuChene, H.R., and Cunningham, K.I., 2006, Tectonic influences on speleogenesis in the Guadalupe Mountains, New Mexico and Texas, *in* Land, L., Lueth, V.W., Raatz, W., Boston, P., and Love, D.L., eds., Caves and karst of southeastern New Mexico: New Mexico Geological Society, Annual Field Conference, p. 211–218.

Ehrhart, J., 2016, Speleogenesis and delineation of megaporosity and karst geohazards through geologic cave mapping and LiDAR analyses associated with infrastructure in Culberson County, Texas: unpublished MS thesis, Stephen F. Austin State University, 159 p.

Ehrhart, J.T., and Stafford, K.W., 2021, Speleogenetic model of evaporite occurrences of the Gypsum Plain utilizing karst mapping and LiDAR analyses in Culberson County, Texas, USA, *in* Johnson, K.S., Land, L., and Decker, D.D., eds., Evaporite karst in the Greater Permian Evaporite Basin (GPEB) of Texas, New Mexico, Oklahoma, Kansas, and Colorado: Oklahoma Geological Survey, Circular 113.

Ernst, R.E., 2014, Large igneous provinces: Cambridge University Press, 653 p.

Harris, A.H., 1985, Late Pleistocene vertebrate paleoecology of the west: University of Texas Press, 293 p.

Hentz, T.F., and Henry, C.D., 1989, Evaporite-hosted native sulfur in Trans-Pecos Texas: relation to late phase Basin and Range deformation: Geology, v. 17, p. 400–403.

Hill, C.A., 1996, Geology of the Delaware Basin, Guadalupe, Apache and Glass Mountains: New Mexico and west Texas: Midland, Permian Basin Section of the SEPM, 480 p.

Keith, S.B., 1982, Paleoconvergence rates determined from K_2O/SiO_2 ratios in magmatic rocks and their application to Cretaceous and tertiary tectonic patterns in southwestern North America: Geological Society of America, Bulletin, v. 93, p. 524–532.

Kelley, V.C., 1971, Geology of the Pecos Country, southeastern New Mexico: New Mexico Bureau of Mines and Mineral Resources, Memoir 24, 78 p.

Kirkland, D.W., 2014, Role of hydrogen sulfide in the formation of cave and karst phenomena in the Guadalupe Mountains and western Delaware Basin, New Mexico and Texas: National Cave and Karst Research Institute, Special Paper 2, 77 p.

Kirkland, D.W., and Evans, R., 1976, Origin of limestone buttes, Gypsum Plain, Culberson County, Texas: American Association of Petroleum Geologists, Bulletin, v. 60, p. 2005–2018.

Klimchouk, A., 2007, Hypogene speleogenesis: hydrogeological and morphometric perspective: National Cave and Karst Research Institute, Carlsbad, NM, Special Paper No. 1, 106 p.

Lindsey, R.F., 1998, Meteoric recharge, displacement of oil columns and the development of residual oil intervals in the Permian Basin, *in* DeMis, W.D., and Nelis, M.K., eds., The search continues into the 21st century: West Texas Geological Society, p. 271–273

Majzoub, A., Stafford, K.W., Brown, W.A., and Ehrhart, J.T., 2017, Characterization and delineation of gypsum karst geohazards using 2-D electrical tomography, Culberson County, Texas, USA: Journal of Environmental and Engineering Geophysics, v. 22, n. 4, p. 441–420.

Morris, J., 2018, Physical and chemical controls on suffosion development in gypsic soil, Culberson County, Texas: unpublished MS thesis, Stephen F. Austin State University, 60 p.

Morris, J., Stafford, K., and Farrish, K., 2021, Physical and chemical controls on suffosion development in gypsic soil, west Texas, *in* Johnson, K.S., Land, L., and Decker, D.D., eds., Evaporite karst in the Greater Permian Evaporite Basin (GPEB) of Texas, New Mexico, Oklahoma, Kansas, and Colorado: Oklahoma Geological Survey, Circular 113.

Nance, R., 1993, Application of the standard tablet method to a study of denudation in gypsum karst, Chosa Draw, southeastern New Mexico: unpublished MS Thesis, University of Northern Colorado, Greely, CO, 82 p.

Polyak, V.J., McIntosh, W.C., Guven, N., and Provencio, P., 1998, Age and origin of Carlsbad Caverns and related caves from 40Ar/39Ar of alunite: Science, v. 249, p. 1919–1922.

Polyak, V., and Provencio, P.P., 2000, Summary of the timing of sulfuric-acid speleogenesis for Guadalupe caves based on ages of alunite: Journal of Cave and Karst Studies, v. 62, n. 2, p. 72–74.

Sares, S.W., 1984, Hydrologic and geomorphic development of a low relief evaporite karst drainage basin, southeastern New Mexico: unpublished MS Thesis, University of New Mexico, Albuquerque, NM, 123 p.

Scholle, P.A., Goldstein, R.H., and Ulmer-Scholle, D.S., 2004, Classic upper Paleozoic reefs and bioherms of west Texas and New Mexico: Socorro, New Mexico Institute of Mining and Technology: 166 p.

Shields, J., 2018, Speleogenetic evolution and geologic remote sensing of the Gypsum Plain, Eddy County, New Mexico: unpublished MS Thesis, Stephen F. Austin State University, 161 p.

Stafford, K. W., 2013, Evaporite karst and hydrogeology of the Castile Formation: Culberson County, Texas and Eddy County, New Mexico, *in* Land, L., Doctor, D.H., and Stephenson, J.B., eds., Proceedings of the 13th Multidisciplinary Conference on Sinkholes and the Engineering and Environmental Impacts of Karst: National Cave and Karst Research Institute, Carlsbad, NM, Symposium 2, p. 123–131.

Stafford, K.W., Brown, W., Ehrhart, J., Majzoub, A., and Woodard, J., 2017, Evaporite karst geohazards in the Delaware Basin, Texas: review of traditional karst studies coupled with geophysical and remote sensing characterization: International Journal of Speleology, v. 46, n. 2, p. 169–180.

Stafford, K.W., Ehrhart, J.T., Majzoub, A., Shields, J., and Brown, W., 2018, Unconfined hypogene evaporite karst: west Texas and southeastern New Mexico, USA: International Journal of Speleology, v. 47, n. 3, p. 293–305.

Stafford, K.W., Land, L., Klimchouk, A, and Gary, M., 2009, The Pecos River hypogene speleogenetic province: a basin-scale karst paradigm for eastern New Mexico and west Texas, *in* Stafford, K.W., Land, L., and Veni, G., eds., Advances in hypogene karst studies: National Cave and Karst Research Institute, Carlsbad, NM, Symposium 1, p. 121–135.

Stafford, K.W., Nance, R., Rosales-Lagarde, L., and Boston, P.J., 2008a, Epigene and hypogene karst manifestations of the Castile Formation: Eddy County, New Mexico and Culberson County, Texas, USA: International Journal of Speleology, v. 37, n. 2, p. 83–98.

Stafford, K.W., Rosales-Lagarde, L., and Boston, P.J., 2008c, Castile evaporite karst potential map of the Gypsum Plain, Eddy County, New Mexico and Culberson County, Texas: A GIS methodological comparison: Journal of Cave and Karst Studies, v. 70, n. 1, p. 35–46.

Stafford, K.W, Ulmer-Scholle, D., and Rosales-Lagarde, L., 2008b, Hypogene calcitization: evaporite diagenesis in the western Delaware Basin: Carbonates and Evaporites, v. 23, n. 2, p. 89–103.

Woodard, J., Brown, W., and Stafford, K., 2021, Geophysical delineation of megaporosity and fluid migration pathways for geohazard characterization within the Delaware Basin, Culberson County, Texas, *in* Johnson, K.S., Land, L., and Decker, D.D., eds., Evaporite karst in the Greater Permian Evaporite Basin (GPEB) of Texas, New Mexico, Oklahoma, Kansas, and Colorado: Oklahoma Geological Survey, Circular 113.

Physical and Chemical Controls on Suffosion Development in Gypsic Soil, West Texas

Jonah Morris and Kevin Stafford
Department of Geology, Stephen F. Austin State University, Nacogdoches, Texas

Kenneth Farrish
Division of Environmental Science, Stephen F. Austin State University, Nacogdoches, Texas

ABSTRACT.—In the Gypsum Plain of southwestern New Mexico and west Texas, suffosion processes have encouraged road failure through dissolution and transport in gypsic soils; however, no prior research has been conducted within the Delaware Basin in regard to these processes. These phenomena were evaluated in both field and laboratory settings to assess the parameters of suffosion development associated with Ranch to Market (RM) 652 in Culberson County, Texas, where infrastructure extends across Castile and Rustler strata. Field studies simulated surficial ponding in various gypsic soils and correlated suffosion potential with soil composition and thickness. Soluble fractions of gypsic soils were delineated through geochemical analyses, further expanding upon the soil descriptions published in the Culberson County Soil Survey, a third-order soil survey (Soil Survey Staff, 2013). Suffosion modeling replicated processes observed in the field through repeated infiltration of Dellahunt and Elcor soils—soil piping and subsidence were induced within suffosion models. Lineaments inferred as solutional fractures were delineated using color-infrared (CIR) images to determine regional suffosion potential. Results obtained from this research were used to form a conceptual model of suffosion development to better mitigate damage imposed on infrastructure in evaporite-karst terrains. Regions with thick, heterogeneous soils of low-to-moderate gypsum content (10–70%) and moderate fracture densities (100–800 m/km^2) are optimal for suffosion development. This model should be considered for future infrastructure projects in not only for the Gypsum Plain, but also for other arid environments with significant evaporite karst and gypsic soils.

INTRODUCTION

In northern Culberson County, Texas, dissolution of indurated gypsite (gypsic soil) and gypsum bedrock has caused substantial damage to infrastructure, primarily in the form of road failures (Stafford and others, 2017). The Gypsum Plain of southeastern New Mexico and west Texas (Fig. 1) is well recognized for extensive epigene and hypogene karst development, but suffosion processes have become a growing concern related to geohazards in recent years (Stafford and others, 2017). Large sections of Ranch to Market (RM) 652 and other infrastructure within the region have been subjected to road base failure as suffosion piping transports saturated fluids and sediments into underlying karst, predominantly during brief, intense precipitation events. Suffosion is capable of operating at rapid rates in gypsite (Stafford, 2016) and its influence on anthropogenic and environmental regimes may not immediately manifest at the surface. No dedicated studies have been previously conducted of suffosion processes in the Gypsum Plain and it is imperative that methods are developed to evaluate suffosion potential for future construction projects, as this region is one of the most abruptly developing petroleum sectors with intense infrastructure usage in North America (Stafford and others, 2017).

Suffosion features are developed by transport of saturated, unconsolidated sediments through soil piping (White, 1988). Laminar transport of fine material

Morris, Jonah; Stafford, Kevin; and Farrish, Kenneth, 2021, Physical and Chemical Controls on Suffosion Development in Gypsic Soil, West Texas, *in* Johnson, K. S.; Land, Lewis; and Decker, D. D. (eds.), Evaporite Karst in the Greater Permian Evaporite Basin (GPEB) of Texas, New Mexico, Oklahoma, Kansas, and Colorado: Oklahoma Geological Survey, Circular 113, p. 165–176.

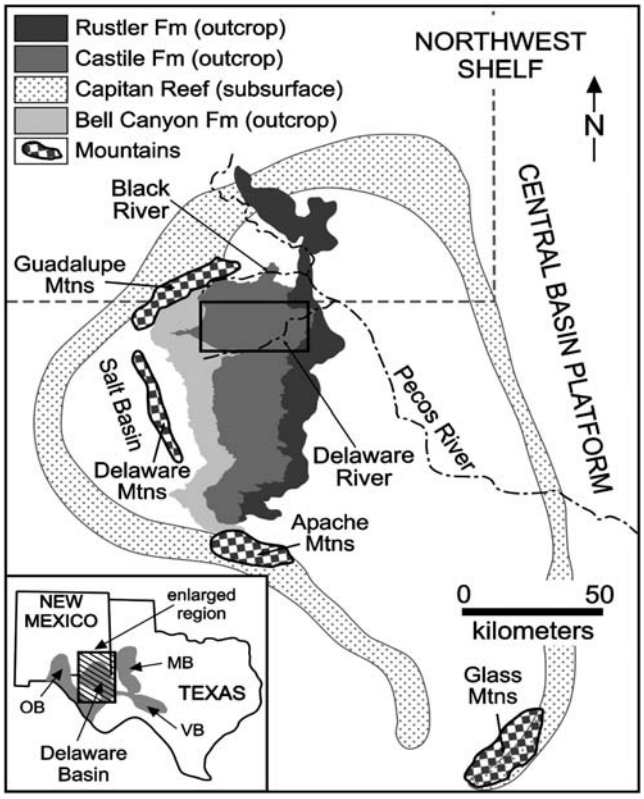

Figure 1. Study area outlined in black box with general location of Guadalupian and Ochoan strata in the Delaware Basin region and associated geomorphology and surficial hydrology (modified from Stafford and others, 2018).

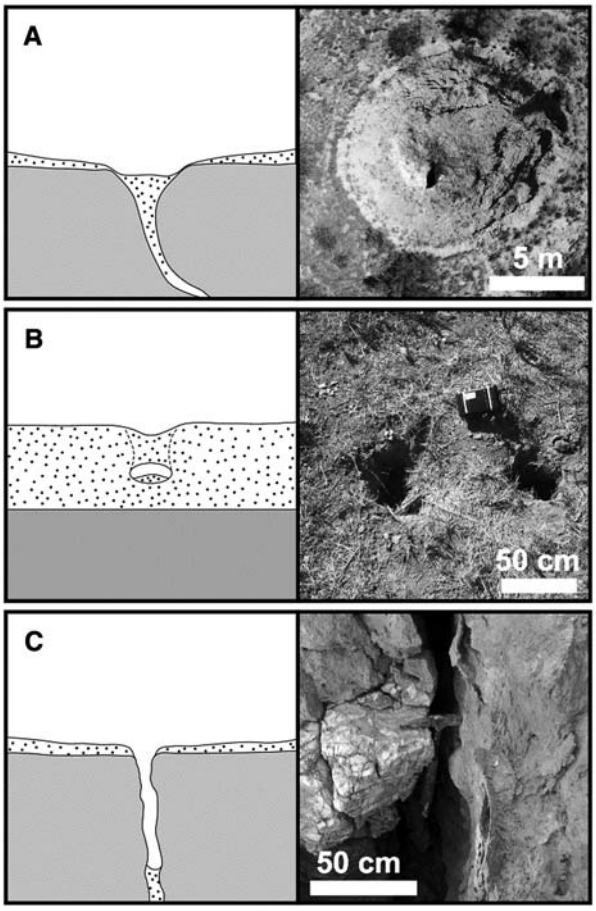

Figure 2. Suffosion features present in the Gypsum Plain including cross-sectional models on right and field examples on left: (A) sediments are funneled into an open cover-collapse sinkhole and transported through karstified gypsum bedrock; (B) lateral soil-piping transports sediments through gypsite macropores; (C) sediments are transported into solutional fractures widened by gypsite/gypsum dissolution.

through adjacent sediments initiates classic soil piping—pipes spread and connect with underlying karst (Gunn, 2004). Changes in the water table and rapid groundwater flow can induce collapse by transporting sediments through karstified formations and undermining overlying strata (Palmer, 2007). Flooding of low relief areas promotes subsidence by transporting soil through vertical pipes and fracture zones (White, 1988). Solutional fractures are important for evaporite karst development (White, 1988) and discharge from underlying karst may also cause flooding (Palmer, 2007). Infiltration through thick unconsolidated or allogenic material can induce suffosion depressions (Ford and Williams, 2007), whereas sink collapse is less probable in thin soils or bedrock (Palmer, 2007). Suffosion processes commonly influence the development of existing karst features and induce cover collapse proximal to infrastructure in karst environments (Ford and Williams, 2007).

In the Gypsum Plain, soil caves develop from suffosion (Fig. 2) and dissolution of soluble minerals (Stafford and others, 2017). Some soil caves can be laterally extensive and contain isolated chambers several meters in diameter. Preferential flow through indurated soils and evaporite dissolution of the soluble fraction form lateral and vertical soil pipes associated with bedrock solutional conduits and fractures at depth (Stafford and others, 2017). Ascending fluids from Guadalupian aquifers migrate through fractured Castile evaporites (Stafford and others, 2017) and some hypogene features exhibit artesianlike discharge following prolonged precipitation that can be masked by surficial deposits susceptible to suffosion (Stafford and others, 2018).

Parameters related to suffosion development in gypsite were evaluated in this study along approximately 35 km of RM 652 starting at the intersection of US 62/180 to the west in Culberson County, Texas (Fig. 1). This study area was investigated as a proxy for suffosion geohazard development within the greater region as RM 652 bisects the entire Gypsum Plain from west to east. Field-based analyses included infiltration testing

coupled with suffosion characterization, including lab-based and remote-sensing analyses. Physical suffosion modeling and chemical analyses of representative gypsite samples were conducted in the laboratory. GIS analyses focused on spatial delineation of evaporite karst and fractures proximal to infiltration sites. Regional suffosion potential in the Gypsum Plain may be quantified with an application of the methods introduced below.

GEOLOGIC SETTING

Situated between the Delaware Mountains to the west, Rustler Hills to the east, Guadalupe Mountains to the north, and Apache Mountains to the south, the Gypsum Plain is a low relief region that forms the central and western parts of the Delaware Basin (Fig. 1). The Delaware Basin formed during the late Paleozoic due to reactivation of Precambrian basement faults and uplift of the Central Basin Platform during the Ouachita Orogeny (Hill, 1996). Precipitation ranges from 20 to 40 cm $year^{-1}$—most occurs during late summer, intense storm events (Hill, 1996). The Gypsum Plain crops out over ~2,600 km^2 as Ochoan strata, primarily the Castile Formation (Kirkland and Evans, 1976). Castile evaporites are Late Permian, deep-water, stratified basin deposits (Kendall and Harwood, 1989; Stafford, 2013) that formed as open marine circulation ceased in the Delaware Basin during the late Guadalupian (Hill, 1996). Castile strata are conformable with the underlying Bell Canyon Formation, unconformable with the overlying Salado Formation, and do not extend beyond the basin margins (Hill, 1996). The Castile Formation is massive to laminated gypsum/anhydrite interbedded with halite with extensive intrastratal solutional removal within the western outcrop region (Henrickson and Jones, 1952; Hill, 1996). Castile evaporites increase in thickness from west to east, reaching 480 m thick in the subsurface (Kelley, 1971; Stafford and others, 2008a) with strata dipping 3–5 degrees northeast as a result of past tectonism (Hill, 1996).

Evaporite karst development is promoted by high sulfate and halide solubility (Stafford and others, 2008b) which commonly leads to subsidence, intrastratal collapse, and brecciation. Gypsum solubility (2.531 g L^{-1} at 20°C) is four orders of magnitude greater than calcite (1.5 mg L^{-1}), with more rapid solution kinetics in gypsum than in anhydrite (Klimchouk, 1996). Rock volume increases, as anhydrite converts to gypsum; most mature gypsum rocks in near-surface exposures originate from hydration of anhydrite, whereas sulfate mineral transitions promote the development of endokinetic fissuring (Klimchouk, 1996). Anhydrite dominates at depth (>450m), whereas gypsum is most common near the surface (Klimchouk, 1996). Past and present evaporite dissolution affects the entire Delaware Basin, creating a complex speleogenetic history for the region (Hill, 1996). Stafford and others (2017) classified Castile karst features into the following: intrastratal dissolution, hypogene caves, hypergene caves, and suffosion caves.

Guadalupian siliciclastics provide groundwater that ascends through Castile evaporites and encourages hypogene speleogenesis (Stafford and others, 2018). Intrastratal dissolution forms brecciated structures through hypogene processes coupled with subsequent collapse of evaporite strata (Stafford and others, 2008c). Hypergene caves are small, laterally limited features with openings that decrease in average cross-sectional area within short distances beyond surface interfaces (Stafford and others, 2017). Suffosion caves are generally too small for human entry (Stafford and others, 2008c), but large soil chambers have been documented that form when connected to larger voids in gypsum bedrock (Stafford and others, 2017). Both natural and anthropogenic sources induce preferential soil piping in the Gypsum Plain (Stafford and others, 2017). The largest karst features of the Castile Formation developed through hypogene processes at the boundary of the Bell Canyon Aquifer, but most features exhibit variable degrees of epigene overprinting (Stafford and others, 2008b).

Surface drainage is perennial near the Pecos River, semiperennial near the Black River, and ephemeral at creeks and arroyos (Hill, 1996). The Pecos River flows across the Delaware Basin's backreef, reef, and basin strata, and its tributaries—the Black and Delaware rivers—are contained within the interior of the Delaware Basin (Hill, 1996). The Gypsum Plain's only perennial channel is the Delaware River, but petroleum and ranching operations commonly draw from water sources provided by Quaternary alluvial deposits throughout the region (Stafford and others, 2018). Flash floods are commonly channeled into arroyos during intense storms (Stafford and others, 2018) and transmitted into the subsurface through evaporite karst interface features (Hill, 1996).

Subsequent to intense precipitation, breached hypogene karst and subsidence valleys overlying fractured bedrock exhibit artesianlike discharge at decadal intervals (Stafford and others, 2018). These conditions are promoted, as recharge to the underlying Bell Canyon Aquifer raises the potentiometric surface within the Castile Formation, exceeding the land surface as artesian discharge (Stafford and Faulkner, 2016). Infrastructure in areas with artesianlike discharge are subjected to considerable damage, as gypsum laminae are leached from underlying bedrock and overlying gypsic soils are saturated (Stafford and others, 2018).

GYPSIC SOILS

The western outcrop region of the Castile Formation weathers into a dull, gray–white gypsum soil (gypsite) in the Gypsum Plain (Hill, 1996). Gypsite is composed of

gypsum and/or anhydrite mixed with insoluble sediments (McGregor, 1954); deposits form as chemical sediments in semiarid-to-arid climates (Arakel and McConchie, 1982). Gypsiferous soils result from both physical and chemical vadose diagenesis of existing gypsum strata with subaerial exposure (Arakel and McConchie, 1982). Gypsic crusts develop on exposed bedrock because of repeated gypsum dissolution and reprecipitation (Stafford and others, 2008b). The change from a cold, humid climate in the Pleistocene to the present arid climate has resulted in the Gypsum Plain's current soil distribution (Hill, 1996; Stafford and others, 2017). Humid conditions brought alluvium to the base of the Delaware Basin; terrace alluvium accumulated in the Pecos River Valley and soil horizons developed in the drier periods (Hill, 1996). Flooding of the Pecos River and its tributaries has distributed graveled alluvium throughout the region (Hill, 1996). These alluvial and gypsic soils overlie bedrock in several areas and range from decimeters to several meters thick (Stafford and others, 2017).

In an extensive, third-order survey, Soil Survey Staff (2013) classified soils varying in gypsum content with textures ranging from graveled alluvium to gypsiferous loam and fine sand throughout the Gypsum Plain (Fig. 3). Soil horizons that contain high gypsum content are generally thin, whereas low-to-moderate gypsum content is common in thick, heterogeneous soil profiles. The Bissett-Rock Outcrop Complex (BID) consists of 65% Bissett soils (Lithic Ustic Haplocalcids) weathered from graveled limestone residuum and 25% limestone rock outcrops in areas with 3–16% slopes. The Bissett-Rock Outcrop Complex (BIE) in areas with 10–30% slopes has a similar composition of 65% Bissett soils and 30% limestone rock outcrops. The Culberspeth–Chilicotal Complex (CVC) consists of 65% Culberspeth soils (Calcic Petrocalcids) weathered from graveled alluvium/colluvium and 30% Chilicotal soils (Ustic Haplocalcids) weathered from graveled limestone pedisediment in areas with 1–8% slopes—this complex is located at the western margin of the study area proximal to BID and BIE complexes. Monohans (MHA) soils (Typic Calcigypsids) form from calcareous and gypsiferous alluvium in areas with 0–2% slopes and are proximal to the Delaware River with Walkerwells (WAB) soils (Ustifluventic Haplocambids) derived from alluvial deposits of gypsum and sandstone—gypsum content varies from 0 to 40%. These soils constitute about 6% of the total study area.

The remaining 94% of the study area is dominated by gypsiferous loams. Dellahunt (DEB) soils (Ustic Calcigypsids) weather from alluvial deposits of gypsum and sandstone in areas with 0–5% slopes, and Elcor (ELC/ELE) soils (Lithic Haplogypsids) weather from gypsum residuum in areas with 1–30% slopes. The Dellahunt–Neimahr–Joberanch Complex (DNB) consists of 30% Dellahunt soils, 25% Neimahr soils (Lithic Ustic Haplocambids), and 25% Joberanch soils (Ustic Petrogypsids), all of which are weathered from alluvial deposits of gypsum and sandstone. The Elcor–Dellahunt–Pokorny

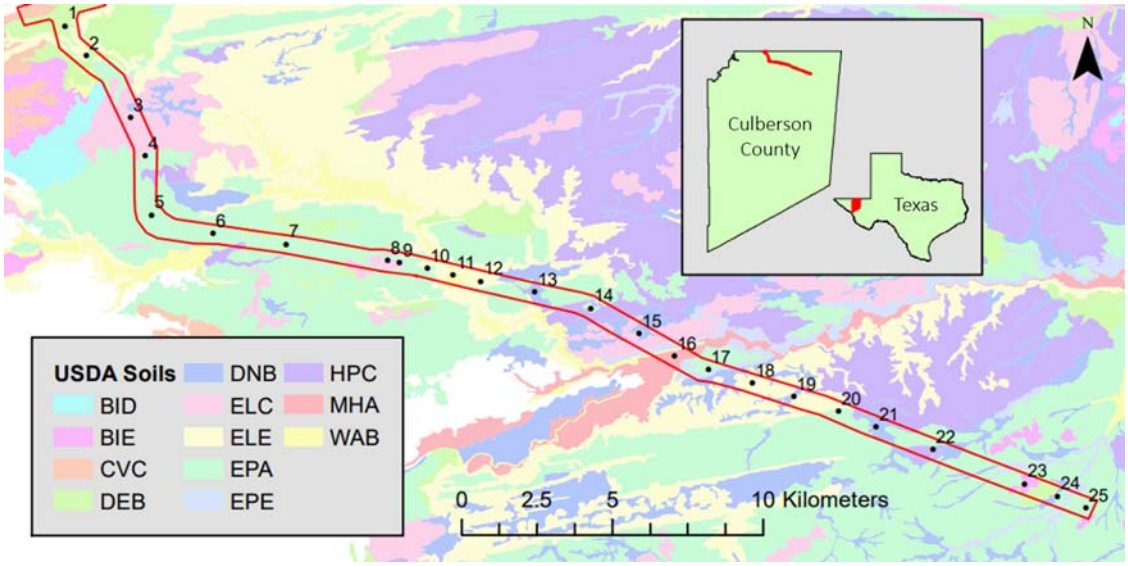

Figure 3. Soil map of the detailed soil units derived from the Culberson County Soil Survey (Soil Survey Staff, 2013): BID (Bissett-Rock Outcrop Complex); BIE (Bissett-Rock Outcrop Complex); CVC (Culberspeth–Chilicotal Complex); DEB (Dellahunt Silt Loam); DNB (Dellahunt–Neimahr–Joberanch Complex); ELC (Elcor Gypsiferous Loam); ELE (Elcor Gypsiferous Loam); EPA (Elcor–Dellahunt–Pokorny Complex); EPE (Elcor–Pokorny–Hollomex–Walkerwells Complex); HPC (Hollebeke–Pokorny Complex); MHA (Monohans Fine Sandy Loam); and WAB (Walkerwells Silty Clay Loam).

Complex (EPA) consists of 35% Elcor soils, 30% Dellahunt soils, and 25% Pokorny soils (Ustic Petrogypsids) in areas with 0–2% slopes. The Elcor–Pokorny-Hollomex–Walkerwells Complex (EPE) forms in areas with 0–30% slopes and consists of 30% Elcor soils, 30% Pokorny soils, 15% Hollomex soils (Ustic Haplogypsids), and 15% Walkerwells soils. The Hollebeke–Pokorny Complex (HPC) consists of 45% Hollebeke soils (Ustic Petrogypsids) and 35% Pokorny soils in areas with 1–8% slopes. Undifferentiated gypsiferous loams of the Elcor, Dellahunt, and/or Pokorny soil series contain 60–90%, 0–10%, and 0–95% gypsum content, respectively. However, these soils are undifferentiated as complexes in the soil mapping in ~ 53% of the study area and are effectively inseparable in the third-order Culberson County Soil Survey, where map units are mostly associations and complexes, with some coassociations and undifferentiated groups. This variation in soluble fractions inhibits the development of suffosion models for the region from existing soil delineations based on soluble content and complicates geoengineering throughout the region, as soil classification is too broadly characterized.

METHODOLOGY

Combined field and laboratory methodologies were developed to evaluate suffosion processes in the Gypsum Plain. Field studies quantified conditions associated with surficial ponding and infiltration in variable gypsite deposits. Laboratory analyses identified the composition of soluble fractions and composition of gypsic soils. Physical suffosion modeling was designed to replicate suffosion processes observed in field conditions within variable mediums and temporally through repeated infiltration analyses. Delineation of fractures, surficial karst manifestations, and regional suffosion potential were conducted through GIS analyses for correlation of observed suffosion phenomena.

Beginning at the intersection of US 62/180, field analyses were conducted at 25 locations along the first ~35 km of RM 652 within the Castile outcrop area. Field analyses were conducted over a 3-day period without prior precipitation for more than 28 days, and infiltration rates were measured along with soil electrical conductivity, moisture, and temperature. At each site, three Turf-Tec infiltration rings were installed into gypsite deposits within the right-of-way of RM 652 but distal to the road in minimally disturbed soils—triplicate infiltration analyses were conducted at each infiltration ring site and all infiltration rates were averaged for analyses. GroLine HI98331 EC Tester and Extech M0750 soil moisture meters were used to collect electrical conductivity/temperature and moisture data, respectively. Soil electrical conductivity, moisture, and temperature were measured at each infiltration ring both before and after infiltration testing. Infiltration rates were correlated with soil classifications designated by USDA (2013) soil surveys. Soil electrical conductivity was assessed between unsaturated and saturated conditions.

Geochemical analyses were conducted on representative soil samples to delineate soluble fractions (Stafford, 2017). Analysis samples were extracted from well-mixed soils, oven dried at 40°C until no mass changes were observed to prevent dehydration of gypsum to anhydrite and dissolved in deionized water for 24 hr with shaker-induced agitation—sample mass was limited to 0.5 g to ensure complete dissolution of soluble minerals (e.g., sulfate minerals) in 250 mL of deionized water. Major cations/anions and TDS were determined from filtered solutions with ICP-MS (Inductively Coupled Plasma Mass Spectrometry) at the Stephen F. Austin State University—Soil, Plant, and Water Analysis Laboratory; acid titrations were conducted with a Mettler Toledo EasyPlus Titrator to determine carbonate/bicarbonate concentrations. Geochemical analyses identified three major soil variants based largely on sulfate content (Fig. 4): 1) low sulfate content; 2) moderate sulfate content; and 3) high sulfate content.

Suffosion modeling was conducted with bulk samples gathered from field Sites 4 and 20. Both gypsite samples are classified by the USDA (2013) as part of the Elcor–Dellahunt–Pokorny Complex (EPA)—these soils constitute 94% of the study area. EPA soils are undifferentiated with gypsum contents that range from 0 to 95%, thus considerable variation exists among soils (Fig. 5). Sites 4 and 20 soils contain 10% and 80% gypsum content, respectively—Site 4 samples represent the Dellahunt soil series with low gypsum content (10%) and

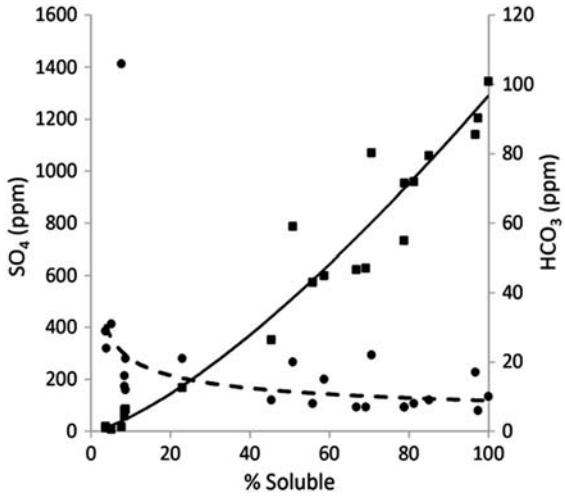

Figure 4. Solubility values of gypsite samples collected from field infiltration sites. Filled circles and dashed line represent HCO_3^+ concentrations, whereas squares and solid line represent SO_4^{2+}.

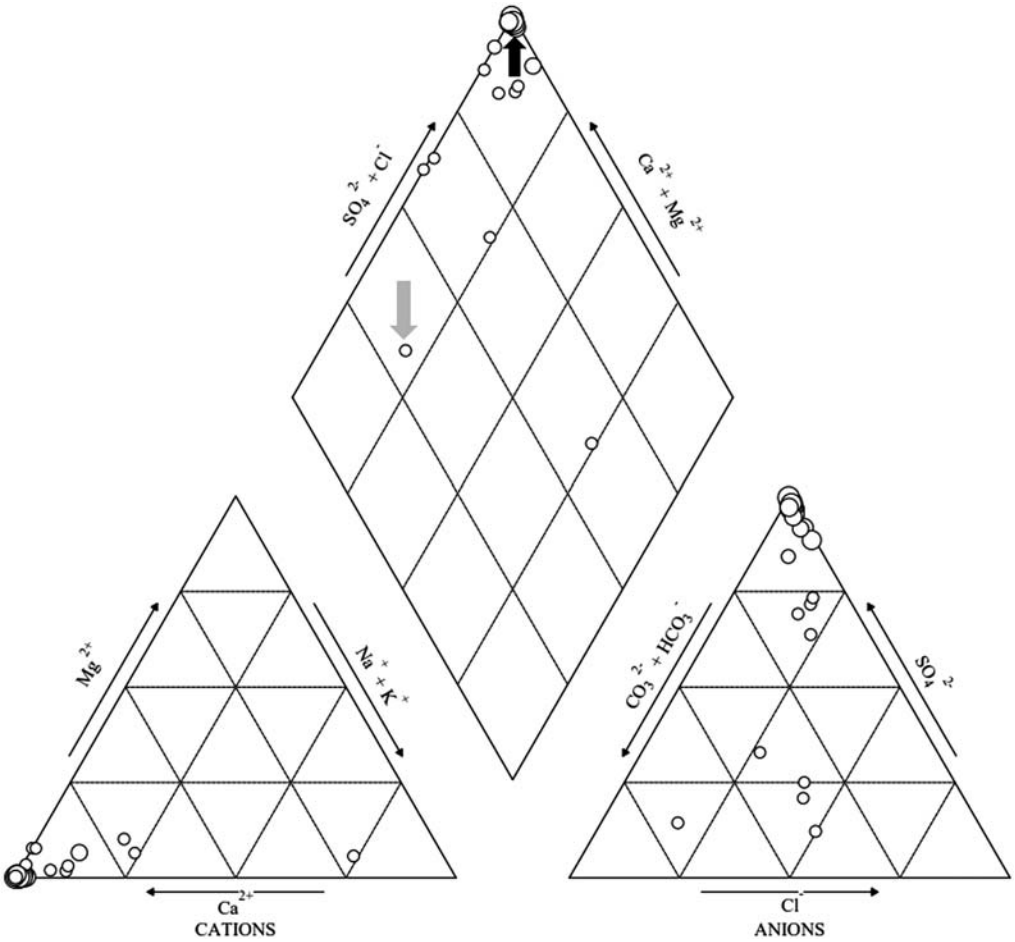

Figure 5. Piper diagram of gypsite samples collected from field infiltration sites—the point designated by the gray arrow is representative of the Dellahunt soil series and the point designated by the black arrow is representative of the Elcor soil series. Larger points indicate greater TDS (Total Dissolved Solids) values.

Site 20 samples represent the Elcor soil series with high gypsum content (>70%).

Physical infiltration modeling was conducted with gypsite that was homogenously mixed and sieved (2 mm) before being packed into butyrate cylinders 10 cm in height and 5 cm in diameter—tubes filled with homogenous soil were percussion-packed with a 1.5 kg cylinder dropped 20 times from height of approximately 30 cm. Filled cylinders were placed in vertical positions and connected to individual water reservoirs by polyethylene tubing to simulate vadose fluid migration induced by surficial ponding (Fig. 6). Water flow was restricted to a maximum rate of 1 mL/s, allowing 100 mL of deionized water to infiltrate through samples with minimal mechanical mass removal. Fluids and mobilized sediments were gravity-drained through a central exit point 1 mm in diameter into collection containers. Dissolved solids, insoluble sediments and suffosion models were oven-dried at 40°C until no mass change was measured, removing soil moisture without converting gypsum to anhydrite. Drying of sediment-packed columns between infiltration analyses was performed to simulate field conditions where soils are saturated during monsoonal rain events and subsequently dried because of high evaporation in the natural arid environment. Soil mass and volume of suffosion models were measured prior and subsequent to infiltration—sediments removed from the system were weighed after the oven-drying phase. Three iterations of this process were conducted with 18 replicate samples for each soil type (i.e., Dellahunt and Elcor soils).

Raster images with 50 cm resolution were used to map lineaments interpreted as fractures in gypsum bedrock/soil to define potential regions of increased suffosion potential within the study area. Feature selection included lineaments defined by linear vegetative growth (Stafford, 2018) and dismissed features related to anthropogenic activity (i.e., buried utility cables, roads, and fences). Lineament orientations and lengths were calculated in ArcGIS and rose diagrams were generated in GeoRose to evaluate spatial variability of fracture intensity. Lineament densities were calculated as line

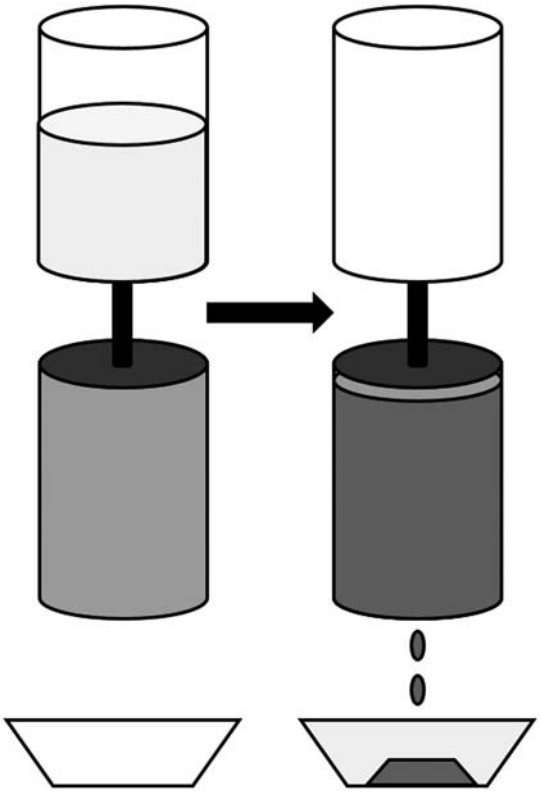

Figure 6. Diagram of suffosion modeling and sediment/solute removal: light-gray in the top left cylinder represents water, medium-gray in the bottom left cylinder represents unsaturated gypsite, dark-gray in the bottom right cylinder represents saturated gypsite, and dark grey in bottom right trapezoid represents sediment and saturated fluids transported out of the system as sediment/solute.

densities in ArcGIS. LiDAR (Light Detection and Ranging) data of sinkhole delineation conducted by Ehrhart (2016) were coupled with mapped lineaments and used to examine suffosion potential correlated with karst conduits in soils associated with infiltration field sites. Ehrhart (2016) delineated natural sinkholes with depths greater than 10 cm using LiDAR data with a horizontal resolution of 30 cm and vertical resolution of 10 cm—anthropogenic features were manually removed from the data set. Sinkhole densities were calculated as kernel densities in ArcGIS.

RESULTS AND DISCUSSION

Suffosion potential was measured according to physical and chemical parameters evaluated in representative samples of gypsic soil. Field analyses demonstrated the relationship between suffosion potential and soil thickness/type. Geochemical delineation of gypsic soils further characterized the broad soil descriptions published in the third-order Culberson County Soil Survey (Soil Survey Staff, 2013). Suffosion modeling correlated suffosion potential with the soluble/insoluble fractions of gypsite. Fracture and sinkhole delineations were coupled with soil thickness to analyze suffosion potential on a regional scale.

Field Analyses

Field infiltration sites were located within the following USDA (2013) designated soil types: two sites in DEB; three sites in DNB; four sites in ELC; two sites in ELE; 11 sites in EPA; one site in HPC; one site in MHA; and one site in WAB (Fig. 3). Soils that contain the Elcor, Dellahunt, and/or Pokorny series dominate the study area—these gypsiferous loams constitute ~94% of total area. The highest (4.7 mm min^{-1}) and lowest (0.5 mm min^{-1}) infiltration rates were measured from DEB and MHA soils, respectively. DEB soils are moderate alkaline silt loams formed from gypsum rock and sandstone, whereas MHA soils are moderate alkaline fine sands derived from calcareous and gypsiferous alluvium (Soil Survey Staff, 2013). The remaining sites (88%) shared an average infiltration rate of ~1.4 mm min^{-1}. Moderate-to-high infiltration rates were observed in thick, heterogeneous soil mixtures, whereas infiltration was limited in thin, fine soils overlying bedrock. Indurated gypsite promoted horizontal infiltration, as fluids came into contact with underlying gypsic cements, and heterogeneous soils allowed vertical infiltration in the absence of high soluble fractions. At Site 11, active suffosion was induced as several liters of water infiltrated through a previously unknown macropore during infiltration testing, forming a "whirlpool", as sediments were flushed into the subsurface, whereas other infiltration rings within 1 m exhibited slow infiltration rates, thus indicating the potential for extreme local heterogeneity of suffosion phenomena and permeability. Suffosion geohazards are more probable in thick, heterogeneous soils that promote moderate infiltration.

Soil electrical conductivity and moisture values were low prior to infiltration, ranging from 0.0 to 0.25 mS cm^{-1} and 0 to 10%, respectively. Most soil moisture readings increased beyond 20% during infiltration and all soil electrical conductivity readings surpassed 0.25 mS cm^{-1} (Fig. 7). These increases indicate that infiltrated fluids reached near saturation with respect to sulfate in gypsite deposits and that soluble ions were quickly mobilized. Areas where soil moisture increased beyond 40% exhibited gypsite compositions with significant clay content that favored soil swelling over vertical infiltration. A direct correlation exists between soil electrical conductivity and moisture throughout the study area, suggesting that moisture content is directly associated with clay content—organic content is extremely low in most soil series within the Gypsum Plain.

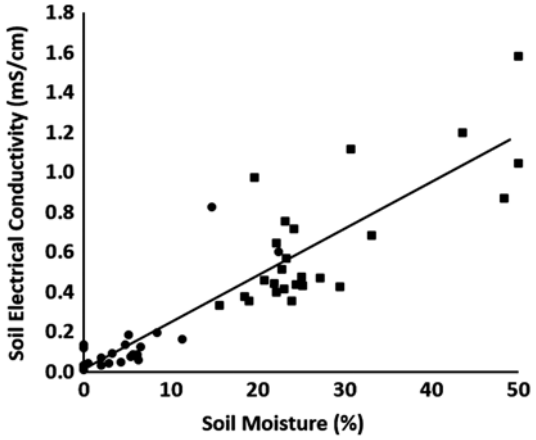

Figure 7. Values of soil electrical conductivity and soil moisture both prior (circles) and subsequent (squares) to infiltration studies. The trend line reflects the average increase of soil electrical conductivity, as sulfate saturation increases (r^2=0.80).

Geochemical Analyses

Over 70% of soluble fractions in most soils within the study area are composed of gypsum, but some chloride and carbonate minerals are present (Fig. 5). In general, chloride and carbonate ions in the study area are most concentrated near the surface due to dissolution and vertical transport of calcium sulfates into deeper soils or speleogenetic features. Calcium sulfates are also leached at depth when coupled with karst features. TDS (Total Dissolved Solids) of soils indicate solubilities exceeding 80% within the region with greater concentrations of soluble fractions at depth.

Soils in the study area can be grouped into three classifications based on their geochemical compositions: fluvial deposits, graveled alluvium, and gypsiferous loams. Sediments deposited by the Delaware River (fluvial deposits) exhibit the lowest soluble sulfate composition (<10%) and total solubility as a result of flooding and surface flow through unconsolidated deposits. Graveled alluviums at the western and eastern edges of RM 652 also have low solubilities and greater chloride/carbonate (>50%) concentrations—these soils are weathered from limestone soil parent materials transported by the Black River. Gypsiferous loams contain the highest concentrations of calcium sulfates (>50%), but varying amounts of chloride and carbonate minerals were present. Greater concentrations of carbonate/chloride ions are generally in gypsiferous loams with thick soil profiles that are proximal to fluvial deposits. Mixing of alluvial and gypsic soils forms heterogeneous mixtures that promote infiltration and dissolution of soluble fractions (gypsum). Soils with almost 100% calcium sulfate compositions appear to be derived in situ from underlying gypsum bedrock and form as thin, indurated gypsite that reduces infiltration and ion mobilization.

Suffosion Modeling

In general, suffosion models exhibited considerable increases in bulk density between initial conditions and the first iteration of infiltration—Dellahunt models increased in density by ~12% and Elcor models increased by ~11%. Dellahunt models transported greater amounts of sediment than Elcor models, but greater consolidation was observed in samples from Elcor soils. Porosities increased (1%) in Dellahunt models, as infiltration was repeated, whereas Elcor models decreased (3%) in porosity with repeated infiltration.

During the first infiltration iteration, Dellahunt and Elcor suffosion models exhibited consolidation and mass removal as deionized water flowed through the system (Fig. 8). Some dissolved solutes were removed from the system with insoluble fractions, but most were redistributed during infiltration and cemented around grains after oven-drying, occluding pore space. Consolidation continued in Dellahunt models with replicate infiltration analyses producing little decrease in porosity, indicating that microconduits formed during the subsequent iterations—mass removal decreased because of secondary grain cementation. Minimal increase in consolidation paired with decreased porosity indicates that fluids were not able to readily migrate through Elcor models during the replicate infiltrations, as permeability was reduced. Precipitated gypsum removed initial porosity, as models were dried.

Dellahunt soil permeability decreased with repeated infiltration modeling, but soils developed connected micropores coupled with cemented horizons that restricted vertical fluid flow as a result of relocation and precipitation of gypsum. This was evident from increased porosity and decreased consolidation between infiltration iterations and observable microconduits, which would provide inception horizons for suffosion piping. Infiltration ceased because of consolidation and gypsum reprecipitation after repeated iteration modeling in Elcor soils. Increased consolidation removed porosity between insoluble grains; reprecipitation removed secondary porosity formed by dissolution in the initial iteration.

Modeling demonstrated that suffosion processes are dependent on geochemical variations in gypsite. Dellahunt soils were more effective than Elcor soils in transporting sediment through suffosion processes. Dissolution of soluble fractions promotes soil pipe formation, but adequate insoluble material is needed to structurally support conduit permeability. In addition, excessive evaporite content reduces porosity, as sulfates are redistributed around insoluble grains and conduits in repeated wetting/drying phases as is common in arid environments. Although suffosion processes are encouraged in gypsite with low-to-moderate soluble fractions, Elcor samples experienced considerable, rapid consolidation and reflected compositions that favor general

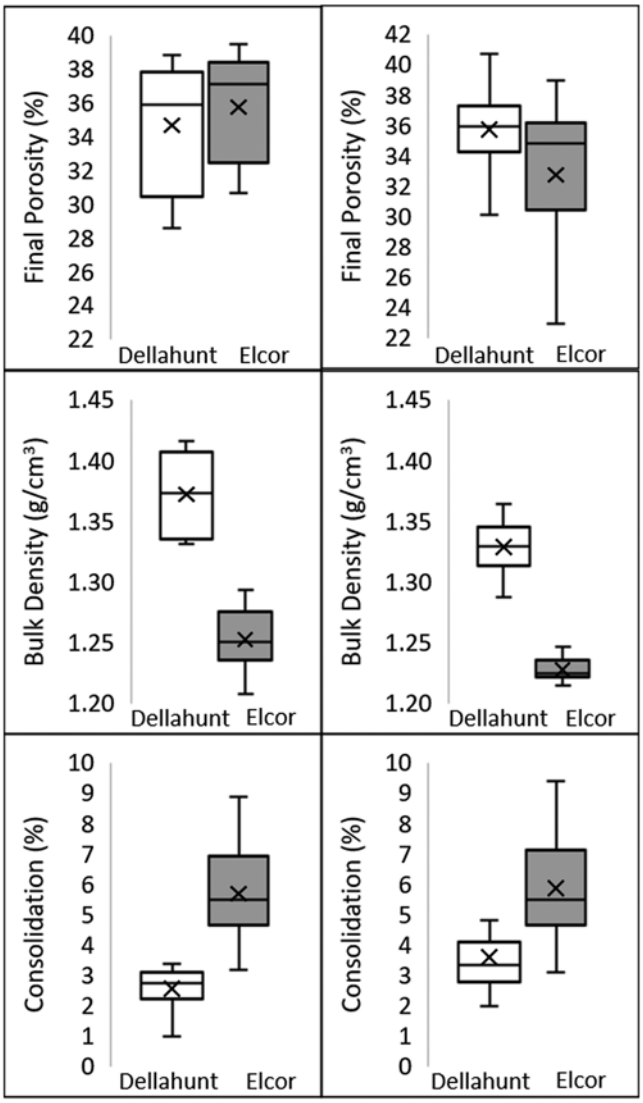

Figure 8. Results of suffosion modeling with Dellahunt (n=12) and Elcor (n=18) soil models. The left column shows the results of the initial iteration and the right column shows the results of the final iteration. White boxes represent the Dellahunt soil series, whereas gray boxes represent the Elcor soil series—median values of each data set are indicated by the horizontal line and averages are indicated by the "x" mark.

subsidence. Geohazards related to suffosion most likely result from a combination of both processes, but models indicate that the development of macropores within indurated gypsite is essential for continued suffosion and the development of potential geohazards.

GIS Analyses

Suffosion features in the Gypsum Plain occur through a combination of physical piping of unconsolidated sediment and dissolution of soluble soil fractions, but soil pipes are not the sole mechanisms of creating suffosion geohazards; fractures and sinkholes coupled to soils transport sediment into underlying karst as well (Fig. 2) by providing outlets for removal of insoluble sediments and saturated waters. Overland flow during intense precipitation flushes gypsite into void spaces provided by solutional fractures and conduits in gypsum bedrock which form the dominant coupling mechanism for enhanced suffosion development within the Gypsum Plain. Solutional fractures at the contact between gypsum bedrock and gypsic soils have commonly been correlated with suffosion features proximal to infrastructure in Castile evaporites (Ehrhart, 2016).

Stafford and others (2017) demonstrated that GIS studies can correlate vegetative growth patterns and available moisture content in evaporite karst environments through CIR (Color InfraRed) and NDVI (Normalized Difference Vegetation Index) analyses. In this arid environment, linear vegetative growth near fractures in thin soil indicate regions of greater moisture flux—fracture delineation is more difficult in soils with greater thicknesses and more uniform soil infiltration (Stafford and others, 2017). In total, 1,159 lineaments were mapped with general orientations at NW–SE and N–S within the study area (Fig. 9). An N–S lineament trend is dominant in the westernmost section of the study area, whereas NW–SE trends are observed to the east; similar fracture trends have been observed in caves and subsurface conduits (Stafford and others, 2008c), indicating that these lineaments accurately reflect local brittle deformation.

LiDAR analyses (Ehrhart, 2016) identified the locations of ~ 4,539 natural sinks within the study area—sinkholes are the most prevalent karst landform of the Castile outcrop region (Stafford and others, 2008c)

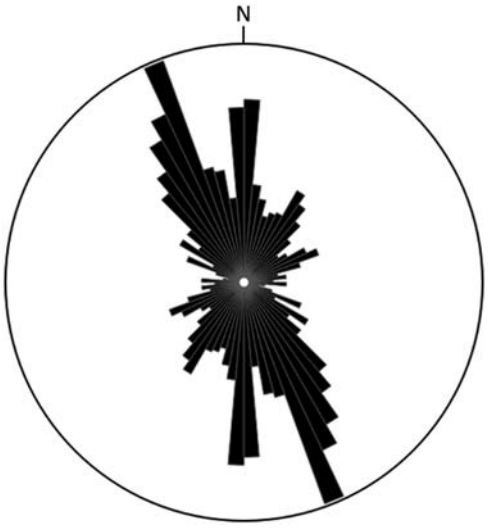

Figure 9. Orientations of lineaments (n=1159) delineated as solutional fractures proximal to RM 652.

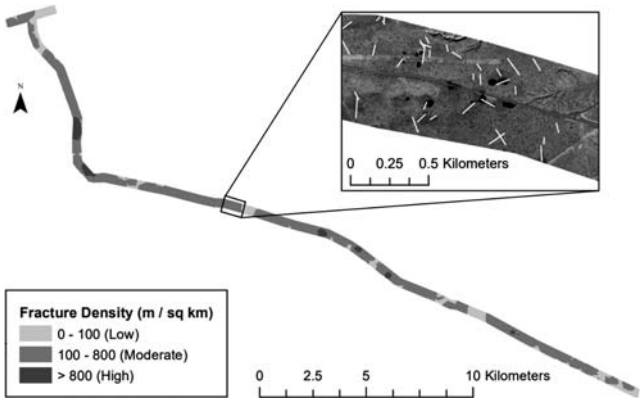

Figure 10. Densities of lineaments inferred as solutional fractures in gypsum strata proximal to RM 652. The inset shows CIR imagery with solutional fractures, as white lines and sinkholes derived from LiDAR analyses as black polygons.

and form due to solutional incision of meteoric water or collapse of strata overlying subsurface voids (White, 1988). Stafford and others (2008c) concluded that about 55% of sinks within the Castile outcrop resulted from collapse, whereas the remaining 45% were solutional sinks overprinted by surficial processes. Suffosion processes are capable of operating in all sinks of the Gypsum Plain to some degree, because most sinks were filled by gypsite as a result of climate shift from the humid Pleistocene to the arid Holocene. Filled sinks commonly have conduits obstructed by sediment infilling, allowing for sediment transport without direct observation as meteoric water infiltrates through indurated gypsite or as fluctuations in the water table disrupt sediments and increase drainage. Sinks without open, direct conduits into underlying karst develop suffosion features along permeable interfaces between gypsum bedrock and gypsite as dissolution of soluble fractions redistributes soluble ions and insoluble sediments within features.

Fracture and sinkhole densities correlate well with each other throughout the region (Fig. 10). The highest densities are commonly in areas with exposed gypsum bedrock, whereas lower densities are in thick alluvial deposits or proximal to major fluvial bodies, such as the Delaware River. Thin, indurated soils may not promote pipe development, but suffosion processes operate in solutional fractures and sinkholes during intense storms. Sediments are transported beneath the surface as overland flow and shallow vadose flow drains through these suffosion features and open sinks into deeper cavities of Castile evaporites. Water table fluctuations and groundwater flow also remove sediments that restrict sinkhole drainage, allowing suffosion processes to enhance existing collapse structures. However, suffosion potential is greatest in areas with moderate fracture and sinkhole densities. Fractures are most noticeable where soils are thin and bedrock exposed, but moderate fracture densities indicate soil thicknesses that support soil pipe development. In these areas, suffosion processes operate through all three mechanisms.

CONCLUSIONS

Suffosion features are considerable hazards to infrastructure and human life in the Gypsum Plain and are detrimental to transportation and industry operations. However, combined field and laboratory methods were effective in characterizing suffosion potential in evaporite strata and providing data for improved management of infrastructure in susceptible areas. Suffosion potential in the Gypsum Plain was determined through studies associated with soil composition, soil thickness, and delineation of solutional fractures and evaporite karst.

The compositions of gypsic soils influence suffosion and can be evaluated according to infiltration rates and soluble fractions present. Regions that promote moderate infiltration rates (1.5–2.3 mm min^{-1}) are optimal for suffosion development when soluble content is moderate. High infiltration rates remove soluble fractions needed to support conduits formed through soil piping, and low infiltration rates cannot transport insoluble sediment into underlying karst. Soil thicknesses are commonly related to soil types—heterogeneous mixtures form deep soil profiles, whereas thin soils overlying bedrock are high in gypsum and clay content. Soil piping is most effective in soils with low-to-moderate gypsum content (10–70%), whereas soils with high gypsum content (>70%) are more inclined toward subsidence through consolidation—further refinement of suffosion potential would be possible with more detailed characterization of soil composition beyond the general, broad characterizations reported by Soil Survey Staff (2013). Soils with high gypsum content are not preferable for soil piping because of insufficient insoluble sediment needed for the structural support of pipes. Solutional fractures and evaporite karst provide paths for fluid and sediment transport, which thus increase suffosion potential. However, high fracture densities correlate with thin soil cover which precludes suffosion development. Regions with moderate fracture (100–800 m km^{-2}) and karst (100–800 features km^{-2}) densities are most susceptible to suffosion processes, because associated soils are thick enough to induce soil piping and are coupled with high permeability bedrock structures. Suffosion potential (Fig. 11) is greatest in thick, heterogeneous soils with low-to-moderate gypsum content (10–70%) and moderate fracture densities (100–800 m km^{-2}).

The methods introduced in this study were economic and effective for discerning areas susceptible to suffosion processes near RM 652, and can be extended to other regions with gypsic soils coupled to evaporite karst. Future construction and mitigation plans should

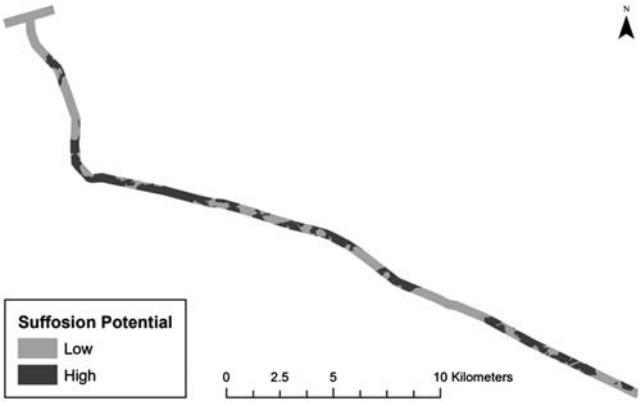

Figure 11. Map of regional suffosion potential proximal to RM 652. High potential areas meet all three criteria (moderate infiltration rates, low-to-moderate gypsum content, and moderate fracture densities), whereas low potential areas fail to meet these criteria.

consider suffosion potential when operating in the Gypsum Plain or in areas with significant evaporite karst and/or gypsic soils—delineating suffosion potential can reduce costs for infrastructural maintenance and reduce human endangerment. Field infiltration studies coupled with geochemical analyses provided an effective approach for characterizing soil compositions and thicknesses, whereas suffosion modeling demonstrated how the ratio between soluble and insoluble fractions of gypsic soils affect suffosion development. Solutional fracture delineation through GIS analyses was useful for determining suffosion potential in sparsely vegetative areas, and its effectiveness was substantiated through correlation between fracture and evaporite karst development. It is probable that studies conducted in other evaporite karst environments will produce similar results with the above methodologies.

ACKNOWLEDGEMENTS

The authors thank the Texas Department of Transportation (TxDOT) and Stephen F. Austin State University for partial funding of this research. Jon Ehrhart, Lillian O'Shay and Jessica Shields provided generous field support throughout this project. The comments of reviewers are greatly appreciated in the improvement of this manuscript during the revision process. Appreciation is expressed to Wesley Brown for his review of this manuscript and helpful contributions to its improvement.

REFERENCES CITED

Adams, J.E., 1965, Stratigraphic-tectonic development of the Delaware Basin: American Association of Petroleum Geologists, Bulletin, v. 49, p. 2140–2148.

Arakel, A.V., and McConchie, D., 1982, Classification and genesis of calcrete and gypsite lithofacies in paleodrainage systems of inland Australia and their relationship to carnotite mineralization: Journal of Sedimentary Research, v. 52, p. 1149–1170.

Barker, C.E., and Pawlewicz, M.J, 1987, The effects of igneous intrusions and higher heat flow on the thermal maturity of Leonardian and younger rocks, western Delaware Basin, Texas, *in* Glass Mountains: SEPM Guidebook, p. 69–83.

Ehrhart, J.T., 2016, Speleogenesis and delineation of megaporosity and karst geohazards through geologic cave mapping and LiDAR analyses associated with infrastructure in Culberson County, Texas: unpublished MS thesis, Stephen F. Austin State University, 66 p.

Ford, D., and Williams, P., 2007, Karst hydrogeology and geomorphology: John Wiley and Sons Ltd., 562 p.

Gunn, J., 2004, Encyclopedia of caves and karst science: Taylor and Francis Books, 902 p.

Hendrickson, G.E., and Jones, R.S., 1952, Geology and groundwater resources of Eddy County, New Mexico: New Mexico Bureau of Mines and Mineral Resources, Groundwater Report 3. 109 p.

Hill, C.A., 1996, Geology of the Delaware Basin, Guadalupe, Apache and Glass Mountains: New Mexico and West Texas: Permian Basin Section—SEPM, Midland, TX, 480 p.

Keller, G.R., Djeddi, R., and Hills, J.M., 1980, A regional geological and geophysical study of the Delaware Basin, New Mexico and West Texas: New Mexico Geological Society, Guidebook, v. 31, p. 105–111.

Kelley, V.C., 1971, Geology of the Pecos County, Southeastern New Mexico: New Mexico Bureau of Mines and Mineral Resources, Socorro, New Mexico, 78 p.

Kendall, A.C., and Harwood, G.M., 1989, Shallow-water gypsum in the Castile Formation – significance and implications, *in* Subsurface and outcrop examination of the Capitan shelf margin, northern Delaware Basin, San Antonio, Texas: SEPM Core Workshop, v. 13, p. 451–457.

Kirkland, D.W., and Evans, R., 1976, Origin of limestone buttes, Gypsum Plain, Culberson County, Texas: American Association of Petroleum Geologists, Bulletin, v. 60, p. 2005–2018.

Lee, M.K., and Williams, D.D., 2000, Paleohydrology of the Delaware Basin, western Texas: overpressure development, hydrocarbon migration, and ore genesis: American Association of Petroleum Geologists, Bulletin, v. 84, p. 961–974.

McGregor, D.J., 1954, Gypsum and anhydrite deposits in southwestern Indiana: Indiana Department of Conservation, v. 8, 24 p.

Palmer, A.N., 2007, Cave geology: Cave Books, 454 p.

Soil Survey Staff (USDA). 2013. Soil survey of Culberson County, Texas: Natural Resources Conservation Service.

Stafford, K.W., 2013, Evaporite karst and hydrogeology of the Castile Formation: Culberson County, Texas and Eddy County, New Mexico, *in* Land, L., Doctor, D.H., and Stephenson, J.B., eds., Proceedings of the 13th Multidisciplinary Conference on Sinkholes and the Engineering and Environmental Impacts of Karst: National Cave and Karst Research Institute, Carlsbad, NM., Symposium 2, p. 123–131.

Stafford, K.W., 2016, 2016 karst geohazard characterization of RM 652: phase two of karst development and geohazards associated with RM 652 in Culberson County, Texas: Report to El Paso District Office of Texas Department of Transportation, 94 p.

Stafford, K.W., 2017, 2017 karst geohazard characterization of RM 652: phase three of karst development and geohazards associated with RM 652 in Culberson County, Texas: Report to El Paso District Office of Texas Department of Transportation, 45 p.

Stafford, K.W., 2018, 2018 karst geohazard characterization of RM 652: phase four of karst development and geohazards associated with RM 652 in Culberson County, Texas: Report to El Paso District Office of Texas Department of Transportation, 21 p.

Stafford, K.W., Rosales-Lagarde, L., and Ulmer-Scholle, D., 2008a, Hypogene calcitization: evaporite diagenesis in the western Delaware Basin: Carbonates and Evaporites, v. 23, p. 89–103.

Stafford, K.W., Boston, P.J., and Rosales-Lagarde, L., 2008b, Castile evaporite karst potential map of the Gypsum Plain, Eddy County, New Mexico and Culberson County, Texas: a GIS methodological comparison: Journal Cave and Karst Studies, v. 70, no. 1, p. 83–98.

Stafford, K.W., Boston, P., and Rosales-Lagarde, L., 2008c, Epigene and hypogene gypsum karst manifestations of the Castile Formation: Eddy County, New Mexico and Culberson County, Texas, USA: International Journal of Speleology, v. 37, p. 83–98.

Stafford, K.W., and Faulkner, M.S., 2016, Engineering geohazards in hypogene evaporite karst, Castile Formation, West Texas, *in* Chaves, T., and Reeling, P., eds., Proceedings of DeepKarst 2016. Origins, resources, and management of hypogene karst: National Cave and Karst Research Institute, Carlsbad, New Mexico, Symposium 6, p. 131-132.

Stafford, K.W., Brown, W.A., Ehrhart, J.T., Majzoub, A.F., and Woodard, J.D., 2017, Evaporite karst geohazards in the Delaware Basin, Texas: review of traditional karst studies coupled with geophysical and remote sensing characterization: International Journal of Speleology, v. 46, p.169–180.

Stafford, K.W., Brown, W., Ehrhart, J., Majzoub, A., and Shields, J., 2018, Unconfined hypogene evaporite karst: West Texas and southeastern New Mexico, USA: International Journal of Speleology, v. 47, p. 293–305.

White, W.B., 1988, Geomorphology and hydrology of karst terrains: Oxford University Press, 464 p.

Geophysical Delineation of Megaporosity and Fluid Migration Pathways for Geohazard Characterization within the Delaware Basin, Culberson County, Texas

Jonathan Woodard, Wesley Brown, and Kevin Stafford
Department of Geology, Stephen F. Austin State University,
Nacogdoches, Texas

ABSTRACT.—Differential dissolution of gypsum within the Delaware Basin poses a significant threat to infrastructure that society depends on. The study area is located in Culberson County, Texas, and traverses a distance of approximately 54 kilometers along RM 652 within the Gypsum Plain, which is situated on the northern margin of the Chihuahua Desert, and includes outcrops of Castile and Rustler strata that host karst geohazards. Regions of karst geohazard potential have been surveyed proximal to the study area in evaporites throughout the Castile Formation outcrop; minimal hazards, in comparison to the Castile Formation, have been documented in the Rustler Formation. A TR-5 OhmMapper capacitively-coupled resistivity (CCR) meter was used to acquire resistivity data for geohazard characterization. This study utilized a traditional dipole–dipole array, with an electrode spacing of 2.5 meters between receivers and a transmitter offset of 2.5 meters. This geometric configuration, combined with medium analyzed, allowed for resistivity readings to be recorded up to approximately 5 meters deep. Data acquisition was recorded with the OhmMapper attached to a vehicle moving at approximately 3 kilometers per hour and transmitting and receiving once per second (approximately 1 meter per sample). Resistivity data was processed using AGI's EarthImager 2D inversion software. Capacitively coupled resistivity has shown to be effective in locating karst geohazards in the shallow subsurface.

INTRODUCTION

The Delaware Basin of west Texas and southeastern New Mexico is the northern most extension of the Chihuahuan Desert and is often referred to as the Gypsum Plain (Hill, 1996). Throughout the Gypsum Plain, significant karst-geohazard manifestations have proven to be detrimental for infrastructure maintenance. The research area, Ranch to Market (RM) 652, is a 54-kilometer section of roadway located on the northeastern edge of Culberson County, Texas (Fig. 1). The dominant outcrop within the study area is the evaporitic Castile Formation, with moderate outcrop exposures of the Rustler Formation in the eastern part of the study area (Fig. 2). Significant amounts of surficial karst phenomena commonly develop throughout the evaporite Castile Formation. Subsequent geohazards form from karsting, often characterized as sinkholes, solution conduits, and subsidence features (Stafford and others, 2008).

Karst features that have substantial cover may not be easily identified by traditional mapping techniques, satellite imagery, or aerial photos (Neukum and others, 2010). Because of the length of the study area, a noninvasive, capacitively coupled resistivity technique was used to locate the shallow karst phenomena beneath asphalt pavement without surficial expressions. This method has been proven in numerous studies to be a reliable technique in locating near-surface karst manifestations, with similar studies being conducted in Florida and Europe (e.g., Garman and Purcell, 2004; Vadillo and others, 2012; Samyn and others, 2014).

Known areas of significant road failure, and the abundance of karst geohazard surface expressions, justified imaging this section of roadway in Culberson County, Texas. A continuous electrical resistivity survey was conducted for approximately 54 kilometers on the westbound lane of RM 652. Six sites exhibiting geophysical anomalies that were verified through excavation are

Woodard, Jonathan; Brown, Wesley; and Stafford, Kevin, 2021, Geophysical Delineation of Megaporosity and Fluid Migration Pathways for Geohazard Characterization within the Delaware Basin, Culberson County, Texas, *in* Johnson, K. S.; Land, Lewis; and Decker, D. D. (eds.), Evaporite Karst in the Greater Permian Evaporite Basin (GPEB) of Texas, New Mexico, Oklahoma, Kansas, and Colorado: Oklahoma Geological Survey, Circular 113, p. 177–187.

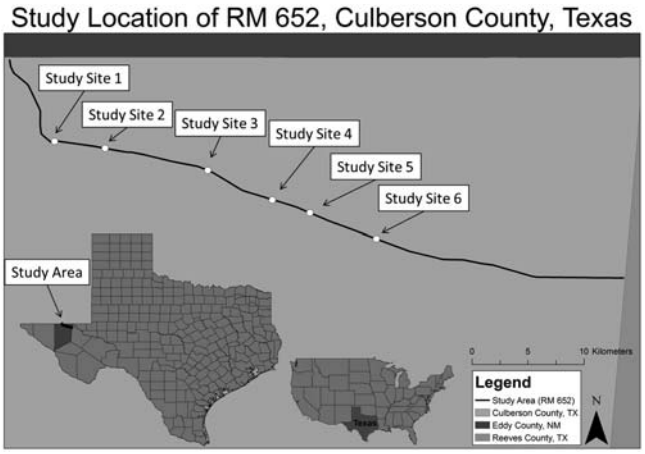

Figure 1. Geographic location of the study area; RM 652 is black line that stretches across the northeastern corner of Culberson County, Texas.

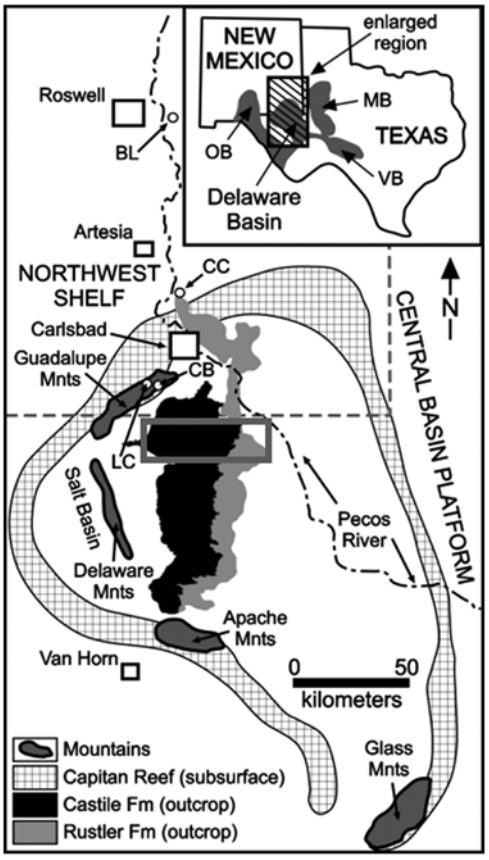

Figure 2. Map showing geographic orientation of the Delaware Basin with respect to Texas. The general study area is identified by the gray box, and primary geologic features of the region are outlined (modified after Stafford and others, 2008).

presented in this manuscript to demonstrate the practicality and efficiency of using a continuous, alternating current (AC), resistivity method to image near-surface karst phenomena.

GEOLOGIC SETTING

The Delaware Basin of west Texas and southeastern New Mexico (Fig. 2) was a restricted Permian evaporite intracratonic basin outlined by a 600–700 kilometer reef complex (Hill, 1996). During Late Mississippian and Early Permian time, the convergence of Laurasia and Gondwana resulted in the formation of Pangea. Subsequent block faulting along Precambrian zones of weakness formed the Permian Basin, which is structurally subdivided into the Midland Basin, Central Basin Platform, and Delaware Basin. Increased sediment loading aided in further separating the Delaware Basin from the Central Basin Platform (Adams, 1962). Subsidence in the Pennsylvanian-Early Permian dominated the depositional environment throughout the Permian, which caused the Delaware Basin to experience deep-water deposition until the end of Guadalupian time (Ross, 1981). During Guadalupian time, carbonates formed the rim of the Delaware Basin margin and siliciclastic material was deposited into the deep basin. Extensive reef growth encircled the Delaware Basin during Ochoan time, which restricted flow of open-marine waters, by closure of the Hovey Channel, creating a deep saline lake and conditions conducive for evaporite deposition. While the Castile Formation is restricted to the Delaware Basin, subsequent deposition of Salado and Rustler formations capped the entire region, including surrounding basins (Scholle and others, 2004).

Throughout the early Mesozoic, the Delaware Basin was tectonically inactive and relatively stable. This tectonic quiescence ended during the late Mesozoic when the Laramide Orogeny caused regional uplift and tilting of the basin strata approximately 3–5° to the east-northeast. Following the Laramide Orogeny, a change from compression to extension occurred within the region, leading to the Basin and Range Phase, which is subdivided into three stages that affected the Delaware Basin: Transition Stage, Main Uplift Stage, and Quaternary Stage. Block faulting on the western side of the Delaware Basin during the Transition Stage is responsible for the down-drop of the Salt Basin (Hill, 1996). During the Main Uplift Stage, a shift of maximum stress, from east-northeast to west-northwest, formed northeast-trending, graben-boundary faults in the basin (Hentz and Henry, 1989). Throughout the Quaternary Stage, border faults continued to be active, with continued movement along the Salt Basin Quaternary faults (Hill, 1996).

Climate change within the Delaware Basin has had a profound impact on the modern geomorphic nature of the Gypsum Plain, as the climate shifted from cool and wet in the Pleistocene to dry and arid in the Holocene. Today, the average precipitation ranges from 20 to 40 cm, with an average annual temperature of 24°C and average summertime high of 40°C. Rainfall typically

occurs between May and October; however, over half of the rain falls between July and September as short-duration, monsoonal-type storm events (Sares, 1984).

KARST DEVELOPMENT

The Delaware Basin hosts one of the most extensive developments of surficially expressed, gypsum karst in North America. Sinkholes, caves, and underground drainage systems are typical throughout the landscape (Hill, 1996). Gypsum outcrops generally only survive in arid climates; thus sinking stream patterns in gypsum karst tend to be small, dry arroyos that terminate into swallow holes or open caves (White, 1988).The highly soluble nature of evaporite rocks of the Castile Formation is primarily responsible for the abundance of karst throughout the Gypsum Plain. Karst expressions occur to a lesser degree in the carbonate Rustler strata because they are more resilient to dissolution effects. The former widespread, halite-rich Salado Formation has undergone extensive surficial weathering and erosion in outcrop, and it has been mostly dissolved in the shallow subsurface by intrastratal dissolution, thereby creating a solutional contact between the Castile and Rustler formations (Stafford and others, 2008). Throughout the Gypsum Plain, hypergene processes dominate the surficial geomorphic evolution of surface rocks, while hypogene processes appear to control the diagenetic evaporite alteration and general speleogenetic evolution (Stafford and others, 2016).

Sinkholes, solution fractures, and caves are abundant throughout the study area, forming under the influences of dissolution and suffosion. Sinkholes formed by descending water typically exhibit more lateral development and form a series of dendritic arroyos that converge and drain into the sink, while collapse sinkholes generally have steeper margins and are normally near-circular in shape (Stafford and others, 2008). Individual caves that have been investigated throughout the Castile Formation show an intricate speleogenetic history that includes hypergene and hypogene origins (Stafford and others, 2016). Hypergene caves form from meteoric processes near the surface and are frequently found throughout the Gypsum Plain; however, they are usually expressed as isolated features with collapsed and filled sinkholes. Hypergene caves also have a tendency to form in areas where surficial gypsic soil comes into contact with gypsum bedrock. Usually, these hypergene-soil caves are either filled with soil, or they rapidly decrease in size away from the entrance area; thus limiting field surveys to within a few tens of meters. However, in some cases these soil caves will connect to caves formed in gypsum bedrock, which suggests that the bedrock caves provide a preferential flow path for water and insoluble soil residues to drain (Stafford and others, 2008). Hypogene caves do not have a direct connection with surface environment activity and meteoric waters at the time of formation and thus form from dissolution caused by rising fluids in confined systems (Stafford and others, 2008). Differences in hydraulic pressure gradients drive dissolution through convection; fluids from lower, pressurized aquifers will flow upward to areas of a lower hydraulic pressure regime, which is often the regional base level (Tóth, 1999).

ELECTRICAL RESISTIVITY ANALYSES

The G858 OhmMapper resistivity system, by Geometrics Inc., TR-5 configuration with a traditional dipole–dipole array was used to collect continuous resistivity data along the 54 kilometer traverse of RM 652 on the west-bound lane, of which six locations, each approximately 160 meters long, are presented in this manuscript (Fig. 1). The TR-5 configuration dipole–dipole array uses one pair of current-emitting electrodes (transmitter), and five pairs of potential electrodes (receivers), connected by a nonconductive tow-link cable. The resistivity meter was attached to a vehicle and towed at a pace of ~3 km/h, while simultaneously collecting GPS data with an average geometric resolution of approximately 50 cm. A 5-m operator isolator cable, 2.5-m dipole cables, and a 2.5-m nonconductive tow-link rope configuration were used (Fig. 3). This electrode geometry enabled recordings to be taken at an effective depth of penetration of approximately 5 meters, at a resolution of approximately one sample at five different depths per meter. The OhmMapper system utilizes a working frequency of approximately 16.5 Khz that is transmitted and received through the dipole cables (Geometrics, 2016). Remote- and arid-location factors of the Gypsum Plain reduced concern of bad data quality normally caused by shallow skin depth and cultural noise.

Resistivity recordings and GPS data points were quality checked in MagMap2000, a preinversion software program by Geometrics, before importing data into the inversion program (Geometrics, 2001). Data inversion was executed in EarthImager 2D, a product of Advanced Geosciences Incorporated (AGI). A smooth model inversion was chosen because of its dependability and ability to generate clear resistivity boundaries (AGI, 2007). The resistivity profiles rendered by inversion were terrain-corrected against data extracted from a digital elevation model, which was constructed from LiDAR data and processed in ArcGIS. LiDAR data was acquired with a horizontal resolution at 0.3 to 0.4 meters, with 10 centimeters vertical resolution (Ehrhart, 2016).

Study Site 1 (160 meter segment)

Study Site 1 was chosen because of significant anomalous patterns found within the profile (Fig. 4A, 5A).

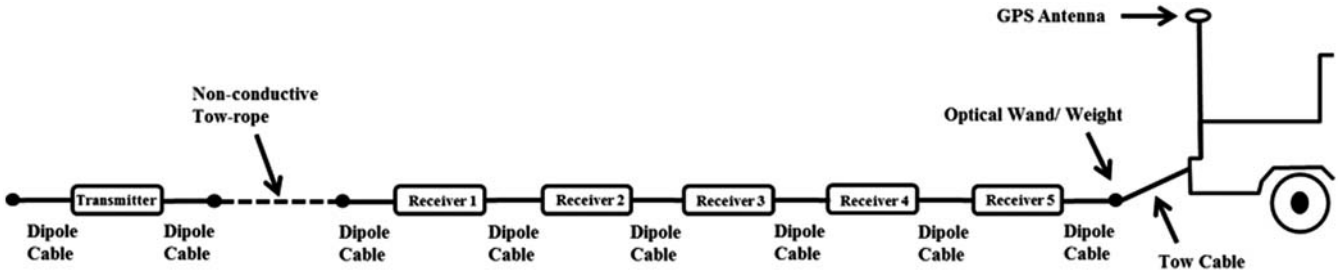

Figure 3. Diagram of OhmMapper TR-5 resistivity meter configuration used and electrode geometries. This image shows a TR5 configuration, with a transmitter (Tx) and five receivers (Rx) that allow for five depths of investigation while continuously collecting resistivity data along a single traverse.

Road failure and water ponding commonly occur above areas indicated to be collapse and/or void features; deeper resistivity surveys were required to further characterize collapse features. However, interpretations of "Cave 1" were confirmed through field-check excavation, and other anomalous signatures that corresponded to its pattern were interpreted to be similar features (Fig. 6A). Traditionally, caves are defined by their ability to allow for human entry; however, this study extends the definition of caves to even include features that are just large enough to allow the passage of a substantial amount of sediment and fluid. This "Cave 1" feature was approximately 30 cm tall, 2 meters wide, and partially filled with water-saturated soil and void space traversing directly under the roadway. Surface runoff at the site flows to the northeast; surface expressions on the southern road margin collect runoff and sediment transporting it under the roadway.

Study Site 2 (160 meter segment)

Study Site 2 was selected for excavation to confirm anomalous patterns seen in profile (Fig. 4B) and significant water ponding during the monsoonal season. Differential dissolution of gypsic soil, used as original roadbase material during construction, resulted in filled sink features and preferential soil piping under and along the survey path (Fig. 5B). Through field excavations, interpretations of this filled sink were verified, along with many soil-piping features (Fig. 6B). This resistivity method was able to document many filled sink geohazards that do not have surficial expression connecting directly to subsurface conduits that would otherwise reveal their presence. These sites represent areas of preferential ponding and increased infiltration, leading to increased dissolution of the gypsic soil road base.

Study Site 3 (160 meter segment)

Study Site 3 was selected for field evaluations so that anthropogenic enhancement effects could be included in road failure characterization. The resistivity profile along this segment indicated significant void space (Fig. 4C). This anomaly occurred proximal to a "toe wall" (i.e., concrete-reinforced vertical barrier at the margin of the road) that was designed to direct water away from the roadway and to maintain infrastructure stability, which was verified by site excavation (Fig. 5C). A large conduit, approximately 11 cm in diameter, was uncovered at an approximate depth of 1.5 m in the trench (Figure 6C). During excavation, substantial water and sediment drained through this solution conduit in the gypsum bedrock as field excavations were underway, indicating an extensive dissolution network beneath the road at depth. Anomalous patterns, such as the ones identified at Study Site 3, were seen on resistivity profiles in areas associated with "toe walls" and drainage-retention berms throughout the study.

Study Site 4 (160 meter segment)

Brecciation is common within the Castile Formation, and resistivity profiles at Study Site 4 show significant anomalous patterns where analyses pass through a roadcut within a breccia pipe (Fig. 5D; Fig.7A). This study site was located on a topographic high and descended down-slope perpendicular to the margin of the exposed breccia pipe, which likely extends through the entire thickness of the Castile Formation. These features are generally recemented after collapse and most often exhibit low permeability conditions within the breccia core; but they frequently possess higher permeability characteristics on their outer margins (Fig. 6D). Brecciation within the study area seems to be a result of intrastratal dissolution of evaporites by hypogenic speleogenesis, where a void was formed at depth and stoped upward (Stafford and others, 2008; Figure 9A).

Study Site 5 (160 meter segment)

Study Site 5 exhibited a resistivity profile that contained significant soil piping anomalous patterns that matched previously excavated locations (Fig. 5E; Fig. 7B). As the roadway was elevated substantially in this location during construction, the resistivity profile does not penetrate deep enough to identify a soil/rock

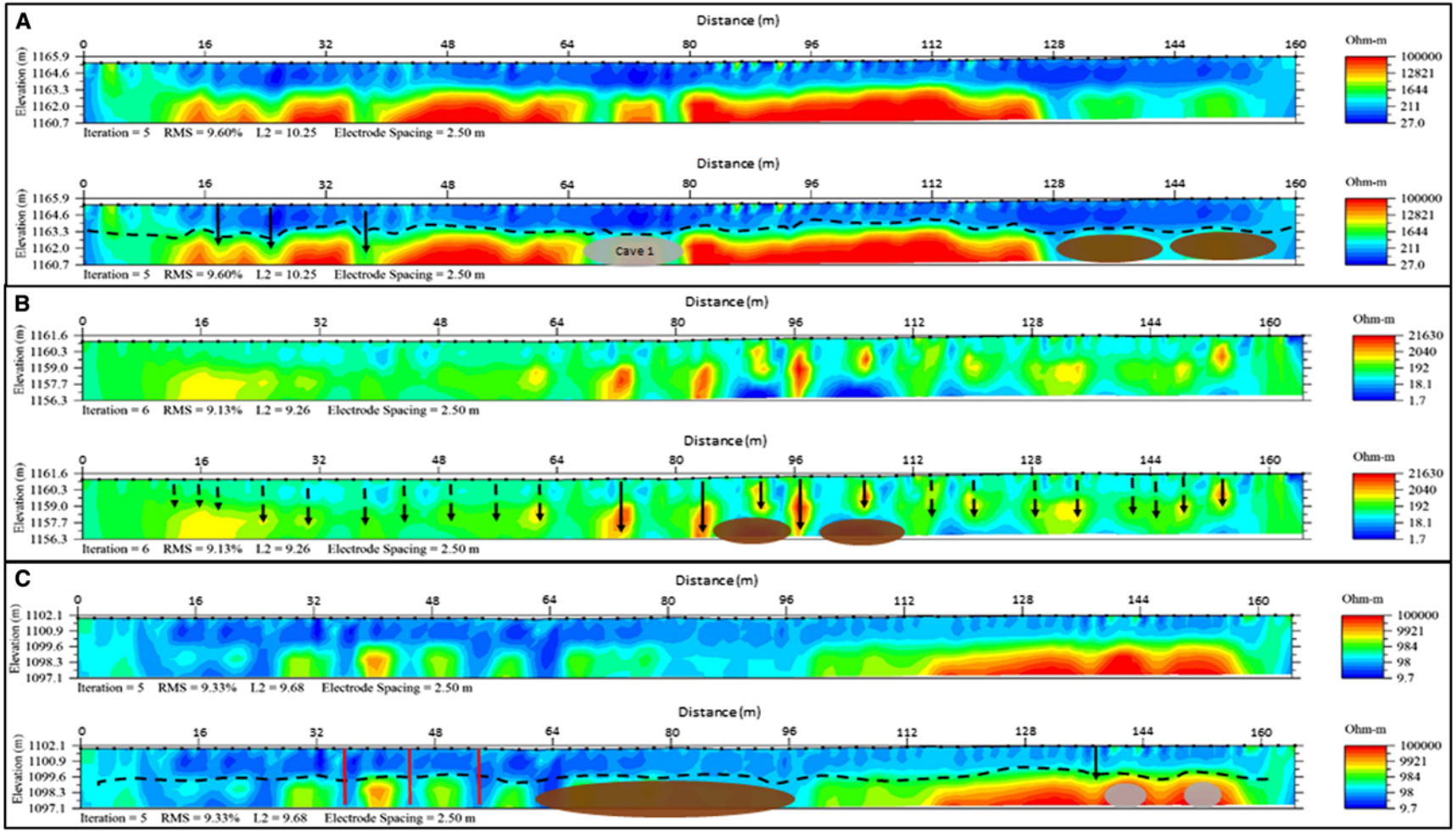

Figure 4. Resistivity inversion profiles displayed at a 2:1 vertical to horizontal scale. (A) Site 1 inverted and interpreted section. RMS error = 9.60%, iteration = 5 (black dashed line is the soil–rock contact, black arrows are solution conduits, brown polygons are leached zones, and gray polygon is Cave 1); (B) Site 2 inverted and interpreted section. RMS error = 9.13%, iteration = 6 (black solid arrows are solution conduits, black dashed arrows are soil piping, and brown polygons are filled sinks); C) Site 3 inverted and interpreted section. RMS error = 9.33%, iteration = 5 (black dashed line is soil–rock contact, black arrows are solution conduits, red lines are fractured rock, brown polygon is filled sink, and gray polygons are cave locations).

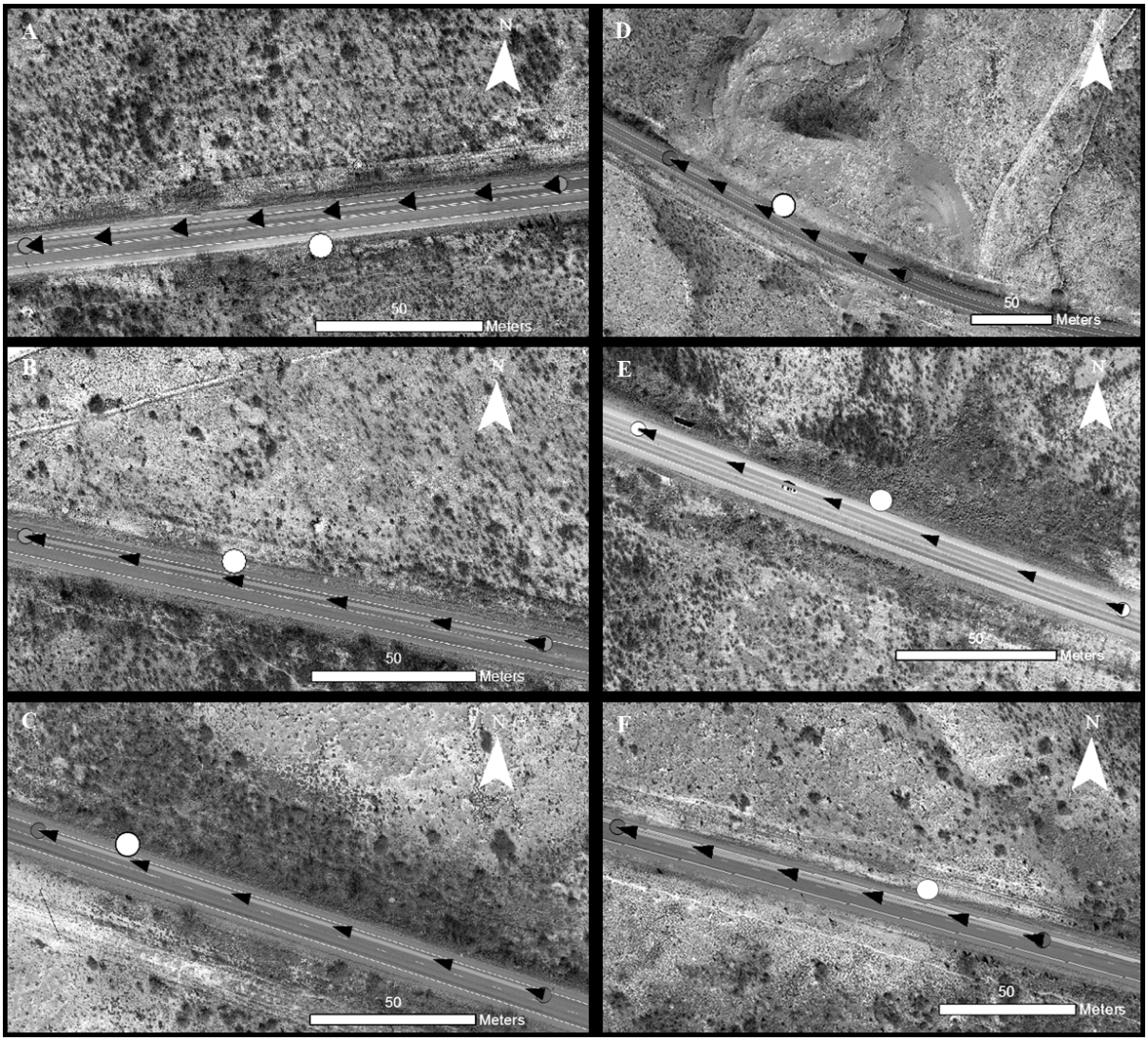

Figure 5. Excavation locations are marked by the circle, survey path is marked by black arrows which indicate survey direction, and the scale bars represent 50 meters on the surface. (A) Study Site 1; (B) Study Site 2; (C) Study Site 3; (D) Study Site 4; (E) Study Site 5; and (F) Study Site 6.

contact, but it does indicate areas of soil piping and water retention. The differential dissolution of gypsic soil used in the original roadbase construction exhibits preferential soil piping. This piping enhances degradation of infrastructure and can lead to a higher soil-moisture retention, which promotes disaggregation of asphalt at the surface (Fig. 6E).

Study Site 6 (160 meter segment)

Study Site 6 was chosen because of a trend of anomalous patterns observed in previous excavations that matched solution conduits, fractured rock, filled sinks, and cave locations (Fig. 5F; Fig. 7C). Surface expressions of solution conduits populated this road segment and are indicated in the resistivity profile below. These surficial karst features allow for suffosion processes to remove surface sediments and, in this case, the road itself (Fig. 6F).

KARST PHENOMENA DISCUSSION

Karst topography throughout the Gypsum Plain develops through natural processes that can be intensified by anthropogenic structures. Karst terrains commonly display complex systems that communicate between geomorphological, hydrogeological, and stratal diagenesis (Stafford and others, 2008). Suffosion processes dominate regions of dense karst geohazard potential and are most likely connected to deeper karst features that allow fluid and sediment transport. During monsoon seasons, heavy rain events dissolve highly susceptible

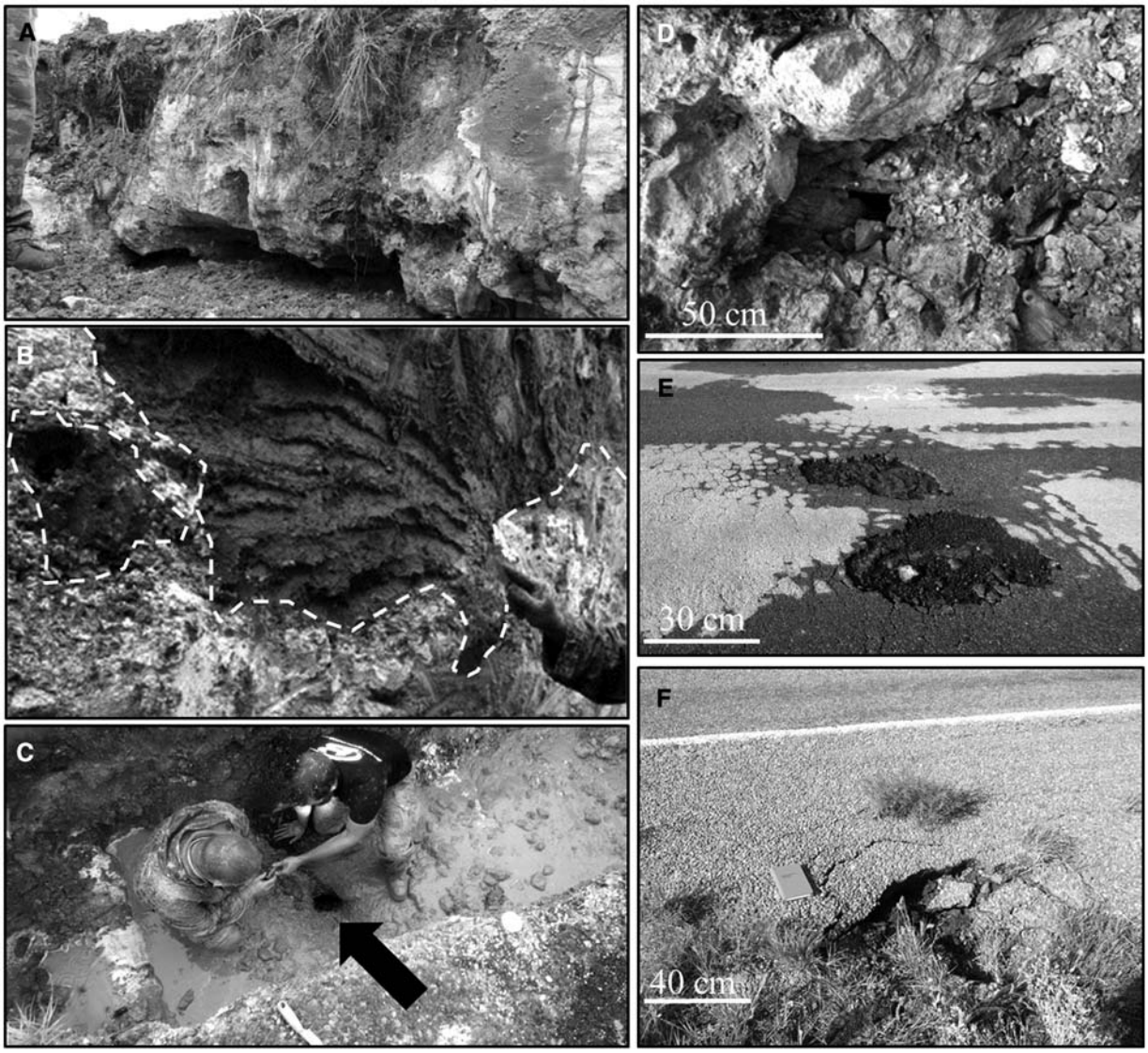

Figure 6. (A) Photo of "Cave 1" at Study Site 1 partially filled with soil and extending directly beneath RM 652; (B) photo of filled sink feature along with preferential soil piping at Study Site 2 outlined by the white dashed lines; (C) photo of solution conduit likely enhanced by anthropogenic structures is indicated by the black arrow at Study Site 3; (D) photo of brecciation at Study Site 4 exhibiting pathways of preferential fluid flow throughout collapse feature; (E) photo of roadway failure along survey path induced by soluble nature of gypsic road base at Study Site 5; and (F) photo of a solution conduit expressed at Study Site 6; features such as this express themselves along the roadway as a result of dissolution and suffosion.

evaporite rocks and widen solution fractures in gypsum bedrock. This solutional widening leads to greater suffosion piping rates of gypsic soil and induces failures, along with subsidence, under the margins and traverse path of the road within the study area.

Anthropogenically enhanced karst features are largely because of traditional road-construction techniques during infrastructure development and subsequent maintenance stages. In areas along the road, complex resistivity profiles correlated well with areas containing a concrete "toe wall" and retention-berm emplacement, despite their purpose to redirect flow away from the thoroughfare. Instead of maintaining roadway integrity, these practices caused water to preferentially infiltrate into the highly soluble, gypsic road-base materials, dissolving the high gypsic content, allowing for focused flow paths to form and increase permeability. This gradual increase in flow, coupled with heavy traffic, can accelerate dissolution of gypsum bedrock and suffosion, causing void geohazards to manifest, leading to collapse and road failure.

In survey locations such as Study Site 2 and Study Site 5, where the road has been elevated with gypsic soil fill,

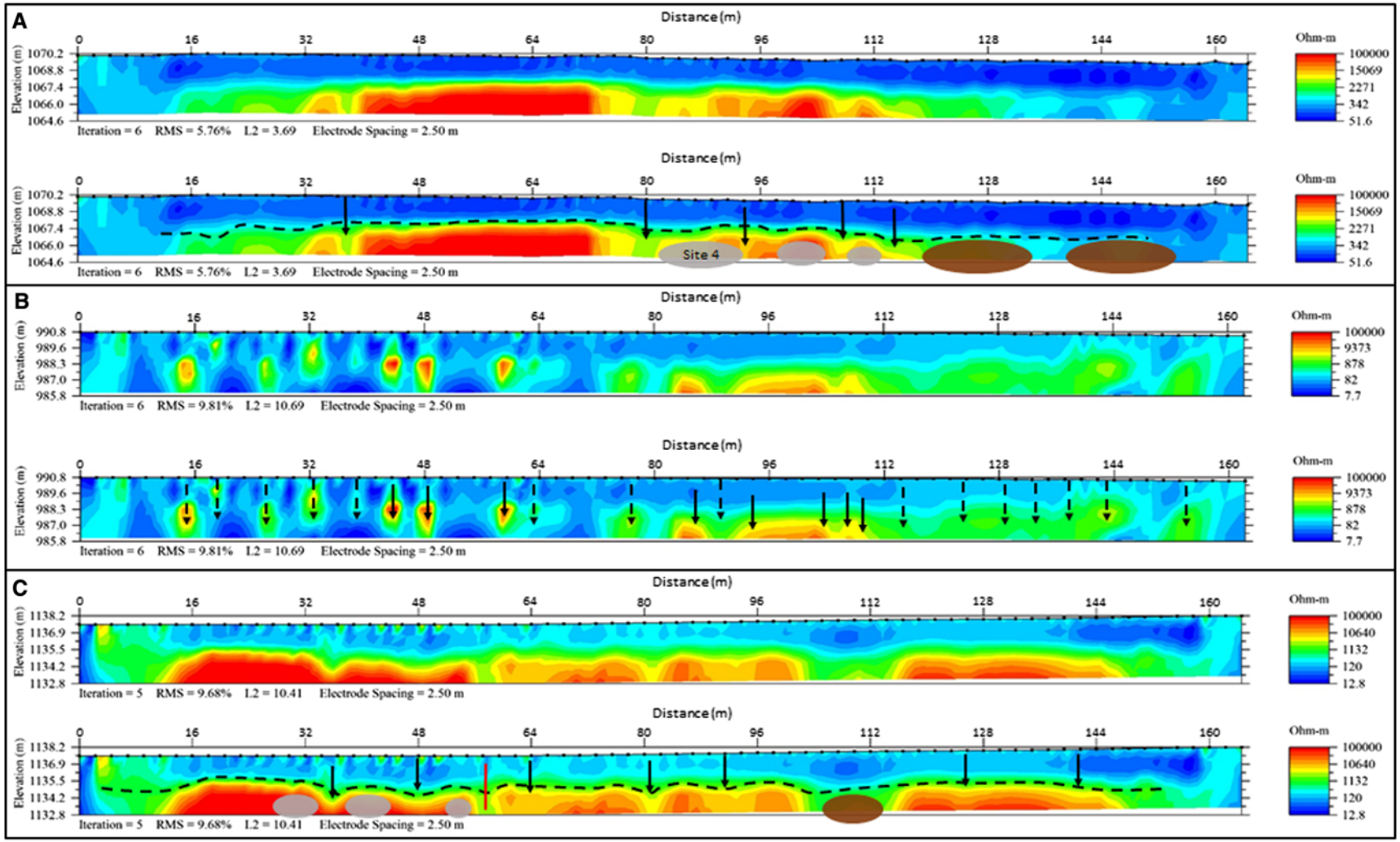

Figure 7. Resistivity inversion profiles displayed at a 2:1 vertical to horizontal scale. (A) Site 4 inverted and interpreted section. RMS error = 5.76%, iteration = 6 (black dashed line is soil–rock contact, black solid arrows are solution conduits, brown polygons are road fill, and gray polygons are breccia-tion); (B) Site 5 inverted and interpreted section. RMS error = 9.81%, iteration = 6 (black solid arrows are solution conduits, and black dashed arrows are soil piping); (C) Site 6 inverted and interpreted section. RMS error= 9.68%, iteration = 5 (black dashed line is soil-rock, brown polygons are road fill, and gray polygons are solution conduits).

the soil–rock contact is not seen in resistivity profiles. However, significant piping and frequent sinks are found in areas where gypsic roadbase is abundant. These features lead to an increase in subsidence that can be seen on the surface, especially during rain events when water ponding occurs. Profiles containing greater gypsic soil than bedrock tend to have lower resistivity readings, but this is most likely because of soil water retention, which continues to weaken the road above it.

Surveys containing soil–rock contact layers show signs of significant dissolution and degradation of gypsum bedrock. Study Sites 1, 3, and 6 contain signature

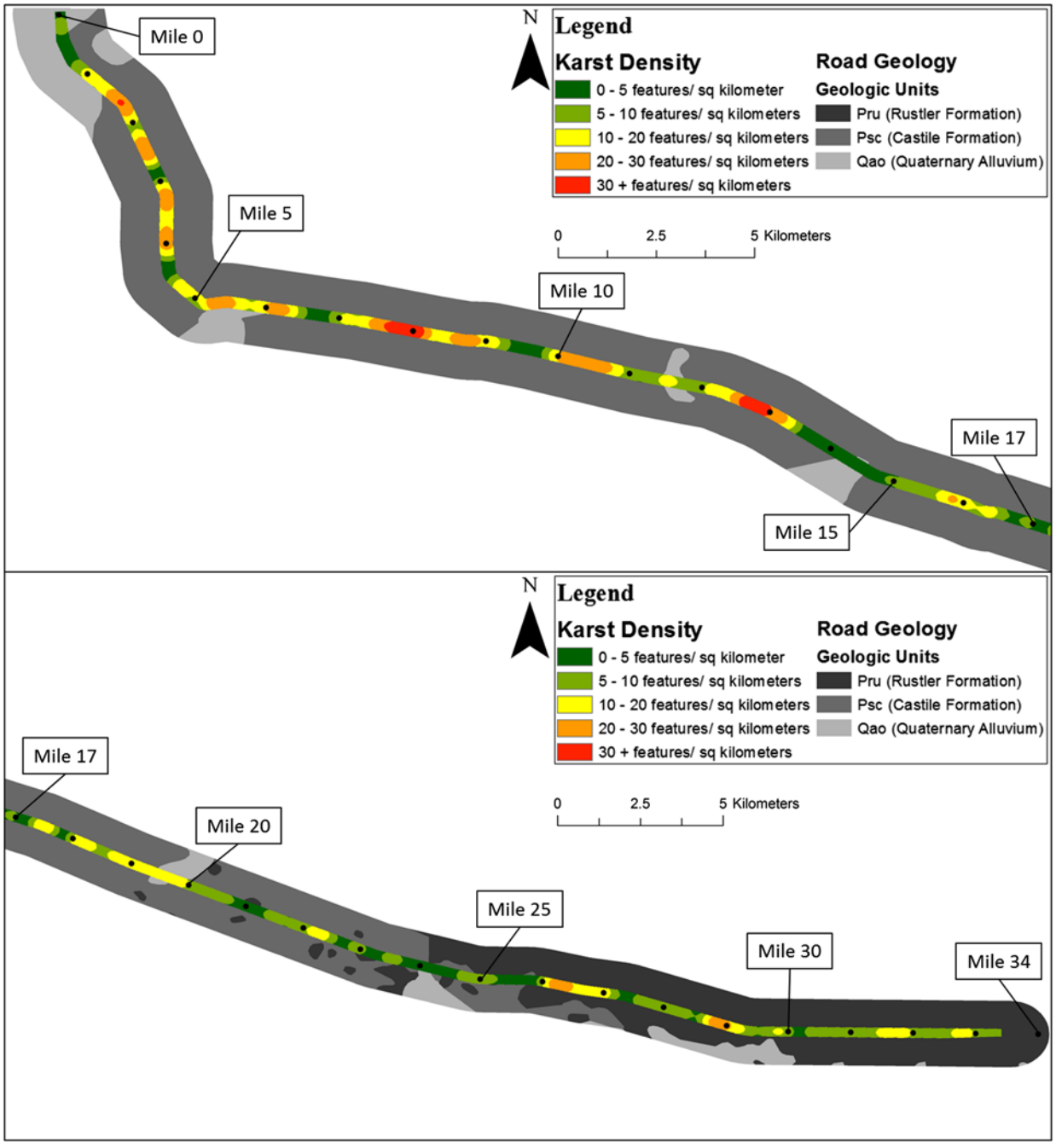

Figure 8. Maps of the study area illustrating the spatial density of karst phenomena delineated by "CCR" methods and the geologic formations associated with karsting. The density was measured by calculating the occurrence of individual geohazards per square kilometer. **Top)** Contains the beginning of the study area where RM 652 intersects US highway 62/180 and ends at TxDOT reference mile marker 17. **Bottom)** begins with TxDOT reference mile marker 17 and ends at TxDOT reference mile marker 34.

anomalies that match surface expressions of fractured gypsum bedrock that are solutionally widening. These fractures enable greater fluid migration, contributing to proximal suffusion processes and formation of caves under the roadway. At Study Site 1, the excavation location was on the opposite side of the road from the interpreted resistivity profile, which was chosen to illustrate karst-feature communication under the road through a network of passageways.

Zones of brecciation are common throughout the Castile Formation; however, they vary in their origin. Blanket breccias frequently occur laterally over wide regions as thin layers, while breccia pipes are vertically extensive but laterally limited (Stafford and others, 2008). A roadcut at Study Site 4 exposes a breccia pipe that is represented as a topographic high, with abrupt changes in resistivity occurring along the margins of the roadcut. While the cores of these features appear well-cemented, high permeability appears to be dominant along the margin of breccia pipes. Further dissolution and collapse of brecciated zone margins will lead to increased piping and fracturing, allowing for a perpetuating cycle of increased dissolution at these locations along RM 652.

The karst-density distribution along the study area varies according to geologic properties of shallow rocks and anthropogenic enhancements perpetuating suffusion and dissolution. These destructive geologic features predominate on the western side of the study area, where the Castile Formation crops out (Fig. 8). Individual geohazards delineated through "CCR" methods are most likely underestimated, compared with the total amount of existing features. Therefore, a statistical analysis was executed based on hazard density to achieve a more accurate representation of geohazard occurrences. Karst development typically suggests a fractal pattern where positioning of large-scale phenomena perpetually repeats at smaller scales (Stafford and others, 2016).

CONCLUSION

Karst features pose a significant threat to infrastructure within the Delaware Basin. The 54-kilometer-long segment of RM 652 that traverses Culberson County is experiencing severe degradation because of differential compaction and dissolution of soluble soil/rock in the subsurface, preferential piping of roadbase material, and general suffosion processes. Furthermore, traditional engineering techniques used to control surface-water drainage have enhanced the formation of karst in the study area. Numerous karst surface expressions have been surveyed along the study area and in adjacent private properties (Ehrhart, 2016). Large sinks, solutional fractures, and caves are forming a network of conduits throughout the study area, which enhance subsurface fluid flow along with road failure. Field excavations confirm capacitively coupled resistivity to be a successful noninvasive method in locating significant karst features, while being a cost-effective and time-efficient method to cover long distances. These 2D resistivity surveys, along with hydrogeologic knowledge of the area, were crucial in interpretation and characterization of the study area.

The use of noninvasive, geophysical methods to characterize subsurface phenomena, such as karst, should be used to aid in development and maintenance of infrastructure. This method can provide insight into significant problems in the subsurface that could otherwise remain undetected and cause catastrophic failure and financial burden.

ACKNOWLEDGMENTS

This research was partially funded by the Texas Department of Transportation (TxDOT), with support from the Department of Geology at Stephen F. Austin State University. The authors are thankful for the generous field assistance of individuals that made this work possible: Aaron Eaves, Adam Majzoub, and Niko Welch. Appreciation is expressed to Melinda Faulkner for her review of this manuscript and helpful contributions to its improvement.

REFERENCES CITED

Adams, J.E., 1962, Foreland Pennsylvanian rocks of Texas and eastern New Mexico, *in* Branson, C.C., ed., Pennsylvanian system in the United States: American Association of Petroleum Geology, Tulsa, OK, p. 372-384.

AGI, 2007, Instruction Manual for EarthImager 2D Resistivity and IP Inversion Software: Austin, TX, Advanced Geosciences, Inc., 139 p.

Ehrhart, J.T., 2016, Speleogenesis and delineation of megaporosity and karst geohazards through geologic cave mapping and LiDAR analyses associated with infrastructure in Culberson County, Texas: unpublished MS thesis, Stephen F. Austin State University, 148 p.

Garman, K.M., and Purcell, S.F., 2004, Applications for Capacitively Coupled Resistivity Surveys in Florida: The Leading Edge, Vol. 23, No. 7, p. 697-698.

Geometrics, 2001, Geometrics Operation Manual: OhmMapper TR1, 29005-01, Rev. F. 134 p.

Geometrics, 2016, OhmMapper: <http://www.geometrics.com/geometrics-products/geometrics-electro-magnetic-products/ohm-mapper>. Accessed December 13, 2016.

Hentz T.F., and Henry, C.D., 1989, Evaporite-hosted native sulfur in Trans-Pecos Texas: Relation to late-phase Basin and Range deformation: Geology, Vol. 17, p. 400-403.

Hill, C.A., 1996, Geology of the Delaware Basin, Guadalupe, Apache and Glass Mountains: New Mexico and West Texas: Permian Basin Section – SEPM, Midland, TX, 480 p.

Neukum, C., Grutzner, C., Azzam, R., and Reicherter, K., 2010, Mapping buried karst features with capacitive-coupled resistivity system (CCR) and ground penetrating radar (GPR): Advances in Research in Karst Media, p. 429-434.

Ross, C.A., 1981, Pennsylvanian and Early Permian history of the Marathon Basin, West Texas, *in* Pearson, B.T., ed., Marathon-Marfa region of West Texas: Permian Basin Section – SEPM, Guidebook 81-20, p. 135-144.

Samyn, K., Mathieu, F., Bitri, A., Nachbaur, A., and Closset, L., 2014, Integrated geophysical approach in assessing karst presence and sinkhole susceptibility along flood-protection dykes of the Loire River, Orléans, France: Engineering Geology, Vol. 183, p. 170-194.

Sares, S.W., 1984, Hydrologic and geomorphic development of a low relief evaporite karst drainage basin, southeast New Mexico: unpublished MS thesis, University of New Mexico, 123 p.

Scholle, P.A., Goldstein, R.H., and Ulmer-Scholle, D.S., 2004, Classic Upper Paleozoic reefs and bioherms of West Texas and New Mexico: New Mexico Institute of Mining and Technology, Socorro, NM, 166 p.

Stafford, K., Nance, R., Rosales-Lagarde, L., and Boston, P., 2008, Epigene and hypogene gypsum karst manifestations of the Castile Formation: Eddy County, New Mexico and Culberson County, Texas, USA: International Journal of Speleology, Vol. 37, p. 83-98.

Stafford, K.W., Brown, W., Ehrhart, J., Majzoub, A., and Woodard, J., 2016, 2016 Karst Geohazard Characterization of RM 652: Phase Two of Karst Development and Geohazards Associated with RM 652 in Culberson County, Texas: Report to El Paso District Office of Texas Department of Transportation, 94 p.

Tóth, J., 1999, Groundwater as a geologic agent and overview of the causes, processes, and manifestations: Hydrogeology Journal, Vol. 7, p. 1-14.

Vadillo, I., Benavente, J., Neukum, C., Grutzner, C., Carrasco, F., Azzam, R., Liñán, C., and Reicherter, K., 2012, Surface geophysics and borehole inspection as an aid to characterizing karst voids and vadose ventilation patterns (Nerja research site, S. Spain): Journal of Applied Geophysics, doi: https://doi.org/10.1016/j.jappgeo.2012.03.006.

White, W.B., 1988, Geomorphology and hydrology of karst terrains: Oxford University Press, New York, 464 p.

Speleogenetic Model of Evaporite-Karst Occurrences of the Gypsum Plain Using Karst Mapping and LiDAR Analyses in Culberson County, Texas, USA

Jon T. Ehrhart and Kevin W. Stafford
Department of Geology, Stephen F. Austin State University,
Nacogdoches, Texas

ABSTRACT.—The Gypsum Plain of the Delaware Basin hosts approximately 1800 km^2 of Castile Formation outcrop with extensive evaporite-karst development. Karst studies on the distribution and speleogenetic evolution of Castile strata began within the last decade with ever-increasing data resolution. This study combines physical field surveys with the analyses of high-resolution (~30-cm accuracy) LiDAR data to create a karst model across the region. The idealized model considers speleogenesis (hypogene and epigene), density of karst features, lithology, and connection between the local hydrostratigraphy and regional hydrogeology. Field studies involved physical mapping of 20 km^2 of the Gypsum Plain from the Castile's western outcrop to where it dips into the subsurface to the east, including the documentation of surfically expressed karst phenomena and mapping of all enterable caves for morphological assessment. Hypogene and epigene caves are surfically expressed across the region and indicate that many caves have been affected by multistage epigenetic development or multistage hypogenetic development with epigenetic overprinting. LiDAR data were processed to create digital-elevation models (DEM) and to determine the effectiveness/accuracy of field surveys compared to remote-sensing techniques. Previous works in the area determined that remote sensing preserved roughly 36% of all karstic features found through physical field surveys. However, because of the advancements in remote-sensing accuracy, this study determined that on average, LiDAR analysis allows for the identification of almost seven times more karstic features than physical surveys over a given area.

INTRODUCTION

The Gypsum Plain of west Texas hosts a plethora of karstic exposures that have only recently been investigated in detail within the last decade (Stafford, 2008a, b). The area has been affected by significant dissolution throughout geologic history which has resulted in the formation of a highly karstic and cavernous landscape. The larger and more famous carbonate caves of the Capitan Formation, such as Carlsbad Caverns and Lechuguilla Cave to the north, have been extensively studied because of their largely complex and expansive cave systems. The widespread evaporite karst of the Permian Gypsum Plain has traditionally been overlooked and generally understudied. This is despite the fact that karst features of the Delaware Basin provide some of the most prominent displays of gypsum karst in North America. Within the Delaware Basin, the primary formation that hosts cavernous porosity is the soluble gypsum and anhydrite of the Castile Formation. Because of the highly soluble nature, the Castile Formation has undergone a significant amount of dissolution for deposition and contains extensive cave and karst features (Stafford and others, 2008b). The caves found within the Castile Formation formed by both epigene and hypogene processes; however, understanding the timing of when each dissolution process affected the Castile can be difficult, as many hypogene caves have been heavily overprinted by epigene processes. Throughout the Castile, karst features vary from surficial karren, sinkholes, and solution breccias to large complex caves that have been affected by multiple processes (Stafford, 2008a). The objective of this study is to improve evaporate-karst characterization within the Delaware Basin by creating an idealized karst

Ehrhart, Jon T.; and Stafford, Kevin, 2021, Speleogenetic Model of Evaporite-Karst Occurrences of the Gypsum Plain Using Karst Mapping and LiDAR Analyses in Culberson County, Texas, USA, *in* Johnson, K. S.; Land, Lewis; and Decker, D. D. (eds.), Evaporite Karst in the Greater Permian Evaporite Basin (GPEB) of Texas, New Mexico, Oklahoma, Kansas, and Colorado: Oklahoma Geological Survey, Circular 113, p. 189–200.

model. This model provides a look at the variability in speleogenetic evolution and the hydrologic framework that exists across the Gypsum Plain in relation to the geomorphic landscape.

Study Area

Located in the Delaware Basin, the study area sits atop an extremely large depocenter where over a billion years of the rock record is preserved, ranging from the 1.3 by old Precambrian basement to the less than 10,000 ybp Holocene sediments (Hill, 1996). The Delaware Basin is bound on its periphery by a series of exposed reef structures: to the west by the Apache Mountains, to the north by the Guadalupe Mountains, to the south by the Glass Mountains, and to the east by the Central Basin Platform. The large Gypsum Plain that encompasses the area is primarily blanketed by the Ochoan Castile and Rustler deposits at the surface (Fig. 1). Specifically, this study focuses on the northern part of Culberson County, Texas, extending ~35 km south of the New Mexico border and 50 km west to east across the Castile outcrop region, encompassing the region of Ranch to Market Road (RM) 652 (Fig. 1). The study area was selected as a representative subsection of the Gypsum Plain to investigate the variations in karst development in line with stratal dip that trends west to east.

Physiographically, the study area is located on the eastern edge of the Basin and Range province and northern edge of the Chihuahuan Desert. The Trans-Pecos region is primarily a desert/semiarid environment with scant precipitation, rapid evaporation, moderate winters, and afternoon showers in spring months. The Gypsum Plain receives less than 300 mm of precipitation per year (Beuchner, 1950), where average temperature is less variable than the rainfall, with mean summer temperatures ranging from 24°C to 30°C; however, temperatures can reach upwards of 38°C.

Geologic Setting

Late Permian sequences in the Delaware Basin are divided into two main series: Guadalupian Series (271–260 mya) and Ochoan Series (260–251 mya) (Adams, 1965) (Fig. 2). The Guadalupian Series represents deposition of a thick, clastic, basin-filling facies with approximately 900–1200 m of total sediment (Hills, 1984). During this time, the periphery of the basin was dominated by reef growth where the reef crest rose approximately 500 m above the basin floor. The central part of the basin was dominated by sandstones and siltstones, the marginal areas by limestone deposits, and the backreef formed evaporite lagoons (Adams, 1965). Continued subsidence provided accommodation space for the central basin formations such as the Cherry Canyon, Brushy Canyon, and Bell Canyon to be deposited. These formations represent the clastic-dominated, primarily terrigenous, sediments that were deposited during episodic sea-level fluctuations during the Guadalupian when shelf environments were subaerially exposed (Scholle and others, 2004). In the closing stages of the Guadalupian, the Permian Basin became relatively tectonically stable and

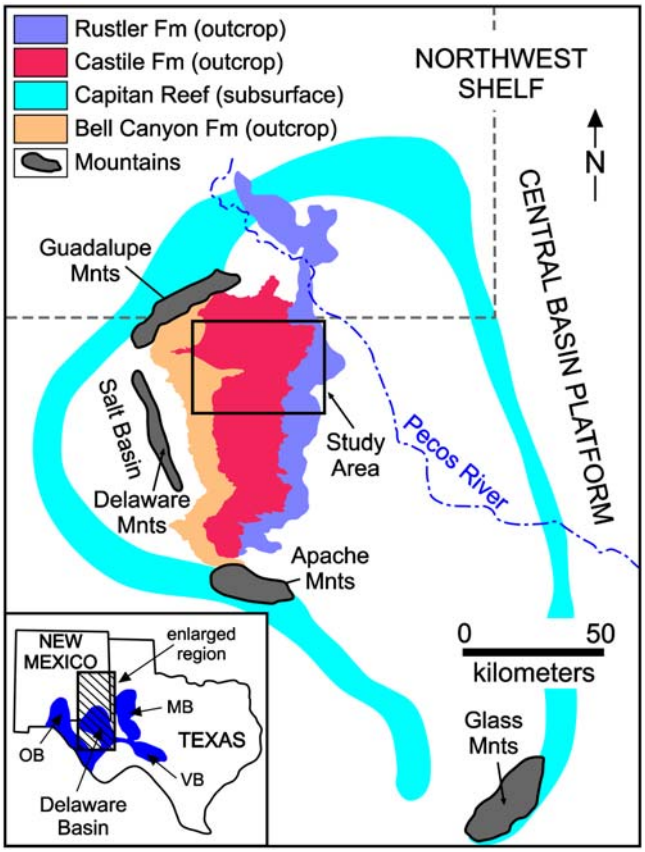

Figure 1. Regional map displaying the generalized location of Permian strata outcrops within the Gypsum Plain and study area outlined (modified from Stafford and others, 2008a).

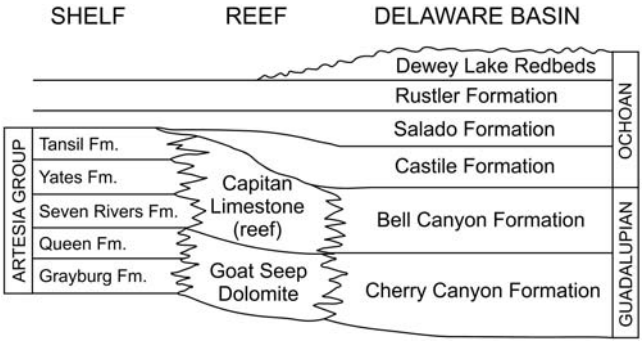

Figure 2. Stratigraphic section from the Shelf (North) to Delaware Basin (South) of lithologic units within the study area (adapted from Scholle and others, 2004).

carbonate sedimentation was terminated (Adams, 1965). Scholle and others (2004) postulate that this is largely due the increased basin restriction that began near the end of the Guadalupian.

Following the Guadalupian, Ochoan evaporite formations were deposited (260–251 mya). Although there are many controversial aspects regarding the exact depositional mechanisms that affected the Delaware Basin at the onset of the Ochoan (Kirkland, 2003), it is widely accepted that continual restriction of evaporite seas from the open ocean resulted in deposition of the first phase of evaporite filling within the Delaware Basin. This closure marks the onset of Ochoan time and the commencement of Castile Formation deposition, which reaches approximately 550 m in thickness in the northern basin (Scholle and others, 2004). The Castile consists of millimeter-scale interbedded laminae of gypsum, anhydrite, organic matter, and calcite. Interbedded layers have been interpreted as varves and represent seasonal salinity fluxes (Scholle and others, 2004). The distinct characteristic of large-scale laterally continual laminations and a lack of shallow water sedimentary structures suggest that the Castile was deposited in deep water that ultimately filled the entire basin (Scholle and others, 2004).

The Castile Formation grades conformably into the Salado which extends far beyond the margins of the Delaware Basin and crosses the Guadalupian reef and shelf facies forming an unconformity boundary (Kelley, 1971; Hill, 1996). The Salado Formation contains laminated halite, anhydrite, sylvite, other evaporites, and minor amounts of siliciclastic material, but does not generally appear in outcrop throughout the Delaware Basin because of its highly soluble nature (Scholle and others, 2004). Rustler strata cap Salado deposits and mark the final evaporite sequence deposited during the Ochoan. During this time, sea-level incursion and subsequent transgressions and regressions deposited cyclic layers of large-scale limestone–dolomite and anhydrite–gypsum deposits (Hill, 1996).

Following Ochoan time, the Delaware Basin began to shift from a marine sedimentation depocenter to a positive area dominated by clastic sedimentation. During the late Cretaceous to early Tertiary, the Laramide Orogeny permanently uplifted the region above the sea level (Hill, 1996), tilting the Delaware Basin eastward approximately 3–5° and elevating it 1.2 km above the sea level on the western side, where it remains today (Horak, 1985). Subsequent to the Laramide uplift, Basin and Range extension commenced and lasted from 30 mya to present, producing conjugate jointing and fault sets oriented approximately N75E and N15W throughout the Gypsum Plain (Nance, 1993). Many of the karstic developments within the Gypsum Plain have been a product of these conjugate fractures as well as Quaternary climate change. During the middle-to-late Pleistocene, the climate in the Delaware Basin alternated between drier and warmer periods to colder and moister periods (Hill, 1996). Today, the Gypsum Plain has transitioned back into an arid, dry climate. However, because of the highly soluble nature of the Gypsum Plain, the current landscape displays many geomorphic traces of its previously wetter history.

METHODOLOGY

To characterize karst evolution across the Gypsum Plain, traditional cave surveys were coupled with remote-sensing analyses to investigate the spatial distribution of karst features and to assess the hydrogeological controls on speleogenesis. Spatial analyses of solutional conduits were accomplished through traditional cave mapping, overland surface mapping, and the analyses of remote-sensing LiDAR data (Light Detection and Ranging). Data collection and analyses were focused proximal to roads within the study area in conjunction with a large geohazard characterization project by the Texas Department of Transportation. Traverse-based surveys were conducted across the Gypsum Plain from west to east in northern Culberson County. The survey area ran along a 55-km stretch of RM652 within 100 m of the right of way. The 13.1 km^2 of total surface survey was conducted at 20-m traverse spacing, and all karst features identified greater than 10 cm in diameter were recorded and classified in the field. All caves discovered large enough for human entry were entered and mapped using standard cave surveying techniques. Morphometric features and lithologic variations were noted within surface surveys and cave maps to assist in speleogenesis assessment.

LiDAR data used for this study included approximately 20 km^2 of data acquired in approximately 300-m wide swaths along RM652 in northern Culberson County. Data have an average horizontal resolution of ~30 cm and vertical resolution of 10 cm for bare earth LiDAR returns. From these data, the delineation of sinkholes was accomplished through the processing of "fill-difference" digital elevation models (DEMs) to identify areas topographically lower than the surrounding land surface. All sinkhole features less than 10 cm in depth were removed, as they fell below the resolution of data. However, depressions associated with roadway construction and other man-made features such as ponds were also identified through LiDAR processing; these anthropogenic/nonkarst features were removed manually. Final data reduction resulted in a map that contains natural sinkholes (i.e., karst features) as determined by LiDAR analyses. Density plots were calculated based on some features per square kilometer to interpret lateral variability in regional karst development.

KARST MORPHOLOGY

The presence of both hypogene and epigene karst development has been documented throughout the Gypsum Plain (Stafford and others, 2008a). The caves identified in this study display morphologies indicative of both multistage epigenetic and multistage hypogenic development with epigenetic overprinting. Epigenetic caves tend to be solutionally entrenched and strongly controlled by fractures, whereas hypogene manifestations are driven by proximity to lithologic variability and are expressed as larger voids. In addition to surface dissolution (sinkholes, shallow caves, and depressions), more evidence of extensive dissolution can be seen throughout the study area in the form of diagenetic alterations (e.g., intrastratal brecciation and evaporite calcitization). The following examples of karst development are not intended to be an exhaustive list of all caves identified in this study; instead, they are provided as representative examples to showcase the variation in karst development across the Gypsum Plain.

Epigene Karst

Epigene cave development within the study area is divided into two main categories, vadose and phreatic morphologies. In this study, several of the cave systems identified displayed morphologic features indicative of epigene development. Epigene caves that formed within the vadose zone are expressed largely as fracture-oriented conduits dominated by increased entrenchment and abundant small-scale scallops. Morphologically, vadose caves maintain relatively narrow passage apertures (relative to height) and are generally laterally limited to 10s of meters in length, as illustrated in Nikad Cave and JC Gypsum Hole (Figs. 3A and 3B) in this study. Nikad Cave is associated with an entrenched 40-m-long, 30-m-wide arroyo and a 2500-m^2 watershed. The entrance is 1 m wide within laminated gypsum bedrock and the cave is humanly passable for 28 m as a single, relatively straight, horizontal passage. Passage width tapers from 1 m wide at its entrance to less than 30 cm wide at the end of the survey. JC Gypsum Hole exhibits a similar morphology, with an inward reducing aperture and increased entrenchment along a fracture that trends along the cave ceiling (Fig. 4F). It is 35 m long and drains a watershed covering 10,000 m^2. As these caves form and water originating as overland flow becomes saturated, the solutional aggressivity is reduced. Lateral cave development is reduced, as saturated fluids recharge along fracture planes. This geomorphic expression in vadose epigene caves (quickly reducing aperature) is consistent with the dissolution characteristics of sulfates (Klimchouk, 2000).

Death Tube Cave and Lillcher Cave are complex multistage epigenetic caves formed originally in the phreatic zone, but later exposed to vadose overprinting (Figs. 3C and 3D). Death Tube Cave is a classic example of an epigene phreatic tube overprinted by vadose processes with more than 200 m of low gradient passage development (Fig. 3C). The elliptical morphology of the majority of the cave indicates that its formation occurred when the water table was significantly higher than it is currently, and that the vadose overprinting observed is the result of local base level drop. Vadose entrenchment is much more significant within the first 30 m of the cave; entrenchment has not substantially affected the remainder of the cave where only small deviations from elliptical passages are present and passage floors are commonly armored with thick clay deposits (Fig. 4G). The known cave terminates in a sump, but throughout the low gradient passage, various "bathtub rings" of organic material are present, indicating that the majority of the cave remains in the epiphreatic zone, although vadose overprinting is active near the arroyo-entrenched entrance.

Lillcher Cave development began with preferential dissolution along fractures within the phreatic zone, forming a simple dendritic morphology of elliptical tubes with a surveyed length and depth of 116 m and 17 m, respectively, that terminates in a sump (Fig. 3D). Entrances and inlet tubes are morphologically comparable with phreatic tubes having formed initially as elliptical tubes that were later entrenched by vadose processes (Fig. 4D). The cave currently exhibits three entrances, all of which have been heavily entrenched. In the lower part of the cave, the most heavily entrenched passage serves as the junction of other major conduits. In this area, a room largely developed within gypsic soil attests to a period of intense vadose entrenchment in the past. Here, original void space was infilled with secondary sediments that were subsequently eroded to produce a cave chamber partially formed within both gypsum bedrock and gypsic soil. Upper parts of sinkhole entrances are composed of 1–3-m-thick sequences of gypsic soil that are being funneled into the entrances. It is probable that the room in the lower part of the known cave is another sinkhole entrance that was completely plugged by sediment in the past and subsequently infilled. Effectively, Lillcher Cave originally formed in the phreatic zone and was then exposed to vadose overprinting at some time in the distant past, likely during the Pleistocene, and subsequently infilled with gypsic soils/sediments during recent climatic shifts. Today, the system is equilibrating with the current climate and sinkhole fills are being piped into the cave. Thus, Lillcher Cave remains in a transitional vadose/phreatic environment, but exhibits evidence of at least two distinctively different episodes of vadose entrenchment.

Although soil piping is a common occurrence throughout the Gypsum Plain, the formation of suffosion

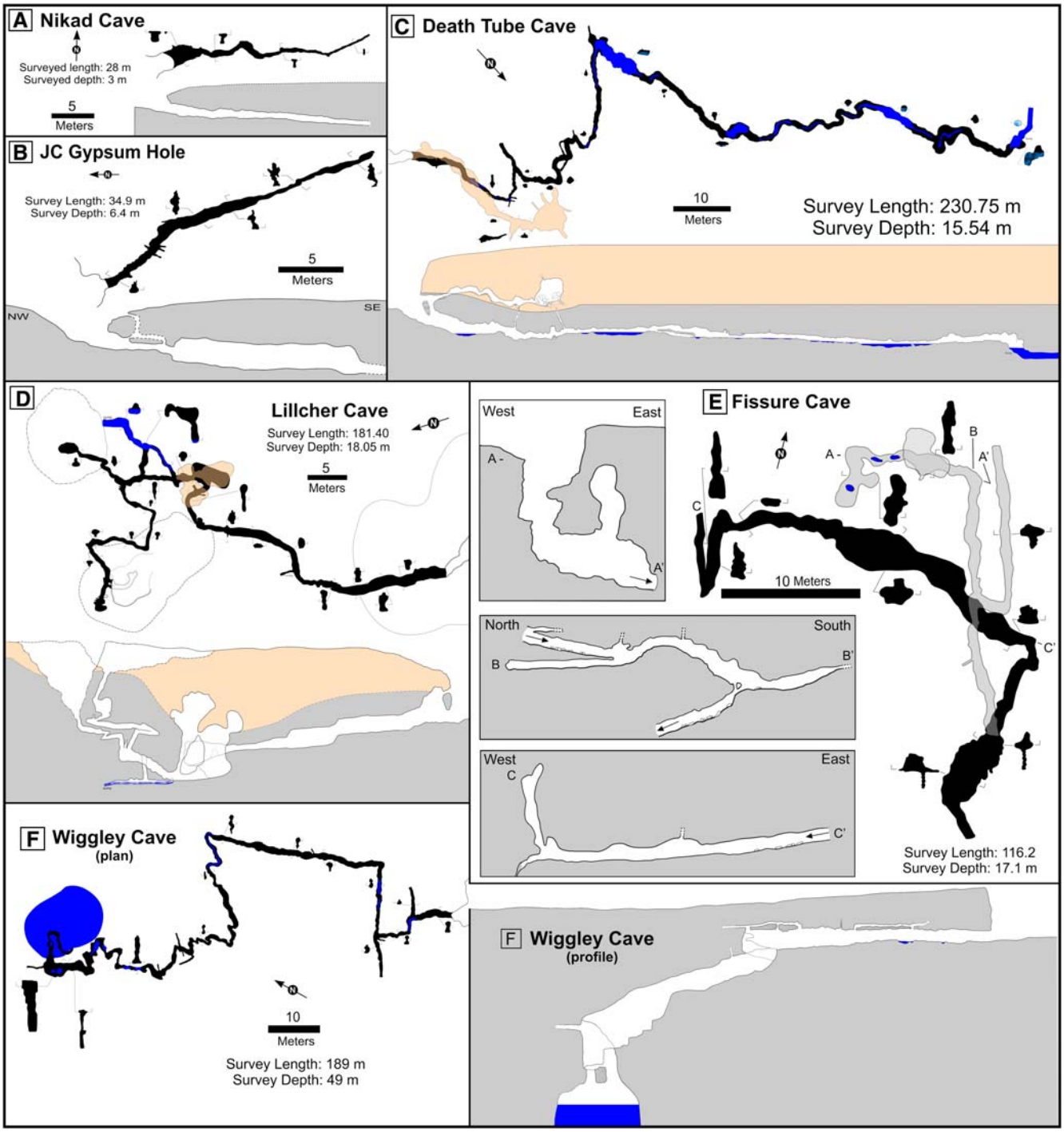

Figure 3. Simplified cave maps that represent typical epigene vadose (3A: Nikad and 3B: JC Gypsum Hole), epigene phreatic (3D: Lillcher and 3C: Death Tube), and hypogene (3F: Wiggley and 3E: Fissure) developments that were surveyed across the study area in both plan and profile views. Parts of Lillcher and Death Tube caves are suffosion features as represented in tan color in plan and profile views; blue indicates water at time of survey.

caves is the least documented occurrences of karst in the area. These caves form as small-to-large-scale sediment piping features and can exhibit much larger passages and spatial extent than previously thought. Filled sinks that are actively opening through suffusion (like those seen in Lillcher Cave) are not uncommon. The upper passage of Death Tube Cave formed along the bedrock/gypsic soil contact which acts as a significant differential permeability horizon. This horizontal contact is intercepted by vertical fractures that follow a similar trend to the lower

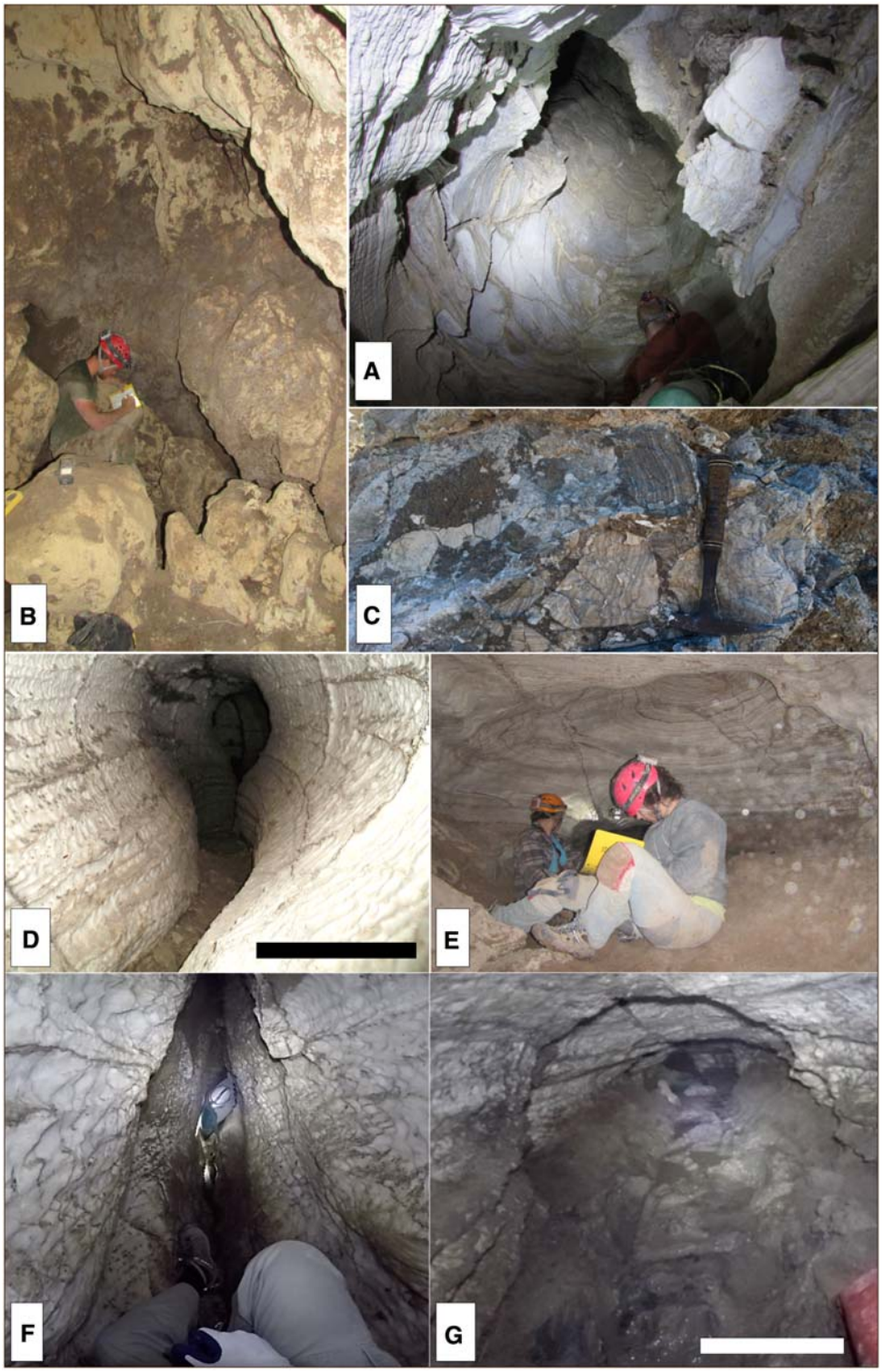

Figure 4. Epigenetic and hypogenetic morphological features found throughout the study area: (A) large hypogene dome (Fissure Cave); (B) soil suffosion chamber (Upper Death Tube Cave); (C) brecciated zone (Breccia Pipe); (D) phreatic tube overprinted by entrenchment (Lillcher Cave); (E) cupolas in relict passage (Fissure Cave); (F) epigene vadose entrenchment (JC Gypsum Hole Cave); and (G) elliptical phreatic tube (Death Tube Cave) Note: black and white bars represent 50 cm.

passage where suffosion products are being piped into. It is likely that this 40-m-long soil cave formed during backflooding events when fluids are injected laterally along the gypsum/soil contact at the entrance and vertically from fractures connecting soil and bedrock parts of the cave. Fluidization of partially lithified sediments resulted in upward stoping and soil cave formation (Fig. 4B) in the upper chamber of Death Tube Cave. A series of 25-cm-diameter inlet piping tubes in the soil cave ceiling follow a fracture and appear to have formed as small-scale piping features during normal precipitation events.

The examples above represent greater complexity of epigene cave development than has been previously documented in the Castile Formation. Significant epigene cave development within the phreatic zone has not been previously reported. In addition, prior to this study, extensive suffosion caves were unreported in this region. However, current research suggests that suffosion caves may extremely be common and can reach a significant size, provided that there is a sufficient outlet for the removal of insoluble clastic particles, either through a cave conduit as described above, or through highly fractured media.

Hypogene Karst

In contrast to epigene cave development, hypogenic caves form in semiconfined systems based on pressure and density gradients and are not directly associated with surficial processes during formation. As suggested by Klimchouk (2007), the identification of hypogene karst can be difficult because of the nature of their origin; hypogene caves can only be explored by cavers after they have been breached or decoupled from the environment in which they formed and commonly exhibit epigenetic overprinting. The primary criteria for identifying these hypogenetic features are the caves morphological expression and hydrostratigraphic position (Klimchouk, 2007). Hypogene caves likely comprise more than half of the total cave development throughout the Gypsum Plain, but surficial expression through surface denudation breaching is spatially limited (Stafford and others, 2008b). Although hypogenic caves are common across the Gypsum Plain, they are somewhat atypical of most reported hypogene manifestations (e.g., Klimchouk, 2007) in that complex maze caves are largely undocumented. Instead, single riser features are most prevalent.

In this study, several of the cave systems identified displayed morphologic features indicative of hypogene development. Fissure and Wiggley caves are typical hypogene features of the Gypsum Plain with morphologies composed primarily of large, single, ascending passages with numerous cupolas, ceiling channels, and domes which are indicative of ascending fluids (Figs. 3E and 3F). These cave examples occur on the western edge of the Gypsum Plain where the contact with underlying Bell Canyon clastics is less than 60 m. Although they are not the most extensive hypogene caves known in the Castile Formation, they share similar morphologic and hydrostratigraphic characteristics to much larger hypogenetic caves found within the area (Stafford and others, 2008a).

Wiggley Cave, similar to Border Cave in the proximal region (TSS, 2016), is 189 m long, 49 m deep, and gives access to a lower level lake room. The cave is heavily entrenched by vadose overprinting which forms a meandering canyonlike passage that ranges from 2 m tall near the entrance to over 15 m tall in the lower parts. The ceiling of Wiggley Cave remains level for extended sections as an elliptical tube with common cupolas connected by an undulating ceiling channel. In several sections, small pits occur which correlate directly with larger ceiling domes and show consistent morphologies of upward migrating fluids along the ceiling with subsequent vadose floor entrenchment. The lowest cave part descends from a dome pit into a lake room of indefinite depth and approximately 20 m in diameter. Anecdotal reports from divers of other similar lake rooms in the area indicated that these features can extend more than 40 m deep. Wiggley Cave was formed by ascending fluid sourced from the underlying Bell Canyon Aquifer as a large dissolution chamber formed near the Bell Canyon and Castile contact. In addition to the lake room, the cave exhibits a single riser tube that follows fracture planes. Once the surface was breached, vadose entrenchment significantly overprinted the cave and it currently has an associated watershed of approximately 60,000 m^2.

Fissure Cave has a surveyed length of 116 m and depth of 17 m (Fig. 3E), forming a multilevel and fracture-controlled hypogene cave that is moderately overprinted by vadose entrenchment. At Fissure Cave's inception, fractures provided pathways for ascending fluids with preferential lateral migration along soluble gypsum laminae. Lower level passages contain large domes and abundant cupolas. The majority of ceilings and walls are completely smooth from ascending waters in a sluggish flow regime (Fig. 4E). In upper parts of the cave, large domes extend more than 5 m as vertical risers (Fig. 4A) and it is probable that the entrance pit was simply the tallest of these domes and first to be breached by denudation. The cave exhibits minimal vadose overprinting in the entrance region which is comparable to the associated small drainage area of less than 3000 m^2. The lower parts of the cave exhibit solutionally widened fractures too small for human passage, but likely connect to additional hypogene chambers or conduits, and potentially a base-level lake similar to Wiggley Cave. Both Fissure and Wiggley caves exhibit vastly different morphologies when compared to their epigene counterparts. However, because of current epigene overprinting, the

recognition of specific morphometric features and analyses of the hydrogeologic environment were critical criteria assessed in determining speleogenesis.

In addition to cave development, the diagenetic alteration/dissolution of host strata is common in the Delaware Basin. Intrastratal dissolution commonly results in large-scale collapse horizons containing "blanket-dissolution breccias" in the Delaware Basin (Anderson and others, 1972). Lateral dissolution breccia forms, as halite interbeds are dissolved and overlying gypsum cannot be supported and collapses. Dissolution breccias can be traced across the basin and have been correlated with still present halite interbeds located in the subsurface in the eastern Delaware Basin (Anderson and others, 1978). In addition to lateral dissolution, vertical dissolution can form breccia pipes where ascending fluids drive dissolution through density convection. As void space is created at depth, overlying strata collapse into voids and upward stoping proceeds vertically, as additional dissolution and collapse enhance vertical brecciation (Fig. 4C) (Anderson and Kirkland, 1980).

SPELEOGENETIC MODEL OF THE GYPSUM PLAIN

Karst development varies from west to east across the Gypsum Plain in the direction of regional dip and stratal thickening. As shown in Fig. 5, this variation is present in the case of geomorphological differences, karst density (both epigene and hypogene), and proximity to differing lithologies. Along the western edge of the Gypsum Plain, the Castile Formation thins to nonexistence along the updip solutional margin. Moving from west to east, the Castile Formation progressively increases in thickness, as the unit dips into the subsurface, and is armored by overlying strata that prevent denudation.

Caves in the western Gypsum Plain, where the Bell Canyon is relatively close to the land surface, are typically expressed as hypogene caves with variable epigene overprinting. Because of the Laramide uplift, strata dips 3–5° east/northeast in the Delaware Basin (Lee and Williams, 2000) and groundwater recharge into basin clastics beneath Castile evaporites quickly shifts to a confined system with elevated hydraulic pressure. Locally, gypsum strata thickness in the western Gypsum Plain ranges from over 100 to 0 m where Bell Canyon outcrops and groundwater recharge occurs. However, valleys and topographic lows within the Gypsum Plain are commonly lower than surface exposures of Bell Canyon clastics, creating potentiometric lows within the system toward which confined fluids migrate. It is likely that potentiometric pressures are elevated in the western part of the study area where overland flow recharge into Bell Canyon clastics is the most intense because of the Delaware Mountains watershed. Consequently, hypogene caves are commonly documented throughout the western flank of the Gypsum Plain (Fig. 5). This is not to say that hypogene caves do not form further east; instead, it suggests that hypogene karst development is simply more aggressive in the western parts. It is probable that there is significant hypogene dissolution at the lower boundary of Castile strata throughout the region and hypogene caves simply appear more common in the west because of a greater incidence of breaching.

In addition to hypogene cave development, the presence of vertical breccia pipes further suggests the presence of significant upward fluid migration throughout the region. Lee and Williams (2000) suggest that these brecciated zones result from solutionally aggressive waters sourced from the Bell Canyon Aquifer that rise by density convection to create significant void space. The collapse of these deep-seated caverns then stope toward the land surface (Anderson and others, 1978). Unlike the hypogenetic caves, breccia pipes are surficially expressed throughout the study area as resistant topographic highs; they are surficial manifestations of deep-seated collapses that have stoped upward. Consistent with brecciated zones found in the study area, similar pipes have been documented to extend through the entire thickness of the Castile Formation in the central Delaware Basin (Hill, 1996). These breccia pipes support the concept that hypogene speleogenesis is active across the Gypsum Plain, but it is focused on the Bell Canyon/Castile contact. Because the Castile evaporites semiconfine the underlying clastic aquifers, hypogene karst development remains isolated from epigene karst until hypogene features are breached by surface denudation and transition into an epigene environment.

Relatively shallow epigene karst is widespread throughout the Gypsum Plain but most common in the eastern parts of the study area, where epigene processes have not been captured by breached hypogene caves. Breached hypogene caves that exhibit accelerated epigenetic overprinting are most common in the western part of the study area. In the central and eastern part of the Gypsum Plain, no shallow surficial expressions of epigene karst connected to larger hypogene occurrences were identified. Thus, these fracture driven caves are vertically restricted and display typical reducing apertures and moderate entrenchment commonly associated with pure epigene evaporite caves formed in the vadose zone (Fig. 5). However, moving even further east across the study area, caves are expressed as multistage epigenetic caves formed within both the vadose and phreatic zones. The occurrence of epigenic caves formed within the phreatic zone indicates that perched aquifers and more complex groundwater systems exist within the Castile Formation than previously recognized. It is probable that independent shallow groundwater systems have developed throughout the eastern region of the study

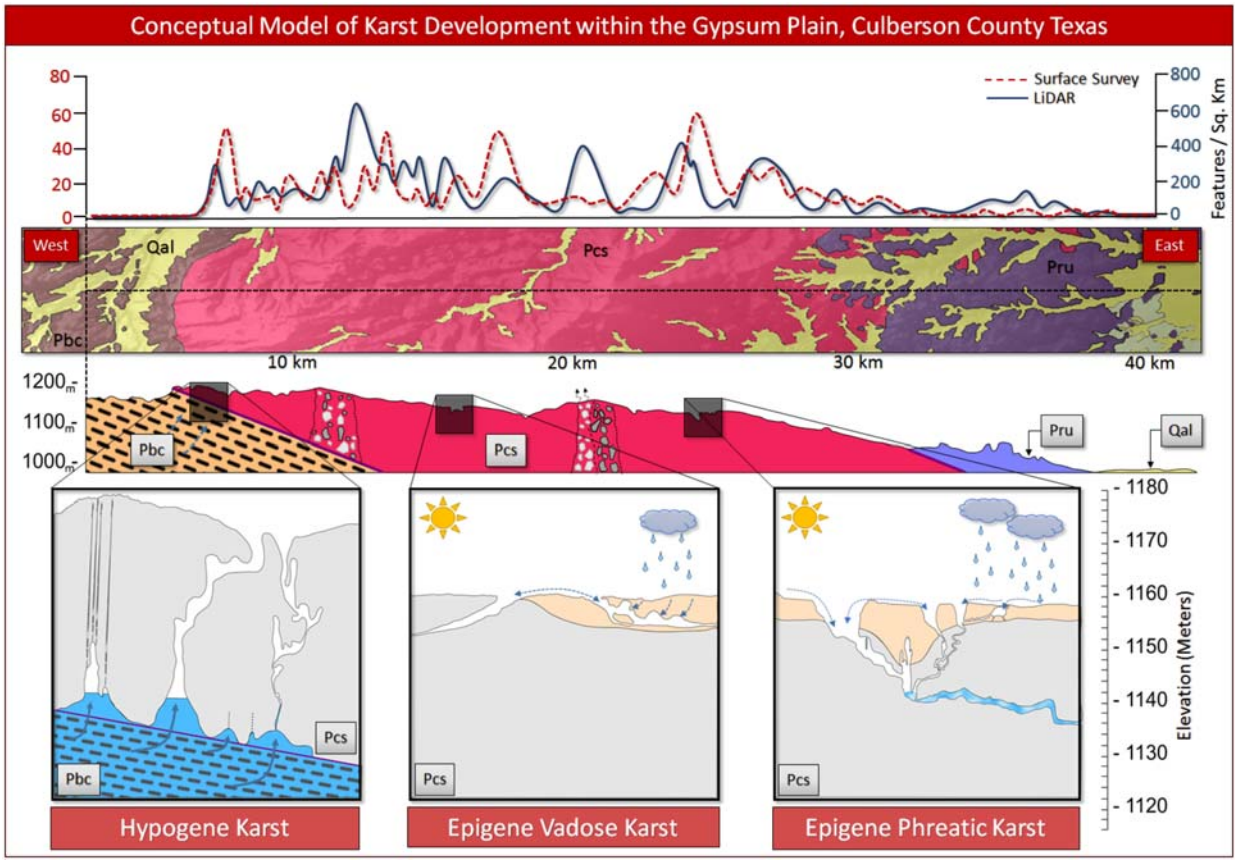

Figure 5. Idealized model of karst development across the Gypsum Plain (Pbc = Bell Canyon Formation, Pcs = Castile Formation, Pru = Rustler Formation, Qal = Quaternary Alluvium); top graph displays the frequency of surface karst manifestations per square kilometer identified by surface surveys (red) and LiDAR analyses (blue); middle diagram displays the cross-sectional relationship between Castile Formation and its bounding formations. Lower diagrams display a representation of the variability in karst development type (i.e., hypogene/epigene) across the study area.

area to accommodate local groundwater recharge and to direct it toward the Delaware River.

Suffosion cave occurrences are much more common in the central and eastern parts of the study area and are usually associated with epigenetic caves (Fig. 5). Bedrock conduits provide pathways for soil removal from the system, but are small enough to limit flow and increase residence time of soil fluids. Increased residence time promotes the dissolution of the gypsic soil fraction resulting in the development of soil caves that are a hybrid of dissolution and suffosion processes; these occurrences create relatively large soil chambers and domes with smooth walls. To the west, located near hypogene occurrences, soil caves are highly subdued. Hypogene caves in this area have the ability to recharge waters rapidly after breaching and the water residence time in soil is greatly reduced, as it flows quickly through the breached system. The suffosion process typically requires infilling of sinks or draping of sediments over pre-existing caves or solutionally widened fractures. Breached hypogene caves that have been exposed to epigene processes receive little or no infilling because of their ability to quickly transport sediments into the subsurface, resulting in less infilling and less suffosion.

In addition to variations in specific karst features from west to east, the overall density of features varies as well. Most surficially expressed karst identified by either field survey or LiDAR analyses are located within the Castile Formation (Fig. 5). Karstic occurrences drop dramatically beyond Castile outcrops within the study area. The Bell Canyon contains no known karst features, as it is predominantly a siliciclastic unit. Karst features within the Rustler Formation are subdued, as this unit is primarily composed of limestone/dolomite and is less soluble than the Castile. LiDAR analyses revealed significantly more karst features than surface surveys, because shallow filled sinks coupled with denser vegetation can preclude the identification of subtle karst features in the field; however, features identified through LiDAR analyses have been systematically checked and all field verifications indicate that extremely shallow and/or surficially small features are true karst features.

CONCLUSIONS

Previous research indicated that >10,000 individual karst features dominated by hypogene processes exist within the Gypsum Plain, with increased karst development along the western edge of the outcrop area (Stafford and others, 2008b). This study further expands upon these findings with increased data resolution and develops a conceptual model for karst spatial distribution (Fig. 5). Karst development appears most predominantly on the western edge of the basin because of intense hypogene karst breaching. At this location, potentiometric pressures in the underlying Bell Canyon Aquifer are highest and Castile thinning from surface denudation is greatest. Breccia pipes occur throughout, as large-scale hypogene dissolution at the Bell Canyon/Castile contact has created stoping features. The central part of the Gypsum Plain is dominated by shallow, fracture-controlled epigene caves formed in the vadose zone. The eastern part of the Castile outcrop exhibits more complex epigene caves of phreatic origin. These phreatic caves are commonly associated with shallow perched aquifers and are likely coupled to the entrenchment of significant fluvial systems (e.g., Delaware River) that bisect the Gypsum Plain.

Only a decade ago, the highest resolution remote-sensing data within the region were 10-m accuracy DEMs and 1-m accuracy digital orthophotos (DOQ). Based on the findings of this study, the previous estimations of karst occurrences in the Gypsum Plain by Stafford and others (2008b) vastly underestimated the region's potential for karst development; this original estimation can easily be increased by at least an order of magnitude and possibly two orders of magnitude. The original study conducted by Stafford and others (2008b) concluded that by analyzing remote-sensing data (DOQ), only 36% of karst features over a given area were identified when compared to what could be identified through physical land surveys. However, in this study, 42 karstic features were identified per square kilometer through physical land surveys and over 270 karstic features were identified per square kilometer through high-resolution LiDAR analyses (Figs. 5 and 6A). This value extrapolated over the entire Gypsum Plain results in an estimation of approximately 500,000 surficially expressed karst features within the Castile outcrop alone. Compared to traditional surveys in the area, physical surface mapping revealed ~15% of all karst detected through high-resolution (~30-cm accuracy) LiDAR analyses. In other words, advances in the resolution and accuracy of

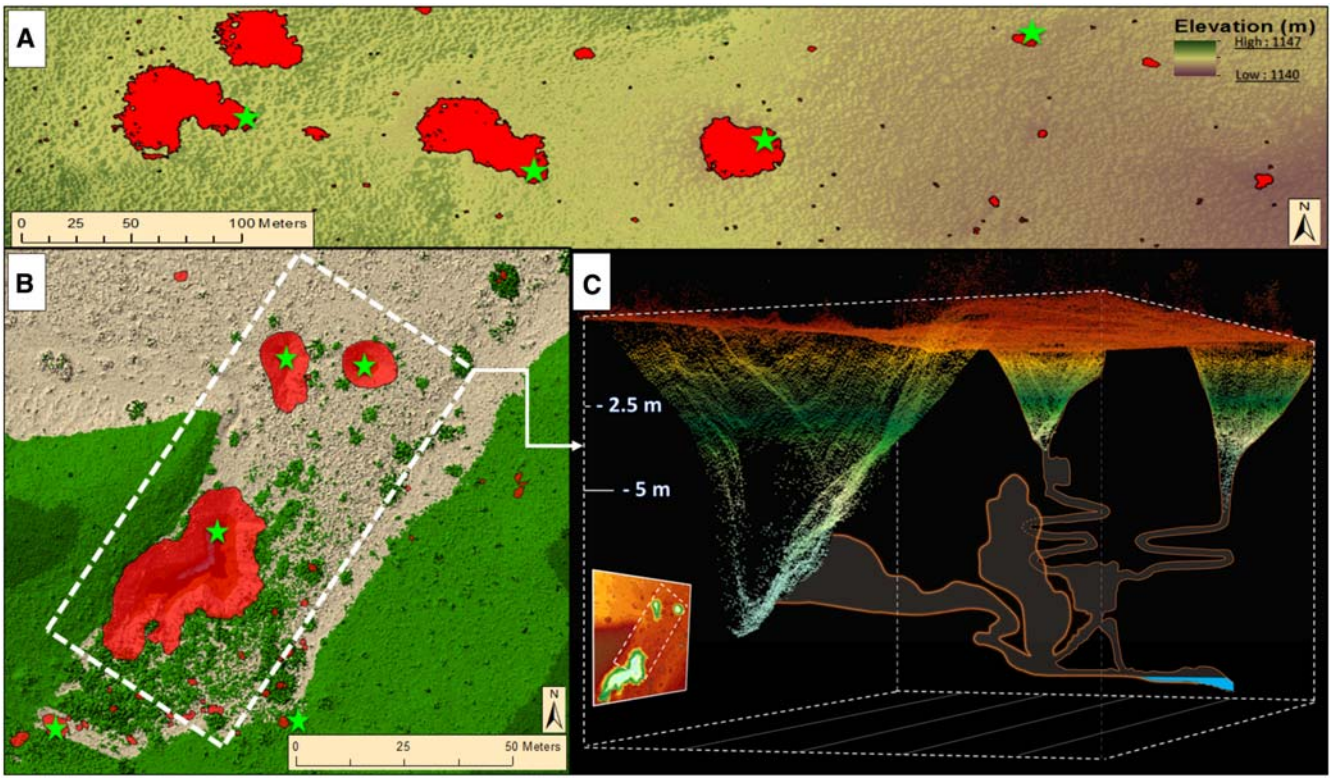

Figure 6. LiDAR analyses. (A) Depicts the discrepancies in karst manifestation identification of surface walks (green stars) and LiDAR analyses (red); (B) LiDAR and DEM analyses enhance identification of depressions surrounded by dense vegetation (small isolated depressions in red); and (C) 3D view of LiDAR point cloud data of the entrances into Lillcher Cave with simplified cave map from survey data (orange) (vertical exaggeration is 2X).

remote-sensing data indicate that LiDAR is almost seven times more effective at identifying surficial karst manifestations when compared to physical land surveys.

In addition to the increased accuracy of remote-sensing data collection in recent years, LiDAR has become much more efficient in its ability to be manipulated to reveal features that would otherwise be missed when doing physical surface surveys. Karstic features that are either shallow, small in diameter, or surrounded by vegetation can now be identified with ease and their associated drainage basins can be more easily assessed (Figs. 6A and 6B).

One of the most important factors of LiDAR analyses within this study is its ability to detect open conduits into the subsurface. Karst depressions identified through DEM analyses may or may not contain open conduits into the subsurface. Depressions identified by DEM analyses were reinvestigated using LiDAR point cloud 3D and cross-sectional views. If the 3D views were interpreted to contain open conduits into the subsurface, as shown in Fig. 6C, these caves were flagged to be investigated and mapped during fieldwork. The rapid advancements in remote-sensing technologies are enabling a better visualization of karstic surface and subsurface relationships. The ability to specifically detect and target karst features with significantly increased efficiency opens the door to conducting karst studies and understanding regional speleology on a much larger scale than traditional survey methods. Identifying the exact scale, location, and quantity of deep-seated hypogene caves was outside of the scope of this research; it is certain that, within the subsurface, the number of karst occurrences that have yet to be exposed is significantly higher than current estimates indicate, and will surely provide for exciting research in the future.

ACKNOWLEDGEMENTS

This research was partially funded by the Texas Department of Transportation with support from the Department of Geology at Stephen F. Austin State University. The authors are indebted to the following field assistants that made this work possible: Ashley Landers, Adam Majzoub, Lillian O'Shay, Jessica Shields, and Nikota Welch. Appreciation is expressed to Wesley Brown for his review of this manuscript and helpful contributions to its improvement.

REFERENCES CITED

Adams, J.E., 1965, Stratigraphic-Tectonic Development of Delaware Basin: American Association of Petroleum Geologists, Bulletin, v. 49, no. 11, p. 2140–2148.

Anderson, R.Y., Dean, W.E., Kirkland, D.W., and Snider, H.I., 1972, Permian Castile varved evaporite sequence, West Texas and New Mexico: Geological Society of America, Bulletin, v. 83, p. 59–85.

Anderson, R.Y., Kietzke, K.K., and Rhodes, D.J., 1978, Development of Dissolution Breccias, Northern Delaware Basin, New Mexico and Texas: New Mexico Bureau of Mines and Mineral Resources, Circular 159, p. 47-52.

Anderson, R.Y., and Kirkland, D.W., 1980, Dissolution of salt deposits by brine density flow: Geology, v. 8, p. 66–69.

Buechner, K.H., 1950, Life History, Ecology, and Range of The Pronghorn Antelope in Trans-Pecos Texas: The University of Notre Dame, The American Midland Naturalist. v. 52, no. 2. 266 p.

Hill, C.A., 1996, Geology of the Delaware Basin, Guadalupe, Apache, and Glass Mountains, New Mexico and West Texas: Society of Economic Paleontologists and Mineralogists, Permian Basin Section, Publication no. 96-39, 480 p.

Horak, R.L., 1985, Trans-Pecos tectonism and its affects on the Permian Basin, *in* Dickerson, P.W., and Muelberger, W.R., eds., Structure and Tectonics of Trans-Pecos Texas: Midland, Texas, West Texas Geological Society, p. 81–87.

Kelley, V.C., 1971, Geology of the Pecos Country, Southeastern New Mexico: New Mexico Bureau of Mines and Mineral Resources, Socorro, New Mexico, Memoir 24, 75 p.

Klimchouk, A.B., 2000, Speleogenesis under deep-seated and confined setting, *in* Klimchouk, A., Ford, D.C., Palmer, A.M., and Dreybrodt, W. (eds.), Speleogenesis: Evolution of Karst Aquifers: National Speleological Society, Huntsville, p. 244-260.

Klimchouk, A.B., 2007, Hypogene Speleogenesis: Hydrogeological and Morphogenetic Perspective: National Cave and Karst Research Institute, Special Paper no. 1, Carlsbad, NM, 106 p.

Kirkland, D.W., 2003, An explanation for the varves of the Castile evaporites (upper Permian), Texas and New Mexico, USA: Sedimentology, v. 50, p. 899–920.

Lee, MK., and Williams D.D., 2000, Paleohydrology of the Delaware Basin, western Texas: overpressure development, hydrocarbon migration, and ore genesis: American Association of Petroleum Geologists, Bulletin, v. 84, no. 7, p. 961–974.

Nance R., 1993, Application of the standard tablet method to a study of denudation in gypsum karst, Chosa Draw, southeastern New Mexico: unpublished M.S. Thesis, University of Northern Colorado, Greely, CO, 82 p.

Scholle, P.A., Goldstein R.H., and Ulmer-Scholle D.S., 2004, Classic upper Paleozoic reefs and bioherms of west Texas and New Mexico: New Mexico Institute

of Mining and Technology, Socorro, NM, Open-file Report 504, 166 p.

Stafford, K.W., Nance, R., Rosales-Lagarde, L., and Boston, P., 2008a, Epigene and hypogene gypsum karst manifestations of the Castile Formation: Eddy County, New Mexico and Culberson County, Texas, USA: International Journal of Speleology, v. 37, p. 83–98.

Stafford K.W., Rosales-Lagarde L., and Boston P.J., 2008b, Castile evaporite karst potential map of the Gypsum Plain, Eddy County, New Mexico and Culberson County, Texas: a GIS methodological comparison: Journal of Cave and Karst Studies, v. 70, no. 1, p. 35–46.

Stafford, K.W., Ulmer-Scholle, D., and Rosales-Lagarde, L., 2008c, Hypogene calcitization: Evaporite diagenesis in the western Delaware Basin: Carbonates and Evaporites, v. 23, p. 89–103.

Texas Speleological Survey, 2016, WallsMap: Texas Speleological Survey proprietary karst database. Texas Speleological Survey, Austin, Texas.

A Novel Approach to Delineating Lithologic Variability of a Karsted Landscape Using CIR Imagery and GIS Analyses, Eddy County, New Mexico

Jessica Shields and Kevin W. Stafford
Department of Geology, Stephen F. Austin State University,
Nacogdoches, Texas

ABSTRACT.—Traditional characterization of karsted terrains involves costly field studies that require months, if not years, of physical field mapping and data collection to complete. This characterization process may be made more efficient by the preliminary identification of areas of interest through careful analysis of geologic maps. Karst features of the Gypsum Plain of southeastern New Mexico and West Texas range from decimeters to tens of meters in scale, requiring highly detailed maps in order for this preliminary analysis technique to be of use. However, maps of the area currently available feature little to no detail of lithologic variability or mineralization. Advances in remote-sensing technologies allow for the production of geologic maps through an increased ability for mineral identification from satellite imagery, most commonly based on hyperspectral data. However, commercially available hyperspectral sensors offer extremely low spatial resolution compared to 50-cm resolution multispectral data available, as well as being more costly and difficult to process. The following novel approach to delineating detailed lithologic variability of a landscape may be employed through the performance of a maximum likelihood classification of color-infrared imagery. WorldView-2 satellite imagery was used in this study for its high 50-cm spatial resolution, to provide a more efficient and cost-effective method of karst identification and lithologic characterization for use in research and natural resource management. Based on comparison with control points acquired in the field and extensive a priori knowledge of the study area, results were deemed highly accurate and are currently being used to aid in ongoing karst studies.

INTRODUCTION

Traditional characterization of karsted terrains entails the costly, time-consuming process of physical field mapping to identify and collect data concerning landscape features. Consequentially, remote-sensing methodologies are actively being pursued as a more cost-effective means of resource management. The Gypsum Plain of southeastern New Mexico and West Texas is the site of extensive karst development within Permian evaporite facies, hosting variable karst manifestations ranging in scale from millimeters to kilometers (Stafford, 2008a). Specific features are commonly associated with unique lithologies or topographic features, allowing for preliminary identification through the use of surficial geologic maps. However, existing geologic maps of the area have poor resolution, featuring the general expected lithology with little detail and no variation in mineralogy (Fig. 1). Advances in satellite imaging technology have allowed for the possibility of land mapping and feature extraction to be performed by image classification of raster cells based on their corresponding radiometric properties, commonly reducing the need for extensive groundwork whereas allowing for coverage of greater areas (Hamideh, 2014).

Commonly, hyperspectral data are used in studies concerning the delineation of surface geologic materials because of increased spectral resolution and some available channels with extremely narrow bandwidths, allowing for greater accuracy in the identification of specific mineral types (Harris and others, 2011). However, commercially available hyperspectral sensors lack refined spatial resolutions necessary in the identification of small karst features and lithologic variability (less than a few

Shields, Jessica; and Stafford, Kevin, 2021, A Novel Approach to Delineating Lithologic Variability of a Karsted Landscape Using CIR Imagery and GIS Analyses, Eddy County, New Mexico, *in* Johnson, K. S.; Land, Lewis; and Decker, D. D. (eds.), Evaporite Karst in the Greater Permian Evaporite Basin (GPEB) of Texas, New Mexico, Oklahoma, Kansas, and Colorado: Oklahoma Geological Survey, Circular 113, p. 201–212.

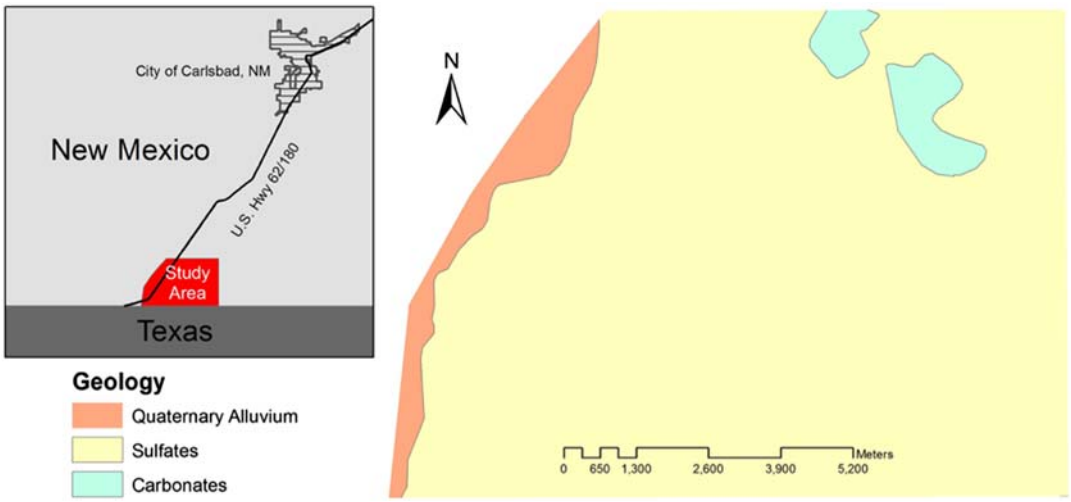

Figure 1. Traditional geology map of the study area created on a small scale of 1:500,000 (adapted from Green and Jones, 1997).

Sensor Name	Type	Spectral Range	Spectral Resolution	Spatial Resolution
LANDSAT 7	Optical-Multispectral; Satellite-borne	0.4 to 2.35 µm and 10.4 to 12.5 µm	65 to 260 nm and 380 nm (pan)	30 m (60 m TIR; 15 m Pan)
ASTER	Optical-Multispectral; Satellite-borne	0.52 to 0.86 µm; 1.60 to 2.43 µm; 8.125 to 11.65 µm	60 to 100 nm; 40 to 70 nm; 350 nm	15, 30 and 90 m
QuickBird	Optical-Multispectral; Satellite-borne	0.45 to 0.90 µm		0.60 m Pan; 2 and 44 m Mss
WorldView-2	Optical-Multispectral; Satellite-borne	Pan. 0.45-0.8; VNIR 0.4 to 1.0 µm		0.5 m
HYPERION	Optical-Hyperspectral; Satellite-borne	0.35 to 2.5 µm	~ 15 nm	30 m
CASI	Optical-Hyperspectral; Airborne	0.4 to 1.1 µm	~ 20 nm	up to 1.23 m (crosstrack)
HyMap	Optical-Hyperspectral; Airborne	0.4 to 2.5 µm	~ 20 nm	3 to 10 m
PROBE-1	Optical-Hyperspectral; Airborne	0.4 to 2.5 µm	~ 20 nm	3 to 10 m

Figure 2. Primary satellite sensors offering commercially available imagery data and corresponding relevant technical specifications (adapted from Harris and others, 2011).

m^2 in size) across a landscape, whereas commercially available, multispectral sensors offer increased spatial resolutions of 50 cm or less (Fig. 2). The Gypsum Plain consists primarily of evaporite and carbonate facies with little vegetation, as it is located in the semiarid, southwestern United States. Top-of-atmosphere reflectance values of the main lithogroups (e.g., sulfates, carbonates, and siliciclastics) present exhibit a significant enough

variation that increased spectral ranges and concentrated values of the hundreds of bands comprising hyperspectral data are not required for the basic discrimination of major features across the study area.

This study is a novel approach to the production of classified satellite imagery displaying surface geologic features using WorldView-2 color-infrared imagery products of the visible and near-infrared spectrum caused by the commercial availability of 50-cm spatial resolution. Computer-assisted processing of color-infrared (CIR) satellite imagery was performed to produce a surface geology map through a supervised maximum likelihood classification of surface reflectance values for the entire study area to delineate lateral variations in lithology less than 1-m wide and aid in the identification of corresponding karst features across the Gypsum Plain. This study is the first of its kind to use WorldView-2 high-resolution multispectral satellite imagery to map the lithologic variability of the Gypsum Plain and, based on published literature review, the first to be attempted in any evaporite karst terrain.

The study area is located in southeastern Eddy County, New Mexico and encompasses approximately 100 km^2 of land managed by the U.S. Department of the Interior, Bureau of Land Management (BLM). The area is commonly referred to as the Yeso Hills area of the Gypsum Plain in the northwestern part of the Delaware Basin (Fig. 3) and is situated along the northern edge of the Chihuahuan Desert, along the southwestern margin of the Great Plains physiographic region. The Gypsum Plain is dominated by evaporites of the Ochoan Castile Formation, as well as residual remnants of the Salado and Rustler formations and minor secondary limestones (Hill, 1996). Annual precipitation in the region ranges from 150 to 400 mm, with an average temperature of 24°C, resulting in sparse, drought-tolerant vegetation (Stafford, 2015). Evaporite karst features, including surficial karren, sinkholes, and caves, are abundant within the Castile Formation caused by the high solubility of gypsum, resulting in a complex karst system that presents unique land management concerns.

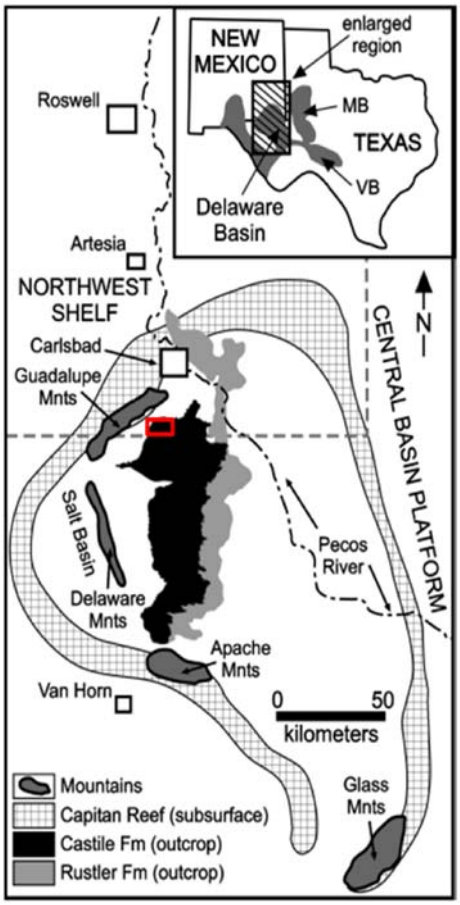

Figure 3. Location of the study area in relation to the surrounding Gypsum Plain comprised of the Rustler and Castile formations, and the greater Delaware Basin, delineated by the subsurface extent of the Capitan Reef and associated outcrops in various mountain ranges. Study area outlined in red (modified from Stafford and others, 2008a).

GEOLOGIC SETTING

The assimilation of Pangea during the late-Paleozoic led to the division of the Permian Basin and formation of the intracratonic Delaware Basin with limited connection to the open marine sea (Dickenson, 1981; Hill, 1996). The Gypsum Plain is developed within the northwestern part of the Delaware Basin and consists primarily of varved, laminated to massive anhydrite/gypsum, interbedded with halite, of the late Permian (early Ochoan) Castile Formation (Dietrich and others, 1995; Hill, 1996; Stafford and others, 2008b). The Castile represents a classic deep-water deposit within a large, stratified, brine-water basin (Adams, 1944) formed following marine disconnectivity at the end of Guadalupian time (Adams, 1972). The Castile overlies the sandstone/siltstone of the Bell Canyon Formation and was deposited beneath the Salado and Rustler evaporite formations of the basin (Fig.4). Residual remnants of the continental Dewey Lake Red Beds, subsequently deposited above the Rustler Formation at the end of the Permian, mark the end of Permian marine deposition within the Delaware Basin and the transition to a combination of sabkha to delta-eolian such as environmental fluctuations until subaerial exposure dominated throughout the Mesozoic.

Cretaceous deposition of siliciclastics within the basin included the interbedded sandstone/conglomerate of the Cox Sandstone, anomalously located within the study area (Hill, 1996). Until the late Cenozoic, the basin experienced little tectonic activity and limited, sporadic deposition of sediments, followed by a period of aerial exposure, uplift and erosion of the late-Miocene

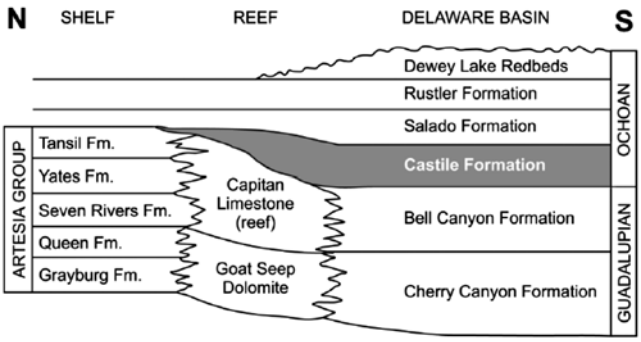

Figure 4. Major lithologic units of the Delaware Basin deposited during the middle-to-late-Permian with the dominant karst-bearing unit, the Castile Formation, highlighted in grey (adapted from Scholle and others, 2004).

associated with the formation of the western Rio Grande Rift (Kirkland, 2014). Therefore, surface exposures within the Gypsum Plain consist of the following lithologies: gypsum, calcite (limestone), dolomite (dolostone), siliciclastics (sandstone and conglomerates), gypsic soils, and weathering byproducts of all lithologies.

Gypsum, the most common bedrock in the study area, promotes extensive karst development because of its high solubility (2.53 g/L) combined with near-linear solution kinetics. Whereas, most bedrock in the study area is covered by a thin, secondary gypsic crust (Fig. 5A) and a variety of surficial karren occur in areas of exposed bedrock, including: rillenkarren (Fig. 5B), spitzkarren (Fig. 5D), kamenitzas, and tumuli. Karren may crop out across a few mm^2 to m^2 in area, but is generally



Figure 5. Common surficial karst manifestations within lithologies of interest across the study area: A) gypsic crust precipitate commonly deposited across a large part of the study area; B) rillenkarren formed on Castile gypsum; C) small-scale closed sinkhole formed caused by subsurface collapse within alluvium; D) spitzkarren formed on Castile gypsum; E) open sinkhole containing the entrance to Green Moss Cave formed within the Castile gypsum; and F) closed sinkhole formed within alluvium acting as host to a dense cluster of grasses native to the Gypsum Plain.

limited in size. Sinkholes are prolific, appearing as the dominant geomorphic karst manifestation and ranging in average size from decimeters to tens of meters in diameter. Filled sinkholes formed either by collapse of subsurface features or by transport of sediment manifest as closed depressions (Fig. 5C). Open sinkholes (Fig. 5E) are generally connected to solutional conduits or cave entrances and may range from shallow, elliptical depressions to laterally elongated, incised arroyos. Sinkholes are commonly associated with partial to complete infilling by alluvium deposits and associated dense vegetation because of the higher moisture content available in these unconsolidated fill materials (Fig. 5F). Caves and solutional conduits are widespread and commonly fracture controlled, ranging from small isolated features to complex forms that may significantly extend, both laterally and vertically (Stafford and others, 2008a). For a general review of hydrologically active karst manifestations within the Gypsum Plain, see Stafford and others (2008a).

Karst mounds, paleokarst erosional remnants formed by the collapse and infill of strata overlying subsurface karst voids (Bachman, 1980), sporadically occur across the Gypsum Plain, including several mounds that have been identified in the eastern part of this study area. Karst mounds represent areas of cavernous porosity within the Castile gypsum and overlying Salado salts that underwent collapse in the past and experienced infilling by overlying strata that subsequently created topographic highs by differential weathering of surrounding gypsum during more recent surface denudation (Bachman, 1980; Hill, 1996). Karst mounds are generally less than 100 m in diameter with a low relief of 3–9 m (Hill, 1996). Steep-sided hills composed of Rustler strata (Fig. 6A) are found clustered along the periphery of the eastern half of the study area, at an average height and diameter of 5 m. K Hill (Fig. 6B) provides a more complex example of these paleokarst phenomena and consists of karstic slump debris from the Rustler Formation, in addition to rotated and down dropped blocks of the Dewey Lake and Cox formations, creating an erosional positive relief structure approximately 18-m high in the central part of the study area (Crawford, 1993). The Cox, Dewey Lake Red Beds, and Rustler formations within the study area solely manifest as karst mounds and have not been identified in situ at any localities.

Areas of the Gypsum Plain have undergone significant mineralogic diagenesis resulting in calcitized evaporites, which generally manifest as isolated masses at the land surface or laterally extensive surface horizons. Ascending light hydrocarbons, likely methane, reduced calcium sulfate to limestone throughout the Ochoan evaporites via either Bacterial Sulfate Reduction or Thermal Sulfate Reduction (Stafford and others, 2008c; Kirkland and Evans, 1976). Isolated limestone buttes, also known as "Castile Buttes" (Fig. 6C), crop out across

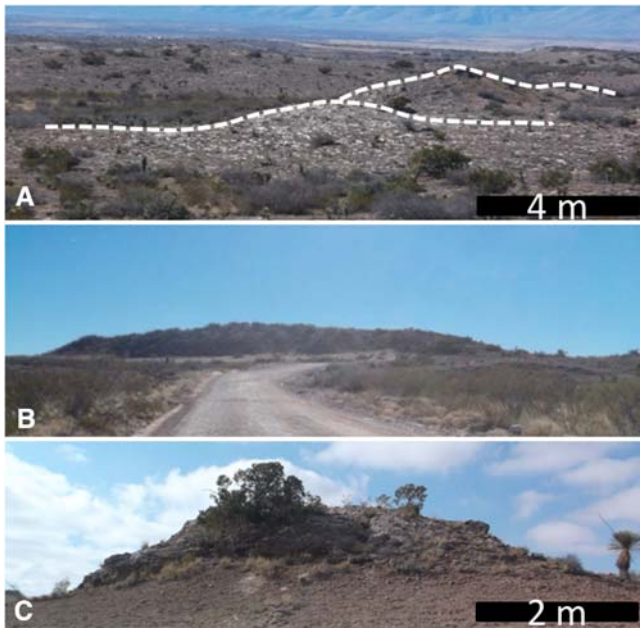

Figure 6. Karst mounds and areas exhibiting secondary calcitization: A) karst mounds (delineated with dashed white lines) primarily consisting of Rustler strata; B) K Hill, the largest karst mound in the study area consisting of Rustler, Dewey Lake Red Beds and Cox strata; D) small Castile butte located within the study area consisting of brecciated Castile gypsum that has been calcitized.

the Gypsum Plain as a product of differential weathering of these calcitized zones, creating topographic highs ranging from a few m^2 to tens of thousands of m^2 in area, and a maximum height of 40 m (Kirkland and Evans, 1976; Stafford and others, 2008c). Laterally extensive limestone sheets are present as residual brecciated clasts at the surface or as intact linear sheets dipping into the subsurface, generally where surrounding gypsum has been dissolved leaving less soluble calcitized residuum. Limestone sheets may range from a few decimeters to up to 2 m in thickness and can crop out over thousands of m^2 (Stafford and others, 2008a). Float of secondary limestone, small clasts of brecciated rock displaced by surface processes, may be localized to areas where the limestone is exposed at the surface or may cover wide areas of the landscape. Calcitization processes and mineral conversion of associated sulfur-ore deposits have also produced secondary selenite occurrences through near-surface oxidation which manifest as linear features, fracture fillings, and lenticular masses (Stafford, 2008c).

MULTISPECTRAL IMAGERY DATA SET AND CHARACTERIZATION

The use of remote-sensing data to discriminate between and identify surficial lithologies for the purpose

of geologic mapping is a well-established practice (Van der Meer and others, 2012). A variety of optical sensor data are available for this purpose, featuring varying spectral and spatial ranges and resolutions appropriate for different purposes and methodologies (Fig. 2). Today, hyperspectral data are most commonly employed in regional bedrock characterization because of greater spectral resolution and range allowing for increased ability and accuracy for identifying earth materials, such as mineral groups and lithotypes, across lithologically variable landscapes for the purpose of mineral mapping and exploration (Harris and others, 2011; Kruse, 2015; Van der Meer and others, 2012). However, limited spatial resolution of commercially/publicly available data from hyperspectral sensors prevents small-scale outcrops and features from being discernible across an image, making it unsuited for the identification of small lithologic changes associated with karst features such as those present within the study area investigated and greater Gypsum Plain. Hyperspectral imagery data are also difficult to obtain and process, costly, and exhibit great redundancy in data (Kruse, 2015). Currently, the highest resolution, commercially available hyperspectral data is 30-m Hyperion satellite-borne data or that obtained via unmanned aerial vehicles (UAVs) equipped with a camera capable of collecting hyperspectral data. The use of UAVs in conjunction with hyperspectral cameras pose their own set of problems, including the high cost of both the platform and camera, time and possible travel required for collection of data and the ability of the user to operate the UAV effectively, to name a few. Conversely, multispectral data are less expensive/ commonly free, less redundant and widely publicly available in increased spatial resolutions of up to 50 cm or less.

Karstic features targeted by this study generally occur on the centimeters to meter scale and associated surficial lithologic variability is common over short lateral distances; therefore, more refined spatial resolution was required for lithologic mapping for improved natural resource management. As shown in Fig. 2, of commercial imagery available for purchase, WorldView-2 satellite imagery features the highest multispectral resolution available at 0.5 m (Harris and others, 2011). Traditionally, CIR imagery is used to differentiate vegetation health across a target area through the use of band rationing techniques (Wolf, 2010; Hamideh and others, 2014). However, the geologic remote-sensing community has traditionally used visible-to-near-infrared imagery for lithologic and structural mapping. In addition, working with a limited number of bands such as only those present within CIR data sets reduces extraneous data redundancy brought on by the overlap of adjacent channels in each sensor (van der Meer and others, 2012).

WorldView-2 CIR satellite imagery, acquired on September 27, 2016, was purchased by Stephen F. Austin State University, Department of Geology for use in this study, chosen for its 50-cm spatial resolution of generated products. Orthorectification and radiometric corrections were performed prior to purchase and imagery acquisition, including a dark offset subtraction and nonuniformity correction (Updike and Comp, 2010). Atmospheric corrections were performed, including conversion of raw digital numbers to top-of-atmosphere spectral radiance, and subsequently top-of-atmosphere reflectance using ArcGIS 10.2 following the process outlined by Updike and Comp (2010).

IMAGE CLASSIFICATION

Before performing image classification, a control point database was established for all documented surficial lithology types and karst features present within the study area. Ten, 1-km^2 grids divided into traverse lines spaced at 50-m intervals were randomly selected across the study area and systematically mapped to develop detailed representative maps of lithologic and geomorphic variability. Based upon data collected through field mapping of each gridded control site, combined with a priori knowledge of the area and known geology, ten unique sample classes were established for image analyses comprising the majority of the surface lithologies and features within the study area: 1) alluvium; 2) algal crust; 3) surficial gypsite precipitates; 4) dense vegetation manifesting commonly as bushes one-quarter to several m^2 in area; 5) calcitized breccia zones or float; 6) exposed Castile gypsum bedrock; 7) residual Cox strata; 8) residual Dewey Lake Red Beds strata; 9) residual Rustler strata; and 10) surface bodies of water. Subsequent to field mapping, additional areas suspected of representing each of the ten established classes were systematically identified across the entirety of the study area to evaluate feature class variability using Google Earth Pro. Locations of identified features were recorded and physically verified in the field to supplement field data attained from detailed physical mapping of gridded sites. Once verified for accuracy, GPS coordinates were established for 106 control points representing each lithology or lithologic feature of interest across the entire study area, not including bushes/large vegetation features (Fig. 7). These control points were used to create training samples and establish reflectance values of the corresponding CIR raster cells. Vegetation-related control points were established directly within the original CIR imagery products to account for the temporal change associated with vegetation life cycle and actual physical existence of features both on the ground and within the image.

Computer-assisted processing was employed via ArcGIS for Desktop 10.2 software to produce a Maximum Likelihood Classification (MLC) of the CIR imagery acquired for use within this study. Based on the control

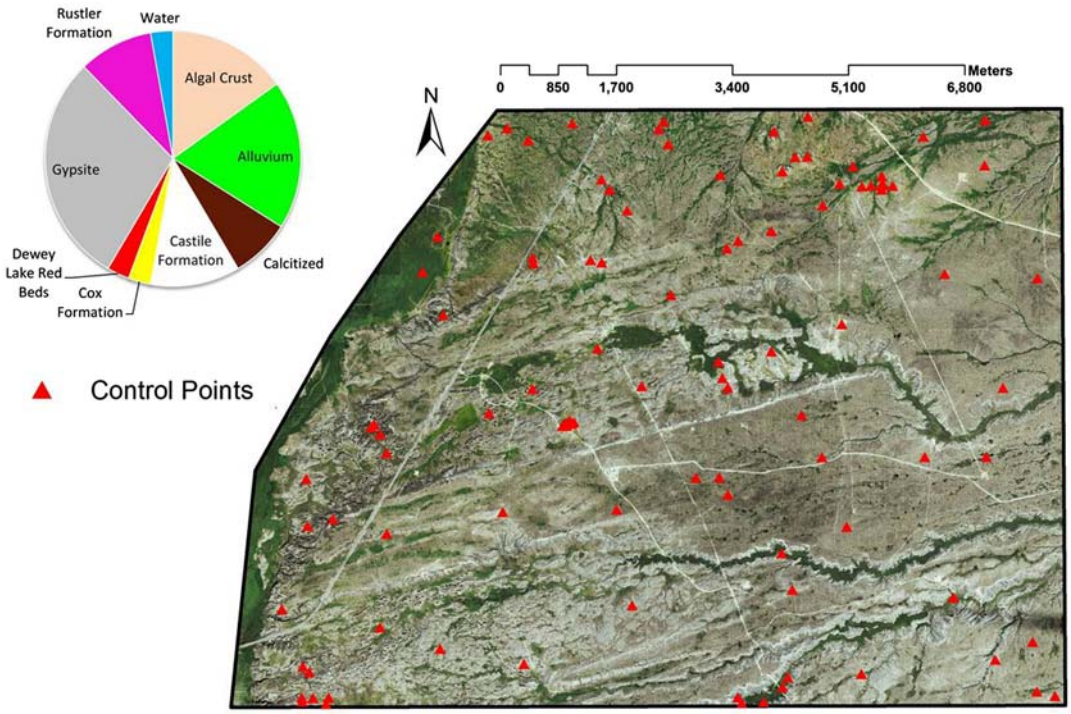

Figure 7. Location of each control point identified and field checked for nine of the ten classes used for later classification of the color-infrared data set (control points were not established for "Vegetation"). Chart (top left) details some control points across the landscape corresponding to each class identified in the field.

points previously established in the field, areas corresponding to each lithology type were specified and surface reflectance values extracted in the form of training samples. A signature file was created, in which each individual class was assigned the mean vector and covariance matrices of the collective cells comprising the specific training sample and used to perform a maximum likelihood classification of each raster cell within the study area. The final product consisted of an output classified raster in which each cell was assigned a class based on the value of the cell.

Parameters specified for the creation of the MLC included a priori probability weighting and specification of a reject fraction. Several cells comprising the training samples used to produce the signature file for raster cell classification was specified to be proportional to some cells of that class across the output classification raster; this was based on the relative number of control points corresponding to each class recorded across the study area as proportional percent of the study area covered by that lithology. A "confidence value" was calculated during MLC ranging from 0.05% to 100%, indicating the confidence with which each raster cell is assigned a class value. Those cells with a confidence value of 5% or less were rejected and assigned no cell value during image classification. Vegetation masks the individual spectra of the rock or soil in which it is growing; therefore, requiring values identified as 'Vegetation' to be reclassified relevant to this study. Further processing of the MLC raster was performed by assigning 'Vegetation' values to the class of their nearest neighbor based on Euclidean distance.

Three sites of specific interest were selected for more detailed assessment within the study area (Fig. 8A) based on the presence of multiple significant karst-related manifestations and a high density of control points present to assess method accuracy. Site one (Fig. 8B) features large areas of exposed calcitized blanket breccia, a Castile butte, small mounds covered by algal crust and grass-filled depressions separated by a significant amount of gypsite in which several karstic sinkholes have been identified. The second site (Fig. 8C) is focused on the carbonates of K Hill, surrounded by gypsite and exposed gypsum containing multiple small epigene karst features. Site three (Fig. 8D) was chosen for the presence of several karst mounds of the Rustler Formation separated by gypsite.

Figure 9 displays the final classified images produced for the three sites of specific interest, whereas Fig. 10 is that of the entire study area. Correlation of the control points used to create training samples indicates that 61% of points were classified with absolute accuracy. Discrepancies in lithologies most commonly occurred between cells classified as the Rustler Formation and

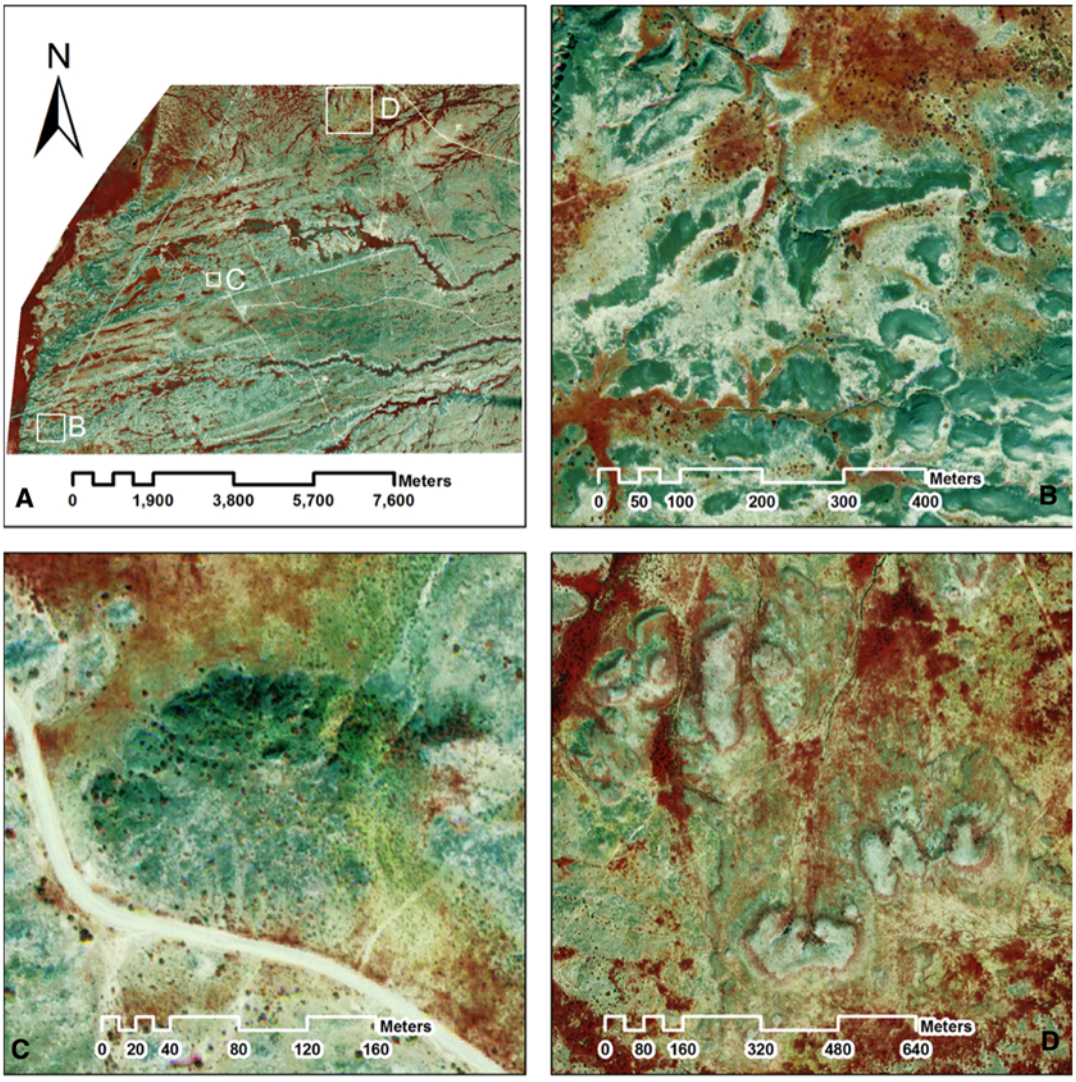

Figure 8. Color-infrared imagery of selected sites of interest evaluated, including: A) relative location of three sites within larger study area (see Figure 1 for reference location of Figure 8A); B) clustered area of exposed calcitized breccia and one of the two Castile buttes located in the study area; C) K Hill karst mound remnant of paleocavern breccia infilling; and D) clustered area of karst mounds composed of Rustler collapse strata.

Gypsite, which is consistent with field observations where Rustler Hills are almost always capped by well-developed gypsite. Figure 11 indicates that this is due in part to the similarity in reflectance values indicated by the two lithologies. Areas of gypsite not associated with Rustler across the study area (but classified as so) are caused by the similar reflectance values. In addition, the Cox Formation and Dewey Lake Red Beds are difficult to distinguish from one another because of the same similarity in mean reflectance values that exhibited between classes. Both the Cox and Dewey Lake contain mixed siliciclastics with similar chemical compositions, thus similar reflectance values. Visual comparison with Google Earth Pro imagery was used to evaluate the overall accuracy of the area which showed strong a priori agreement with knowledge of the study area. All control point values misclassified were clusters of only a few cells, less than a few m^2, located within a greater area of the control point lithology.

Postdepositional alteration of gypsum caused by high solubility and ease of weathering has resulted in the existence of a thin gypsic residue across the landscape of the Gypsum Plain (Watson, 1982). Spectral sensors employed in the collection of CIR data only collect data concerning surface reflectance characteristics, indicating that many of the signatures collected have been influenced by the weathered, surficial residue (Harris and others, 2011) inhibiting the comparison of values across the image observed with standard laboratory-based values for carbonates and evaporites for accuracy.

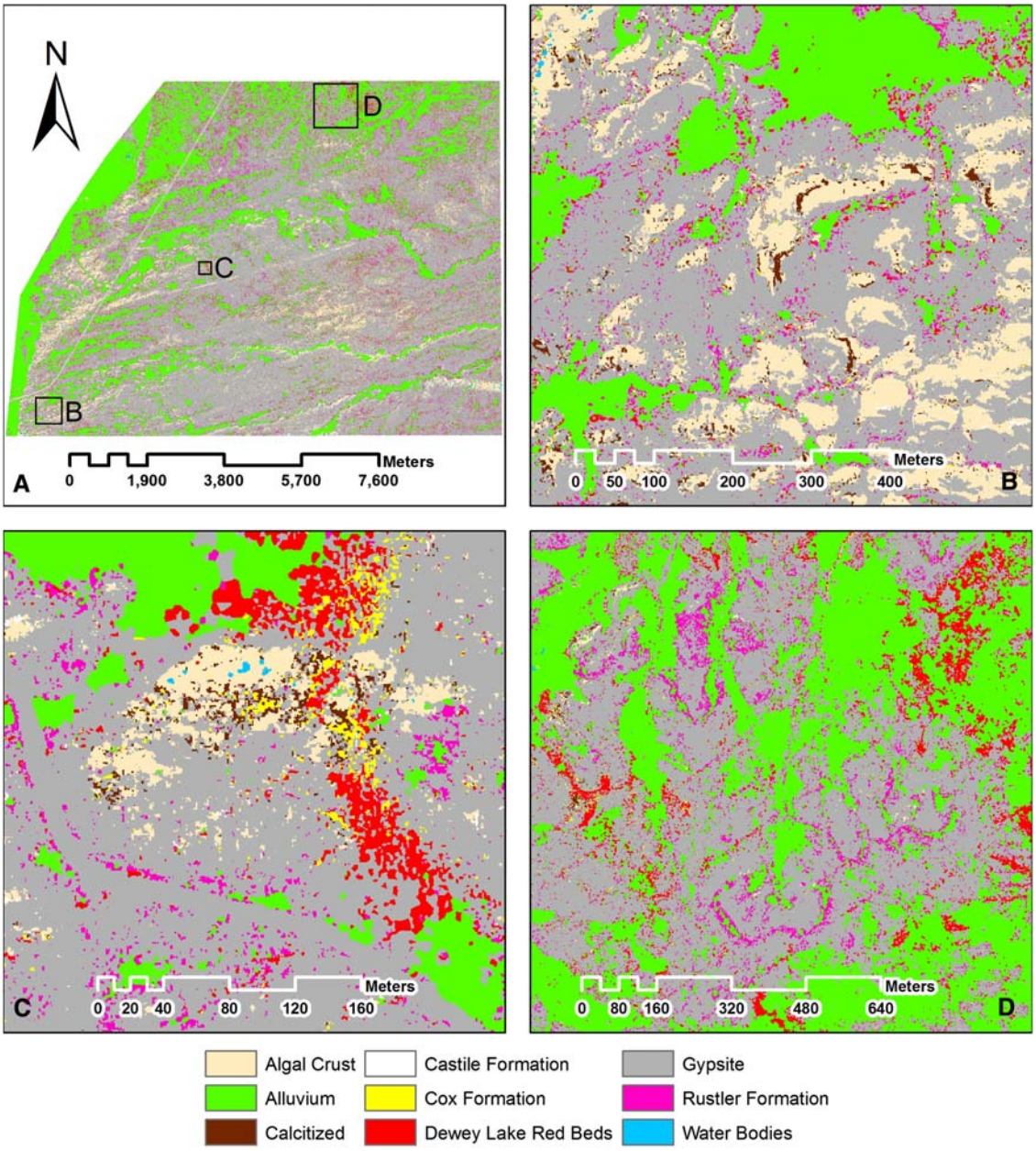

Figure 9. Final maximum likelihood classification rasters produced for each of the three areas of interest from Figures 2–7: A) relative location of three sites within larger study area (see Figure 1 for reference location of Figure 9A); B) clustered area of exposed calcitized breccia and one of the two Castile buttes located in the study area; C) K Hill karst mound remnant of paleocavern breccia infilling; and D) clustered area of karst mounds composed of Rustler collapse strata.

CONCLUSIONS

Surface geologic maps created through the classification of spectral reflectance values across a landscape via satellite imagery are a more efficient approach to the characterization of the lithologic variability within the karsted landscape of the Gypsum Plain of the Delaware Basin than traditional methods commonly employed. Results of this study enabled efficient and largely effective geologic mapping of the entire 100-km^2 study area (Fig. 11), which could be extended throughout the entire Gypsum Plain and is currently being used for improved delineation of likely regions of more intense karst development, including caves and paleokarst features. High spatial resolution is especially important in the creation of such products, resulting in the use of multispectral data rather than hyperspectral data in this study based on current technology of commercially available data. Based on the training sample values and classification

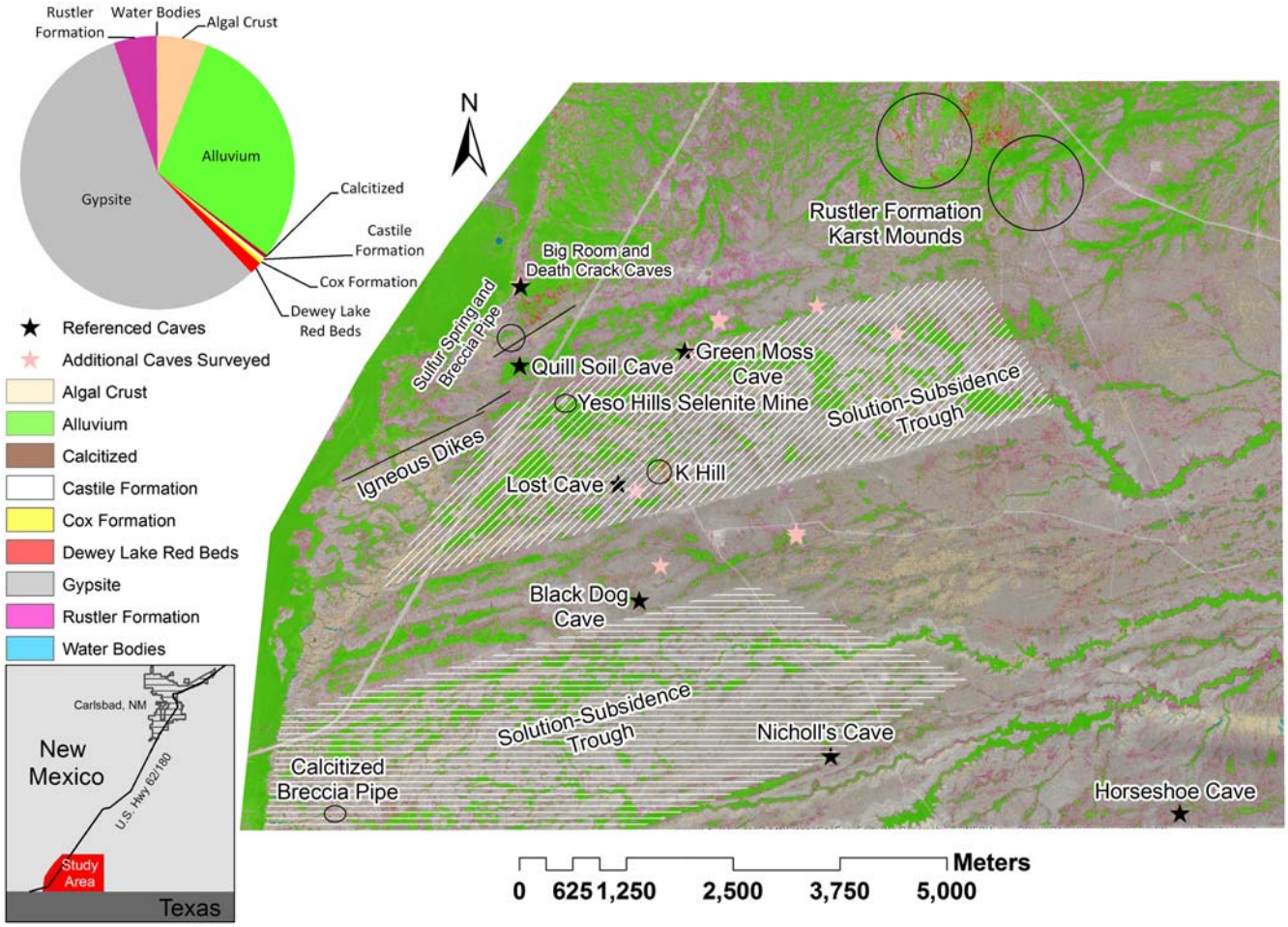

Figure 10. Final lithologic surface map of the study area based on the maximum likelihood classification performed.

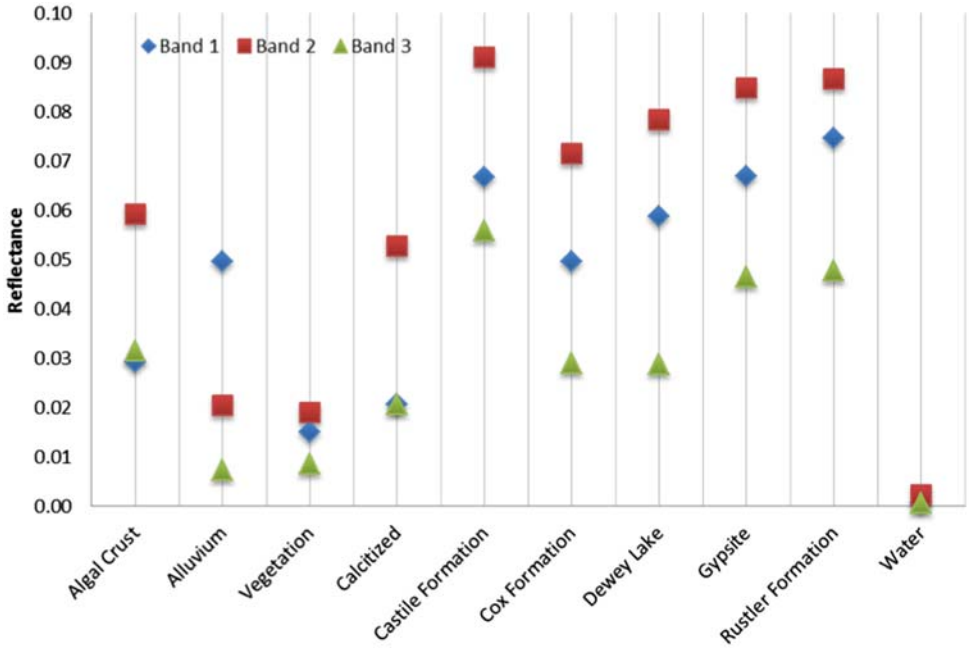

Figure 11. Graph displaying the mean reflectance value of each band for the corresponding class' training samples. Note distinct reflectance values for most sample classes.

parameters used, the methods employed in this study produced a more accurate representation of the study area based on comparison with control points, Google Earth Pro imagery and familiarity with the area, than traditional, published geologic maps of the region indicate (Fig. 1).

Differences in control point values and classified cell values were the product of extremely similar reflectance values across multiple bands of the CIR imagery caused by similar chemical composition of actual or constantly associated lithologies and were almost always individual to small clusters of cells located in a greater area of the correct lithology; the confusion between Rustler and gypsite lithologies, where gypsite thinly mantles Rustler strata, being the exception. The use of such remotely sensed map products as those developed in this study allows for targeted survey and identification of karst features, rather than methodical surveys that commonly take months to years of field observations to complete, thus increasing field efficiencies and reducing potential assessment costs.

The creation of surface geologic maps via less expensive, less time-consuming processes such as satellite image classification for the characterization and use in identification of geologic variability across a karsted landscape is useful to entities such as the Bureau of Land Management or other agencies for a more efficient approach to natural resource management. Greater availability and decreased cost of multispectral data than that of hyperspectral, as well as simplified pre- and postclassification image processing allows for the use of proposed methods by a greater community and lower skill and experience levels with remote sensing. As technologies increase, hyperspectral imagery analyses will likely be used for even greater accuracy (especially of cells pertaining to Rustler/gypsite and Cox/Dewey Lake issues) of remotely sensed geologic mapping within the Gypsum Plain and similar arid environments, but currently, commercially available, satellite-based hyperspectral imagery resolution is too poor. New and rapidly advancing UAV technologies will provide significant opportunities for improved geologic characterization within complex karst systems such as the Gypsum Plain in the near future, but likely require a significantly higher cost to be obtained, as well as all issues previously specified.

REFERENCES CITED

Adams, J.E., 1944, Upper Permian Ochoa series of Delaware Basin, West Texas and southeastern New Mexico: American Association of Petroleum Geologists, Bulletin, v 28, p. 1596–1625.

Adams, J.E., 1972, Semi-cyclicity in the Castile anhydrite, *in* Elam, J.G., and Chuber, S., eds., Cyclic sedimentation in the Permian Basin: West Texas Geological Society, Special Publication 72-60, p.196–202.

Bachman, G.O., 1980, Regional Geology and Cenozoic History of the Pecos Region, Southeastern New Mexico: US Geological Survey, Open-File Report no. 80-1099, 117 p.

Crawford, J.E., 1993, K Hill and the Yeso Hills selenite occurrence, *in* Love, D.W., Hawley, J.W., Kues, B.S., Adams, J.W., Austin, G.S. & Barker, J.M., eds., Cyclic sedimentation in the Permian Basin: New Mexico Geological Society, Guidebook, v. 44, p. 8–10.

Dickenson, W.R., 1981, Plate tectonic evolution of the southern Cordillera: Arizona Geological Society Digest, v. 14, p. 113–135.

Dietrich, J.W., Owen, D.E., Shelby, C.A., & Barnes, V.E., 1983, Geologic atlas of Texas, Van Horn- El Paso sheet: University of Texas Bureau of Economic Geology, v.36, 1 p.

Green, G.N., and Jones, G.E., 1997, The Digital Geologic Map of New Mexico in ARC/INFO Format: U.S. Geological Survey Open-File Report 97-0052, 9 p.

Harris, J., Wickert, L., Lynds, T., Behnia, P., Rainbird, R., Grunsky, E., McGregor, R., and Schetselaar, E., 2011, Remote Predictive Mapping 3. Optical Remote Sensing - A Review for Remote Predictive Geological Mapping in Northern Canada: Geoscience Canada, v. 38, no. 2, p. 49–84.

Hamideh, N., Beecham, S., Anderson, S., and Nagler, P., 2014, High spatial resolution WorldView-2 imagery for mapping NDVI and its relationship to Temporal Urban Landscape Evapotranspiration Factors: Journal of Remote Sensing, v.6, p. 580–602.

Hill, C.A., 1996, Geology of the Delaware Basin, Guadalupe, Apache and Glass Mountains: New Mexico and West Texas: Midland, Permian Basin Section of the SEPM, Publication 96-39, 480 p.

Kirkland, D.W., 2014, Role of hydrogen sulfide in the formation of cave and karst phenomena in the Guadalupe Mountains and western Delaware Basin, New Mexico and Texas: National Cave and Karst Research Institute, Special Paper 2, 77 p.

Kirkland, D.W., and Evans, R., 1976, Origin of limestone buttes, Gypsum Plain, Culberson County, Texas: American Association of Petroleum Geologists, Bulletin, v. 60, p. 2005–2018.

Kruse, F.A., 2015, Integrated visible and near-infrared, shortwave infrared, and longwave infrared full-range hyperspectral data analysis for geologic mapping: Journal of Applied Remote Sensing, v. 9, no. 1, p. 096005-1–096005-17.

Stafford, K.W., 2015, Evaluation of Existing Geologic Conditions along RM 652: Initial Characterization

of Karst Geohazards Associated with RM 652 in Culberson County, Texas: Texas Department of Transportation, p. 1–71.

Stafford, K.W., Nance, R., Rosales-Lagarde, L., and Boston, P.J., 2008a, Epigene and hypogene karst manifestations of the Castile Formation: Eddy County, New Mexico and Culberson County, Texas, USA: International Journal of Speleology, v. 37, n. 2, p. 83–98.

Stafford, K.W., Rosales-Lagarde, L., and Boston, P.J., 2008c, Castile evaporite karst potential map of the Gypsum Plain, Eddy County, New Mexico and Culberson County, Texas: A GIS methodological comparison: Journal of Cave and Karst Studies, v. 70, n. 1, p. 35–46.

Stafford, K.W., Ulmer-Scholle, D., and Rosales-Lagarde, L., 2008b, Hypogene calcitization: evaporite diagenesis in the western Delaware Basin: Carbonates and Evaporites, v. 23, n. 2, p. 89–103.

Updike, T., and Comp, C., 2010, Radiometric use of WorldView-2 imagery: Digital Globe Technical Note, p. 17.

Van der Meer, F.D., van der Werff, H.M., van Ruitenbeek, F.J., Hecker, C.A., Bakker, W.H., Noomen, M.F., van der Meijde, M., Carranza, E.J.M., de Smeth, J.B., Woldai, T., 2012, Multi- and hyperspectral geologic remote sensing: A review: International Journal of Applied Earth Observation and Geoinformation, v.14, no. 1, p. 112–128.

Watson, A., 1982, The origin, nature and distribution of gypsum crusts in deserts: unpublished Ph.D. dissertation, Wolfson College, University of Oxford, England, 669 p.

Wolf, A., 2010, Using WorldView 2 VIS-NIR MSI Imagery to Support Land Mapping and Feature Extraction Using Normalized Difference Index Ratios: International Society for Optics and Photonics, p. 8390.

Evaporite Karst in the Permian Rustler, Salado, and Castile Formations at Red Bluff Dam on the Pecos River, Loving and Reeves Counties, Texas

Kenneth S. Johnson
Retired Geologist, Oklahoma Geological Survey,
Norman, Oklahoma

Richard A. Shoemaker
Retired Engineer, HDR Engineering, Inc.,
Buena Vista, Colorado

John Charlton
HDR Engineering, Denver, Colorado

Cris Parker
HDR Engineering, Austin, Texas

ABSTRACT.—Red Bluff Dam and Reservoir, located on the Pecos River between Loving and Reeves Counties in west Texas, has been losing water since impoundment began in early 1937 —mainly due to seepage through evaporite-karst features beneath the dam. Water flows through collapse structures and brecciated-karst zones in the Permian-age Rustler Formation, which is the bedrock beneath most parts of the dam, and through Quaternary deposits of weakly to strongly cemented sand and gravel that locally lie between the base of the dam and bedrock. In the Red Bluff area, the Rustler Formation consists mainly of interbedded dolomite, gypsum, and shale, and it probably also contained some layers of salt (halite) that have been dissolved by ground water. The dam has undergone three grouting programs: the most recent being completed in December 2014.

Rocks in the Rustler and overlying Dewey Lake Formations at Red Bluff are largely brecciated, mainly due to dissolution of salt and gypsum within the Rustler Formation and in the underlying Permian Salado and Castile Formations. The high solubility of these evaporites enables karst features, such as dissolution channels, cavities, sinkholes, breccias, and collapse structures, to form readily in gypsum and salt, and this can result in slow subsidence or sudden collapse of overlying strata.

Collapse breccias are exposed in the Rustler and Dewey Lake Formations in the dam and spillway area, and also occur beneath parts of the dam itself. As seepage from the reservoir flows in and around the breccia, it can further dissolve the gypsum and dolomite blocks to enhance karst features that allow even more circulation of ground water. In general, gypsum karst is an important factor in any dam's ability (or inability) to hold water, because dams built upon gypsum karst generally experience at least some loss of reservoir water.

The loss of water from the reservoir is mainly due to the following: 1) dissolution of salt and/or gypsum beds in the Rustler, Salado, and Castile Formations; 2) collapse and chaotic disruption of gypsum and dolomite units in the Rustler Formation; 3) development of karst features within the gypsum and dolomite units and collapsed blocks of the Rustler Formation; and 4) probable seepage through Quaternary sands and gravels, chiefly beneath the northeast side of the dam.

Johnson, Kenneth S.; Shoemaker, Richard A.; Charlton, John; and Parker, Cris, 2021, Evaporite Karst in the Permian Rustler, Salado, and Castile Formations at Red Bluff Dam on the Pecos River, Loving and Reeves Counties, Texas, *in* Johnson, K. S.; Land, Lewis; and Decker, D. D. (eds.), Evaporite Karst in the Greater Permian Evaporite Basin (GPEB) of Texas, New Mexico, Oklahoma, Kansas, and Colorado: Oklahoma Geological Survey, Circular 113, p. 213–232.

INTRODUCTION

This study examines the regional and local geologic setting of the Permian-age Rustler Formation and associated rocks in the Delaware Basin of west Texas and southeast New Mexico (Figs. 1, 2) and how these rocks relate to leakage problems at Red Bluff Dam on the Pecos River in west Texas. The Rustler Formation and the underlying Salado and Castile Formations are characterized by an abundance of soluble gypsum and salt beds that locally are partly or totally dissolved to produce collapse structures, chaotic features, and breccia in rocks that immediately underlie Red Bluff Dam and Reservoir.

The study embraces the area around the small community of Red Bluff and the Red Bluff Dam, located in Loving and Reeves Counties, Texas, as well as areas farther east in Loving County, where the Rustler and underlying formations are not as extensively dissolved and disrupted as they are beneath the dam. The study focuses on: 1) the dissolution of salt and gypsum in the Rustler and underlying formations; 2) the regional and local distribution, thickness, and structure of the Rustler Formation; and 3) the effects that dissolution and collapse of the Rustler Formation have on the loss of water beneath Red Bluff Dam.

This report is part of a larger drilling and testing study carried out by HDR Engineering, Inc. (HDR), to establish a grouting program that will eliminate, or at least minimize, loss of lake water through breccia, through gypsum- and dolomite-karst features, and through Quaternary deposits that underlie the dam (Charlton and others, 2021). The dam and reservoir are owned and operated by Red Bluff Water Power Control District for water supply, irrigation, flood control, and recreation purposes. Appreciation is expressed to Dr. Lewis Land, geologist with the National Cave and Karst Research Institute, for his review and constructive comments on an early draft of this report.

GEOLOGIC SYSTEM	Formations and Members	
QUATERNARY AND TERTIARY	Pecos Alluvium, Dissolution-Trough Fill, and Gatuña Formation	
TRIASSIC	Dockum Group	
PERMIAN	Dewey Lake Formation	
	Rustler Formation	Forty-Niner
		Magenta Dolomite
		Tamarisk
		Culebra Dolomite
		Los Medaños (proposed formal name for "unnamed lower member")
	Salado Formation	
	Castile Formation	
	Older Permian Formations	

Figure 1. Generalized stratigraphic column for the Rustler Formation and overlying and underlying strata in the vicinity of Red Bluff Reservoir (modified from Powers and Holt, 1999; Ewing and others, 2012).

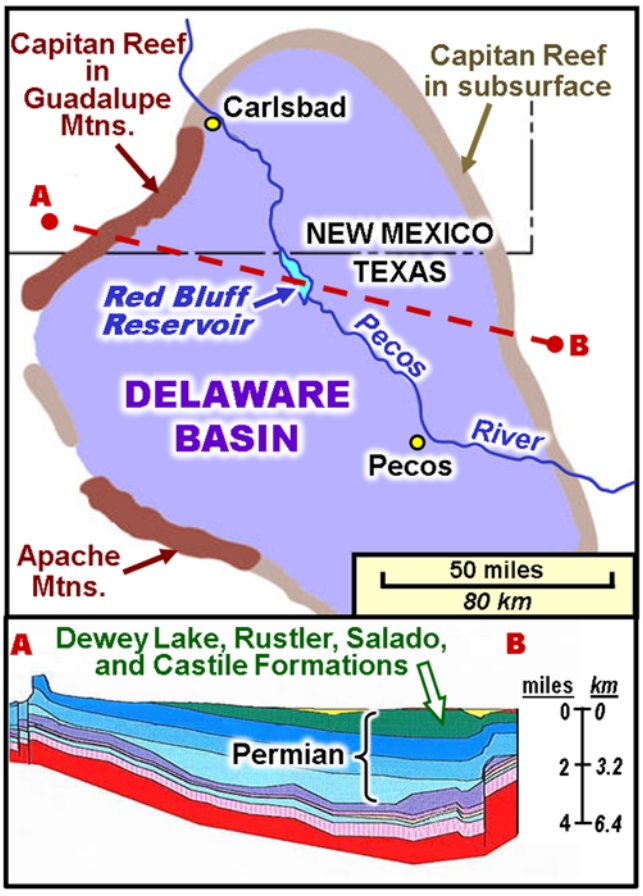

Figure 2. Delaware Basin map and structural cross section showing thick accumulation of Permian and older sedimentary rocks. Dewey Lake, Rustler, Salado, and Castile Formations (green) are thinner to the west, largely because of dissolution of salt beds within these formations. These evaporite formations overlie older, nonevaporite Permian formations (blue) throughout the Delaware Basin.

Literature Search

The surface geology of the dam and reservoir area was originally mapped and described by Komie (1952) and subsequently mapped by AGRA (1994). Also, a regional, generalized map was prepared by the Texas Bureau of Economic Geology (Eifler, 1976).

Regional studies of salt deposits in the Delaware Basin include those of Pierce and Rich (1962), Snider (1966), Johnson and Gonzales (1978), Ege (1985), and Hill (1996). Regional studies of gypsum and anhydrite deposits in the Delaware Basin include those of Withington (1962), Snider (1966), Anderson and others (1972), Johnson and others (1989), and Hill (1996).

Regional studies of evaporite dissolution and karst features in the Delaware Basin include those by Maley and Huffington (1953), Olive (1957), Johnson and Gonzales (1978), Lambert (1983), Bachman (1984), Hill (1996, 2003), Martinez and others (1998), Johnson (2003a), Land (2013), Stafford (2013), and Stafford and Nance (2018). Studies of the hydrogeology of the Rustler aquifer include those of Ashworth (1990), Boghici and Van Broekhoven (2001), and Ewing and others (2012). The study by Ewing and others (2012) was conducted to document the development of a three-dimensional groundwater model for the Rustler Aquifer in west Texas and southeast New Mexico: this report is especially valuable because it includes excellent maps showing the regional structure and thickness of the Rustler Formation throughout Loving and northern Reeves Counties.

Cores of the Rustler Formation within 25 miles of Red Bluff Dam are described by Vine (1963), Eager (1983), and Hentz and others (1989).

Field Studies

During field studies in May 2012, we examined outcrops of the Culebra Dolomite and collapsed gypsum blocks of the Rustler Formation, as well as chaotic blocks of red shales and siltstones of the Dewey Lake Formation. These collapsed blocks show a high degree and randomness of collapse, disruption, and disorientation of rock units in the vicinity of the dam. Based upon field studies and examination of previous reports, we recommended the drilling of five additional cores (Reference Boreholes, RB–1 to RB–5) to establish a framework of the dolomite, gypsum, and other rock units that extend down as much as 200 feet beneath the dam and spillway. This drilling program was approved by the Red Bluff Water Power Control District and completed late in July 2012. The drilling was performed by Cutting Edge Core Drilling of Elgin, Texas, and John Charlton logged the boreholes.

Geophysical-log Study

Study of the subsurface distribution, thickness, and structure of gypsum beds in the area required examining the geophysical logs of 46 oil and gas tests, most of which were drilled within 6 miles of the dam. Logs of some wells drilled as much as 25 miles east of the dam were also examined to determine the amount and distribution of salt and gypsum layers in the Rustler, Salado, and Castile Formations where they have not been dissolved. Recognition of gypsum beds and associated rock types on geophysical logs is well established (Alger and Crain, 1966; Nurmi, 1978; Johnson, 2021). Of special value for the current geophysical-log study was the regional subsurface investigation of the stratigraphy of the Castile, Salado, and Rustler Formations by Snider (1966).

Three factors that limit the full usefulness of geophysical logs in the vicinity of Red Bluff Dam are 1) many of the logs do not show information about rock formations in boreholes at depths shallower than about 1,000 feet (the depth at which intermediate casing is commonly set); 2) although some of the well logs record information about rock units as shallow as 10–100 feet below the land surface, many of these wells have only a single log (such as only a gamma-ray log), and it can be difficult to interpret the types of rock when only a single log is available; and 3) because of the collapse and chaotic nature of rocks in the Rustler and Salado Formations near the dam, it can be difficult to correlate specific rock units from one well to another and to identify the top and bottom of the Rustler on the geophysical logs.

RESULTS OF STUDY

Main results of this study are divided into the following discussions: 1) main types of rocks in the area; 2) dissolution of gypsum and salt; 3) the regional character of the Rustler and underlying formations; 4) the local character of the Rustler Formation; and 5) other local rocks and deposits in the vicinity of the dam.

Main Rocks and Deposits in the Red Bluff Area

Permian sedimentary rocks that crop out in the Red Bluff area are mainly dolomite and gypsum, along with layers of red-brown shale, siltstone, and sandstone—all of which were deposited in the central part of the Delaware Basin (Figs. 1, 2). The bedrock formation at the dam is the Rustler Formation, and it contains all of these rock types. In addition, thick deposits of salt (halite) and gypsum/anhydrite (gypsum and/or anhydrite) are present in the underlying Salado and Castile Formations beneath the dam and farther to the east, at depths of several hundred to several thousand feet below the land surface (Figs. 3, 4). In the Red Bluff Dam area, most of these salt beds, and some of the gypsum/anhydrite beds, have been dissolved from the Rustler, Salado, and Castile Formations in Late Tertiary and Quaternary

times (Ewing, 2012), resulting in collapse and disruption of Rustler strata.

Permian shales, siltstones, and sandstones typically are not as hard and competent as the interbedded gypsum/anhydrite and dolomite, and they tend to weather more readily in outcrops. Most of these clastic sedimentary rocks are red brown in color, although some are gray, brown, and tan.

Surficial materials over much of the Red Bluff area are Quaternary-age deposits of sand, clay, and conglomerate. These sediments were laid down as alluvium by Pecos River and its tributaries. In addition, there are local deposits of gypsite, which is an unconsolidated, earthy variety of gypsum that commonly is intermixed with clay, dirt, and sand. Gypsite is not a hard rock, like gypsum, and it is not a part of the dissolution and water-loss problem at Red Bluff Dam.

Breccias are also locally present as a rubble of large and small chaotic blocks of rock that here result from dissolution of underlying rocks (salt or gypsum). These collapse breccias have fallen into underlying cavities or caves, and the original cavity could have been tens or even hundreds of feet below the resultant breccia. Collapse breccias here can consist of chaotic blocks or fragments of gypsum, dolomite, shale, siltstone, and sandstone: the void spaces between these blocks can be air- or water-filled, or they are filled with clay, silt, or sand that has been washed into the voids.

Dissolution of Gypsum and Salt

Gypsum and salt are evaporite rocks, and they are readily dissolved by groundwater—as long as the water is not saturated with calcium sulfate (for gypsum dissolution) or sodium chloride (for salt dissolution). In fact, gypsum and salt are, respectively, about 150 and 7,500 times more soluble than limestone or dolomite (Martinez and others, 1998). Such high solubilities enable subsurface dissolution channels and sinkholes to form in evaporite rocks in a matter of only days, weeks, or years, and this can result in slow subsidence or catastrophic collapse of overlying strata (Fig. 4). Most of the dissolution of salt and gypsum in the Rustler, Salado, and Castile Formations in the region occurred during Late Tertiary and Quaternary times (Ewing and others, 2012), and it certainly is still going on.

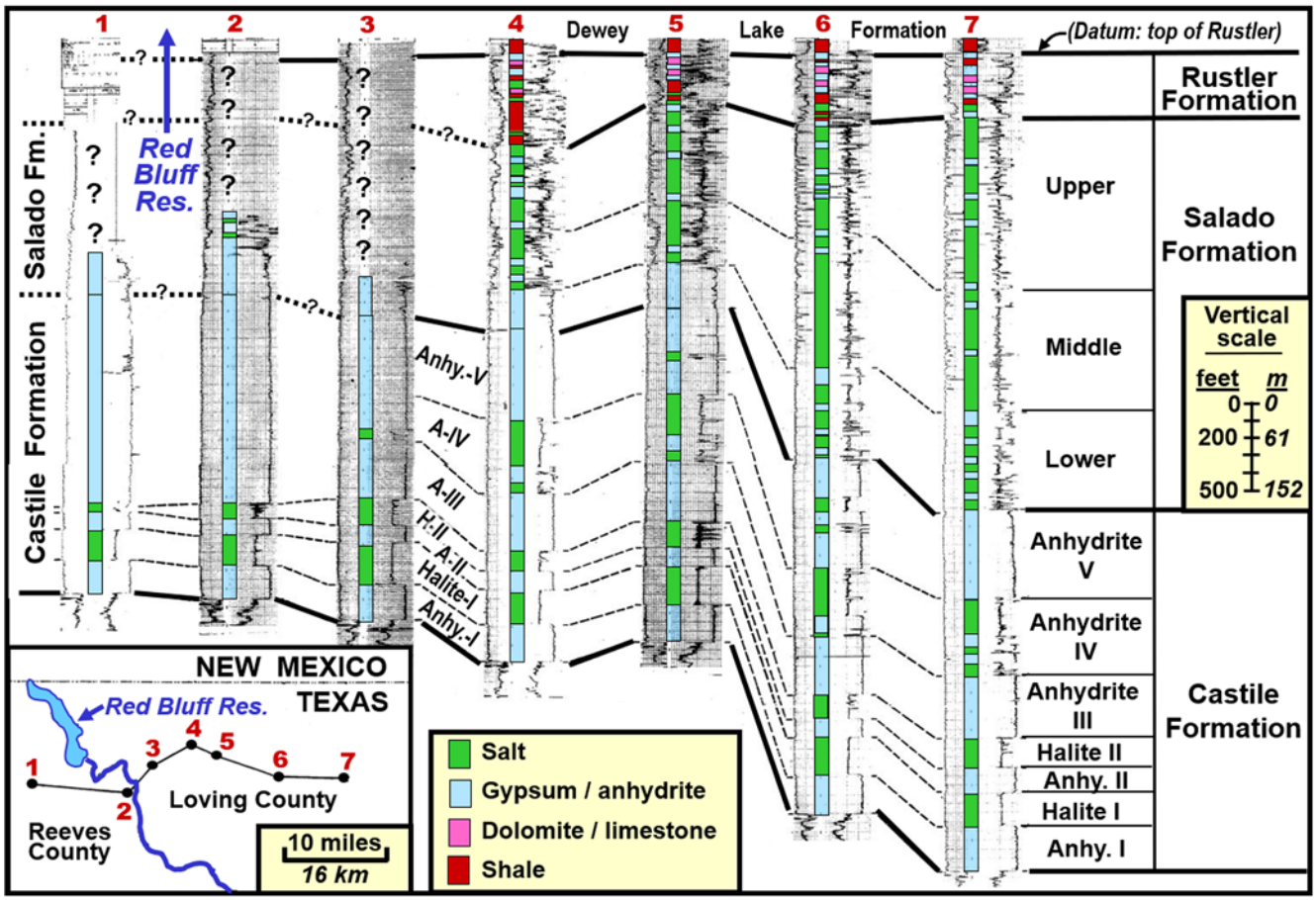

Figure 3. Stratigraphic cross section of Rustler, Salado, and Castile Formations in Loving and Reeves Counties, Texas (modified from Snider, 1966). Numbering of wells (1–7) is unique to this cross section.

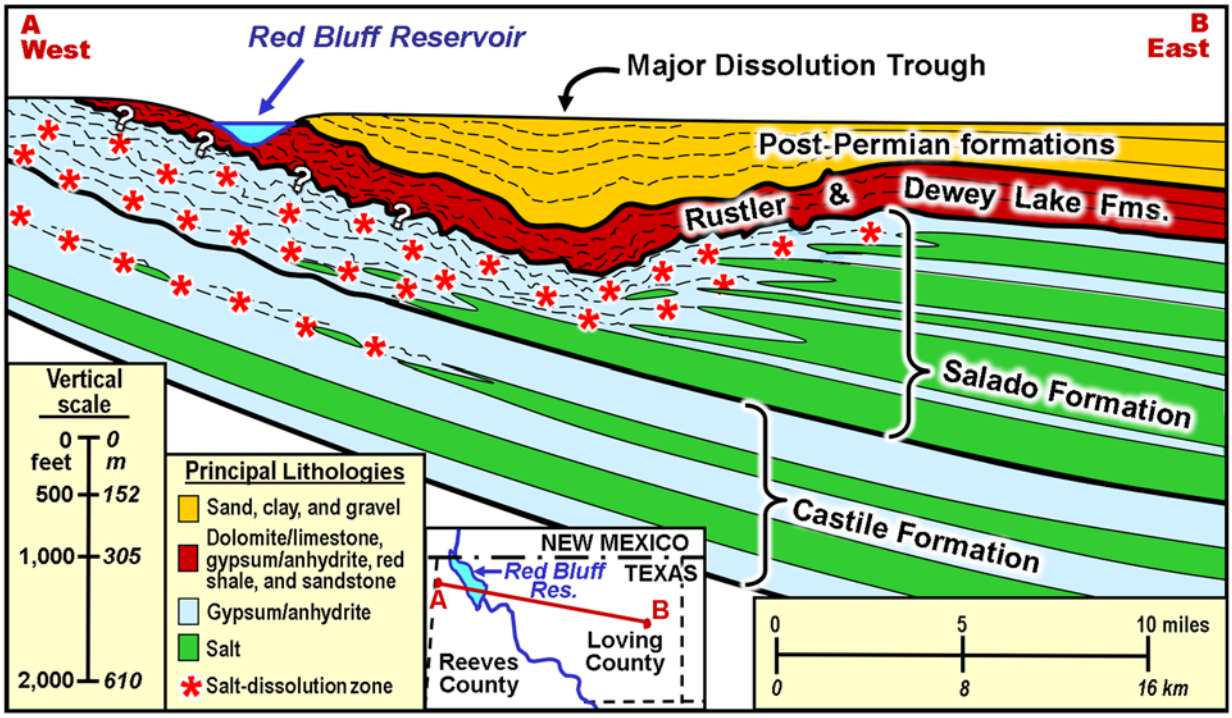

Figure 4. Generalized structural cross section A–B showing dissolution of salt in the Salado and Castile Formations beneath the Rustler and Dewey Lake Formations in Loving and Reeves Counties, Texas. Based upon data in Snider (1966), Martinez and others (1998), field investigations, and Figure 3 of this report.

Gypsum is a moderately soluble rock. It is susceptible to being partially or totally dissolved by groundwater and to developing "karst features," such as caves, sinkholes, and underground water courses (Johnson, 1996, 2003a, 2008a; Stafford, 2013; Stafford and Nance, 2018). Gypsum and/or anhydrite are abundant in the Rustler, Salado, and Castile Formations, and they underlie all parts of the Red Bluff Dam area (Fig. 4). Gypsum also crops out near the dam, in the spillway area and locally in the impoundment area just upstream of the dam. It is also very likely that gypsum crops out in many areas that are inundated by the reservoir. Small amounts of gypsum also occur as intergranular gypsum, as gypsiferous cement, and as thin veins in some of the Rustler dolomite, shale, siltstone, and sandstone units in the Red Bluff area (AGRA, 1994; HDR Reference Boreholes). Intergranular gypsum, gypsiferous cement, and gypsum veins can be dissolved locally and can allow small-scale seepage, but their contribution to water loss is not considered very high.

Salt is a highly soluble rock. It is significant to this study because the Salado and Castile Formations contain abundant subsurface salt beds in the area; the Rustler Formation probably also contained salt beds in the Red Bluff area, and it still contains salt farther east in Loving County (Fig. 3). Local dissolution of these salt beds has caused extensive collapse structures in the Rustler and overlying Dewey Lake Formations in the vicinity of Red Bluff Dam (Fig. 4) and in most of the western half of the Delaware Basin.

Exposed collapse structures, formed by dissolution of salt and/or gypsum in the Red Bluff area, contain broken fragments, or breccia, of Rustler and Dewey Lake strata, and the chaotic nature of this rock enhances groundwater circulation and dissolution of the gypsum immediately below the dam. Several exposures of large-scale collapse breccia are in the dam and spillway area, and small-scale collapse breccia is present in several of the HDR Reference Borehole cores (Fig. 5).

Gypsum karst is an important factor in a dam's ability to hold water. Dams built upon gypsum karst generally experience some loss of reservoir water, and this can even result in collapse and failure of the dam (Johnson, 2008b). Where gypsum karst is present beneath a dam, water can penetrate and enlarge the karst features and may escape from the reservoir. Several articles and books have been published on properties of dam foundations built upon gypsum deposits (James and Lupton, 1978; James and Kirkpatrick, 1980; Chen and Wu, 1983; Milanović, 2000, 2018; Fell, 2005; Johnson, 2008b; Cooper and Gutiérrez, 2013; Milanović and others, 2019).

Several examples of gypsum-karst problems and dams in the United States are McMillan Dam (New Mexico), Quail Creek Dike (Utah), Upper Mangum Dam (Oklahoma), Anchor Dam (Wyoming), and Horsetooth and Carter Lake Dams (Colorado) (Johnson, 2008b).

McMillan Dam, on the Pecos River upstream of Carlsbad, NM, experienced leakage into gypsum-karst features in the Seven Rivers Formation during its entire life, from 1908 to 1991 (Cox, 1967). Quail Creek Dike failed in 1989 in part because of flow of water through an undetected gypsum-karst unit beneath an earth-fill embankment (James and others, 1989; O'Neill and Gourley, 1991; Payton and Hansen, 2003). The long-studied Upper Mangum Dam was abandoned before construction, because of extensive gypsum karst in the abutments and impoundment area (Johnson, 2003b). Anchor Dam, built in 1960, has significant drainage of water from the reservoir because of earth fissures, sinkholes, and gypsum karst that underlie the impoundment area (Jarvis, 2003). Horsetooth and Carter Lake Reservoirs, built upon gypsum-bearing strata in the 1940s, developed sinkholes and seepage loss of water in the 1980s and 1990s (Pearson, 2002).

Regional Character of the Rustler and Underlying Formations

The Rustler Formation consists of interbedded dolomite, limestone, gypsum, anhydrite, shale, siltstone, and sandstone (Ewing and others, 2012). Salt is locally present in the Rustler to the east, in eastern Loving County and beyond, but it is probably all removed by dissolution in the Red Bluff area. Salt has also been described in the Rustler in the northern Delaware Basin, near the Waste Isolation Pilot Plant (WIPP) site (Powers and others, 2006). Regional subsurface studies just east of the dam show that the Rustler now consists of gypsum/anhydrite, dolomite/limestone, shale, and some beds of salt (Fig. 3). Because of dissolution of salt and gypsum in the Rustler, Salado, and Castile Formations, most of the Salado, Rustler, and Dewey Lake strata in western Loving County and northern Reeves County are disrupted and brecciated (Fig. 4).

The Rustler Formation in Loving, Reeves, and Culberson Counties is subdivided into five members (Figs. 1, 5). Because of lateral variation in deposition of the Rustler Formation, all the members are not readily recognized in all parts of the region. The Magenta and Culebra Dolomites are generally widespread, and locally they are limestones or dolomitic limestones. Gypsum or anhydrite is fairly widespread in the Rustler, but these beds are more discontinuous than the dolomites. Because of dissolution of Salado salts, Rustler strata are highly

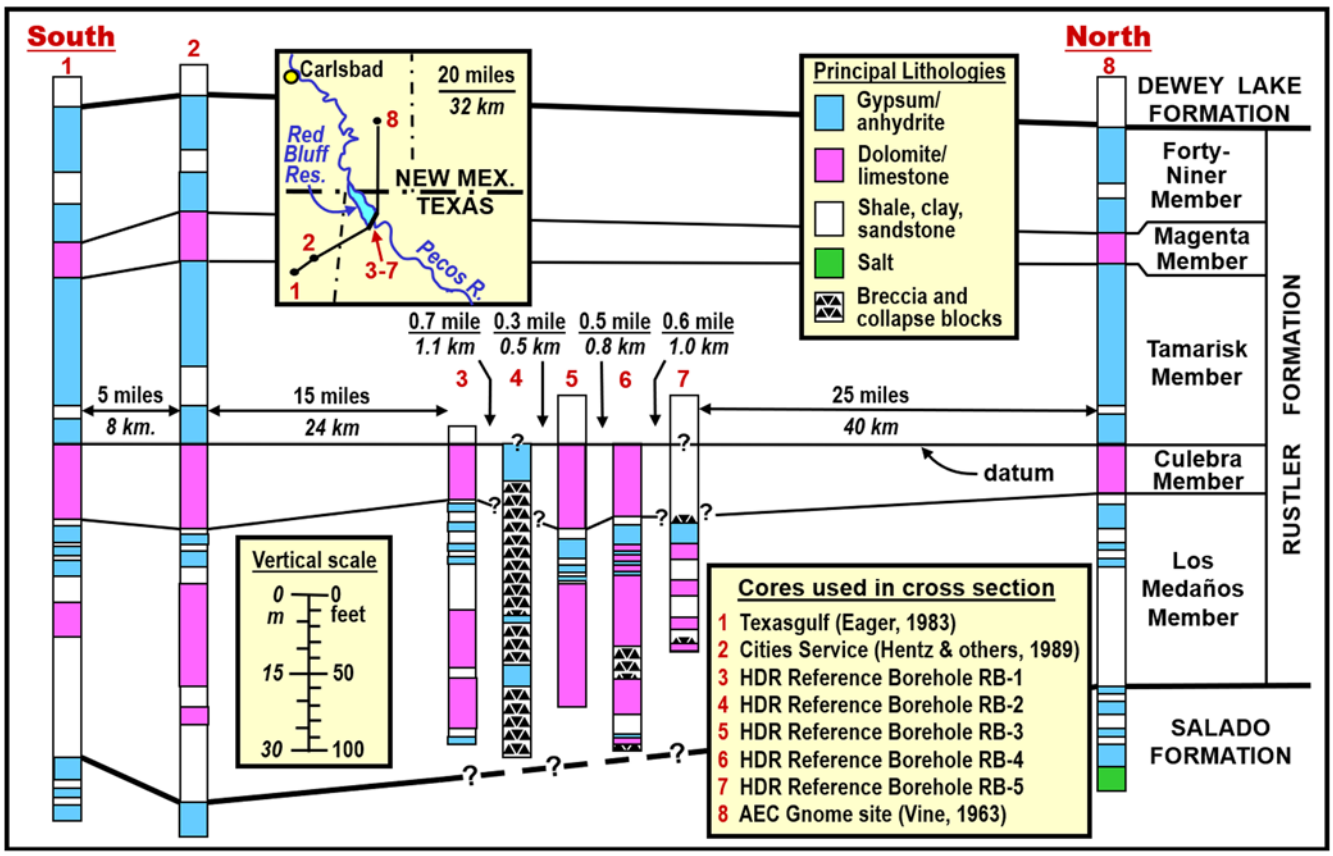

Figure 5. Stratigraphic cross section showing regional cores of the Rustler Formation from Culberson County, TX (south), to Eddy County, NM (north), and all five of the HDR Reference Boreholes (RB–1 through RB–5) at Red Bluff Dam. Numbering of wells (1–8) is unique to this cross section.

chaotic westward across the region, and it is difficult or impossible to recognize individual rock units of the Rustler is some areas (Figs. 3, 4). Rustler strata below the Culebra Dolomite farther north have been referred to as Nash Draw Member or Malaga Member by some workers, but we are unable to recognize them near Red Bluff and have adopted the simpler classification of Los Medaños Member (Figs. 1, 5).

About 25 miles north of Red Bluff, in Nash Draw, the Rustler formation was cored in 1958 by the Atomic Energy Commission (AEC) at the "Gnome Site" (Fig. 5, core #8). The Forty-Niner and Tamarisk Members both contain abundant gypsum, and the Los Medaños Member contains some gypsum (Vine, 1963). Gypsum is also reported in the Rustler Formation still farther north at the WIPP site (Powers and others, 2006), located about 25 miles east of Carlsbad and 33 miles north of Red Bluff.

The Rustler was also cored at two sites in Culberson County to the southwest, where the cores were taken as part of a sulfur-exploration program. One core was drilled by Texasgulf, Inc., at a site about 20 miles southwest of Red Bluff (Eager, 1983), and the other core was drilled by Cities Service Company at a site about 15 miles southwest of Red Bluff (Hentz and others, 1989) (Fig. 5, cores #1, 2). Here also the Forty-Niner and Tamarisk Members contain abundant gypsum, and minor amounts of gypsum are present in the Los Medaños Member. These two cores, and the AEC core at the Gnome Site, provide excellent data on the regional character of the Rustler within 15–25 miles of Red Bluff, so they are shown here in comparison with the HDR Reference Boreholes (RB–1 through RB–5) drilled at Red Bluff Dam in July 2012 (Figs. 5, 6).

The most-detailed geologic map of the Red Bluff area (Fig. 6) was prepared by Komie (1952): it shows that most of the area is mantled by Quaternary deposits, with only a few outcrops of bedrock. Because of sparse bedrock exposures, the locations of RB–1, 3, and 4 were chosen where we would encounter the Culebra Dolomite at shallow depth in each borehole, and we hoped we could establish the sequence of rock units that should be beneath the Culebra throughout the length of the dam. Any variation from this established sequence in other boreholes would be an anomaly and probably would be because of collapse that results from dissolution of underlying salt and gypsum beds.

Figure 5 shows all five of the HDR Reference Boreholes and illustrates the complex geology beneath the dam. Because of the regional abundance of gypsum

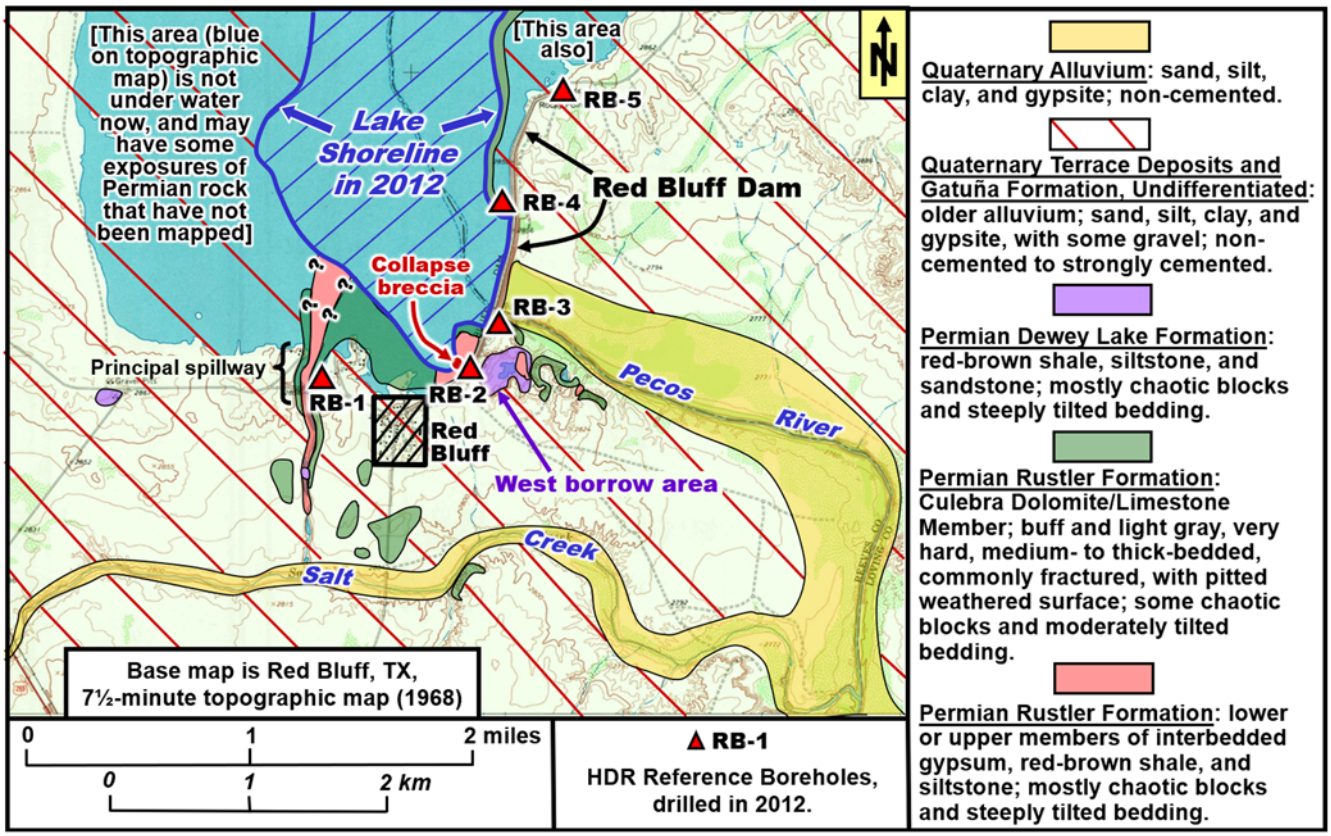

Figure 6. Generalized geologic map of Red Bluff Dam area. Based upon Komie (1952), AGRA (1994), and field observations made by authors of this report. Lake was smaller during field studies in 2012 than what is shown on published base map.

above the Culebra, and the paucity of gypsum below, we interpret that gypsum blocks in the collapse breccia drilled in RB–2 were dropped down from the overlying Tamarisk (and perhaps the Forty-Niner) Member. The chaotic nature of the geology beneath parts of the dam in this cross section affirms the complexity documented by AGRA (1994, see their Fig. 4.3, modified here as our Fig. 7).

A structure-contour map on top of Anhydrite I in the lower part of the Castile Formation (Fig. 8) shows that strata below the dissolution zone near Red Bluff dip gently to the east at about 90 feet per mile, or a dip of about 1º. All strata above this datum should also dip gently to the east across the area, except for the effect of dissolution of overlying salts (and gypsum/anhydrite) in the upper Castile, and in the Salado and Rustler Formations. Dissolution of these evaporites has caused considerable collapse and brecciation of the Salado and Rustler Formations, making it difficult to correlate rock layers or formation contacts in the immediate vicinity of Red Bluff Dam. Geophysical logs used to prepare Figure 8 are listed in Table 1 and were numbered on the map for simplicity.

A regional map showing structural contours on top of the Rustler Formation (Fig. 9) demonstrates how complex the structure is above the Castile Formation. The map, compiled from geophysical logs by Ewing and others (2012), shows sharp changes in elevation of the top of the Rustler within relatively short distances (a similarly complex structure map was prepared by Hiss, 1976). For example, instead of a gentle regional dip of about 90 feet per mile to the east (as in Fig. 8), the top of the Rustler in north-central Loving County plunges down at least 600 feet to the *west* within a distance of about 2 miles into a dissolution trough. And west of this trough the dip of the Rustler top is quite irregular throughout Loving and Reeves Counties. The cause of the dissolution trough and the irregularity of the Rustler structure is mainly dissolution of salt in the Salado Formation, and secondarily is dissolution of salt in the Castile and Rustler Formations (Figs. 3, 4). Most of the salt dissolution here probably occurred in Late Tertiary and Quaternary times (Ewing and others, 2012), but some Salado salt was also being dissolved at other places as early as during Salado time (Johnson, 1993; Holt and Powers, 2010). Complexity and structural chaos of

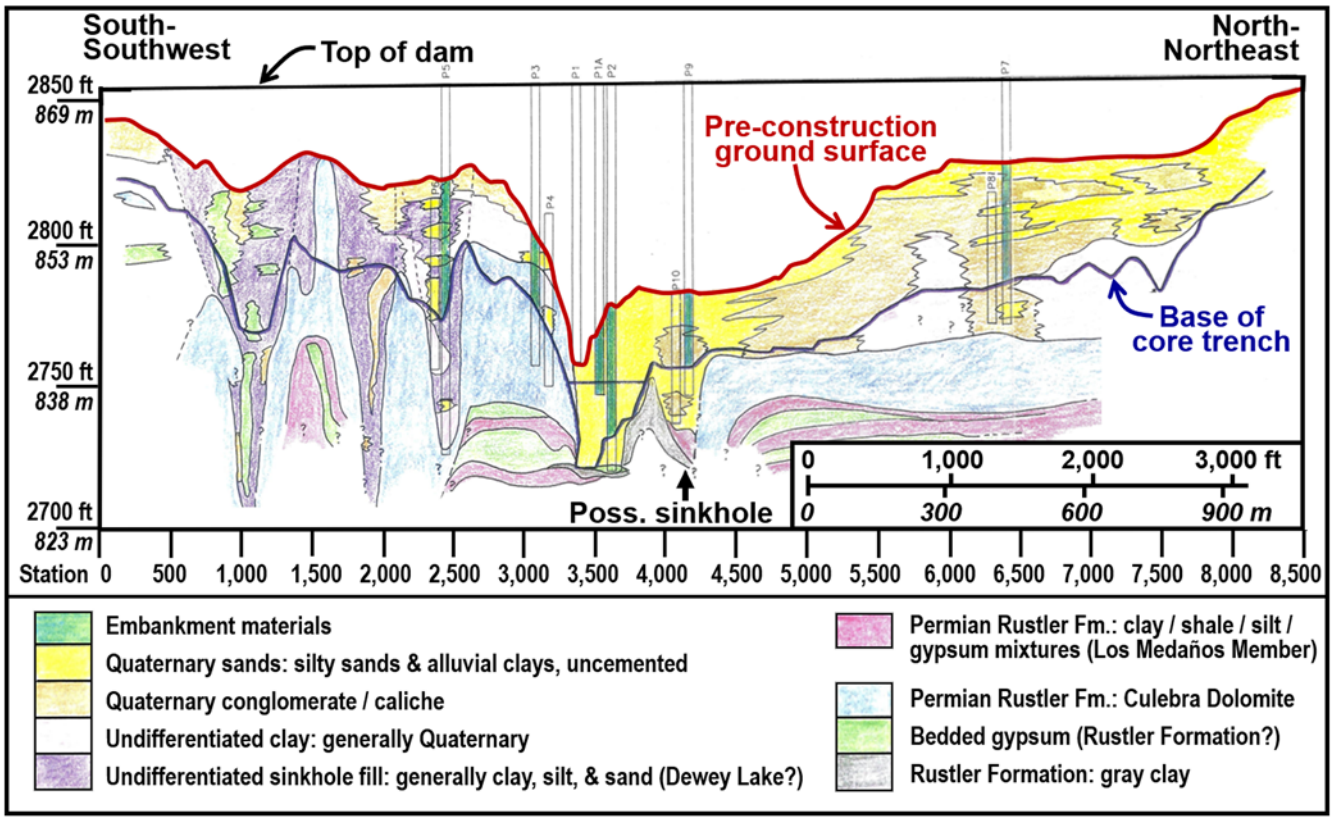

Figure 7. Conceptual cross section along Red Bluff Dam alignment, based upon historic borehole logs and excavations (modified from AGRA, 1994, figure 4.3). The complex geology of the dam foundation (particularly on left side of diagram) is mainly because of dissolution of underlying salt and gypsum layers, and resultant collapse and brecciation of overlying strata. Rustler bedrock in the right half of the cross section is probably as complex as in the left half.

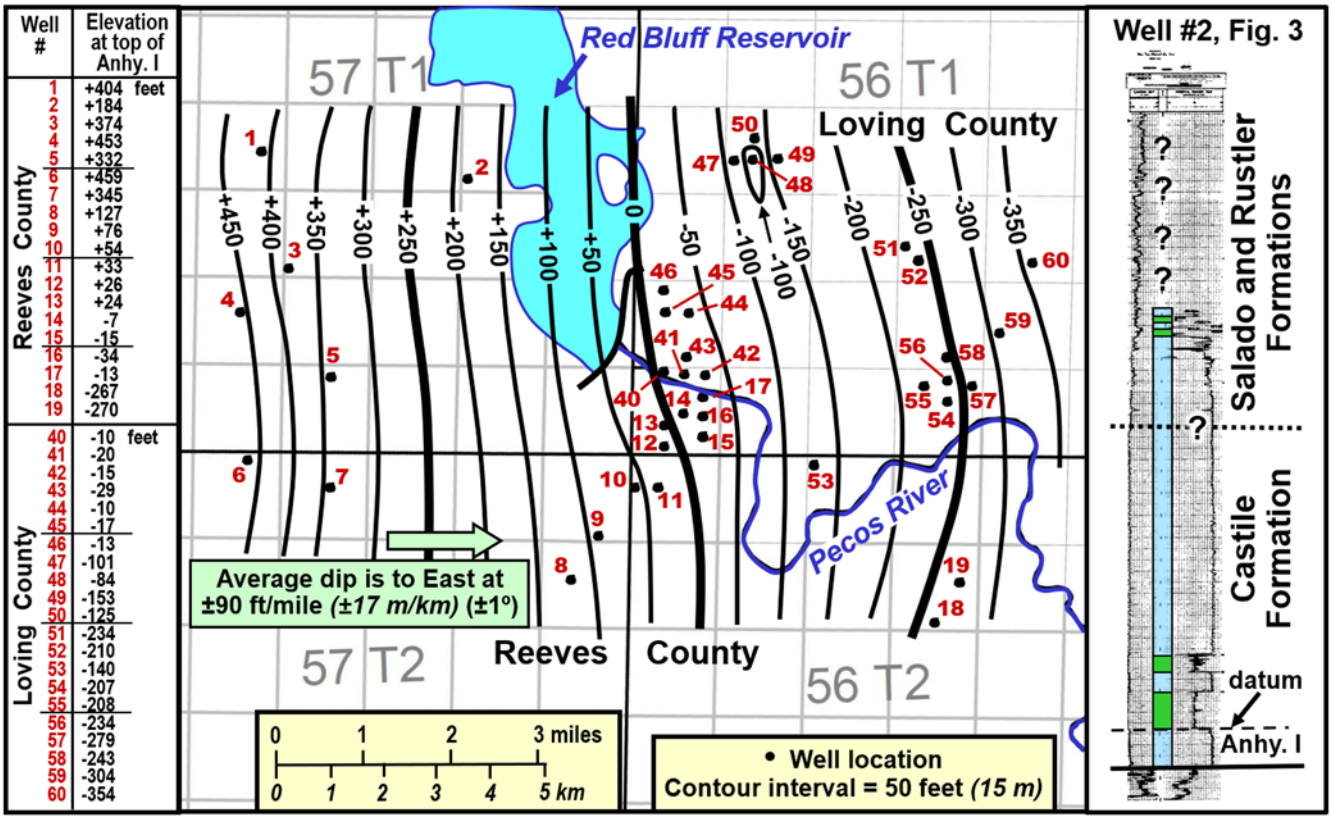

Figure 8. Structure-contour map on top of Anhydrite I in the Red Bluff Reservoir area. The datum (top of Anhydrite I) is just above the base of the Castile Formation, as shown on electric log to the right. Wells are identified in Table 1.

Rustler strata are well displayed in cross sections at and near the Red Bluff Dam (Figs. 3, 4, 5, 7).

Another map compiled by Ewing and others (2012) shows considerable variation in the thickness of the Rustler Formation in the region (Fig. 10). This variation results partly from dissolution of Rustler evaporites. Also, determining the base of the Rustler on geophysical logs (and therefore the thickness of the Rustler) in western Loving County and Reeves County can be difficult, because where the Salado salt has been dissolved, the collapse residue can be mistaken for similar material in the lower part of the Rustler (Ewing and others, 2012).

Local Character of the Rustler Formation

Outcrops of the Rustler Formation consist of dolomite, limestone, gypsum, and shale in the Red Bluff area. Although the formation contains five members in much of the Delaware Basin (Fig. 1), the chaotic nature of the geology around Red Bluff Dam makes it possible to definitely recognize only the Culebra Dolomite Member. Other random outcrops in the Rustler, such as the gypsum and shale, cannot be reliably assigned to a specific member in most outcrops. Figures 11, 12, and 13 show outcrops of mostly collapsed parts of the Rustler and Dewey Lake Formations in the vicinity of the dam, and Figure 14 shows cores of brecciated rock recovered in the HDR Reference Boreholes.

Culebra Dolomite Member

In the Red Bluff area, the most conspicuous exposures of Rustler strata are those of the Culebra Dolomite Member (Figs. 11, 12A). The Culebra is the most resistant rock unit in the Rustler Formation near Red Bluff, and it crops out extensively at several sites: just upstream of the dam; along the main spillway; adjacent to the (decommissioned) power plant; near the west borrow area; and several places south of the community of Red Bluff (Fig. 6). Because of dissolution of underlying salt and gypsum beds, the Culebra has been dropped into underlying cavities to form tilted blocks that commonly dip in various directions at angles of 15° to 30° (Figs. 11, 12A).

The chaotic nature of the Culebra (and all other units in the Rustler) is very well shown in Figure 5 and in the conceptual cross section along the dam alignment that was prepared earlier by AGRA (Fig. 7). These cross sections show the complexity of the local geology that results from dissolution of underlying salt (and gypsum) deposits and collapse of overlying strata into a chaotic jumble. It is likely that the true nature of the local geology beneath the dam is even more complex than what was

TABLE 1.—Oil and gas wells used to compile structure-contour map on top of Castile Formation Anhydrite I (Fig. 8). Well numbers (1–66) assigned by authors. API numbers are unique identifiers for each well drilled in the United States. Wells 61–66 are east of area in Figure 8, but were useful in identifying undissolved salt and gypsum layers.

Well #	API #	Operator Name	Lease Name	Well #	County
1	42389101250000	ORLA PETCO INC	TXL NCT B	4	REEVES
2	42389101370000	RITCHIE JMC	RD BLUFF CNTRIST 26	1-26	REEVES
3	42389314250000	ORLA PETCO INC	AGNES	2	REEVES
4	42389314030000	TEXACO INCORPORATED	REEVES `AD` FEE	2	REEVES
5	42389319450000	TEXACO INCORPORATED	REEVES `BU` FEE	5	REEVES
6	42389321120000	GRAYSTONE EXPL CORP	BURNER	9608	REEVES
7	42389102370000	J E H OILS	CONOCO-STATE	1	REEVES
8	42389321960000	SYNERGY OIL&GAS INC	LASELL STATE	1	REEVES
9	42389322630000	PENN VRGNIA OIL&GAS	MATHEWS NORTH PVOG	1	REEVES
10	42389315650000	CONOCO INCORPORATED	TUNSTILL O&L	4	REEVES
11	42389315170000	CONOCO INCORPORATED	TUNSTILL O&L	2	REEVES
12	42389315240000	TEXACO INCORPORATED	REEVES `BJ` FEE	1	REEVES
13	42389317050000	TEXACO INCORPORATED	REEVES `BJ` FEE	2	REEVES
14	42389320450000	MANZANO OIL CORP	TXL `43`	4	REEVES
15	42389320850000	MANZANO OIL CORP	TXL `43`	8	REEVES
16	42389320820000	MANZANO OIL CORP	TXL `43`	7	REEVES
17	42389320720000	MANZANO OIL CORP	TXL `43`	6	REEVES
18	42389325020000	CHAPARRAL ENERGY LLC	TUNSTILL JACK STATE	11	REEVES
19	42389324790000	CHAPARRAL ENERGY LLC	TUNSTILL JACK STATE	10	REEVES
40	42301310140000	MANZANO OIL CORP	TXL `43`	5	LOVING
41	42301309880000	MANZANO OIL CORP	TXL `43`	1	LOVING
42	42301309970000	MANZANO OIL CORP	TXL `43`	2	LOVING
43	42301309680000	J R P RESOURCES INC	JOHNSON `B42`	12	LOVING
44	42301309250000	RICHMOND PETRLM INC	JOHNSON `B42`	2	LOVING
45	42301309490000	RICHMOND PETRLM INC	JOHNSON `B42`	4	LOVING
46	42301309430000	RICHMOND PETRLM INC	JOHNSON `B42`	3	LOVING
47	42301314420000	CHAPARRAL ENERGY LLC	TXL	2905	LOVING
48	42301314130000	CHAPARRAL ENERGY LLC	TXL	2902	LOVING
49	42301314170000	CHAPARRAL ENERGY LLC	TXL	2904	LOVING
50	42301314010000	CHAPARRAL ENERGY LLC	TXL	2901	LOVING
51	42301312970000	CHAPARRAL ENERGY LLC	JOHNSON 34 `A`	1	LOVING
52	42301300450000	TEXACO INCORPORATED	LAGO UNIT	1	LOVING
53	42301303860000	TEXACO INCORPORATED	KROM HAROLD	1	LOVING
54	42301311570000	CHAPARRAL ENERGY LLC	HACIENDA STATE	1046	LOVING
55	42301312050000	CHAPARRAL ENERGY LLC	HACIENDA STATE	3046	LOVING
56	42301313160000	CHAPARRAL ENERGY LLC	HACIENDA STATE	4046	LOVING
57	42301311450000	CHAPARRAL ENERGY LLC	TYLER STATE	1-46	LOVING
58	42301311980000	CHAPARRAL ENERGY LLC	FRASER TXL E	1	LOVING
59	42301311630000	CHAPARRAL ENERGY LLC	JOHNSON W D	32	LOVING
60	42301311520000	CHAPARRAL ENERGY LLC	FRASER TXL	8	LOVING
61	42301307730000	ROSEWOOD RES INC	RRI STATE	108	LOVING
62	42301308330000	MARATHON OIL COMPANY	NORTH MASON UNIT	1503	LOVING
63	42301010030000	GERMANY&PAGE&GULF	TXL B 35	1	LOVING
64	42301009580000	SUTTON R E GULF	TXL 41	1	LOVING
65	42301000590000	CALTO OIL PAGE P GLF	TXL AL 5	1	LOVING
66	42301009920000	WILSON EXPL CO	GS BRUNSON	1	LOVING

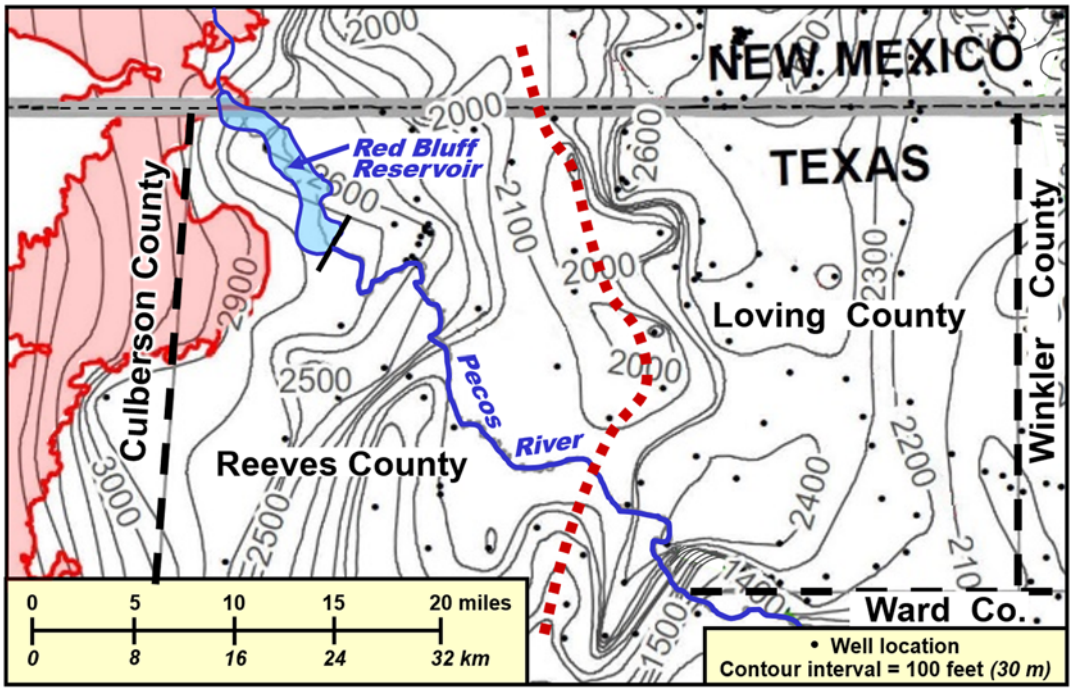

Figure 9. Structure-contour map on top of Rustler Formation (from Ewing and others, 2012). Structure is highly complex, mainly because of dissolution of salt beds in the underlying Salado Formation. Regional dip near Red Bluff Reservoir *should be* to the east at ±90 feet per mile (see Fig. 8). Rustler is chaotically dropped at least 600 feet (±180 m), from 2,600 feet down to less than 2,000 feet, in a major dissolution trough (dashed red line in center of map). Red shaded area in west is outcrop of Rustler Formation, according to Ewing and others (2012).

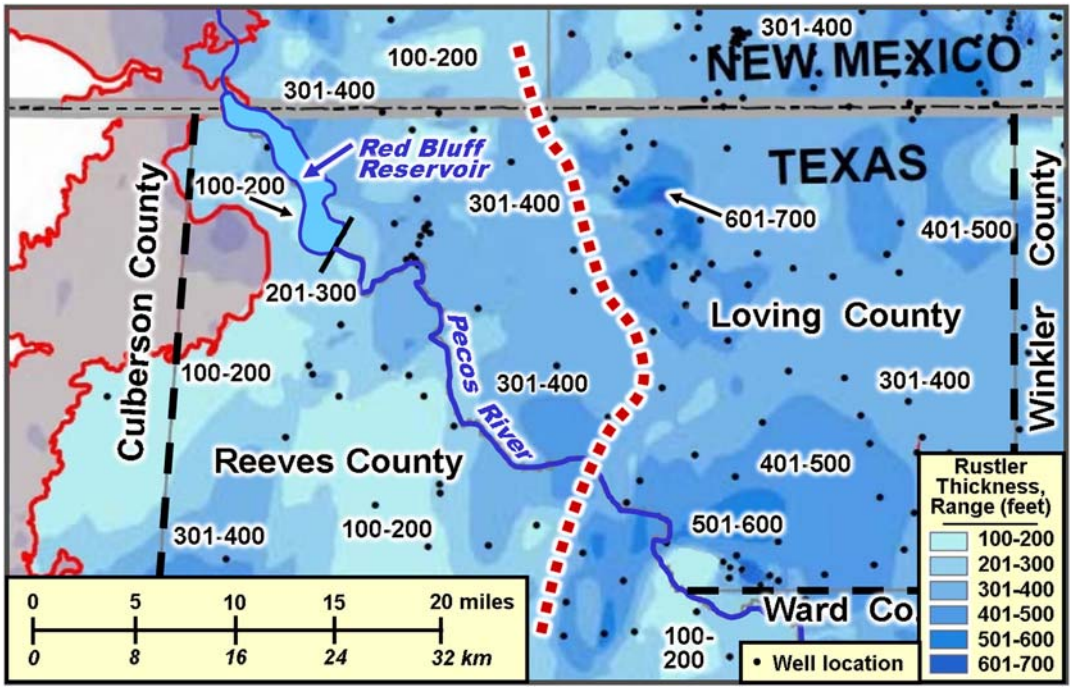

Figure 10. Thickness map of the Rustler Formation (modified from Ewing and others, 2012). Colors are areas of equal thickness, in 100s of feet (30 m). Thickness is highly variable, mainly because of dissolution of salt beds in the underlying Salado Formation and resultant collapse of the Rustler Formation. Locally, the Rustler thins abruptly by 200 to 400 feet (61-122 m), from 601 to 700 feet down to 301–400 feet, in a major dissolution trough (dashed red line in center of map). Red shaded area in west is outcrop of Rustler Formation, according to Ewing and others (2012).

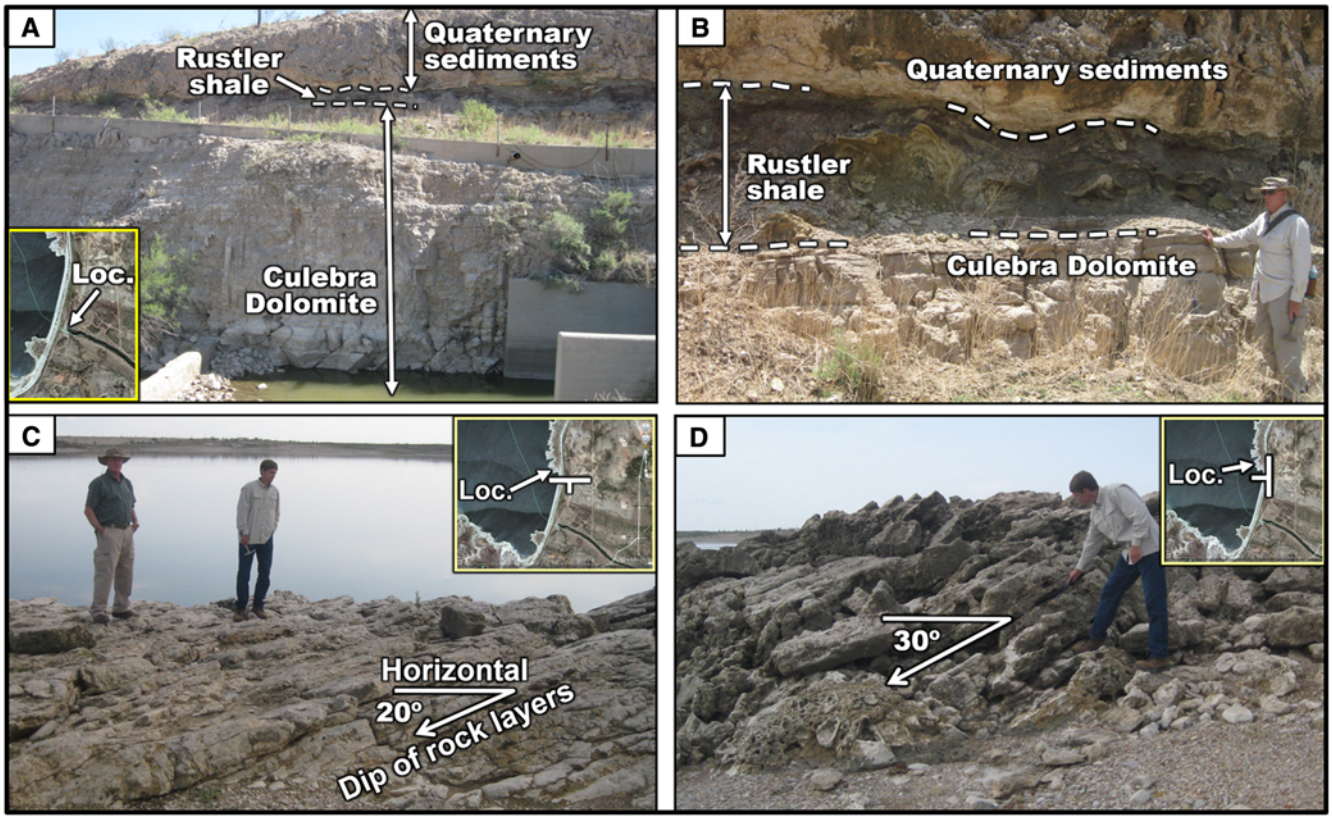

Figure 11. Views of Culebra Dolomite at Red Bluff Dam. A) Nearly horizontal Culebra, Rustler, and Quaternary strata at decommissioned power plant of dam. Culebra here contains two sets of fractures that are: 1) vertical and 2) dip about 45° down to the left (east-southeast). B) Close-up of upper part of Figure 11A, showing contorted bedding in Rustler shale between Culebra Dolomite and Quaternary sediments. C) Tilted block of Culebra Dolomite dips to the south at 20°. D) Tilted block of Culebra Dolomite (300 feet north of Figure 11C) dips to the west at 30°.

shown by AGRA (Fig. 7). The geology of Permian rocks beneath the Quaternary deposits on the right-hand (northeast) side of Figure 7 is probably as complex as it is beneath the left-hand (southwest) side, but there were not enough deep boreholes to show this when that cross section was prepared.

The Culebra appears to be little disturbed and nearly horizontal, at several places, including: at the decommissioned power plant (Figs. 11A, 11B); in the main spillway just north of the spillway gates; and south of the community of Red Bluff—but these are the exceptions. In places the Culebra is a true dolomite, whereas elsewhere it is a dolomitic limestone or even a limestone (hence, our occasional use of the term "dolomite/limestone").

In the Red bluff area, the Culebra commonly is buff, yellowish-gray or olive-gray, very hard, medium- to thick-bedded, fine-grained dolomite or dolomitic limestone. It locally contains inclusions of gypsum and calcite (Komie, 1952). In places it contains vugs and other pore spaces, because of dissolution of preexisting salt and/or gypsum originally deposited within the dolomite; this is similar to observations farther north at the WIPP Site, about 25 miles east of Carlsbad, NM (Powers and others, 2006). The Culebra is 35–55 feet thick in Reference Boreholes 1, 3, and 4 (Fig. 5) and is approximately 55 feet thick in local outcrops examined by Komie (1952). Where it is much thinner than 55 feet near Red Bluff Dam, this undoubtedly results from local erosion, dissolution, or collapse of some of the unit.

Being a somewhat water-soluble rock, the Culebra may locally be karstic and contain small or large solution cavities or passageways. Also, there are places where the Culebra is fractured or jointed (Fig. 11A), and these fractures can be pathways through which water can travel. Therefore, where the Culebra is fractured or karstic, it may contain openings that allow water to exit the reservoir and pass under the dam.

Gypsum

The second most conspicuous rock in the Rustler in the Red Bluff area is gypsum. Gypsum here is white, light- to medium-gray, or can even have a reddish hue (caused by iron oxides). In some places it is massive, and elsewhere it is thin-bedded. Regionally, gypsum is

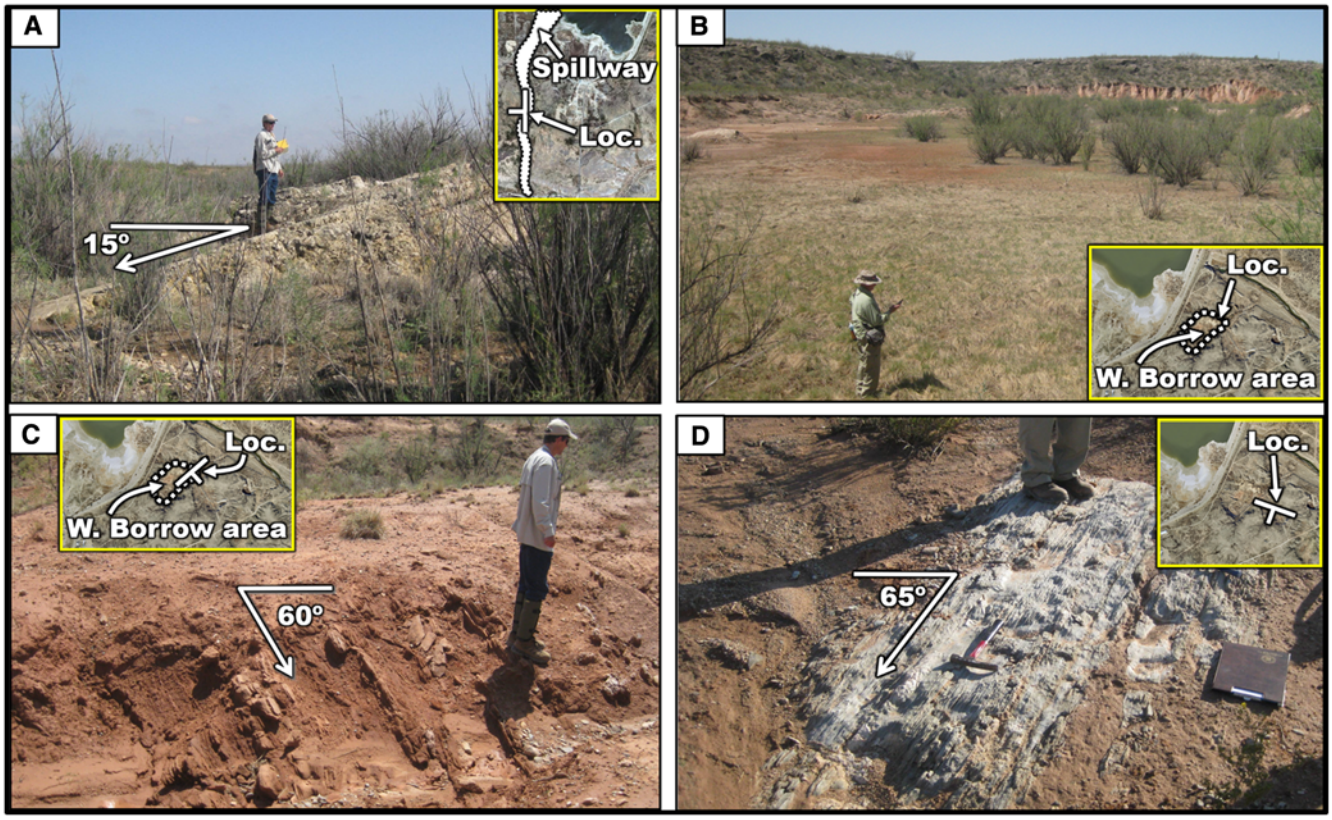

Figure 12. Views of collapse features near Red Bluff Dam. A) Tilted block of Culebra Dolomite dips to the west at 15° in dam spillway. B) View looking southwest over west borrow area, which contains many collapsed blocks of Dewey Lake Formation overlain by Quaternary conglomerate (in background). C) Collapsed block of Dewey Lake Formation redbeds (shale and siltstone) that dip to the southeast at 60° in west borrow area. D) Collapsed block of gypsum in Rustler Formation dips to the south-southwest at 65°, just east of the west borrow area.

present in the Forty-Niner, Tamarisk, and Los Medaños Members of the Rustler Formation (Fig. 5), and the same is probably true in the Red Bluff area. However, the chaotic nature of the Rustler beneath and near the dam (Figs. 4, 5, 7) makes it difficult to assign most of the gypsum beds or blocks to a particular member of the Rustler Formation. Komie (1952) reports that the thickness of individual gypsum units exposed in the area ranges from 8 to 27 feet, whereas RB–1 through RB–5 encountered gypsum units (or blocks) 3–22 feet thick (Fig. 5). Some of the gypsum units in the Reference Boreholes are probably collapsed blocks and may not represent the true thickness of the gypsum before its collapse. Examples of collapse blocks or fragments of gypsum are shown in Figures 12D, 13, and 14.

The most dramatic example of collapse breccia in the Red Bluff area is exposed on the south shore of the lake, just upstream of Red Bluff Dam station 1,500 (Figs. 13, 14A–C). At this site, chaotic blocks of gypsum are randomly oriented in an area that extends at least 200 feet in a N 30º E direction and at least 110 feet in a N 60º W direction: this collapse breccia, normally covered by lake water, was visible in 2012 because of an exceptionally low lake level and, unfortunately, may not be visible when lake levels rise. The bedding in various blocks of gypsum and other rock types here dips at angles of 20º to 90º in all directions, and individual exposed blocks are 1–27 feet across (Fig. 13).

Collapse blocks here result from dissolution of underlying beds of salt (and probably also some gypsum) and chaotic collapse of the Rustler Formation to form a collapse breccia. The gypsum blocks may be part of any of the Rustler members (Forty-Niner, Tamarisk, or Los Medaños Members), but they are so jumbled up that their true stratigraphic position cannot be determined. The full thickness or depth of this collapse breccia is not known, but RB–2 (intentionally drilled in the collapse breccia) remained in breccia to its total depth of 200 feet (Figs. 5, 14A–C). This area of collapse breccia is adjacent to an "area of surfacing seepage" just downstream of the dam, as noted by AGRA (1994) in their Figure 2.1 and as described in their Table 4.1.

Additional evidence of collapse breccia at, and beneath, the dam was presented by AGRA (Fig. 7). Borings and other interpretations by AGRA show areas of collapse breccia (AGRA called them "collapse structures")

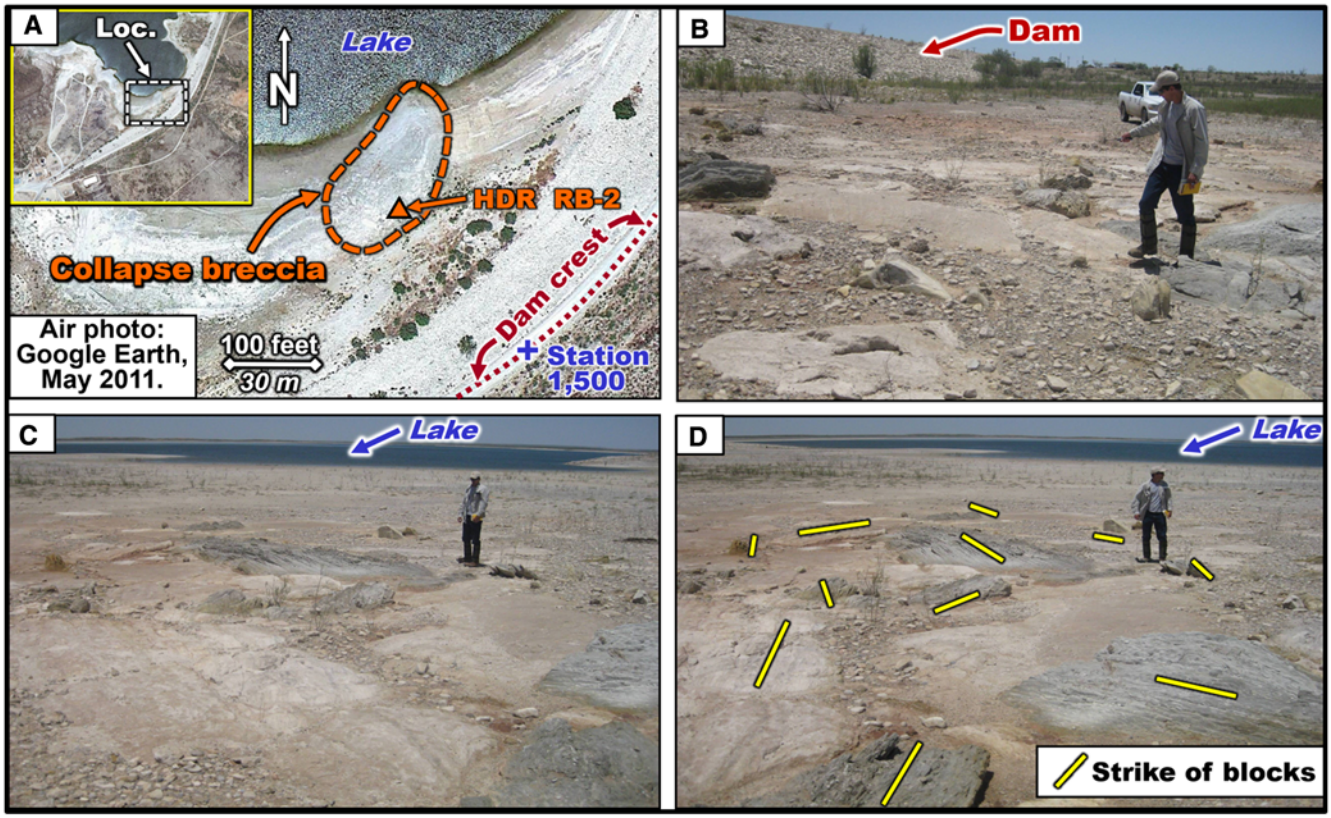

Figure 13. Views of collapse breccia near station 1,500 of Red Bluff Dam. A) Collapse breccia, exposed along south shore of lake during low water level, covers an area of 200 by 110 feet, and was drilled to a depth of 200 feet in the HDR RB–2 core. B) View, looking south, of collapse breccia consisting of gypsum and other rocks in blocks 1–27 feet across. C) Another view, looking north, of same collapse breccia with blocks of gypsum and other rocks. D) Another view, looking north, of same collapse breccia showing strike direction of strata in individual blocks of rock that dip in all directions at angles of 20° to 90°.

almost continuously on the left side of Figure 7, between dam stations 800 and 2,650: this part of the dam is adjacent to the collapse breccia described above, just upstream of dam station 1,500 (HDR RB–2; Figs. 5, 6, 13, 14A–C).

Gypsum is a moderately water-soluble rock—much more soluble than dolomite or limestone—and thus it is the most karstic rock in outcrops and shallow subsurface in the Red Bluff area. Some of the typical karst features, such as sinkholes and caves, are not evident in local outcrops, but there certainly are underground cavities and openings within, or adjacent to, gypsum layers or collapsed blocks. This is evident because of the many notations about a "cavity" or "void," 1–3 feet high, in the logs of boreholes and grout holes drilled beneath, or adjacent to, the dam (Reed and Associates, 1978). Similar cavities or voids are also noted in descriptions of HDR's RB–1 through RB–5 and grout holes drilled in the current grouting program (Charlton and others, 2021).

Karst features in gypsum may be a significant source of water loss beneath Red Bluff Dam. Because of the local abundance of gypsum, its moderate solubility, and the chaotic nature of gypsum blocks in the area, there are ample opportunities for water to seep down to, and into, any cracks, cavities, or other openings in (or adjacent to) the gypsum. And because of gypsum's solubility, water that is unsaturated with respect to calcium sulfate will further dissolve the gypsum and may enlarge any openings in the rock, thus enhancing and increasing the flow of water over time.

Shale, Siltstone, and Sandstone

Shale, along with siltstone and sandstone, make up the remainder of rocks locally present in the Rustler Formation. These rocks or sediments are rarely seen in local outcrops, but have been drilled and cored in many of the boreholes in the dam foundation (Reed and Associates, 1978). They are described as shale, clay, siltstone, and/or sandstone that are in various colors, including tan, red, brown, gray, dark gray, and olive gray. These types of sedimentary rocks are present in all members of the Rustler Formation in the region (except the Culebra and

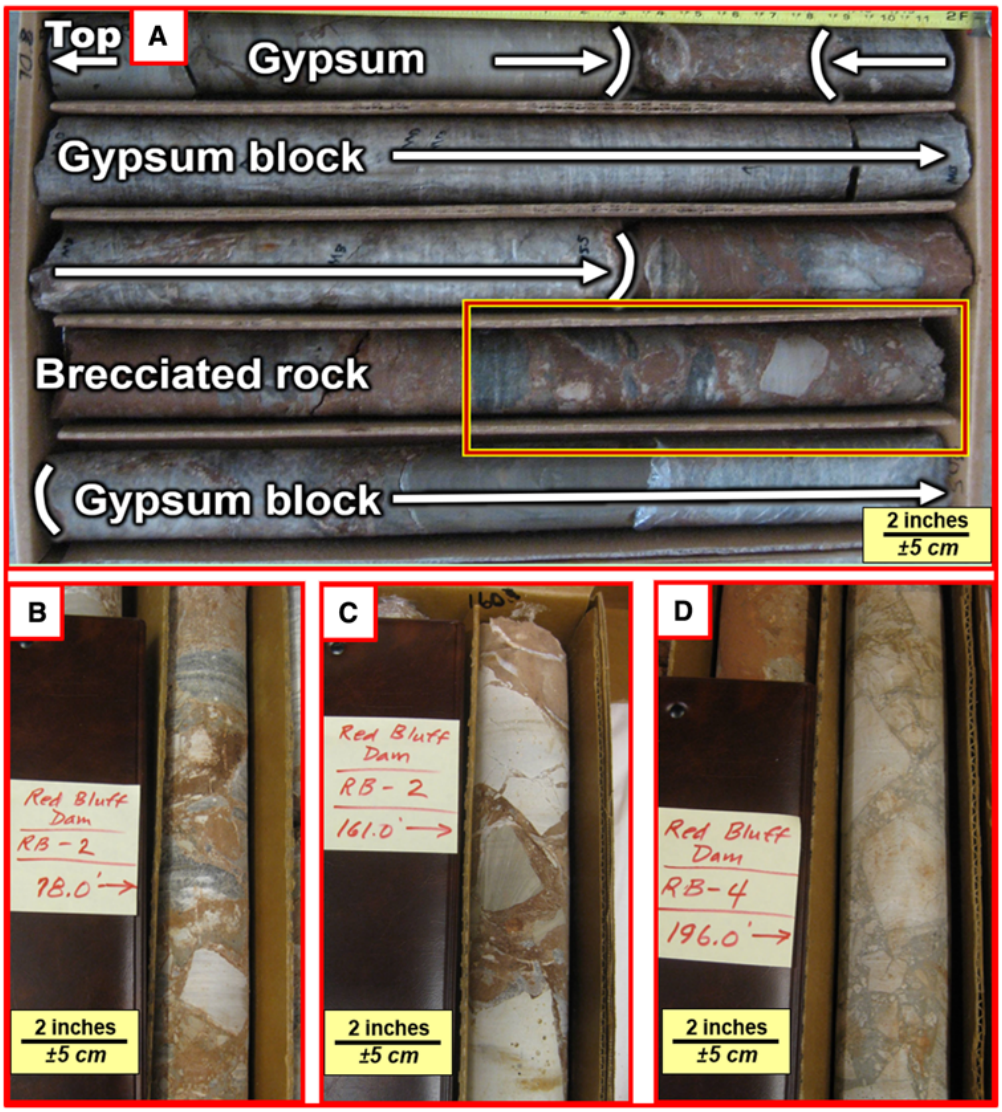

Figure 14. Brecciated rock in NX cores (about 2.15 inches in diameter) drilled in collapse breccia near station 1,500 of Red Bluff Dam (borehole HDR RB–2) and at northeast end of dam (borehole HDR RB–4). A) A 2-foot-long box of core (depth, 70.5 to 80.5 feet) from RB–2 contains large blocks of gypsum, as well as small-scale brecciated rock (outlined in red). B) Small-scale brecciated rock in core from RB–2 includes angular fragments of gypsum, dolomite, and shale recemented in a matrix of red-brown mudstone (marker is 78.0 feet deep). C) Similar small-scale breccia in core from RB–2 (marker is 161.0 feet deep). D) Similar small-scale breccia in core from RB–4 (marker is 196.0 feet deep).

Magenta Dolomite Members), but, because of the chaotic nature of the Rustler in the Red Bluff area, in most cases it is impossible to assign these rocks to any particular member.

One outcrop where a shale unit can be reliably assigned is at the Power Plant (Figs. 11A, 11B). At this site, several feet of contorted shale in the Rustler Formation directly overlies the Culebra Dolomite and therefore is part of the Tamarisk Member. The highly contorted bedding within this shale probably results from dissolution of preexisting gypsum and/or salt layers that were interbedded with, or were directly beneath, the shale.

Other Local Rocks and Deposits

Other rocks and deposits near and beneath Red Bluff Dam are 1) the Salado and Castile Formations that underlie the Rustler; 2) the Dewey Lake Formation that overlies the Rustler; and 3) Quaternary deposits that blanket and overlie Permian rocks in most of the area.

Salado and Castile Formations

Beneath the Rustler Formation are the salt and gypsum/anhydrite units of the Salado and Castile Formations (Figs. 1, 3–5). They are not exposed anywhere

within perhaps 10 miles of the dam, but they have a profound influence on the local geology, at and near the dam. Because of dissolution of salt and gypsum/anhydrite within these formations (Fig. 4), the Rustler Formation has been chaotically disrupted, and it is very difficult to recognize individual Rustler rock units in outcrops or correlate them in the many boreholes that have been drilled—the one exception being the Culebra Dolomite, which is conspicuous in outcrops and is generally recognizable in boreholes. Because of extensive dissolution within the Salado, it is also very difficult to recognize the top and base of the formation near the dam (Fig. 3), and therefore only units in the Castile Formation are clearly recognizable.

Dewey Lake Formation

The Dewey Lake Formation, which directly overlies the Rustler Formation regionally, as well as at and near the dam (Figs. 1, 3–6), is mostly reddish-brown shale and siltstone (Figs. 12B–C). It is the youngest Permian-age formation in the Delaware Basin. The Dewey Lake is poorly exposed in the vicinity of the dam, but it has a reported thickness of about 110 feet in nearby parts of Loving County (Komie, 1952); he described the scattered exposures of Dewey Lake, located some 3–5 miles north of the dam, as "remnants interred as fill in tremendous sinkholes" (Komie, 1952, p. 17).

Exposures of the Dewey Lake Formation near the dam (Fig. 6) are located: 1) in the west borrow area; 2) in a small area about 0.3 mile south of the main spillway; and 3) in a quarry located about 1.25 miles west of the community of Red Bluff. In each of these locations, Dewey Lake strata are highly disrupted and chaotic as a result of dissolution of underlying salt and gypsum/anhydrite units.

The west borrow area (shale was excavated here for the core of the dam) is a substantial area of collapse containing numerous exposures of chaotic blocks of Dewey Lake redbeds that dip at moderate to steep angles in various directions (Figs. 12B–C). Although these exposures were not originally recognized as Dewey Lake strata by Komie (1952), they were later recognized by AGRA (1994), and we agree with the AGRA interpretation. It is possible that some of the collapse features in the west borrow area are connected with the collapse breccia of Rustler gypsum blocks northwest of dam station 1,500, inasmuch as these collapse areas are only a couple of hundred feet apart, on opposite sides of the dam (Fig. 6).

The small collapse block of reddish-brown shale and siltstone, located about 0.3 mile south of the main spillway (Fig. 6), is believed to be an exposure of the Dewey Lake Formation. It has all the lithologic characteristics of the Dewey Lake, and the 20-foot-wide block dips at an angle of 70º.

The third known local exposure of Dewey Lake strata is in a quarry, or pit, about 1.25 miles west of the Red Bluff community. At this site, one exposure of Dewey Lake redbeds dips toward S 30º E at an angle of about 40º. The Dewey Lake here is overlain unconformably by Quaternary sediments.

Quaternary Deposits

Quaternary deposits include a variety of sands, silts, clays, gravels, and other sediments laid down in rivers, streams, and lakes or ponds that covered Permian bedrock during the Quaternary Period. They include present-day alluvium along the banks and floodplains of Pecos River and Salt Creek, as well as terrace deposits and the Gatuña Formation. These sediments are noncemented to strongly cemented, and they mantle, overlie, and conceal the great complexity that exists in the Rustler and other bedrock formations at most places near the dam (Figs. 6, 7, 11A–B). Aside from Pecos River and Salt Creek alluvium, the other Quaternary deposits are not differentiated on the geologic map (Fig. 6).

It is likely that some of the seepage, particularly on the northeast side of the dam, is flowing through the weakly to strongly cemented layers of Quaternary silt, sand, and conglomerate (Fig. 7). AGRA (1994, p. 27) reports that shallow groundwater is found in boreholes all along the toe of the dam along its northeast extent, and much of the water appears to be following flow paths under the core and cutoff trench of the dam. This results in shallow-water or surface seepage at points downstream of the dam at several places between dam stations 4,000 and 7,000 (AGRA, 1994, see their Figure 2.1).

Gypsite, a Quaternary deposit, is an earthy variety of gypsum that forms by precipitation of gypsum crystals in lakes or ponds whose water is supersaturated with calcium sulfate that has been weathered and eroded from nearby Permian gypsums. It is a noncemented deposit that typically contains clay, silt, and/or sand washed into the lake or pond during precipitation. Gypsite deposits in the area are up to 10–20 feet thick. Gypsite is no particular problem, as far as loss of water from Red Bluff Reservoir. It may be present in the foundation on the northeast side of the dam (on the right side of Fig. 7), but it would be interspersed with layers of noncemented sand, silt, and clay, and should be no more of a problem than any of the sands with which it is associated.

CONCLUSION: LOSS OF WATER BENEATH RED BLUFF DAM

The main causes of water loss beneath Red Bluff Dam appear to be because of the following: 1) dissolution of salt and/or gypsum beds in the Rustler, Salado, and Castile Formations; 2) collapse and chaotic disruption of gypsum, dolomite, and other rocks in the Rustler

Formation; 3) development of karst features within the gypsum and dolomite units and collapsed blocks of the Rustler Formation; and 4) probable seepage through Quaternary sands and gravels, chiefly beneath the northeast side of the dam.

Dissolution of salt and/or gypsum in the Rustler, Salado, and Castile Formations has led to subsidence and collapse of overlying strata—particularly in the Rustler Formation (Figs. 4, 7). As a result, the Rustler and overlying Dewey Lake Formations have been chaotically dropped into underground solution cavities to form several collapse breccias, such as the one observed just northwest of dam station 1,500 (Figs. 13, 14A–C), and other collapse features at various places adjacent to the dam, in the spillway, and in the west borrow area (Figs. 11, 12). Such chaotic brecciation has contorted and fractured the Culebra Dolomite and the many gypsum beds in the Rustler (Fig. 7), opening up numerous pathways for water to seep through the breccia. Movement of groundwater through the fractures and breccia zones, and through other areas underlain by gypsum, causes karst development in the water-soluble rocks, and this further enables water to flow beneath the dam.

The main area for this water loss appears to be on the southwest side of the dam, between stations 800 and 2,650, producing surface seepage that flows through the west borrow area and into the Pecos River. It is also possible that similar breccia zones, karst features, and flow paths underlie the northeast side of the dam, but data are inconclusive at this time. Beneath the northeast side of the dam, the weakly to strongly cemented sands and gravels (Fig. 7) apparently are permeable enough to allow lake water to seep under the dam between dam stations 4,000 and 7,000, and this water then surfaces and flows through the east borrow area and into the Pecos River.

REFFERENCES CITED

AGRA, 1994, Red Bluff Dam geotechnical investigation and piezometer installation project, Red Bluff, Texas: unpublished report *submitted to* HDR Engineering, Inc., Austin, TX, from AGRA Earth & Environmental, Inc., El Paso, TX, as AGRA E&E Job No. E94-4067, 35 p., plus Appendices A–G.

Alger, R.P., and Crain, E.R., 1966, Defining evaporite deposits with electric well logs, *in* Rau, J.L., ed., Second symposium on salt: Cleveland, Northern Ohio, Geological Society, Vol. 2, p. 116-130. http://www.ross-crain.com/freepubs/1966-2%20Defining%20Evaporite%20Deposites%20With%20Electrical%20Well%20Logs%20%20NOGS-SALT%20Alger-Crain.pdf

Anderson, R.Y., Dean, W.E., Jr., Kirkland, D.W., and Snider, H.I., 1972, Permian Castile varved evaporite sequence, west Texas and New Mexico: Geological Society of America Bulletin, Vol. 83, p. 59-86. https://www.wipp.energy.gov/library/CRA/2009_CRA/references/Others/Anderson_et_al_1972_Permian_Castile.pdf

Ashworth, J.B., 1990, Evaluation of ground-water resources in parts of Loving, Pecos, Reeves, Ward, and Winkler Counties, Texas: Texas Water Development Board, Report 317, 51 p. http://www.twdb.texas.gov/publications/reports/numbered_reports/doc/R317/R317.pdf

Bachman, G.O., 1984, Regional geology of Ochoan evaporites, northern part of Delaware Basin: New Mexico Bureau of Mines and Mineral Resources, Circular 184, 22 p. https://geoinfo.nmt.edu/publications/monographs/circulars/downloads/184/Circular-184.pdf

Boghici, R., and Van Broekhoven, N.G., 2001, Hydrogeology of the Rustler aquifer, Trans-Pecos Texas, *in* Mace, R.E., Mullican, W.F., III, and Angle, E.S., eds., Aquifers of west Texas: Texas Water Development Board Report 356, p. 207-225. https://www.twdb.texas.gov/publications/reports/numbered_reports/doc/R356/Ch15_Rustler.pdf

Charlton, J., Ostrowsky, J., Shoemaker, R.A., and Johnson, K.S., 2021, Design and implementation of a grout program in an evaporite-karst foundation, Red Bluff Dam, Loving and Reeves Counties, Texas, *in* Johnson, K.S., Land, L., and Decker, D.D., eds., Evaporite karst in the Greater Permian Evaporite Basin (GPEB) of Texas, New Mexico, Oklahoma, Kansas, and Colorado: Oklahoma Geological Survey, Circular 113.

Chen, F., and Wu, M, 1983, Investigation of the engineering properties of a dam foundation containing gypsum seams: Rock Mechanics and Rock Engineering, Vol. 16, No. 4, p. 275-280.

Cooper, A.H., Gutiérrez, F., 2013, Dealing with gypsum karst problems: hazards, environmental issues, and planning, *in* Shroder, J., ed. In chief, Frumkin, A., ed., Treatise on Geomorphology: Academic Press, San Diego, CA, Vol. 6, Karst Geomorphology, pp. 451–462. https://www.researchgate.net/publication/262373474

Cox, E.R., 1967, Geology and hydrology between Lake McMillan and Carlsbad Springs, Eddy, County, New Mexico: U.S. Geological Survey, Water-Supply Paper 1828, 48 p. https://pubs.usgs.gov/wsp/1828/report.pdf

Eager, G.P., 1983, Core from the lower Dewey Lake, Rustler, and upper Salado Formations, Culberson County, Texas, *in* Shaw, R.L., and Pollan, B.J., eds., Permian Basin cores—a workshop: Permian Basin Section, S.E.P.M. Core Workshop #2, p. 273-283.

Ege, H.R., 1985, Maps showing distribution, thickness, and depth to salt deposits of the United States: U.S.

Geological Survey, Open-File Report 85–28, 11 p., map scale, 1:2,500,000. https://pubs.er.usgs.gov/publication/ofr8528

Eifler, G.K., Jr., Geologic Atlas of Texas, Pecos Sheet: Texas Bureau of Economic Geology, scale 1:250,000.

Ewing, J.E., Kelley, V.A, Jones, T.L., Yan, T, Singh, A., Powers, D.W., Holt, R.M., and Sharp, J.M., 2012, Groundwater availability model report for the Rustler aquifer: Texas Water Development Board, Draft Final Report, about 400 p. https://www.twdb.texas.gov/groundwater/models/gam/rslr/RSLR_GAM_Report.pdf

Fell, R., 2005, Geotechnical engineering of dams: A.A. Balkema, Leiden, New York, 912 p.

Hentz, T.F., Price, J.G., and Gutierrez, G.N., 1989, Geologic occurrence and regional assessment of evaporite-hosted native sulfur, Trans-Pecos Texas: Texas Bureau of Economic Geology, Report of Investigations No. 184, 70 p.

Hill, C.A., 1996, Geology of the Delaware Basin, Guadalupe, Apache, and Glass Mountains, New Mexico and west Texas: Society of Economic Paleontologists and Mineralogists, Permian Basin Section, Publication No. 96–39, 480 p.

Hill, C.A., 2003, Intrastratal karst at the Waste Isolation Pilot Plant site, southeastern New Mexico, *in* K.S. Johnson and J.T. Neal, eds., Evaporite karst and engineering/ environmental problems in the United States: Oklahoma Geological Survey Circular 109, p. 197-209. http://ogs.ou.edu/docs/circulars/C109.pdf

Hiss, W.L., 1976, Structure of the Permian Ochoan Rustler Formation, southeast New Mexico and west Texas: New Mexico Bureau of Mines and Mineral Resources, Resource Map 7, scale 1:500,000. https://geoinfo.nmt.edu/publications/maps/resource/downloads/7/RM-7.pdf

Holt, R.M., and Powers, D.W., 2010, Evaluation of halite dissolution at a radioactive waste disposal site, Andrews County, Texas: Geological Society of America Bulletin, v. 122, p. 1989-2004.

James, A.N., and Lupton, A.R.R., 1978, Gypsum and anhydrite in foundations of hydraulic structures: Geotechnique, Vol. 28, No. 3, p. 249-272.

James, A.N., and Kirkpatrick, I.M., 1980. Design of foundations of dams containing soluble rocks and soils: Quarterly Journal of Engineering Geology, Vol. 13, p. 189-198.

James, R.L., Catanach, R.B., O'Neill, A.L., and Von Thun, J.L., 1989, Investigation of the cause of Quail Creek Dike failure: Unpublished report of the Independent Review Team to Norman H. Bangerter, Governor of Utah, 155 p.

Jarvis, T., 2003, The money pit: karst failure of Anchor Dam, Wyoming, *in* K.S. Johnson and J.T. Neal, eds., Evaporite karst and engineering/environmental problems in the United States: Oklahoma Geological Survey Circular 109, p. 271–278. http://ogs.ou.edu/docs/circulars/C109.pdf

Johnson, K.S., 1993, Dissolution of Permian Salado salt during Salado time in the Wink area, Winkler County, Texas, *in* D.W. Love and others, eds., Carlsbad region, New Mexico and west Texas: New Mexico Geological Society Guidebook, 44th Annual Field Conference (October 6–9, 1993), p. 211-218. https://www.researchgate.net/publication/268385405

Johnson, K.S., 1996, Gypsum karst in the United States, in A. Klimchouk and others, eds., Gypsum karst of the world: International Journal of Speleology, v. 25, nos. 3–4, p. 183-193. https://scholarcommons.usf.edu/ijs/vol25/iss3/13/

Johnson, K.S., 2003a, Evaporite-karst problems in the United States, *in* K.S. Johnson and J.T. Neal, eds., Evaporite karst and engineering/environmental problems in the United States: Oklahoma Geological Survey Circular 109, p. 1-20. http://ogs.ou.edu/docs/circulars/C109.pdf

Johnson, K.S., 2003b, Gypsum karst and abandonment of the Upper Mangum Damsite in southwestern Oklahoma, *in* K.S. Johnson and J.T. Neal, eds., Evaporite karst and engineering/environmental problems in the United States: Oklahoma Geological Survey Circular 109, p. 85-94. http://ogs.ou.edu/docs/circulars/C109.pdf

Johnson, K.S., 2008a, Evaporite-karst problems and studies in the USA: Environmental Geology, Vol. 53, No. 5, p. 937-943. https://www.researchgate.net/publication/225519191

Johnson, K.S., 2008b, Gypsum-karst problems in constructing dams in the USA: Environmental Geology, Vol. 53, No. 5, p. 945-950. https://www.researchgate.net/publication/226513928

Johnson, K.S., 2021, Identification of gypsum, anhydrite, and salt on geophysical logs in the Greater Permian Evaporite Basin, *in* Johnson, K.S., Land, L., and Decker, D.D., eds., Evaporite karst in the Greater Permian Evaporite Basin (GPEB) of Texas, New Mexico, Oklahoma, Kansas, and Colorado: Oklahoma Geological Survey, Circular 113.

Johnson, K.S., and Gonzales, S., 1978, Salt deposits in the United States and regional characteristics important for storage of radioactive wastes: prepared for Union Carbide Corp., Nuclear Division, Oak Ridge National Laboratory, Office of Waste Isolation, Y/OWI/SUB-7414/1, 188 p. Also available from: Oklahoma Geological Survey, Open-File Report 18-2018. http://www.ou.edu/content/dam/ogs/documents/data/OF18-2018.pdf

Johnson, K.S., Gonzales, S., and Dean, W.E., 1989, Distribution and geologic characteristics of anhydrite deposits in the United States, *in* W. E. Dean and K. S. Johnson, eds., Anhydrite deposits of the United States and characteristics of anhydrite important for storage of radioactive wastes: U.S. Geological Survey Bulletin 1794, p. 9–90. https://pubs.usgs.gov/bul/1794/report.pdf

Komie, K.E., 1952, Geology of Red Bluff Lake area, Loving and Reeves Counties, Texas: unpublished M.S. Thesis, The University of Texas, 73 p.

Lambert, S.J., 1983, Dissolution and evaporites in and around the Delaware Basin, southeastern New Mexico and west Texas: Sandia National Laboratory, Albuquerque, New Mexico, SAND 82–0461. https://pdfs.semanticscholar.org/19b4/e083b9d9d611677ef0860ac31ca4a764286f.pdf?

Land, L., 2013, Evaporite karst in the Permian Basin region of west Texas and southeastern New Mexico: the human impact, *in* Land, L., Doctor, D.H., and Stephenson, J.B., eds., Sinkholes and the engineering and environmental impacts of karst–Proceedings of the thirteenth multidisciplinary conference, Carlsbad, NM, May 6 through 10, 2013: National Cave and Karst Research Institute, Carlsbad, NM, p. 113-121. http://scholarcommons.usf.edu/cgi/viewcontent.cgi?article=1119&context=sinkhole_2013

Maley, V.C, and Huffington, R.M., 1953, Cenozoic fill and evaporite solution in the Delaware Basin, Texas and New Mexico: Geological Society of America, Bulletin, v. 64, p. 539-546.

Martinez, J.D., Johnson, K.S., and Neal, J.T., 1998, Sinkholes in evaporite rocks: American Scientist, v. 86, No. 1 (January–February), p. 38-51. https://www.researchgate.net/publication/250968543

Milanović, P.T., 2000, Geologic engineering in karst: Zebra Publishing Ltd., Belgrade, Yugoslavia, 347 p.

Milanović, P.T., 2018, Engineering karstology of dams and reservoirs: CRC Press, Taylor and Francis Group, Boca Raton, FL, 356 p.

Milanović, P.T., 2019, Maksimovich, N., and Meshcheriakova, O, 2019, Dams and reservoirs in evaporites: Springer Nature Switzerland, 156 p.

Nurmi, R.D., 1978, Use of well logs in evaporite sequences, *in* Dean, W.E., and Schreiber, B.C., eds, Marine evaporites: Society of Economic Paleontologists and Mineralogists, SEPM Short Course No. 4 held in Oklahoma City, p. 144-176.

O'Neill, A.L., and Gourley, C., 1991, Geologic perspectives and cause of the Quail Creek Dike failure: Bulletin of Association of Engineering Geologists, Vol. 27, No. 2, p. 127-145.

Olive, W.W., 1957, Solution-subsidence troughs, Castile Formation of Gypsum Plain, Texas and New Mexico: Geological Society of America, Bulletin, Vol. 68, p. 351-358.

Payton, C.C., and Hansen, M.N., 2003, Gypsum karst in southwestern Utah: failure and reconstruction of Quail Creek Dike, *in* K.S. Johnson and J.T. Neal, eds., Evaporite karst and engineering/environmental problems in the United States: Oklahoma Geological Survey Circular 109, p. 293-303. http://ogs.ou.edu/docs/circulars/C109.pdf

Pearson, R.M., 2002, Gypsum karst of the Lykins Formation and effects for Colorado Front Range water projects; Horsetooth and Carter Lake Reservoirs: Geological Society of America, Abstracts with Programs, Vol. 34, No. 6, p. 216.

Pierce, W.G., and Rich, E.I., 1962, Summary of rock salt deposits in the United States as possible storage sites for radioactive waste materials: U.S. Geological Survey, Bulletin 1148, 91 p. https://pubs.er.usgs.gov/publication/b1148

Powers, D.W., and Holt, R.M., 1999, The Los Medaños Member of the Permian (Ochoan) Rustler Formation: New Mexico Bureau of Geology & Mineral Resources, New Mexico Geology, Vol. 21, No. 4, p. 97-103. https://geoinfo.nmt.edu/publications/periodicals/nmg/21/n4/nmg_v21_n4_p97.pdf

Powers, D.W., Holt, R.M., Beauheim, R.L., and Richardson, R.G., 2006, Advances in depositional models of the Permian Rustler Formation, southeastern New Mexico, *in* Land, L., Lueth, V.W., Raatz, W., Boston, P., and Love, D.W., eds., Caves & karst of southeastern New Mexico: New Mexico Geological Society, Fall Field Conference, Guidebook 57, p. 267-276. https://www.wipp.energy.gov/library/CRA/2009_CRA/references/Others/Powers_et_al_2006_Advances_in_Depositional_Models.pdf

Reed, E.L., & Associates, 1978, Inspection and grouting Red Bluff Dam, Pecos River, Reeves and Loving Counties, Texas: unpublished report prepared for Red Bluff Water Power Control District, Pecos, Texas, 20 p. plus illustrations, boreholes and grouting records, and water analyses.

Snider, H.I., 1966, Stratigraphy and associated tectonics of the Upper Permian Castile–Salado–Rustler evaporite complex, Delaware Basin, west Texas and southeast New Mexico: unpublished Ph.D. dissertation, University of New Mexico, Socorro, NM, 196 p.

Stafford, K.W., 2013, Evaporite karst and hydrogeology of the Castile Formation: Culberson County, Texas, and Eddy County, New Mexico, *in* Land, L., Doctor, D.H., and Stephenson, J.B., eds., Sinkholes and the

engineering and environmental impacts of karst–Proceedings of the thirteenth multidisciplinary conference, Carlsbad, NM, May 6 through 10, 2013: National Cave and Karst Research Institute, Carlsbad, NM, p. 123-131. https://pdfs.semanticscholar.org/fa26/e653bc2c3ae95007f83dde9a1d4eab38211d.pdf

Stafford, K.W., and Nance, R.G., 2018, Evaporite karst of west Texas: Delaware Basin, *in* Stafford, K.W., and Veni, G., eds., Hypogene karst of Texas: Texas Speleological Survey, Monograph 3, p. 36-50. https://www.texasspeleologicalsurvey.org/PDF/Hypogene_Karst_of_Texas.pdf

Vine, J.D., 1963, Surface Geology of the Nash Draw Quadrangle, Eddy County, New Mexico: U.S. Geological Survey, Bulletin 1141–B, 46 p. https://pubs.er.usgs.gov/publication/b1141B

Withington, C.F., 1962, Gypsum and anhydrite in the United States, exclusive of Alaska and Hawaii: U.S. Geological Survey, Mineral Investigations Resource Map MR–33.

Design and Implementation of a Grout Program in an Evaporite-Karst Foundation, Red Bluff Dam, Loving and Reeves Counties, Texas

John Charlton
HDR Engineering, Denver, Colorado

Jenn Ostrowsky
Utah State University, Logan, Utah

Richard A. Shoemaker
Retired Engineer, HDR Engineering, Inc., Buena Vista, Colorado

Kenneth S. Johnson
Retired Geologist, Oklahoma Geological Survey, Norman, Oklahoma

ABSTRACT.—Red Bluff Dam is a high-hazard, 9000-ft-long embankment dam located in west Texas on the Pecos River. The dam and the reservoir it impounds are owned and operated by the Red Bluff Water Power Control District and provide irrigation water for seven irrigation districts in the area. Construction of the dam began in late 1934 and was completed in 1936 under the engineering supervision of the Public Works Administration. Impoundment of the reservoir began in late 1936. Soon after initial filling of the reservoir, extensive seepage was noted at various locations along the toe and on the downstream slope of the dam. The District performed grouting operations in 1973 and 1978 to address seepage through multiple zones of the foundation.

The geology of the site includes the Permian-age Rustler Formation (dolomite, gypsum, and shale at the site) and Quaternary deposits of weakly to strongly cemented sand, gravel, and clay. Extensive collapse structures, resulting from dissolution of layers of evaporites (salt and/or gypsum) in the underlying Rustler, Salado, and Castile Formations, exist within the dam foundation. Site investigations were performed in 2012 and 2013 that included geologic mapping, core drilling, and piezometer installation. Data from these investigations, combined with existing data from previous grouting operations and site investigations, were used to develop a comprehensive geologic model of the site and to design an effective grouting program aimed at mitigating the most critical seepage zones.

The grout program was designed, and contract documents were prepared based on data from previous studies and grouting programs, as well as the 2012 and 2013 site investigations. The grout program criteria were to provide optimal grouting of the dam foundation while protecting the embankment dam. Grouting began in February of 2014 with The Judy Company as the contractor and was completed in January of 2015. This paper presents details of the grout program, geologic conditions encountered during grouting, revisions of the grout program based on field conditions to maximize the effectiveness of the foundation grouting, and the use of data from the grout program to develop additional treatment measures for ongoing seepage mitigation for the dam.

Charlton, J.; Ostrowsky, J.; Shoemaker, R. A.; and Johnson, K. S., 2021, Design and Implementation of a Grout Program in an Evaporite-Karst Foundation, Red Bluff Dam, Loving and Reeves Counties, Texas, *in* Johnson, K. S.; Land, Lewis; and Decker, D. D. (eds.), Evaporite Karst in the Greater Permian Evaporite Basin (GPEB) of Texas, New Mexico, Oklahoma, Kansas, and Colorado: Oklahoma Geological Survey, Circular 113, p. 233–245.

INTRODUCTION

Red Bluff Dam is an existing 'Large', 'High' hazard dam located in Texas on the Pecos River within the Rio Grande River Basin, approximately six miles south of the New Mexico state line (Figure 1). The maximum height of the dam at the river is 106 ft and, at the current reservoir conservation pool elevation of 2828.2 ft (NAVD88), the reservoir contains nearly 146,000 ac-ft of water. The 9200-ft-long dam and reservoir it impounds are owned and operated by the Red Bluff Water Power Control District (the District) in Pecos, Texas, and provide irrigation water for seven irrigation districts in Reeves, Loving, Ward, and Pecos Counties.

Construction of the dam began in late 1934 under the engineering supervision of the Public Works Administration. The dam was completed in late 1936, and in early 1937 a large flood filled the reservoir to its original conservation pool capacity (approximately 310,000 ac-ft). Soon after this rapid initial filling of the reservoir, extensive seepage was noted at various locations along the toe and on the downstream slope of the dam. And so began the 77-yr-long history of monitoring seepage and grouting the foundation of Red Bluff Dam.

Aside from overtopping, because of inadequate spillway capacity, internal erosion or "piping" from seepage through or beneath earthen embankments is the most common cause of dam failures. Experience has shown that adverse seepage and piping conditions can be difficult to detect. When seepage and piping conditions reach the point where detection is finally made, the failure mechanism is often advanced to a stage that leaves little or no time to implement remedial measures.

The geology beneath Red Bluff Dam is very complex, and major portions of the dam are founded on rock formations that are composed of water-soluble minerals and rocks (gypsum, anhydrite, limestone, dolomite). The complex foundation and long-term seepage conditions (and near failure of the dam in 1973) increase the potential for a catastrophic failure and release of the reservoir at any time, and likely with little or no advance warning. Periodic "maintenance" grouting of the dam's foundation will need to be performed by the District as part of the regular operation and maintenance plan for the remainder of the dam's useful life.

HDR Engineering, Inc. (HDR) has served as the District's consultant for various projects at Red Bluff Dam since early 1994. Most recently (since 2009) HDR has been working with the District on dam safety update projects that were necessitated by a dam safety and security inspection of the project conducted on February 26, 2008 by the Texas Commission on Environmental Quality (TCEQ) Dam Safety Program staff (see references) and by Texas dam safety rule changes that became effective on January 1, 2009. Those projects have consisted of a study to update the hydrology and hydraulics (H&H) and to assess the overall spillway capacity: dam-breach analyses, including downstream inundation mapping; preparation of an emergency action plan; documentation of required operation and maintenance procedures for the project; and continuing efforts to record and interpret instrumentation readings at the dam.

The foundation grouting work addressed by this report was not mandated by TCEQ Dam Safety; however, TCEQ has advised the District that reservoir impoundment above the spillway's concrete overflow crest (against the 15-ft-tall radial gates) should not be done until work is performed to reduce foundation seepage at the dam. In fact, the District recently hired a contractor to "lock" the spillway gates in the fully opened position by installing steel brackets in the sidewalls of each spillway bay to prevent closing the gates. If in the future the District decides to rehabilitate and begin using the gates again, the resulting maximum conservation pool capacity of the reservoir would nearly double to 286,000 ac-ft.

The grouting work undertaken in 2014 was actually the third grouting program completed at the dam. The first program was conducted in 1973, after subsidence was discovered along a major section of the upstream shell of the dam. This work was followed by a second program in 1978. The results of the first two grouting programs have been documented in reports prepared in 1974 and 1978 by Ed L. Reed & Associates (1978). In addition to the 1973 and 1978 grouting programs, AGRA Earth and Environmental completed piezometer installations and a review of all grouting and construction data to develop a geologic profile of the dam (AGRA, 1994).

SITE GEOLOGY

Bedrock in the Red Bluff area consists of dolomite, dolomitic limestone, and gypsum, along with layers of red-brown shale, siltstone, and sandstone. At the dam (Figure 2), Permian strata relevant to the dam foundation include the following: shale and siltstone of the Dewey Lake Formation; dolomite, dolomitic limestone, and gypsum, along with layers of red-brown shale, siltstone, and sandstone of the Rustler Formation; and deeper underground are beds of salt and gypsum/anhydrite in the Castile and Salado Formations. Dissolution of these salt beds, and some of the gypsum/anhydrite beds from the Rustler, Salado, and Castile Formations, has resulted in collapse and disruption of overlying Rustler and Dewey Lake strata. Large breccia/collapse zones have completely displaced and rotated blocks of Dewey Lake and Rustler strata. The breccia/collapse zones can consist of blocks of gypsum, dolomite, shale, siltstone, and sandstone. Much of the space between blocks is filled with clay that has been washed into, and deposited in, the spaces. The cross section in Figure 3, based

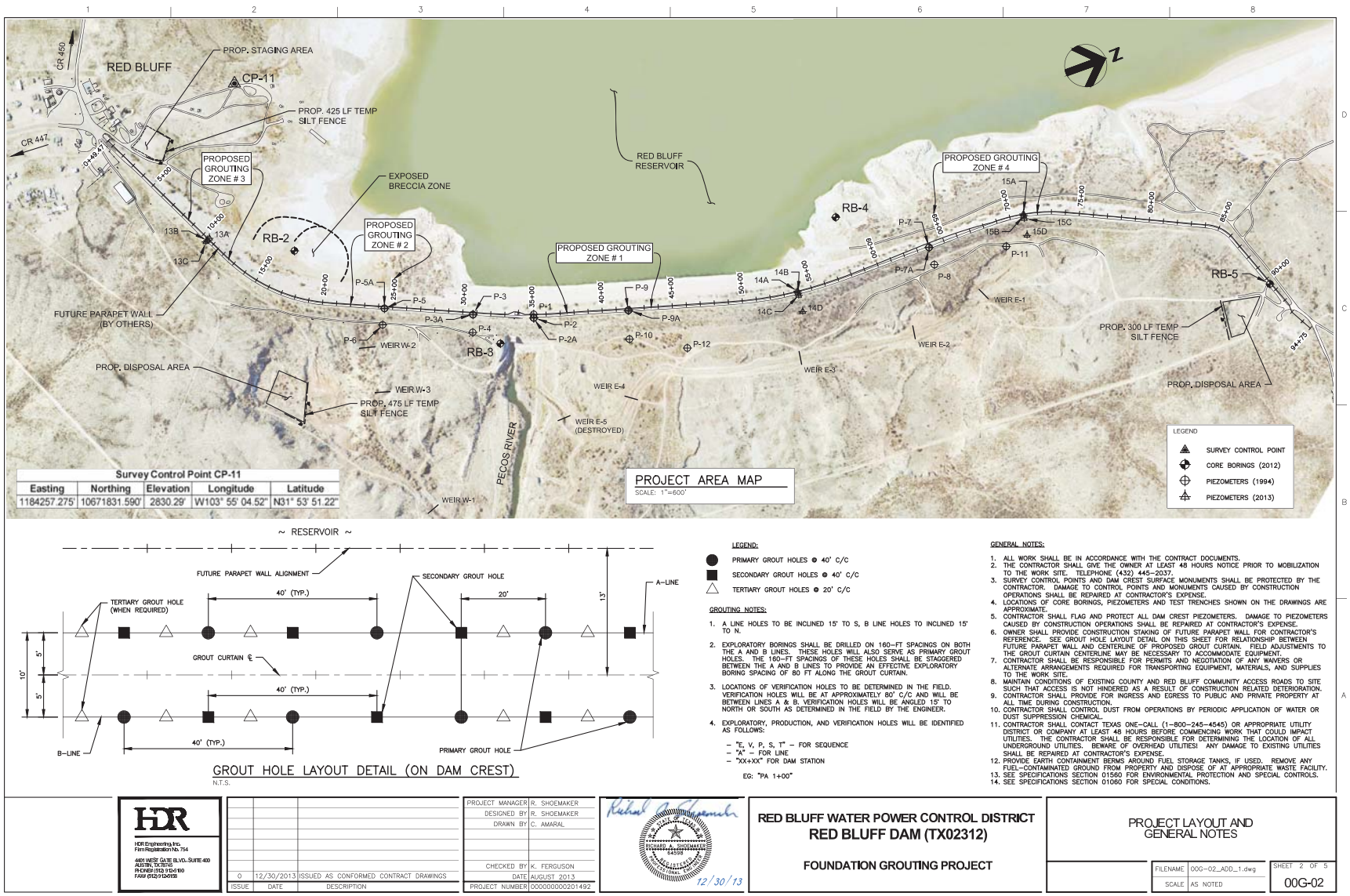

Figure 1. Plan view of the Red Bluff Dam showing 2014 grouted zones 1, 2, and 4.

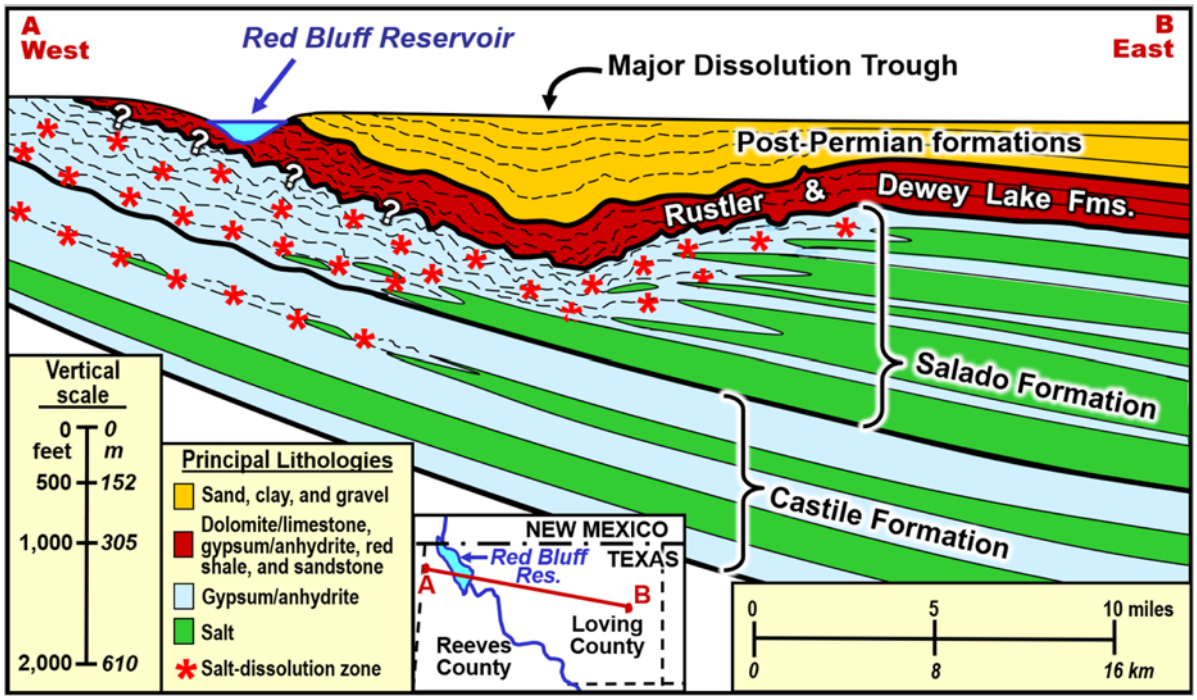

Figure 2. Generalized structural cross section A—B through Red Bluff Dam showing dissolution of salt in the Salado and Castile Formations beneath the Rustler and Dewey Lake Formations in Loving and Reeves Counties, Texas. The Rustler Formation contains soluble gypsum beneath the dam. From Johnson and others (2021).

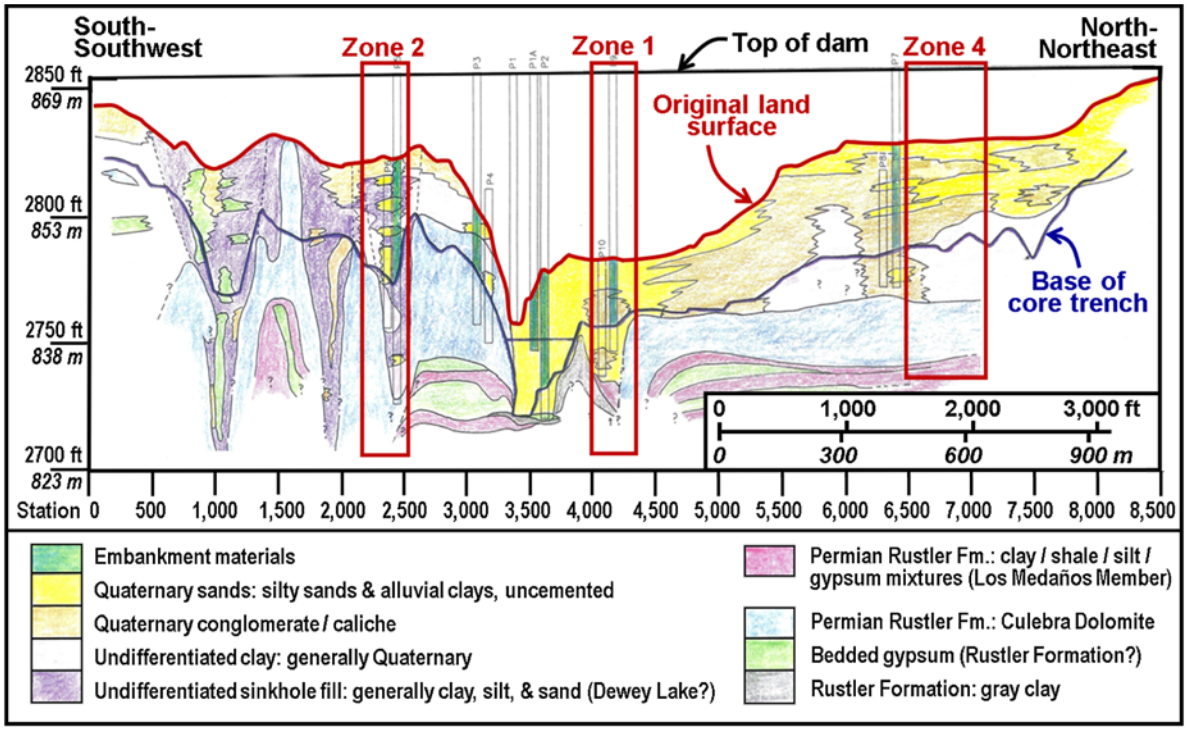

Figure 3. Conceptual cross section along Red Bluff Dam alignment, based upon historic borehole logs and excavations (modified from AGRA, 1994, Figure 4.3). The complex geology of the dam foundation (particularly on the left side of the diagram) is mainly due to dissolution of underlying salt and gypsum layers, and resultant collapse and brecciation of overlying strata. Rustler bedrock in the right half of the cross section is probably as complex as in the left half. All materials between original land surface and base of core trench were removed during construction of the dam. Also shown are zones 1, 2, and 4 for the grout program of 2014 to 2015 (Figures 4, 5, 6, 7).

upon data available in 1994, shows the great complexity of the geology at the dam that resulted from dissolution of underlying salt and gypsum and chaotic collapse of overlying strata.

Some of the youngest sediments in the area, the Tertiary Gatuña Formation and Quaternary terrace deposits and alluvium, consist of sand, silt, clay and gravel, with zones of variably cemented sands and gravels that in some zones are very hard and well cemented, while other zones contain soft silt and clay. These locally derived materials were deposited in depressions caused by dissolution of evaporites of the Rustler and Salado Formations as well as surface erosional features. Still younger deposits of sand (some windblown), silt, clay, and gravel are widespread and vary in thickness across the area where the Gatuña or Rustler deposits have been eroded and redeposited.

GROUT PROGRAM PHASED APPROACH

In early 2012, the District decided that since grouting at the dam was last performed back in 1978, a maintenance-grouting program should be developed for the dam's foundation. HDR Engineering, Inc. was subsequently instructed to prepare a scope of work for the development of the new grouting program. HDR Engineering, Inc. developed a three-phased approach for this program. The objective of the approach was to build on previous grouting programs at the dam through updated technologies, instrumentation data analysis, retaining specialized expertise, and using lessons learned from similar projects to develop a targeted, cost-effective grouting program for the foundation and abutments of the dam. The three phases were as follows:

1. Phase 1 – Review of existing geologic literature, aerial photographs, oil and gas well logs, previous grouting data, existing borehole data, and instrumentation readings. Conduct a detailed, multi-day field reconnaissance. Develop regional and local geologic models to be used to prepare recommendations for a Phase 2 exploratory drilling and testing program at targeted areas in the dam foundation and abutments.
2. Phase 2 – Perform exploratory drilling, water-pressure testing and geophysical surveys, which would be used to refine the local geologic model into a site-specific model of the dam's foundation and abutments.
3. Phase 3 – Prepare contract documents, technical specifications, and design drawings for a targeted, cost-effective grouting program. Bids would then be solicited from pre-qualified geotechnical specialty contractors to perform the grouting.

During the Phase 1 field reconnaissance performed in 2012, it was determined that the drilling of geologic reference borings on the order of 150 to 200 ft deep in the vicinity of the dam would greatly enhance the understanding of the site geology. Sites for four proposed 200-ft deep borings were selected at locations across the dam site that were believed to have a high probability of encountering the "typical" stratigraphic sequence, as expected in the region, based upon the review of existing geologic literature, oil and gas well logs, and information obtained during the field reconnaissance. A fifth boring site was selected to investigate the depth and characteristics of a major geologic collapse feature upstream of the dam in the vicinity of the 1973 subsidence event. The reference borings were completed in August of 2012.

Given the complexity of the local geology, it became apparent after Phases 1 and 2 that additional drilling and water pressure testing (Phase 3) would have limitations in better defining the complex and variable dam foundation. Significant funds could have been spent by the District to conduct a Phase 3 exploration program that would not provide sufficient data to assist in better understanding the dam foundation and appropriate grouting design. Therefore, on completion of Phases 1 and 2, it was HDR's recommendation that Phase 3 be eliminated and the District consider proceeding directly into the grouting program. The District concurred with this plan and also felt that having a grouting contractor on-site was a prudent course of action, should problems develop during drilling and water pressure testing. Phase 3 then became the design and bidding phase again.

GROUT PROGRAM DESIGN

HDR and the District identified two specific needs to assist with the design of the grouting program: (1) the need to conduct a formal, 1-day potential-failure-mode analysis (PFMA) to classify modes from high to low probability and prioritize areas of the foundation for grouting; and (2) the need to install additional piezometers in the dam and foundation.

Given the seepage history at Red Bluff Dam, the PFMA was limited to seepage-related mechanisms that could potentially initiate dam failure and/or complete or partial loss of the reservoir. In a geologic environment comprised of soluble evaporite rocks and karst features, undetected erosion and chemical processes may be at work in the foundation that could adversely impact support of the dam and seepage control in the foundation. The objectives of the PFMA for Red Bluff Dam were (1) to assist in identifying and prioritizing specific zones of the dam's foundation to be grouted in light of potential financial constraints; and (2) determine the need for, and location of, additional piezometers to provide pre- and post-grouting data for evaluating the effectiveness of the grouting program.

The installation of 11 new piezometers in the dam and foundation at Stations 10+50, 54+00, and 71+00 was completed in July of 2013. These piezometers proved

helpful for monitoring water levels in the dam and foundation before, during, and after the 2014 grouting work, as well as providing additional geotechnical data on the dam and foundation.

The PFMA effort and subsequent data from the new piezometers helped to identify and prioritize proposed areas for grouting. On conclusion of Phases 1 and 2 (HDR's December 2012 Report), the following locations of the dam were recommended for grouting, based on the results of dam-crest monument surveys, piezometer readings, and seepage observed in the vicinity of weirs W-1, E-1, and E-2:

- Sta. 8+00 to 16+00;
- Sta. 34+00 to 42+00;
- Sta. 52+00 to 56+00; and
- Sta. 60+00 to 72+00.

These limits also generally corresponded to the recommendations for future grouting presented in the May 1991 U.S. Bureau of Reclamation Special Technical Report, which included Stations 8+00 to 12+00; 36+00 to 54+00; and 68+00 to 72+00.

On conclusion of the Phase 3 design work and the PFMA session, a total of eight proposed areas across the dam were identified and prioritized for grouting. These eight areas represent 4500 linear feet of the dam, or approximately 50% of the total length of the dam. Details on these areas are presented in Table 1.

The District's budgetary considerations at the time dictated that the proposed grouting work not exceed approximately US $2 million. Given this budget, and an estimated cost for the drilling and grouting, HDR proceeded with the preparation of design and contract documents for the District to advertise the first four grout zones for bids. These four zones represent 2000 linear feet of the proposed 4500 linear feet of the dam identified for grouting. The documents prepared included drawings, technical specifications, a prequalification request package, a bid form, and contract documents. HDR Engineering, Inc. stated in these documents that the proposed grouting program was an exploratory program that stressed data collection and real-time monitoring of grouting operations aimed at better defining the dam foundation geology.

CONSTRUCTION TIMELINE

The construction contract for the project was awarded to The Judy Company (TJC). HDR Engineering, Inc. represented the District during construction by providing construction contract administration and on-site construction observation services for the project.

In early to mid-September 2013, a significant rain event occurred in the Carlsbad, New Mexico area, resulting in flooding along the Pecos River upstream of Red Bluff Reservoir. Inflows from this flood raised the reservoir level approximately 11 ft from elevation 2801.5 to 2812.5 ft-msl between September 13 and October 6, 2013. Readings being collected by the new piezometers soon after this flood indicated that water pressures in the foundation at grout zone 4, both upstream and downstream of the dam centerline, were responding very quickly to the increased reservoir level. Water levels in the new piezometers at grout zone 3 appeared to be less responsive to the increased reservoir level.

As a result, HDR discussed reprioritizing grout zones 3 and 4 with the District and TJC, to make zone 4 part of the 'Base Bid' work, while moving zone 3 to the 'Additive Bid' work. The total length of zone 4 was 700 ft (Sta. 65+00 to 72+00), while the length of zone 3 was only 400 ft (Sta. 8+50 to 12+50). HDR Engineering, Inc. proposed replacing zone 3 in the 'Base Bid' with 500 ft of zone 4 (Sta. 67+00 to 72+00), because the bottom of the proposed grout curtain elevation was 25 ft

TABLE 1.—Recommended Grout Zones

Grout Zones (by Priority)	Begin Sta.	End Sta.	Bottom of Grout Curtain Elevation
1	37+50	43+50	2700 (FT-NGVD 1929)
2	22+00	25+00	2710
3	8+50	12+50	2715
4	65+00	72+00	2740
5	43+50	56+00	2710 to 2725
6	12+50	16+00	2710
7	60+00	65+00	2750
8	33+50	37+50	2700

shallower in zone 4 compared to zone 3. The 'Additive Bid' work then became grout zone 3 and 200 ft of zone 4 (Sta. 65+00 to 67+00).

Drilling and grouting began on February 3, 2014. During the course of the work, it became apparent that the original contract period of 195 days for substantial completion (July 16, 2014), plus 30 days for final completion, was not going to be sufficient. The District granted several contract extensions over the course of the project. A major rain event and subsequent flooding severely impacted the project site beginning on September 19, 2014. The spillway engaged at the dam for the first time since 1987, which blocked both access roads to the dam until October 12, 2014. As a result of the flood, the District temporarily suspended work for 30 days from September 19 to October 18, 2014.

The grouting project was completed on December 18, 2014, 350 days after Notice to Proceed. In the end, 1570 linear feet (LF) of dam was grouted under the Phase 4 program instead of the 2000 linear feet that was planned during design and bidding. This included

- 640 LF of zone 1 (Sta. 37+10 to 43+50);
- 360 LF of zone 2 (Sta. 21+60 to 25+20); and
- 570 LF of zone 4 (Sta. 67+00 to 72+70).

The location of the three grouted zones on the 1994 AGRA geologic profile is presented in Figure 1.

GROUT PROGRAM IMPLEMENTATION

Construction began with the drilling of exploratory borings in zone 2 and installation of multi-port sleeve pipe (MPSP) standpipes in the embankment to just below (approximately 6 in. below) the embankment/foundation interface. The contractor's initial plan was to install standpipes and begin grouting in zone 2, then begin operations in zone 1 while work in zone 2 continued, and finally begin work in zone 4 after zones 2 and 1 were completed. As drilling and grouting progressed, the lessons learned with each hole were incorporated to adjust the drilling, MPSP standpipe installation, and grouting methods. The overall goal during work in each zone became reducing borehole collapse problems to allow grouting of the foundation treatment zone using the most cost-effective and efficient process available. The Judy Company recorded grout-take rates, pressure, and grout-mix properties for all grouting operations. In addition, TJC geologists logged core from exploratory borings, cuttings from rotary and sonic drilling, and recorded the injection pressure and pumping rate for all water pressure (Lugeon) tests for each grout stage. These efforts allowed the grouting program to be investigatory as well as remedial. Discussions on the conditions encountered in each grout zone and key issues are presented below in chronological order of the grouting by the contractor.

Grout Zone 2 (Sta. 21+60 to 25+50) Conditions/ Issues Encountered During Grouting

The dam foundation strata in the 360 linear feet of zone 2 consist primarily of dolomite (Rustler Formation) (some gypsum at the southern extent of the zone), with a cover of sedimentary material (Gatuña and/or recent alluvium) of variable thickness (Figure 4). The dolomite varies in strength from very hard to soft, with these hard to soft zones interbedded, and it is also intensely fractured. The top elevation of the dolomite is inconsistent, and two low areas are present that extend from Station 22+40 to 23+20 and Station 24+00 to 25+20. These low areas in the top of the Rustler may be a result of collapse due to dissolution of underlying evaporites, erosion of the surface prior to deposition of the Gatuña, or both. The overlying Gatuña/recent alluvium sediments consist of silt, clay, fine- to coarse-grained sand, gravel, and variably cemented sand and gravel conglomerate.

During initial drilling and grouting in zone 2, the dam foundation conditions presented challenges to MPSP installation, drilling, and grouting. The specified drilling and grouting methods were modified to more effectively inject grout into the foundation as described in the following paragraphs.

Throughout most of zone 2, the specified drilling and grouting procedure consisted of drilling, at an inclination of 15 degrees, through the embankment using rotary sonic equipment and installing the MPSP standpipe into what was identified as the foundation material directly below the bottom of the embankment, followed by gravity grouting of the embankment/foundation interface. Following installation of the standpipe, drilling proceeded below the embankment with an initial protective downstage grouting zone, at low pressure, of up to 20 ft directly below the embankment interface. Drilling then continued to the design depth of 152 ft below the top of the dam, followed by upstage grouting of the open hole. Using this specified method, the contractor experienced several issues, as described below:

- During production drilling below the MPSP standpipe, nearly all grout holes that were left open were later found to be unstable. Below the bottom of embankment, and above sound rock (Culebra Dolomite), the surficial Gatuña Formation was unstable and contributed to (a) the frequent collapse of grout holes; (b) successive re-drilling; (c) ineffective injection of grout; (d) difficult packer placement during water pressure testing and grouting; and (e) lost tooling. This contributed to delays to TJC's work schedule. With continued re-drilling and the use of downstage grouting in many of the holes, the grout holes were eventually held open and grouted to closure.
- As an attempt to combat the problem of collapsing holes, the MPSP standpipe installation was

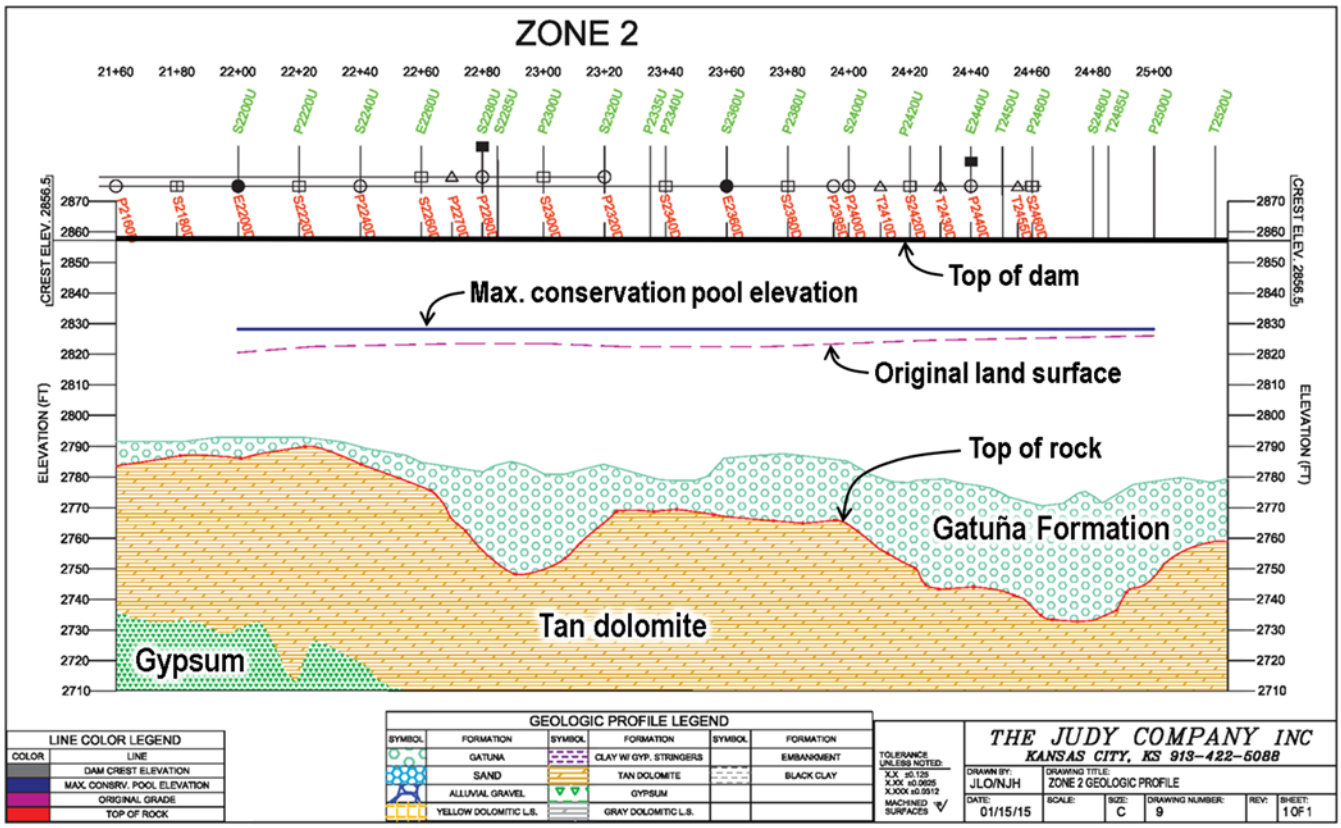

Figure 4. Zone 2 geologic profile, based on grout program data (from The Judy Company, 2015).

modified so that the pipe would be extended below the bottom of the embankment and through the variable Gatuña sediments into what was interpreted as sound, intact rock (typically Culebra Dolomite). While this procedure reduced borehole stability problems in the Gatuña, further grout-hole instability issues occurred in areas of intensely fractured, soft, and decomposed bedrock. Grouting was completed with several iterations of re-drilling and downstage re-grouting, eventually achieving closure.

- In response to collapsing hole conditions, the contractor attempted to drill steel casing to total depth, and grout from the bottom of this casing, progressively pulling up casing and grouting in 10- to 20-ft stages. This proved to be effective for the most part, but progress was slow. In areas where very soft foundation conditions were encountered (e.g., unconsolidated, soil-like deposits in the Gatuña), material would migrate into the hole as the casing was extracted, making it very difficult to grout effectively. Seating packers just below the bottom of the steel casing for pressure testing and grouting was also problematic.
- Areas in zone 2 that accepted high grout quantities were found in both the surficial Gatuña Formation and dolomite bedrock. The areas of high grout take are presented in Table 2.
- An evaluation of the geologic cross section and grout-take data reveals that the Gatuña Formation took roughly 36% of the total grout used in zone 2. The dolomite bedrock took the remaining 64%.
- Review of the grout-take data indicates an approximate 85% reduction in grout takes from primary to tertiary order holes as presented in Table 3.

Grout Zone 2, Key Observations

- Foundation materials in zone 2, including both the surficial Gatuña Formation and weathered Culebra Dolomite bedrock, were found to be problematic in maintaining an open hole during both downstage and upstage grouting. Extending the bottom of the MPSP standpipe through the softer Gatuña deposits to the top of bedrock reduced borehole stability issues within the Gatuña. Grouting through ports in the standpipe from the interface zone at the bottom of the embankment to the top of bedrock proved to be the most effective means of grouting the Gatuña Formation.
- The variable nature of the foundation geology was confirmed.
- Areas in the foundation that accepted higher grout quantities were generally characterized as: (a) dolomitic bedrock (Culebra) within subsidence zones;

TABLE 2.—Zone 2 – Summary of High Grout-Take Areas

Stations	Elevation (ft-msl)	Geologic Description
21+60 to 22+80	2740–2770	Culebra Dolomite
24+00 to 24+60	2740–2770	Gatuña Formation
24+00 to 25+20	2710–2740	Dolomite within subsidence zone

TABLE 3.—Zone 2 – Summary of Average Grout Takes per Foot*

Hole Order	Total Grout Takes	
	Gal/ft	Sacks/ft
Primary/ Exploratory	16.2	1.00
Secondary	5.6	0.33
Tertiary	2.7	0.14

*Modified from Table 3, The Judy Company (2015).

and (b) the in-filled, surficial deposit (Gatuña) overlying subsidence zones.

- A well-cemented, hard conglomerate layer caps the Gatuña in zone 2 and mostly defines the bottom of the original cutoff trench excavation.
- Unconsolidated sediments beneath this conglomerate layer comprise the majority of the Gatuña.
- Grout injection quantities decreased from primary- to tertiary-order holes, indicating zone 2 approached closure and may generally be considered a successful grouting program.

Grout Zone 1 (Sta. 37+10 to 43+50) Conditions/ Issues Encountered During Grouting

The dam foundation across zone 1 consists of gypsum and dolomite (dolomitic limestone) of the Rustler Formation, sporadic cover of Gatuña conglomerate and sediments, and alluvial sands and clay (Figure 5). The dolomite varies from a yellowish-brown (intensely weathered) to gray dolomite. Gypsum underlies the dolomite from Station 39+50 to 40+70 at elevations ranging from 2705 to 2710 ft-msl. At approximately Station 41+20, the elevation of the top of the gypsum abruptly changes to elevation 2730 to as high as elevation 2750 ft-msl. The gypsum unit persists to the northern extent of zone 1 at Station 43+50. It is not fully understood if the gypsum noted from Station 39+50 to 40+70 and that observed from Station 41+20 to 43+50 are the same unit, with the southern extent of the gypsum at a lower elevation due to a subsidence/collapse feature.

Overlying the foundation bedrock from Station 37+10 to 39+50 is alluvial material consisting of predominantly fine-grained sand with limited zones of coarse-grained sand to cobble-sized material at the base of the sequence (from Station 38+20 to 39+30). The sand is capped by a layer of black, moderately stiff to stiff clay from Station 37+10 to 39+50. The black clay was observed intermittently through the rest of zone 1. The origin of this clay layer is not understood.

Drilling and grouting were accomplished in zone 1 with installation of the MPSP at the base of the embankment and extended to the top of sound rock, as modified in zone 2.

Areas in zone 1 that accepted high grout quantities were generally found in the gray dolomitic limestone and near the contact of the yellow dolomitic limestone and tan dolomite at the north end of the zone. These specific areas are presented in Table 4.

Evaluation of the geologic cross section and grout-take data indicates that of the total grout injected at zone 1, the gray dolomitic limestone took approximately 57% of the total grout, the gypsum 15%, the tan dolomite 14.5%, the yellow dolomitic limestone 13%, and the sand and gravel 0.5%. This indicates the majority of the grout was injected into the dolomitic rock mass in strata that are heavily fractured and weathered.

Review of the grout data presented in Table 5 shows an approximate 72% reduction in grout take from primary- to tertiary-order holes.

Grout Zone 1, Key Observations

- Foundation materials in zone 2, including both the surficial Gatuña Formation and Culebra Dolomite bedrock, were found to be problematic in maintaining an open hole during downstage and upstage grouting. The extension of the MPSP system into sound bedrock in zone 1 minimized borehole stability issues in overlying material.
- The largest grout takes were in the dolomitic limestone and gypsum. The alluvium encountered from Station 37+10 to 39+50 did not take significant grout quantities.
- The Gatuña is limited in thickness and extent when compared to zone 2.
- Grout injection quantities decreased from primary- to tertiary-order holes, indicating that zone 1 approached closure and may be considered a successful grouting program.

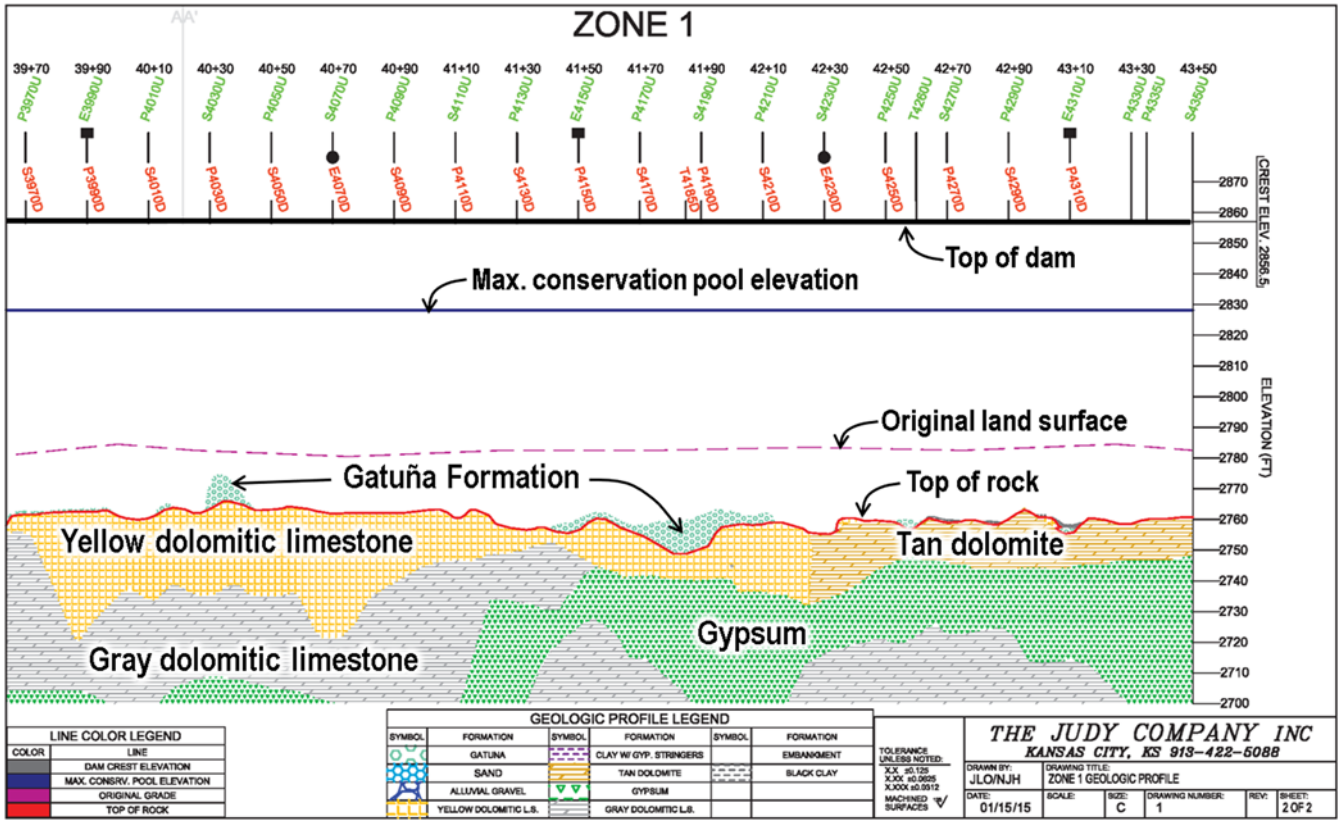

Figure 5. Zone 1 geologic profile, based on grout program data (from The Judy Company, 2015).

TABLE 4.—Zone 1 – Summary of High Grout-Take Areas*

Stations	Elevations (ft)	Geologic Description
37+30 to 37+90	2700–2720	Gray Dolomitic Limestone
38+70 to 39+10	2720–2740	Contact of Gray Dolomitic Limestone, Tan Dolomite, Clay, and Gravel.
39+30 to 39+90	2730–2750	Gray Dolomitic Limestone
42+10 to 42+50	2740–2760	Contact of Yellow Dolomitic Limestone and Tan Dolomite

*Information from The Judy Company (2015).

Grout Zone 4 (Sta. 67+00 to 72+70) Conditions Encountered During Grouting

Foundation conditions along zone 4 can be divided into two segments: (1) in the south segment (Figure 6), Station 64+60 to 70+40 consists of tan dolomitic limestone bedrock of the Rustler Formation, covered by the Gatuña Formation that ranges in thickness from 35 to greater than 60 ft; and (2) the north segment (Figure 7), from Station 70+40 to the north limit of zone 4 at

TABLE 5.—Zone 1 – Summary of Average Grout Takes per Foot

Hole Order	Total Grout Takes	
	Gal/ft	Sacks/ft
Primary/Exploratory	18.8	1.11
Secondary	12.3	0.71
Tertiary	5.2	0.28

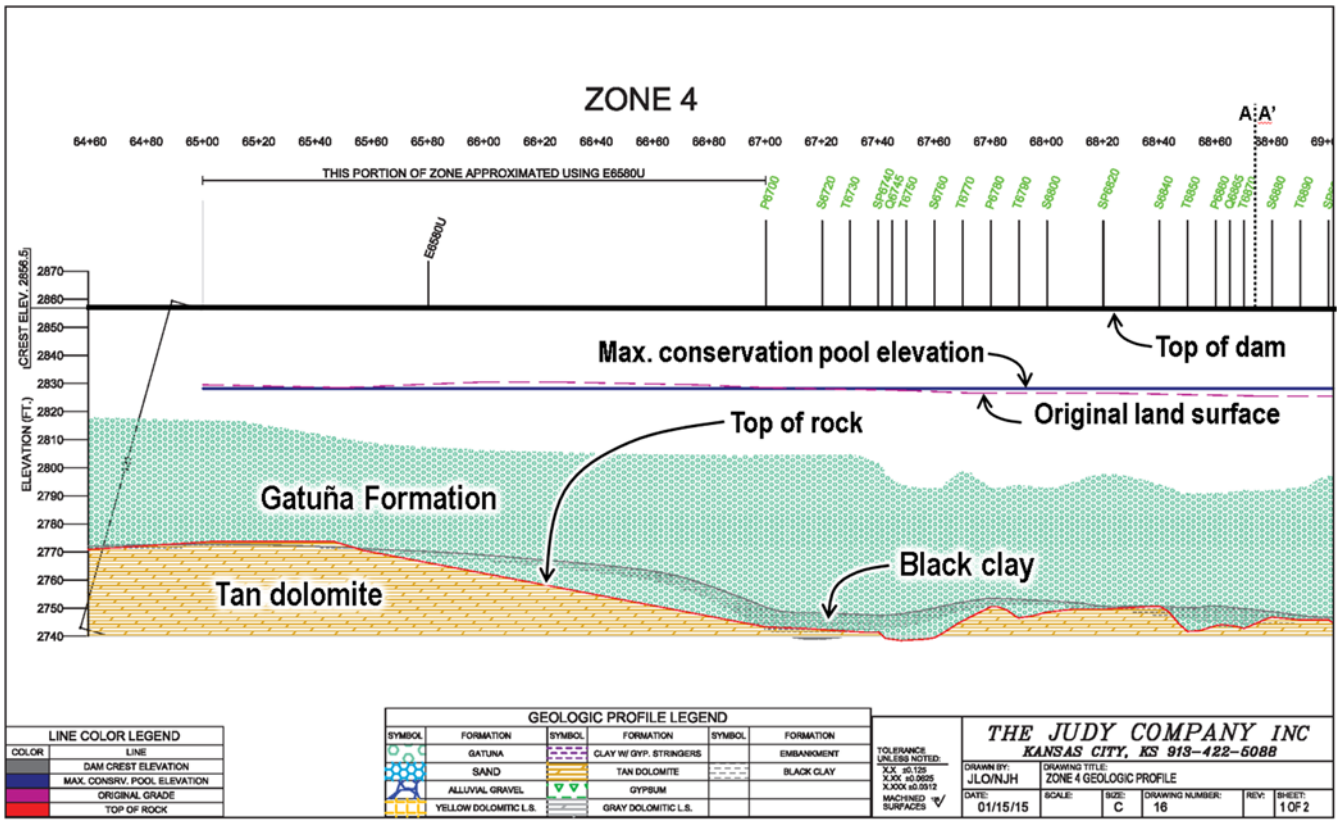

Figure 6. Zone 4 geologic profile (south segment), based on grout program data (from The Judy Company, 2015).

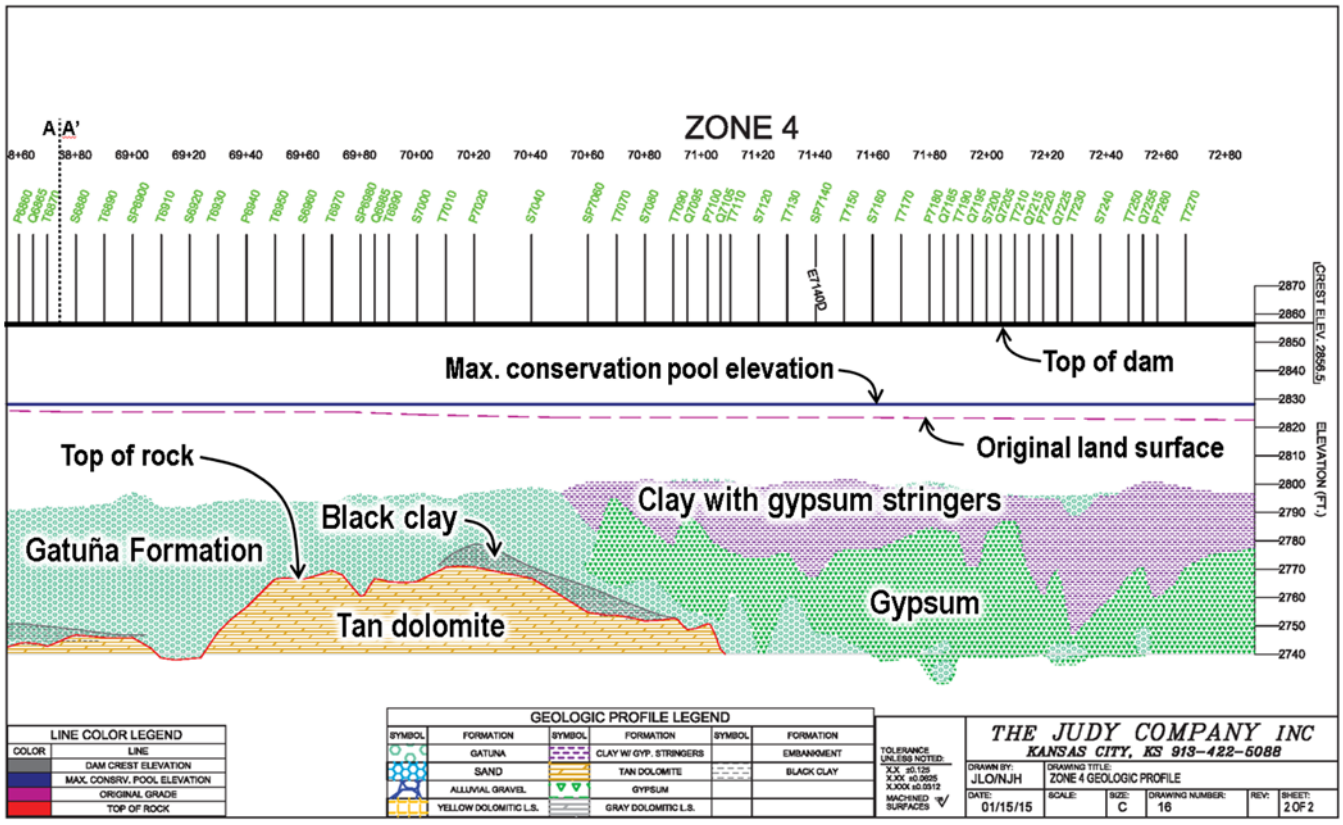

Figure 7. Zone 4 geologic profile (north segment), based on grout program data (from The Judy Company, 2015).

TABLE 6.—Zone 4 – Summary of High Grout-Take Areas*

Stations	Elevations (ft)	Geologic Descriptions
6735–6780	2740–2790	Dissolution Features; Weathered Dolomite; Gatuña
6840–6905	2740– 2790	Dissolution Features; Weathered Dolomite; Gatuña
6920–7000	2740–2800	Dissolution Features; Weathered Dolomite; Gatuña
7075–7115	2740–2785	Dissolution Features; Weathered Dolomite; Gatuña; Clay/Gypsum
7180–7270	2740–2800	Dissolution Features; Clay and Gypsum

*Information from The Judy Company (2015).

Station 72+70, consists of gypsum and overlying clay (with gypsum stringers), and minimal, laterally inconsistent Gatuña cover. Interpretation of the drilling logs places the Gatuña below the gypsum from Station 70+70 to 71+60. This interpretation would indicate that a very large subsurface channel has been in-filled with Quaternary detritus. Most notable in zone 4 is the system of large voids from approximately Station 71+60 to Station 72+70, near the northern extent of zone 4 (Figure 7).

In zone 4, the grout-line layout was modified, with consideration given to the remaining contract funds at the time and expediting drilling and grouting operations. Based on continued borehole instability issues at zone 2, and the absence of evidence in zones 1 and 2 that subvertical fractures act as integral seepage paths, a decision was made to use a single row of vertical grout holes in zone 4. The final spacing included primary holes on 40-ft centers, secondary holes on 20-ft centers, tertiary holes on 10-ft centers, and quaternary holes on 5-ft centers. Multi-port sleeve pipe standpipes were extended into the foundation to full design depth (117 ft below top of the dam), with sleeve-ports spaced 2.5 ft along the standpipe in the foundation zone for pressure testing and grout injection. Grout isolation bags were installed on the standpipes at the embankment/foundation interface and at prominent geologic contacts in the foundation, as determined by the contractor's geologist in the field. There were typically no more than three isolation bags on any one individual standpipe.

The most notable grout takes in zone 4 were concentrated at the north end (Sta. 71+80 to 72+70) (Figure 7). This portion of zone 4 is characterized by gypsum, large voids, and clay with gypsum stringers. This zone may be within a large subsidence feature filled with a weathered gypsum blocks from younger, previously overlying gypsum beds, entrained clay, and more recent infill material in solution features that have historic connection with surface water. Other areas throughout zone 4 that accepted high grout quantities were also characterized by subsidence and dissolution features. These areas are presented in Table 6.

TABLE 7.—Zone 4 – Summary of Average Grout Takes per Foot*

Hole Order	Total Grout Takes	
	Gal/ft	Sacks/ft
Primary/Exploratory	27.1	1.9
Secondary	20.3	1.4
Tertiary	15.1	1.0
Quaternary	29.5	2.1

*Modified from Table 3, The Judy Company (2015).

By evaluating the geologic cross section and grout-take data, it is estimated that the gypsum took roughly 54%, the Gatuña 25%, the tan dolomite 17%, and the clay about 3% of the total grout injected in zone 4. Worth note is that 54% of the grout injected in zone 4 went into gypsum, a rock that is characterized dissolution due to seepage action; the amount of some of the grout takes suggests the presence of large voids and significant seepage pathways in this foundation material.

In review of the grouting data presented in Table 7, there was an approximate 47% reduction in grout takes from primary- to tertiary-order holes. However, grout takes increased significantly in quaternary-order holes, indicating the presence of large voids and/or seepage pathways in these areas.

CONCLUSIONS

- The modified full-depth, ported MPSP system installed in vertical borings and single-row grout curtain layout proved to be partially effective within the zone 4 treatment zone. There were reduced issues with grouting operations that were related

to borehole stability when compared to zones 1 and 2.

- There was a reduction in grout takes from primary- to tertiary-order holes, and then an increase in average grout take for quaternary-order holes. This was observed primarily in the gypsum at the northern end of zone 4, as well as within some quaternary holes drilled into the Gatuña Formation.
- Areas in the foundation described as subsidence or dissolution features were characterized by high grout takes, indicating potential seepage pathways. High amounts of grout were accepted by the weathered dolomite underlying the subsidence or dissolution features and the infilling surficial deposit.
- Grout injection quantities generally decreased from primary- to tertiary-order holes, indicating that zone 4 may have been approaching closure. However, grout takes increased or remained comparable to tertiary holes with the addition of quaternary holes in areas that had high grout take in tertiary holes. The grout takes seem to indicate that the zone 4 grouting program was mostly successful, with the exception of the north end (Sta. 71+80 to 72+70) of the zone, where multiple quaternary holes were drilled and took large quantities of the thickest grout mixes (D and E).

REFERENCES

AGRA, 1994, Red Bluff Dam geotechnical investigation and piezometer installation project, Red Bluff, Texas: unpublished report *submitted to* HDR Engineering, Inc., Austin, TX, *from* AGRA Earth & Environmental, Inc., El Paso, TX, as AGRA E&E Job No. E94-4067, 35 p., plus Appendices A–G.

Johnson, K.S., Shoemaker, R.A., Charlton, J., and Parker, C., 2021, Evaporite karst in the Permian Rustler, Salado, and Castile Formations at Red Bluff Dam on the Pecos River, Loving and Reeves Counties, Texas, *in* Johnson, K.S., Land, L., and Decker, D.D., eds., Evaporite karst in the Greater Permian Evaporite Basin (GPEB) of Texas, New Mexico, Oklahoma, Kansas, and Colorado: Oklahoma Geological Survey, Circular 113.

Reed, E.L., & Associates, 1978, Inspection and grouting Red Bluff Dam, Pecos River, Reeves and Loving Counties, Texas: unpublished report prepared for Red Bluff Water Power Control District, Pecos, Texas, 20 p. plus illustrations, boreholes and grouting records, and water analyses.

The Judy Company, 2015, Foundation grouting project, Red Bluff Dam Texas: unpublished report *submitted to* HDR Engineering, Inc., Austin, TX, *from* The Judy Company, Inc., Kansas City, Kansas.

Permian Blaine and San Andres Formations of Western Oklahoma and Palo Duro Basin of Texas: Their Correlation and Evaporite Karst

Kenneth S. Johnson
Retired Geologist, Oklahoma Geological Survey,
Norman, Oklahoma

ABSTRACT.—The Permian Blaine Formation outcrops of western Oklahoma are a series of gypsum, dolomite, and shale units that can be correlated directly into the San Andres Formation in the Palo Duro Basin of north-central Texas. This was first established during extensive studies in the subsurface of the Palo Duro Basin, and the current paper affirms this correlation with a series of 6 geologic columns in major areas of the two-state region. Bed-by-bed correlation of gypsum beds in the Blaine and San Andres Formations shows that individual beds can be traced in outcrops over an area about 600 km north-south and as much as 200 km east-west: these individual beds also extend in subsurface to the west and north another couple hundred kilometers, or so, and thus they have a great areal extent. Where these same strata are in subsurface in the Anadarko and Palo Duro Basins, sulfate beds are commonly anhydrite, not gypsum, and moderately thick to thick beds of salt (halite) overlie some of the gypsum/anhydrite beds. In both outcrops and in subsurface, soluble gypsum/anhydrite and salt are locally or extensively dissolved, leading to typical karst development in the evaporite beds.

In outcrops, the Blaine Formation in its type area (Blaine County, in northwest Oklahoma) is about 30 m thick, and consists of three principal gypsum beds; in southwest Oklahoma, the Blaine is about 50 to 60 m thick, and consists of nine principal gypsum beds, most of the additional gypsums being in the upper part of the formation; and still farther to the southwest, in north-central Texas, additional gypsum beds at the base and the top of the formation swell its thickness to more than 150 m (giving rise to these outcrops being called the "Blaine of Texas"). In most areas, individual gypsum/anhydrite beds of the Blaine or San Andres are 3 to 9 m thick; the dolomite beds range from less than 1 m to almost 5 m thick, and the shales are generally 1 to 9 m thick.

Salt karst has a profound effect on Permian and overlying strata in the region. In subsurface, substantial amounts of salt are present in the Blaine Formation and associated strata in the Anadarko Basin of Oklahoma, and in the San Andres Formation in the Palo Duro Basin. These thick salt units are partially or totally dissolved in most places where they are at depths of less than about 200 to 300 m. This has produced many collapse structures and related features where the salt has been dissolved in both the Anadarko and Palo Duro Basins in the past. Evidence that salt dissolution is an on-going process is the presence of numerous salt springs and salt flats located on outcrops of the Blaine and associated strata on the flanks of the Anadarko Basin, and on the east side of the Palo Duro Basin in southwest Oklahoma and north-central Texas.

Gypsum karst is widespread in the Blaine Formation of western Oklahoma and north-central Texas: it is best developed where the Blaine consists mainly of thick gypsum beds interbedded with thin shales. Western Oklahoma and north-central Texas are among the best areas in the United States for the study of gypsum karst, including caves, sinkholes, springs, disappearing streams, and karst aquifers. Oklahoma has a total of 201 recorded gypsum caves in the Blaine, with 152 in northwest Oklahoma and 49 in southwest Oklahoma. In just the Palo Duro Basin portion of north-central Texas,

Johnson, Kenneth S., 2021, Permian Blaine and San Andres Formations of Western Oklahoma and Palo Duro Basin of Texas: Their Correlation and Evaporite Karst, *in* Johnson, K. S.; Land, Lewis; and Decker, D. D. (eds.), Evaporite Karst in the Greater Permian Evaporite Basin (GPEB) of Texas, New Mexico, Oklahoma, Kansas, and Colorado: Oklahoma Geological Survey, Circular 113, p. 247–277.

the "Blaine of Texas" has a total of 106 recorded gypsum caves. Extensive karst in the gypsum and dolomite of the Blaine Formation has produced an important aquifer, where sulfate-rich ground water is produced for irrigation in both southwest Oklahoma and north-central Texas.

INTRODUCTION

In good exposures or shallow cores, the Permian Blaine Formation is a series of cyclic rock units, wherein each cycle consists of (in ascending order) dolomite, gypsum (or anhydrite), red–brown shale, and then green–gray shale leading to the next overlying cycle; in the deeper subsurface, salt (halite) may also be present above the gypsum/anhydrite unit. However, in some areas, mainly in southwest Oklahoma and north-central Texas, gypsum and salt beds are partially or totally missing because of dissolution, or Blaine strata may have collapsed because of dissolution of interbedded or underlying gypsum and/or salt beds. As a result of this dissolution of evaporites, as well as facies changes, wherein dolomite or gypsum beds "disappear" laterally by grading into shales, there has been some uncertainty in regional correlations over the years.

To establish regional correlations, geologic columns are herein shown for 6 sites or areas in the Anadarko and Palo Duro Basins depicting the stratigraphy of the Blaine and San Andres Formations and associated strata (Fig. 1). In compiling these 6 geologic columns, the author relied on detailed studies based on core data and/or excellent outcrops in three areas: 1) northwest Oklahoma (Fay and others, 1962; Fay, 1964; Johnson, 2019c); 2) southwest Oklahoma (Scott and Ham, 1957; Johnson, 1967, 1990a, 1990b, 2019b); and 3) north-central Texas (Pendery, 1963; Jones, 1971; Hovorka and Granger, 1988; Johnson, 2019a). These three areas are in the central part of the Greater Permian Evaporite Basin (GPEB), as defined by Johnson (2021).

Appreciation is expressed to Dr. Susan D. Hovorka, geologist with the Texas Bureau of Economic Geology, for her review and constructive comments on an early draft of this report.

CORRELATION OF BLAINE AND SAN ANDRES FORMATIONS

In western Oklahoma and north-central Texas, the Blaine is a group of gypsum beds that can be conveniently grouped together, and thus, the top and base of the Blaine Formation are not the same throughout the Anadarko and Palo Duro Basins. In addition, a different nomenclature for gypsum and dolomite units has developed in different areas, because correlation or equivalence of units was not established until long after a local nomenclature had been developed in each area. Where first named and described in Blaine County, northwest Oklahoma, the Blaine Formation is about 30 m thick and consists of three main gypsum beds. In southwest Oklahoma, the Blaine is 50–60 m thick and consists of nine gypsum beds; the base of the Blaine here is the same gypsum unit as in northwest Oklahoma (but with a different name), and some closely spaced gypsum beds (not present in northwest Oklahoma) are embraced in the upper part of the Blaine Formation. Similarly, some gypsum beds both above and below the Blaine of southwest Oklahoma are included within the "Blaine of Texas," where the total thickness is as much as 150 m.

Blaine and San Andres evaporites and associated redbeds (the underlying Flowerpot and overlying Dog Creek Shales) of Oklahoma and north-central Texas

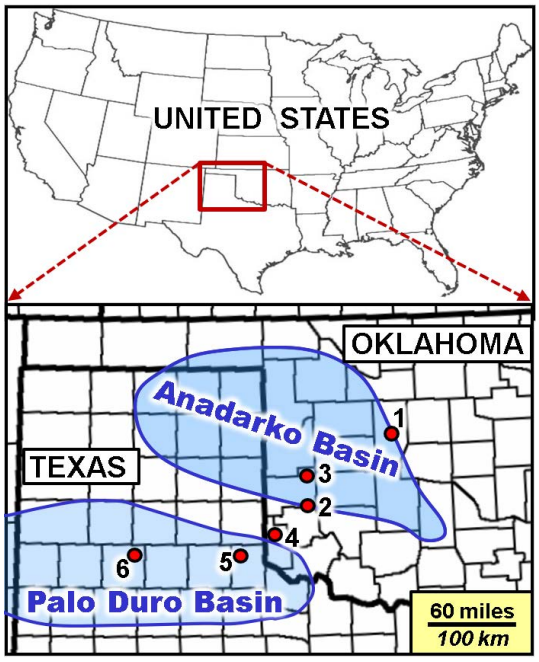

Figure 1. Map of western Oklahoma and Texas Panhandle showing the Anadarko and Palo Duro Basins and the location of 6 geologic columns that depict the stratigraphy and correlation of the Blaine and San Andres Formations. Locations on map: 1) Blaine County (Fig. 3); 2) southeast Beckham County (Fig. 4); 3) northeast Beckham County (Fig. 5); 4) Harmon County (Fig. 6); 5) Childress County (Fig. 7); and 6) Swisher County (Fig. 8).

are located in the central part of the GPEB, and are the lateral equivalents of San Andres carbonates, which are far to the south and west (Presley, 1981, cross section B–B´). The lateral gradation of the San Andres carbonates into the San Andres/Blaine evaporites from the south to the north and northeast is as follows: 1) from the Midland Basin, the thick San Andres carbonates grade into the thick San Andres evaporite sequence of the Palo Duro Basin; 2) farther north and east, only the middle gypsum and dolomite units of the San Andres persist into the Blaine Formation of southwest Oklahoma, whereas evaporites in the lower and upper parts of the San Andres grade into shales and salts of the Flowerpot and Dog Creek Formations, respectively; and 3) still farther northeast, the uppermost gypsum beds of the Blaine in southwest Oklahoma grade laterally into Dog Creek shales, and only three main gypsum beds persist into the Blaine of northwest Oklahoma.

The Blaine Formation of western Oklahoma is equivalent to the middle division and unit 5 of the lower division of the San Andres Formation in the Palo Duro Basin (Fig. 2). This correlation was partly shown in the cross sections by Presley (1981b) and McGookey and others (1988), and was most clearly demonstrated and stated in Fracasso and Hovorka (1986, p. 28) and in Figure 4 of Hovorka and Granger (1988). The current paper contains geologic columns of the Blaine and/or San Andres Formations in 6 areas in western Oklahoma and the Palo Duro Basin (Fig. 1), affirming equivalence of the gypsum (or anhydrite) and dolomite beds from one area to another. The region containing gypsum outcrops of the Blaine Formation in Oklahoma and Kansas, and the "Blaine of Texas," extends at least 600 km north–south, and as much as 200 km east–west. The full extent of tracing individual gypsum/anhydrite beds of the Blaine Formation westward into the subsurface of the Oklahoma Panhandle, Kansas, and Colorado is not yet fully established, but individual beds probably extend another couple of hundred kilometers to the west and north.

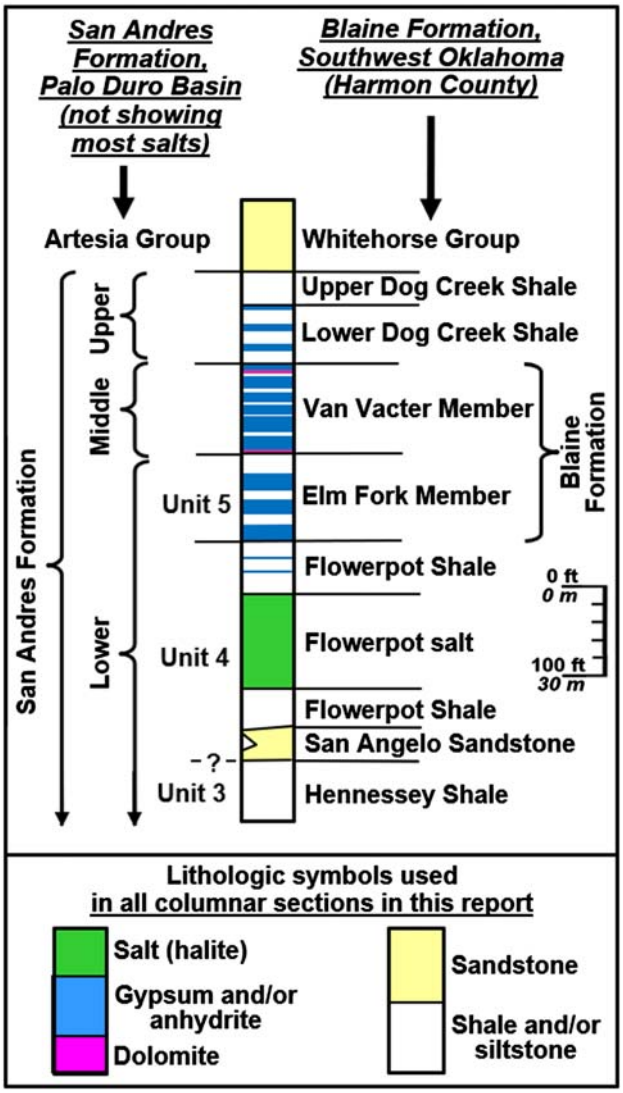

Figure 2. Geologic column showing general correlation of Blaine Formation and associated strata in southwest Oklahoma with San Andres Formation units in the Palo Duro Basin of the Texas Panhandle. Based upon data presented in geologic columns 1–6 in this report.

Blaine Formation in Blaine County, Northwest Oklahoma (Fig. 3)

The Blaine Formation is named for exposures in Blaine County, Oklahoma (Gould, 1902, 1905), and more recent comprehensive studies of the Blaine Formation in that area were carried out by Fay and others (1962) and Fay (1964). Geologic column 1, representing the formation in Blaine County, is given in Figure 3: here, Fay considered the Blaine as all strata from the Cedar Springs Dolomite Bed, at the base, through the Shimer Gypsum Member at the top. Throughout northwest Oklahoma, the three main gypsum beds are the Medicine Lodge, Nescatunga, and Shimer Beds, whereas the Kingfisher Creek Bed is relatively thin, or even absent. The Blaine Formation is 25–30 m thick in Blaine County and most parts of northwest Oklahoma. All strata below the Whitehorse Group that are shown in Figure 3 are in the El Reno Group (Fay and others, 1962; Fay, 1964).

While proposing the term "Blaine" in northwest Oklahoma, Gould (1902) also proposed the name "Greer" Formation, western division, for a series of (what he thought were younger) thick gypsum and shale strata in Greer County of southwest Oklahoma: hence, a separate nomenclature was established for the formation and for individual beds in the two different parts of the State. Subsequent work by Sawyer (1924) and Gould (1924) identified a broad syncline in Permian rocks of western Oklahoma—the Anadarko syncline (now called the Anadarko Basin)—and established that the "Blaine"

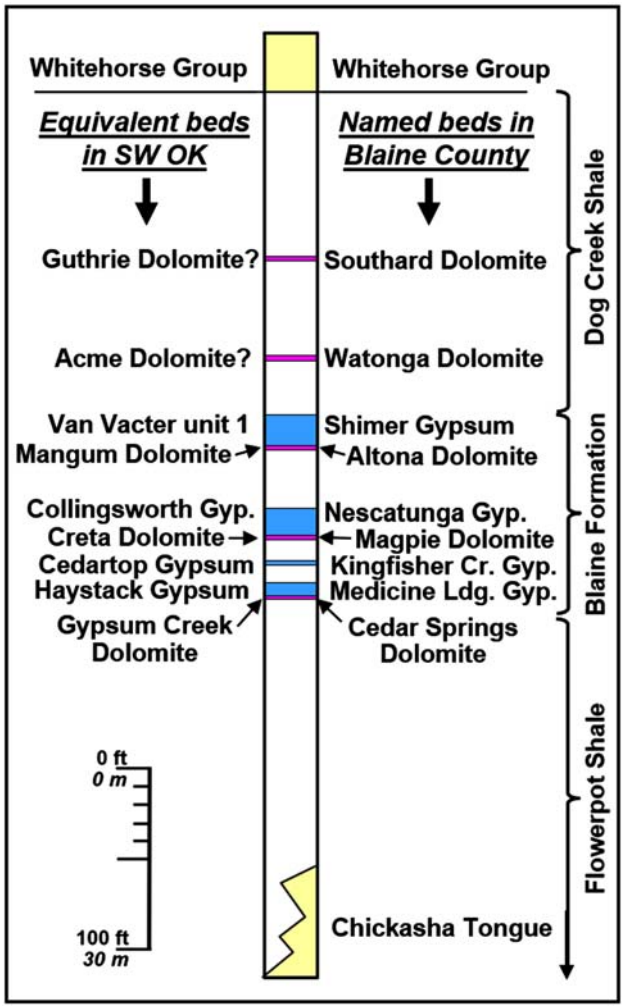

Figure 3. Geologic column 1, showing outcrops of Blaine Formation and associated strata in Blaine County, Oklahoma (on right), which is a composite of two measured sections: Fay and others (1962, measured section XI), and Fay (1964, measured section 21). Also shown (on left) are the names of the same beds in southwest Oklahoma: correlation of Guthrie and Acme Dolomites are probable, but not proven.

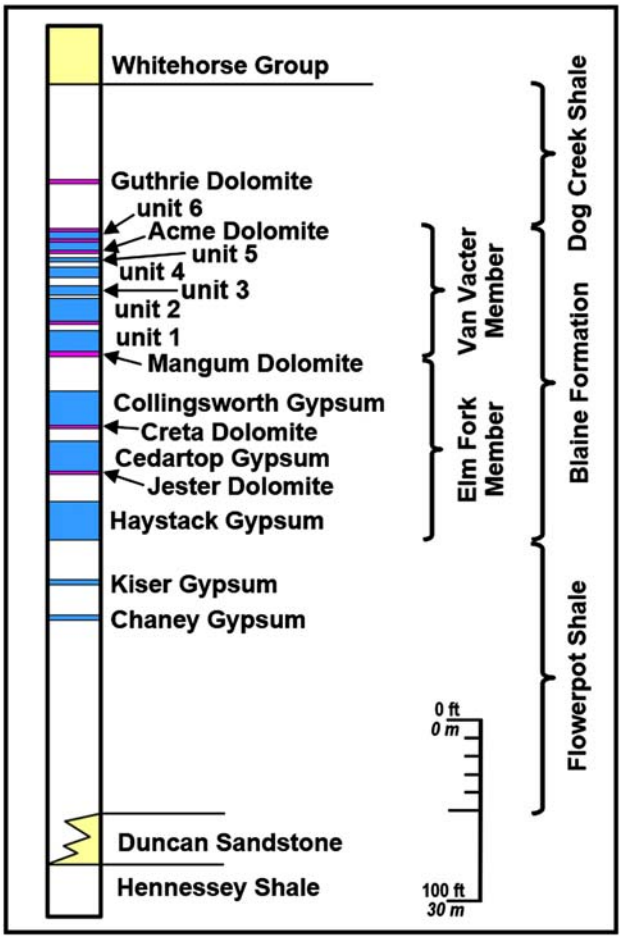

Figure 4. Geologic column 2, showing Blaine Formation and associated strata in outcrops and shallow subsurface of southeast Beckham County, Oklahoma. Composite column derived from: outcrop data in Scott and Ham (1957; measured sections 6, 7, 8, and 15); description of Carter core by Johnson (1967, p. 226–229); and final nomenclature by Johnson (1990a).

and "Greer" were equivalent units. The name "Blaine Formation" was subsequently applied in both areas, but the separate and dual nomenclature for individual gypsum and dolomite beds had been established and was retained. Subsequent subsurface study of geophysical logs throughout the Anadarko Basin has proved equivalence of the various beds and members in the two areas, and the equivalent names in southwest Oklahoma are shown on the left side of Figure 3. Although not definite, it is likely that the Watonga and Southard Dolomites of Blaine County are equivalent to the persistent Acme and Guthrie Dolomites, respectively, of southwest Oklahoma and north-central Texas.

Blaine Formation in Southeast Beckham County, Southwest Oklahoma (Fig. 4)

The Blaine Formation in southwest Oklahoma originally included all strata from the base of the Chaney Gypsum to the top of the Mangum Dolomite (Gould, 1902, 1905). Scott and Ham (1957) carried out the first detailed study and mapping of the Blaine in this area and established the present-day, basic stratigraphic framework of the Blaine Formation in southwest Oklahoma: they placed the thin Kiser and Chaney Gypsum Beds and associated thick shales in the underlying Flowerpot Shale, and the two thick gypsum beds that they identified above the Mangum Dolomite were named the Van Vacter Member of the Blaine Formation. Johnson (1967) recommended dividing the Blaine into the Van Vacter Member (to include the Mangum Dolomite), above, and the

Elm Fork Member, below; then, Johnson (1990a) formally divided the Blaine into those two members, along with several additional formal and informal units within the members (Fig. 4).

Work by Johnson (1967, Carter core) involved coring the Blaine Formation near the Van Vacter type locality and proving that it contained not 2, but 6 noncontinuous and traceable gypsum beds (Johnson, 2019b), each of which is typically underlain by a dolomite. These 6 gypsum/anhydrite and dolomite beds are informally referred to as units 1 through 6, in ascending order: exceptions to this informal nomenclature in the Van Vacter Member are the well-established formal names of the Mangum and Acme Dolomite Beds. Thickness of the Blaine Formation along the south flank of the Anadarko Basin typically ranges from 45 to 60 m (Johnson, 1967).

Geologic column 2 (Fig. 4) summarizes the stratigraphic succession first proposed by Gould, modified by Scott and Ham, and completed by Johnson for southwest Oklahoma. Figure 3 shows the correlation of individual beds of the Blaine Formation in southwest Oklahoma with those same units in Blaine County, northwest Oklahoma.

Flowerpot Shale in this area is similar to its occurrence and character in Blaine County, although two thin but widespread gypsums, the Kiser and Chaney Gypsum Beds, each less than 1 m thick, are traceable throughout southwest Oklahoma and into north-central Texas.

The Duncan Sandstone in the area of geologic column 2 (Fig. 4) is near the distal (western) end of its distribution: the formation increases in thickness to the east, toward its source area east of the Anadarko Basin. The term Duncan Sandstone is given to these strata north of the Wichita Mountains, whereas the term San Angelo Sandstone is given to equivalent strata south of the Wichita Mountains, in southwest Oklahoma and north-central Texas.

All strata from the base of the Duncan Sandstone to the top of the Dog Creek Shale make up the El Reno Group of western Oklahoma, as proposed originally by Becker (1930), who proposed it as a formation, and Schweer (in Brown, 1937), who changed it to group status.

Blaine Formation (subsurface) in Northeast Beckham County, Southwest Oklahoma (Fig. 5)

In the subsurface of the Anadarko Basin of western Oklahoma, the Flowerpot, Blaine, and Dog Creek Formations contain thick units of salt (halite) (Fig. 5). Salt occurs in the upper part of the Flowerpot Shale (the Flowerpot salt), in several parts of the Blaine Formation, and in the lower part of the Dog Creek Shale (the Yelton salt): collectively, this sequence of salts and interbedded gypsum/anhydrite, dolomite, and shale is referred to as the Beckham evaporites (Jordan and Vosburg, 1963).

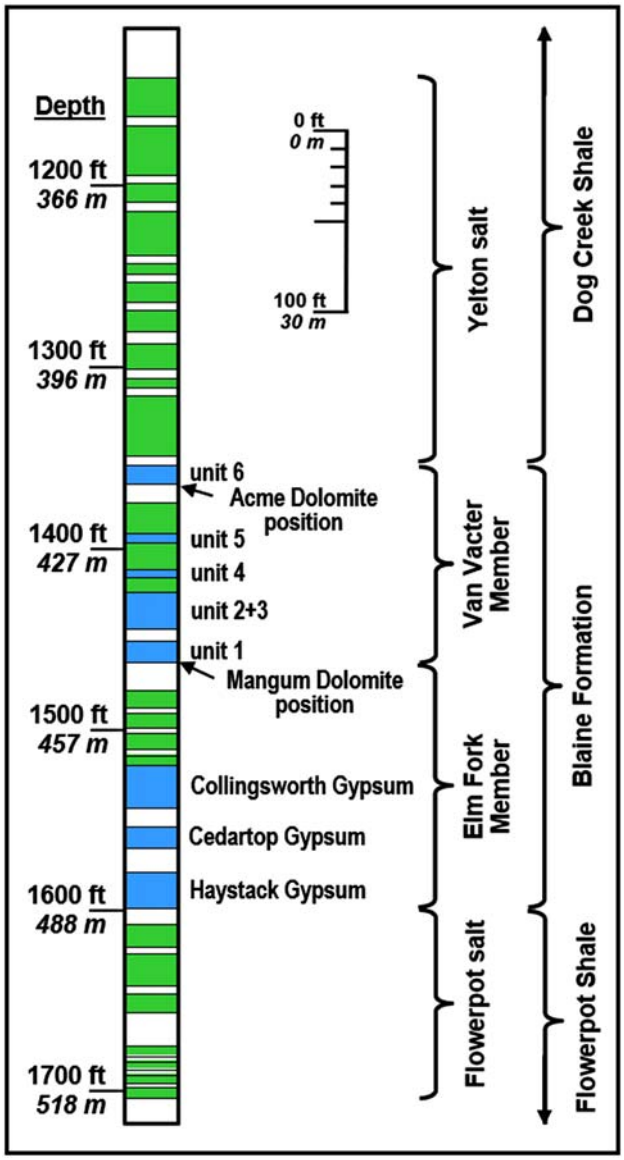

Figure 5. Geologic column 3, showing Blaine Formation and associated strata in the deep subsurface of the Anadarko Basin in northeast Beckham County, Oklahoma. Composite of cores and geophysical logs of wells drilled by Shell Oil Co. on the Yelton lease in sec. 15, T. 10 N., R. 21 W. Modified from Jordan and Vosburg (1962, Fig. 13). Although no dolomite beds were described in the borehole, most (or all?) dolomites are probably present at the base of gypsum/anhydrite beds (as they are beneath gypsum beds in nearby outcrops). All strata from the base of the Flowerpot salt to the top of the Yelton salt are referred to as the Beckham evaporites.

It is noteworthy that the middle Blaine salt, located between the Collingsworth Gypsum and the Mangum Dolomite (Nescatunga Gypsum and Altona Dolomite in northwest Oklahoma), is present in the subsurface far to the west (Texas and Oklahoma Panhandles) and

to the north (western Kansas and eastern Colorado). Based upon cores, and interpretation of geophysical logs of petroleum tests in the subsurface of northeast Beckham County, the gypsum/anhydrite beds in the Blaine Formation part of the Beckham evaporites are readily correlated with those same beds in outcrops and cores about 20 km to the south (Fig. 4), on the south flank of the Anadarko Basin. Where the Blaine Formation contains salt beds in the deep Anadarko Basin, it ranges from 50 to 75 m thick (Johnson, 1967).

The Shell Oil Co. No. 1–LPG Yelton well was drilled in 1953 for underground storage of Liquified Petroleum Gas in a single dissolution cavity created in the salts between Van Vacter anhydrite unit 2+3 and unit 6 (Fig. 5). Cores of a part of the Yelton salt in that well are described as consisting of coarse-crystalline salt, with thin (average, 18 cm thick) interbeds of brown shale that comprise about 20% of the unit (Jordan, 1959; Jordan and Vosburg, 1963). No description is provided for the salt unit in the Blaine Formation in the No. 1–LPG Yelton core, but it may be similar in character to the Yelton salt.

Dolomites at the base of anhydrite units of the Blaine Formation in original descriptions of the No. 1–LPG Yelton cores are not mentioned, but it is reasonable to expect that such dolomite units, so widespread in outcrops to the south (especially the normally thick Mangum and Acme Dolomites), persist into the subsurface nearby, and just were not recognized in the core examination.

Blaine Formation in Harmon County, Southwest Oklahoma (Fig. 6)

Nomenclature for the maximum development of the Flowerpot, Blaine, and Dog Creek Formations in southwest Oklahoma is shown in Figure 6; these strata, along with the underlying Duncan/San Angelo Sandstone, make up the El Reno Group in southwest Oklahoma (Scott and Ham, 1957; Johnson, 1967, 1990a). The San Angelo Sandstone in Harmon and Jackson Counties is equivalent to the Duncan Sandstone on the north side of the Wichita Uplift (Fig. 4). The geologic column for Harmon County (Fig. 6) is representative of the Blaine Formation and associated strata in the Hollis–Hardeman Basin, which is the eastern extension of the Palo Duro Basin of Texas. Thickness of the Blaine Formation in this area ranges from about 55 to 60 m (Johnson, 1967, 2019b).

Strata from the Chaney Gypsum Bed up through the Mangum Dolomite Bed are extensively exposed in southwest Oklahoma, and they have been easily recognized and correlated throughout the area. However, gypsum beds of the Van Vacter Member are another story: the thick gypsum units are poorly exposed in most areas (largely because of partial or total dissolution and/or collapse), and were not recognized as 6 noncontinuous

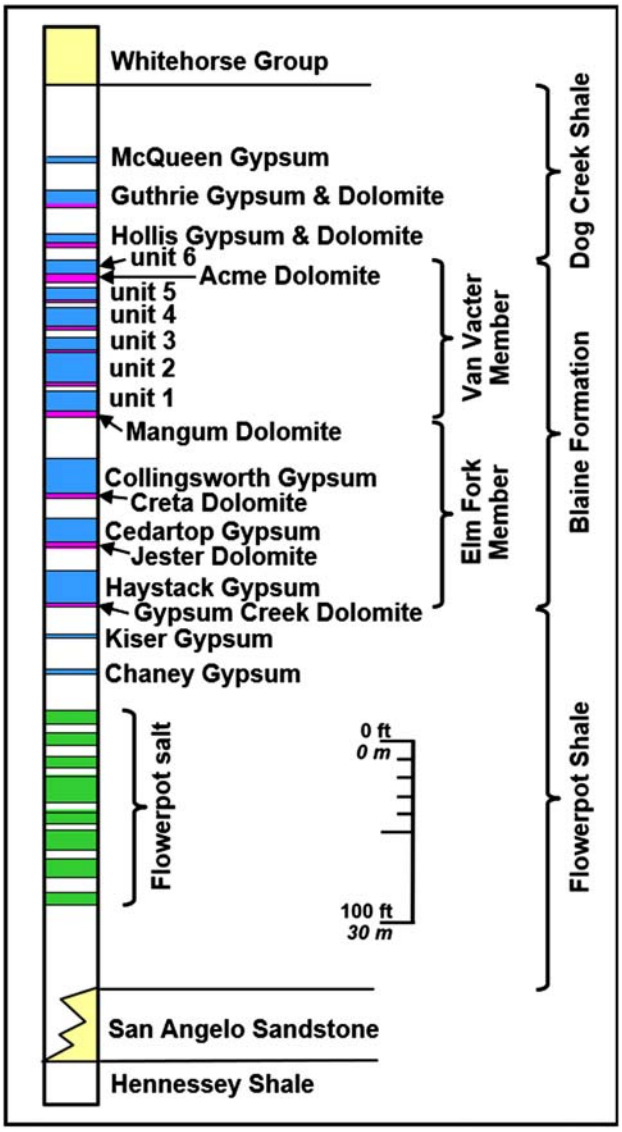

Figure 6. Geologic column 4, showing Blaine Formation and associated strata in outcrops and subsurface of Harmon County, Oklahoma. Composite column derived from data in Johnson (1967, 1989, 2019b), based on outcrops, cores, and geophysical logs.

stratigraphic units until cores and detailed stratigraphic tests were obtained (Johnson, 1967, 1990a, 2019b). We now know that each of the 9 main gypsum beds making up the Blaine Formation in southwest Oklahoma is underlain by a dolomite bed at most sites. Conspicuous and mappable gypsums and dolomites in the Elm Fork Member have each been named, whereas the gypsums and dolomites in the Van Vacter Member are given an informal status (i.e., gypsum unit 1, dolomite unit 2, gypsum unit 2, etc.), with the exception of the Mangum and Acme Dolomite Beds, which are readily recognized in outcrops and are correlated throughout southwest Oklahoma and north-central Texas.

Blaine Formation in Childress County, North-Central Texas (Fig. 7)

Comprehensive study of cores and outcrops in the Jonah Creek–Salt Creek area of northwest Childress County, Texas, was carried out by me in cooperation with the U.S. Army Corps of Engineers (Tulsa District) in the early 1970s to determine the source of salt-water contamination in this part of the Prairie Dog Town Fork Red River drainage (Johnson, 1981, 2019a). Results of this study show a great similarity of the stratigraphy of the Blaine and Dog Creek Formations in this area (Fig. 7) to the same units in southwest Oklahoma (Fig. 6). The main difference is inclusion of an upper dolomite/gypsum unit (unit 7) at the top of the Van Vacter Member of the Blaine Formation. The thickness of the Blaine Formation in Childress County is about 60 to nearly 70 m, where it lacks salt interbeds: it is about 75m thick where it contains salt in the subsurface of Motley County, just to the southwest (Johnson, 2019a).

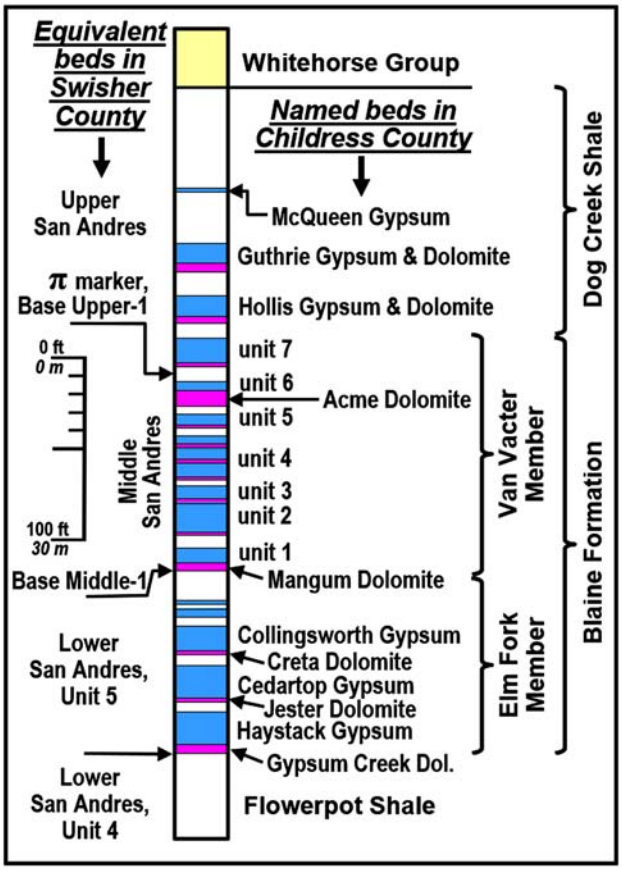

Figure 7. Geologic column 5, showing Blaine Formation and associated strata in outcrops and shallow subsurface of northwest Childress County, Texas (on right). Composite column based on outcrops and cores, as shown in Johnson (2019a, plate 7). Also shown (on left) are the names of the same beds in the San Andres Formation in subsurface of the Palo Duro Basin in northeast Swisher County (Fig. 8); salt beds in Swisher County are omitted here to simplify correlations.

Addition of thick gypsum beds at the top and bottom of the Blaine Formation is a long-standing treatment of the formation in Texas: gypsum and dolomite beds in the upper Flowerpot and lower Dog Creek of southwest Oklahoma increase in thickness and abundance to the south and west into north-central Texas, and these beds are commonly included in what is called the "Blaine of Texas" (Roth, 1945; Pendery, 1963; Jones, 1971; Johnson, 2018). In fact, the 1:250,000-scale geologic maps of north-central Texas (the Plainview, Lubbock, Big Springs, and San Angelo sheets of the Geologic Atlas of Texas, published by the Texas Bureau of Economic Geology) show the "Blaine of Texas" embraces all strata from the top of the San Angelo Sandstone to the base of the Whitehorse Group. With this expanded concept of the Blaine (top of San Angelo to base of Whitehorse), the thickness of the "Blaine of Texas" ranges from about 150 to almost 215 m in areas south of Childress County (Jones, 1971).

All strata in north-central Texas from the base of the San Angelo Sandstone to the top of the Dog Creek Shale (base of Whitehorse Group) were placed in the Pease River Group by Roth (1945), and this has been followed by Pendery (1963), Jones (1971), Hentz and Brown (1987), and others working in the area. Therefore, the Pease River Group of Texas is equivalent to the El Reno Group of western Oklahoma.

Stratigraphically equivalent units in the San Andres Formation in the Palo Duro Basin are shown on the left side of geologic column 5 (Fig. 7). This correlation of beds was most clearly demonstrated and stated in Fracasso and Hovorka (1986, p. 28) and in Figure 4 of Hovorka and Granger (1988), and is supported by my own work in correlating the Blaine Formation on geophysical logs from southwest Oklahoma into the Palo Duro Basin. Correlation of the base of the lower San Andres unit 5 with the base of the Haystack Gypsum (or Gypsum Creek Dolomite) is unquestionable, as is correlation of the base of the middle San Andres (M-1) with the base of the Van Vacter Member (the Mangum Dolomite Bed). Correlation of the base of the upper San Andres (the Pi [π] marker bed) with shale between units 6 and 7 of the Van Vacter Member is highly probable, although it may, after more detailed work, be proven to be equivalent to the shale below the Acme Dolomite or perhaps above gypsum unit 7 of the Van Vacter.

San Andres Formation in Swisher County, North Texas (Fig. 8)

Geologic column 6 (Fig. 8) is representative of parts of the lower, middle, and upper San Andres Formation in cores that were drilled by the U.S. Department of Energy in the late 1970s and early 1980s at 10 locations in the

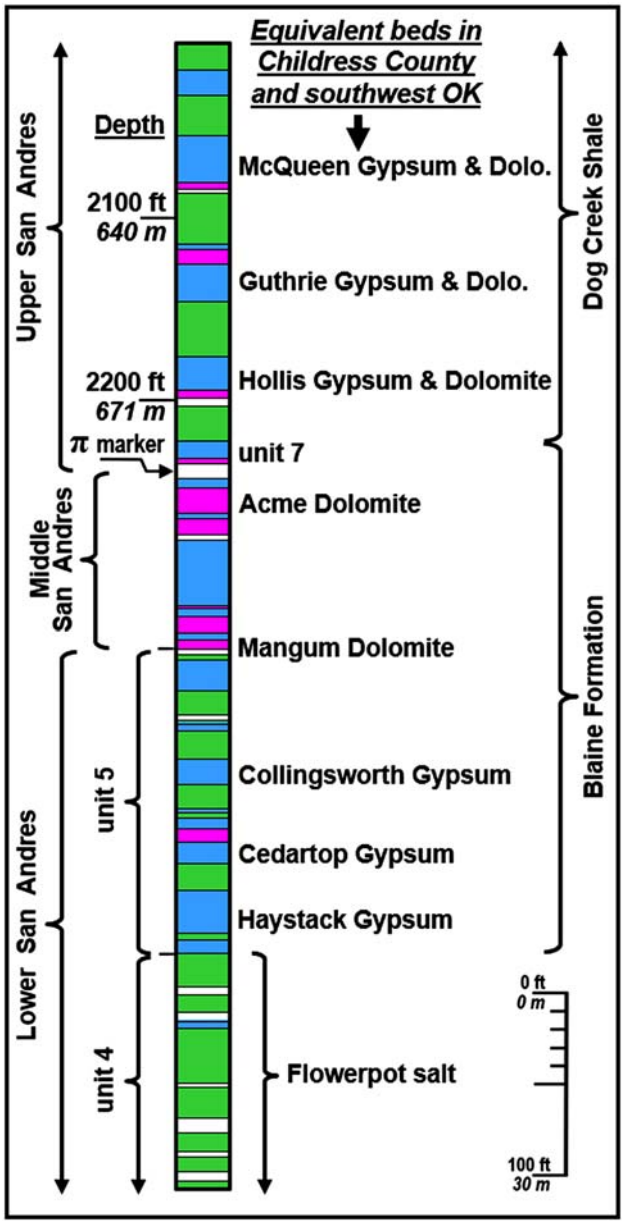

Figure 8. Geologic column 6, showing the San Andres Formation (on left) in the subsurface of the Palo Duro Basin in northeast Swisher County, Texas. Based on core descriptions of the D.O.E.–Gruy Federal, D.M. Grabbe No. 1 well, shown in McGowan (1981, plate 1), and correlations of Hovorka and Granger (1988). Also shown (on right) are the names of the same beds and formations in Childress County, Texas, and southwest Oklahoma.

Palo Duro Basin: the cores were drilled as part of a program to evaluate the potential for developing a nuclear-waste repository deep underground in salt beds of the San Andres Formation. Illustrated in Figure 8 is the DOE–Gruy Federal D.M. Grabbe No. 1, drilled in northeast Swisher County, Texas, in 1981; lithology of this core is reproduced from McGowan (1981, Plate 1). Originally, the San Andres Formation in the Palo Duro Basin was informally divided into just lower and upper divisions, but in later work (Fracasso and Hovorka, 1986; Hovorka and Granger, 1988), the lower part of the upper division was separated out as the middle San Andres (Fig. 8). The Blaine Formation part of the San Andres here is about 85 m thick.

Although detailed correlation of some individual gypsum/anhydrite and dolomite beds within the Blaine Formation breaks down westward across the Palo Duro Basin, there is unquestioned equivalence of the base of lower San Andres unit 5 to the base of the Blaine Formation in southwest and northwest Oklahoma. In addition, the base of the middle San Andres in the Palo Duro Basin is definitely equivalent to the Mangum Dolomite in southwest Oklahoma and to the Altona Dolomite in northwest Oklahoma. In addition, there is a high probability that the base of the upper San Andres (the Pi [π] marker bed) is equivalent to the shale below Van Vacter Member unit 7 in Childress County, Texas, and is stratigraphically close to the Acme Dolomite in southwest Oklahoma and the Watonga Dolomite in northwest Oklahoma.

The Pi (π) marker bed is a persistent rock layer in the upper part of the San Andres Formation throughout southeast New Mexico (Pitt and Scott, 1981), and it has been traced eastward across the Palo Duro Basin to the shallow subsurface of north-central Texas (Ramondetta, 1982; Fracasso and Hovorka, 1986; Hovorka and Granger, 1988). The Pi marker has been described in various areas as a siltstone bed (Pit and Scott, 1981) or a siltstone and fine sandstone bed (Fracasso and Hovorka, 1886). Its value is that on geophysical logs it is a sharp, high-gamma-ray peak at the base of the upper San Andres Formation: 1) it can be correlated over great distances from southeast New Mexico to the eastern Palo Duro Basin; 2) it is essentially equivalent to the top of the Blaine Formation in southwest Oklahoma; and 3) it is probably equivalent to strata just above the Watonga Dolomite in northwest Oklahoma.

EVAPORITE KARST IN BLAINE AND SAN ANDRES FORMATIONS

Salt and gypsum beds in the Blaine Formation and associated strata in western Oklahoma have been dissolved naturally at many places, and the same is true for salt and gypsum beds in the San Andres Formation in the Palo Duro Basin of Texas. Fresh ground water circulates down to salt and gypsum in these formations, dissolves some or all of the evaporites, and produces karst features, such as sinkholes, collapse structures, breccia pipes, caves, natural bridges, disappearing streams, and salt springs. In some places, dissolution is not highly focused: instead, and it removes gypsum or salt somewhat uniformly over moderate-to-large areas, producing

sheetlike dissolution of the evaporite with, perhaps, little disturbance of overlying strata, except for subsidence or settling.

The process for dissolution of evaporites was discussed by Johnson (1981) with reference to salt dissolution, but the guidelines also apply to gypsum dissolution. He stated that ground water in contact with salt or gypsum will dissolve some of the rock, providing that the water is not already saturated with NaCl or $CaSO_4$, respectively (Fig. 9). For extensive dissolution to occur, it is necessary for the resulting brine to be removed from the evaporite rock, or else the brine becomes saturated and the dissolution process stops. Four basic requirements for dissolution of salt or gypsum are: 1) a deposit of salt or gypsum against which, or through which, water can flow; 2) a supply of water unsaturated with NaCl or $CaSO_4$, respectively; 3) an outlet whereby the resulting brine can escape; and 4) energy, such as a hydrostatic head or density gradient, to cause water to flow through the system (Johnson, 1981). When all four requirements are met, dissolution of salt or gypsum can be quite rapid, in terms of geologic time. A brief discussion on the development of sinkholes in North America was given by Martinez and others (1998).

Recent discussions of widespread evaporite karst in the Blaine Formation and associated strata in western Oklahoma are presented by Johnson (2003a, 2013), and in the San Andres Formation in the Palo Duro Basin by Gustavson and others (1980a, 1980b, 1982) and Simpkins and others (1981). The current report will show examples of salt karst and gypsum karst in this large region.

Salt Karst

Western Oklahoma and the Texas Panhandle contain a thick sequence of salt-bearing evaporites in the Blaine Formation and associated strata and in the San Andres Formation (Fig. 10). The Oklahoma occurrences have been mapped and described by Jordan and Vosburg (1963), Johnson (1967, 1976), and Johnson and Gonzales (1978). Similar thick deposits of salt in the San Andres Formation in the Palo Duro Basin are described and shown on maps and cross sections by Presley (1981a, 1981b, 1987), Ramondetta (1982), Fracasso and Hovorka (1986), McGookey and others (1988), and Hovorka (1990). These thick salt units typically are partially or totally dissolved where they are at depths of less than about 200 to 300 m. Evidence that salt dissolution is an on-going process is the presence of numerous salt springs and salt flats located on outcrops of the Blaine and associated strata on the flanks of the Anadarko Basin in Oklahoma (Ward, 1961; Johnson, 2019c, 2019d), and on the east side of the Palo Duro Basin in north-central

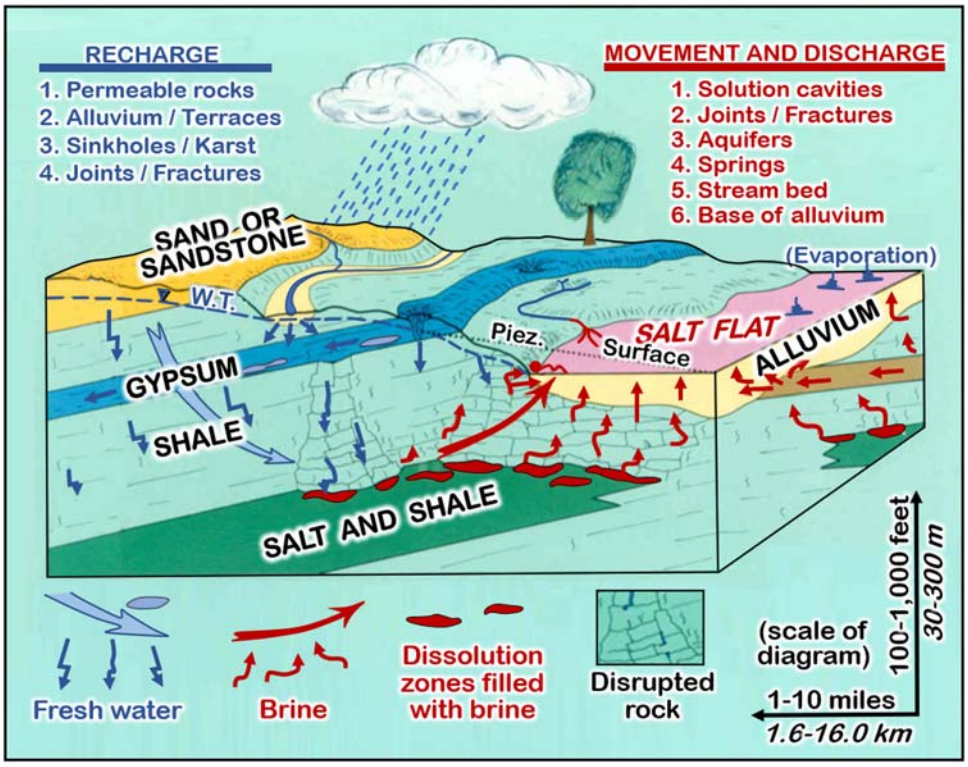

Figure 9. Schematic diagram showing circulation of fresh water and brine in areas of salt dissolution in western Oklahoma and north-central Texas (modified from Johnson, 1981, 2019a).

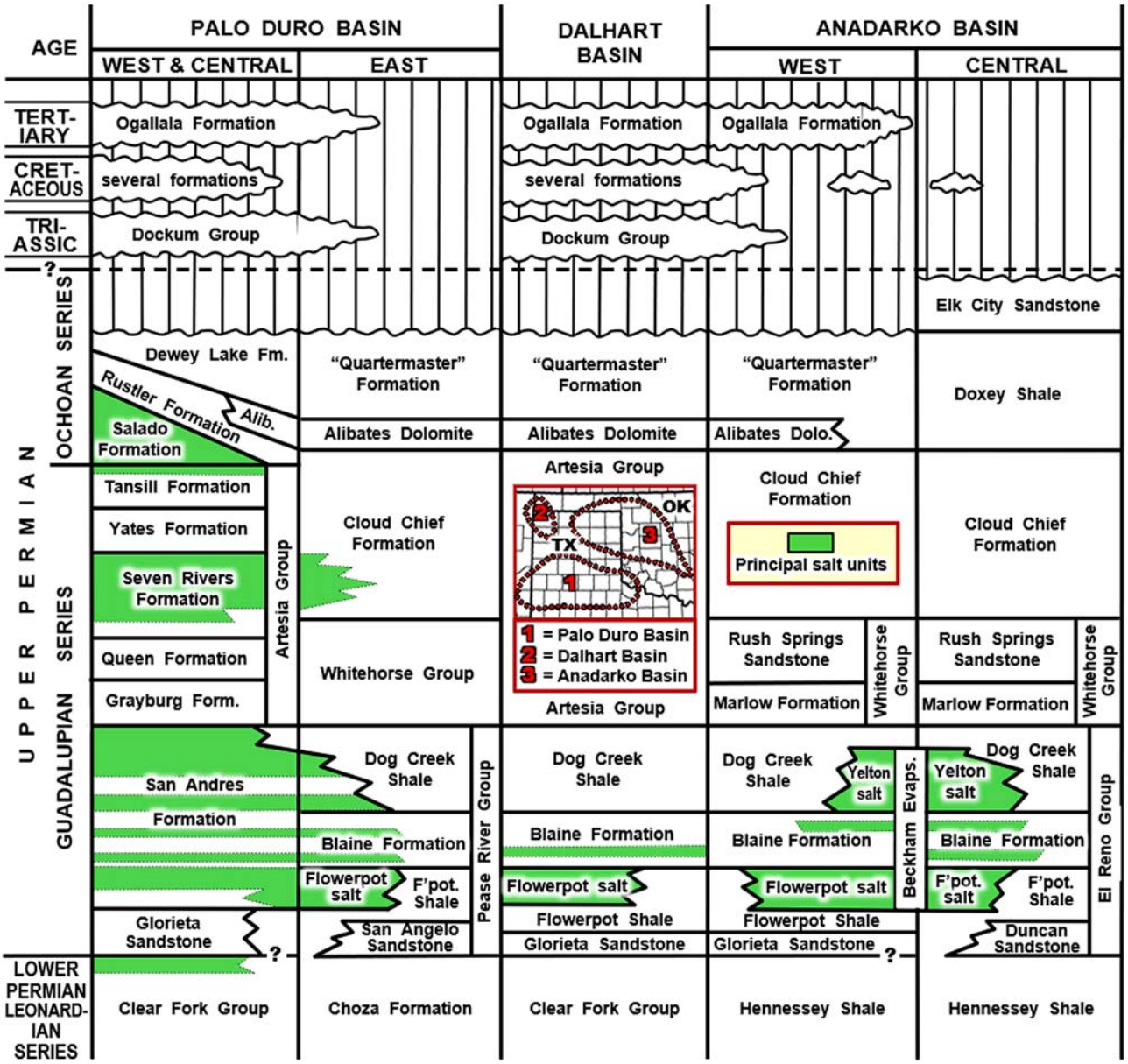

Figure 10. Stratigraphic nomenclature of Upper Permian and younger strata in western Oklahoma and Texas Panhandle, showing main salt units in green (modified from Johnson, 1976). Some workers have placed the Glorieta, San Angelo, and Duncan Sandstones in the Leonardian Series.

Texas (Ward, 1961; Johnson, 1981, 2019a; Richter and Kreitler, 1986).

Below are discussions of salt karst in the Blaine Formation and associated strata in areas a, b, and c in Oklahoma (Fig. 11). These are followed by discussions of salt karst in the San Andres Formation of Texas in: 1) the Palo Duro Basin and 2) a separate study in the east Palo Duro Basin area.

Area a

In area a, the deep Anadarko Basin preserves a thick sequence of salt-bearing evaporites in the Blaine Formation and associated strata (Fig. 5) that are partly dissolved where they extend to shallower depths of the basin (Fig. 12): these salt-bearing units are (in ascending order) the Flowerpot salt, Blaine Formation, and Yelton salt—which collectively are referred to as the Beckham evaporites (Jordan and Vosburg, 1963). The Beckham evaporites are up to 250 m thick in eastern Beckham County, along the axis of the basin, and the salt units tend to be dissolved at depths less than about 200–300 m.

Normally, outcropping strata in the Anadarko Basin dip at an angle of less than one degree (less than 10 m/km) toward the axis of the basin. However, dissolution of salt has resulted in some collapse structures, and in those

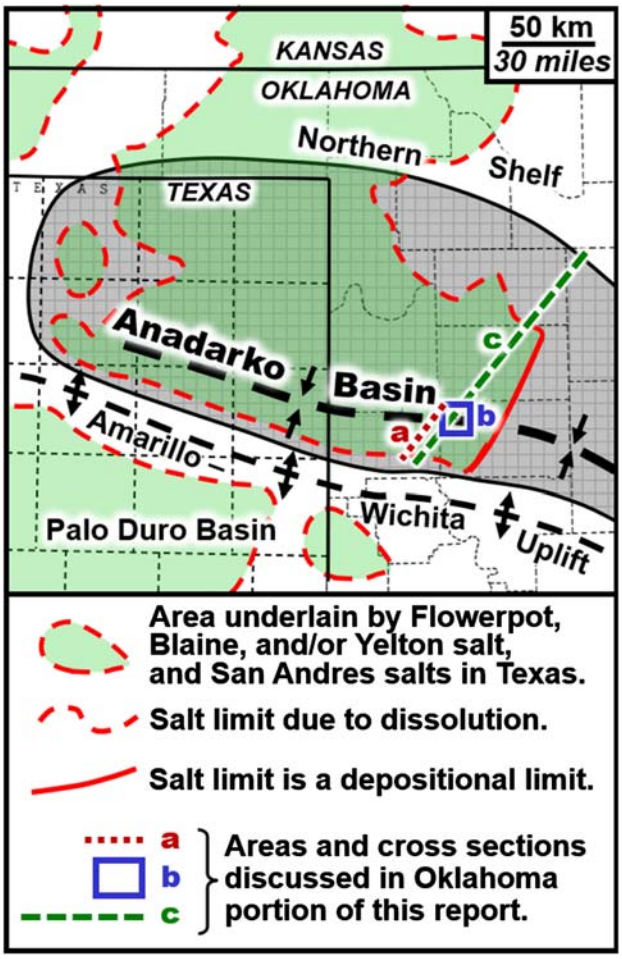

Figure 11. Map of Anadarko Basin in western Oklahoma and Texas Panhandle showing areas underlain by, and dissolution limits of, the Flowerpot, Blaine, and/or Yelton salts (modified from Johnson, 2013). Also shown are three areas and cross sections of salt dissolution in Oklahoma that are discussed in this report (areas a, b, and c).

areas underlain by salt karst the overlying strata have subsided, settled, or collapsed into the underground cavities (Fig. 12, lower cross section). This has resulted in disturbed bedding in outcropping rocks, and locally Permian rocks dip at angles of up to 30°, or more. Disturbed bedding and collapse structures caused by salt karst in the Oklahoma part of the Anadarko Basin can be seen in outcrops of overlying Permian units (the Cloud Chief, Doxey, and Elk City Formations), as represented in the lower cross section in Figure 12, and as breccia pipes and other collapse features of Cretaceous rocks at scattered locations on the north flank of the Anadarko Basin (see "Area b" and "Area c," below).

The Yelton salt is the youngest salt unit in the Anadarko Basin, and it ranges in depth from about 200 m to nearly 400 m along and near the axis of the Anadarko Basin (Jordan and Vosburg, 1963; Johnson, 1963, 1967). This salt is partly or totally dissolved on the flanks of the basin, and overlying strata have collapsed into the salt-karst cavities (Fig. 12, lower cross section). The thickness, distribution, and sharp termination of the Yelton salt at its dissolution limits have been mapped by Jordan and Vosburg (1963) and Johnson (1963, 1967). Collapse structures and disturbed bedding in outcropping Cloud Chief, Doxey, and Elk City strata that overlie the dissolution zone have been well documented in field studies by Smith (1964), Richardson (1970), Zabawa (1976), Moussavi-Harami (1977), Suneson (2012), and Johnson (2013). Whereas strata overlying the Yelton salt along and near the axis of the Anadarko Basin are still essentially flat lying (dips of less than one degree), chaotic-bedding features are common to the north and south, where the Yelton salt has been dissolved and overlying strata have collapsed.

Area b

Area b, referred to as the Canute–Burns Flat area in Johnson (2013), is an excellent area to examine dissolution of the Yelton salt and resultant subsidence and collapse of overlying strata (Fig. 13). Here, the Yelton salt is typically 50–70 m thick, but it thins sharply to the north and east because of dissolution, and is totally missing within several kilometers. As a result of salt dissolution, there is a significant difference in the attitude (dip) of outcropping rocks in the area underlain by the Yelton, as compared to nearby areas where the Yelton is totally dissolved. Mapping of the surface geology here by Richardson (1970) showed that outcrops above the Yelton are essentially horizontal, whereas his study, and that of Johnson (2013), showed that Permian strata overlying the salt-dissolution area typically dip erratically at angles of 5–30°, and that Cretaceous and Permian strata in the same area occur as scattered chaotic collapse blocks or breccia pipes (Fig. 14): breccia pipes here are cylindrical or irregular columns of broken rock (rubble) that have dropped into deep-seated, salt-dissolution cavities. Disruption of outcropping strata because of Yelton-salt dissolution on the north flank of the Anadarko Basin is also shown in Figure 12 (lower cross section).

Cretaceous strata once covered the area, but have now been entirely removed by erosion, except where they have been preserved in breccia pipes as down-dropped blocks of limestone and sandstone (Suneson, 2012; Johnson 2013) (Fig. 14B). These breccia pipes typically are less than 0.4 hectare (1 acre) in size, and it appears that Cretaceous strata have dropped some 50 m, or more, and are now juxtaposed against various Permian formations on the north flank of the Anadarko Basin.

Area c

Area c refers to a cross section (Figs. 11, 15) from the deep Anadarko Basin to the northern shelf where cores

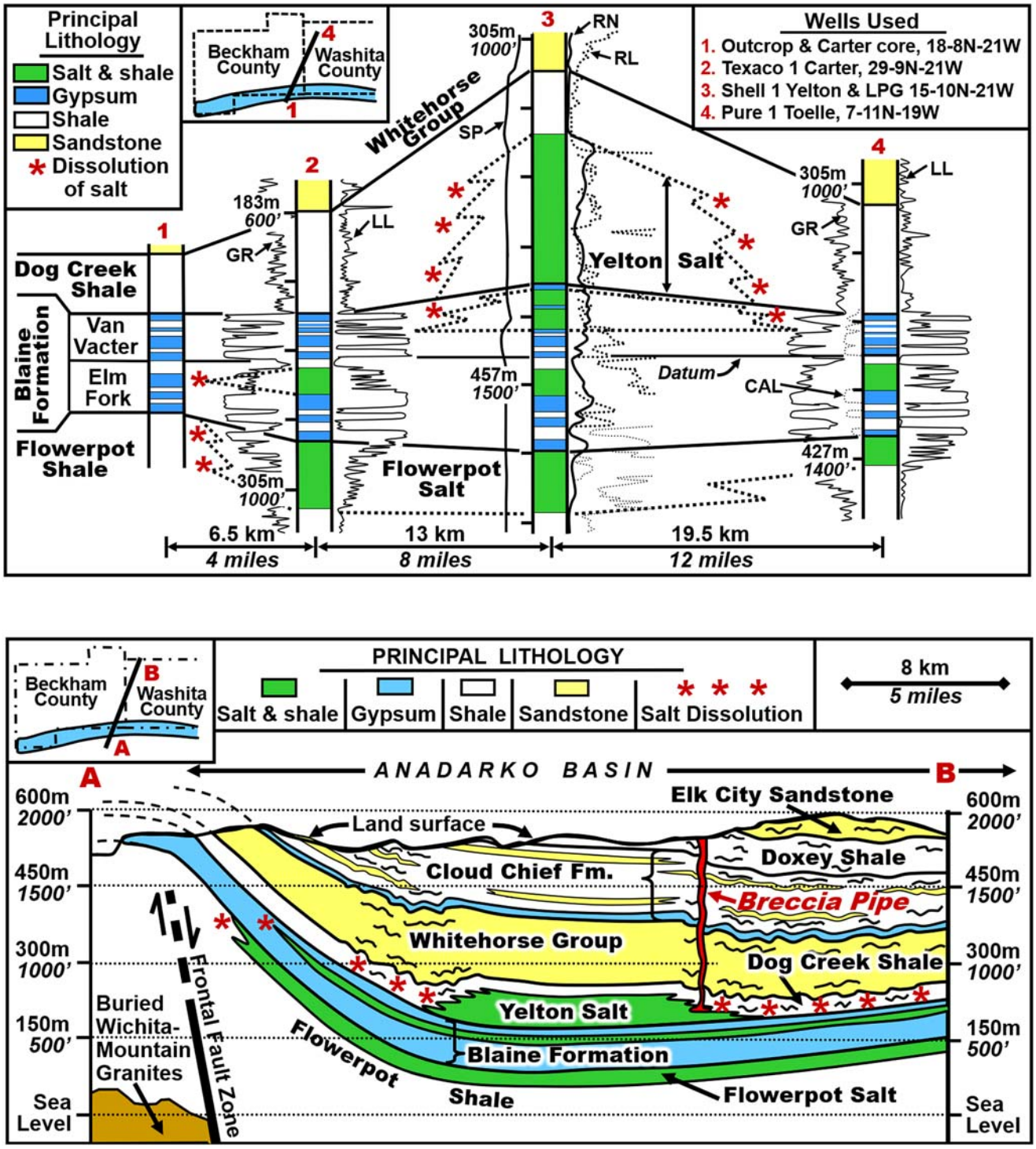

Figure 12. Cross sections showing dissolution of Permian salt units in eastern Beckham and western Washita Counties, Oklahoma (from Johnson, 2013). Upper and lower cross sections are along the same alignment: upper cross section is stratigraphic; lower cross section is structural. This is "cross section a" in Figure 11.

drilled at Canton Lake Dam contain about 30 m of brecciated Dog Creek Shale that results from dissolution of Yelton salt, or salt in the Blaine Formation, that once extended about 100 km northeast of its present limits (Fig. 16) (Johnson, 2017). Brecciated Dog Creek at Canton Lake Dam rests directly on the Shimer Gypsum, the top bed of the Blaine Formation in northwest Oklahoma (Fig. 3), and shows that at one time salt layers in the Yelton salt, or in the Van Vacter Member of the Blaine Formation, extended well beyond their present limits

in the deep parts of the basin. Further evidence of the previous presence of these salts are the large areas containing scattered collapse blocks of Cretaceous rocks in Washita, Custer, and Dewey Counties (Fig. 15), as mapped or described by Stanley (2002), Johnson and others (2003), Fay (2010), Suneson (2012), and Johnson (2013, 2017).

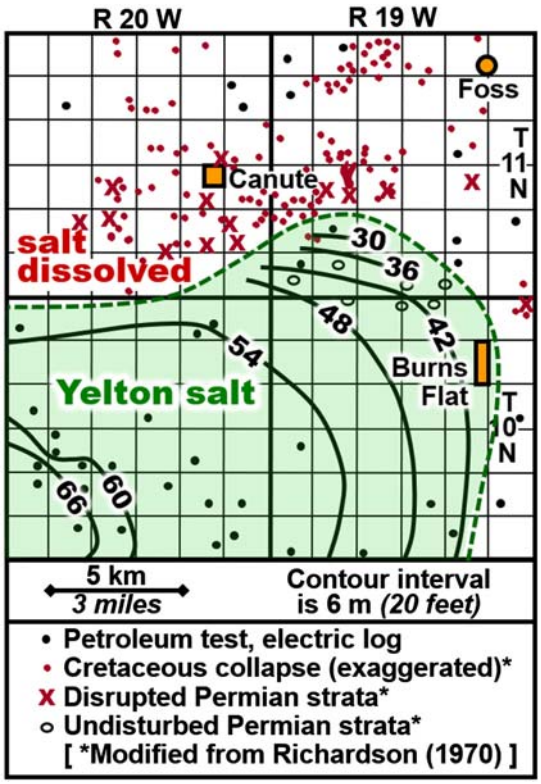

Figure 13. Map showing thickness of Yelton salt (green), and the area of salt dissolution and collapse of overlying strata in the Canute–Burns Flat area of northwest Washita County, Oklahoma. Cretaceous collapse structures are mostly less than 0.4 hectare (1 acre). From Johnson (2013, 2017). This is "area b" in Figure 11.

Breccia cored at Canton Lake Dam consists of angular fragments of shale, siltstone, sandstone, dolomite, and gypsum that range in size from about 0.5 cm to 15 cm across, and are surrounded by, and recemented in, a matrix of clay, shale, or sandstone (Fig. 17) (Johnson 2017). Many cores were drilled at the dam site during three phases of investigation, and breccia was reported in the lower part of the Dog Creek in virtually all the cores. The brecciated zone is about 15 m below the land surface at the dam site. If karst or collapse features are present nearer to the land surface at the dam, they are now masked by Quaternary deposits or the earthen dam itself: however, photographs (taken during dam construction in 1946) of excavations show that upper Dog Creek strata appear to be disrupted and undulate as much as 6–9 m within short distances, and these look like subsidence, collapse, and sinkhole features that would result from dissolution and collapse of underlying Dog Creek strata (Johnson, 2017).

It is likely that a moderate amount of bedded salt (either Yelton salt or salts in the Van Vacter Member of the Blaine Formation) originally existed in a large area of Washita, Custer, and Dewey Counties, reaching all the way to Canton Lake Dam area. That salt was dissolved by ground water, resulting in fracturing, subsidence, and brecciation of interbedded and overlying strata: this produced layers of brecciated Dog Creek Shale, as were cored at Canton Lake Dam, as well as breccia pipes that preserve Cretaceous collapse blocks elsewhere in the Anadarko Basin.

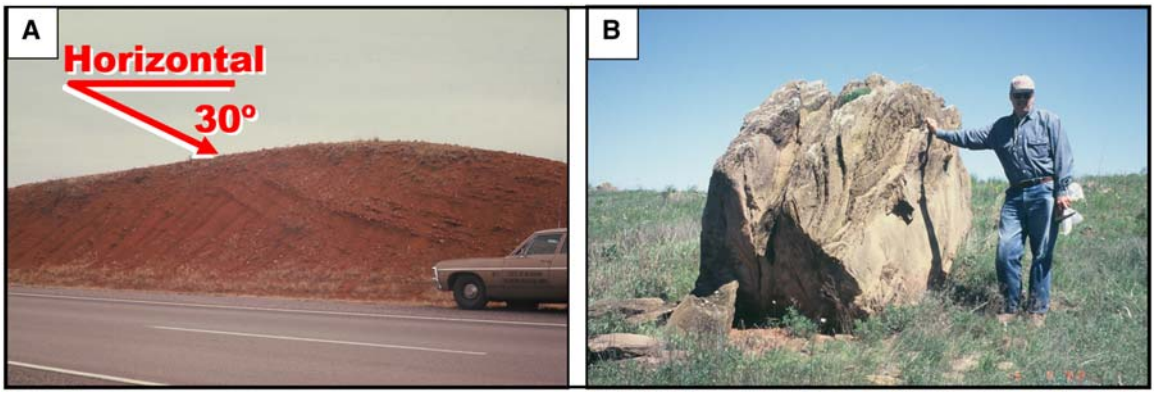

Figure 14. Collapse structures because of dissolution of the Yelton salt in the Anadarko Basin, where Permian strata unaffected by salt dissolution normally dip at angles of less than 1°. A) Large masses of Permian strata (Doxey Shale here) are tilted and dip at angles of up to 30° where salt dissolution occurred beneath a large area: masses are up to 2–4 hectares (5–10 acres). B) Other collapse features are breccia pipes or chimneys, where blocks of Cretaceous limestone and sandstone drop down in areas generally less than 0.4 hectare (1 acre), and are juxtaposed with Permian outcrops.

Palo Duro Basin

Johnson (1976) made a study of the thickness, depth, and distribution of Permian salt deposits in the Texas Panhandle and western Oklahoma to determine if the region might contain an area suitable for the underground disposal of high-level radioactive wastes: he recommended that, of the three basins studied (Anadarko, Palo Duro, and Dalhart Basins), parts of the Palo Duro Basin appeared to have salt deposits most likely to meet the criteria for hosting a radioactive-waste repository. The U.S. Department of Energy then contracted (in 1977) with the Bureau of Economic Geology (BEG) at The University of Texas at Austin, along with several engineering and consulting firms, to conduct extensive geologic and hydrologic studies related to salt deposits in the Palo Duro Basin.

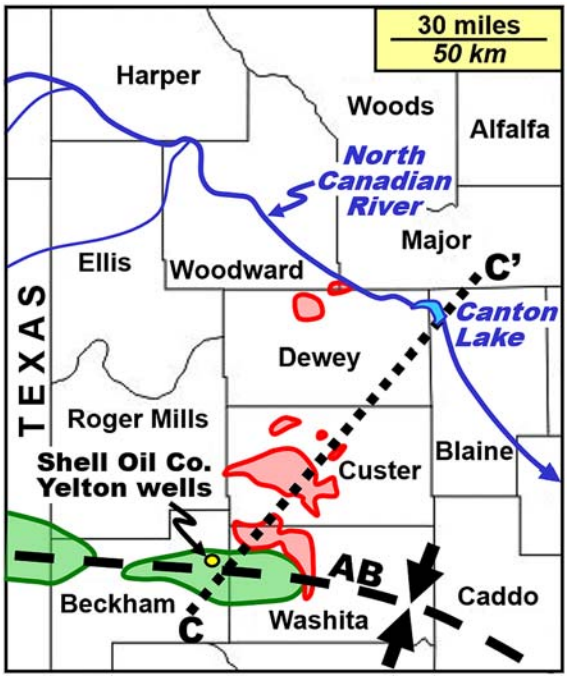

Figure 15. Map of northwest Oklahoma showing: 1) axis of the Anadarko Basin (AB); 2) areas still underlain by the Yelton salt (green); 3) location of Shell Oil Co. Yelton wells (see also Figs. 5, 12); 4) areas with multiple breccia pipes and collapse blocks of Cretaceous rocks in Washita, Custer, and Dewey Counties (red); 5) Canton Lake, where breccia was encountered in Permian strata during dam construction; and 6) location of cross section C–C' (see Fig. 16), which is "cross section c" in Figure 11. From Johnson (2017).

In 1987, the U.S. Congress amended the Nuclear Waste Policy Act to focus only on the Yucca Mountain Site in Nevada, and further study of Palo Duro Basin as a potential repository site ceased. However, a wealth of information was obtained and published by BEG on the Permian salt deposits of the Palo Duro Basin during their studies, and one of the major foci was on the geology and dissolution phenomena of salts in the San Andres Formation. Among those reports are Gustavson (1979, 1982, 1986a), Gustavson and others (1980a, 1980b, 1982), Presley (1980, 1981a, 1981b), Simpkins and others (1981), Collins (1984), Goldstein and Collins (1984), and Gustavson and Finley (1985).

Maps showing distribution of the San Andres salts, and areas where those salts are partly or totally dissolved, were prepared by Presley (1981a), and are simplified here in Figure 18. Salt is abundant in the San Andres Formation. Net salt thickness ranges from about 15 to 120 m in the lower San Andres, and from about 30 to 90 m in the upper San Andres. The top of these salts is about 900 m below the land surface in the south (deep) part of the Palo Duro Basin, and it rises to depths as shallow as 150–330 m in the east and north parts of the basin (Presley, 1981a): at

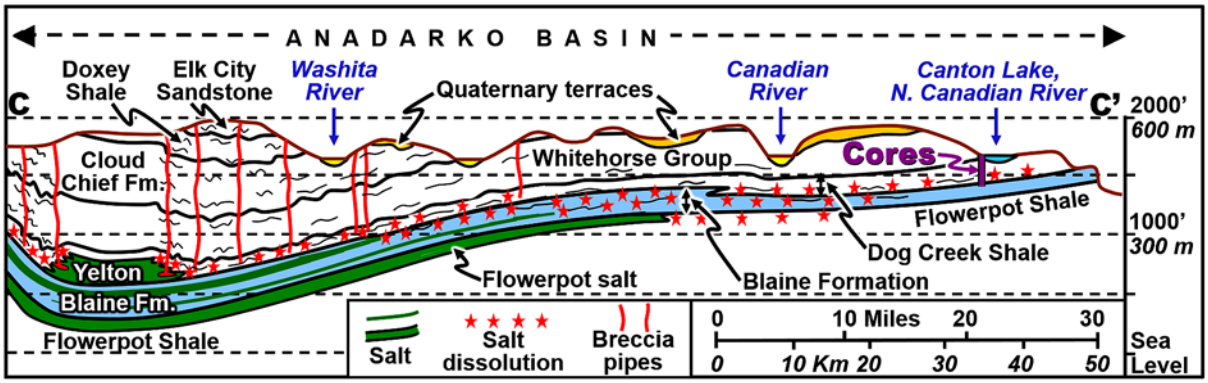

Figure 16. Cross section C–C' from axis of Anadarko Basin (left) to the northern shelf area (right). Permian salt units, still present in the deep subsurface, are dissolved at shallower depths, causing brecciation and collapse of overlying strata. Breccia pipes (schematically located) locally reach the present land surface and contain collapse blocks of Permian and Cretaceous strata. Cores at Canton Lake Dam (right side of cross section) contain collapse breccia (see Fig. 17) resulting from dissolution of Yelton or Blaine salt beds, previously present in the area. Location of "cross section c" shown in Figures 11 and 15. From Johnson (2017).



Figure 17. Three boxes containing 4 m (13 feet) of core from borehole BL–3, drilled on left spillway abutment of Canton Lake Dam in Blaine County, Oklahoma. Top of core is 40.2 m (132.0 feet) deep, and bottom is 44.2 m (145.0 feet) deep. Core shows brecciated Dog Creek Shale, with fragments of shale, siltstone, dolomite, and gypsum that are recemented in a matrix of clay, shale, and sandstone. Rock is brecciated because of collapse resulting from dissolution of underlying salt in the Yelton salt, and/or salts in the upper part of the Blaine Formation (see right side of Fig. 16). From Johnson (2017).

these shallow depths, ground-water dissolution of salt occurs (Fig. 9), and the San Andres and overlying strata are fractured, disrupted, and chaotically dropped. Collapse features above San Andres dissolution zones include breccias, breccia pipes, faults, sinkholes, and complex folds (Gustavson and others, 1980b).

Cross sections by Presley (1981a, b) (Figs. 19, 20) show clearly the dissolution of San Andres salts as they rise from 900-m depths in the deep Palo Duro Basin to shallower depths on the east and north margins of the basin (see location of cross sections in Fig. 18). Both are stratigraphic cross sections, with the datum being the top of the San Andres Formation, or equivalent strata at the top of the Blaine Formation, or gypsum/anhydrite in the lower part of the Dog Creek Shale. Salts in the upper San Andres and unit 5 of the lower San Andres (Fig. 19) are dissolved in eastern Armstrong County—and parts of Briscoe, Hall, and Motley Counties (Fig. 18). The upper San Andres salt is about 280 m (800 ft) deep, and well preserved, in wells #19 and #22 (Fig. 19); but these salts are dissolved about 30 km to the east, where they would be about 150 m (500 feet) deep in well #43. In addition, in a similar manner, the remaining salts in the lower San Andres are all dissolved at depths of about 150 m (between wells #31 and #9), within a distance of about 35 km (Fig. 19).

Another cross section (Fig. 20) extends from the deep Palo Duro Basin on the south, up over the Oldham Nose

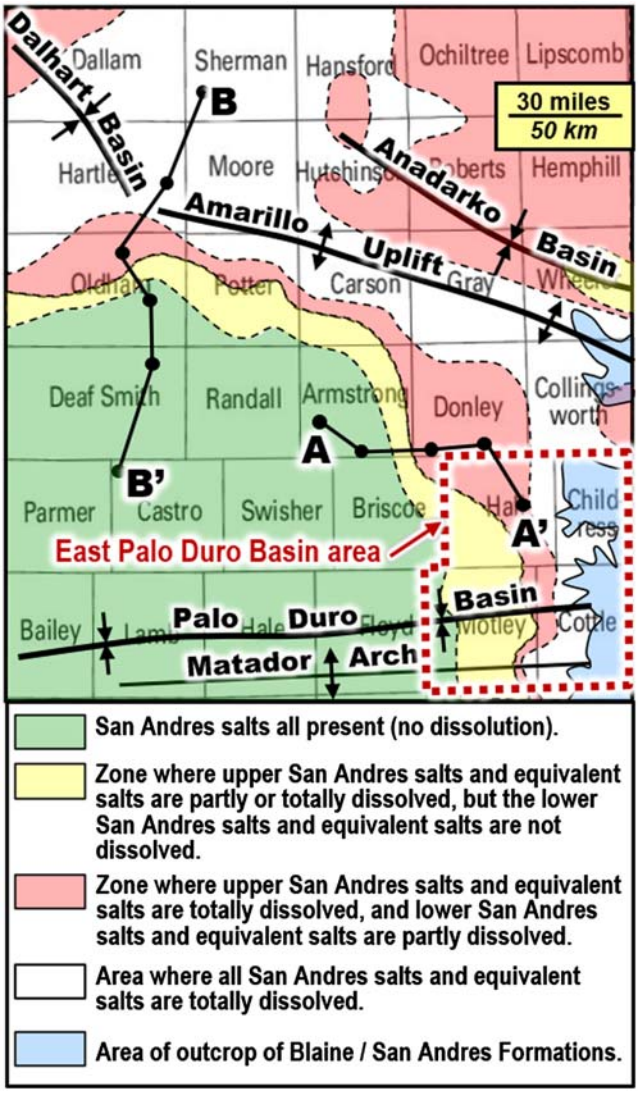

Figure 18. Map showing zones of salt dissolution in the lower and upper San Andres Formation in the Palo Duro and Dalhart Basins (Presley, 1981a), and in the equivalent Blaine Formation and associated strata in the Anadarko Basin (Jordan and Vosburg, 1963; Johnson, 1976). Salt beds of the San Andres Formation in the Palo Duro Basin are dissolved where they approach the eastern outcrops (A–A', Fig. 19), and where they go over the Amarillo Uplift to the north (B–B', Fig. 20). The "East Palo Duro Basin area" is shown in Figure 21.

(a westward extension of the Amarillo Uplift), and into the Dalhart Basin on the north. This cross section shows dissolution of the San Andres salts where they now would be about 300–400 m below the current land surface. However, salt dissolution here probably occurred during Ogallala deposition, in Tertiary time (Gustavson and others, 1980b; Gustavson and Finley, 1985; Gustavson, 1986a) when those salts were much closer to what was then the land surface—this paleodissolution probably occurred when the salt units were then at a depth of 200–300 m. Most of this salt dissolution occurred in Oldham County, with about 260 m of salt being removed between well #2 in Deaf Smith County and well #33 in Hartley County.

Gustavson and others (1980b) noted that the regional extent of salt dissolution in the northern Palo Duro Basin is also shown by a map drawn on the base of the Ogallala Formation, a heterogeneous sequence of 60–180 m of fluvial and windblown sands, silts, clays, and gravels deposited and reworked from streams that flowed eastward from the Rocky Mountains during Miocene–Pliocene times. Large, closed subsidence basins, up to about 300 km^2 and over 100 m deep, developed during sedimentation of the Ogallala above areas of San Andres salt dissolution, and this attests that dissolution of San Andres salts has spanned late Tertiary through Quaternary (and modern) times (Gustavson, 1986a). In fact, Gustavson (1986a) also pointed out that development and location of about 200 km of the length of the Canadian River Valley in New Mexico and the Texas Panhandle follows the path of an east-northeast-trending subsidence trough formed by dissolution of Permian salts on the north side of the Palo Duro Basin.

East Palo Duro Basin area

The east Palo Duro Basin area (Figs. 18, 21) embraces four Texas counties wherein salts in the Flowerpot, Blaine, and Dog Creek Formations are currently being dissolved to produce several major salt plains and salt springs. Salt dissolution in this area was first discussed by Johnson (1981), and then was more fully discussed by Richter and Kreitler (1986) and Johnson (2019a). Present-day distribution of these salt units is largely controlled by surface drainage and depth to the salt layers, with the salt beds being dissolved at depths less than about 150–240 m. However, I believe that, in the past, all parts of this four-county area were underlain by salt beds in one or more of the three salt-bearing units mentioned above.

Brine forms by ground water dissolving salt in the Flowerpot, Blaine, and Dog Creek Formations, and the brine then migrates laterally and upward through interconnected aquifers to the surface (Fig. 9). Joint systems, fault-flexure zones, sinkholes, cavities/caves, and collapse features are the probable pathways for major upward and lateral movement of brine. This process has been going on intermittently or continuously for a long time, perhaps several hundred thousand years, or longer, with brine being emitted at different sites in the area as the salt was being dissolved in various parts of the four-county area.

Field studies show that sinkholes are common in some areas where the "Blaine of Texas" and the Whitehorse Group crop out on the east and northeast side of the

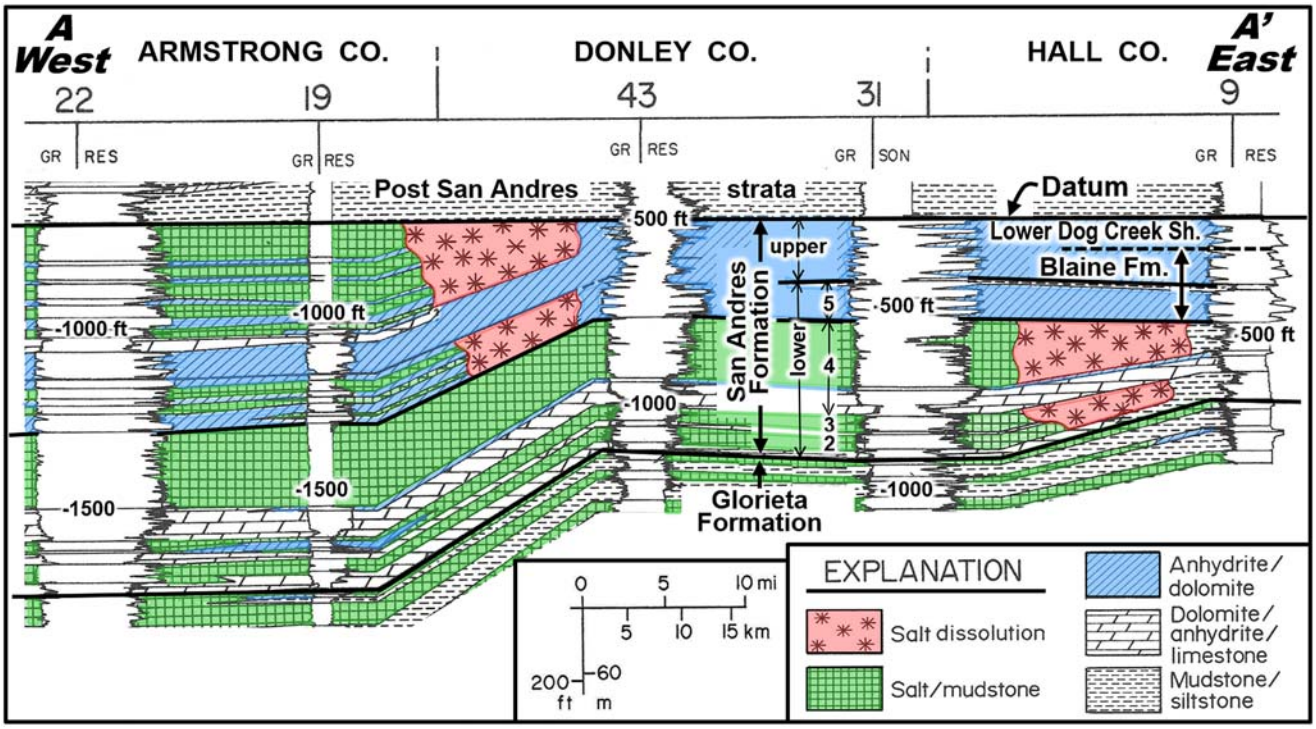

Figure 19. Regional stratigraphic cross section A–A' showing transition of part of the San Andres Formation to the Blaine Formation in the Palo Duro Basin (modified from Presley, 1981b); depths are in feet. Salt beds of the San Andres in the Palo Duro Basin are all dissolved where they approach the eastern outcrops in north-central Texas. Location of cross section shown in Figure 18.

Palo Duro Basin, and these can have an adverse impact on highways and other construction and cultural features in the area (Simpkins and others, 1981; Gustavson, 1986b). For example, Simpkins and others (1981) identified more than 400 sinkholes and undrained depressions on aerial photographs in Hall County alone: these sinkholes are up to 100 m wide and 15 m deep. In addition, they recognized 11 active fractures and faults that they associate with salt dissolution and collapse.

Gypsum Karst

An overview of processes and distribution of gypsum karst throughout the United States was given by Johnson (1996), but western Oklahoma and north-central Texas are among the best regions in the United States for the study of gypsum karst, including caves, sinkholes, springs, disappearing streams, and karst aquifers. The region containing gypsum outcrops of the Blaine Formation and the "Blaine of Texas" extends about 600 km north–south and as much as 200 km east–west (part of which is shown in Fig. 22). Karst features are best developed where the Blaine is mainly thick gypsum beds with thin shale interbeds. Early development of porosity in the Blaine occurs chiefly in dolomite beds and in the lower part of each overlying gypsum unit; locally, dolomite porosity is so extensive that the rock is honeycombed and has only a skeletal framework supporting the voids (Johnson, 2003a). Therefore, gypsum cavities are most common at and near the contact with underlying dolomites. In places, the cavities are developed along local joints, fractures, and bedding planes in the gypsum (Fig. 23A), but there are no known regional orientation patterns.

Examples of gypsum karst, caves, and local dissolution/collapse structures are given in Figure 23. Figure 23A shows the preferential early dissolution of gypsum along joints and bedding planes: such openings are enlarged because of further dissolution by through-flowing waters, and by abrasion, because of sand, gravel, and other materials being carried in the waters. Figure 23B indicates the size of some of the sinkholes that can lead into local caves and underground water courses. Figures 23C and 23D show collapse structures and tight folds that result from dissolution of salt and gypsum in the Blaine Formation and underlying strata in the shallow subsurface along Prairie Dog Town Fork Red River in Texas. Figures 23E and 23F are interior views of two caves in the Blaine Formation of southwestern Oklahoma.

Both gypsum and dolomite beds of the Blaine Formation are commonly karstic in outcrops and shallow subsurface of western Oklahoma and north-central Texas. Gypsum beds in the Blaine Formation typically are 3–9 m thick throughout the region. Dolomite beds in

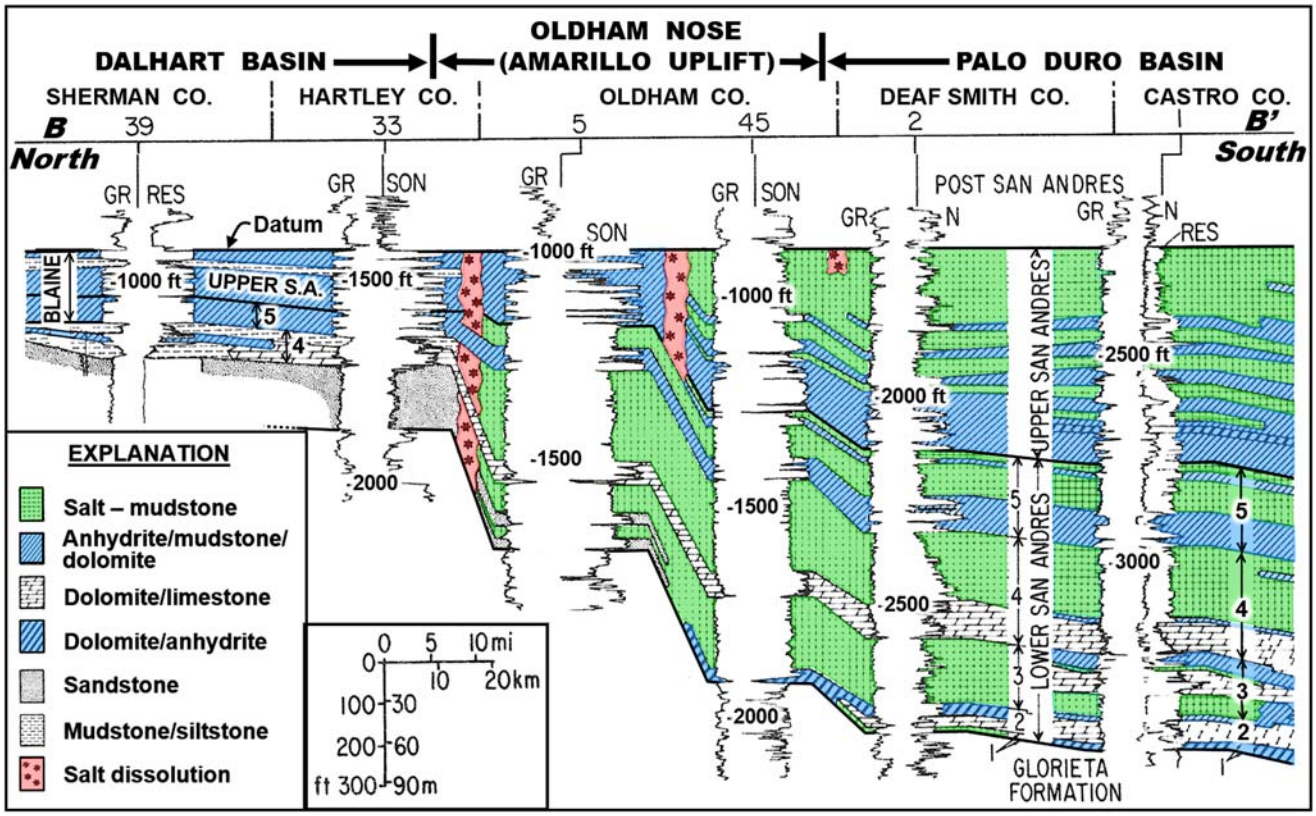

Figure 20. Regional stratigraphic cross section B–B' showing transition of the San Andres Formation in the Palo Duro Basin (right) to the Blaine Formation in the Dalhart Basin (modified from Presley, 1981a); depths are in feet. Salt beds of the San Andres in the deep Palo Duro Basin are all dissolved where they approach, and extend over, the Oldham Nose/Amarillo Uplift. Location of cross section shown in Figure 18.

the Blaine of western Oklahoma typically are less than 1 m thick, but locally reach 2 m: in Texas, they are typically 1–3 m thick, and locally are almost 5 m thick (Pendery, 1963; Jones, 1971). Most karst features in the Blaine Formation are developed in the gypsum beds, but in southwest Oklahoma and north-central Texas, the dolomite beds are also karstic and, along with the gypsum beds, are significant sources of irrigation water.

Below are examples of gypsum karst in the Blaine Formation, including: 1) development of caves; 2) aquifers; and 3) problems in siting of dams.

Gypsum Caves in Blaine Formation

Gypsum caves are widespread and quite common in the Blaine Formation of western Oklahoma and north-central Texas. Oklahoma has a total of 201 recorded caves in the Blaine (Table 1), with 152 in northwest Oklahoma and 49 in southwest Oklahoma. In just the Palo Duro Basin part of north-central Texas, the "Blaine of Texas" has a total of 106 recorded gypsum caves (Table 1); there are another 16 recorded gypsum caves farther south in King and Stonewall Counties, Texas (Johnson, 2018).

Discussions of gypsum caves in the Blaine of western Oklahoma are by Myers and others (1969), S. Bozeman (1987, 2002), Johnson (1989, 1990b, 2003a, 2011, 2018), Bozeman and Bozeman (2002), J. Bozeman (2003), Christenson and others (2003), Miller and others (2003), and Tarhule and others (2003). Most studies of gypsum caves in the Blaine Formation in Oklahoma have been carried out by members of the Central Oklahoma Grotto (COG), chiefly by members John and Sue Bozeman of Oklahoma City. The major outlet for COG research is in 21 volumes of *Oklahoma Underground*, a journal they publish intermittently (see "Publications/News" and then "Oklahoma Underground Publications" on their website: http://okcavers.com/). In addition, on the COG website is an interesting movie/slide show on "Western Oklahoma Gypsum Caves" that gives tours and discussions of several major caves, including Alabaster Caverns and D.C. Jester Cave.

Discussions of gypsum karst and caves in north-central Texas are by McGregor and others (1963), Reddell and Russell (1963), Galegar and DeGeer (1969), Brown (1987), Elliott and Veni (1994), and Johnson (2018). The Texas Speleological Association (TSA) is the major source of data on caves in Texas: *The Texas*

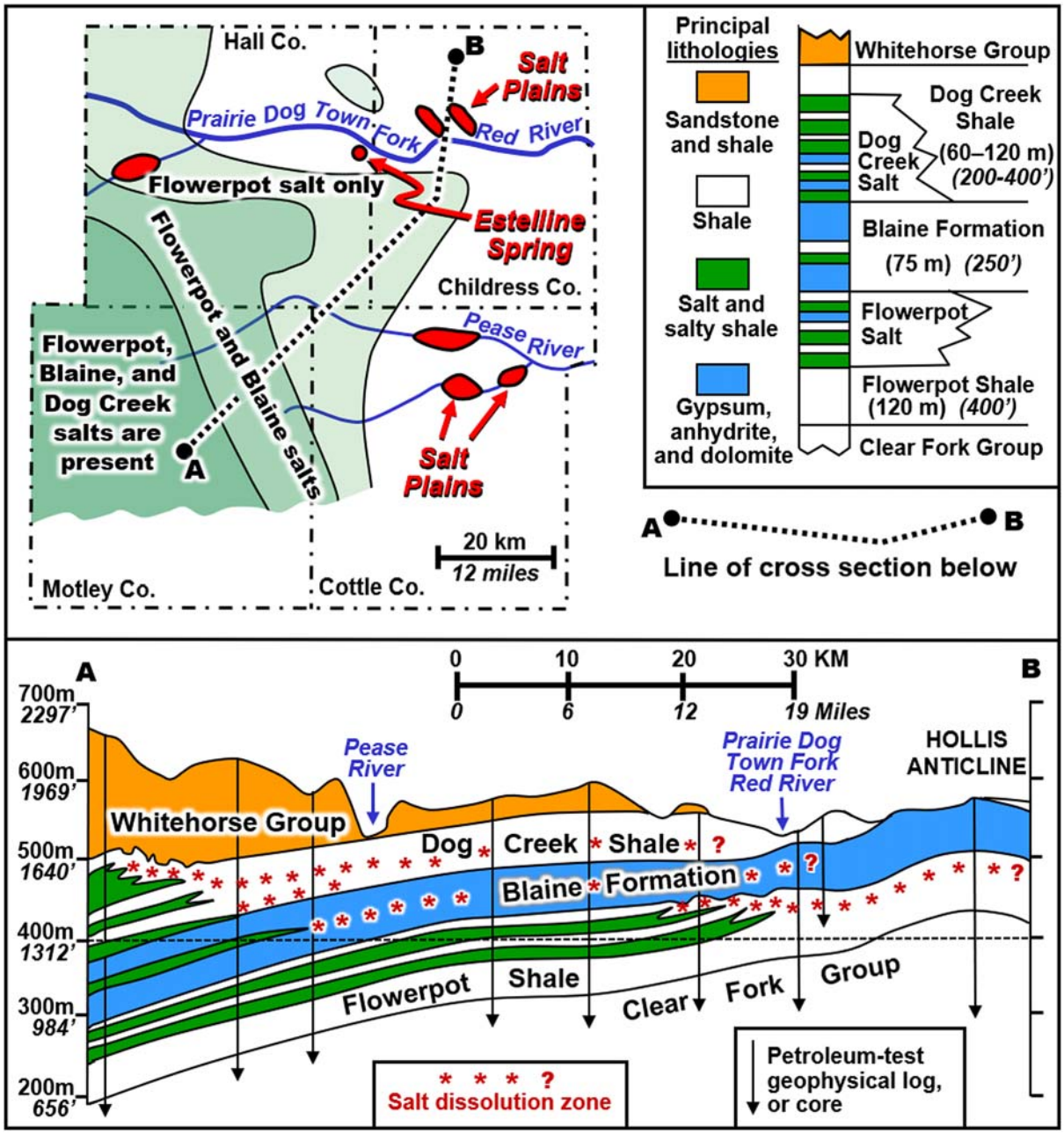

Figure 21. Generalized map, columnar section, and cross section showing evaporites and salt-dissolution zones in Blaine Formation and associated strata in East Palo Duro Basin area of north-central Texas (from Johnson, 2019a). Original lateral extent of each salt unit (and extent of dissolution zones) is uncertain. Location of East Palo Duro Basin area shown in Figure 18.

Caver is published quarterly by TSA, and copies are available online at: https://www.cavetexas.org/TSA/TC_Online/ Below are brief discussions of five caves in western Oklahoma and north-central Texas: Alabaster Caverns, Selman Cave, D.C. Jester Cave, Estelline Spring, and Walkup Cave (Fig. 22).

Alabaster Caverns. Alabaster Caverns State Park (Figs. 22, 24) hosts the best-known cave in Oklahoma or north-central Texas (Myers and others, 1969; Central Oklahoma Grotto, 1985; Johnson, 2011, 2018). This northwest Oklahoma cave is 1,873 m long: it is the 19th longest gypsum cave in the United States, and the 66th longest gypsum cave in the world (Table 2). Cavern development is almost wholly in the Medicine Lodge Gypsum Bed, and the cave has a maximum width of 18 m and a maximum height of 15 m.

The main passage consists of three sections, each of nearly equal length (Fig. 24): 1) a collapse section near the entrance; 2) a middle section with domes in

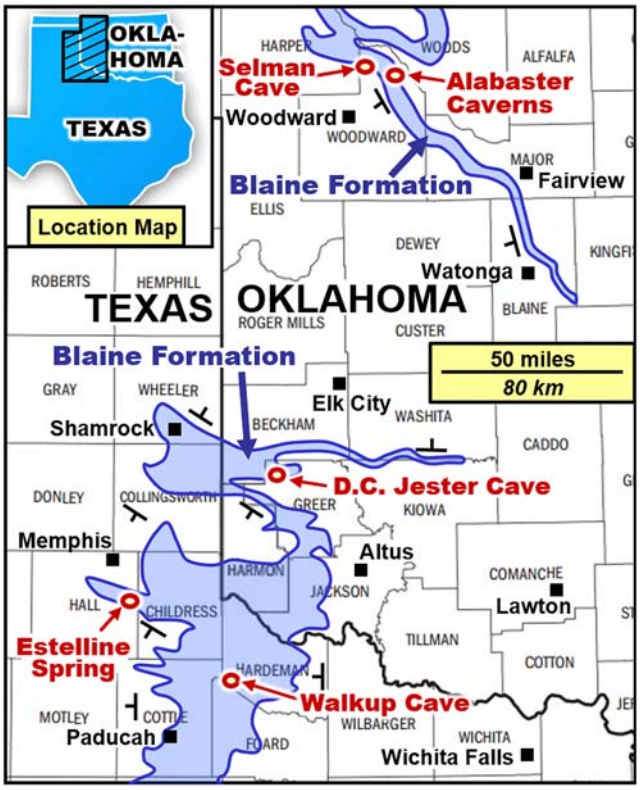

Figure 22. Map of western Oklahoma and north-central Texas showing outcrops of Blaine Formation, four gypsum caves and one spring described in this report, and general strike and dip of Blaine Formation (modified from Johnson, 2018).

the roof; and 3) a channel section at the end. The collapse section is characterized by large gypsum, shale, and selenite boulders that have fallen from the roof. At the beginning of this section, the Rotunda (the largest room in the cave) extends from the Flowerpot Shale, on the floor, all the way through the Medicine Lodge Gypsum, and ends at the base of the Nescatunga Gypsum Bed. In the middle section, the ceiling contains many domes, and at the land surface in this section is a cluster of sinkholes that funnel rainwater down into the cave. In the channel section, the roof, walls, and floor of the cave are smooth and well-polished, showing how abrasion by the underground stream helped form the cavern.

Selman Cave. The Selman Cave System (Fig. 22) became an outdoor living laboratory and field station in 1998 when about 130 ha (325 acres) of land was acquired, through donation and purchase, by the University of Central Oklahoma (UCO) to establish the Selman Living Laboratory (SLL). Located in northwest Oklahoma, about 16 km southwest of the town of Freedom, it has been used for UCO classes and research on ecology, mammalogy, ornithology, plant taxonomy, freshwater biology, entomology, mycology, and herpetology. The website for the SLL is: https://sites.uco.edu/cms/sll/

Geologic data on the Selman Cave System, summarized by Bozeman (2002, 2003), shows that cave development is nearly restricted to the thick Medicine Lodge and Nescatunga Gypsum Beds and the intervening shale. The main passageway consists of wide, high tunnels with a meandering stream underfoot. It contains a breakdown-boulder room 18 m tall, and several domes up to 12 m high, along with some passages that require stooping or crawling. With a length of 4,794 m (Table 2), it is the 19th longest gypsum cave in the world and the 3rd longest gypsum cave in the United States (after D.C. Jester Cave [below], and Parks' Ranch Cave in New Mexico); there are more than 25 separate entrances to the cave system.

D.C. Jester Cave. Jester Cave, located in Greer County, southwest Oklahoma (Figs. 22, 25, 26), is the longest gypsum cave in the United States, and also the 8th longest gypsum cave in the world (Table 2). The main passage is 2,413 m long, but its many known side passages are a total of 7,652 m long: thus, the total length of cave system is 10,065 m. This brief discussion is based largely on the comprehensive report by Bozeman (1987), and shorter reports on the geology by Johnson (1989, 1990b, 2003a, 2018).

Almost all parts of the main cave are formed in the 5-m-thick gypsum unit 1 of the Van Vacter Member (Figs. 23E, 25). Instead of the passages being mainly long and straight, they typically are angulate, with sharp bends and some broad, sweeping curves (Fig. 26). Many of the passages are elliptical in cross section, although they are quite variable. The main passage typically is 6–15 m wide and 1.5–6 m high; side passages typically are 1.5–3 m wide and 0.6–3 m high. The alignment of various segments of Jester Cave suggests the cave's flow may be controlled by several sets of joints or fractures; the main segments are oriented between N10ºW and N30ºW, with other cave segments oriented N60ºE, N30ºE, and N60ºW. Karst in the area is extensive, and there are more than 70 separate known entrances to Jester Cave.

Estelline Spring. Estelline Spring is a unique cave/sinkhole/spring: it is a major salt-water spring issuing from a sinkhole in the alluvium of Prairie Dog Town Fork Red River, about 1.6 km east of the town of Estelline, in north-central Texas (Figs. 21, 22, 27). The few published data on Estelline Spring are contained in Ward (1961), Galegar and DeGeer (1969), Gustavson and others (1982), and Johnson (2018). A special study of this sinkhole was carried out by the U.S. Army Corps of Engineers (USACE), because it was the source of high-salinity brine (a flow of 127 L/sec that released 450 metric tons of salt per day) that degraded the quality of water in the Red River system farther downstream (Galegar and DeGeer, 1969).

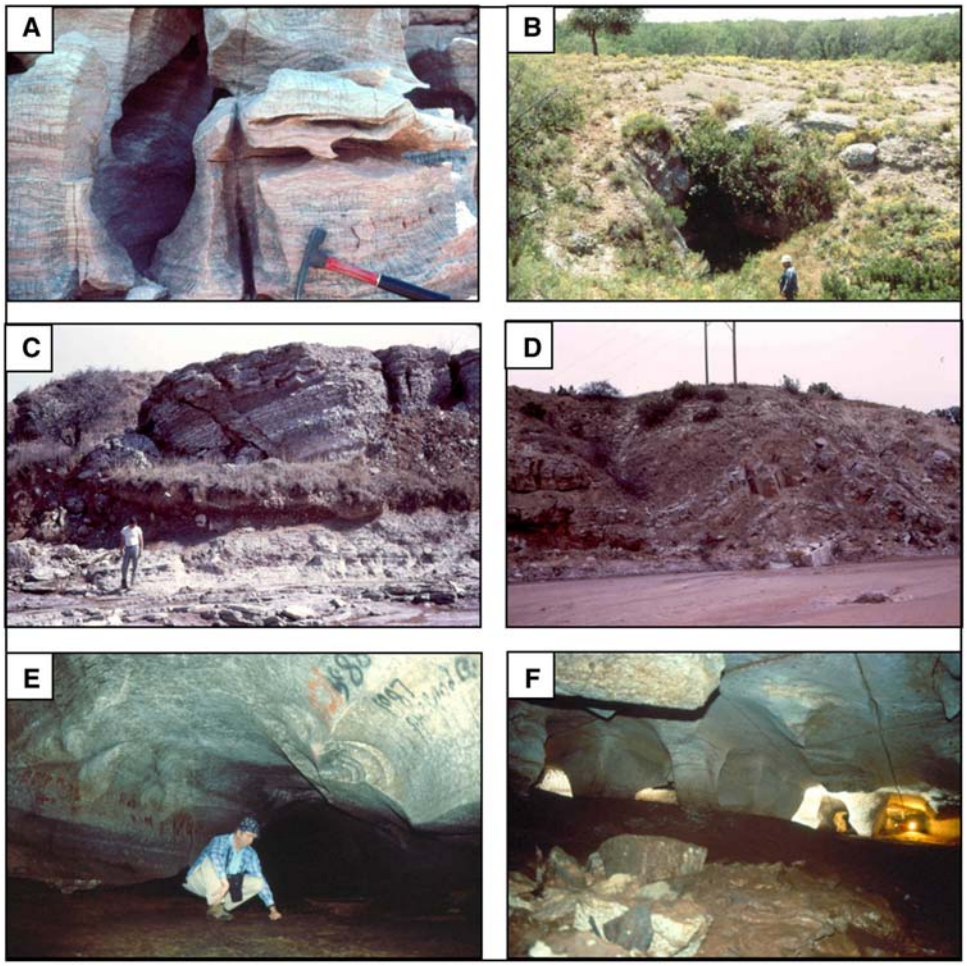

Figure 23. Gypsum karst, sinkholes, and caves in western Oklahoma and north-central Texas (from Johnson, 2018). A) Karst in Cloud Chief Gypsum (Late Guadalupian) in western Oklahoma, with dissolution most pronounced along joints (vertical here) and bedding planes (horizontal here). B) Gypsum sinkhole in Blaine Formation, southwest Oklahoma. C & D) Dissolution of salt and gypsum causes collapse block (C) and tight fold (D) in Blaine Formation along Prairie Dog Town Fork Red River, Texas. E) Interior of D.C. Jester Cave in unit 1 of the Blaine Formation, Greer County, Oklahoma. F) Interior of Cascade Spring Cave, Blaine Formation, in Greer County, Oklahoma. Photos A through D by the author; E and F by John and Sue Bozeman.

TABLE 1.—Number of recorded gypsum caves in Blaine Formation of western Oklahoma and north-central Texas. Oklahoma data provided by Sue and John Bozeman, Central Oklahoma Grotto, Oklahoma City, in July, 2015; Texas data from Texas Speleological Survey (2019 [list updated November 22, 2016]).

OKLAHOMA		TEXAS	
Beckham	6	Childress	38
Blaine	14	Collingsworth	30
Greer	38	Cottle	20
Harmon	5	Foard	0
Major	58	Hall	1
Woods	15	Hardeman	14
Woodward	65	Wheeler	3
TOTAL	201	TOTAL	106

SCUBA divers determined the shape, depth, and volume of the brine-filled cavity (Fig. 27). The cavity is about 11,038 m^3, and they measured the cavity to a depth of 38 m, where they reached a small, unpassable opening about 0.6 by 0.9 m wide; beyond this point, the cavity extends to an unknown size and depth (Galegar and DeGeer, 1969). Based upon my own studies of the local geology around Estelline Spring, carried out on behalf of the USACE, I believe that the two dolomite units in the cavity (Fig. 27) are the Hollis Dolomite (below) and the Guthrie Dolomite (above).

To stop the flow of brine from Estelline Spring, the USACE built an impervious, circular dike around the spring in 1963. The dike, 104 m in diameter and 3 m high, completely suppressed flow from the spring when water within the dike rose and imposed a head

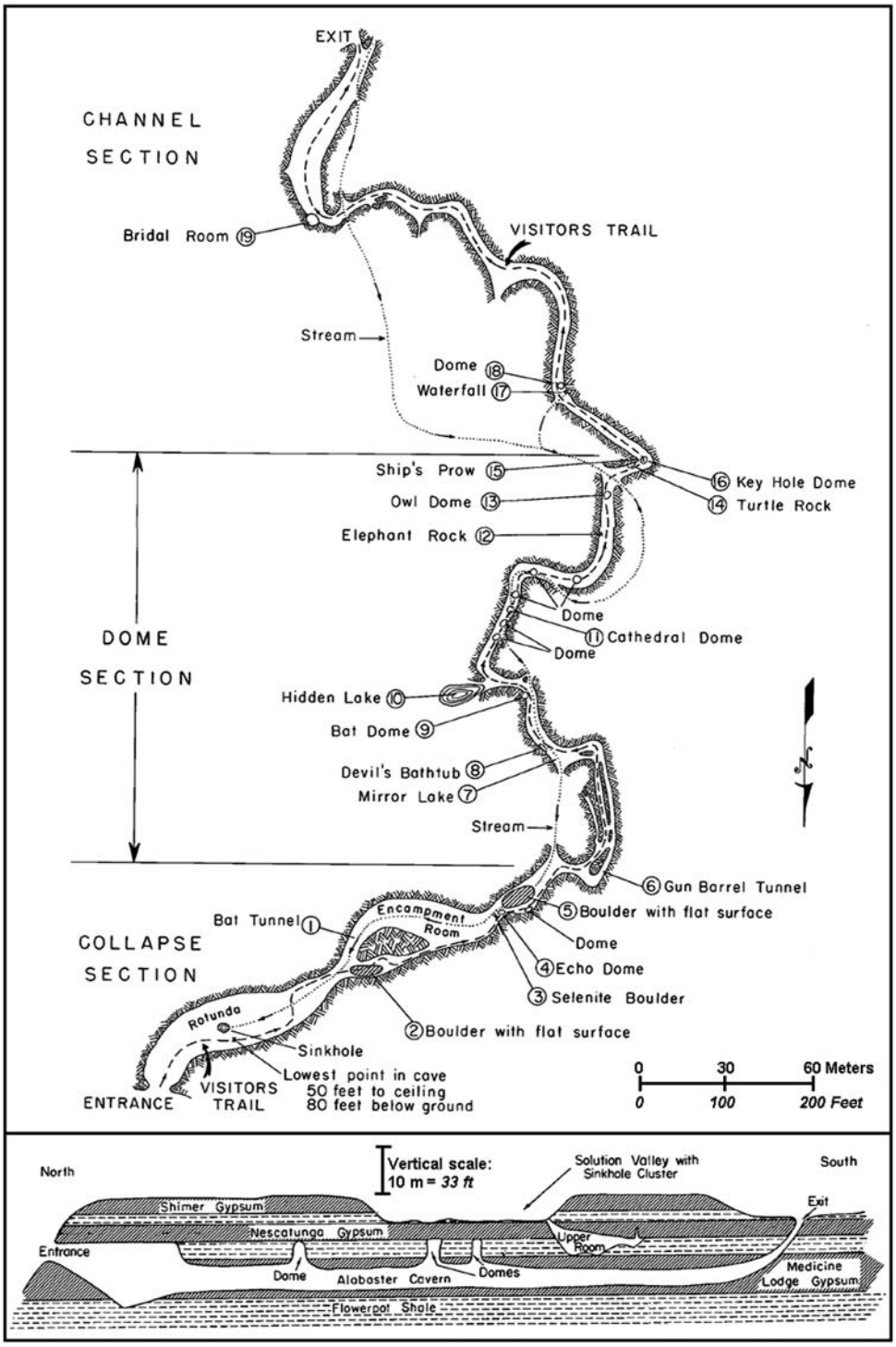

Figure 24. Alabaster Caverns map (above) and cross section (below), in Woodward County, Oklahoma (Myers and others, 1969). Main cave is developed in the thick Medicine Lodge Gypsum Bed of the Blaine Formation. On map, note that north is oriented toward the bottom.

of 1.7 m above local ground level (Galegar and DeGeer, 1969). Although the flow of brine from Estelline Spring was stopped by the dike, the highly karstic nature of the local bedrock, and the high permeability of the overlying alluvium, undoubtedly must allow at least some of the brine to exit the main cavity and seep to the surface elsewhere in the vicinity.

Walkup Cave. Walkup Cave, with a length of 1,188 m, is the third longest gypsum cave in north-central

Texas, and the 93rd longest gypsum cave in the world (Table 2). Good sources of information about Walkup Cave are Reddell and Russell (1963), Brown (1987), and Elliott and Jorden (*in* Elliott and Veni, 1994, p. 211–212); these are summarized by Johnson (2018). Location of the cave is shown in Figure 22, and a map of the cave is shown in Figure 28.

TABLE 2.—Gypsum caves in the Blaine Formation of western Oklahoma and north-central Texas that are among the longest caves in the world (from Bob Gulden, www.caverbob.com "world [sic] longest gypsum caves" compiled July 01, 2019).

#	CAVE NAME	STATE	COUNTY	LENGTH MILES	LENGTH METERS
8	D.C. Jester Cave ★	OK	Greer	6.254	10,065
19	Selman Cave ★	OK	Woodward	2.979	4,794
39	Horseshoe Valley Cave	OK	Greer	1.715	2,760
51	Nescatunga Cave	OK	Major	1.490	2,398
52	Bingham Cave	OK	Woodward	1.478	2,379
63	Sculpture Cave	OK	Major	1.194	1,922
66	Alabaster Caverns ★	OK	Woodward	1.164	1,873
69	West Clutch Cave	TX	Childress	1.111	1,788
71	Pearl Cave	OK	Woodward	1.097	1,765
75	Widow Cave	OK	Major	1.052	1,693
83	Pothooks Cave	TX	Childress	0.938	1,510
93	Walkup Cave ★	TX	Hardeman	0.738	1,188
100	Conical Sink Cave	TX	Childress	0.664	1,069
113	Root Cellar Cave	TX	Childress	0.397	639
119	Upper Hinton Creek Cave	TX	Collingsworth	0.336	541
129	Collapse Cave	TX	Cottle	0.227	365
133	Little Crystal Cave	TX	Hardeman	0.202	325
136	Big Mouth Cave	TX	Wheeler	0.186	299

= rank in length among gypsum caves in the world, as of July 1, 2019.
★ = cave discussed in current report.

Walkup Cave captures water from a stream to the north, and funnels it to the south, through the cave system, and into the Pease River. Water entering the Main Entrance travels about 110 m and reaches Division Room (or "Decision" Room), where the passage divides: the right branch is a small crawlway leading to a large sink with multiple entrances, beyond which there are two short caves—Boulder Passage and Short Cave; the left (main) branch from Division Room starts out as a passage that is 3–3.5 m wide and 2–3 m high, and it continues as a fairly open system for the next several hundred meters. Near the south end of the cave, it makes a complex loop that crosses under itself (lower left part of Fig. 28); the loop, about 90 m long, forms the Big Room, with the lower part of the loop being about 4 m below the upper.

Blaine Aquifer in Southwest Oklahoma and North-Central Texas

Karstic conditions in the Blaine Formation make it an aquifer in parts of southwest Oklahoma and north-central Texas. Because of the high total dissolved solids (TDS) in the water, it is unacceptable as drinking water, but is extensively used for irrigation. Discussions of the Blaine aquifer in parts of Harmon, Jackson, and Greer Counties of southwest Oklahoma are by Schoff (1948), Steele and Barclay (1965), Johnson (1990b, 2003a, 2019b), Runkle and McLean (1995), Runkle and others (1997), and Osborn and Eckenstein (1997). In southwest Oklahoma, the Blaine is largely flushed of its salt (NaCl) content, and it provides irrigation water for cotton, wheat, and other crops that can tolerate a moderate-to-high calcium-sulfate ($CaSO_4$) content.

Water in the Blaine aquifer in southwest Oklahoma has a TDS generally ranging from 1,500 to 6,000 mg/L,

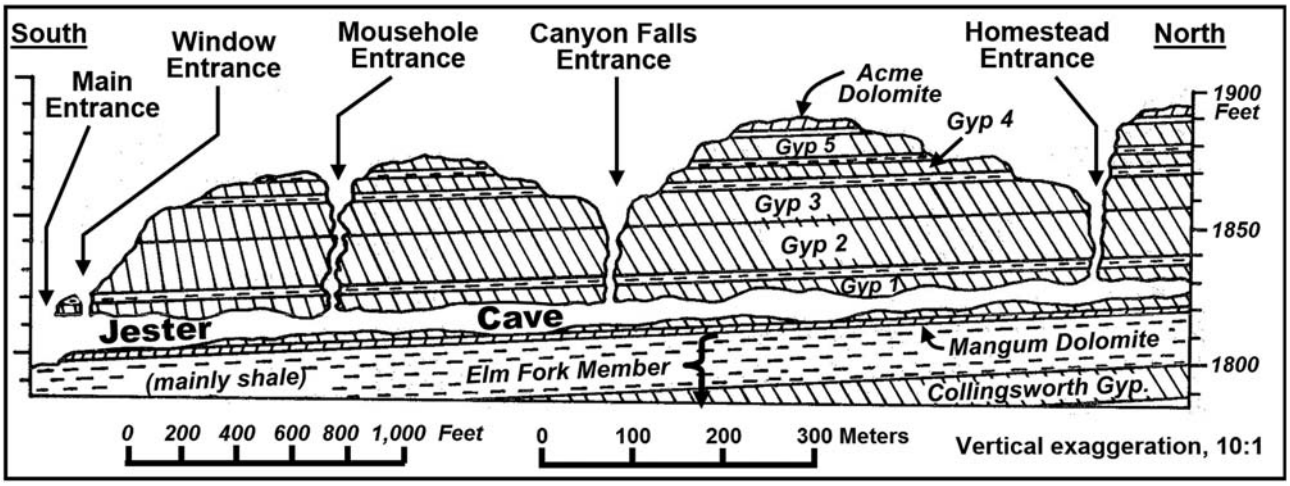

Figure 25. D.C. Jester Cave, Greer County, Oklahoma. Schematic cross section shows that cave is developed in gypsum bed 1 of the Van Vacter Member of the Blaine Formation (after Bozeman, 1987; Johnson, 1990b).

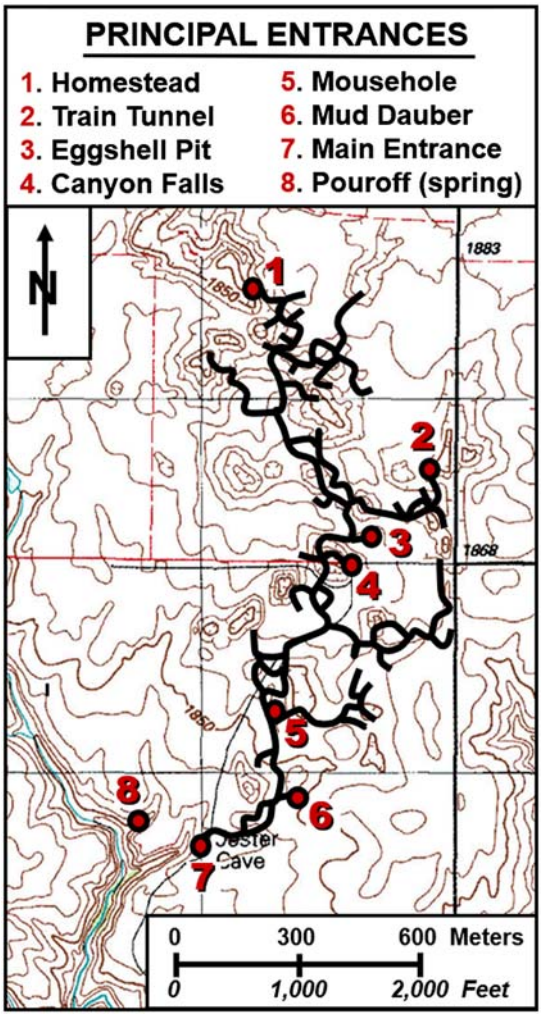

Figure 26. D.C. Jester Cave, Greer County, Oklahoma. Simplified map shows surveyed passages and main entrances (after Bozeman, 1987; Johnson, 1990b).

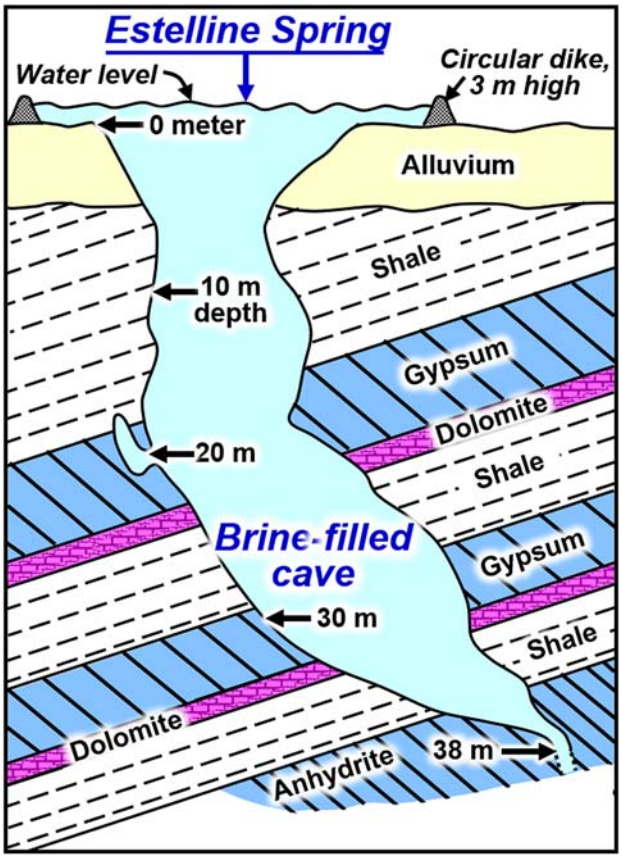

Figure 27. Cross section of brine-filled cave beneath Estelline Spring, Hall County, Texas: based upon divers using SCUBA gear (after Galegar and DeGeer, 1969). At depth of 38 m, cave diameter is less than 1 m; total depth unknown.

and averaging about 3,100 mg/L (Johnson, 2019b), and only at a few places are chloride concentrations high enough to damage crops. Permeability in the aquifer is attained by extensive dissolution and porosity in some of the dolomite beds, as well as cavernous conditions in some of the gypsum beds. Irrigation wells, in an area of about 2,500 km^2, typically are 15–100 m deep and commonly yield 1,000–8,000 L/min. Because of the importance of this aquifer in the area, a recharge-demonstration project was carried out to show the feasibility and effectiveness of recharging the Blaine aquifer with surface runoff (Osborn and Eckenstein, 1997). Recharge was accomplished by intercepting surface runoff and channeling that water, by gravity flow, down wells or sinkholes, and into cavities in the aquifer.

The Blaine aquifer in north-central Texas has been described by Runkle and McLean (1995), Runkle and others (1997), and Hopkins and Muller (2011). Because salt is still present in the Blaine Formation and associated strata in parts of this area (Fig. 21), the produced groundwater is suitable mainly for salt-tolerant crops, livestock, and selected industrial use: the salt content of waters in the Blaine is discussed by Richter and Kreitler (1986). TDS exceeds drinking-water standards in 97% of samples tested by Hopkins and Muller (2011), and the median TDS concentration of all samples is 2,835 mg/L. Although the median TDS here is lower than in southwest Oklahoma, the relatively higher salt content means that this water is generally classified as slightly saline: the salt content is the main factor limiting use of the water. Karstic conditions exist in the "Blaine of Texas" all the way from Wheeler County on the north to Fisher County on the south (Hopkins and Muller, 2011), a distance of about 120 km. However, almost all the water pumped from the Blaine aquifer in north-central Texas (about 98%) comes from wells in only four counties in the northern part of the aquifer: Childress, Collingsworth, Hardeman, and Cottle Counties (see Fig. 22 for location of two of these counties).

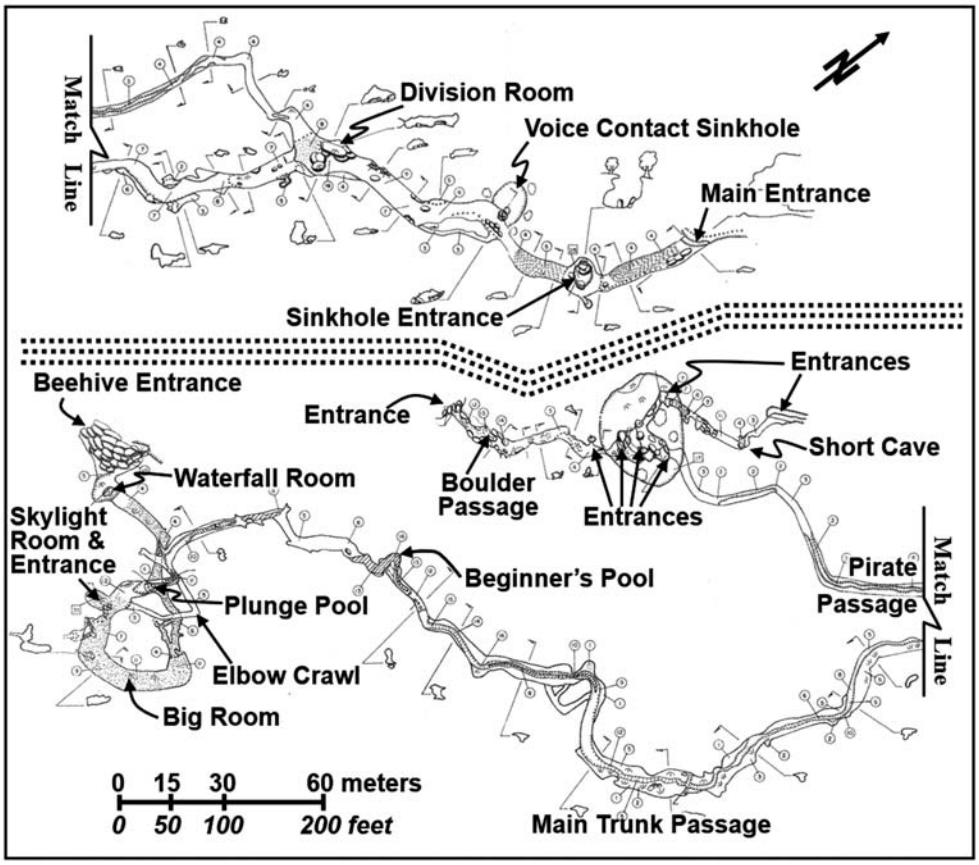

Figure 28. Walkup Cave, Hardeman County, Texas, showing floor plan (after Texas Speleological Survey, unpublished data).

Gypsum-Karst Problems in Siting of Upper Mangum Dam

Engineering-geology assessment of the initially proposed Upper Mangum Damsite in an area of gypsum karst in the Blaine Formation in Greer County, southwest Oklahoma, showed that the site is unsuitable and should be abandoned (Johnson, 2003b, 2008). This damsite, about 14 km west of Mangum on the Salt Fork Red River (Fig. 29), had been investigated and evaluated by the U.S. Bureau of Reclamation since 1937, in hopes of providing water for irrigation, flood control, and recreation. The Blaine Formation here is about 60 m of gypsum, with thin interbeds of dolomite and shale: nearby outcrops show abundant karst features, such as caves, sinkholes (Fig. 23B), disappearing streams, and springs. Extensive karst features in the area should have terminated the project early on, but the topography was so attractive along this stretch of Salt Fork Red River: both proposed abutments are high and form a narrow water gap between them, and thus, the size (length) of the dam would be quite small. In all early studies, it was realized that karstic foundation conditions were marginal, at best, but it was always hoped that an engineering solution could be found to resolve these problems.

In the early 1990s, the U.S. Army Corps of Engineers, Oklahoma Water Resources Board, and citizens of Mangum launched a final investigation. In 1999, I was asked to evaluate the geologic/karst data, based on all previous data and the results of coring and pressure testing of five new boreholes (each 40–60 m deep) drilled along the proposed dam alignment in 1995 and 1999 (Fig. 29). This final assessment (Johnson, 2003b) showed that open cavities, clay-filled cavities, and other karst features are abundant in and near the abutments, and that fluid losses (in each 3-m interval that was pressure tested) ranged from 60 to 250 L/min in most tests, and in one borehole the losses were 1,600–5,300 L/min. The final borehole, BH-1-99, was drilled in the stream valley: it encountered cavities and vugs in each of each of the gypsum and dolomite beds, and the drill rig lost circulation from a depth of 7.5 m to the bottom of the hole—indicating the presence of one or several cavities that could accept a large amount of water. BH-1-99 then drilled into a 0.6-m-high cavity at the top of the Flowerpot salt, and, at a depth of 39 m, entered an artesian zone that caused salt water to flow up through the borehole to the land surface (Johnson, 2003b).

As a result of this final set of studies, it was recommended to abandon the Upper Mangum Damsite, and

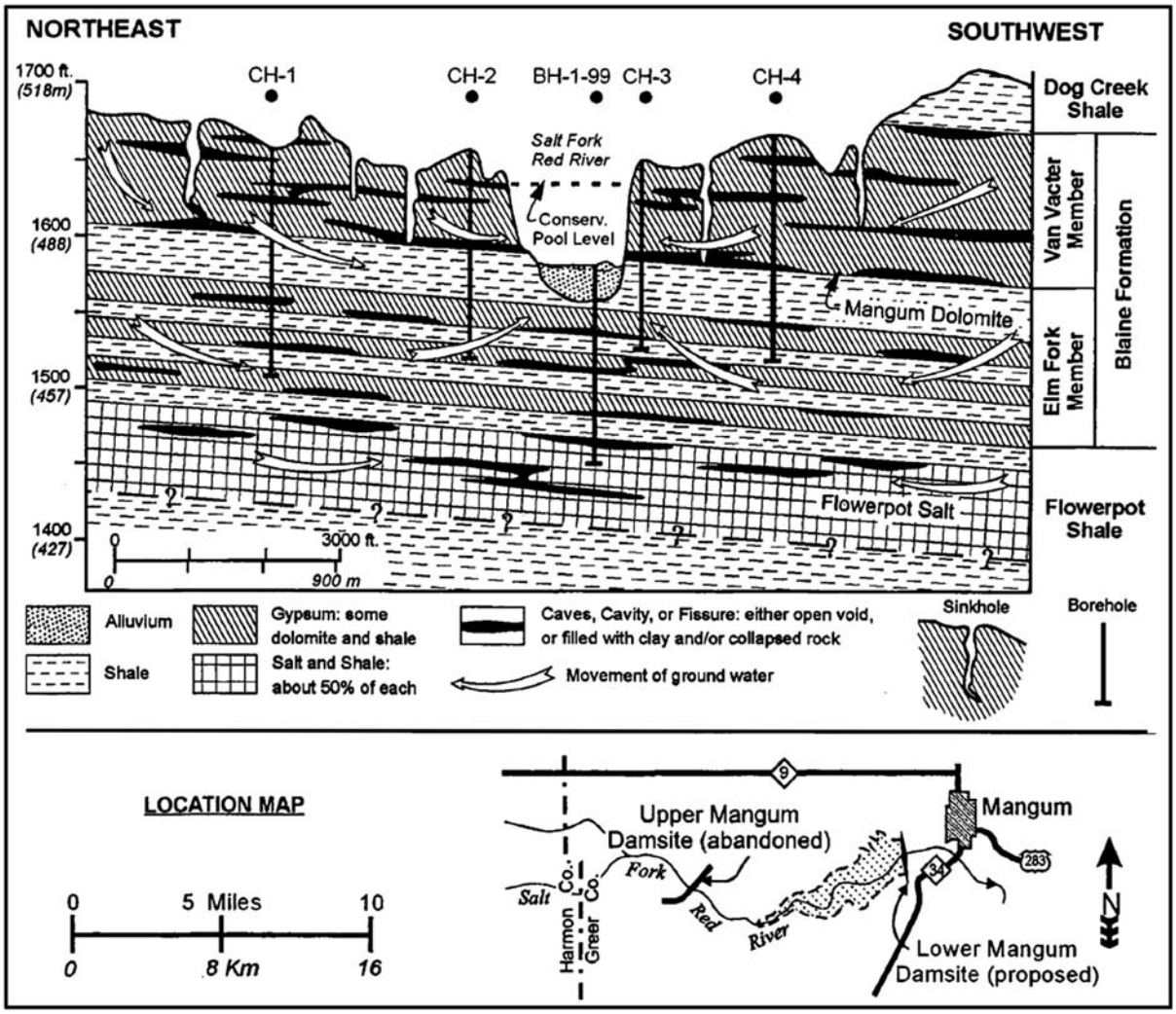

Figure 29. Schematic cross section along alignment of proposed Upper Mangum Dam, looking downstream (Johnson, 2003b). Although the topography was favorable at the site, extensive karst features (interpretive caves, cavities, fissures, and sinkholes shown here) in gypsum, dolomite, and salt led to its abandonment.

seek a more suitable site farther east on Salt Fork Red River, where bedrock for the dam and the impoundment area would be completed in the underlying Flowerpot Shale (Johnson, 2003c). The newly proposed Lower Mangum Damsite is just 3 km southwest of Mangum: it is outside of the area of gypsum karst in the Blaine Formation, and is beyond (east of) the dissolution limits of the Flowerpot salt.

REFERENCES CITED

Becker, C.M., 1930, Structure and stratigraphy of southwestern Oklahoma: American Association of Petroleum Geologists, Bulletin, Vol. 14, p.47-55.

Bozeman, J., 2003, Exploration of western Oklahoma gypsum caves, *in* K.S. Johnson and J.T. Neal, eds., Evaporite karst and engineering/environmental problems in the United States: Oklahoma Geological Survey Circular 109, p. 57-64. http://ogs.ou.edu/docs/circulars/C109.pdf

Bozeman, S. (ed.), 1987, The D.C. Jester Cave System: Central Oklahoma Grotto, Oklahoma City, Oklahoma Underground, Vol. 14, 56 p.

Bozeman, S. (ed.), 2002, The Selman Cave System: Central Oklahoma Grotto, Oklahoma City, Oklahoma, Oklahoma Underground, Vol. 20, 44 p.

Bozeman, J, and Bozeman, S., 2002, Speleology of gypsum caves in Oklahoma: Carbonates and Evaporites, Vol. 17, No. 2, p. 107-113.

Brown, K., 1987. Walkup Cave revisited. The Texas Caver, Vol. 32, No. 4, p. 76-79, 85. http://www.karstportal.org/FileStorage/Texas_Caver/1987-v32-n04.pdf

Brown, O.E., 1937, Unconformity at base of Whitehorse formation, Oklahoma: American Association of Petroleum Geologists, Bulletin, Vol. 21, p.1534-1553.

Central Oklahoma Grotto, 1985, The Caves of Alabaster Caverns State Park: Central Oklahoma Grotto, Oklahoma City, Oklahoma Underground, Vol. 12, 23 p.

Christenson, S, Hayes, C., Hancock, E., and McLean, J., 2003, Correlating the location of a cave passage in gypsum karst to a highway right-of-way using a cave radio: *in* K.S. Johnson and J.T. Neal, eds., Evaporite karst and engineering/environmental problems in the United States: Oklahoma Geological Survey Circular 109, p. 65-70. http://ogs.ou.edu/docs/circulars/C109.pdf

Collins, E.W., 1984, Styles of deformation in Permian Strata, Texas Panhandle: The University of Texas at Austin, Bureau of Economic Geology, Geological Circular 84–4, 32 p.

Elliott, W.R., and Veni, G., *eds.*, 1994, The Caves and Karst of Texas: A Guidebook for the 1994 Convention of the National Speleological Society with Emphasis on the South-Western Edwards Plateau: Huntsville, Alabama, National Speleological Society, 342 p.

Fay, R.O., 1964, The Blaine and related formations of northwestern Oklahoma and southern Kansas: Oklahoma Geological Survey, Bulletin 98, 238 p. http://ogs.ou.edu/docs/bulletins/B98.pdf

Fay, R.O., 2010, Preliminary geologic map of the Foss Reservoir 30' X 60' quadrangle, Beckham, Custer, Dewey, Ellis, and Roger Mills Counties, Oklahoma: Oklahoma Geological Survey, Oklahoma Geological Quadrangle Map OGQ–78A. Scale 1:100,000. http://ogs.ou.edu/docs/OGQ/OGQ-78A-color.pdf

Fay, R.O.; Ham, W.E.; Bado, J.T.; and Jordan, L., 1962, Geology and mineral resources of Blaine County, Oklahoma: Oklahoma Geological Survey, Bulletin 89, 252 p. http://ogs.ou.edu/docs/bulletins/B89.pdf

Fracasso, M.A., and Hovorka, S.D., 1986, Cyclicity in the Middle Permian San Andres Formation, Palo Duro Basin, Texas Panhandle: The University of Texas at Austin, Bureau of Economic Geology, Report of Investigations No. 156, 48 p.

Galegar, W.C., and DeGeer, M.W., 1969, Measuring subsurface spring flow with radiotracers: Proceedings of the American Society of Civil Engineers, Vol.95, No. SA6, p. 1097-1103.

Goldstein, A.G., and Collins, 1984, Deformation of Permian strata overlying a zone of salt dissolution and collapse in the Texas Panhandle: Geology, Vol. 12, No. 5, p. 314-317.

Gould, C.N., 1902, General geology of Oklahoma: Oklahoma Department of Geology and Natural History, Biennial Report No. 2, p. 17–74

Gould, C.N., 1905, Geology and water resources of Oklahoma: U.S. Geological Survey, Water Supply Paper 148, p. 39–71.

Gould, C.N., 1924, A new classification of the Permian redbeds of southwestern Oklahoma: American Association of Petroleum Geologists, Bulletin, Vol. 8, p. 322-341.

Gustavson, T.C., 1979, Salt dissolution, *in* Dutton, A.P., and others, 1979, Geology and geohydrology of the Palo Duro Basin, Texas Panhandle: The University of Texas at Austin, Bureau of Economic Geology, Geological Circular 79–3, p. 87-93.

Gustavson, T.C., 1980, Rates of salt dissolution, *in* Gustavson, T.C., and others, 1980, Geology and geohydrology of the Palo Duro Basin, Texas Panhandle: The University of Texas at Austin, Bureau of Economic Geology, Geological Circular 80–7, p. 71–75.

Gustavson, T.C., 1982, Structural control of major drainage elements surrounding the Southern High Plains, *in* Gustavson, T.C., and others, 1982, Geology and geohydrology of the Palo Duro Basin, Texas Panhandle: The University of Texas at Austin, Bureau of Economic Geology, Geological Circular 82–7, p. 176–182.

Gustavson, T.C., 1986a, Geomorphic development of the Canadian River Valley, Texas Panhandle: an example of regional salt dissolution and subsidence: Geological Society of America, Bulletin, Vol. 97, p. 459-472.

Gustavson, T.C., ed., 1986b, Geomorphology and Quaternary stratigraphy of the Rolling Plains, Texas Panhandle: The University of Texas at Austin, Bureau of Economic Geology, Guidebook 22, 97p.

Gustavson, T.C., and Finley, R.J., 1985, Late Cenozoic geomorphic evolution of the Texas Panhandle and northeast New Mexico—Case studies of structural controls on regional drainage development: The University of Texas at Austin, Bureau of Economic Geology, Report of Investigations No. 148, 42 p.

Gustavson, T.C., Finley, R.J., and Baumgardner, R.W., Jr., 1980a, Preliminary rates of slope retreat and salt dissolution along the eastern Caprock Escarpment of the Southern High Plains and in the Canadian River Valley, *in* Gustavson, T.C., and others, 1980, Geology and geohydrology of the Palo Duro Basin, Texas Panhandle: The University of Texas at Austin, Bureau of Economic Geology, Geological Circular 80–7, p. 76-82.

Gustavson, T.C., Finley, R.J., and McGillis, K.A., 1980b, Regional dissolution of Permian salt in the Anadarko, Dalhart, and Palo Duro Basins of the Texas Panhandle: The University of Texas at Austin, Bureau of Economic Geology, Report of Investigations No. 106, 40 p.

Gustavson, T.C., Simpkins, W.W., Alhades, A., and Hoadley, A., 1982, Evaporite dissolution and

development of karst features on the Rolling Plains of the Texas Panhandle: Earth Surface Processes and Landforms, Vol. 7, p. 545-563.

Hentz, T.F., and Brown, L.F., Jr., 1987, Geologic atlas of Texas, Wichita Falls–Lawton sheet: The University of Texas at Austin, Bureau of Economic Geology, scale 1:250,000.

Hopkins, J., and Muller, C., 2011, Water quality in the Blaine Aquifer: Texas Water Development Board, Report 376, 40 p. http://www.twdb.texas.gov/publications/reports/numbered_reports/doc/R376_Blaine.pdf

Hovorka, S.D., 1990, Sedimentary processes controlling halite deposition, Permian Basin, Texas: unpublished Ph.D. Dissertation, The University of Texas at Austin, 393 p.

Hovorka, S.D., and Granger, P.A., 1988, Subsurface to surface correlation of Permian evaporites—San Andres–Blaine–Flowerpot relationships, Texas Panhandle, *in* W.A. Morgan and J. A. Babcock, eds., Permian rocks of the Midcontinent: Midcontinent SEPM, Special Publication No. 1, p. 137-159.

Johnson, K.S., 1963, Salt in the El Reno Group (Permian), Elk City area, Beckham and Washita Counties, Oklahoma: University of Oklahoma, Biennial Geological Symposium, 8th, Proceedings, p. 79–92. https://www.researchgate.net/publication/306374740

Johnson, K.S., 1967, Stratigraphy of the Permian Blaine Formation and associated strata in southwestern Oklahoma: unpublished Ph.D. Dissertation, University of Illinois, 247 p.

Johnson, K.S., 1976, Evaluation of Permian salt deposits in the Texas Panhandle and western Oklahoma for underground storage of radioactive wastes: unpublished report submitted to Union Carbide Corporation, Oak Ridge National Laboratories, Office of Waste Isolation, Y/OWI/Sub–4494/1, 73 p. Also available from: Oklahoma Geological Survey, Open-File Report 19–2018. http://www.ou.edu/content/dam/ogs/documents/data/OF19-2018.pdf

Johnson, K.S., 1981, Dissolution of salt on the east flank of the Permian Basin in the southwestern U.S.A.: Journal of Hydrology, Vol. 54, p. 75-93. https://www.researchgate.net/publication/245098253

Johnson, K.S., 1989, Geology of Jester Cave: NSS News, National Speleological Society, Huntsville, AL, Vol. 47, No. 1, p. 11-17. https://www.researchgate.net/publication/307970029

Johnson, K.S., 1990a, Standard outcrop section of the Blaine Formation and associated strata in southwestern Oklahoma: Oklahoma Geological Survey, Oklahoma Geology Notes, Vol. 50, p. 144-168. http://www.ogs.ou.edu/pubsscanned/NOTES/GN-V50N5.pdf

Johnson, K.S., 1990b, Hydrogeology and karst of the Blaine gypsum–dolomite aquifer, Southwestern Oklahoma: Oklahoma Geological Survey Special Publication 90–5, 31 p. http://ogs.ou.edu/docs/specialpublications/SP90-5.pdf

Johnson, K.S., 1996, Gypsum karst in the United States: International Journal of Speleology, Vol. 25, No. 3–4, p. 183-193. file:///C:/Users/ksjoh/Downloads/GypsumkarstintheUnitedStates.pdf

Johnson, K.S., 2003a, Evaporite karst in the Permian Blaine Formation and associated strata of western Oklahoma, *in* K.S. Johnson and J.T. Neal, eds., Evaporite karst and engineering/environmental problems in the United States: Oklahoma Geological Survey, Circular 109, p. 41-55. http://ogs.ou.edu/docs/circulars/C109.pdf

Johnson, K.S., 2003b, Gypsum karst and abandonment of the Upper Mangum Damsite in southwestern Oklahoma, *in* K.S. Johnson and J.T. Neal, eds., Evaporite karst and engineering/environmental problems in the United States: Oklahoma Geological Survey Circular 109, p. 85-94. http://ogs.ou.edu/docs/circulars/C109.pdf

Johnson, K.S., 2003c, Gypsum karst as a major factor in the design of the proposed Lower Mangum Dam in southwestern Oklahoma, *in* K.S. Johnson and J.T. Neal, eds., Evaporite karst and engineering/environmental problems in the United States: Oklahoma Geological Survey Circular 109, p. 95-111. http://ogs.ou.edu/docs/circulars/C109.pdf

Johnson, K.S., 2008, Gypsum-karst problems in constructing dams in the USA: Environmental Geology, Vol. 53, No. 5, p. 945-950. https://www.researchgate.net/publication/226513928

Johnson, K.S., 2011, Alabaster Caverns State Park: Oklahoma City Geological Society, Shale Shaker, Vol. 62, No. 2, p. 108-112. https://www.researchgate.net/publication/306373810

Johnson, K.S., 2013, Salt karst and collapse structures in the Anadarko Basin of Oklahoma and Texas, *in* L. Land, D.H. Doctor, and J.B. Stephenson, eds., Sinkholes and the engineering and environmental impacts of karst–Proceedings of the thirteenth multidisciplinary conference, Carlsbad, NM, May 6 through 10, 2013: National Cave and Karst Research Institute, Carlsbad, NM, p. 103-112. http://scholarcommons.usf.edu/cgi/viewcontent.cgi?article=1118&context=sinkhole_2013

Johnson, K.S., 2017, Evaporite karst and collapse breccia in Permian strata, Canton Lake Dam, Blaine County, Oklahoma: Oklahoma Geological Survey, Oklahoma Geology Notes, Vol. 76, No. 3, p. 5-18. http://ogs.ou.edu/docs/geologynotes/GN-V76N3.pdf

Johnson, K.S., 2018, Gypsum caves of north Texas and western Oklahoma, *in* Stafford, K.W., and Veni, G., eds., Hypogene karst of Texas: Texas Speleological Survey, Monograph 3, p. 111-122. https://www.texasspeleologicalsurvey.org/PDF/Hypogene_Karst_of_Texas.pdf

Johnson, K.S., 2019a, Salt in Permian Flowerpot, Blaine, and Dog Creek Formations is dissolved to create salt plains in Childress, Hall, Cottle, and Motley Counties, Texas, and northern Harmon County, Oklahoma: Oklahoma Geological Survey, Open-File Report OF1–2019, 34 p. http://www.ou.edu/content/dam/ogs/documents/data/OF1-2019.pdf

Johnson, K.S., 2019b, Blaine aquifer in the Hollis Basin of southwest Oklahoma: structure-contour map and stratigraphic/hydrologic data: Oklahoma Geological Survey, Geologic Map GM-45, scale 1:125,000. http://ou.edu/content/dam/ogs/documents/GMs/GM-45%20map.pdf

Johnson, K.S., 2019c, Geology of salt plains on the Cimarron River in northwest Oklahoma: Big Salt Plain, Little Salt Plain, Salt Creek Canyon, and Okeene Salt Plain: Oklahoma Geological Survey, Open-File Report OF2–2019, 50 p. http://www.ou.edu/content/dam/ogs/documents/data/OF2-2019.pdf

Johnson, K.S., 2019d, Geologic studies, natural-brine emissions, and hourglass-selenite crystals at Great Salt Plains on Salt Fork Arkansas River, Northwest Oklahoma: Oklahoma Geological Survey, Open-File Report OF3–2019, 29 p. http://www.ou.edu/content/dam/ogs/documents/data/OF3-2019.pdf

Johnson, K.S., 2021, Overview of evaporite karst in the Greater Permian Evaporite Basin (GPEB) of TX, NM, OK, KS, and CO, *in* Johnson, K.S., Land, L.A., and Decker, D.D., eds., Evaporite karst in the Greater Permian Evaporite Basin (GPEB) of Texas, New Mexico, Oklahoma, Kansas, and Colorado: Oklahoma Geological Survey, Circular 113.

Johnson, K.S., and Gonzales, S., 1978, Salt deposits in the United States and regional characteristics important for storage of radioactive waste: prepared for Union Carbide Corp., Nuclear Division, Oak Ridge National Laboratory, Office of Waste Isolation, Y/OWI/SUB-7414/1, 188 p. Also available from: Oklahoma Geological Survey, Open-File Report 18–2018. http://www.ou.edu/content/dam/ogs/documents/data/OF18-2018.pdf

Johnson, K.S., Stanley, T.M., and Miller, G.W., 2003, Geologic map of the Elk City 30' X 60' quadrangle, Beckham, Custer, Greer, Harmon, Kiowa, Roger Mills, and Washita Counties, Oklahoma: Oklahoma Geological Survey, Oklahoma Geological Quadrangle Map OGQ–44. Scale 1:100,000. http://ogs.ou.edu/docs/OGQ/OGQ-44-color.pdf

Jones, J.O., 1971, The Blaine Formation of North Texas: unpublished Ph.D. Dissertation, University of Iowa, 173 p.

Jordan, L, 1959, Underground storage in salt, Elk City Field: Oklahoma Geological Survey, Oklahoma Geology Notes, Vol. 19, No. 2, p. 32-34. http://ogs.ou.edu/docs/geologynotes/GN-V19N2.pdf

Jordan, L.; and Vosburg, D.L., 1963, Permian salt and associated evaporites in the Anadarko Basin of the western Oklahoma–Texas Panhandle region: Oklahoma Geological Survey, Bulletin 102, 76 p. http://ogs.ou.edu/docs/bulletins/B102.pdf

Looney, J., 2011, The history of Oklahoma caves: American Spelean History Association, The Journal of Spelean History, Vol. 45, No. 1, p. 10-25. http://caves.org/section/asha/issues/139.pdf

McGookey, D.A., Gustavson, T.C., and Hoadley, A.D., 1988, Regional structural cross sections, mid-Permian to Quaternary strata, Texas Panhandle and eastern New Mexico: Distribution of evaporites and areas of evaporite dissolution and collapse: The University of Texas at Austin, Bureau of Economic Geology, Cross Sections, CS0008, 17 p., 12 cross sections.

Martinez, J.D., Johnson, K.S., and Neal, J.T. 1998, Sinkholes in evaporite rocks: American Scientist, Vol. 86, No. 1 (January–February), p. 38-51. https://www.researchgate.net/publication/250968543

McGowen, J.H., 1981, Depositional sequences and associated sedimentary diagenetic facies: an ongoing investigation of salt-bearing core, Swisher County, Texas, in Gustavson, T.C., and others, 1981, Geology and geohydrology of the Palo Duro Basin, Texas Panhandle: The University of Texas at Austin, Bureau of Economic Geology, Geological Circular 81–3, p. 90-92 and plate 1.

McGregor, D.R., Pendery, E.C., and McGregor, D.L., 1963, Solution caves in gypsum, north-central Texas: Journal of Geology, Vol. 71, p. 108-115.

Miller, G., Dewers, T., and Tarhule, A., 2003, Laser positioning and three-dimensional digital mapping of gypsum karst, western Oklahoma: *in* K.S. Johnson and J.T. Neal, eds., Evaporite karst and engineering/environmental problems in the United States: Oklahoma Geological Survey Circular 109, p. 71-75. http://ogs.ou.edu/docs/circulars/C109.pdf

Moussavi-Harami, R., 1977, Areal geology of Cordell area, central Washita County, Oklahoma: unpublished MS Thesis, University of Oklahoma, 76 p.

Myers, A.J., Gibson, A.M., Glass, B.P., and Patrick, C.R., 1969, Guide to Alabaster Cavern and Woodward County, Oklahoma: Oklahoma Geological Survey, Guidebook 15, 38 p. http://ogs.ou.edu/docs/guidebooks/GB15.pdf

Osborn, N.I., and Eckenstein, E., 1997, Blaine gypsum groundwater recharge demonstration project data report: Oklahoma Water Resources Board, Technical Report 97–4, 308 p. https://www.owrb.ok.gov/studies/reports/reports_pdf/tr97_4_blaine_gypsum.pdf

Pendery, E.C., III, 1963, Stratigraphy of Blaine Formation (Permian), north-central Texas: American Association of Petroleum Geologists, Bulletin, Vol. 47, No. 10, p. 1828-1839.

Pitt, W.D., and Scott, G.L., 1981, Porosity zones of lower part of San Andres Formation, east-central New Mexico: New Mexico Bureau of Geology and Mineral Resources, Circular 179, 19 p. https://geoinfo.nmt.edu/publications/monographs/circulars/downloads/179/Circular-179.pdf

Presley, M.W., 1980, Upper Permian salt-bearing stratigraphic units, in Gustavson, T.C., and others, 1980, Geology and geohydrology of the Palo Duro Basin, Texas Panhandle: The University of Texas at Austin, Bureau of Economic Geology, Geological Circular 80–7, p. 12-23.

Presley, M.W., 1981a, San Andres salt stratigraphy and salt purity, *in* Gustavson, T.C., and others, 1981, Geol-ogy and geohydrology of the Palo Duro Basin, Texas Panhandle: The University of Texas at Austin, Bureau of Economic Geology, Geological Circular 81–3, p. 33-40.

Presley, M.W., 1981b, Middle and Upper Permian salt-bearing strata of the Texas Panhandle: lithologic and facies cross sections: The University of Texas at Austin, Bureau of Economic Geology, Cross Sections, CS0003, 10 p., 7 cross sections.

Presley, M.W., 1987, Evolution of Permian evaporite basin in Texas Panhandle: American Association of Petroleum Geologists, Bulletin, Vol. 71, No. 2, p. 167-190.

Ramondetta, P.J., 1982, Facies and stratigraphy of the Sn Andres Formation, northern and northwestern shelves of the Midland Basin, Texas and New Mexico: The University of Texas at Austin, Bureau of Economic Geology, Report of Investigations No. 128, 56 p.

Reddell, J.R., and Russell, W.H., 1963, The caves of northwest Texas: Texas Speleological Survey, Vol. 1, No. 8, 56 p. http://www.texasspeleologicalsurvey.org/PDF/TSS_Volume1/TSS%201(8)%20compressed.pdf

Richardson, J.L., 1970, Areal geology of western Washita County, Oklahoma: unpublished MS Thesis, University of Oklahoma, 67 p.

Richter, B.C., and Kreitler, C.W., 1986, Geochemistry of salt-spring and shallow subsurface brines in the Rolling Plains of Texas and southwestern Oklahoma: The University of Texas at Austin, Bureau of Economic Geology, Report of Investigations No. 155, 47 p.

Roth, R., 1945, Permian Pease River Group of Texas: Geological Society of America, Bulletin, Vol. 56, p. 893-908.

Runkle, D.L., Bergman, D.L., and Fabian, R.S., 1997, Hydrologic data for the Blaine aquifer and associated units in southwestern Oklahoma and northwestern Texas: U.S. Geological Survey, Open-File Report 97–50, 213 p. https://pubs.usgs.gov/of/1997/0050/report.pdf

Runkle, D.L., and McLean, J.S., 1995, Steady-state simulation of ground-water flow in the Blaine aquifer, southwestern Oklahoma and northwestern Texas: U.S. Geological Survey, Open-File Report 94–387, 92 p. https://pubs.usgs.gov/of/1994/0387/report.pdf

Sawyer, R.W., 1924, Areal geology of a part of southwestern Oklahoma: American Association of Petroleum Geologists, Bulletin, Vol. 8, p. 312-321.

Schoff, S.L., 1948, Ground-water irrigation in the Duke area, Jackson and Greer Counties, Oklahoma: Oklahoma Geological Survey, Mineral Report 18, 10 p. http://ogs.ou.edu/docs/mineralreports/MR18.pdf

Scott, G.L., Jr., and Ham, W.E., 1957, Geology and gypsum resources of the Carter area Oklahoma: Oklahoma Geological Survey, Circular 42, 64 p. http://ogs.ou.edu/docs/circulars/C42.pdf and http://ogs.ou.edu/docs/circulars/C42PII.pdf

Simpkins, W.W., Gustavson, T.C., Alhades, A.B., and Hoadley, A.D., 1981, Impact of evaporite dissolution and collapse on highways and other cultural features in the Texas Panhandle and eastern New Mexico: The University of Texas at Austin, Bureau of Economic Geology, Geological Circular 81–4, 23 p.

Smith, A.H., 1964, Areal geology of Elk City area, Beckham and Roger Mills Counties, Oklahoma: unpublished MS Thesis, University of Oklahoma, 64 p.

Stanley, T.M., 2002, Geologic map of the Woodward 30' X 60' quadrangle, Ellis, Dewey, Roger Mills, and Woodward Counties, Oklahoma: Oklahoma Geological Survey, Oklahoma Geological Quadrangle Map OGQ–40. Scale 1:100,000. http://ogs.ou.edu/docs/OGQ/OGQ-40-color.pdf

Steele C.E., and Barclay, J.E., 1965, Ground-water resources of Harmon County and adjacent parts of Greer and Jackson Counties, Oklahoma: Oklahoma Water Resources Board, Bulletin 29, 96 p.

Suneson, N.H., 2012, Custer County oysters: Oklahoma City Geological Society, Shale Shaker Vol. 62, No. 6, p. 422-429. https://www.yumpu.com/en/document/read/11973193-

Tarhule, A., Dewers, T., Young, R., Witten, A., and Halihan, T., 2003, Integrated subsurface-imaging

techniques of detection cavities in the gypsum karst of Oklahoma: *in* K.S. Johnson and J.T. Neal, eds., Evaporite karst and engineering/environmental problems in the United States: Oklahoma Geological Survey Circular 109, p. 77-84. http://ogs.ou.edu/docs/circulars/C109.pdf

Texas Speleological Survey, 2019, Texas County Karst Totals: Texas Speleological Survey website. https://www.texasspeleologicalsurvey.org/deeplong/countytotals.php

Ward, P.E., 1961, Geology and ground-water features of salt springs, seeps, and plains in the Arkansas and Red River basins of western Oklahoma and adjacent parts of Kansas and Texas: U.S. Geological Survey, Open-File Report 63–132, 94 p. https://pubs.er.usgs.gov/publication/ofr63132

Zabawa, P.J., 1976. Investigation of surficial structural geology of portions of Beckham, Custer, Roger Mills, and Washita Counties, Oklahoma: unpublished MS Thesis, University of Oklahoma, 98 p.

Delhi Sinkhole and Watonga Sinkhole Caused by Gypsum Karst in the Permian Blaine Formation of Western Oklahoma

Kenneth S. Johnson
Retired Geologist, Oklahoma Geological Survey, Norman, Oklahoma

ABSTRACT.—Two notable sinkholes have formed in the past 63 yr because of gypsum karst in the Permian Blaine Formation of western Oklahoma. The Delhi Sinkhole, located in Beckham County, southwest Oklahoma, formed in 2011: it was originally 12 m wide and 12 m deep and eventually reached a diameter of 18 m. The Watonga Sinkhole, located in Blaine County, northwest Oklahoma, formed in 1957: it reached a diameter of 14 m and a depth of 5.2 m. Both sinkholes formed in open fields where about 15 to 30 m of Quaternary terrace deposits and dune sands overlie the gypsum beds. The Blaine Formation consists of multiple gypsum beds, about 3 to 6 m thick, interbedded with shale beds, 1–10 m thick, and thin dolomites. Total thickness of the formation is about 60 m in the southwest part of the State and about 30 m in the northwest.

INTRODUCTION

Permian gypsum crops out extensively in western Oklahoma, and locally, the gypsum contains sinkholes, caves, disappearing streams, and other typical karst features. The most extensive of these gypsum outcrops are in the Blaine Formation, which is widespread in both the southwest and northwest parts of the State (Fig. 1). Although karst features are common in outcrops of the Blaine Formation, historic development of sinkholes is rare: when sinkholes do form, it causes concern for local citizens, and can even garner regional and state-wide interest. The current paper describes two gypsum-karst sinkholes that formed in the Blaine Formation of western Oklahoma: 1) the Delhi Sinkhole, which formed in 2011 near the town of Delhi, in Beckham County, southwest Oklahoma; and 2) the Watonga Sinkhole (formerly the "Foley sink"), which formed in 1957 near the town of Watonga, in Blaine County, northwest Oklahoma (Fig. 1). These surface sinks reached 18 and 15 m wide, respectively, and fortunately, they both formed in plowed farmland, so there were no deaths, injuries, or loss of infrastructure.

The Blaine Formation consists of a series of white gypsum beds, commonly 3–6m thick, interbedded with redbed shales and siltstones that typically are 1–10 m thick; each of the gypsum beds is commonly underlain by a dolomite bed that is 1 cm to more than 1 m thick (Fig. 2). Total thickness of the Blaine Formation in

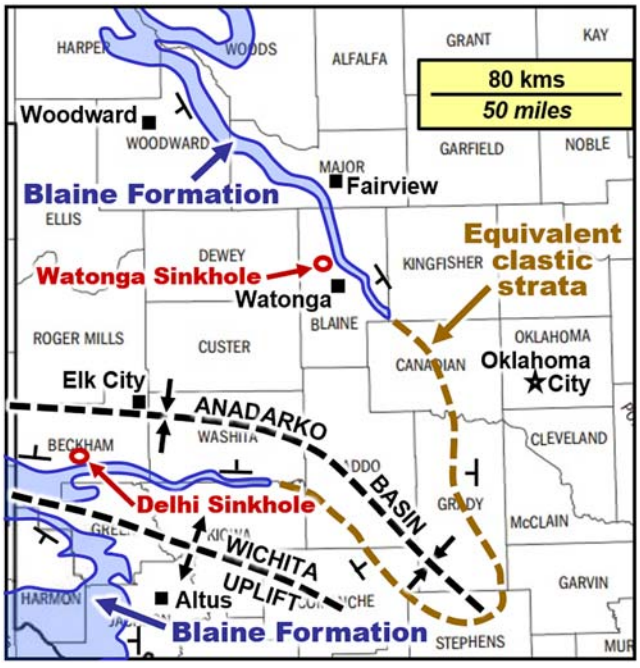

Figure 1. Map of western Oklahoma showing: 1) location of Delhi and Watonga Sinkholes, 2) outcrops of thick gypsum beds in the Blaine Formation, 3) outcrops of clastic strata equivalent to the Blaine Formation, 4) axis of Anadarko Basin in outcropping Permian strata, and 5) axis of Wichita Uplift.

Johnson, Kenneth S., 2021, Delhi Sinkhole and Watonga Sinkhole Caused by Gypsum Karst in the Permian Blaine Formation of Western Oklahoma, *in* Johnson, K. S.; Land, Lewis; and Decker, D. D. (eds.), Evaporite Karst in the Greater Permian Evaporite Basin (GPEB) of Texas, New Mexico, Oklahoma, Kansas, and Colorado: Oklahoma Geological Survey, Circular 113, p. 279–284.

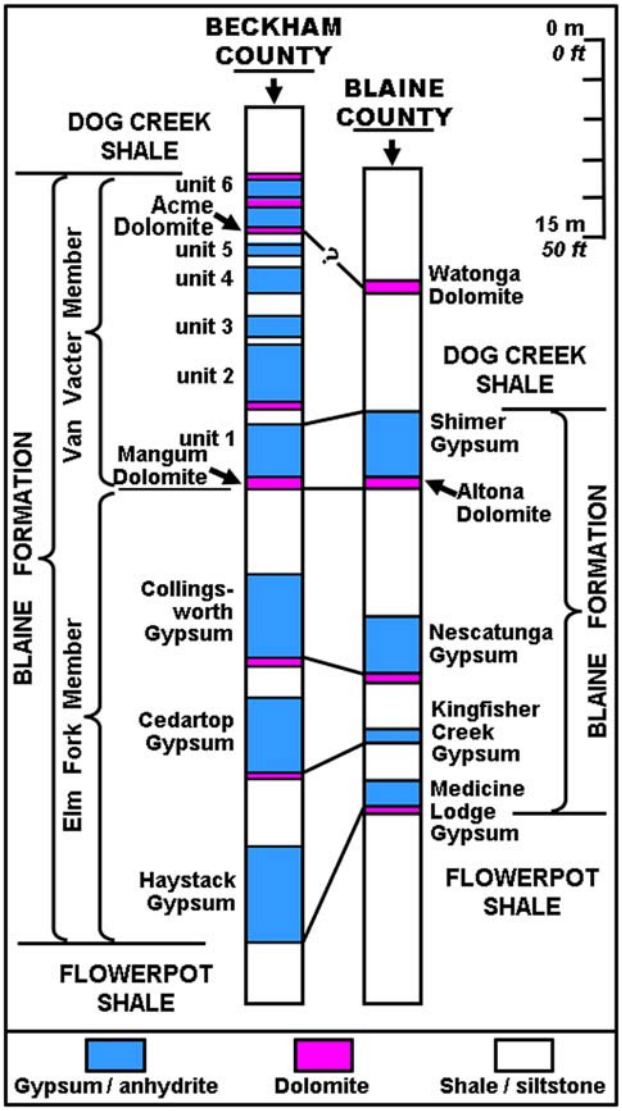

Figure 2. Geologic columns showing stratigraphy and correlation of gypsum beds of Blaine Formation in Beckham and Blaine Counties, Oklahoma (modified from Johnson, 2021b). Stratigraphic datum is Mangum and Altona Dolomites. Gypsum units 2 through 6 in Beckham County grade laterally into the Dog Creek Shale between Beckham and Blaine Counties.

outcrops is about 60 m in southwest Oklahoma and about 30 m in northwest Oklahoma. Nomenclature for the individual gypsum and dolomite beds of the Blaine differs in southwest and northwest Oklahoma, because they were originally thought to be two different formations: it was not until the early 1920s that it was realized that they were outcrops of the same formation on the north and south flanks of the then-newly recognized Anadarko Basin, but the dual nomenclature for beds in the Blaine Formation was retained (summarized in Johnson, 2021b). All gypsum beds in the upper part of the Van Vacter Member of southwest Oklahoma grade laterally into shales in the subsurface of the Anadarko Basin, and these shales comprise the lower part of the Dog Creek Shale on the north flank of the basin.

Appreciation is expressed to TGS, the Houston-based company with the largest online well-log database, for permission to access their files of geophysical logs of petroleum tests in the area north of Delhi. Data obtained from those logs aided me in establishing the character and distribution of the Blaine and Flowerpot Formations in that area. An earlier report by Johnson (2003b) describes gypsum karst in the Blaine Formation throughout western Oklahoma, and recent overviews of gypsum caves in the Blaine Formation of western Oklahoma are presented by Bozeman (2003) and Johnson (2018).

DELHI SINKHOLE, BECKHAM COUNTY, SOUTHWEST OKLAHOMA

The Delhi Sinkhole formed on, or just before, Novem-ber 16, 2011, in a cultivated field about 1.8 km north of the small community of Delhi, in south-central Beckham County (Figs. 3, 4). Larger towns in the area are Sayre, about 12 km north of the sink, and Erick, about 17 km to the west. The location of the sink is 185 m north and 23 m east of the SW corner of sec. 6, T. 8 N., R. 23 W. (35°11'29.99" N, 99°40'36.74" W). At the time the sink formed, it was referred to as the "Sayre Sink" in some of the press releases. The Delhi Sinkhole was originally 12 m wide and 12 m deep, but by October, 2012, it had expanded to a diameter of about 15 m (Fig. 3B): by early in 2020, it reached about 18 m wide and the sides had partly caved in, thus, partially filling the sinkhole.

Formation of the Delhi Sinkhole undoubtedly is caused by dissolution of gypsum beds in the upper part of Blaine Formation (in the Van Vacter Member) (Fig. 5). Unfortunately, there are no borehole records available at or near the sink, so the precise depth and size of the underground gypsum cavity are unknown. At the sinkhole, the Blaine Formation is mantled by an unknown thickness (probably about 15 to 20 m) of Quaternary terrace deposits and dune sands, so it is impossible to determine which gypsum beds are present in the shallow subsurface. I assume that the main cavity is developed in the thicker gypsum unit 1 and/or units 2+3 of the Van Vacter Member, because the land surface originally collapsed to a depth of 12 m. The underlying Flowerpot salt is present to the north, in the Anadarko Basin (Fig. 5), but there are no data to suggest that the Flowerpot salt extends beneath the Delhi Sinkhole. The original 12-m diameter of the sink is consistent with those forming over gypsum cavities (see Watonga Sinkhole, below), whereas sinkholes forming because of salt dissolution and collapse typically have a diameter of about 100 m, or more (see Johnson, 2021a, for

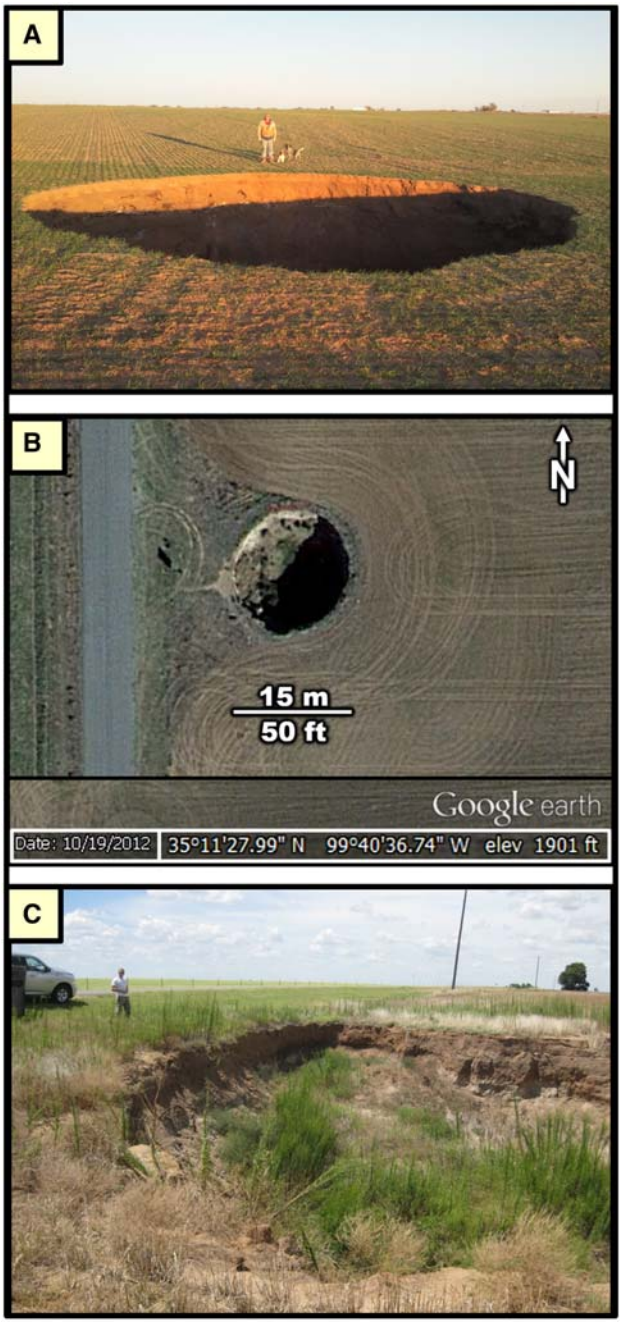

Figure 3. Photos of Delhi Sinkhole in Beckham County, southwest Oklahoma. A) Ground view of sink shortly after formation on, or just before, November 16, 2011; sink was about 12 m wide and 12 m deep. B) Google Earth view of sinkhole in October 2012; sink was about 15 m wide. C) Ground view of sinkhole in July 2016 shows that the sides have partly caved in, partially filling the sink. Sink is now (early 2020) about 18 m wide.



Figure 4. Geologic map of Delhi area, Beckham County, Oklahoma, showing Delhi Sinkhole and two wells used in cross section A–B, which is shown in Figure 5. Lower Blaine and upper Blaine are, respectively, the Elm Fork and Van Vacter Members of the Blaine Formation. Map modified from Johnson and others (2003).

descriptions of numerous salt-dissolution sinkholes in the Greater Permian Evaporite Basin--GPEB).

Gypsum karst is widespread in outcrops just to the south and southwest of Delhi. Murphey (1958) made a field study of these extensive Blaine Formation outcrops in what he called the "Erick Area," and he observed sinkholes, natural bridges, and caves throughout the area. Murphey (1958, p. 55) stated: "Caves vary in size and length throughout the [Erick] area, the largest being 15 to 20 feet [4.6 to 6.1 m] from floor to ceiling. The length of caves varies from a few hundred yards [meters] to more than a mile [1.6 km], the longest being Jester Caves." The presence of underground cavities and caves was further attested by Murphey (1958, p. 55): "Water

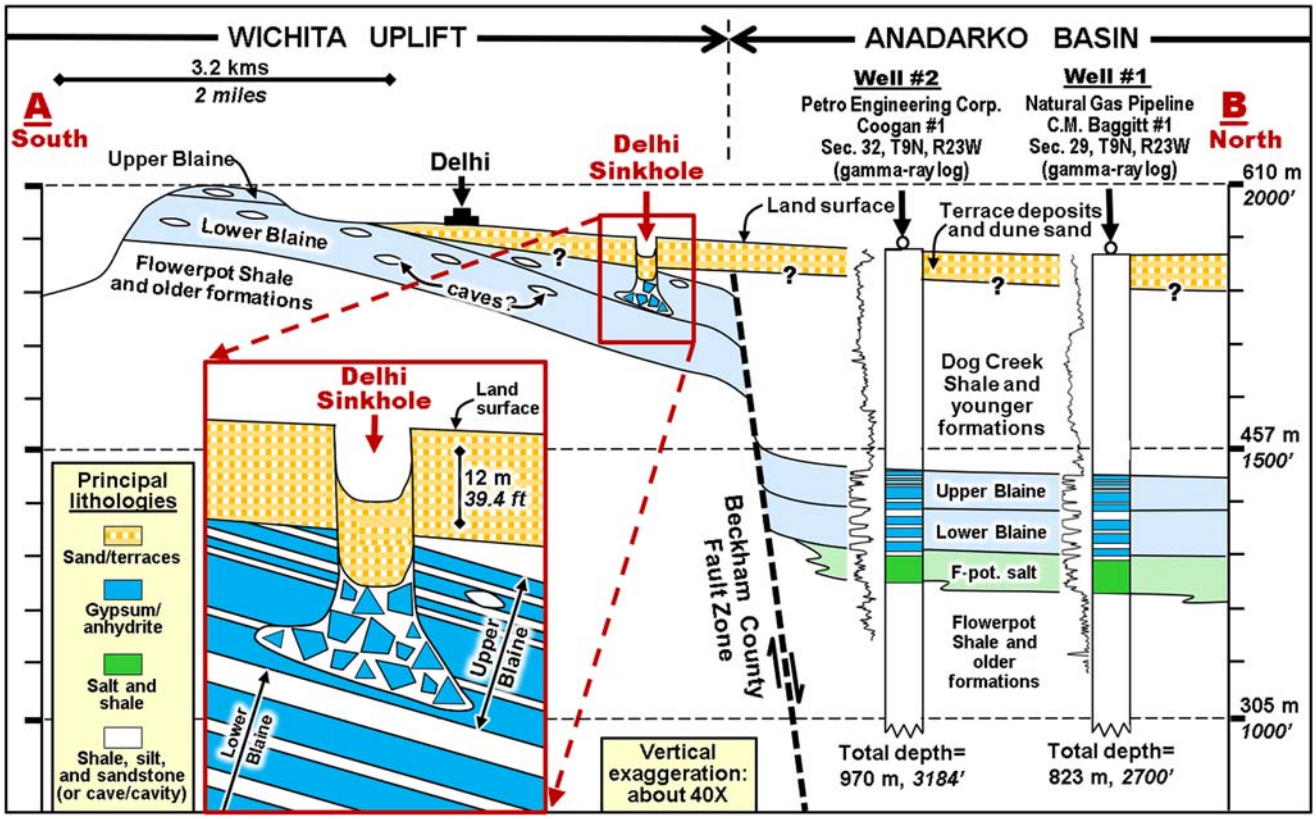

Figure 5. Cross section A–B through the Delhi Sinkhole in Beckham County, southwest Oklahoma, showing probable sinkhole configuration and hypothetical caves in the Blaine Formation; lower Blaine and upper Blaine are, respectively, the Elm Fork and Van Vacter Members of the Blaine Formation. Size of sinkhole is exaggerated horizontally. Location of cross section shown in Figure 4.

wells drilled in this area often record drops of the drill bit in excess of 6 feet [1.8 m]. This is due to penetration of an underground channel." Murphey also noted that the Erick Area contains clay- or sand-filled cracks, crevices, and cavities that formed by dissolution of gypsum, followed by deposition of the clay or sand from water flowing through the void spaces. He stated (p. 60) that "this phenomenon is noticeable in all gypsum outcrops in this area." The Delhi area, including the Delhi Sinkhole and nearby lands covered by terrace deposits and dune sands, are underlain at shallow depths (about 3 to 20 m deep) by these same karstic gypsum beds that crop out extensively just several kilometers to the south (Fig. 4).

The presence of topographic depressions elsewhere in the Delhi area suggests that there may be earlier sinkholes that are now largely masked by terrace deposits and dune sand. Examination of the Delhi 1:24,000-scale topographic map (contour interval about 3 m) shows more than 30 closed depressions within about 3 km of the Delhi Sinkhole. Admittedly, terrace deposits and dune sands commonly contain closed depressions formed as wind blowouts, but it is also possible that some of these depressions may be the sites of earlier, gypsum-karst sinkholes that now are partly, or mostly, filled in by wind-blown sands. Terrace deposits here are an excellent aquifer, and they can provide a good supply of fresh water that percolates down and dissolves the gypsum.

The Beckham County Fault Zone, as shown in Figure 5, is a normal fault or fault zone in Permian rocks that overlie a deep-seated basement fault. Ham and others (1964, Plates I and II) mapped an east–west basement fault along the south side of secs. 31 and 32, T. 9 N., R. 23 W., about 1 to 2 km north of the Delhi Sinkhole. The top of basement rock here drops down to the north about 600 m across the fault (from about -770 m elevation to about -1,370 m), and this fault is also transmitted up through overlying Permian strata. Johnson (1995) noted the following: 1) about 50 faults or flexures have been mapped in the Blaine Formation and associated strata in southwest Oklahoma; 2) many, or most of the surface structures are known to overlie similar, deep-seated structures; and 3) all surface faults are presumed to be normal, inasmuch as the several fault planes that can be observed are normal and have dips of about 60 to 65°. Therefore, the Beckham County Fault Zone is shown here as a normal fault, with a throw of between 30 and 60 m in the Blaine Formation.

WATONGA SINKHOLE, BLAINE COUNTY, NORTHWEST OKLAHOMA

Fay (1958) described a similar sinkhole that formed on December 10, 1957, about 5 km northwest of the town of Watonga, in Blaine County, northwest Oklahoma (Fig. 6), on land owned by Mrs. Anna Foley: he also mentioned three older sinkholes located about 225 m northeast of the herein-named Watonga Sinkhole (previously referred to by Fay as the "Foley sink"). The location of the sink is 228 m north and 172 m east of the SW corner of sec. 2, T. 16 N., R. 12 W. (35°53'12.57" N, 98°27'10.50" W). The depression reached about 14 m wide and 5.2 m deep (Fig. 7), with large cracks parallel to the edge of the hole, but it is now largely filled in by the landowner. The sink formed in Quaternary terrace deposits and dune sands, about 30 m above the Shimer Gypsum Bed at the top of the Blaine Formation (Fig. 8). The Shimer Gypsum is typically 5–6 m thick in the area. Quaternary deposits here are sand and gravel of unknown thickness, but probably as much as 20–30 m thick: terrace deposits here unconformably overlie Permian strata, which could include some of the Dog Creek Shale that overlies the Shimer Gypsum. Terrace deposits are an excellent aquifer in the area, and thus can provide a good supply of fresh water for gypsum dissolution.



Figure 6. Geologic map of Watonga area, Blaine County, Oklahoma, showing Watonga Sinkhole and cross section C–D, which is shown in Figure 8. Map modified from Fay (2010).

Fay (1958) concluded (and I concur) that dissolution occurred in the Shimer Gypsum Bed, and that the Watonga Sinkhole and other nearby collapse structures occurred above underground cavities in the Shimer. The Shimer Gypsum contains caves and natural springs in Roman Nose State Park, located just 5 km north of Watonga Sinkhole. Although dissolution of salt is the cause of some sinkholes in the Greater Permian Evaporite Basin (Johnson, 2021a), there is no evidence of salt in the Dog Creek, Blaine, or underlying Flowerpot strata in the area: the nearest salt in any of these formations is about 50 km to the southwest, where the Flowerpot salt is present (Jordan and Vosburg, 1963, Plate III, Map B). In addition to the sinkholes on Foley land, Fay also noted that several reports in the local Watonga newspaper mentioned former sinks having formed in the general area. No additional studies have been carried out to better understand the Watonga Sinkhole or other sinks in the area.

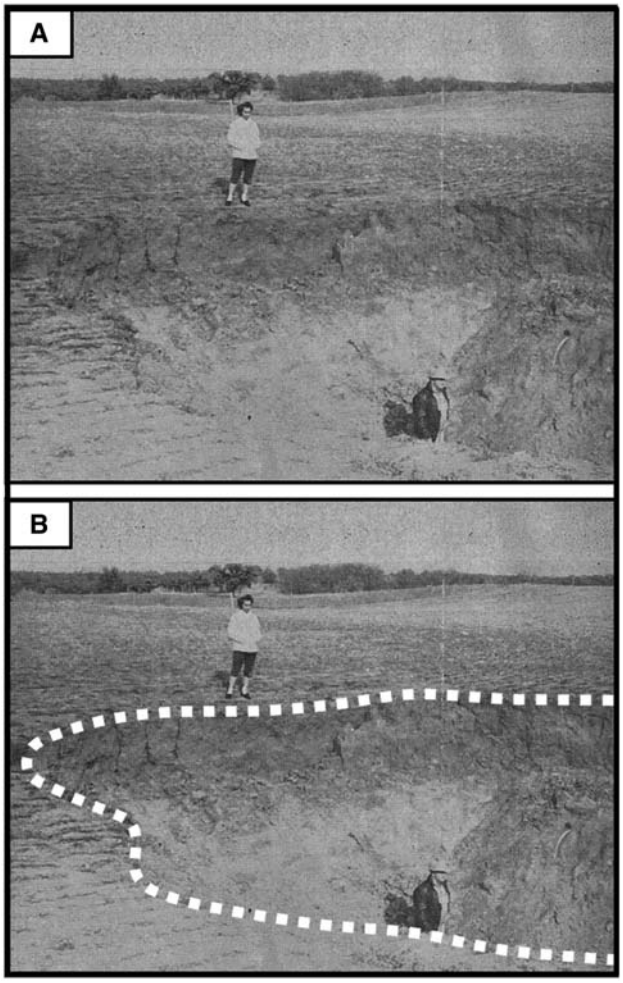

Figure 7. A) Closeup view of half of Watonga Sinkhole in Blaine County, Oklahoma (from Fay, 1958). Woman is standing at rim of sinkhole, and man is standing in bottom of sinkhole, about 5.2 m deep. B) Same photo as above, with rim of sinkhole marked by dotted white line.

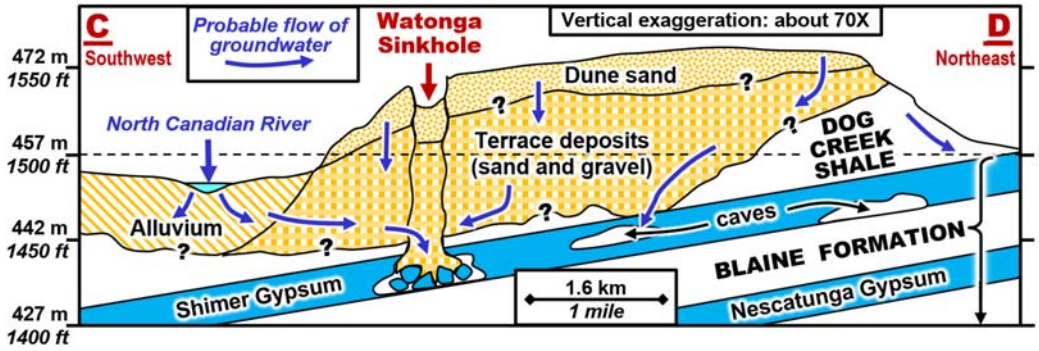

Figure 8. Cross section C–D through the Watonga Sinkhole in Blaine County, northwest Oklahoma, showing probable groundwater movement, possible caves, and collapse of overlying strata into a cavity formed in the Shimer Gypsum Bed at the top of the Blaine Formation (modified from Fay, 1958). Size of sinkhole is exaggerated horizontally. Location of cross section is shown in Figure 6.

REFERENCES CITED

Bozeman, J., 2003, Exploration of western Oklahoma gypsum caves, *in* Johnson, K.S., and Neal, J.T., eds., Evaporite karst and engineering/environmental problems in the United States: Oklahoma Geological Survey, Circular 109, p. 57-64. http://ogs.ou.edu/docs/circulars/C109.pdf

Fay, R.O., 1958, A recent sink hole in central Blaine County, Oklahoma: Oklahoma Geology Notes, Vol. 18, No. 3, p. 58-64.

Fay, R.O., 2010, Preliminary geologic map of the Watonga 30' X 60' quadrangle, Blaine, Caddo, Canadian, Custer, Dewey, and Kingfisher Counties, Oklahoma: Oklahoma Geological Survey, Oklahoma Geologic Quadrangle OGQ–77A, scale, 1:100,000. http://ogs.ou.edu/docs/OGQ/OGQ-77A-color.pdf

Ham, W.E., Denison, R.E., and Merritt, C.A., 1964, Basement rocks and structural evolution of southern Oklahoma: Oklahoma Geological Survey, Bulletin 95, 302 p. http://ogs.ou.edu/docs/bulletins/B95.pdf (text only, no plates)

Johnson, K.S., 1995, Surface structures in Permian strata of southwestern Oklahoma as indicators of deep-seated structures, *in* Johnson, K.S., ed., Structural styles in the southern Midcontinent, 1992 symposium: Oklahoma Geological Survey, Circular 97, p. 288-292. http://ogs.ou.edu/docs/circulars/C97.pdf; Reprinted in 1996: Swindler, D.L., and Williams, C.P., compilers, Transactions of the 1995 AAPG Mid-Continent Section meeting, Tulsa, Oklahoma: Tulsa Geological Society, p. 135–139.

Johnson, K.S., 2003, Evaporite karst in the Permian Blaine Formation and associated strata of western Oklahoma, *in* Johnson, K.S., and Neal, J.T., eds., Evaporite karst and engineering/environmental problems in the United States: Oklahoma Geological Survey, Circular 109, p. 41-55. http://ogs.ou.edu/docs/circulars/C109.pdf

Johnson, K.S., 2018, Gypsum caves of north Texas and western Oklahoma, *in* Stafford, K.W., and Veni, G., eds., Hypogene karst of Texas: Texas Speleological Survey, Monograph 3, p. 111-122. https://www.texasspeleologicalsurvey.org/PDF/Hypogene_Karst_of_Texas.pdf

Johnson, K.S., 2021a, Overview of evaporite karst in the Greater Permian Evaporite Basin (GPEB) of TX, NM, OK, KS, and CO, *in* Johnson, K.S. Land, L., and Decker, D.D., eds., Evaporite karst in the Greater Permian Evaporite Basin (GPEB) of Texas, New Mexico, Oklahoma, Kansas, and Colorado: Oklahoma Geological Survey, Circular 113.

Johnson, K.S., 2021b, Permian Blaine and San Andres Formations of western Oklahoma and Palo Duro Basin of Texas: their correlation and evaporite karst: *in* Johnson, K.S., Land, L., and Decker, D.D., eds., Evaporite karst in the Greater Permian Evaporite Basin (GPEB) of Texas, New Mexico, Oklahoma, Kansas, and Colorado: Oklahoma Geological Survey, Circular 113.

Johnson, K.S., Stanley, T.M., and Miller, G.W., 2003, Geologic map of the Elk City 30' x 60' Quadrangle, Beckham, Custer, Greer, Harmon, Kiowa, Roger Mills, and Washita Counties, Oklahoma: Oklahoma Geological Survey, Oklahoma Geologic Quadrangle Map OGQ–44, scale 1:100,000. http://ogs.ou.edu/docs/OGQ/OGQ-44-color.pdf

Jordan, L., and Vosburg, D.L., 1963, Permian salt and associated evaporites in the Anadarko Basin of the western Oklahoma–Texas Panhandle region: Oklahoma Geological Survey, Bulletin 102, 76 p. http://ogs.ou.edu/docs/bulletins/B102.pdf (text only, no plates)

Murphey, C.W., 1958, Areal geology of the Erick Area, Beckham and Greer Counties, Oklahoma: unpublished MS thesis, University of Oklahoma, Norman, Oklahoma, 102 p.

Oklahoma Geological Survey Circular 113, 2021

This Time It's Natural: Sinkhole Under Interstate 135 in McPherson County, Kansas

Neil M. Croxton
Kansas Department of Transportation,
Salina, Kansas

ABSTRACT.—In 2012, a small area of subsidence was noticed forming beneath the northbound lanes of Interstate 135 in central Kansas. The settlement is centered near a pier on a bridge overpass. The overpass carries rural traffic on a gravel secondary named Shawnee Road; the sinkhole is presently referred to as the Shawnee Road Sink. Shallow sinkholes are common in this part of Kansas; they are associated with the natural dissolution of the Hutchinson Salt Member along its subsurface dissolution front. Regular monitoring since September, 2012, has verified that the settlement continues. As the clearance beneath the bridge will be compromised by regrading the highway, the Kansas Department of Transportation has decided to remove the structure and close the county road at that location. Demolition and reconstruction of the area are scheduled to begin in September 2020.

INTRODUCTION

Sinkholes are a part of life in a three-county area of McPherson, Rice, and Reno Counties in central Kansas. Random, unpredictable, and unstoppable settlement affects houses, businesses, cultivated fields—and highways (Photo 1). Natural dissolution of the vast and deep Hutchinson Salt Member cannot be prevented. Although they generally form gradually, and therefore commonly are not dangerous, the sinkholes are disruptive and can be expensive to cope with.

The Kansas Department of Transportation (KDOT) has been long aware of the presence and causes of salt-related sinkholes. In 1966, two active sinkholes were found beneath Interstate 70 in Russell County during the highway's construction (Croxton, 2002, 2003). The Hutchinson Salt Member is 300 feet thick at that location, and its top is over 1200 feet below the surface. Unplugged oil wells are the cause for those sinkholes—the drilling opened a path for groundwater to flow over the salt and dissolve it. The two Interstate 70 sinkholes, plus an additional one, which has recently begun



Photo 1. Two shallow sinkholes 2 miles north-northwest of the subject area. The sinkhole to the right is affecting a house foundation (behind trees).

Croxton, Neil M., 2021, This Time It's Natural: Sinkhole Under Interstate 135 in McPherson County, Kansas, *in* Johnson, K. S.; Land, Lewis; and Decker, D. D. (eds.), Evaporite Karst in the Greater Permian Evaporite Basin (GPEB) of Texas, New Mexico, Oklahoma, Kansas, and Colorado: Oklahoma Geological Survey, Circular 113, p. 285–293.

moving again, continue to cause headaches for KDOT, 50 years later.

The sinkholes in McPherson, Rice, and Reno counties are caused by the natural dissolution of this same salt unit. Small sinkholes regularly develop under highways in this area. Such sinkholes are monitored by performing periodic surveys along the length of the highway, and fill is added as needed to maintain an acceptable profile. Typically, the rate of settlement is not constant, and years of movement can be interrupted by a period of relative stability. After many years—commonly at least 10 years and up to 25 years—the settlement stops altogether.

Seismic reflection surveys by the Kansas Geological Survey since the 1980s have increased our understanding of the process that causes the sinkholes. Such a survey in 2006 helped the agency plan the alignment of a four-lane highway, changing the location of an overpass on K-61 near the town of Inman. But the Geology Section of the Kansas DOT realizes that subsidence in this area is a risk that has the potential to damage infrastructure.

The author would like to thank the following individuals for their assistance with this paper: George Edmonson, KDOT Maintenance Supervisor; Jeff Geist, P.G., KDOT Engineering Geologist; Kyle Halverson, P.G., KDOT Chief Geologist; Greg Ludvigson, PhD, Kansas Geological Survey; Scott Otipoby—KDOT Graphic Design Supervisor; and Lynn Watney, PhD, Kansas Geological Survey.

GEOLOGY OF THE PROJECT

Northern McPherson County is underlain by the extensive, Permian-age Wellington Formation. This unit is over 500 feet thick at the sinkhole location, and the upper part is marine shale that is approximately 10 feet below the surface at the site. It consists of red and gray shale, with thin irregular limestone and siltstone beds.

Also within the Wellington Formation, 150–200 feet below the land surface, is the Hutchinson Salt Member. It is composed of halite with an unusually small amount of interbedded shale impurities—on average, only about 20%. This member was formed from evaporites deposited in the northeast arm of a sea located during the Middle Permian Period (Drawing 1). Cycles of encroachment and evaporation across 37,000 square miles of what is now central and south-central Kansas left salt over 500 feet thick at the center of the basin (Drawing 2). In northern McPherson County, the Hutchinson Salt Member originally measured nearly 200 feet thick.

Uplift and tilting during the late Permian or early Triassic periods were centered in the Missouri Ozarks and caused a westward structural dip of the older rocks in central and eastern Kansas (Merriam, 1963). This tilting of the Wellington Formation and subsequent erosion have brought the salt close enough to the surface that groundwater is actively dissolving its eastern edge (Drawing 3). This dissolution front extends north-south

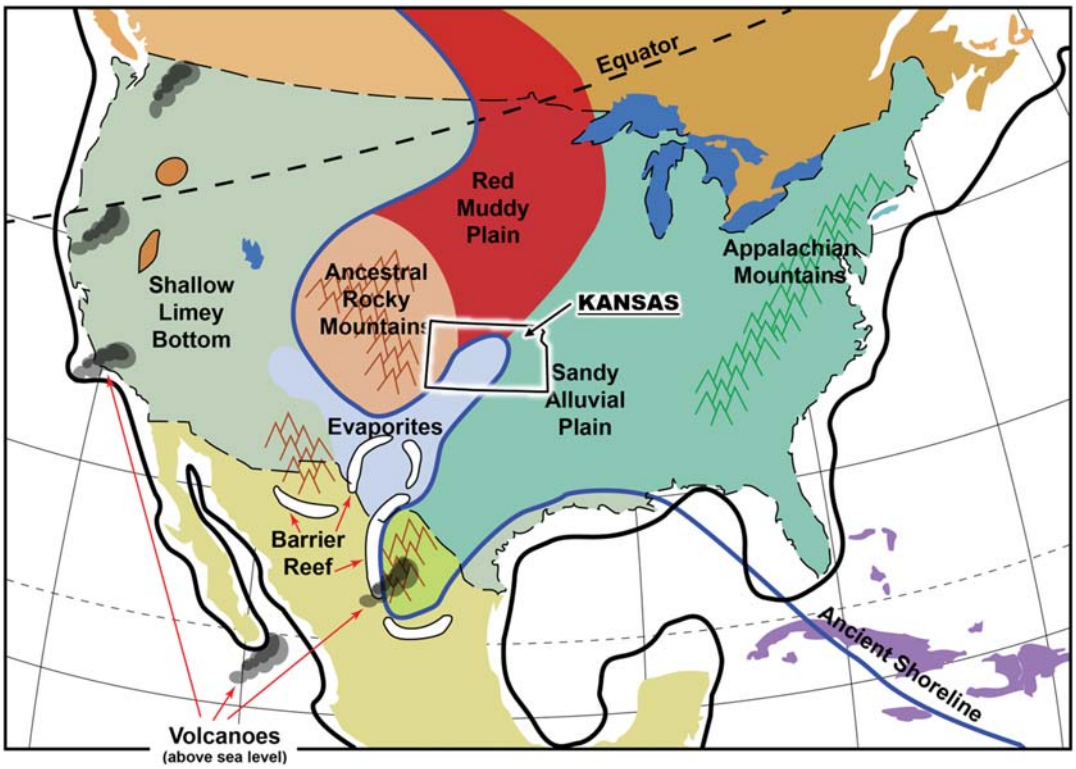

Drawing 1. Middle Permian geography, after Dott and Batten (1981).

through McPherson County (Drawing 4) and is responsible for the formation of the broad north-south valley between McPherson and Wichita. Natural dissolution of the salt has resulted in the formation of countless shallow sinkholes throughout McPherson, Rice, and Reno Counties.

Where bedrock is near the surface, as it is at the interstate bridge, subsidence is caused by the slow downward movement of intact blocks of the shale that overlies the salt bed. Whereas the collapse material just above the dissolving salt may be jumbled, shallower beds can evidently maintain strength to bridge the void, at least for a while. The collapse is therefore expressed only by these upper beds sagging slightly (Drawing 5). This is what we believe is occurring at the Shawnee Road Sink.



Drawing 2. Isopach lines showing thickness, in feet, of the Hutchinson Salt Member, after Walters (1978).

THE BRIDGE AND THE INVESTIGATION

In early 2012, the Highway Maintenance Supervisor for the Lindsborg area noticed a depression on Interstate 135 immediately south of the Shawnee Road overpass, which is located 6 miles south of the McPherson/Saline County line, near milepost 71 (Drawing 6). Being familiar with these types of sinkholes, KDOT Maintenance notified staff surveyors; surveys began that fall and have continued every six months since. Surveys are run along each lane of the interstate and along the handrail and centerline of the bridge.

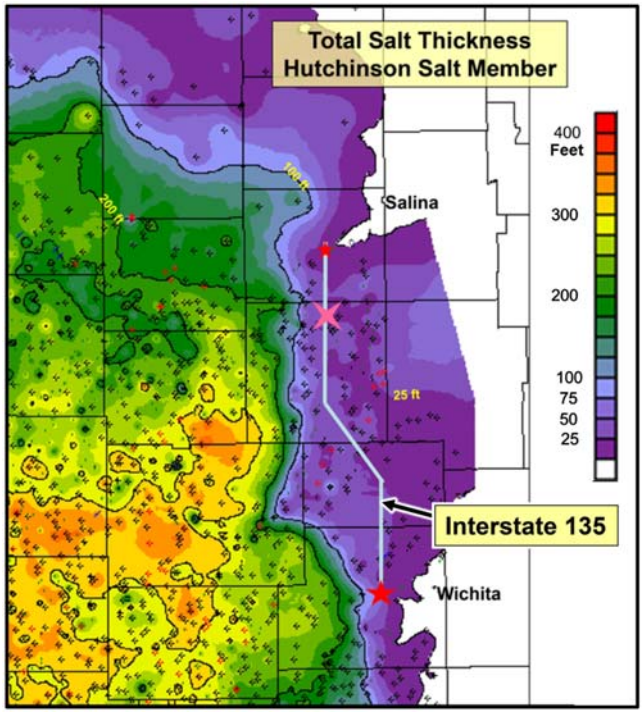

Drawing 4. Thickness of the Hutchinson Salt Member showing eastern dissolution front, Interstate 135, and Shawnee Road Sink (X).

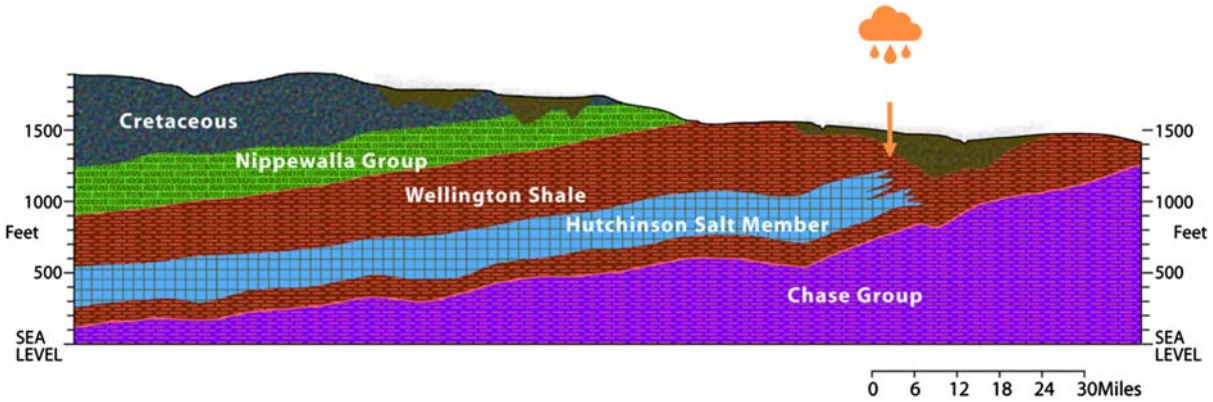

Drawing 3. Generalized section across central Kansas, showing structural dip to west. Vertical exaggeration 100x. After Walters (1978).

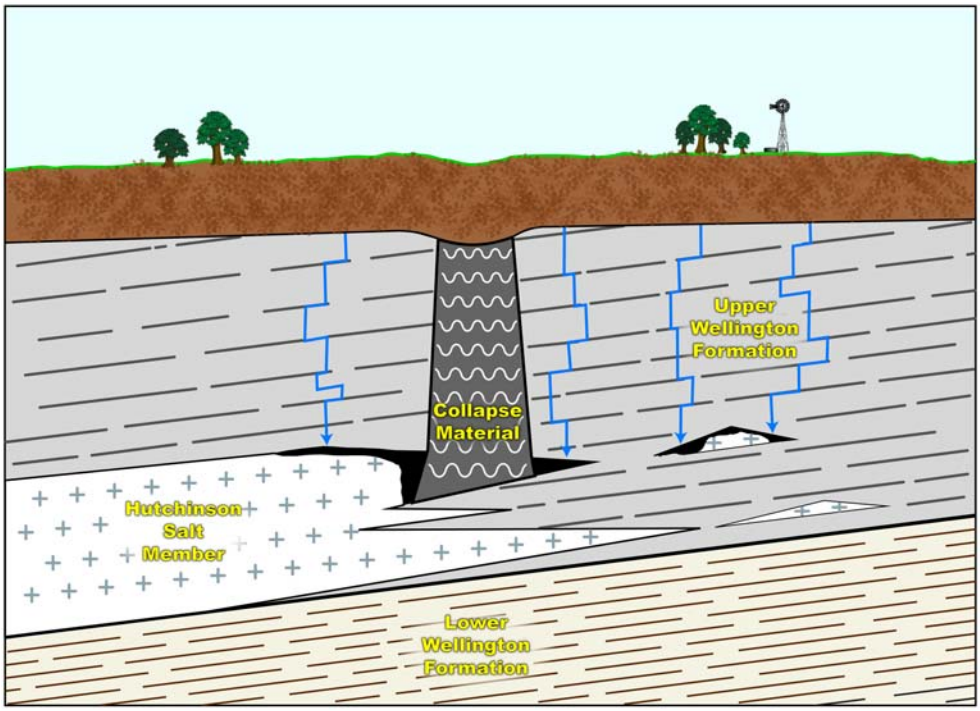

Drawing 5. Generalized section of salt dissolution and subsidence along the eastern limits of the Hutchinson Member. We believe that subsurface dissolution of salt is also happening at Shawnee Road.

The bridge on Shawnee Road was built in 1968 as part of the original interstate project. It is a three-pier structure with concrete girders (Photo 2). The pier foundation is spread footings bearing on the shallow Wellington Formation shale. Abutments are supported by steel piling. Shawnee Road is an unpaved county road and carries very low traffic—probably less than 20 vehicles a day.

By 2016, subsidence had increased enough that the bridge was obviously being affected. Both railings had noticeable dips (Photo 3). There was a significant low area along the south railing over the northbound lanes. After rains, this area held water (Photo 4); the maintenance supervisor noted that he could have ice-skated on the deck during the winter. KDOT knows from experience that concrete bridges will deform plastically if the subsidence below it is slow. For the time being, KDOT was not worried about the integrity of the bridge.

At least as concerning as the bridge, however, was the effect on the interstate roadbed beneath it. The northbound pavement had dropped 4 inches in 4 years, in addition to the unknown amount of subsidence that occurred before monitoring began. A visible and growing depression was now noticeable when driving just south of the bridge (Photo 5). Eventually, the area would need to be rebuilt, to preserve visibility and prevent standing water during heavy rain. Adding fill to the roadbed is impossible if there is a bridge overhead, because a vertical clearance beneath that bridge must be maintained. If the bridge is sinking, too, then the road cannot be raised. Shawnee Road had KDOT's attention.

In January 2017, the Geology Section of the KDOT was asked to conduct a drilling investigation in the vicinity of the bridge and sinkhole. A total of 23 power-auger soundings and one core hole were completed (Photos 6, 7, 8). A contour map on the top of the shale was created (Drawing 7), showing that the subsidence was centered just north of the east pier. The bedrock appears to have dropped about 5 feet, although the bridge has not moved nearly that much. The original bridge foundation geology logs from 1967 were consulted and a top-of-bedrock map created from those soundings. From that investigation, which was not as extensive, it does appear that the shale has dropped about 4 feet near the east pier. Why the bridge itself does not reflect an equally severe a drop is not known.

Recovered cores showed no unusual weathering of the shale, nor was there any indication of void spaces (Photo 9). The only interesting feature of the rock cores was the many high-angle and vertical fractures. This is unusual and may be an indication of the stresses within the block of bedrock that is settling into the void. Our report to the State Bridge Office in Topeka explained the mechanism by which the sinkhole was forming and noted that the settlement would likely continue into the near future.

At about this time, KDOT contracted with the engineering department of Kansas State University to analyze the stresses within the bridge. That report concluded that some parts of the structure were being stressed beyond its design. Reinforcing the bridge was possible but was not a long-term solution if the subsidence continued.



Drawing 6. Map of central Kansas, showing the location of the Shawnee Road Sink (star).


Photo 2. The Shawnee Road bridge in 2020, looking north.

THE PROJECT

Both lanes of the interstate continued to settle (Drawing 8). In April, 2019, KDOT officials met to discuss what to do about the bridge. Chief Geologist Kyle Halverson summarized the history of the site, explained the geology, and concluded by recommending the bridge be removed. In May, a project was created. Plans were developed to detail the removal of the bridge and part

of the approach fill. Because of the stresses built up within the concrete, trying to remove the bridge in pieces could be dangerous. Interstate 135 will therefore be temporarily closed, and the bridge dropped by explosives. By winter of 2020, this project will be underway. The current cost estimate is $300,000.



Photo 3. The south railing of Shawnee Road bridge, looking east, 2020.

THE FUTURE

Once the Shawnee Road bridge has been removed, the roadbed of Interstate 135 can be regraded to its original profile. If the settlement continues, water will begin to pond adjacent to the highway—first intermittently, then perhaps permanently (Photo 10). Fill can be added indefinitely to retain the desired grade line. At some point, however, KDOT is certain that the subsidence will stop. How long that takes cannot be known.

The Russell County subsidence has taught KDOT personnel that the traveling public can take a sudden interest in geology when the word "sinkhole" is mentioned regarding a highway. Once it becomes known that KDOT is removing the bridge because a sinkhole has formed beneath it, some will be concerned about the safety of the interstate. Newspapers and television stations may ask for interviews. Those KDOT representatives close to the project should be prepared to explain what is happening and why the agency feels there is no danger to the public.

REFERENCES CITED

Croxton, N.M., 2002, Subsidence on Interstate and 70 in Russell County, Kansas, related to salt dissolution—a history: The Professional Geologist, v. 39, no. 8, p. 2-7.

Croxton, N.M., 2003, Subsidence on Interstate 70 in Russell County, Kansas, related to salt dissolution—a history, *in* Johnson, K.S., and Neal, J.T., eds., Evaporite karst and engineering/environmental problems in the United States: Oklahoma Geological Survey, Circular 109, p. 149-155. http://ogs.ou.edu/docs/circulars/C109.pdf

Dott, R.H., and Batten, R.L., 1981, Evolution of the Earth: 3rd Edition, McGraw-Hill, 573 p.



Photo 4. Looking east across the Shawnee Road bridge, 2020.



Photo 5. The northbound lanes of Interstate 135 beneath Shawnee Road bridge, 2020.

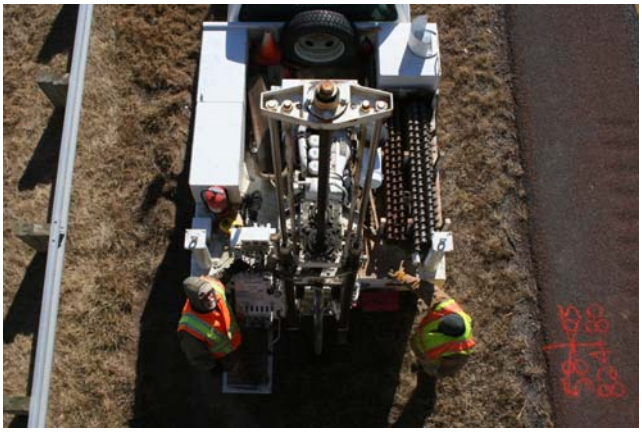

Photo 6. Drilling at Shawnee Road bridge in early 2017.



Photo 7. Drilling at Shawnee Road bridge in early 2017.



Photo 8. Drill cuttings, showing the weathered shale close to the surface.

Merriam, D.F., 1963, The geological history of Kansas: Kansas Geological Survey, Bulletin 162, 317 p.

Walters, R.F., 1978, Land subsidence in central Kansas related to salt dissolution: Kansas Geological Survey, Bulletin 214, 82 p.

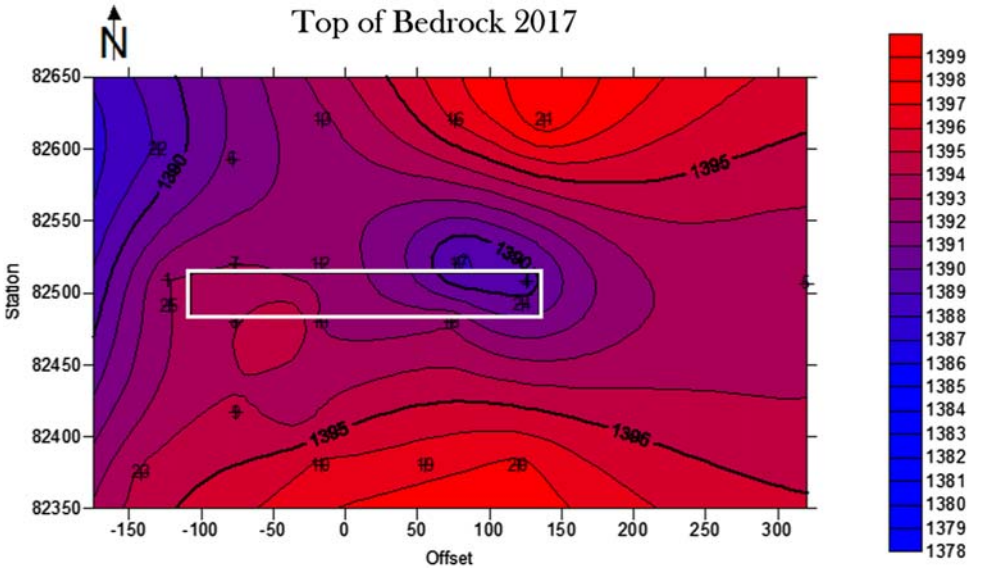

Drawing 7. Contour map on the top of bedrock at the Shawnee Road sink, based on drill soundings in 2017. Elevations in feet above sea level. Bridge footprint is outlined in white.



Photo 9. The recovered cores. Notice both the good recovery and fractured rock.

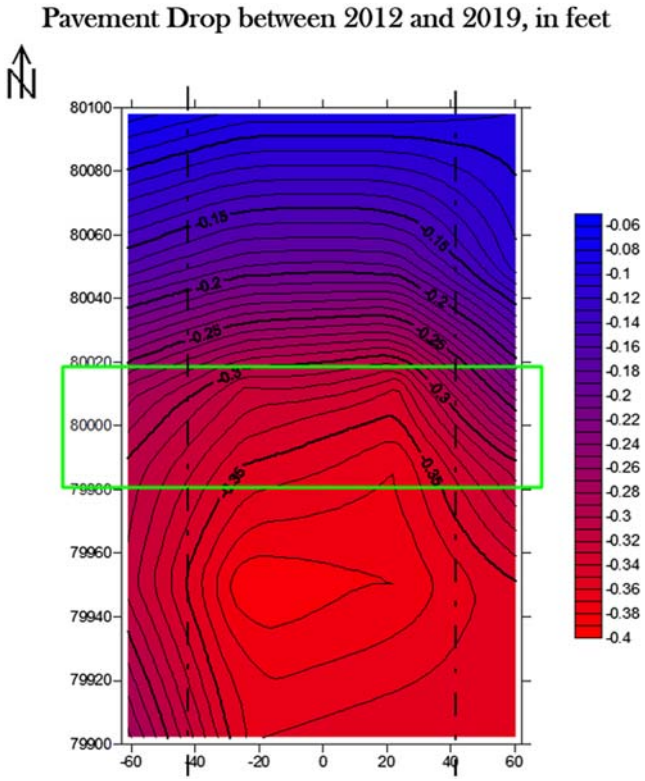

Drawing 8. Interpolated contour map in feet of subsidence at Shawnee Road sink, based on pavement elevations between September 2012 and September 2019. Bridge footprint is outlined in green.

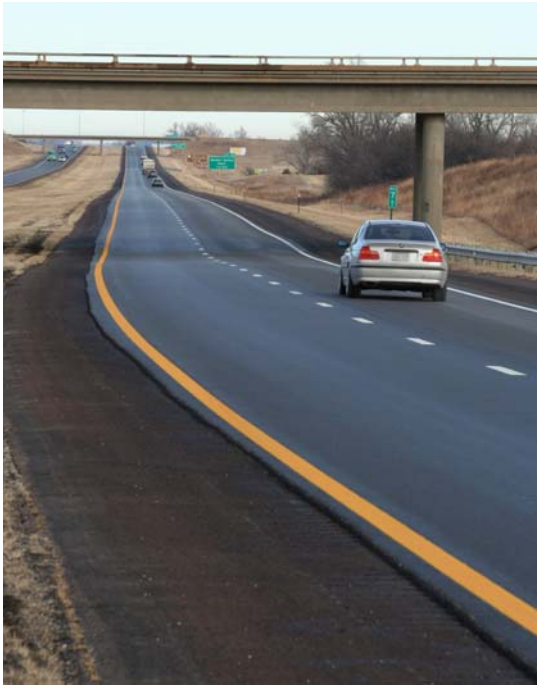

Photo 10. The northbound lanes at Shawnee Road bridge in 2020. If settlement continues, water will begin to pond in the ditches here.

Karst Feature Predictability Models Within Barber County, Kansas

G.M. Kelner
Department of Geosciences, Fort Hays State University, Hays, Kansas

K.L. Gauvey
Department of Earth and Planetary Sciences, The University of Tennessee at Knoxville, Knoxville, Tennessee

J.B. Sumrall
Department of Geosciences, Fort Hays State University, Hays, Kansas

ABSTRACT.—The Gypsum Hills in Barber County, Kansas, is known to have karst features, such as caves and sinkholes. This study created two predictive models for karst features. Features that were previously identified were used to aid in the creation of a predictive model, along with Light Detection and Ranging (LiDAR) and Advanced Spaceborne Thermal Emission and Reflection Radiometer (ASTER) imagery. Only one privately owned ranch in Barber County was used for this study because of time constraints. The predictive models for karst features will be useful for future exploration of karst features on this property. Understanding the distribution and occurrence of karst features will help landowners mitigate risk, such as collapse leading to structural damage and aquifer contamination.

These karst feature predictability models encompass the use of the ESRI ArcMap software platform. The data for this model consist of slope and aspect, nearest neighbor elevation, Normalized Difference Vegetation Index (NDVI), land cover/land use, distance to geomorphic features, subsurface geology, and other attributes calculated in ArcMap. Other software platforms were also used in the creation of these models [Microcomputer Digital Elevation Models (MicroDEM), System for Automated Geoscientific Analyses (SAGA) GIS, and Environment for Visualizing Images (ENVI) for imagery analysis]. To test these models, features were identified using the sink-fill function in ArcMap on hillshade layers generated from LiDAR data. Field validation of these models successfully identified 52% of the validation points as having karst features, as well as 12 additional points in high probability areas that were visited. A total of 38 additional points (a 51% increase in the karst database) were added to the karst inventory for the property. The future use of this model will likely be limited to Barber County, Kansas; however, the techniques and approaches used by these two models may be useful in creating future predictive models in other karst areas.

INTRODUCTION

The Gypsum Hills of Barber County, Kansas, hosts a variety of karst features (Gauvey, 2019). Understanding the distribution and occurrence of karst features will help landowners mitigate risk (e.g., collapse leading to structural damage, dam failures, and aquifer contamination). The goals of this study comprised 1) create a predictive model for karst features using Geographic Information Systems (GIS) and remote sensing; 2) create a karst-hazard map using GIS and the predictive model; and 3) refine the geologic constraints that lead to karst formation in the study area. The karst predictive model will also be useful for future exploration of features in Barber County, such as caves, which may contain rare or threatened organisms.

Kelner, G.M.; Gauvey, K.L.; and Sumrall, J.B., 2021, Karst Feature Predictability Models Within Barber County, Kansas, *in* Johnson, K. S.; Land, Lewis; and Decker, D. D. (eds.), Evaporite Karst in the Greater Permian Evaporite Basin (GPEB) of Texas, New Mexico, Oklahoma, Kansas, and Colorado: Oklahoma Geological Survey, Circular 113, p. 295–304.

Geographic Setting

Barber County is located in southcentral Kansas (Fig. 1). The landscape of Barber County is rugged and heavily influenced by the rivers and water features within the area. There are buttes and mesas that can be seen throughout the area, which are formed by the Medicine Lodge Gypsum (Benison and others, 2015). The area also contains a large number of drainage valleys, locally referred to as draws (large) and washes (small), that are formed and controlled by the water flowing through the area. This landscape is known as the physiographic region of Kansas called the 'Red Hills' or 'Gypsum Hills'. Much of the area within the study area is used as rangeland and is leased to prospective people for livestock grazing, as well as hunting use during the applicable seasons during the year. The use of the landscape by livestock creates animal trails that can be useful to navigate the landscape during fieldwork because of the steep draws and washes that are common throughout the area.

The study area within Barber County is located on private ranch property west of Medicine Lodge, Kansas (Fig. 2). The ranch property consists of ~4,000 ac of pasture and rangeland. Exact locations of the ranch and karst features are not given to protect the land and the karst features, as requested by the property owners.

Geologic Background

The geology of Barber County, Kansas, is dominated by the Permian Nippewalla Group. These red-bed evaporite sequences of the Nippewalla Group were classified in the late 1800s and further refined into individual units during the 1930s caused by the exploration of oil and gas (Cragin, 1896, Norton, 1939). Further outcrop and subsurface studies on the Blaine Formation in Kansas and Oklahoma include Kulstad and others (1956), Ham (1960), Fay, (1964), and Johnson (1967). Equivalent-aged rock units to the Nippewalla Group of Kansas, Oklahoma, and the Texas Panhandle were described by Jordan and Vosburg (1963). Petrography of the sediments of the Nippewalla Group in south-central Kansas was described by Swineford (1955).

Nippewalla Group

The Nippewalla Group consists mostly of red beds that were deposited on a broad, flat, arid alluvial–aeolian plain bordering a shallow inland sea (Hills, 1942; Swineford, 1955). The group is primarily composed of siltstones and very fine-grained sandstones, with minor amounts of silty shale and gypsum. The Nippewalla Group is divided into six formations (from bottom to

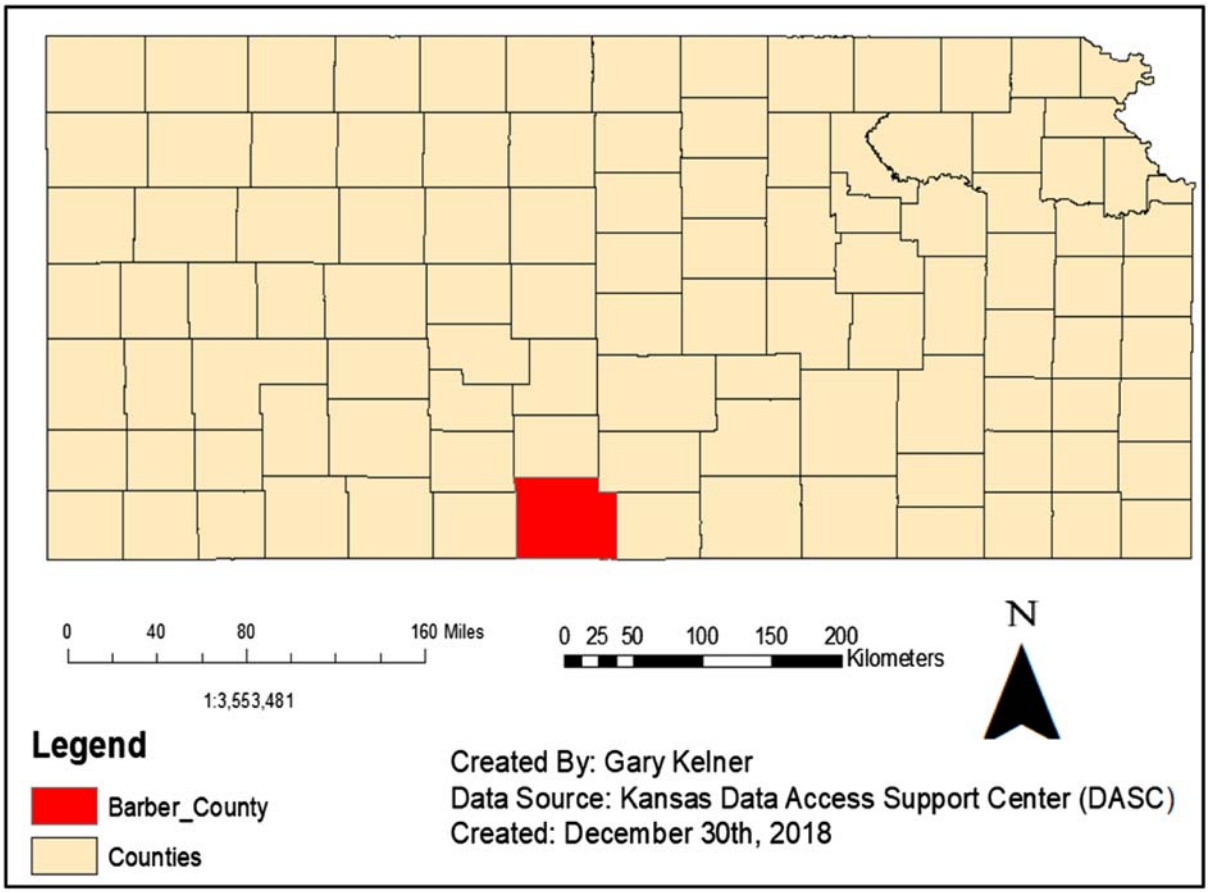

Figure 1. Location of Barber County in southcentral Kansas.

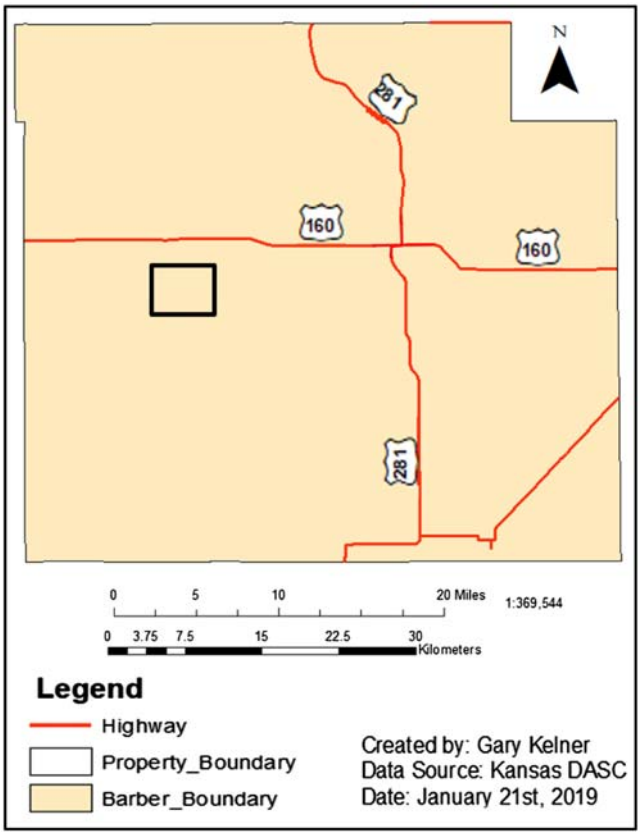

Figure 2. Location of the study area within Barber County, Kansas.

top): Harper Sandstone, Salt Plain Formation, Cedar Hills Sandstone, Flowerpot Shale, Blaine Formation, and Dog Creek Shale. The Dog Creek Shale is commonly grouped with the Blaine Formation, as it lies between the uppermost gypsum of the Blaine and the base of the Whitehorse sandstone.

The Blaine Formation consists of about 50 ft of massive gypsums, thin dolomites, and brown–red shale. The formation is exposed in Barber, Comanche, and Kiowa Counties, and is divided into four members: in descending order, they are the Haskew Gypsum, Shimer Gypsum, Nescatunga Gypsum, and Medicine Lodge Gypsum (Norton, 1939). The Dog Creek Shale, commonly grouped with the Blaine Formation, has a thickness of from 14 to 53 ft (Moore and others, 1951). The Dog Creek Shale consists of thin beds of dark-red silty shale, brown–red and green–gray siltstone, and very fine-grained sandstone, dolomite, dolomitic and gypsiferous sandstone, and gypsum (Swineford, 1955). The Haskew Gypsum, the upper member of the Blaine Formation, consists of less than 1 ft of gypsum; it is underlain by about 5 ft of brown–red shale (Moore and others, 1951). The underlying Shimer Gypsum consists of a 13–23 ft bed of massive gypsum that overlies approximately 1 ft of dolomite (Moore and others, 1951). Beneath the Shimer, or its underlying dolomite, is about 8 ft of red shale, and then the Nescatunga Gypsum, which is about 5 ft thick (Moore and others, 1951). Beneath the Nescatunga is 8 ft of red shale, and then the Medicine Lodge Gypsum: this is the lowest gypsum in this sequence and is the thickest bed of gypsum in Kansas, measuring up to more than 30 ft (Moore and others, 1951). The Medicine Lodge Gypsum grades down into 1 ft of oolitic/pellitic dolomite called the Cedar Springs Dolomite (Fay, 1964). Below the Medicine Lodge Gypsum or its underlying dolomite is the Flowerpot Shale.

GIS and Remote Sensing Applied to Karst Prediction

Field-mapping karst features take a longer amount of time than using the previous data collected from topographic maps (Hubbard, 2003). Morphometry, which is defined as the measurement and analysis of the shape of earth's landforms (Bates and Jackson, 1987), is useful for grouping similar landforms together when mapping karst features (Hyland, 2005; Ford and Williams, 1989). The use of Airborne Laser Swath Mapping (ALSM) has been shown to not be a useful way to map karst features unless a large amount of aerial photography was being used (Seale and others, 2007). Ground-truthing sometimes produces features that must be incorporated into data sets from field mapping (Siart and others, 2009).

Many different tools within the ArcMap software platform can be used in conjunction to create karst feature predictability models. The nearest neighbor distance tool is the most useful when creating predictability maps when the sinkholes are more clustered and the density model is more useful when the sinkholes are dispersed (Galve and others, 2009). The understanding of what controls sinkhole collapse is needed to better create predictability maps for the future and the Normalized Difference Vegetation Index (NDVI) can assist with that understanding (Yilmaz, 2007). The creation of a karst feature predictability model in ArcMap is made considerably easier by combining multiple variables in karst feature prediction, such as the Digital Elevation Model (DEM), satellite imagery as well as elevation, slope, aspect, ground-truthing in the field, and the distance to the drainage feature (Theilen-Willige, 2014; Ozdemir, 2016; and Kresic, 2013). One of the most common methods to predict karst features is using the Logistic Regression tool within ArcMap (Ozdemir, 2016).

When classifying karst features in ArcMap, sediment-filled depressions that were created using the sink-fill tool were separated from vegetation and bare rock by selecting them as a surface class when looking at the variables for karst features (Siart and others, 2009). Using the Topographic Position Index (TPI) to calculate the elevation difference between a point on a DEM and the neighboring pixel is an emerging way to detect karst

features (Doctor and Young, 2013). Creating nested polygons in ArcMap, which are polygons that overlap, represents complex depressions or more than one sinkhole when classifying karst features (Angel and others, 2004). If a complex depression had an innermost polygon, then it would be classified as a singular depression when creating karst feature predictability maps (Angel and others, 2004).

The organizations that use remote-sensing technology have ranged from the National Aeronautics and Space Administration (NASA) to the private citizen (Siegal and Gillespie, 1980). Delineating features on the earth's surface is made considerably easier by the use of remote sensing and Light Detection and Ranging (LiDAR). Reconditioning LiDAR using the watershed analysis tool within ArcMap is one method to detect karst features (Doctor and Young, 2013). Multiple software programs can be used when needed to assist in terrain analysis and recognition, such as System for Automated Geoscientific Analyses (SAGA) GIS and Microcomputer Digital Elevation Models (MicroDEM) (Schillaci and others, 2015).

Study Objectives

The objectives of this study are to 1) create a predictive model for karst features using Geographic Information Systems (GIS) and remote sensing; 2) create a karst hazard map using GIS and the predictive model; and 3) refine the geologic constraints that lead to karst formation in the study area. This work is built upon research projects by: Gauvey and Sumrall (2018), Sumrall and Gauvey (2018), Gauvey and Sumrall (2019), Gauvey and others (2019) and a master's thesis by Gauvey (2019). The reader is encouraged to explore these materials for more information on the exact controls of speleogenesis within Barber County, Kansas.

METHODS AND RESULTS

Multiple software systems were used for this study. The primary software platform used was ArcMap version 10.7.1 by Environmental Systems Research Institute (ESRI). This program aided in the map creation and data analysis for this research. Some of the other software platforms used as needed were MicroDEM, SAGA GIS, and Minnesota Department of Natural Resources (MNDNR) GPS. The software program ENVI 5.1 (32 bit) was used for remote-sensing analysis of the imagery used for this research. It is noted that for the maps of output and validation and all maps that show the location of karst features on the property, roads and other detailed landscape features were purposefully removed in ArcMap to protect the location of these features.

Data Collection and Conditioning

The start of this study first consisted of gathering data for Barber County, Kansas. These data came from multiple online sources: the Kansas Data Access Support Center (DASC), the United States Geological Survey (USGS), the United States Department of Agriculture (USDA), and the National Aeronautics and Space Administration (NASA). These data sets included topographic maps, geologic maps, infrastructure features, land-use maps, digital elevation models (DEM), Landsat and ASTER Imagery, and Light Detection and Ranging (LiDAR) data.

After the data were collected from the various sources, multiple conditioning steps were needed before the predictive models could be created. This included the creation of a geodatabase for file storage and manipulation, digitization of nonelectronic maps (geologic maps), geographic coordinate system reprojection, and mosaicking imagery and DEM raster files to cover the study area. Further conditioning of DEM and LiDAR imagery included various functions conducted in ArcMap, including slope, aspect, hillshade, Normalized Difference Vegetation Index (NDVI), and Sink-Fill calculations. These attributes that were calculated within ArcMap were stored within the geodatabase for later use in the creation of the predictive models.

Creation of Predictive Models

Two predictive models were created in this study to test the influence of various features on karst prediction. These two models were used to create a refined prediction model for field validation. The first model was a non-normalized model that did not account for variation in scale between predictive variables. This model is referred to as the non-normalized model. The second model was normalized and weighted with researcher optimization to determine the most appropriate weightings of predictive class variables. Both models used the following attributes for the prediction of karst features: elevation, slope, aspect, and NDVI. The non-normalized model also used distance to roads, distance to hydrologic features, surface geology, and land use in addition to these features. The normalized/weighted model used distance to the geologic contact between the Blaine and Whitehorse Formations and ASTER Geology calculations (Sabin's Ratio; Ourhzif and others, 2019) in addition to the shared attributes.

Non-normalized Model

This predictive model was created using the raster calculator tool function within the ArcMap Toolbox, which allowed the user to perform mathematical functions with multiple layers. The model consisted of the geographic layers that were identified as being important in surface

karst expression. Conditional functions were used, because this categorizes the output of the variables being inputted into the raster calculator. The output of this raster calculator tool will be the result of the karst feature prediction model.

The first step to create the non-normalized model included creating Conditional Function #1, which involved elevations of known karst features. Conditional Function #1 calculated the elevation range of the karst features for the study area. This was done using the following conditional function:

```
Con(("DEM_Section" > low elevation) & ("DEM_Section"
    < High elevation)), "DEM_Section")
    = outelevationrange_Section
```

The output of this expression creates the elevation range from the lowest elevation to the highest elevation as shown by the DEM which is already in the GIS software.

The next step in the creation of the non-normalized modeled was writing Conditional Function #2, which incorporated land-use data for karst features. Conditional Function #2 used the USDA land-use data. The class of land use that was identified as important for karst feature formation was grass/pasture land. Conditional Function #2 was the following:

```
Con("LandUse_USDA", "outelevationrange_Section", ' ',
    "CLASS_NAME = 'Grass/Pasture' ")
    = outelevationLandUse_Section
```

This function calculated the intersection between elevation ranges of karst features and grass/pasture land cover. This intersection output would be used as the input for the next step of the model.

The next step of creating the non-normalized model was writing Conditional Function #3. This function calculated the intersection between the previous Conditional Function #2 and the distance from streams and farm roads. This calculation attempted to identify karst features associated with surface water and/or collapse. Conditional Function #3 was the following:

```
Con((" farm roads_euclidean distance", < 4828.03)
    & (" hydrology_euclidean distance", < 4828.03),
    " outelevationLandUse_Section")
    = outelevationdistance_section
```

These results identified the intersection between elevation, land use, the distance from roads as well, and the distance from surface water features for potential karst features. The values above were miles converted to meters for use in the ArcMap system.

The next step of creating the non-normalized model was writing Conditional Function #4. This function identified the intersection of karst features within a specific aspect direction and slope with a certain degree with the previous Conditional Function #3 output. Conditional Function #4 was the following:

```
Con((" DEM_Slope", < 50)
    & (" outelevationdistance_section", > 0),
    Con((" DEM_aspect", > 135) &
    (" DEM_aspect", < 225),
    "outelevationdistance_section", 0))
    = outraster_section
```

The results of this calculation showed the intersection of elevation, land use, distances from the roads and hydrologic features, and the aspect/slope of the landscape.

The final step of creating the non-normalized model was writing Conditional Function #5. Conditional Function #5 calculated the intersection of the previous outputs with the NDVI and local geology for karst features. Conditional Function #5 was the following:

```
Con((" geology_units_raster" >= geo unit raster number)
    & (" geology_units_raster", >= geo unit raster number),
    Con((" ndvi_month_section", > 1)
    & (" ndvi_month_section", < 400),
    " outraster_section", 0))
```

After the initial run of this model, Functions 2 through 5 had to be executed again with the land-use class changed in Function 2 to deciduous forest, because this model could only accommodate one land-use class at a time. This second run was then added to the first output (Fig. 3).

Normalized and Weighted Model

The Normalized and Weighted Model used similar input layers; however, additional variables were calculated in addition to those used in the non-normalized model. These additional variables included the distance to the geologic contact between the Blaine and Whitehorse Formations and ASTER Geology calculations (Sabin's Ratio). First, the distance to the geologic contact was calculated using nested buffers of 10 m around the digitized contact vector file within ArcMap. The buffers closest to the geologic contact were given values of 10, and lower values were given as the distance from the contact increased. These nested buffers were converted from vector files to raster files to be used in the raster calculator. This was based on a hypothesis that the geologic contact is an important factor in speleogenesis within Barber County (Gauvey, 2019).

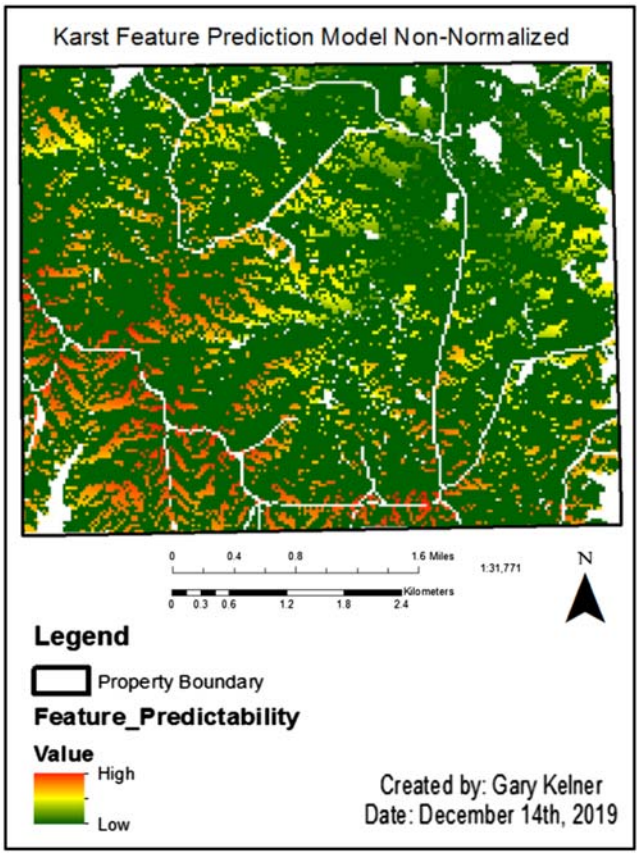

Figure 3. Output for the Non-normalized Model showing high probability values in red and low probability values in green.

Next, Sabin's Ratio was calculated using the Harris Geospatial software platform ENVI (Environment for Visualizing Images) version 5.1 (32 bit). ASTER data from 2007 were acquired and band ratios were used to calculate Sabin's Ratio. There were certain band ratios that were developed to show mineral occurrences on the land surface according to (Ourhzif and others, 2019). Sabin's ratio uses combinations of bands within the ASTER data and the equation is the following: (Band 4/Band 2, Band 6/Band 7, Band 10). The ratios were created using the band ratio tool within the ENVI toolbar, and once the ratios were created, the band math tool was used to add together the resulting ratios to create the final output map. This Sabin's ratio showed the mineral composition of the study area. The following ratio: [(Band 6+Band 9/Band 7+Band 8), (Band 5+Band7/Band6), Band 2/Band 1] created a Red–Green–Blue (RGB) false color image of the ASTER data as the output. The initial false color raster image was reclassified based on having three known geologic materials at the surface (red shale, gypsum/gypsiferous soil, and sandstone). This reclassified output showed the potential gypsum deposits along with other similar units such as the gypsiferous soil that is commonly seen in the study area.

Similar to the non-normalized model, this model used the raster calculator tool function within the ArcMap Toolbox. Prior to inputting these raster files into the calculator, these files were normalized for the highest potential of karst feature prediction. This was accomplished using previously identified karst features (74 karst features identified by Gauvey, 2019) to determine the range in values of every variable input into the model for this select set of training data. To determine the range in values for each variable, a 10 m buffer was created around each known karst feature, and zonal statistics were calculated using ArcMap. This idealized range of each variable allowed for the reclassification of the raster data into normalized data sets with a value of 10 assigned to the range of values associated with the training data (known karst features). Lower values were given to the reclassified data for values outside of the training data. This zonal statistical method using training data was performed on all of the variables input into this model.

Next, normalized variables were evenly weighted to create an initial model; however, this evenly weighted initial model did not perform as expected. This was determined using a preliminary validation data set (containing 15 additional karst features located by the authors) collected after Gauvey (2019) completed her work.

Finally, several efforts were attempted to manually optimize feature prediction using various weightings of variables. This was accomplished by varying the weights of variables until the preliminary validation data set was adequately predicted. The optimized weights were determined to be 34.5% geologic contact, 27.6% ASTER Sabin's Ratio geology, 17.2% elevation, 10.3% Aspect, 6.9% slope, and 3.5% NDVI. When these weights were applied in the raster calculator, the output file was scaled from 1 to 10 with higher values associated with higher predictions for the presence of karst features. The output for the Normalized and Weighted Model is shown in Figure 4.

Comparison of Models and Selection of Data for Field Validation

To compare model outputs for use in selecting locations for field validation, the two models were reclassified within ArcMap. Each reclassification was conducted with two classes using Natural Breaks (Jenks). This produced output raster files with values of one (1) for high prediction or zero (0) for low prediction. The two files were added using the raster calculator to create the model agreement and comparison, as shown in Figure 5. A value of two (2) means that the two models agree in their high predictability, a value of one (1) means that only one

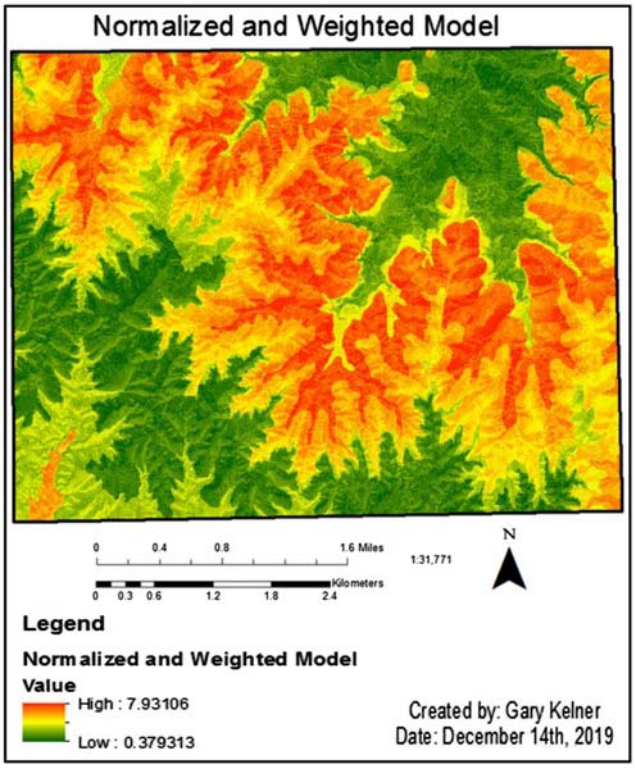

Figure 4. Output for the Normalized and Weighted Model showing high probability values in red and low probability values in green.

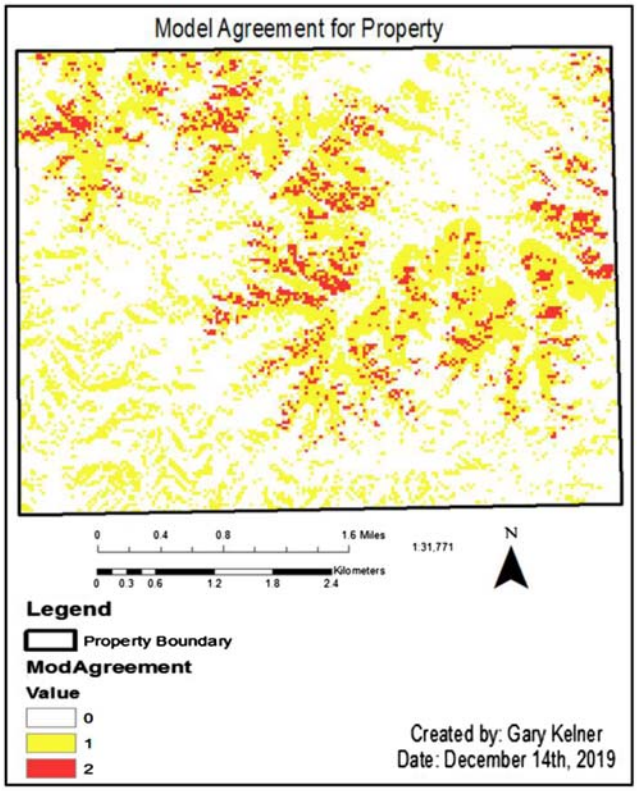

Figure 5. Model agreement for the prediction of features. A value of two (2) is an agreement of the two models of high probability, a value of zero (1) means that one model predicted high probabilities, and a value of zero (0) means that both models agree in a low probability.

model has a high prediction value, and a value of zero (0) means that the two models agree in a low predictability.

To select locations for field validation, a combination of visual assessment of land cover and sink fills using hillshade derived from LiDAR was used. Thousands of points were identified by the sink-fill function; however, when correlation with agreement of high prediction of models was applied, 91 features were viable for validation. These 91 features were visually assessed using Quickbird Imagery of the area, and 50 features were selected based on ease of access, location on the property, and other factors such as the presence of manmade features that were mistakenly identified by the sink-fill function.

Field Validation

Fifty points were selected for field validation of these two models (Fig. 6). Each point was visited during a weekend of fieldwork in November 2019. A software package called Avenza Maps® was used on cell phones and field tablets. This mapping software used georeferenced PDFs created in ArcMap to help locate the validation points. A total of 26 points of those identified of the 50 points were field verified as hosting karst features (52% accuracy). In addition to validating these points, 12 additional features were located using the model output in real time on Avenza Maps®. This was accomplished using the model agreement output overlain on the hillshade to investigate areas that were not identified using the sink-fill function. The total number of points that were field validated using these approaches was 38 (Fig. 7).

DISCUSSION AND CONCLUSIONS

Based on field validation results, these models contribute significantly to the identification of unknown karst features on this property; however, the development of these models is limited to this specific study location. The methods that were used by the two models could easily be replicated in other areas of Barber County, Kansas. It is highly unlikely that these models would be useful in their current form for other gypsum areas of the world. This does not mean that these models do not contribute to our understanding of karst prediction in gypsum karst regions. Instead, the concepts of these models can be modified and individually tailored for other gypsum areas for karst prediction.

The identification of karst features without these predictive models proved to be time consuming and incredibly challenging. Gauvey (2019) identified 74 karst features during 8 months of fieldwork to collect data. The validation of points identified in this study occurred over a weekend of fieldwork in November and identified 51% additional features to the known karst inventory on this vast property. This method has been incredibly successful for locating karst features for this property, and there exists future use of the model on the current property. It is possible that other karst features exist that the sink-fill function would not identify (e.g., caves without a sinkhole entrance), so future work could focus on the other regions that these models predict to have high probabilities of karst features.

After field validation, the models were analyzed to determine what resulted in their failed prediction, especially because most of the points that were negative were clustered in the northwestern-to-north-central part of the property (Fig. 8). This was concerning, because obviously, all of the landscape attributes that favor karst development were present in this area. It was also important to note that additional points were not able to be identified outside of the sink-fill points in this negative region, meaning that a significant amount of fieldwork was conducted without finding any other karst features in this part of the property. In the field, it became apparently obvious why there were no karst features; the bedrock geology (more importantly, the contact between the

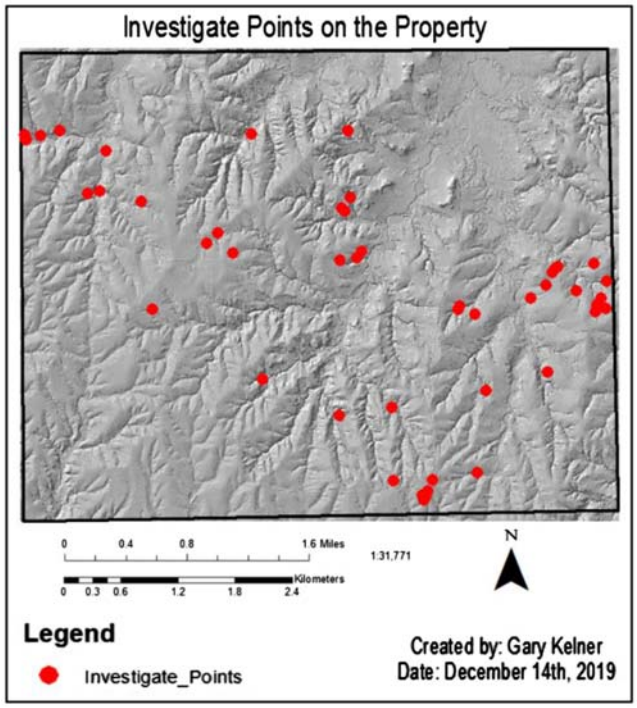

Figure 6. Field validation investigation points identified by the model agreement applied to the sink-fill function.

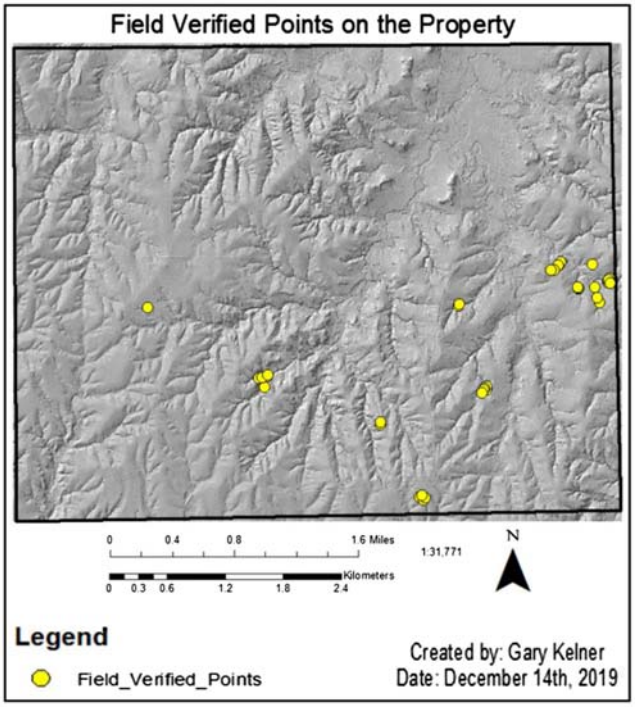

Figure 7. All of the points (38 totally) were identified or verified using the models during field validation.

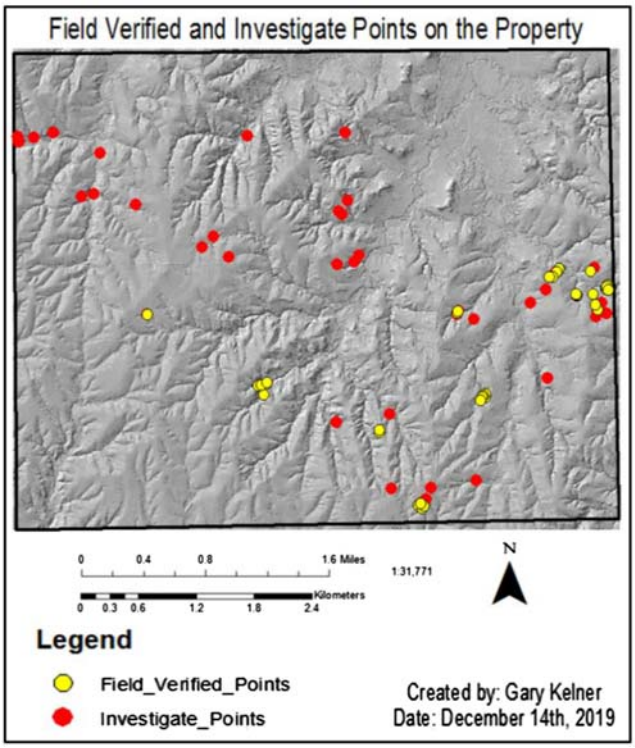

Figure 8. Field-verified points (yellow) and investigate points (red) determined using sink-fill function and models. There were no verified points in the northwest-to-north-central part of the property.

Blaine and Flowerpot Formations) was not where it was mapped by the Kansas Geological Society's detailed geologic map. Instead, a sandstone unit (either the Cedar Hills Sandstone or the Whitehorse Sandstone) and Quaternary Loess were present in this part of the property. The gypsum of the Blaine Formation, which is essential for karst formation, was either 1) covered by this insoluble material, essentially masking its expression on the surface, or 2) removed by surface erosion. Detailed geologic mapping must be conducted to determine the stratigraphic placement of the sandstone identified in this part of the property, which is beyond the scope of this paper.

When combining the mistake in surface geology at the local scale with the sensitivity of the sink-fill function in identifying enclosed sinks of nonkarst origin, the models were actually more accurate than the validation would suggest. If the correct localized geology was input initially into both models, then the northwest-to-north-central part of the property would have received extremely low values resulting from the underlying geology and lack of the geologic contact. This is obviously a limitation of this study; however, detailed field mapping of the localized geology will be the focus of future studies that are currently beyond the scope of this study.

ACKNOWLEDGEMENTS

Funding for the research conducted was partially provided by the Fort Hays State University Graduate Scholarly Experience Grant as well as the Kansas MiniView Grant, which assisted in the purchase of aerial imagery. Funding provided to assist in the presentation of this research at the 2019 Geological Society of America Meeting in Phoenix Arizona was provided by the Geological Society of America South Central Division Student Travel Grant. A special thanks to Dr. Jay Simms for this grant.

Many thanks to Jonathan Camelo, Britta Coleman, Elizabeth Emerson, Nathan Feldcamp, and Alex Lyles. Thank you very much for your assistance with the collection of field data for this project. Appreciation is expressed to Dr. Richard Lisichenko for his review of this manuscript and helpful comments.

REFERENCES CITED

Angel, J.C., Nelson, D.O., and Panno, S.V., 2004, Comparison of a new GIS-based technique and a manual method for determining sinkhole density: An example from Illinois' sinkhole plain: Journal of Cave and Karst Studies, Vol. 66(1), p. 9-17.

Bates, R.L., and Jackson, J.A., 1987, Glossary of geology: American Geological Institute, Alexandria, Virginia, 788 p.

Benison, K.C., Zambito IV, J.J., and Knapp, J., 2015, Contrasting siliciclastic–evaporite strata in subsurface and outcrop: an example from the Permian Nippewalla Group of Kansas, USA. Journal of Sedimentary Research, Vol. 85(6), p. 626-645.

Campbell, C.L., 1963, Permian evaporites between the Blaine and Stone Corral Formations: unpublished MS thesis, University of Kansas, Lawrence, KS, 73 p.

Cragin, F.W., 1896, The Permian System in Kansas: Colorado College Studies, Vol. 6, p. 1-48.

Doctor, D.H., and Young, J.A., 2013. An evaluation of automated GIS tools for delineating karst sinkholes and closed depressions from 1-meter LIDAR-derived digital elevation data, *in* Land, L., Doctor, D.H., and Stephenson, J.B., eds., Sinkholes and the Engineering and Environmental Impacts of Karst: Proceedings of the Thirteenth Multidisciplinary Conference: National Cave and Karst Research Institute, Symposium 2, p. 49-58.

Fay, R.O., 1964, The Blaine and related formations of northwestern Oklahoma and southern Kansas: Oklahoma Geological Survey, Bulletin 98, 238 p.

Ford, D.C., and Williams, P.W., 1989, Karst geomorphology and hydrology: London, Unwin Hyman, 601 p.

Galve, J.P., Gutiérrez, F., Remondo, J., Bonachea, J., Lucha, P., and Cendrero, A., 2009, Evaluating and comparing methods of sinkhole susceptibility mapping in the Ebro Valley evaporite karst (NE Spain): Geomorphology, Vol. 111(3-4), p. 160-172.

Gauvey, K.L., Sumrall, J.B., and Kelner, G.M., 2019, The petrographic controls on gypsum karst speleogenesis in south central Kansas: Geological Society of America, Annual meeting, Phoenix, Arizona, Program with Abstracts.

Gauvey, K., 2019, Gypsum karst speleogenesis in Barber County, Kansas of the Permian Blaine Formation: unpublished MS thesis, Fort Hays State University, Hays, Kansas, 131 p.

Gauvey, K.L., and Sumrall, J.B., 2018, Gypsum karst reconnaissance in Barber County, Kansas of the Permian Blaine Formation: Geological Society of America, Abstracts with Programs, Vol.50, no.6.

Gauvey, K.L., and Sumrall, J.B., 2019, Gypsum karst speleogenesis in south-central Kansas: Geological Society of America, Abstracts with Programs, Vol.51, no.2.

Ham, W.E., 1960, Middle Permian evaporites in southwestern Oklahoma: 21st International Geological Congress, Norden, Report Part 12, p. 138-151.

Hills, J.M., 1942, Rhythm of Permian seas–a paleogeographic study: American Association of Petroleum Geologists, Bulletin, Vol. 26, p. 217-255.

Hubbard, Jr., D.A., 2003, Use of regional sinkhole mapping for sinkhole susceptibility maps, *in* Beck, B.F., ed., Sinkholes and the Engineering and Environmental Impacts of Karst, Huntsville, AL: American Society of Civil Engineers, Ninth Multidisciplinary Conference, p. 61-71.

Hyland, S.E., 2005, Analysis of sinkhole susceptibility and karst distribution in the northern Shenandoah Valley, Virginia: implications for low impact development (LID) site suitability models: unpublished MS thesis, Virginia Tech, Blacksburg, VA, 56 p.

Johnson, K.S., 1967, Stratigraphy of the Permian Blaine Formation and associated strata in southwestern Oklahoma: unpublished PhD dissertation, University of Illinois, Champaign-Urbana, IL, 247 p.

Jordan, L., and Vosburg, D.L., 1963, Permian salt and associated evaporites in the Anadarko Basin of the western Oklahoma–Texas Panhandle Region: Oklahoma Geological Survey, Bulletin 102, 76 p.

Kresic, N., 2013, Water in karst: management, vulnerability, and restoration: New York, McGraw-Hill, 608 p.

Kulstad, R.O., Fairchild, P., and McGregor, D., 1956, Gypsum in Kansas: Kansas Geological Survey, Bulletin 113, 110 p.

Malone, D.J., 1962, Stratigraphic relations and structural significance of the Blaine Formation in the subsurface of southwestern Kansas: unpublished MS thesis, University of Wichita, Wichita, KS, 72 p.

McKee, E.D., Oriel, S.S., and others, 1967a, Paleotectonic investigations of the Permian System of the United States: US Geological Survey, Professional Paper 515, 271 p.

McKee, E.D.; Oriel, S.S., and others, 1967b, Paleotectonic maps of the Permian System: US Geological Survey, Miscellaneous Geologic Investigations Map I-450.

Merriam, D.F., 1958, Preliminary regional structural contour map on top of the Stone Corral Formation (Permian) in Kansas: Kansas Geological Survey, Oil and Gas Investigations 17, map.

Moore, R.C.; and others., 1951, The Kansas rock column: Kansas Geological Survey, Bulletin 89, p. 1-132.

Norton, G.H., 1939, Permian red beds of Kansas: American Association of Petroleum Geologists, Bulletin, Vol. 23, p. 1751-1819.

Ourhzif, Z.; Algouti, A.; and Hadach, F., 2019, Lithological mapping using Landsat 8 OLI and ASTER multispectral data in Imini-Ounilla District South High Atlas of Marrakech: International Archives of the Photogrammetry, Remote Sensing & Spatial Information Sciences, XLII-2/W13, 1255–1262 https://doi.org/10.5194/isprs-archives-XLII-2-W13-1255-2019, 2019

Ozdemir, A., 2016, Sinkhole susceptibility mapping using logistic regression in Karapınar (Konya, Turkey): Bulletin of Engineering Geology and the Environment, Vol. 75(2), p.681-707.

Rascoe, B., Jr., 1968, Permian System in the western Mid-Continent: The Mountain Geologist, Vol. 5, p. 127-138.

Rascoe, B., Jr., and Baars, D.L., 1972, The Permian System, *in* Geologic atlas of the Rocky Mountain Region: Rocky Mountain Association of Geologists, Denver, CO, p. 143-165.

Schillaci, C., Braun, A., and Kropáček, J., 2015, 2.4. 2. Terrain analysis and landform recognition. Geomorphological Techniques (Online Edition).

Schumaker, R.D., 1966, Regional study of Kansas Permian evaporite formations: unpublished MS thesis, Wichita State University, Wichita, KS, 87 p.

Seale, L.D., Florea, L.J., Vacher, H.L., and Brinkmann, R., 2008, Using ALSM to map sinkholes in the urbanized covered karst of Pinellas County, Florida—1, methodological considerations: Environmental Geology, Vol. 54(5), p. 995-1005.

Siart, C., Bubenzer, O., and Eitel, B., 2009, Combining digital elevation data (SRTM/ASTER), high resolution satellite imagery (Quickbird) and GIS for geomorphological mapping: A multi-component case study on Mediterranean karst in central Crete: Geomorphology, Vol. 112(1-2), p.106-121.

Siegal, B.S., and Gillespie, A.R., eds., 1980, Remote sensing in geology: New York, John Wiley, 702 p.

Sumrall, J.B., and Gauvey, K.L., 2018, Sinkhole morphology from the Blaine Formation of Barber County, Kansas: Geological Society of America, Abstracts and Programs, Vol. 50, no. 6.

Swineford, A., 1955, Petrography of Upper Permian rocks in south-central Kansas: Kansas Geological Survey, Bulletin 111, 179 p.

Theilen-Willige, B., Malek, H., Charif, A., El Bchari, F., and Chaïbi, M., 2014, Remote sensing and GIS contribution to the investigation of karst landscapes in NW-Morocco: Geosciences, Vol. 4(2), p. 50-72.

Yilmaz, I., 2007, GIS-based susceptibility mapping of karst depression in gypsum: a case study from Sivas basin (Turkey): Engineering Geology, Vol. 90(1-2), p. 89-103.

Oklahoma Geological Survey Circular 113, 2021

Gypsum Karst in South-Central Kansas

Kaitlyn L. Gauvey and Jonathan B. Sumrall
Department of Geosciences, Fort Hays State University,
Hays, Kansas

ABSTRACT.—Field reconnaissance examining the Permian Blaine Formation and the karst features within those rocks was conducted on two ranches in Barber County, Kansas. Karst features are developed dominantly in gypsum and include caves, sinkholes, losing streams, springs, and other surficial karst features. The Blaine Formation is known as a significant karst unit in Oklahoma; however, little work has been conducted in Kansas. The thickness of the various facies of the Blaine Formation thins from Oklahoma into Kansas from 27 to 15 meters thick (90–50 feet). This study documents the local distribution of karst features and determines the controls on formation, distribution, and surface expression in the Blaine Formation.

INTRODUCTION

Evaporite deposits are sediments that form because of the precipitation of salts out of evaporating water. The primary evaporite rocks are gypsum, anhydrite, and halite. Most evaporite rocks are highly soluble and dissolve by simple ionic dissolution. Karst is a landscape underlain by soluble rock that has dissolved producing karst landforms such as sinkholes, caves, and springs. Evaporite-karst features can form rapidly in a matter of weeks because of the high solubility, whereas carbonate-karst features typically take centuries to develop (Johnson, 1996). Gypsum deposits are found in 32 of the 48 conterminous United States and underlie approximately 35–40% of the land area (Johnson, 1992). Much of the United States midcontinent is composed of Mid-Permian red beds and evaporites as subsurface and surface deposits (Walker, 1967). These evaporites are widely distributed in the United States and most contain karst features (Fig. 1). Quinlan and others (1986) give an overview of evaporite karst in the United States, and White (1988) provides a good overview of karst processes in evaporite rocks.

The landscape of south-central Kansas is dominated by red cedar trees, buttes, mesas, and canyons. The buttes are capped by pale blue-gray gypsum/anhydrite, and their slopes consist of highly friable red mudstone and fine red sandstone (Benison and others, 2015). The underlying evaporites and associated red beds create a topography that does not fit the conventional portrayal of the Great Plains landscape of Kansas. This physiographic region, called the Gypsum Hills, is located in Clark, Comanche, Barber, and Harper Counties of Kansas and is referred to as the Gypsum Hills. The Gypsum Hills is aptly named because of the vast natural gypsum deposits in the area. The National Gypsum Mine in Barber County mines the Medicine Lodge Gypsum member of the Permian Blaine Formation (Benison and others 2015). The Gypsum Hills is also referred to as the Red Hills due to the iron-oxide-rich soil, and the land in this region is mostly used as open rangeland.

The Kansas Geological Survey lists the south-central region of Kansas containing over 200 caves, yet there have been no documented karst studies in south-central Kansas (Young and Beard, 1993). The objective of this

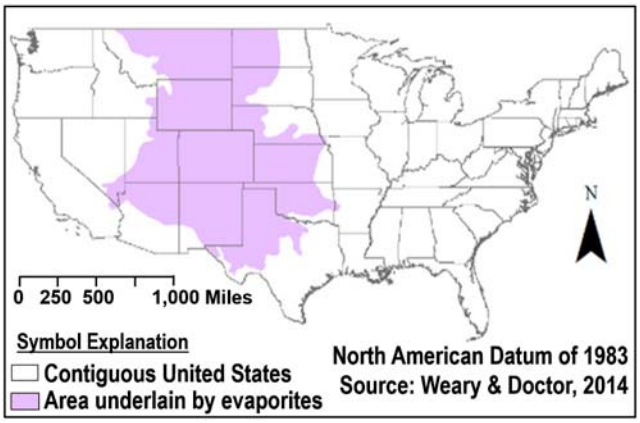

Figure 1. Subsurface evaporite deposits distribution in the western part of United States (modified from Doctor and Weary, 2014).

Gauvey, Kaitlyn L.; and Sumrall, Jonathan B., 2021, Gypsum Karst in South-Central Kansas, *in* Johnson, K. S.; Land, Lewis; and Decker, D. D. (eds.), Evaporite Karst in the Greater Permian Evaporite Basin (GPEB) of Texas, New Mexico, Oklahoma, Kansas, and Colorado: Oklahoma Geological Survey, Circular 113, p. 305–317.

study is to locate and document the local distribution of karst features in Barber County, Kansas to further understand the mechanism of gypsum karst formation within the Permian Blaine Formation (Fig 2). This study also seeks to understand distribution and surface expression of karst features.

GEOLOGIC SETTING

The midcontinent of North America contains extensive Pangean red beds and evaporites, which include the Nippewalla, Quartermaster, Opeche, Chugwater, Spearfish, and Goose Egg strata (Tomlinson, 1916; Mudge, 1967; Walker, 1967; Holdoway, 1978; Turner, 1980; Glennie, 1987; Nance, 1988; Golonka and Ford, 2000; Benison and Goldstein, 2000, 2001; Zharkov and Chumakov, 2001; Roscher and Schneider, 2006; Benison and others, 2015; Johnson, 2021). These evaporites were deposited in the Greater Permian Evaporite Basin (GPEB), extending from west Texas and southeast New Mexico into western Oklahoma, western Kansas, and southeastern Colorado (Johnson, 2021). In Kansas, the mid-Permian Nippewalla Group was deposited in a series of basins (Syracuse Basin, the Hugoton Embayment of the Anadarko Basin, the Cimarron Basin, the Salina Basin, and the Sedgwick Basin) bounded by the Las Animas Arch to the West, and the Nemaha Anticline to the east (Fig. 2) (Merriam, 1962; Maughan, 1967; Mudge, 1967; Holdoway, 1978).

The Nippewalla Group contains alternating bedded evaporites (mainly gypsum), red-bed mudstones, siltstones, and sandstones in outcrop. Much of the Nippewalla Group is found in the subsurface reaching thicknesses greater than 150 m. Surficial outcrops in south-central Kansas and northwestern Oklahoma are thinner due to halite dissolution (Benison and Goldstein, 2001; Benison and others, 2015). The Nippewalla Group is divided into six formations listed in ascending order: the Harper Sandstone, Salt Plain Formation, Flowerpot Shale, Cedar Hills Sandstone, Blaine Formation, and Dog Creek Formation (Fig. 3). Erosion and halite

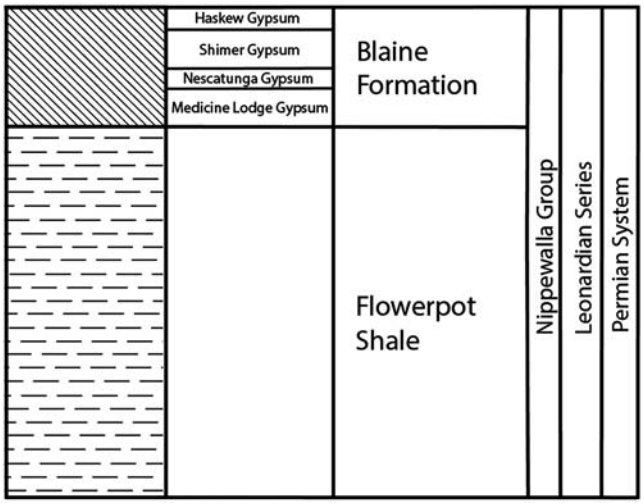

Figure 3. Simplified stratigraphy of the study area (after Norton, 1939).

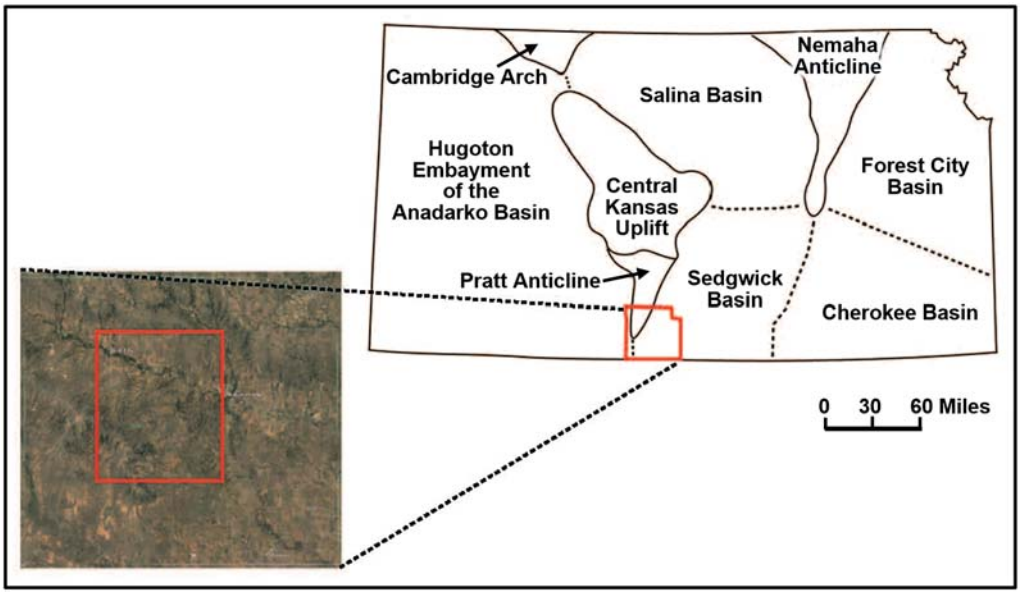

Figure 2. (Left) Aerial photo of the study area shown in red. The Medicine Lodge river runs from the northwest extent of the mapping area into the small town of Medicine Lodge in the east. (Right) Map depicting the structural geology of Kansas. Barber County is located in the south-central region (red). The Hugoton embayment of the Anadarko Basin is located to the West, the Pratt anticline plunges to the south, and the Sedgwick basin is located to the east. Modified from Merriam, 1962.

dissolution have altered the surface exposures so drastically that correlating core with outcrops by lithological association and/or thickness is problematic (Benison and others, 2015). Surficial outcrops of the Nippewalla Group in south-central Kansas total 284 m thick; however, the six formations are relatively similar to one another in lithologies, and thickness estimates in the field area of Kansas and Oklahoma are controversial because of the previously mentioned issues (Holdoway, 1978; Benison 1997a, b; Benison and others, 2015).

Mid-Permian evaporite karst has been intensively studied in western Oklahoma and Texas (Jordan and Vosburg, 1963; McGregor and others, 1963; Myers and others, 1969, Johnson, 1972, 1981, 1986, 1990a, 1990b, 1991, 2003, 2021; Gustavson and others, 1982; Bozeman, 1987; Runkle and Johnson, 1988, Hovorka and Granger, 1988; Bozeman and Bozeman, 2002). Earlier studies dealing with south-central Kansas are by Merriam and Mann (1957) and Young and Beard (1993). Merriam and Mann (1957) discuss notable solution subsidence and collapse features in the Gypsum Hills (most notably the natural bridges). Young and Beard (1993) propose a simplistic model for Kansas gypsum speleogenesis, where solutionally enlarged joints pirate surface water into conduits that extend into nearby canyons, but they did not list any quantitative data or evidence for these claims.

The Greater Permian Evaporite Basin is the site for deposition of the Permian Blaine Formation. There are two prominent gypsum cave systems in Oklahoma: J.C. Jester Cave is located in southwestern Oklahoma, and Alabaster Caverns of Northwestern Oklahoma (Bozeman, 1987; Bozeman and Bozeman, 2002; Bozeman, 2003; Johnson, 1992, 2018). J.C. Jester Cave is one of the longest gypsum caves in the western hemisphere (6.25 Miles) (Bozeman, 1987). Alabaster caverns are a collection of caves in Alabaster Caverns State Park. Caves in this region form in the basal gypsum bed of the Blaine Formation (Johnson, 1996, 2018).

The climate of the region has transitioned into an arid to semiarid desert within the last 10,000 years (Hill, 1996). The region has a humid subtropical climate with hot, humid summers averaging 35°C and cold, dry winters averaging –5 °C (NOAA, 2018). The average annual precipitation is 737 mm (29 inches) with the US average of 990 mm (39 inches) of rain per year (NOAA, 2018).

PERMIAN BLAINE FORMATION OF BARBER COUNTY

Divisions of the Blaine

The Blaine Formation consists of about 15 meters of massive gypsums, thin dolomites, and brown-red shales in south-central Kansas and thickens up to 27 meters in northern Oklahoma (Fay, 1964). Anhydrite, instead of gypsum, is ordinarily present in the Blaine where the unit is more than 10–60 m below the land surface (Johnson, 1992). The Blaine Formation is exposed in Barber, Comanche, and Kiowa Counties of Kansas and is divided into four members in descending order: the Haskew Gypsum, Shimer Gypsum, Nescatunga Gypsum, and Medicine Lodge Gypsum (Norton, 1939) (Fig. 3). The Blaine Formation extends from Kansas across western Oklahoma and into the Texas Panhandle, making it one of the most extensive and easily traced formations of the Permian red beds.

The Haskew Gypsum is the upper member of the Blaine Formation and consists of 0.30 meters (<1ft) of gypsum and 1.5 meters (5 ft) of brown-red shale (Fig. 3). In south-central Kansas, most of the gypsum has been removed by dissolution (Moore and others, 1951). The Shimer Gypsum Member underlies the Haskew Member and consists of 4–7 meters (13–23 ft) of massive gypsum overlying one foot of dolomite; however, much of the gypsum has been removed by dissolution (Moore and others, 1951). The Nescatunga Gypsum Member consists 1.5 meters of gypsum between 8 feet of red shale. The Nescatunga and Shimer Gypsum beds are not present in Barber County (Moore and others, 1951).

The Medicine Lodge Gypsum Member, named after the city of Medicine Lodge in Barber County, is the thickest bed of gypsum in the study area, measuring up to 9 meters (30 feet) (Moore and others, 1951). The Medicine Lodge Gypsum is underlain by 0.30 meter of oolitic/pellitic dolomite called the Cedar Springs Dolomite (Fay, 1964). The Cedar Springs Dolomite grades from an oolitic dolomite into a light gray, fine-grained, non-fossiliferous, dolomitized mudstone (Fay, 1964). The base of the mudstone contains dolomitized pelletoid grains that grade upward into coarse-grained dolomite rhombs with an increase in anhydrite content (Holdoway, 1978). Benison and others (2015) describe a 0.15 m thick carbonate unit as the Microcodium-rich Cedar Springs Dolomite at the base of the Blaine formation. X-ray diffraction (XRD) and petrographic observations by Benison and others (2015) indicated there is no dolomite in this member. The Cedar Springs Dolomite was shown to be composed of subequal parts of calcite crystals (attributed to the Microcodium) and gypsum/anhydrite, with detrital quartz and hematite-rich silt (Benison and others, 2015).

The underlying Flowerpot Shale consists of 55 meters of friable, red-brown gypsiferous shale and thin layers of green-gray silty shale with a few thin beds of sandstone and siltstone (Bayne and others, 1968; Johnson, 1992). The formation is cut by intersecting veins of satin spar gypsum (Bayne and others, 1968). Selenite crystals and satin spar veins are commonly found in eroded

hillsides. Outcrops are restricted to Barber and Comanche Counties (Moore and others, 1951).

Deposition of the Blaine

South-central Kansas was situated between 0°S and 5°S latitude during the mid-Permian (Golonka and others, 1994). The depositional environments of the Nippewalla Group were a series of extremely acid saline ephemeral lakes, mudflats, sandflats, paleosols, and eolian dunes (Benison and others, 1998, 2013; Benison and Goldstein, 2001; Sweet and others, 2013; Foster and others, 2014). The most direct chronological analysis by magnetostratigraphy of the Nippewalla Group, the Dog Creek Shale Formation, suggests deposition during the Leonardian and Guadalupian (276–267 Ma) (Foster and others, 2014).

In central Oklahoma, the Blaine Formation contains bivalve-rich dolomite beds; however, in Kansas, the only carbonates reported are dolomitized mudstones or Microcodium-rich calcretes (Fay, 1964; Benison and others, 2001). Fay (1964) indicates a 0.30 m of light gray oolitic/pelletic dolomite bed at the base of the Medicine Lodge Gypsum. Benison and others (2001) do not identify an oolitic/pelletic dolomudstone, but a Microcodium-rich calcrete located in the red siliciclastics that do not contain dolomite.

STRUCTURAL AND DIAGENETIC HISTORY

Barber County lies on the southern extent of the Pratt Anticline (Fig. 2). The Pratt Anticline is a post-Mississippian extension of the Central Kansas uplift and separates the Hugoton Embayment from the Sedgwick Basin (Merriam, 1962). Cretaceous-aged strata unconformably overlie Permian-aged strata because of the post-Mississippian uplift and subsequent erosion of Triassic and Jurassic-aged strata during the Cretaceous (Western Interior Seaway) (McLaughlin, 1942; Merriam, 1955; Merriam, 1957). Quaternary glacial deposits unconformably overlie Cretaceous-aged strata. Post-Pleistocene glacial and associated fluvial deposits mark a stark change in climate (Norton, 1939).

In the subsurface, the Nippewalla Group contains massively bedded and displacive halite, whereas surficial outcrops of the Permian Nippewalla Group have undergone late-stage dissolution of halite cement (Benison and others, 2015). Gypsum/anhydrite caprocks and slope-forming siliciclastics are clues to past halite cement in the siliciclastics (Benison and others, 2015). Surface section measurements in central Kansas reveal depositional and early diagenetic halite, such as pseudomorphs after displacive and chevron halite. Collapse structures in south-central Kansas are evidence of dissolution of bedded halite close to the surface.

KARST FORMATION IN SOUTH-CENTRAL KANSAS

Young and Beard (1993) documented 205 caves found in Barber County. These caves were reported to be found within or near the walls of canyons, and many of the steep-walled canyons represent unroofed caves. The large dendritic canyons were interpreted to be relict caves that were subsequently unroofed as surface denudation and valley erosion took place. South-central Kansas was known for natural bridges that form by the solution of Permian gypsum (Merriam and Mann, 1957; Young and Beard, 1993; Benison and others, 2015). Many of the famed natural bridges have since collapsed. The Sun City Natural Bridge was the most significant natural bridge in Barber County; it measured 55 feet long (Jewett, 1935), and collapsed in 1962.

MATERIALS AND METHODS

Site Descriptions

Two privately owned ranches located west of Medicine Lodge were used in this study. Property owners have asked not to have their exact geographic location revealed for privacy. Specific cave locations have been removed to protect these features. Property One is located south of US Highway 160 and includes 16 km^2 (4,000 acres) of mostly open rangeland. Bedrock at Property One is mantled with a thin veneer (0.15 m) of clayey loams. Property Two is located north of US Highway 160 and includes over 28 km^2 (7,000 acres) of mostly open range pasture land. The bedrock at Property Two is highly mantled with sandy loam and marks a stark contrast to the thinly mantled Property One just 10 kilometers (6 mi) southeast.

Field Methods

Rock sampling and cave surveying were conducted in the summer of 2018. Previous exploration and documentation of south-central Kansas have been done by members of the Kansas Speleological Society (KSS); however, the KSS has not explored south of Highway 160 (Property One). Rock samples were collected from key outcrops within caves to distinguish petrographic controls on passage morphology. Twelve samples were obtained from the cave ceiling (proto-channels), "ledges," and wall (Fig. 4). These bulk samples were large enough to create one- by two-inch thin sections and leave enough material for mineralogical and geochemical analyses.

Most cave and karst features located were surveyed using standard cave survey techniques as documented by Dasher (1994). Plan sketches and cross sections of each cave were created to document cave passage

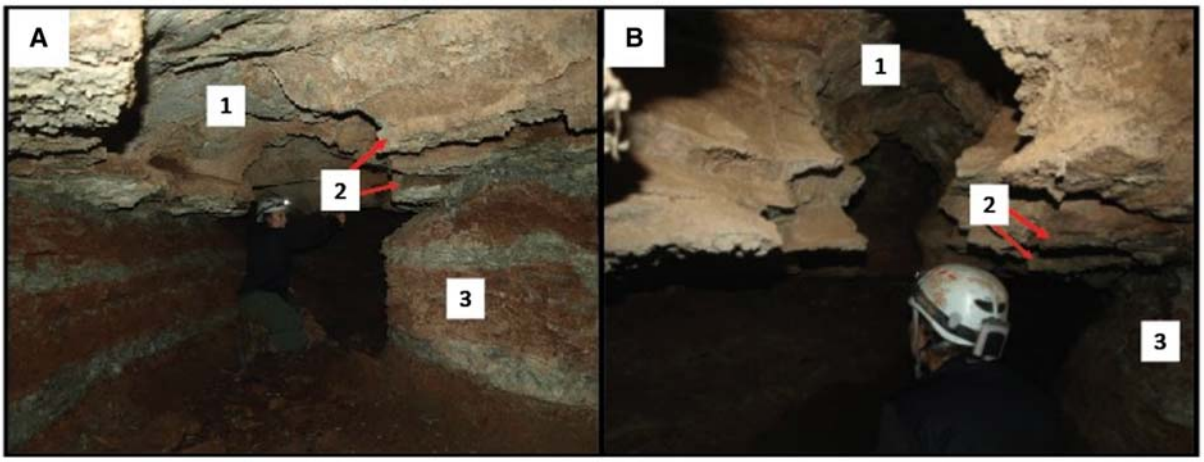

Figure 4. Cave passage morphologies. Left (A) shows 1) Proto-channel, 2) Cave Ledge, 3) Cave wall. Right (B) depicts 1) Proto-channel (tube-shaped), 2) Cave Ledge, 3) Cave wall.

morphology and passage orientation. The locations of karst features were documented with a handheld Global Positioning System (GPS) unit, recorded as UTM coordinates, and stored in a relational database to be used within a Geographical Information System (GIS) to generate maps. Georeferenced LiDAR Data were used to correct erroneous points (Access, 2011).

Laboratory Methods

Twelve samples were made into standard thin sections. Cave "ledge" samples were stained with alizarin red-S to distinguish the presence of dolomite and calcite (Dickson, 1966). Samples were powdered for XRD using a low-speed dental drill and sieved through 250 μm, 125 μm, and 63 μm sieves for routine qualitative evaluation of mineral components. Bulk mineralogy was analyzed for mineralogy using a Rigaku diffractometer with Cu Kα radiation and internal quartz standard.

RESULTS

Field Results

Field reconnaissance identified 62 karst features, including 18 open sinkholes (i.e., caves or smaller solutional conduits that connect directly to sinkholes), 9 filled sinkholes, 14 caves with no associated sinkhole, and 13 springs. Ten of the 18 sinkholes contained caves that were large enough for humans to enter. Caves were developed at the geologic contact between the Medicine Lodge Gypsum Member and the Flowerpot Shale. Filled sinkholes were generally found in the sandy loam mantled material on Property Two. Sinkhole complexes and associated caves were primarily on Property One where the gypsum is exposed or thinly mantled. Cave passage length measures 78 m (256 ft) with vertical extents of 4 m (14 ft). The average cave volume was 35.25 m^3 (1,245 ft^3) with the average cave area being 104 m^2 (1,119 ft^2). Cave entrances are found at the geologic contact between the Medicine Lodge Gypsum and Flowerpot Shale, within sinkholes, or near canyon walls. Cave entrances are formed mainly by cover/ceiling collapse or cliff retreat.

Cave Morphology

On both properties, cave entrances are found near cover-collapse sinkholes or where surface denudation has breached the cave. Entrances typically contain a solutionally enlarged fracture in the gypsum. Cave passages follow joint sets, and where these joint sets meet, passages extend vertically, in some cases up to 4 meters (14 ft) (Fig. 5). Passages are generally short (ranging from to 1.5 to 78 m), straight to slightly sinuous, and are oriented along joints that have sharp, orthogonal bends at joint intersections. Several caves are "through-caves" that have only two entrances (one collection sink and one resurgence) (Jennings 1971; Klimchouk, 1996b).

Passages morphologies are commonly controlled by bedding planes between the Medicine Lodge Gypsum and the Flowerpot Shale (Fig. 4). Tube-shaped proto-conduits or "ceiling channels" form in the Medicine Lodge Gypsum Member, measure 0.3–0.6 meters in diameter, and follow ceiling joints (Fig. 4). Carbonate ledges occur between the Medicine Lodge Gypsum and the Flowerpot Shale. The ledges form resistant beds that protrude out into the cave passage (Fig. 4). The underlying Flowerpot Shale is friable and contains abundant satin spar gypsum stringers, masses of selenite gypsum, and laminations of bleached-gray shale. The Flowerpot Shale portion of the cave passage is commonly wider than the passage developed in overlying strata.

Active water seeps are commonly seen at the contact between the carbonate ledge and the Flowerpot Shale,

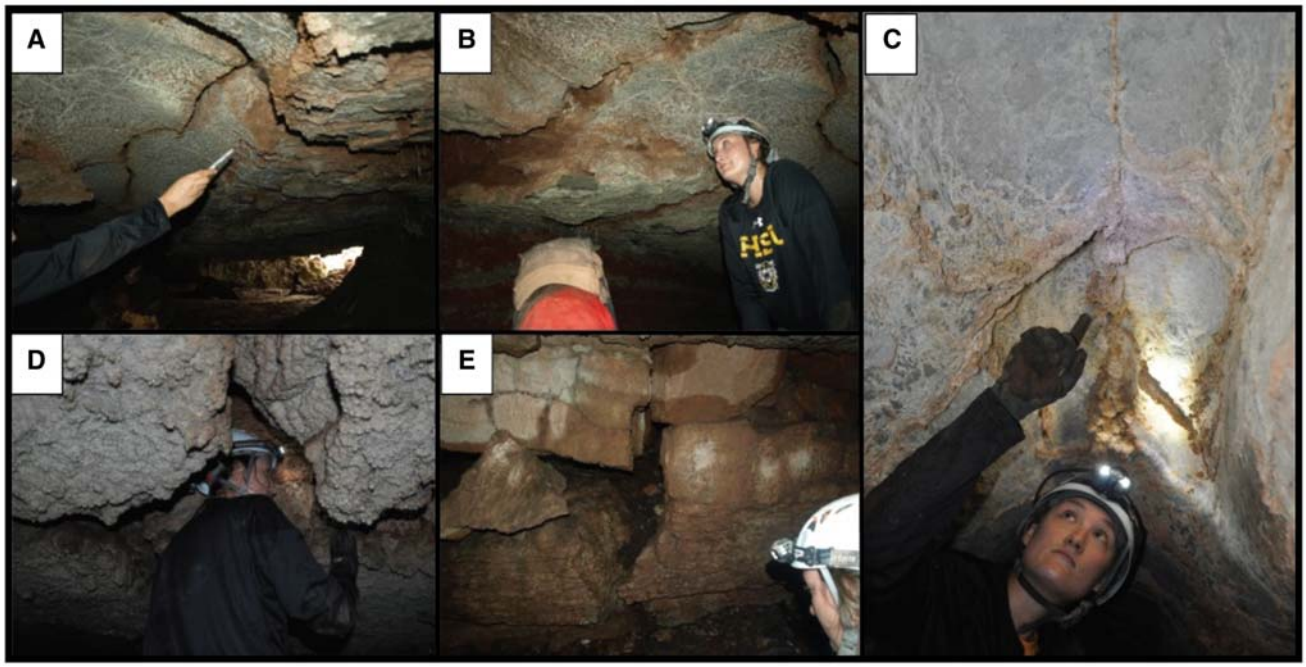

Figure 5. A) and B) Ceiling channel in Medicine Lodge Gypsum following ceiling fracture. C) Ceiling channel in the Medicine Lodge Gypsum following a ceiling fracture. Scallops are observed on the wall. D) Joint set intersection in the Medicine Lodge Gypsum that extends 14- feet vertically. E) Joint set intersection where water is seeping into the cave toward a standing pool of water. Scallops are observed on the walls.

and most caves contain standing pools of water year-round. Scallops were observed on gypsum passage walls and on recent breakdown blocks.

Sinkhole Morphology

Solutional sinks form atop the buttes and mesas within the Medicine Lodge Gypsum. Sinkholes on Property One are expressed far differently than those on Property Two. On Property Two, sinkholes are highly mantled with a sandy aggregate mantle creating an easily identifiable depression. On Property One, the bedrock is exposed with a thin veneer of loamy soil, creating sinkhole complexes that are not easily identified as sinkholes due to their dendritic shape (Fig. 6). Sinkhole complexes form in the upper valley, where slightly mantled material is funneled into solutionally enlarged surface joints (Fig. 7). Joints pirate surface water into sinkholes and surface fractures. Surface water is directed into cave systems, where they flow through the caves into the erosional valleys below.

PETROGRAPHIC AND MINERALOGIC RESULTS

Cave Ceiling

The base of the Medicine Lodge Gypsum is a host for ceiling channel formation. Megascopically, the gypsum is soft, buff to gray, and microcrystalline. Anhedral secondary granular gypsum replacement crystals are abundant in all cave ceiling/proto-channel samples (Fig. 8A). These crystals range in size from 0.05 to 5 mm. Subhedral to anhedral gypsum laths measuring up to 2 mm are scattered throughout (Fig. 8A). Anhedral dolomite inclusions are present measuring up to 2 mm (Fig. 8A). Patchy iron oxide staining is common; however, anhydrite was not identified in any of the samples.

Cave "Ledge"

Megascopically, the carbonate layer is dark gray mudstone. The "ledge" lithology ranges from dolomicrite to laminated peloidal dolomicrite (Fig. 8B). The matrix is composed of anhedral dolomite crystals measuring up to 1 mm and composes > 90% of the samples. These crystals are sucrosic near the base and progressively increase in secondary granular gypsum and iron oxides are moving stratigraphically upward. Euhedral dolomite cements measuring up to 1 mm commonly fill pores. Staining indicates the presence of dolomite, which is confirmed by XRD analysis.

Cave Wall

Megascopically, the cave wall is composed of red to bleached gray shale interbedded with satin spar stringers and selenite crystals. Samples were obtained from more-indurated shale units within the cave passage. Sampling was biased because of poor induration and friability.

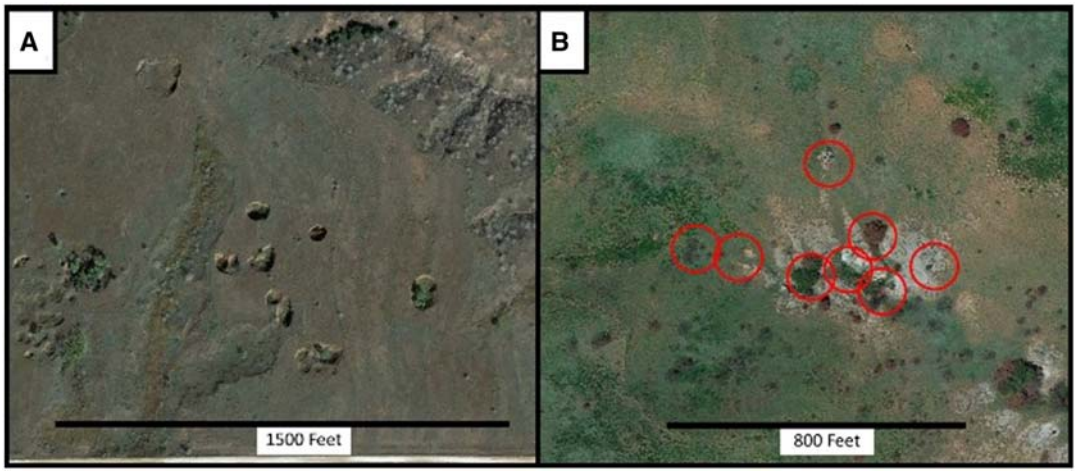

Figure 6. Sinkhole complexes in the two regions of the study area. A) Northern portion of the study area where mantle material is thicker and produces more distinct sinkholes. Notice the two generations of sinkholes. The first generation represents collapse and reworking to form a dendritic pattern. The second generation represents recent collapse because of mining activities in the area. B) Southern portion of the study area when mantle material is thin or lacking. Sinkholes are less noticeable, so their locations have been circled.



Figure 7. Various sinkholes in Barber County. A) Sinkhole complex in a thicker sandy loam-mantled sinkhole complex. These sinkholes do not have bedrock exposed in the bottoms. B) Slightly mantled sinkhole complex with exposed bedrock. Mantled material is a clayey loam. C) Exposed bedrock covers collapse sinkhole. The mantle material has been stripped by surface erosion by the adjacent stream. There is a cave entrance in the bottom of this sinkhole that feeds a stream passage.

In thin section, secondary granular gypsum composes > 90% of the bulk mineralogy. Subhedral satin spar gypsum laths measuring up to 2 mm are found. Subhedral to anhedral dolomites (1 mm) are found. Euhedral anhydrite ghosts are replaced with secondary granular gypsum (Fig. 8C). Insoluble iron oxides commonly fill fractures.

DISCUSSION

In this region of Barber County, cave formation is primarily dependent on the geologic contact between the Medicine Lodge Gypsum and Flowerpot Shale. Solutionally enlarged joints observed on the surface follow the same trend as fractures seen in cave passages

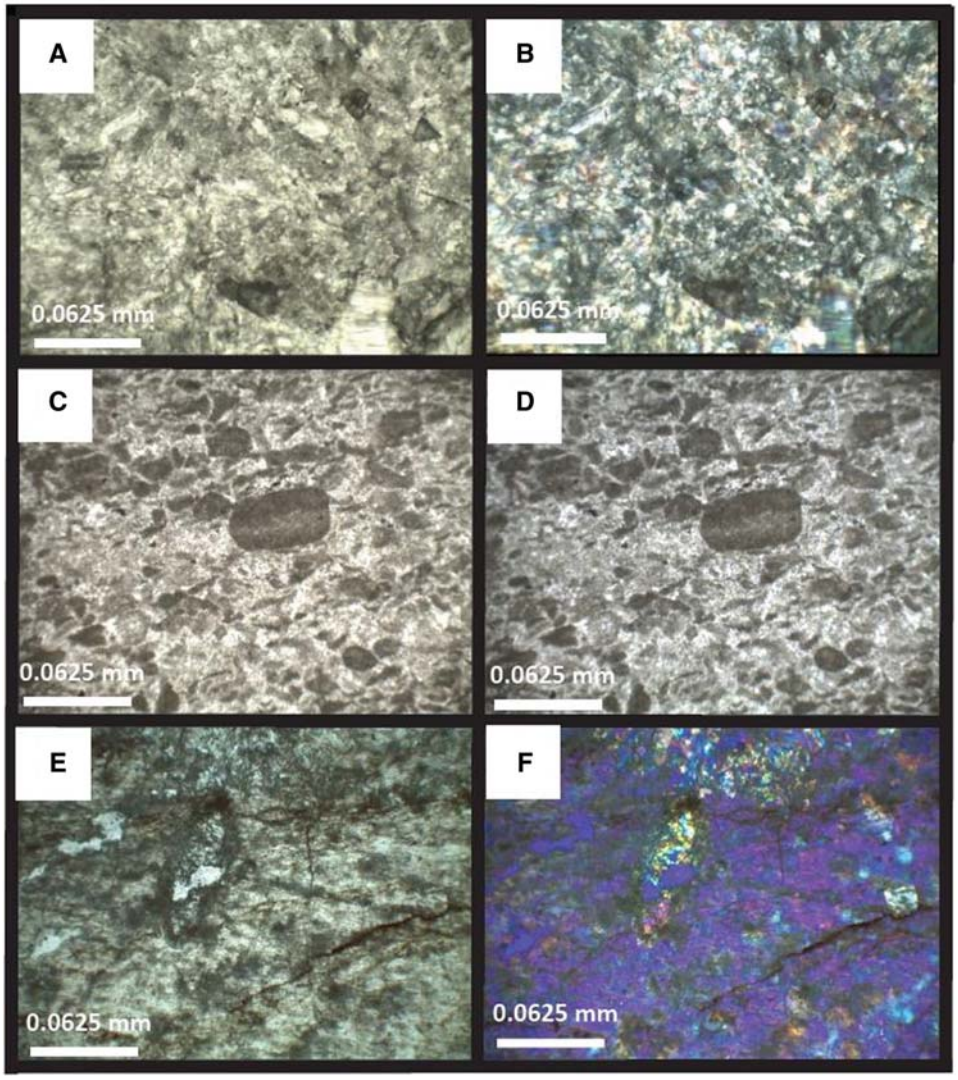

Figure 8. A) Cave ceiling sample in plane polarized light. Secondary granular gypsum matrix with euhedral dolomite inclusions. B) Same cave ceiling sample in cross-polarized light. C) Cave ledge sample in plane-polarized light. Pelloids are laminated and are completely dolomitized with a sucrosic texture. D) Same cave ledge sample in cross-polarized light. E) Cave wall sample in cross-polarized light. An euhedral anhydrite ghost can be observed. The cave wall is mostly composed of selenite gypsum, satin spar gypsum, and Fe-oxide rich clay. Fe-oxides commonly fill fractures. F) Same cave wall sample in cross-polarized light with the gypsum plate inserted. An anhydrite ghost is replaced with secondary granular gypsum.

(Fig. 9). Proto-channels are observed in the Medicine Lodge Gypsum outcrops along (Fig. 4). Surface water is pirated through solutionally enlarged joints and forms conduits within the Medicine Lodge Gypsum (Fig 7). The conduit entrenches into the underlying carbonate layer (Fig. 4). This carbonate layer forms a resistant ledge that is present in every cave. Further entrenchment into the underlying Flowerpot Shale widens the cave passage, creating the "ceiling channel" appearance. The ledge represents the geologic contact between the Cedar Springs Dolomite and the Flowerpot Shale.

X-ray diffraction and petrographic observations of the carbonate layer agreed with Fay (1964) observations of dolomite and gypsum. Fay (1964) described the basal dolomite layer as the Cedar Springs Dolomite to be an oolitic dolomudstone grading into a pelletoid dolomitized mudstone. Petrographic observations did not support the presence of ooids; however, pelloids were observed. This basal carbonate unit is established as the Cedar Springs Dolomite based on XRD and petrographic observations. Benison and others (2015) report XRD and petrographic observations of the Cedar Springs Dolomite as not containing dolomite, but containing calcite-rich Microcodium structures. These findings suggest that Benison and others (2015) were not at the geologic contact between the Medicine Lodge

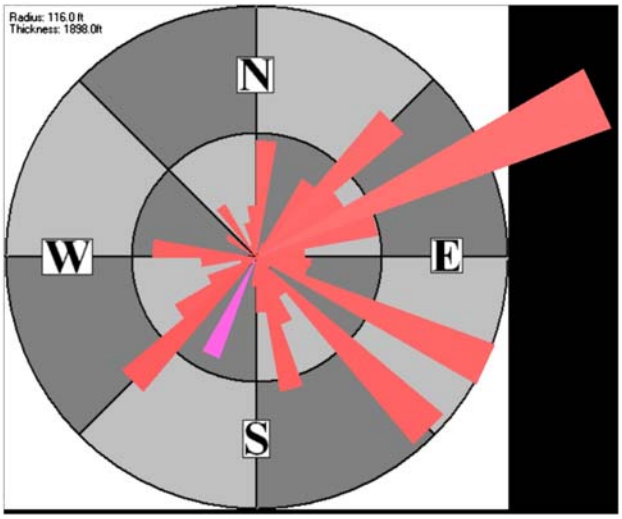

Figure 9. Compass 3D Rose diagram of fractures seen in cave passages. There are a total of 122 passage hots. Surface outcrop joint sets measure: 50W/160 and 40E/030. Cave passages typically follow similar trends because of ceiling fractures. Joint sets that intersect are primarily solutionally enlarged and form upper passages.

Gypsum and Flowerpot Shale. Overall, the stratigraphy of south-central Kansas is difficult to correlate because of the high solubility of the gypsum and underlying gypsiferous shale. Caves in this study form at the geologic contact between the Medicine Lodge Gypsum and Flowerpot Shale. The presence of karst features may be a key in determining stratigraphic location for the region.

A simplistic model for this area's gypsum speleogenesis is proposed (Fig. 10). Cave passage morphology is dependent on solutionally enlarged joints that transmit the overlying mantled material and allogenic water into conduits. Proto-conduits develop at the base of the Medicine Lodge Gypsum and reach the resistant Cedar Spring Dolomite. Vadose entrenchment through the Cedar Springs Dolomite forms a resistant ledge. Further entrenchment into the Flowerpot Shale mechanically erodes the shale layers and dissolves gypsum stringers. Cave passage morphology is mainly dependent on differential erosion between the Flowerpot Shale and the Cedar Springs Dolomite. This study agrees with Young and Beard (1993) model for Kansas gypsum speleogenesis and resulting geomorphology of the area based on field observations. Surface streams are partially pirated by surficial joints in the exposed gypsum and pirated into enlarged joints that flow through caves and exit into the walls of a canyon. In the field, sinkholes and caves form at the upstream end of dendritic canyons and appear to pirate surface water and mantled soil.

Field reconnaissance determined that every upstream end of an erosional valley did not reveal a new cave, as

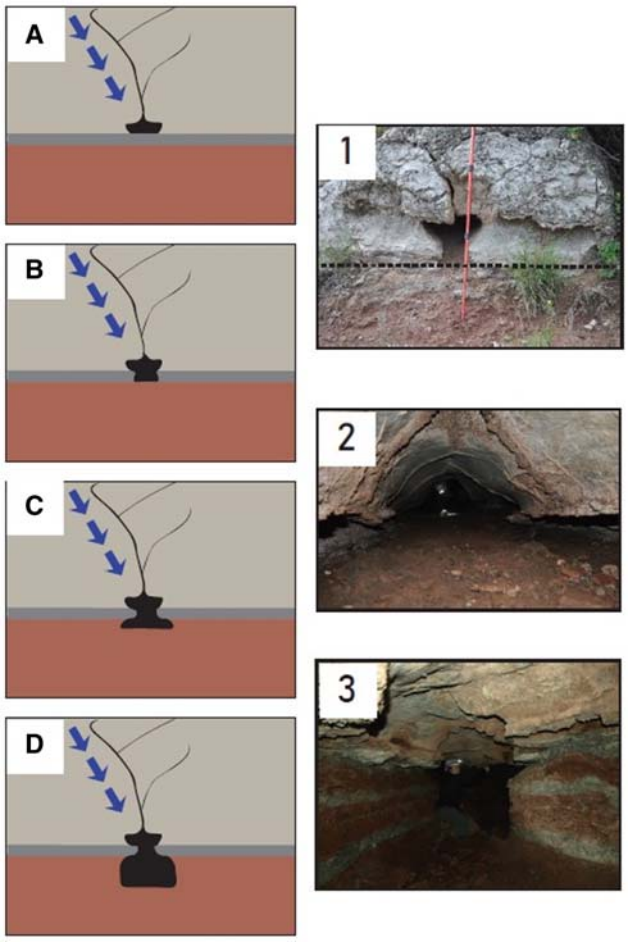

Figure 10. Simplistic model depicting gypsum speleogenesis in Barber County. A) Surface fractures and solutionally enlarge joints. Shown in 1, a proto-channel develops at the geologic contact between the Medicine Lodge Gypsum and Flowerpot Shale (approximate contact in dashed line). B) Vadose entrenchment into the underlying Cedar Springs Dolomite layer. The dolomite forms a resistant ledge seen in 2. C) Further vadose entrenchment into the underlying Flowerpot shale mechanically erodes the shale nearest the dolomite ledge. D) This erosion widens the passage. Erosion and dissolution of gypsum further entrench the passage seen in 3.

Young and Beard (1993) proposed. Exposed outcrops of gypsum in the southwestern portion of Property One did not contain caves. This area has been interpreted to be higher in the Blaine stratigraphic section. Aerial imagery shows an abundance of exposed gypsum bedrock in the southwest (Property One); however, the geologic contact between the Medicine Lodge Gypsum, Cedar Springs Dolomite, and Flowerpot Shale was not present. As documented in this study, cave formation is heavily dependent upon this geologic contact between bedding planes, and no karst features are found without this geologic contact.

Remnant caves, or shelter caves bordering the erosional valleys, are relatively small and contain the same features as a larger cave (i.e., the geologic contact between the Medicine Lodge Gypsum, Carbonate Ledge, and Flowerpot Shale). These caves likely represent larger caves that have been lost to cliff retreat. This process is evident by the large boulders found on the valley floors that are composed of Medicine Lodge Gypsum.

Sinkhole complexes form in the upper valley where mantled material is funneled into solutionally enlarged surface joints (Figs. 6, 7). Joints pirate surface water and soil into sinkholes and surface fractures. Surface water is directed into cave systems and flows into the valleys below through these caves. These karst features appear to be hydrologically connected.

CONCLUSION

This survey of caves and karst landforms adds significantly to the basic knowledge of the geology of this region. Field observations indicate cave formation is dependent on (1) the geologic contact between the Permian Blaine Formation and the underlying Flowerpot Shale, (2) the amount and type of surficial mantle material, and (3) solutionally enlarged fractures that enable water flow.

Surface fractures pirate surface water into solutionally enlarged joints or insurgences. Solutionally enlarged joints are necessary for enlargement of solutional sinks or conduits. Proto-conduits form at the base of the Medicine Lodge Gypsum and entrench into the underlying carbonate layer. Resistant carbonate ledges underlying the Medicine Lodge Gypsum were determined to be the Cedar Springs Dolomite, as described by Fay (1964). Further entrenchment into the underlying Flowerpot Shale widens the passage by mechanical erosion and dissolution of satin spar gypsum stringers.

Various sinkhole morphologies were formed by the amount and type surficial mantle material. Property One was slightly mantled with a thin, clayey loam, whereas Property Two was highly mantled with a thicker sandy loam. These sinkhole complexes form in the exposed gypsum bedrock near the top of valleys and are commonly associated with cave entrances.

Petrologic and XRD observations confirm the presence of dolomite and inclusions of gypsum within the carbonate layer. This carbonate layer was interpreted to be the Cedar Springs Dolomite as described by Fay (1964). Ooids and Microcodium structures were not observed as described by Fay (1964) and Benison and others (2015). Petrographic observations within samples of the cave wall confirm the replacement of anhydrite by gypsum.

The distribution of karst features is controlled by stratigraphy and surface denudation. Insurgent caves entrances are found where bedrock is thinly mantled and are commonly associated with sinkhole complexes that remove mantled material, whereas resurgent cave entrances occur in valley walls. Caves preferentially form at the geologic contact between the Medicine Lodge Gypsum and Flowerpot Shale and contain similar passage morphologies (i.e., proto-conduits, carbonate ledges, widened cave wall). Stratigraphy is difficult to determine because of fast rate of erosion of gypsum and shale beds; however, the presence of karst features at this geologic contact can aid in determining stratigraphy.

It is hoped that this investigation of the caves and karst of Barber County is a valuable addition to the limited literature in this region and also that it can act as a foundation for much- needed further investigation. Future research, including dye tracing, shallow geophysical exploration, sinkhole distribution, and petrographic controls on speleogenesis, will build upon this research.

ACKNOWLEDGMENTS

We would like to thank Dr. James Murowchick from the University of Missouri-Kansas City for analyzing samples used in this study. We would also like to thank the property owners; without their guidance, my vehicle would have remained in a pasture.

REFERENCES CITED

Access, K.D., 2011, Support Center. 2015. State of Kansas GIS Data Access and Support Center.

Bayne, C.K., Goebel, E.D., Jewett, J.M., O'Connor, HG., Swineford, A., and Zeller, D.E., 1968, The stratigraphic succession in Kansas: Kansas Geological Survey, Bulletin 189, 81 p.

Benison, K.C., 1997a, Field descriptions of sedimentary and diagenetic features in red beds and evaporites of the Nippewalla Group (middle Permian), Kansas and Oklahoma: Kansas Geological Survey, Open File Report 97-21, 62 p.

Benison, K.C., 1997b, Acid lake and groundwater deposition and diagenesis in Permian red bed-hosted evaporites, midcontinent, U.S.A.: unpublished Ph.D. dissertation, The University of Kansas, Lawrence, KS, 480 p.

Benison, K.C., 2013, Acid saline fluid inclusions: examples from modern and Permian extreme lake systems: Geofluids, Vol. 13, p. 579-593.

Benison, K.C., and Goldstein, R.H., 2000, Sedimentology of ancient saline pans: an example from the Permian Opeche Shale, Williston Basin, North Dakota, USA: Journal of Sedimentary Research, Vol. 70, p. 159-169.

Benison, K.C., and Goldstein, R.H., 2001, Evaporites and siliciclastics of the Permian Nippewalla Group of Kansas, USA: a case for non-marine deposition in saline lakes and saline pans: Sedimentology, Vol. 48, p. 165-188.

Benison, K.C., and Goldstein, R.H., 2002, Recognizing acid lakes and groundwater in the rock record: Sedimentary Geology, Vol. 151, p. 177-185.

Benison, K.C., Goldstein, R.H., Wopenka, B., Burruss, R.C., and Pasteris, J.D., 1998, Extremely acid Permian lakes and groundwaters in North America: Nature, Vol. 392, p. 911-914.

Benison, K.C., Zambito, J.J., Soreghan, G.S., Soreghan, M.J., Foster, T.M., and Kane, M.J., 2013, Permian red beds and evaporites of the Amoco Rebecca K. Bounds core, Greely County, Kansas: implications for science and industry, *in* Dubois, M.K., Watney, W.L., and Tollefson, J., eds., Mid-Continent Core Workshop: from Source to Reservoir to Seal: Mid-Continent Section, American Association of Petroleum Geologists, Kansas Geological Survey, p. 9-14.

Benison, K.C., Zambito, J.J., and Knapp, J., 2015, Contrasting siliciclastic-evaporite strata in subsurface and outcrop: An example from the Permian Nippewalla Group of Kansas, U.S.A.: Journal of Sedimentary Research, doi: https://doi.org/10.2110/jsr.2015.43

Bozeman, S., ed., 1987, The D.C. Jester Cave system: Central Oklahoma Grotto, Oklahoma City, OK, Oklahoma Underground, Vol. 14, 56 p.

Bozeman, J., 2003, Exploration of western Oklahoma gypsum caves, *in* Johnson, K.S., and Neal, J.T., eds., Evaporite karst and engineering/environmental problems in the United States: Oklahoma Geological Survey, Circular 109, p. 57-64. http://ogs.ou.edu/docs/circulars/C109.pdf

Bozeman, J., and Bozeman, S., 2002, Speleology of gypsum caves in Oklahoma: Carbonates and Evaporites, Vol. 17, No. 2, p. 107-113.

Compass, http://fountainware.com/compass/ Accessed 5/9/2018

Dasher, G. R., 1994. On Station. Huntsville, Alabama 35810-4431, USA: National Speleology Society, Inc.

Fay, R.O., 1964 The Blaine and related formations of northwestern Oklahoma and southern Kansas: Oklahoma Geological Survey, Bulletin 98, 238 p.

Foster, T.M., Soreghan, G.S., Soreghan, M.J., Benison, K.C., and Elmore, R.D., 2014, Climatic and palaeogeographic significance of aeolian sediment in the Middle Permian Dog Creek Shale (Midcontinent U.S.A.): Palaeogeography, Palaeoclimatology, Palaeoecology, Vol. 402, p. 12-29.

Glennie, K.W., 1987, Desert sedimentary environments, present and past: a summary: Sedimentary Geology, Vol. 50, p. 135-165.

Golonka, J., Ross, M.I. and Scotese, C.R., 1994, Phanerozoic paleogeographic and paleoclimatic modeling maps, *in* Embry, A.F., Beauchamp, B. and Glass, D.J., eds, Pangea: Global Environments and Resources: Canadian Society of Petroleum Geologists, Memoir 17, p. 1-47.

Golonka, J., and Ford, D., 2000, Pangean (Late Carboniferous–Middle Jurassic) paleoenvironment and lithofacies: Palaeogeography, Palaeoclimatology, Palaeoecology, Vol. 161, p. 1-34.

Gustavson, T.C., Finley, R.J., and McGillis, K.A., 1980, Regional dissolution of Permian salt in the Anadarko, Dalhart, and Palo Duro Basins of the Texas Panhandle: Texas Bureau of Economic Geology, Report of Investigations 106, 40 p.

Holdoway, K.A., 1978, Deposition of evaporites and red beds of the Nippewalla Group, Permian, western Kansas: Kansas Geological Survey, Bulletin 215, 43 p.

Hovorka, S.D., and Granger, A., 1988, Subsurface to surface correlation of Permian evaporites – San Andres – Blaine – Flowerpot relationships, Texas Panhandle, *in* Morgan, W.A., and Babcock, J.A., eds., Permian rocks of the Midcontinent: Society of Economic Paleontologists and Mineralogists, Special Paper 1, p. 137-159.

Jewett, J.M., 1935, Some measurements at the Sun City Natural Bridge: Kansas Academy of Science, Transactions, Vol. 38, p. 189-190.

Johnson, K.S., 1972, Northwest Oklahoma; Book 2 of Guidebook for geologic field trips in Oklahoma: Oklahoma Geological Survey, Educational Publication 3, 42 p.

Johnson, K.S., 1981, Dissolution of salt on the east flank of the Permian Basin in the southwestern U.S.A.: Journal of Hydrology, Vol. 54, p. 75-93.

Johnson, K.S., 1986, Hydrogeology and recharge of a gypsum-dolomite karst aquifer in southwestern Oklahoma, U.S.A., *in* Gunay, G., and Johnson, I.V., eds., Karst water resources; Proceedings of the International Symposium on Karst Water Resources, Ankara, Turkey, July 7–19, 1985: International Association of Hydrological Sciences, Publication No. 161, p. 343-357.

Johnson, K.S., 1990a, Hydrogeology and karst of the Blaine gypsum-dolomite aquifer, southwestern Oklahoma: Oklahoma Geological Survey, Special Publication 90–5, 31 p.

Johnson, K.S., 1990b, Standard outcrop section of the Blaine Formation and associated strata in southwestern Oklahoma: Oklahoma Geology Notes, Vol. 50. 144-168.

Johnson, K.S., 1991, Guidebook for geologic field trips in Oklahoma: Northwest Oklahoma: Oklahoma Geological Survey, Educational Publication 3, 42 p.

Johnson, K.S.,1992, Evaporite karst in the Permian Blaine Formation and associated strata in western Oklahoma, USA, *in* Back, W., Herman, J.S., and Paloc H., eds., Hydrogeology of selected karst regions: Verlag Heinz Heisse Publishing Co., Hannover, Germany, International Association Hydrogeologists, Vol. 13, p. 405-420.

Johnson, K.S., 1996, Gypsum karst in the United States: International Journal of Speleology, Vol. 25, Nos. 3-4, p. 183-193, https://doi.org/10.5038/1827-806X.25.3.13.

Johnson, K.S., 2003, Evaporite karst in the Permian Blaine Formation and associated strata of western Oklahoma, *in* Johnson, K.S., and Neal, J.T., eds., Evaporite karst and engineering/environmental problems in the United States: Oklahoma Geological Survey, Circular 109, p. 41-55. http://ogs.ou.edu/docs/circulars/C109.pdf

Johnson, K.S., 2018, Gypsum caves of north Texas and western Oklahoma, *in* Stafford, K.W., and Veni, G., eds., Hypogene karst of Texas: Texas Speleological Survey, Monograph 3, p. 111-122. https://www.texasspeleologicalsurvey.org/PDF/Hypogene_Karst_of_Texas.pdf

Johnson, K.S., 2021, Overview of evaporite karst in the Greater Permian Evaporite Basin (GPEB) of TX, NM, OK, KS, and CO, *in* Johnson, K.S., Land, L., and Decker, D.D., eds., Evaporite karst in the Greater Permian Evaporite Basin (GPEB) of Texas, New Mexico, Oklahoma, Kansas, and Colorado: Oklahoma Geological Survey, Circular 113.

Jordan, L., and Vosburg, D.L., 1963, Permian Salt and Associated Evaporites in the Anadarko Basin of the Western Oklahoma–Texas Panhandle Region: Oklahoma Geological Survey, Bulletin 102, 76 p.

McGregor, D.R., Pendry, E.C., and McGregor, D.L., 1963, Solution caves in gypsum, north-central Texas: Journal of Geology, Vol. 71, p. 108-115.

McLaughlin, T.G., 1942, Geology and ground-water resources of Morton County, Kansas: Kansas Geological Survey, Bulletin 40, p. 1-126.

Merriam, D.F., 1955, Jurassic rocks in Kansas: American Association of Petroleum Geologists, Bulletin, Vol. 39, p, 31-46.

Merriam, D.F., 1957, Subsurface correlation and stratigraphic relation of rocks of Mesozoic age in Kansas: Kansas Geological Survey, Oil and Gas Investigations 14, p. 1-25.

Merriam, D.F., 1962, History of Precambrian studies in Kansas: Kansas Academy of Science, Transactions, Vol. 65, No. 4, p. 433-447.

Merriam, D.F., and Mann, C. J., 1957, Sinkholes and related geologic features in Kansas: Kansas Academy of Science, Transactions, Vol. 60, No. 3, p. 207-243.

Mudge, M.R., 1967, Central Midcontinent region, *in* McKee, E.D., and Oriel, S.S., eds., Paleotectonic investigations of the Permian System in the United States: US Geological Survey, Professional Paper 515, p. 97-128.

Moore, R.C., Frye, J.C., Jewett, J.M., Wallace, L., and O'Connor, H.G., 1951, The Kansas rock column: Kansas Geological Survey, Bulletin 89, 132 p.

Myers, A.J., Gibson, A.M., Glass, B.P., and Patrick, C.R., 1969, Guide to Alabaster Cavern and Woodward County, Oklahoma: Oklahoma Geological Survey, Guidebook 15, 38 p.

Nance, H.S., 1988, Interfingering of evaporites and red beds: an example from the Queen/Grayburg Formation, Texas: Sedimentary Geology, Vol. 56, p. 357-381.

NOAA, 2018, National Oceanic and Atmospheric Administration, National Centers for Environmental Information, Climate at a Glance, http://www.ncdc.noaa.gov/cag/ (accessed March 6, 2018).

Norton, G.H., 1939, Permian red beds of Kansas: American Association of Petroleum Geologists, Bulletin, Vol. 23, p. 1751-1819.

Quinlan, J.F., Smith, R.A., and Johnson, K.S., 1986, Gypsum karst and salt karst of the United States of America, *in* Atti Symposio Internationale sul Carsismo Nelle Evaporiti (Proceedings, International Symposium on Karst in Evaporites), Palermo, Italy, October 27–30, 1985: Le Grotte d'Italia (4), v. 13, p. 73-92.

Runkle, D.L., and Johnson, K.S., 1988, Hydrogeologic study of a gypsum-dolomite karst aquifer in southwestern Oklahoma and adjacent parts of Texas, U.S.A., *in* Karst hydrogeology and karst engineering protection: Geological Publishing House, Beijing, China, Proceedings of the IAH 21st Congress, Guilin, China, Vol. 21, Part 2, p. 400-405.

Sweet, A.C., Soreghan, G.S., Sweet, D.E., Soreghan, M.J., and Madden, A.S., 2013, Permian dust in Oklahoma: source and origin for Middle Permian (Flowerpot–Blaine) red beds in western tropical Pangaea: Sedimentary Geology, Vol. 284–285, p. 181-196.

Tomlinson, C.W., 1916, The origin of red beds: a study of the conditions of origin of the Permo-Carboniferous and Triassic red beds of the western United States: Journal of Geology, Vol. 24, p. 28–253.

Turner, P., 1980, Continental red reds: New York, Elsevier, Developments in Sedimentology 29, 562 p.

Walker, T.R., 1967, Formation of red beds in modern and ancient deserts: Geological Society of America, Bulletin, Vol. 78, p. 353-368.

White, W.B., 1988, Geomorphology and Hydrology of Karst Terrains, New York, Oxford University Press, 464 p

White, W.B., 1988, Geomorphology and hydrology of karst terrains: New York, Oxford University Press, 464 p.

Young, J., and Beard, J., 1993, Caves in Kansas: Kansas Geological Survey, Educational Series 9, 48 p.

Zharkov, M.A., and Chumakov, N.M., 2001, Paleogeography and sedimentation settings during Permian–Triassic reorganizations in biosphere: Stratigraphy and Geological Correlation, Vol. 9, p. 340-363.

Oklahoma Geological Survey Circular 113, 2021

Salt Dissolution and the Wallace Sinkhole in the Sharon Springs–Wallace Area, Wallace County, Western Kansas

Kenneth S. Johnson
Retired Geologist, Oklahoma Geological Survey,
Norman, Oklahoma

ABSTRACT.—Salt beds in the Permian Flowerpot and Blaine Formations are extensively dissolved in parts of western Kansas, and this has resulted in development of a number of sinkholes in the region. The current study of evaporite karst in the Sharon Springs–Wallace area in Wallace County focuses on the distribution, thickness, depth, structure, and dissolution of these two salt units, and on their relationship to development of the Wallace Sinkhole, formed in July, 2013, and five earlier-formed sinkholes: the Smoky Basin Cave-in, the Old Maid's Pool, and three sinks in Bradshaw Draw, near the Wallace Sinkhole.

Salt beds in the area probably are mostly displacive halite that developed within a reddish-brown mudstone matrix. The Flowerpot salt is typically 200 to almost 240 ft thick in most of the area, but in the west it is dissolved and all overlying strata are dropped down about 150 - 200 ft across a salt-dissolution front. Salt that occurs in the middle of the Blaine Formation typically ranges from 35 to 50 ft thick in the east half of the area, but is mostly dissolved and missing in the west. Although most of the salt dissolution occurred sometime between Late Cretaceous and Tertiary time, it is still happening locally.

Structural mapping of the area shows a regional dip of strata to the north at less than 1°, but two newly identified faults interrupt this pattern and appear to be related to recent sinkhole development. The depth to the salt ranges from about 2,000 to 2,400 ft in the area, and it appears that faults and/or fractures in overlying strata are allowing fresh ground water to circulate down to the salts and locally cause their dissolution. When a dissolution cavity in the salt becomes too large, the roof of the cavity collapses: this allows overlying rocks to drop into the cavity and form a collapse breccia or breccia pipe that can reach the land surface as a sinkhole that typically has a diameter of about 200 ft.

The Wallace Sinkhole has a diameter of about 200 ft and originally it was about 90 ft deep. Fortunately, it formed in pasture land, and there were no injuries or infrastructure damage. At this site, the middle Blaine salt is about 2,330 ft deep, and the underlying Flowerpot salt is about 2,400 ft deep. This is quite deep for dissolution to occur, but it appears that one of the newly mapped faults extends to the sinkhole and may be a pathway for fresh water to reach and dissolve the salt. Most of the other sinkholes in the area may have a similar origin.

INTRODUCTION

In late July, 2013, a large sinkhole formed in Wallace County, western Kansas, about 9 mi north of the town of Wallace, and 12 mi north–northeast of Sharon Springs (Fig. 1). This sink, informally referred to in the past as the "Wallace," the "Sharon Springs," or the "Wallace County" Sinkhole, is herein named the "Wallace Sinkhole" after the nearest town. The sinkhole developed in an area of sparse drilling for oil and gas or irrigation water, but in an area underlain by Permian-age salt beds in the Flowerpot and Blaine Formations at a depth of about 2,300–2,400 ft. These Permian salt beds are known to be naturally dissolved extensively in parts of western Kansas (Campbell, 1963; Schumaker, 1966; Holdoway, 1978), and thus, dissolution of these salts, and creation of

Johnson, Kenneth S., 2021, Salt Dissolution and the Wallace Sinkhole in the Sharon Springs–Wallace Area, Wallace County, Western Kansas, *in* Johnson, K. S.; Land, Lewis; and Decker, D. D. (eds.), Evaporite Karst in the Greater Permian Evaporite Basin (GPEB) of Texas, New Mexico, Oklahoma, Kansas, and Colorado: Oklahoma Geological Survey, Circular 113, p. 319–335.

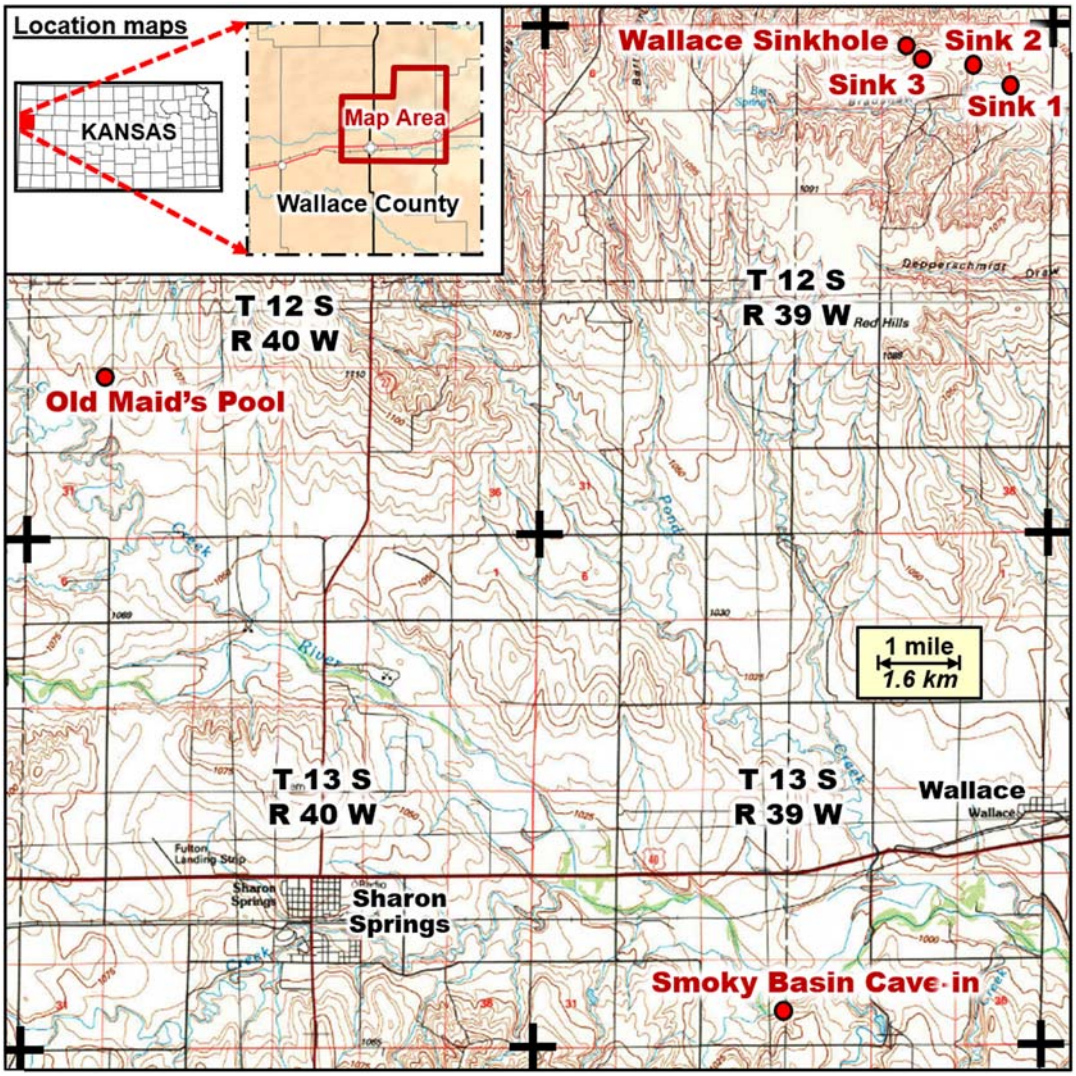

Figure 1. Location of Wallace Sinkhole and five other sinkholes in the Sharon Springs–Wallace area, Wallace County, Kansas. Base map is USGS 1:100,000-scale topographic maps for the Sharon Springs and Goodland quadrangles: both maps prepared in 1985.

a deep-seated cavity that collapsed, was initially believed to be responsible.

Preliminary studies by Lynn Watney of the Kansas Geological Survey (KGS), and early statements by Rex Buchanan, then-Director of KGS, showed a belief that the sinkhole resulted from collapse into a salt-dissolution cavity, and I concur with this early interpretation of salt karst. To evaluate this hypothesis, I undertook a study of salt deposits in the Sharon Springs–Wallace area to show the distribution, thickness, depth, structure, and dissolution of the salt beds, and to relate these data to the location and probable cause of the Wallace Sinkhole and five other sinkholes in the area.

Earlier regional and local studies have provided valuable information for the current study. Primary investigations of several salt units in western Kansas were conducted by Campbell (1963), Schumaker (1966), and Holdoway (1978): they prepared maps showing the thickness and distribution of the salt units, and their data also show the general dissolution limits of each of the salts. General studies or summaries of sinkholes and collapse features in western Kansas were made by Johnson (1901), Schoewe, (1949), Merriam and Mann (1957), Merriam (1963, Appendix D), and Macfarlane and Wilson (2006). Specific reports on sinkholes in Wallace County are by Moore (1926a, b), Russell (1929), Elias (1931), Frye (1950), and Merriam and Mann (1957).

As far as rock terminology used in this report: 1) "salt" in all cases is halite (NaCl); 2) the term "anhydrite" is used, although in some areas, the rock may, in fact, be gypsum; and 3) the word "shale" refers to shale, or to a mix of shale, siltstone, mudstone, and perhaps even some sand: shale is probably dominant, but the true and complete lithology is uncertain.

Appreciation is expressed to the Kansas Geological Survey for having their publications and scans of wireline (geophysical) logs available online: this provided access to a wide range of data needed for this report.

STRATIGRAPHY

Stratigraphy of Wallace County has been described by Elias (1931) and Hodson (1963), and additional studies of salt deposits and/or dissolution in the region are by Schumaker (1966), Holdoway (1978), Zambito and others (2012), and Benison and others (2015). The oldest stratigraphic unit of concern in this study is the Permian Stone Coral Formation, and the youngest is Quaternary alluvium along modern rivers and streams (Fig. 2).

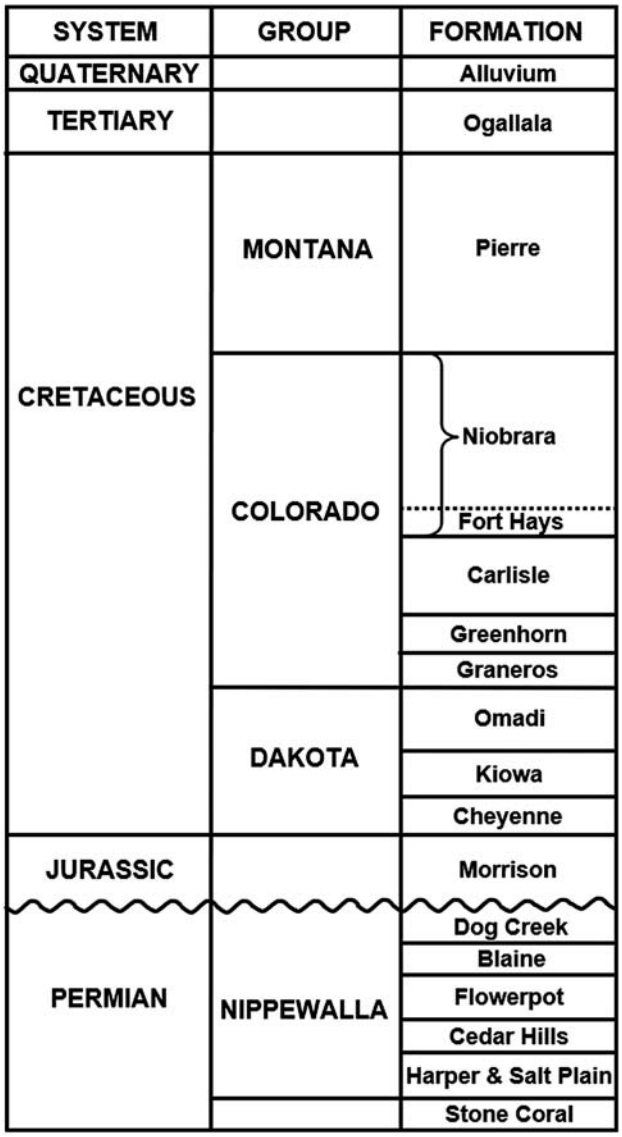

Figure 2. Stratigraphic sequence in Wallace County (after Merriam, 1957; Hodson, 1963; Zeller, 1968). Relative thickness of formations is approximately indicated by height of boxes.

Permian formations of interest in the area are redbeds and evaporites that range from the Stone Coral Formation (oldest) to the Dog Creek Shale (youngest). The Stone Coral Formation is about 30 ft thick and is mostly anhydrite, with about 2–5 ft of salt commonly at the top: this anhydrite is an excellent marker bed throughout most of western Kansas. It is overlain by undifferentiated Harper Sandstone and Salt Plain Formation, which consists of about 70–120 ft of sandstone, siltstone, and shale (Fig. 3). Next above is the Cedar Hills Sandstone: it is 60–80 ft of sandstone, and is capped by 5–10 ft of anhydrite, the Y-anhydrite.

The overlying Flowerpot Formation has two different characteristics in the area: in most of the area, it is 200 to almost 250 ft of salt and shale (the Flowerpot salt), underlain by about 20 ft of Flowerpot Shale; in the west, the salt has been largely or totally dissolved, and the formation consists of about 60–100 ft of shale (Flowerpot Shale), which may contain unknown, but minor, amounts of residual, undissolved salt.

Above the Flowerpot is the Blaine Formation, which generally consists of lower and upper anhydrite/shale units, and a middle salt unit (Fig. 3): the two anhydrite beds in the lower Blaine are equivalent to the Medicine Lodge and Nescatunga Beds of the Blaine Formation in northwest Oklahoma and southwest Kansas; the middle salt unit is comparable to the middle salt above the Nescatunga/Collingsworth Bed of the Anadarko Basin; and the lowest anhydrite in the upper Blaine is correlative with the Shimer Bed of northwest Oklahoma. The thickness of the Blaine Formation is about 80–100 ft, where the middle salt is present, but it thins to about 40–70 ft in the west, where the salt is dissolved. The youngest recognizable Permian unit in the area is the Dog Creek Shale, which is about 100 ft, or more, of shale.

Above Permian strata are the Jurassic Morrison Formation and the Cretaceous Dakota, Colorado, and Montana Groups (Fig. 2). Jurassic and Cretaceous formations are not of special importance to the study, except that the Niobrara Formation is a thick unit (about 600 ft thick) of chalk, with about 60 ft of Fort Hays Limestone at its base; the Pierre Shale is about 600 ft of shale, although the upper part is commonly eroded and overlain by the Ogallala.

The youngest strata in the area are the Tertiary Ogallala Formation and Quaternary alluvium, both of which are important aquifers in Wallace County (Hodson, 1963). The Ogallala consists mainly of fluvial deposits of sand, gravel, silt, and clay: it has a nonuniform thickness of 0–400 ft in the county because of the formation having unconformable contacts at its base and top. Alluvium locally contains sand and gravel deposits in the larger valleys, and in places, it is up to 40–50 ft thick. Some of the groundwater that ultimately migrates

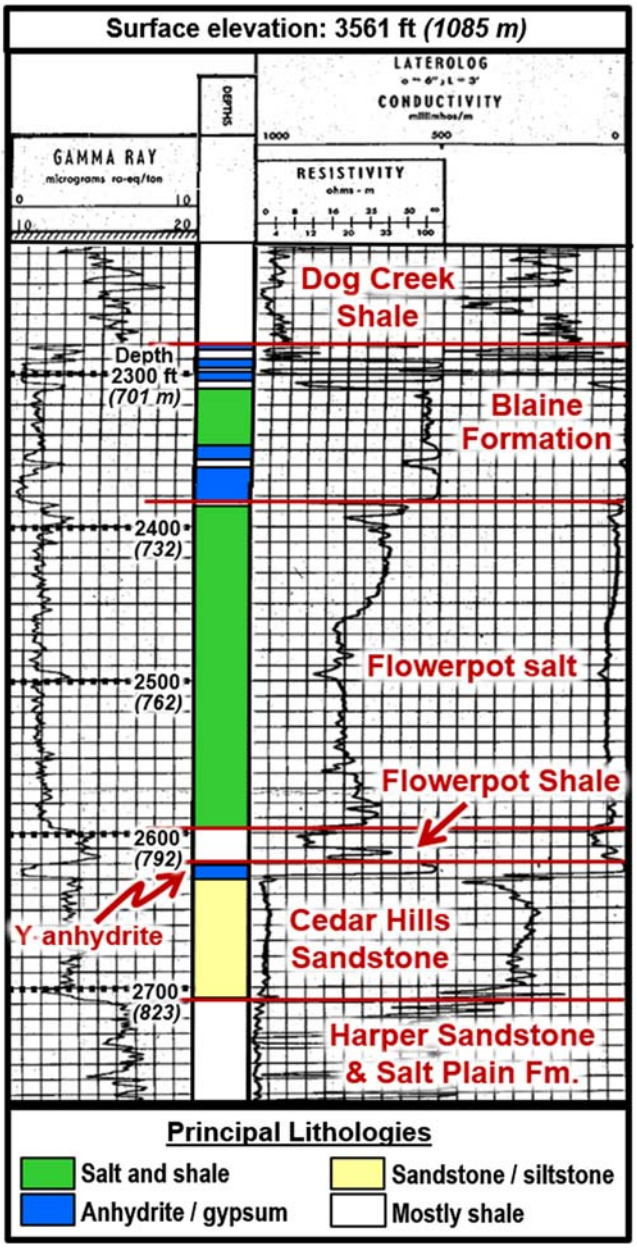

Figure 3. Geophysical log and interpretive lithology of part of the General Crude Oil Co., Delia F. Adams No. 1 well, located 2 mi (3.2 km) south of the Wallace Sinkhole. The well is located in C NE NE, sec. 15, T. 12 S., R. 39 W., and is the closest borehole log to the Wallace Sinkhole.

down to dissolve Permian salt beds certainly must have its origin in these two aquifers.

SUBSURFACE SALT UNITS AND DISSOLUTION

Salt units in the Sharon Springs–Wallace area are in the Permian Flowerpot and Blaine Formations. The General Crude Oil Co., Delia F. Adams No. 1 well, drilled about 2 mi south of the Wallace Sinkhole, shows these two salt units to be 212 and 38 ft thick, respectively (Fig. 3), and the well log is representative of the salt-bearing Flowerpot–Blaine sequence throughout the area. The depth to the salts in the Adams well is 2,310 ft to the middle Blaine salt, and about 2,385 to the Flowerpot salt.

Dissolution of salt units in the area appears to always start with removal of the youngest (uppermost) salt, the middle Blaine salt, and then progresses down to partial and then total removal of salt in the Flowerpot (Fig. 4). The location of wells used in Figure 4, as well as the Adams well and the other cross sections discussed in the report, is shown in Figure 5.

Widespread natural dissolution of salt beneath nonsoluble strata results in interstratal karst, and this can be characterized as sheetlike dissolution. An example of this is widespread removal in the past of the Flowerpot salt in the western part of the study area (Fig. 6), accompanied by settling or subsidence of overlying rock over a fairly large area. In contrast to such widespread salt dissolution, present-day dissolution occurs mainly where an underground cavity is created in a relatively small area: overlying rock then collapses chaotically into the cavity, resulting in a collapse breccia or breccia pipe that can reach the land surface as a sinkhole several hundred feet wide.

There are no known cores of the salt units in the Sharon Springs–Wallace area, and thus the lithology shown in illustrations of this report is based upon interpretation of geophysical logs. However, there are several reports in the region that are based upon examination of cores of Permian rocks, including salts in the Flowerpot and Blaine Formations. Holdoway (1978) describes cores of the Atomic Energy Commission (AEC) test hole 5 in Wichita County, about 30 mi south–southeast of Sharon Springs, and both Zambito and others (2012) and Benison and others (2015) describe cores from Amoco's Rebecca K. Bounds #1 well (RKB well) in Greeley County, about 30 mi south–southwest of Sharon Springs. These two reports provide valuable information about the petrology of the salt units. In addition, both Schumaker (1966) and Holdoway (1978) have provided excellent maps and cross sections of the Flowerpot salt and Blaine Formation throughout western Kansas: the current report provides more-detailed data on these rock units in the Sharon Springs–Wallace area of Wallace County.

Flowerpot Salt

The Flowerpot salt underlies most of the study area, but is largely or totally removed by sheetlike dissolution in the west (Fig. 6). Both Schumaker (1966) and Holdoway (1978) show that the Sharon Springs–Wallace area is near the limits of the Flowerpot salt, and that it is mostly or totally dissolved farther to the west. In the

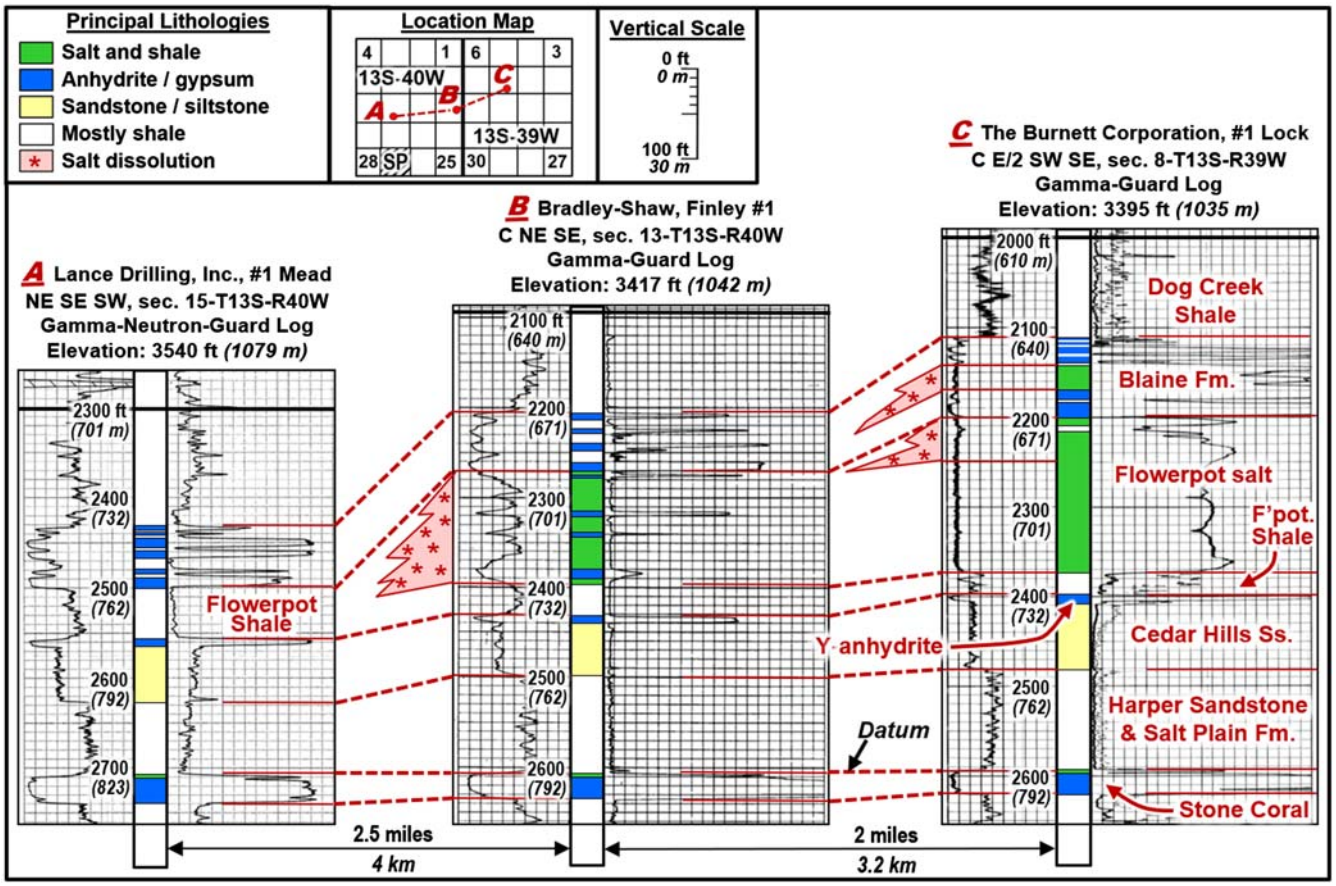

Figure 4. Stratigraphic cross section showing dissolution of uppermost salts just north of Sharon Springs ("SP" on Location Map). Between wells C and B, salt is dissolved in the middle part of the Blaine Formation, and in the upper part of the Flowerpot salt; and between wells B and A, all the remaining Flowerpot salt is dissolved.

current study area, the Flowerpot salt typically is 200 to almost 240 ft thick, where fully developed, and its thickness drops off sharply (in places within just 1 or 2 miles) at the dissolution front, beyond which the Flowerpot Shale contains little or no recognizable salt (Figs. 4, 6). Typically, where the Flowerpot salt is well developed, about 20–30 ft of shale (Flowerpot Shale) separates the salt from the underlying Y-anhydrite of the Cedar Hills Sandstone (Figs. 3, 4); farther west, these 20–30 ft of shale are included with the overlying, salt-deficient strata as the Flowerpot Shale.

The best petrologic descriptions of the Flowerpot salt in the region are based on cores from the AEC #5 and the RKB wells. Flowerpot salt in the AEC #5 well is described as "fine to coarse crystals of halite, intimately associated with red, anhydritic, silty mudstone. The halite is not bedded, but several thin beds of mudstone and anhydrite occur within the sequence . . . Halite in some parts of the Flower-pot [sic], especially lower in the section, appears to have grown within the sediments, displacing soft, silty mud as it grew . . . During halite growth, clay-size impurities were displaced and became concentrated around grain margins" (Holdoway, 1978).

In cores of the RKB well, the Flowerpot "consists almost exclusively of displacive halite within a reddish-orange mudstone matrix with varying ratio of halite to siliciclastics" (Zambito and others, 2012). "Displacive halite" is described by Benison and others (2015) as "a lithology in which red siliciclastic mudstone or sandstone hosts randomly oriented halite crystals," and they note that displacive halite is the dominant form of salt in the RKB core. Examples of salt from the RKB well, with varying degrees of red clastics, are shown in Figure 7: I assume that salts in the Sharon Springs–Wallace area are similar to the range of displacive salts shown in the RKB core.

Therefore, based upon descriptions of the nearest Flowerpot salt cores, those in the AEC and RKB wells, I assume that the Flowerpot salt in the Sharon Springs–Wallace area is an impure, displacive salt with varying amounts of reddish-brown clay and silt. Where the salt is largely or totally dissolved, the Flowerpot sequence has been compressed, caused by the loss of salt and the weight of the overlying rock column, and the remaining shale is only a fraction of the original thickness of the salt unit.

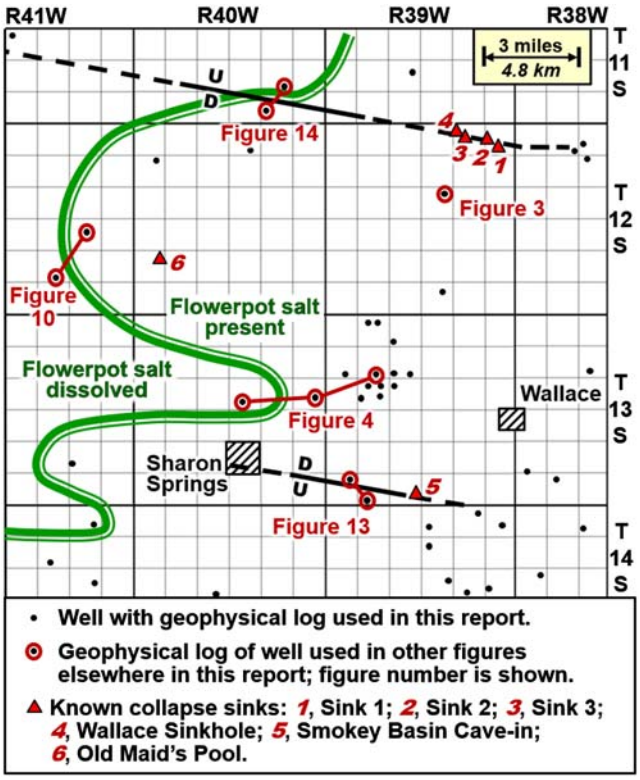

Figure 5. Map showing location of well logs used in this report, and those well logs that are used in other figures in the Sharon Springs–Wallace area. Also shown are known sinkholes, faults, and the approximate dissolution front for the Flowerpot salt (green line).

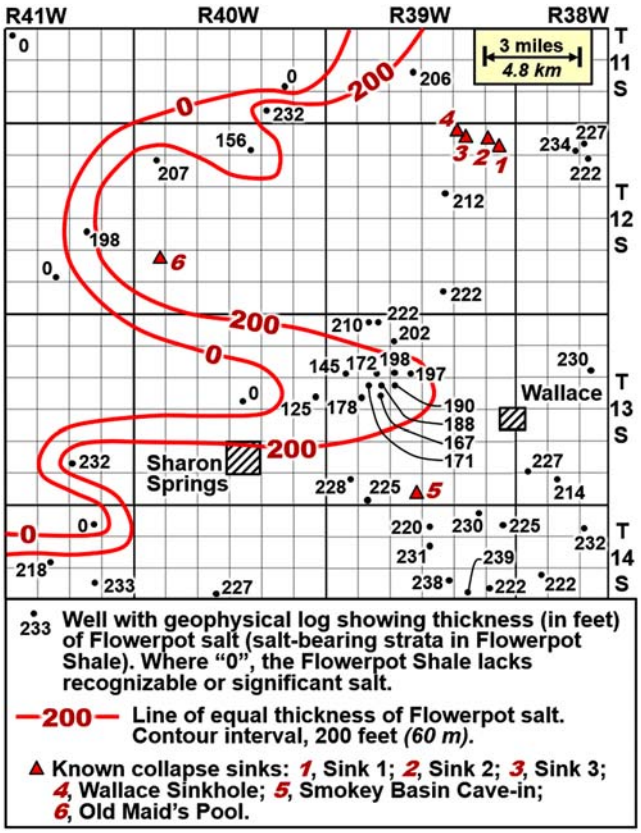

Figure 6. Map showing thickness of the Flowerpot salt in the Sharon Springs–Wallace area.

Benison and others (2015) conducted experiments to determine semiquantitatively how much rock volume and thickness was lost by dissolution of salts in the RKB core. They took six displacive-salt samples, three from the Blaine and three from the Flowerpot, and dissolved them. The salt samples were similar to those shown in Figures 7B, C, and D. Sample thicknesses that they used ranged from 5 to 26.7 vertical centimeters (2–10.5 vertical inches) of core, and aggregated a total 1.1 m (3.6 ft). The amount of rock lost to dissolution by height (thickness) ranged from 53.2 to 88.0%, and averaged 74.2%; the amount of rock lost to dissolution by mass ranged from 68.2 to 95.1%, and averaged 85.5%. The authors noted that samples with a high salt-to-clastics ratio had a higher loss of rock thickness and mass, whereas those with a low salt-to-clastics ratio had a lower, but still significant, loss of rock thickness and mass.

Inasmuch as deep-subsurface dissolution of salt, such as in the Sharon Springs–Wallace area, occurs under a heavy overburden of overlying rocks (generally 2,000–2,500-ft deep), I assume that much of the pore space caused by salt dissolution is closed (compressed and squashed), and that a loss-of-rock percentage at depth would be somewhere between the height and mass data reported by Benison and others (2015). I suspect that with the compaction, the loss of rock thickness after dissolution of displacive salt in the Sharon Springs–Wallace area probably averages somewhere near the midpoint of their two data sets (height and mass data), namely about 80%, and that dissolution of the displacive salt reduces the remaining clastic sequence, on average, to about 20% of the thickness of the original salt unit.

Examination of the thickness of Flowerpot strata in Figure 4 supports my assumption that, in general, dissolution of displacive salt in the study area reduces the thickness of the remaining Flowerpot clastic material to about 20% of the thickness of the original, undissolved salt unit. In well C (Fig. 4), the Flowerpot salt is 174 ft thick, which would compress to 174x0.2=34.8 ft upon dissolution, and the Flowerpot Shale at its base is about 26 ft thick: therefore, the total thickness of postdissolution Flowerpot clastics in well C would be about 60.8 ft. In well B, some of the Flowerpot salt is dissolved, and the remaining 125 ft of salt would compress to 125x0.2=25 ft: the Flowerpot Shale at its base is about 35 ft thick, and thus, the total thickness of postdissolution Flowerpot clastics in well B would be about 60 ft. In well A, all the salt is dissolved, and the total thickness

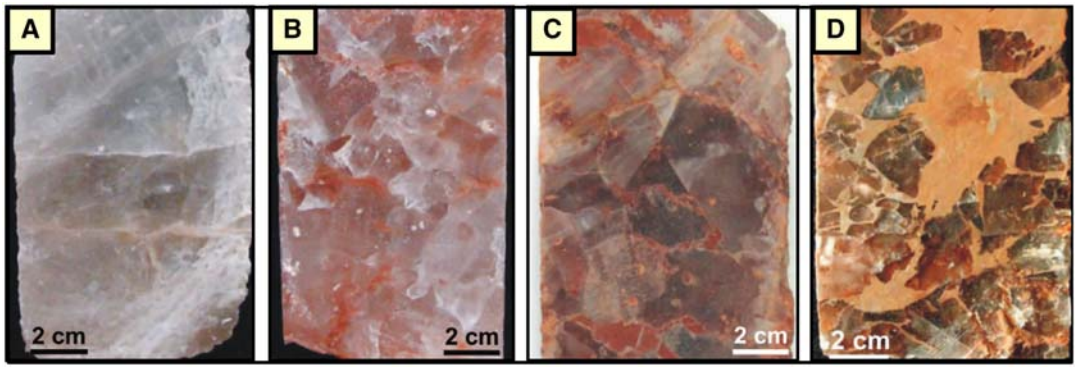

Figure 7. Photos of salt cores from the RKB well, about 30 mi (50 km) south–southwest of the town of Sharon Springs (from Benison and others, 2015). A) Bedded salt in the upper anhydrite/shale unit of the Blaine Formation; high-purity salt, with minor hematite. B) Displacive salt near the top of the middle Blaine salt; it has a high salt-to-clastics ratio. C) Displacive salt in the lower part of the middle Blaine salt; it has a more-typical salt-to-clastics ratio. D) Displacive salt in undifferentiated Harper Sandstone and Salt Plain Formation; it has a low salt-to-clastics ratio.

of the Flowerpot Shale here is 57 ft. Therefore, in well A, where all salt is dissolved, the Flowerpot Shale (57 ft thick) is about as thick as the proposed postdissolution thickness of Flowerpot clastics in well C (60.8 ft) and in well B (60 ft). In other parts of the study area, where it seems that the salt is missing, and the thickness of the residual Flowerpot Shale is more than 20% of the thickness of the Flowerpot salt farther to the east, I assume that not all of the salt is dissolved—but the residual salt is not recognizable on geophysical logs.

Middle Blaine Formation Salt

The total thickness of the Blaine Formation in the study area generally ranges from about 75 to 100 ft thick in the east, and is less than 50 ft thick throughout much of the west (Fig. 8). The formation consists of lower and upper anhydrite/shale units, and a middle salt unit (Figs. 3, 4). Salt in the middle of the Blaine typically ranges from 35 to 50 ft thick in the east half of the study area, and is mostly dissolved and missing in the west (Fig. 9): there are, however, two outlying sites of residual salt in the west, where the salt unit is 20 and 39 ft thick.

The middle Blaine salt is the shallowest salt in the area, and apparently is always the first salt to be dissolved. In addition to the large area of sheetlike, total dissolution in the west, there are several locations in the east where all the salt is removed, despite being surrounded by areas of relatively thick middle Blaine salt. This shows that there are some processes whereby salt-dissolving water is able to percolate/migrate down to the salt to the east of the main dissolution front, and similarly, it is evident that all salt is not removed to the west of the main dissolution front (see residual salt masses in R. 41 W., Fig. 9).

Salt in the middle of the Blaine Formation is widespread in the northern half of the Greater Permian

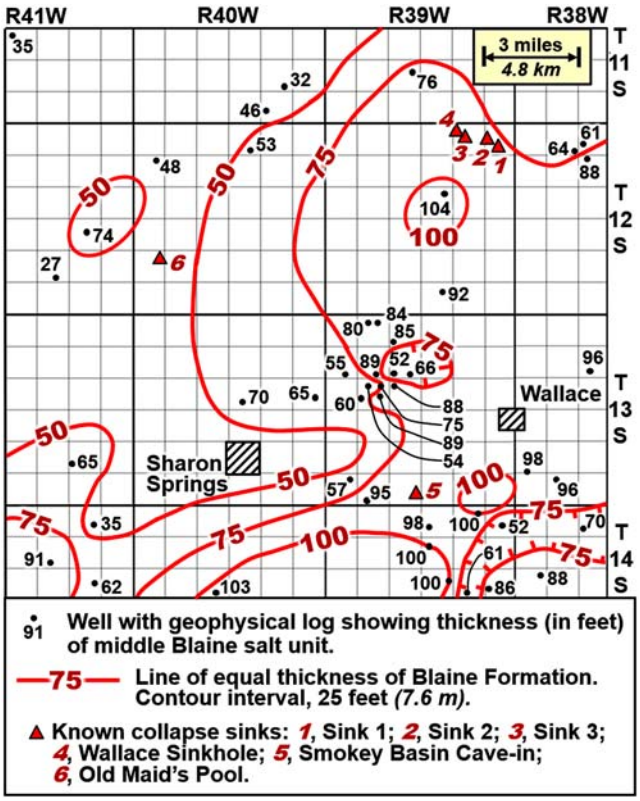

Figure 8. Map showing thickness of the Blaine Formation in the Sharon Springs–Wallace area.

Evaporite Basin, as defined by Johnson (2021a). It is documented in the Anadarko Basin and eastern Palo Duro Basin (Johnson, 2021b), in Baca County, southeast Colorado (Askew, 2013), over the Las Animas Arch in east-central Colorado (Berry, 2018), and in western Kansas (Holdoway, 1978; Zambito and others, 2012; Benison and others, 2015). This salt unit overlies the Nescatunga/Collingsworth Bed, and underlies the Shimer Bed/Van

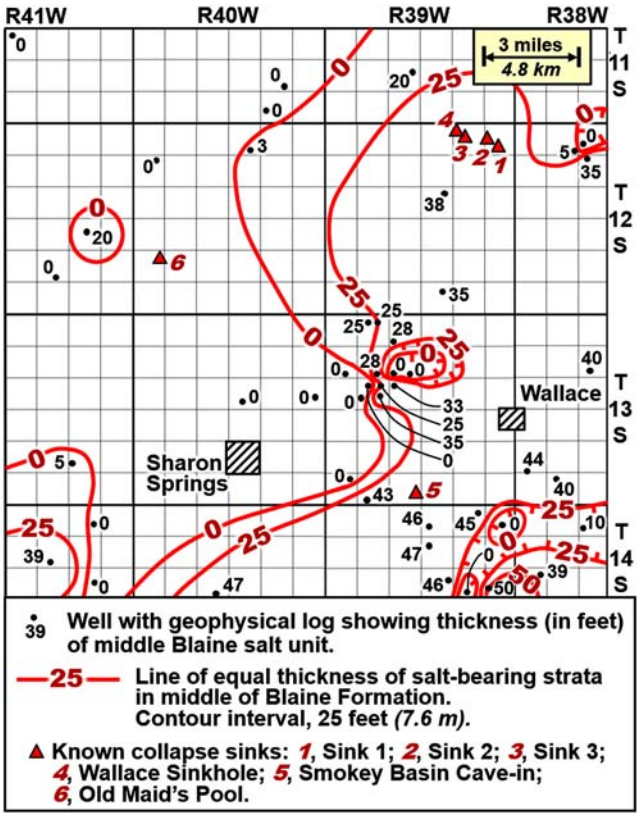

Figure 9. Map showing thickness of salt-bearing strata in the middle of the Blaine Formation in the Sharon Springs–Wallace area.

Vacter unit 1: nomenclature for these individual beds in the Blaine Formation is well established in the Anadarko Basin of western Oklahoma (Johnson, 2021b).

The middle Blaine salt probably consists mainly of displacive halite, similar to what is described in the Flowerpot salt, and similar to what is described in the RKB well (Fig. 7). Benison and others (2015) also describe the presence of several bedded (high-purity) salt layers in the middle and upper units of Blaine, so it is possible that some of the middle Blaine salt in the study area is also bedded salt (Fig. 7A).

Dissolution of the middle Blaine salt is shown in Figure 4. In well C, the middle Blaine consists of 28 ft of salt overlain by about 3 ft of shale. Assuming the same losses in height (thickness) and mass because of salt dissolution as in the RKB well (described above for the Flowerpot salt), the compaction of clastics in well C after dissolution of displacive salt would reduce the thickness of the clastic sequence to about 20% of the original salt unit. Therefore, the middle Blaine salt in well C would compress to 28x0.2=5.6 ft of shale, and, added to the 3 ft of shale above that salt, the postdissolution thickness of these strata should be almost 9 ft thick. In wells A and B, just 4.5 and 2 mi to the west, respectively, the middle unit lacks salt and is about 11 ft thick: close to the nearly 9-ft thickness estimated for the compressed, postdissolution middle Blaine salt in well C.

The Blaine Formation should be about 60–70-ft thick where all the middle Blaine salt has been dissolved, and the overlying beds have merely settled down intact (Fig. 4, wells A and B). However, in some wells where the middle Blaine salt has been dissolved, the Blaine Formation is abnormally thin (less than 60 ft thick in parts of the northwest, as shown in Fig. 8), and some anhydrite beds appear to be thin or missing. This can result from brecciation, collapse, and disruption of Blaine anhydrite beds above a dissolution zone (dissolution of salt in either the Blaine or the Flowerpot), so that the well was drilled through a chaotic interval where one or more of the disrupted anhydrite beds is not penetrated in the borehole. A good example of this is shown in Figure 10, where the Blaine Formation is only 27 ft thick in the Natural Gas Drilling Co., Burk No. 1, and it appears that only two of the six anhydrite beds were penetrated in the borehole (the other anhydrite beds having been disrupted and broken up, or removed by dissolution—at least they were not penetrated in the borehole).

Timing of Salt Dissolution

Dissolution of the Flowerpot and Blaine salts in the Sharon Springs–Wallace area occurred at least some time after deposition of the Fort Hays Limestone at the base of the Late Cretaceous Niobrara Formation. This is affirmed by examination of two wells drilled on either side of the dissolution front of the Flowerpot salt (Fig. 10). The combined thickness of the Flowerpot and Blaine Formations is 296 ft in the Burk 23-1 well, on the right, whereas it is reduced to 120 ft in the Burk No. 1 well on the left: therefore, the thickness of these two formations is reduced by 176 ft as a result of salt dissolution and brecciation. Using the Stone Coral as a stratigraphic datum, we see that all of the marker beds above the Blaine Formation in these two wells are dropped by about 170 ft across the dissolution front, basically the same as the reduced thickness of the Flowerpot and Blaine Formations.

All strata between the top of the Blaine and the base of the Niobrara are essentially of equal thickness on both sides of the dissolution front, and therefore, the dissolution did not occur while these strata were being deposited: that is, not prior to deposition of the lower Niobrara. If dissolution had occurred before Niobrara time, then one or several of the pre-Niobrara formations would be thicker to the west, as it, or they, accumulated a greater thickness by filling in the resulting depression. The lack of shallower, recognizable marker beds in the upper Niobrara, Pierre, or Ogallala Formations in the study area makes it impossible to say more precisely when this dissolution occurred, except that it began after deposition of the Fort Hays Limestone, and is still going on today.

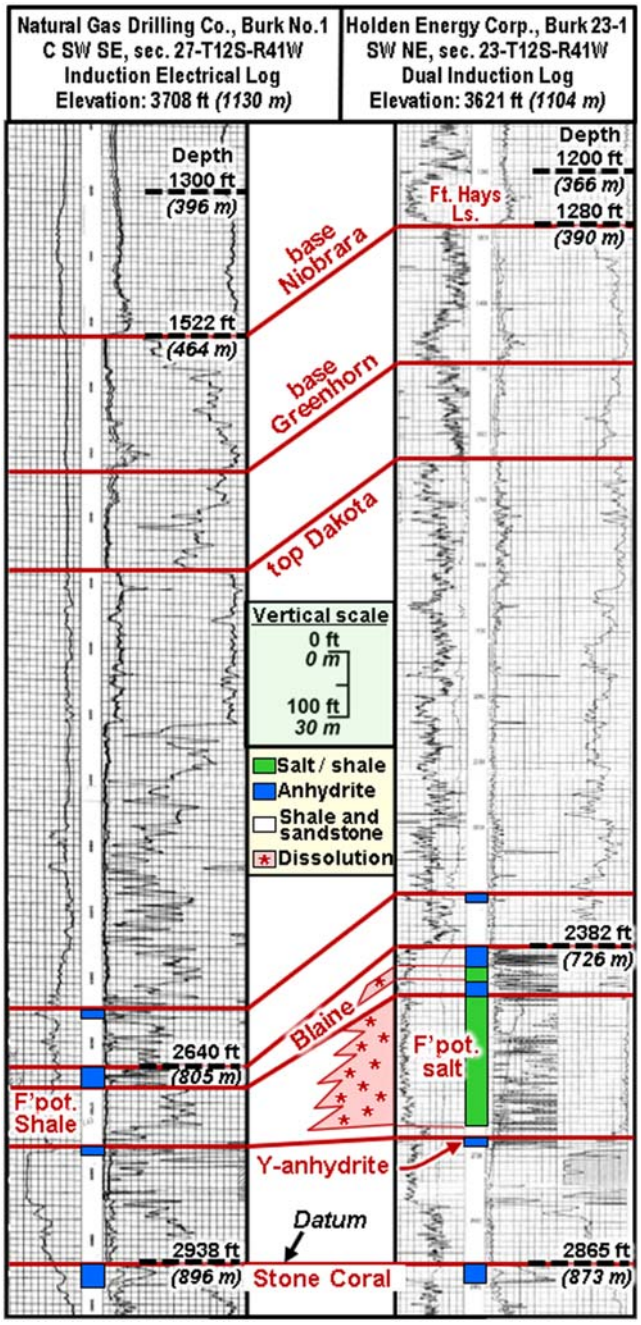

Figure 10. Stratigraphic cross section showing two wells, about 9,000-ft (±2,750 m) apart, in the southeast part of T. 12 S., R. 41 W., where about 176 ft (54 m) of Blaine and Flowerpot salts have been dissolved; datum is top of Stone Coral anhydrite. All strata between the Blaine Formation and the lower Niobrara are uniformly dropped about 170 ft (52 m) across the salt-dissolution front, indicating that salt dissolution occurred at least after early Niobrara (Late Cretaceous) time.

Similar results are observed elsewhere across the dissolution front in the area, supporting the fact that all, or at least most, dissolution of the Flowerpot and Blaine salts here occurred after deposition of the Fort Hays Limestone. In comparing two wells in secs. 2 and 10, T. 14 S., R. 41 W., again using the Stone Coral as the stratigraphic datum, the thickness of the Flowerpot and Blaine Formations, combined, is reduced from 330 to 160 ft across the dissolution front: a reduction of 170 ft. The top of the Blaine Formation drops 170 ft across the dissolution front and the several marker beds (the same as shown in Fig. 10) above the Blaine drop about 200 ft. Inasmuch as the thickness of all strata between the top of the Blaine and the base of the Niobrara increases by only 30 ft across the dissolution zone, it suggests that most of the salt dissolution occurred after Fort Hays deposition; perhaps 30 ft of salt-dissolution-induced subsidence may have occurred sometime between deposition of the Blaine and the start of Niobrara deposition in that part of the area.

Other studies in western Kansas provide similar results on the timing of dissolution of salt and collapse of overlying strata into sinkholes or large subsidence troughs. In general, the major dissolution and collapse occurred after deposition of early Late Cretaceous strata (after Dakota or Fort Hays/Niobrara deposition), and before or during deposition of the Tertiary Ogallala Formation (Macfarlane and Wilson, 2006). This also includes studies in Hamilton County of the Coolidge and Devil's Hole Sinks and the Little Bear Fault (McLaughlin, 1943), and in Meade County of the Crooked Creek and Fowler Faults (Gutentag and others, 1981).

Timing of salt dissolution in the Sharon Springs–Wallace area apparently is not the same as dissolution of these same salts about 35 mi farther west in Colorado. Berry (2018) examined results of a seismic survey in parts of Cheyenne and Kiowa Counties and concluded that dissolution of the middle Blaine salt (therein referred to as "upper Blaine halite") occurred mainly before Taloga deposition (Late Permian), and that dissolution of the Flowerpot salt (therein referred to as "lower Blaine halite") occurred in post-Taloga time, but before deposition of the Dakota Formation (that is, well before Niobrara deposition).

In Baca County, southeast Colorado, Askew (2013) showed that a series of parallel zones of salt-thins in the middle Blaine salt are aligned along a northeast–southwest trend that overlies similarly oriented, deep-seated faults radiating from an Ancestral Apishapa High. He could only conclude that salt dissolution occurred in post-Triassic time, but he suggested that Tertiary tectonism in that area could have reactivated these deep-seated faults, and that this could have provided vertical pathways, whereby near-surface fresh water in the Dakota and Ogallala aquifers could migrate down to the Blaine salt and cause its dissolution.

STRUCTURAL GEOLOGY

The structural geology of strata below the Flowerpot and Blaine salts in the Sharon Springs–Wallace area is relatively simple: the Y-anhydrite, a short distance below the Flowerpot salt, dips gently to the north at about 12–25 ft/mi (about one-eighth to one-fourth of 1°), interrupted by two herein-identified faults (Fig. 11). There are no soluble salts beneath the Y-anhydrite, except for 2–5 ft of salt commonly at the top of the Stone Coral: therefore, this structural datum should accurately represent the structure of Permian strata, excluding the effects of dissolution of Flowerpot and Blaine salts.

Mapping the structure at the top of the Blaine Formation, however, presents a different, more complicated picture (Fig. 12). The top of the Blaine generally dips to the north at about the same rate as the Y-anhydrite, but the simple north dip is interrupted at numerous places by subsidence and collapse into dissolution zones developed in the Flowerpot and middle Blaine salts. The most conspicuous structural feature in the Blaine Formation is in the west, where the top of the Blaine is generally dropped about 150–200 ft across the Flowerpot salt-dissolution zone. This drop is similar to the amount of thinning of the Flowerpot–Blaine sequence across the dissolution front, and clearly results entirely (or almost entirely) from salt dissolution.

Structural cross sections are presented at two places that show displacement of Permian strata across the two newly identified faults: the Sharon Springs Fault, just east of Sharon Springs (Figs. 11, 12, 13), and the Ruggles Draw Fault Zone in the north part of the study area (Figs. 11, 12, 14).

The Sharon Springs Fault has a throw (down to the north) of about 82 ft on top of the Y-anhydrite, and a throw of 113 ft (down to the north) on top of the Blaine Formation, on the basis of two wells that are less than 1 mi apart (Fig. 13). Most of the difference in throw between the two datum beds is caused by dissolution of the middle Blaine salt, inasmuch as the total thickness of the Blaine decreases by 38 ft on the downthrown (north) side. The orientation of the Sharon Springs Fault is unknown at the site of this cross section, but it is

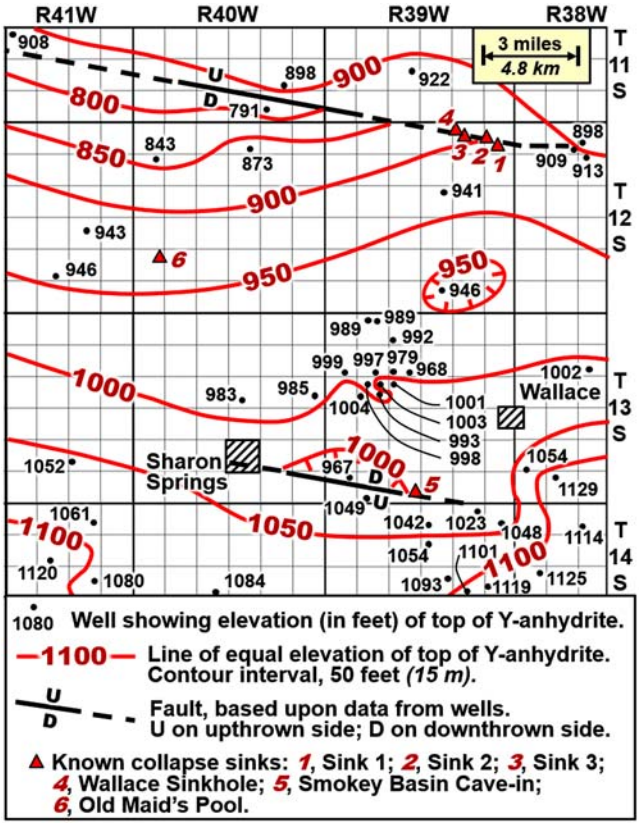

Figure 11. Structure map showing elevation of top of the Y-anhydrite in the Sharon Springs–Wallace area.

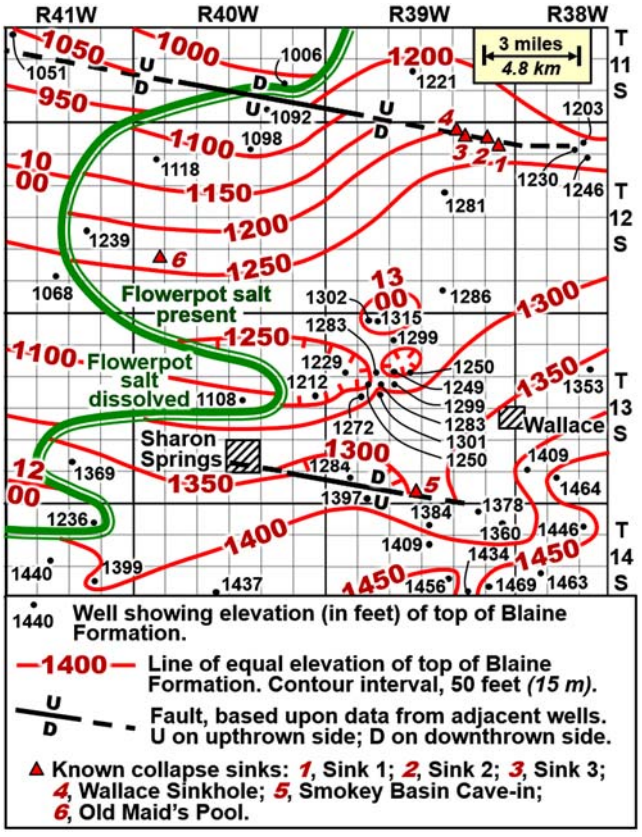

Figure 12. Structure map showing elevation of top of the Blaine Formation in the Sharon Springs–Wallace area. Also shown is the approximate dissolution front for the Flowerpot salt (green line). Ruggles Draw Fault Zone in north is downthrown to the south (see Fig. 11), except in southeast part of T. 11 S., R. 40 W., where dissolution of Flowerpot and middle Blaine salts has caused the top of the Blaine to locally be downthrown to the north (see Fig. 14).

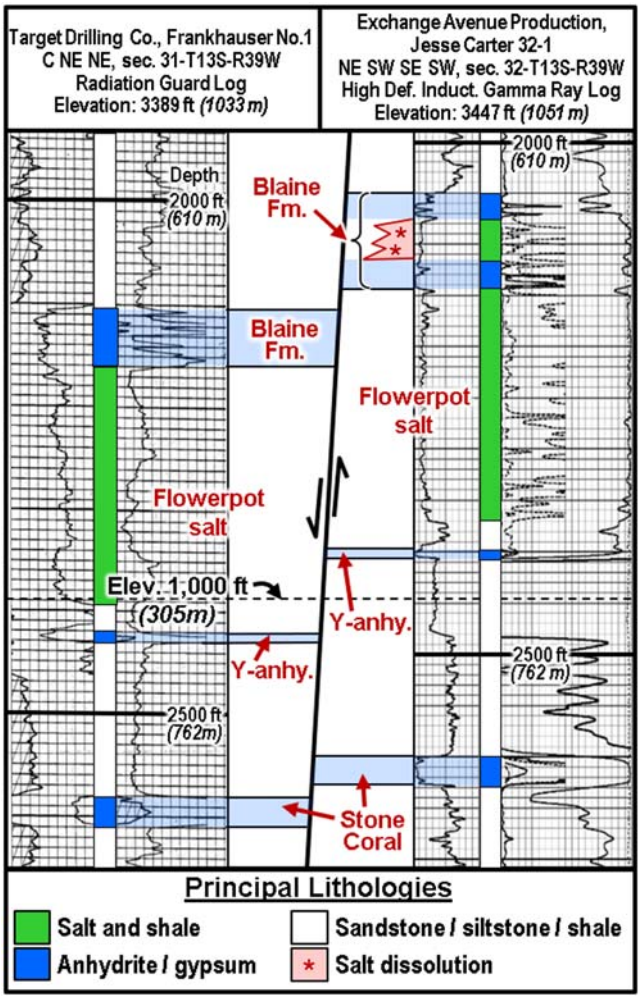

Figure 13. Structural cross section showing Sharon Springs Fault between two wells in southwest part of T. 13 S., R. 39 W. Throw is 82 ft (25 m) at top of Y-anhydrite, and, due to dissolution of the middle Blaine salt, is 113 ft (34 m) at top of Blaine Formation.

possible that it ties in with the Smoky Basin Cave-in (a sinkhole) to the east. A fault was exposed in the wall of this sink, according to both Russell (1929) and Elias (1931), and for this reason, I have chosen to draw the fault with an orientation of S 80° E and have it intersect with the Smoky Basin Cave-in (Figs. 11, 12); the suggested orientation of this fault is further justified by the following discussion of the Ruggles Draw Fault Zone.

The Ruggles Draw Fault Zone is downthrown to the south in strata beneath the Flowerpot Shale, as well as in strata above the Flowerpot in most of the area. However, in a limited area, in the southeast part of T. 11 S., R. 40 W., the Blaine Formation is downthrown to the north, caused by dissolution of the Flowerpot salt (Figs. 12, 14). To explain this complex situation, two structural cross sections are presented across the Ruggles Draw Fault Zone (Figs. 14A, 14B), using two wells that are about 1 mi apart and that straddle the fault zone: these wells are about 1 mi west of the north-trending Ruggles Draw, the nearest surface feature that is named. The cross section shown in Figure 14A is complex, and parts of it are difficult, or impossible, to explain. The Stone Coral is dropped down to the south, with a throw of about 27 ft, and the Y-anhydrite is also down on the south with a throw of about 107 ft. However, the top of the Blaine Formation is raised up on the south by about 85 ft. In addition, the Cedar Hills Sandstone appears to be missing in the F & M well, on the south.

The facts noted above cannot be explained by a single fault separating the two wells, and therefore, a second cross section (Fig. 14B) is presented to more reasonably show the probable faulting between the two wells. In this cross section, the well logs are eliminated to simplify the drawing, but the lithology and depths are the same as in Figure 14A. By showing two faults (faults "a" and "b") between the two wells, it is possible to explain the ambiguities in Figure 14A.

Both faults in the fault zone are normal, downthrown to the south (on the left) in strata below the Flowerpot. However, because of dissolution of the Flowerpot salt between the two wells, the Blaine Formation has been dropped down about 85 ft on the north (on the right), and this makes the upper part of fault "a" appear to be a reverse fault in the Blaine Formation and overlying strata. Fault "a" cuts the F & M well at, or near, the top of the Cedar Hills Sandstone, thus explaining the absence of the Cedar Hills in that well: it also explains 107 ft of throw of the Y-anhydrite. Fault "b" is necessary, because it shows 27 ft of throw of the Stone Coral between the two wells. It is possible that some of the Flowerpot salt is present in the block between the two faults, but it is certainly mostly gone in the Pickrell well on the north. I believe that this second cross section (Fig. 14B) more accurately shows conditions between the two wells, although it is not clear if the Ruggles Draw Fault Zone is a fault zone (multiple faults) elsewhere in the area.

As with the Sharon Springs Fault, the orientation of this Ruggles Draw Fault Zone is unknown at the site of Figure 14. However, inasmuch a series of four sinkholes, located about 6 mi to the east, have a striking alignment of about S 80° E (Fig. 15), it is reasonable to draw the fault zone with that same orientation and have it extended through the area of the Wallace Sinkhole and the other 3 sinks in Bradshaw Draw.

In addition, the Ruggles Draw Fault Zone may extend still farther east, with a slight shift to an east–west orientation, reaching the area of three wells in the northwest part of T. 12 S., R. 38 W.: here, although the Y-anhydrite does not appear to be offset (Fig. 11), the top of the Blaine is dropped down to the north by 27 ft (Fig. 12), and the thickness of the middle Blaine salt (Fig. 9) decreases

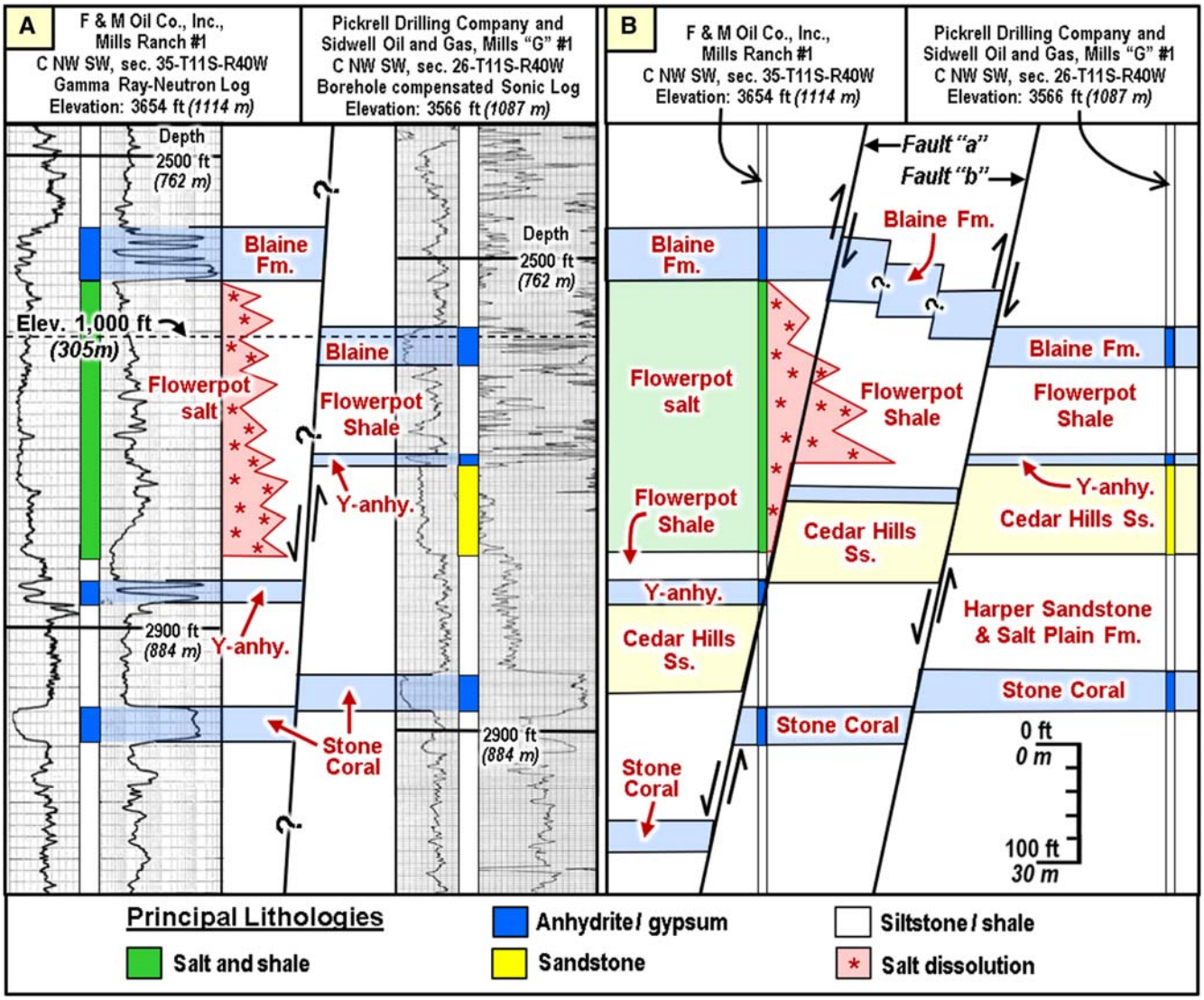

Figure 14. Structural cross sections A and B showing Ruggles Draw Fault Zone between two wells in southeast part of T. 11 S., R. 40 W. A) Simplified cross section with well logs showing throw is 107 ft (33 m) at top of Y-anhydrite, and 86 ft (26 m) (reversed throw) at top of Blaine Formation. This cross section, as drawn, is complex and impossible to explain. B) More reasonable cross section, without geophysical logs, showing a fault zone with two normal faults, downthrown on the left (south), but dissolution of the Flowerpot salt between the two wells causes the Blaine Formation and younger strata to be downthrown on the right (north) of both faults. Fault "a" cuts the F & M well at, or near, the top of the Cedar Hills Sandstone, explaining why, in the F & M well, the Cedar Hills is missing, and why the interval between the Y-anhydrite and Stone Coral is so thin. Some Flowerpot salt may be present in the down-dropped block between the two faults.

sharply to the north, from 35 ft to 0 and 5 ft in a distance of less than half a mile. Although actual fault(s) may not be present in this eastern-most section of the fault zone, joints and/or fractures in the Ruggles Draw zone may be pathways for meteoric water to reach, and dissolve, the middle Blaine salt.

If I am correct in the orientation of the Sharon Springs and Ruggles Draw Faults, then it is likely that 5 sinkholes (Wallace, Sink 1, Sink 2, Sink 3, and Smoky Basin cave-in) are the result of groundwater percolating down faults, fault zones, or associated joints and fractures, creating dissolution cavities in the Blaine and/or Flowerpot salts, resulting in collapse and development of the sinkholes. In addition, water percolating down joints and/or fractures at the east end of the Ruggles Draw Fault Zone is likely the cause of dissolution of the middle Blaine salt in two wells in sec. 4 and 5, T. 12 S., R. 38 W.

In addition to the 2 fault systems identified in the current study, Elias (1931, p. 40) stated that he observed many fissures in outcrops of the Niobrara in Wallace

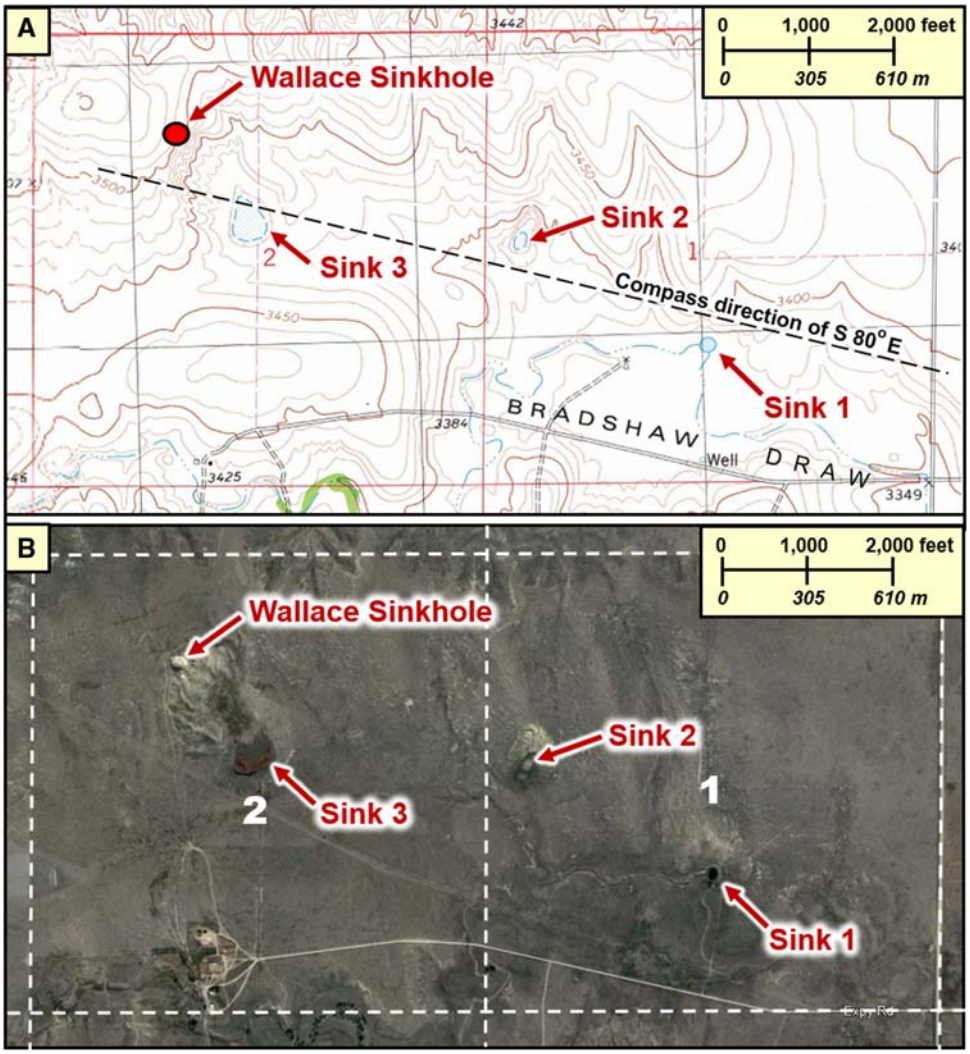

Figure 15. Location of Wallace Sinkhole and three earlier sinkholes in secs. 1 and 2, T. 12 S., 39 W., in Bradshaw Draw, Wallace County, Kansas. These sinkholes are roughly aligned along the compass direction of S 80°E. A) Map is the 1979 USGS 1:24,000-scale topographic map of Harris Draw East, and a small part of Harris Draw West. B) Aerial photograph of same area from Google Earth, dated October 6, 2014.

County. He postulated that these fissures could have been pathways for groundwater to circulate down and dissolve soluble rock.

SINKHOLES IN SHARON SPRINGS–WALLACE AREA

Wallace County has 6 known sinkholes in the Sharon Springs–Wallace area. Three of the sinks, the Wallace Sinkhole, Smoky Basin Cave-in, and Sink 1, have formed since the year 1900, whereas the other three, Old Maid's Pool, Sink 2, and Sink 3, formed at earlier, unknown times. The several reports that have discussed Wallace County sinkholes in the past are by Moore (1926a, b), Russell (1929), Elias (1931), Frye (1950), Merriam and Mann (1957), and Merriam (1963).

Wallace Sinkhole

On July 31, 2013, a large sinkhole was discovered near the center of the northwest quarter of sec. 2, T. 12 S., R., 39 W., about 9 mi north of the town of Wallace, in Bradshaw Draw (Figs. 1, 15, 16). This newly named Wallace Sinkhole had already reached about 200 ft in diameter and about 90 ft deep by that time (Figs. 16A, 16B), and the bottom of the sinkhole was dry—no ponding of water in the bottom. Although it occurred in pasture land and caused no injuries or infrastructure damage, it caused quite a stir and drew statewide interest. The sinkhole became a local attraction for several days, with many people coming to see the new phenomenon. Because of the potential danger, fencing was soon erected around the sink to protect visitors. A series of concentric fractures developed around the south side

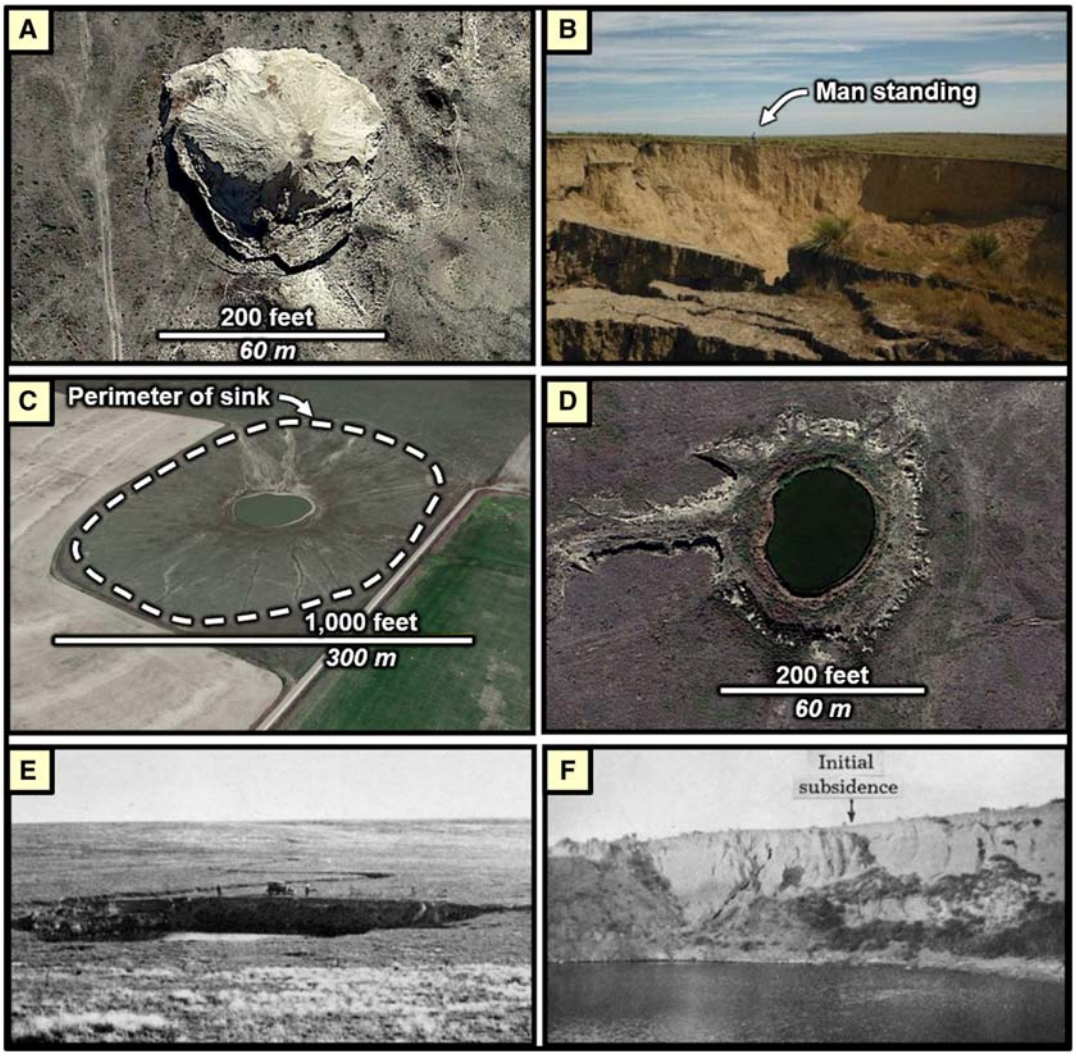

Figure 16. Photos of sinkholes in the Sharon Springs–Wallace area. A) Google Earth vertical view of Wallace Sinkhole, dated October 6, 2014. B) Ground view of Wallace Sinkhole, courtesy Larry Townsend, Wallace County Sheriff. C) Google Earth oblique view of Old Maid's Pool, dated July 10, 2016. D) Google Earth vertical view of Sink 1 in Bradford Draw, dated October 6, 2014. E) View of Sink 1, taken about 1930, some 30 yr after the sinkhole formed (Elias, 1931, Plate XL–B). F) View of Smokey Basin Cave-in, taken about 1930, some 4 yr after the sinkhole formed (Elias, 1931, Plate XL–A).

of the sinkhole, indicating that the hole could become larger by sloughing off of the sides (Fig. 16A). The surface elevation of the sinkhole is about 3,500 ft above sea level (Fig. 15).

Bedrock at the sinkhole is Cretaceous Pierre Shale, but it is mantled by the Pleistocene Peoria and Loveland Formations, and possibly also some thin Tertiary Ogallala Formation (Hodson, 1963): the total thickness of these surficial deposits at the sinkhole is unknown, but probably in the range of 20–50 ft thick. They unconformably overlie the Pierre Shale, which is at least several hundred feet thick, and then about 600 ft of Niobrara Formation (chalk and limestone). Underlying the Niobrara Formation is a series of Cretaceous, Triassic, and Permian strata, as shown in Figures 2 and 10.

Assuming that the elevation of the top of the Blaine Formation is about 1,200 ft (Fig. 12), then the Blaine would be about 2,300 ft deep. Inasmuch as the thickness of the upper Blaine anhydrites is about 30 ft (Fig. 3), then the depth to the middle Blaine salt is about 2,330 ft, and the top of the Flowerpot salt is about 2,400 ft deep. This is quite deep for dissolution to occur, but if the Ruggles Draw Fault Zone (Figs. 11, 12, 14) does extend east to the Wallace Sinkhole area, and if there are associated fractures or other open pathways, then it is possible for fresh groundwater to migrate down the fault zone and dissolve some of the Blaine and Flowerpot salts. If the cavity thus formed became so large that the roof of the cavity ultimately collapsed, then overlying strata would also fall in, forming a

collapse breccia or breccia pipe that reached the land surface as the Wallace Sinkhole.

The size of the sinkhole requires that at least some of the Flowerpot salt has been dissolved beneath the Wallace Sinkhole. Inasmuch as the depth of the surface sink reached at least 90 ft, and the thickness of the middle Blaine salt was originally only about 35–40 ft thick in the area (Figs. 3, 9), dissolution of all the Blaine salts alone could not form a cavity high enough to create the 90-ft-deep sinkhole. Therefore, a significant amount of the Flowerpot salt must have been dissolved locally, despite the fact that more than 200 ft of salt is still present in all the wells surrounding the sinkhole (Fig. 6).

Of additional interest in this area is the thinning and absence of the middle Blaine salt about 4 mi east of the Wallace Sinkhole, in secs. 4 and 5, T. 12 S., R. 38 W. (Fig. 9). In wells that are less than half a mile apart, the salt unit thins from 35 ft on the south, to 0 and 5 ft on the north. This abrupt thinning (dissolution) of the middle Blaine salt occurs along a further extension, at S 80° E, of the Ruggles Draw Fault Zone that apparently passes through the Wallace Sinkhole. The thickness of the Flowerpot salt is quite similar in these three wells (Fig. 6), and thus, salt dissolution has only reached down to the middle Blaine salt: collapse of a cavity only about 35 ft high in the Blaine Formation here apparently is not enough to form a breccia pipe that reaches up to the current land surface (i.e., no sinkhole here).

Other Sinkholes

Several other sinkholes are present in the Sharon Springs–Wallace area, and they are likely to have been formed by dissolution of subsurface salt beds in the Blaine and/or Flowerpot Formations. These additional sinks are Smokey Basin Cave-in, Old Maid's Pool, and Sinks 1, 2, and 3 in Bradshaw Draw.

Smoky Basin Cave-in

The Smoky Basin Cave-in developed on March 9, 1926, on the south side of Smoky Hill River on the section line between secs. 33 and 34, T. 13 S., R. 39 W. (Figs. 1, 16F). Shortly after the collapse, Moore (1926a, b) described the dimensions as 250 by 350 ft wide, and a depth, estimated by early visitors, of 300–500 ft (this depth seems extreme and unreasonable to me). Water then ponded in the sinkhole, and, as an indication of the great size of the underground cavity that collapsed to form the sinkhole, Moore (1926a) stated "Systematic soundings [of the pond] showed a gradual increase in depth of the water to about 50 feet, and then in the middle part of the depression a practically vertical-sided hole in which the depth of water was 165 to 170 feet. The computed volume of the depression is approximately 1.5 million cubic feet." Both Russell (1929) and Elias (1931) noted that a fault was exposed in the wall of the sink, and Russell described it as a normal fault with a throw of 50 ft.

Early views on the origin of Smoky Basin Cave-in attributed it to: 1) dissolution of chalk in the Cretaceous Niobrara Formation, with subsequent collapse of the roof (Moore, 1926a, b; Elias, 1931; Frye, 1950; Merriam and Mann, 1957), and 2) voids being created in the Niobrara during deformation along tensional fault planes (Russell, 1929).

It is certain that the Smoky Basin Cave-in results from dissolution of salt in Blaine and Flowerpot Formations. The middle Blaine salt, locally about 45 ft thick, is completely missing in three nearby wells: 2 mi to the west, 3 mi to the east–southeast, and about 3.5 mi to the south–southeast (Fig. 9). Although there is no evidence of the Flowerpot salt (locally about 225 ft thick) being dissolved in those same three wells, or elsewhere within about 4 mi of the Cave-in (Fig. 6), it is certainly likely that if the Blaine salt is dissolved locally, then some of the upper Flowerpot salt could also be dissolved locally. Dissolution of the middle Blaine salt, and a significant part (or all?) of the Flowerpot salt, is the most likely explanation for the origin of the Smoky Basin Cave-in, inasmuch as the great amount of collapse (soundings of up to 170 ft in the middle of the pool) is too much to result from dissolution of the middle Blaine salt alone. Based on data from nearby wells, the top of the middle Blaine salt in the Smoky Basin Cave-in would be about 1,950 ft deep, and the top of the Flowerpot salt about 2,025 ft deep.

Old Maid's Pool

Old Maid's Pool, located in the northeast corner of sec. 30, T. 12 S., R. 40 W. (Figs. 1, 16C), is a broad, circular depression that now measures about 1,000 by 1,500 ft wide, and is at least 60 ft from the rim down to a permanent pool of water. Moore (1926b) described it as a "nearly circular depression over eighty feet in maximum depth, approximately three eights of a mile in diameter at the rim and holding at the bottom a permanent small lake about three hundred feet wide." He believed that the origin of this sinkhole and the Smokey Basin Cave-in is undoubtedly the same, but that Old Maid's Pool formed perhaps several scores or even hundreds of years earlier: therefore, Moore attributed this sinkhole to dissolution of chalk in the Niobrara Formation, and ultimate collapse of the cavity's roof.

It is likely that dissolution of salt in the Blaine Formation and some (or all?) of the Flowerpot salt is the cause of Old Maid's Pool. The middle Blaine salt is missing in most of the area around this sinkhole, with a residual patch of 20 ft of salt in a well located about 2.5 mi to the west (Fig. 9), and the regional dissolution front of the Flowerpot salt (the "0" thickness line) appears to

be about 2 or 3 mi to the west and south of the sinkhole (Fig. 6). Dissolution of the middle Blaine salt, and a significant part (or all?) of the Flowerpot salt, is the most likely explanation for the origin of the Old Maid's Pool. Data from a nearby well indicate that the top of the middle Blaine salt would be about 2,300 ft deep, and the top of the Flowerpot salt would be about 2,350 ft deep.

Sinks 1, 2, and 3

Sinks 1, 2, and 3 are located in Bradshaw Draw, in secs. 1 and 2, T. 12 S., R. 39 W. (Figs. 1, 15, 16). These sinks, along with the Wallace Sinkhole, are aligned at about S 80° E. Sink 1 was described by Russell (1929) as being a steep-sided hole, only about 10 ft wide 20 yr earlier, with a deep pool in the bottom: he noted that it had enlarged gradually in the 20 yr prior to 1929. It has continued to enlarge, and at present the sinkhole is about 200 ft in diameter (Fig. 16D). Elias (1931) also mentioned Sink 1: he stated that it originated about 1900, and he included a photo of the sink as of about 1930, wherein the sink appears to be about 150 ft wide (Fig. 16E).

Sinks 2 and 3 (Fig. 15) are even more briefly mentioned than Sink 1 by Russell (1929) and Elias (1931). Both sinks are undated, but clearly are older than Sink 1: they have dry bottoms, and their walls are only moderately steep, because of prolonged erosion.

The origin of Sinks 1, 2, and 3 was considered to be dissolution cavities in the Niobrara chalk by Elias (1931), or because of voids created by tensional faulting in the Niobrara by Russell (1929). Because of the alignment of these sinks, Elias suggested that they are possibly arranged along a fault, whereby groundwater is circulating in, and dissolving, the chalk at a depth of about 500 ft.

Based upon current research, however, it is likely that Sinks 1, 2, and 3 were formed in the same way as the Wallace Sinkhole: collapse of overlying strata caused by dissolution of soluble material in the middle Blaine salt and part (or all?) of the Flowerpot salt along the Ruggles Draw Fault Zone. Inasmuch as the surface elevations of the 3 sinks averages about 3,400 ft (Fig. 15), some 100 ft lower than the Wallace Sinkhole, the depth to the middle Blaine salt at the 3 sinks would be about 2,230 ft, and to the top of the Flowerpot salt about 2,300 ft. These sinks, including the Wallace Sinkhole, are along the possible eastward extension of the Ruggles Draw Fault Zone (Figs. 11, 12, 14), and thus, they could have been formed by fresh water migrating down open fault and/or fracture planes and dissolving the salt.

REFERENCES CITED

Askew, R.L., 2013, Distribution of the Permian Blaine Formation salt in the subsurface of the Hugoton Embayment area of Baca County, southeast Colorado: Rocky Mountain Association of Geologists, The Mountain Geologist, Vol. 50, No. 2, p. 65-75.

Benison, K, Zambito, J.J, and Knapp, J.P., 2015, Contrasting siliciclastic-evaporite strata in subsurface and outcrop: An example from the Permian Nippewalla Group of Kansas, U.S.A.: Journal of Sedimentary Research, Vol. 85, No. 6, p. 626-645. https://www.researchgate.net/publication/275214596

Berry, H.D., 2018, Dissolution of Permian salt, Las Animas Arch, Colorado: unpublished MS thesis, University of Louisiana at Lafayette, 96 p.

Campbell, C. L., 1963, Permian evaporites between the Blaine and Stone Corral Formations: unpublished MS thesis, University of Kansas, 73 p.

Elias, M.K., 1931, The geology of Wallace County, Kansas: Kansas Geological Survey, Bulletin 18, 254 p. http://www.kgs.ku.edu/Publications/Bulletins/18/index.html

Frye, J.C., 1950, Origin of Kansas Great Plains depressions: Kansas Geological Survey, Bulletin 86, Part 1, p. 1-20. http://www.kgs.ku.edu/Publications/Bulletins/86_1/index.html

Gutentag, E.D., Lobmeyer, D.H., and Slagle, S.E., 1981, Geohydrology of southwestern Kansas: Kansas Geological Survey, Irrigation Series 7, 73 p. http://www.kgs.ku.edu/Publications/Bulletins/IRR7/index.html

Hodson, W.G., 1963, Geology and ground-water resources of Wallace County, Kansas: Kansas Geological Survey, Bulletin 161, 108 p. http://www.kgs.ku.edu/General/Geology/Wallace/index.html

Holdoway, K.A., 1978, Deposition of evaporites and red beds of the Nippewalla Group, Permian, western Kansas: Kansas Geological Survey, Bulletin 215, 43 p. http://www.kgs.ku.edu/Publications/Bulletins/215/index.html

Johnson, K.S., 2021a, Overview of evaporite karst in the Greater Permian Evaporite Basin (GPEB) of TX, NM, OK, KS, and CO, *in* Johnson, K.S., Land, L., and Decker, D.D., eds., Evaporite karst in the Greater Permian Evaporite Basin (GPEB) of Texas, New Mexico, Oklahoma, Kansas, and Colorado: Oklahoma Geological Survey, Circular 113.

Johnson, K.S., 2021b, Permian Blaine and San Andres Formations of western Oklahoma and Palo Duro Basin of Texas: their correlation and evaporite karst, *in* Johnson, K.S., Land, L., and Decker, D.D., eds., Evaporite karst in the Greater Permian Evaporite Basin (GPEB) of Texas, New Mexico, Oklahoma, Kansas, and Colorado: Oklahoma Geological Survey, Circular 113.

Johnson, W.D., 1901, The High Plains and their utilization: US Geological Survey, 21st Annual Report, Part 4, p. 601-741.

Macfarlane, P.A., and Wilson, B.B., 2006, Enhancement of the bedrock-surface-elevation map beneath the Ogallala portion of the High Plains Aquifer, western Kansas: Kansas Geological Survey, Technical Series 20, 28 p. http://www.kgs.ku.edu/Publications/Bulletins/TS20/ts20.pdf

McLaughlin, T.G., 1943, Geology and ground-water resources of Hamilton and Kearny Counties, Kansas: Kansas Geological Survey, Bulletin 49, 220 p. http://www.kgs.ku.edu/General/Geology/Hamilton/index.html

Merriam, D.F., 1963, The geologic history of Kansas: Kansas Geological Survey, Bulletin 162, 317 p. http://www.kgs.ku.edu/Publications/Bulletins/162/index.html

Merriam D.F., and Mann, C.J., 1957, Sinkholes and related geologic features in Kansas: Kansas Academy of Science, Transactions, Vol. 60, No. 3, p. 207-243. https://digital.lib.usf.edu/SFS0054165/00001

Moore, R.C., 1926a, Note of subsidence near Sharon Springs, Wallace County, Kansas: Kansas Geological Survey, Bulletin 11, p. 95-96. http://www.kgs.ku.edu/Publications/Bulletins/11/05_salt.html

Moore, R.C., 1926b, The subsidence near Sharon Springs, Kansas: Science, Vol. 64, No. 1649, p. 130-131.

Russell, W.L., 1929, Local subsidence in western Kansas: American Association of Petroleum Geologists, Bulletin, Vol. 13, No. 6, p. 606-609.

Schoewe, W.H., 1949, The geography of Kansas, part 2, physical geography (geology): Kansas Academy of Sciences, Transactions, Vol. 52, No. 3, p. 261-333.

Schumaker, R.D., 1966, Regional study of Kansas Permian evaporite formations: unpublished MS thesis, Wichita State University, Wichita, Kansas, 87 p.

Zambito, J.J., Benison, K.C., Foster, T.M., Soreghan, G.S., Soreghan, M.J., and Kane, M., 2012, Lithostratigraphy of Permian red beds and evaporites in the Rebecca K. Bounds core, Greeley County, Kansas: Kansas Geological Survey, Open-File Report 2012–15, 45 p. http://www.kgs.ku.edu/Publications/OFR/2012/OFR12_15/KGS_OF_2012-15.pdf

Zeller, D.E., 1968, The stratigraphic succession in Kansas: Kansas Geological Survey, Bulletin 189, 81 p. http://www.kgs.ku.edu/Publications/Bulletins/189/index.html

Oklahoma Geological Survey Circular 113, 2021

Dissolution of the Permian Flowerpot Salt Beneath the Great Plains Reservoirs, Queens State Wildlife Area, in Kiowa, Prowers, and Bent Counties, Southeast Colorado

Kenneth S. Johnson
Retired Geologist, Oklahoma Geological Survey,
Norman, Oklahoma

ABSTRACT.—The Permian Flowerpot salt has been dissolved beneath the Great Plains Reservoirs in southeast Colorado, and this has resulted in 10 large, natural depressions that are now being used to store water in four major reservoirs. Individual depressions range from 0.6 to 5.0 mi^2. The four major reservoirs, and several smaller ones, are fed by canals developed in the late 1800s to tap the nearby Arkansas River; the stored water is then used for irrigation, wildlife, and recreational purposes. The Flowerpot salt, part of a red-bed and evaporite sequence, is generally 200–245 ft thick and about 1,800–2,000 ft deep in the northeast part of the study area; however, it thins sharply and is mostly dissolved to the southwest, across a major salt-dissolution front. The timing of salt dissolution is not known, but probably started during or after Late Cretaceous time, and persisted until the late Pleistocene or Holocene Epochs. Structure mapping on marker beds below and above the Flowerpot salt also shows the effect of salt dissolution: the lower marker bed dips gently across the site of the dissolution front without being affected, whereas the upper marker bed shows what appears to be a fault that is offset 100–200 ft across the dissolution front.

INTRODUCTION

Prehistoric dissolution of the Permian Flowerpot salt in southeast Colorado has created several large, natural depressions at the earth's surface that are now being used to store water, mainly for irrigation, but also for wildlife and recreational purposes. The focus of the current study is an area called the Great Plains Reservoirs (GPR) that is located in the Queens State Wildlife Area and embraces parts of Kiowa, Prowers, and Bent Counties, Colorado (Figs. 1, 2). A series of four major reservoirs, and several smaller ones, were formed in the late 1800s when the Great Plains Water Company constructed a series of canals to carry water from the Arkansas River into these depressions (Newell, 1901, p. 240–243). At the starting point of the canal system, water enters the Fort Lyon Canal about 3 mi northwest of La Junta, Colorado, and eventually flows through several additional canals to supply water to the various reservoirs in the GPR. La Junta is about 50 mi WSW of the GPR. The Canals and reservoirs are currently managed by the Amity Mutual Irrigation Co., located in Holly, Colorado, and the U.S. Bureau of Land Management. The GPR system of canals and reservoirs is reportedly the most extensive project of its kind in the west.

The four major reservoirs have Cheyenne names: Neegronda ("Big Water"), Neesopah ("Black Water"), Neenoshe ("Standing Water"), and Neeskah ("White Water")—which is also called "Queens." Water depths in the major reservoirs, at capacity, reportedly range from 13 to 25 ft, and sometimes one or several of them may be dry. Water levels fluctuate, because they are filled during the winter and during floods on the Arkansas River, and the water may be drawn down during Spring and Summer irrigation. Three of the major reservoirs are formed by filling of two-to-four adjacent depressions: when water levels are low, we can see that Neeskah, Neenoshe, and Neesopah Reservoirs comprise two, three, and four separate natural-subsidence depressions, respectively. But when water levels are high, these separate, natural depressions are filled to overflowing,

Johnson, Kenneth S., 2021, Dissolution of the Permian Flowerpot Salt Beneath the Great Plains Reservoirs, Queens State Wildlife Area, in Kiowa, Prowers, and Bent Counties, Southeast Colorado, *in* Johnson, K. S.; Land, Lewis; and Decker, D. D. (eds.), Evaporite Karst in the Greater Permian Evaporite Basin (GPEB) of Texas, New Mexico, Oklahoma, Kansas, and Colorado: Oklahoma Geological Survey, Circular 113, p. 337–346.



Figure 1. Map of Colorado showing location of Great Plains Reservoirs study area in parts of Kiowa, Prowers, and Bent Counties.

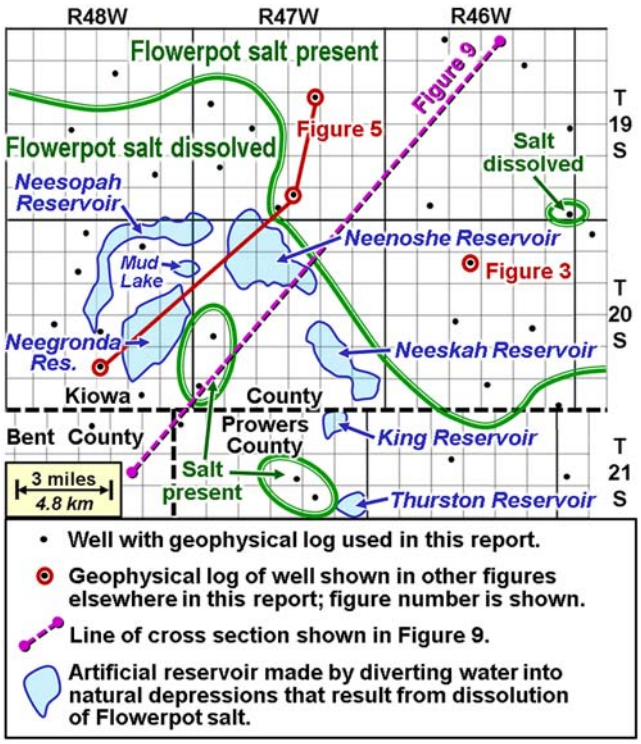

Figure 2. Map of the Great Plains Reservoirs area showing the following: 1) location of well logs used in this report; 2) well logs shown in other figures in the report (Figures 3 and 5); 3) line of cross section in Figure 9; 4) artificial reservoirs at near capacity; 5) county lines; and 6) the approximate limits of Flowerpot salt (green lines), which is mainly present in the northeast part of the area.

and the smaller, depression-filled lakes merge into the three larger reservoirs.

Europeans who settled the area in the late 1800s saw the value of natural depressions in the area for storage of water for irrigation, but the origin of the depressions was unknown. Study of geophysical (electric) logs of petroleum tests in the area has answered the question of the origin of these depressions. A thick sequence of salt (halite), generally 200–245 ft thick and now about 1,800–2,000 ft below the land surface, is present in the Permian Flowerpot Formation just north and east of the depressions: however, most of this Flowerpot salt has been dissolved from the Flowerpot Formation beneath the depressions, and this has resulted in subsidence and collapse of all overlying strata, until the collapse features reached the land surface as natural depressions.

Appreciation is expressed to Dr. Lewis Land, geologist with the National Cave and Karst Research Institute, for his review and constructive comments on an early draft of this report; and to Mr. Terry Howland and Mr. Colin Thompson, with Amity Mutual Irrigation Co., for their review of information about the canals, the reservoirs, and the history of the project. Appreciation is also expressed to the Colorado Oil & Gas Commission, of the Colorado Department of Natural Resources, for having scans of geophysical logs available online: this provided access to the log data needed for this study.

STRATIGRAPHY

Strata of interest in this study are all of Permian age, and range from the Stone Corral, at the bottom, to an unnamed marker bed above the Dog Creek Shale at the top (Fig. 3). These strata are characterized as a "red-bed and evaporite sequence" in the Leonardian and Guadalupian Series. An excellent description of these same strata, in a core drilled about 40 mi to the ENE of the GPR, is given by Zambito and others (2012); this core is from the Amoco Production Company, Rebecca K. Barnes No. 1, drilled in sec. 17, T. 18 S., R. 42 W., Greeley County, Kansas.

The Stone Corral in the study area is typically 30–40 ft of anhydrite, and it is a regionally correlatable rock unit in eastern Colorado and western Kansas; it is equivalent to the Cimarron anhydrite farther south in western Oklahoma and north Texas. The Stone Corral is overlain by 175–200 ft of mostly shale, mudstone, and sandstone of the Salt Plain, Harper, and Cedar Hills Formations, in ascending order. At the top of the Cedar Hills Sandstone is the persistent Y-anhydrite, which typically is 15–30 ft thick.

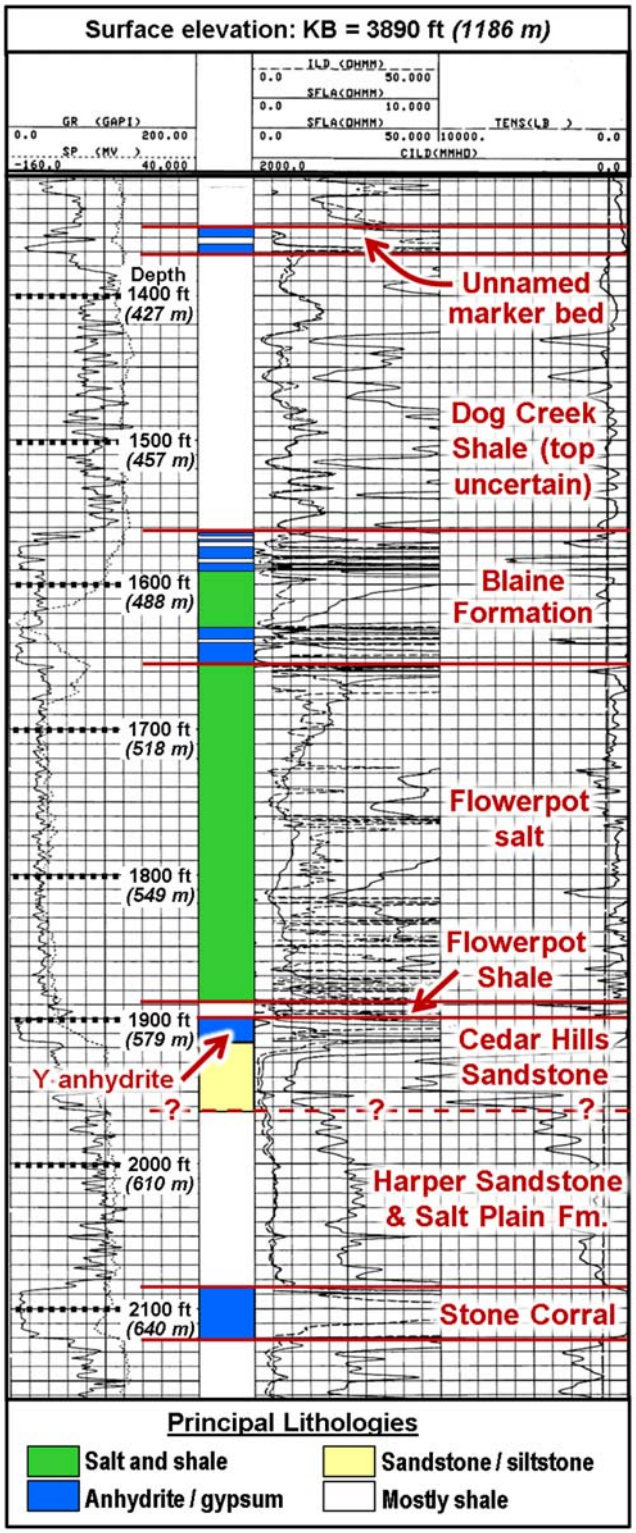

Figure 3. Geophysical log and interpretive lithology of part of the TXO Production Corp., Shouse No. 1 well, located in NE SW NE, sec. 9, T. 20 S., R. 46 W., Kiowa County, Colorado. Log is a "Dual Induction-SFL-GR" log.

Overlying the Y-anhydrite is the Flowerpot Formation that consists of salt and salty shale (Flowerpot salt), and/or shale and mudstone (Flowerpot Shale). The Flowerpot salt is mostly 200–245 ft thick in the northeast part of the study area, but it thins to 105–176 ft thick to the southwest, and then is completely missing in most of the southwest part of the study area (Fig. 4). The "0 feet" thickness line in Figure 4 approximates the dissolution front that separates areas of Flowerpot salt from areas of no salt. In the northeast part of the area, 10–20 ft of Flowerpot Shale normally is present between the top of the Y-anhydrite and the base of the overlying Flowerpot salt, and likewise, about 10 ft of Flowerpot Shale is normally present between the top of the Flowerpot salt and the base of the Blaine Formation (Figs. 3, 5). Southwest of the dissolution front, the salt is mostly missing and the Flowerpot Shale here typically ranges from 25 to 40 ft thick. Two outlying patches of Flowerpot salt are still present beyond the dissolution front, with 10–176 ft of salt and salty shale being present in these outliers (Fig. 4). It is likely that additional residual patches of Flowerpot salt are present in the southwest part of the area, but they were not penetrated in the wells examined for this report (not all wells with geophysical logs in the study area were available for examination).

Above the Flowerpot is the Blaine Formation, a regionally persistent sequence of interbedded gypsum/anhydrite, shale, thin beds of dolomite, and (locally) salt. The formation is recognized in eastern Colorado, western Kansas, western Oklahoma, and much of north

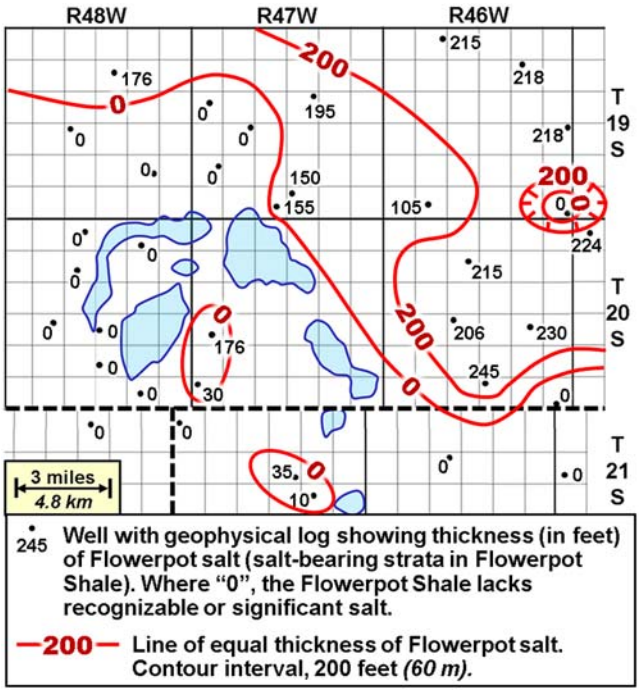

Figure 4. Map showing thickness of the Flowerpot salt in the Great Plains Reservoirs area.

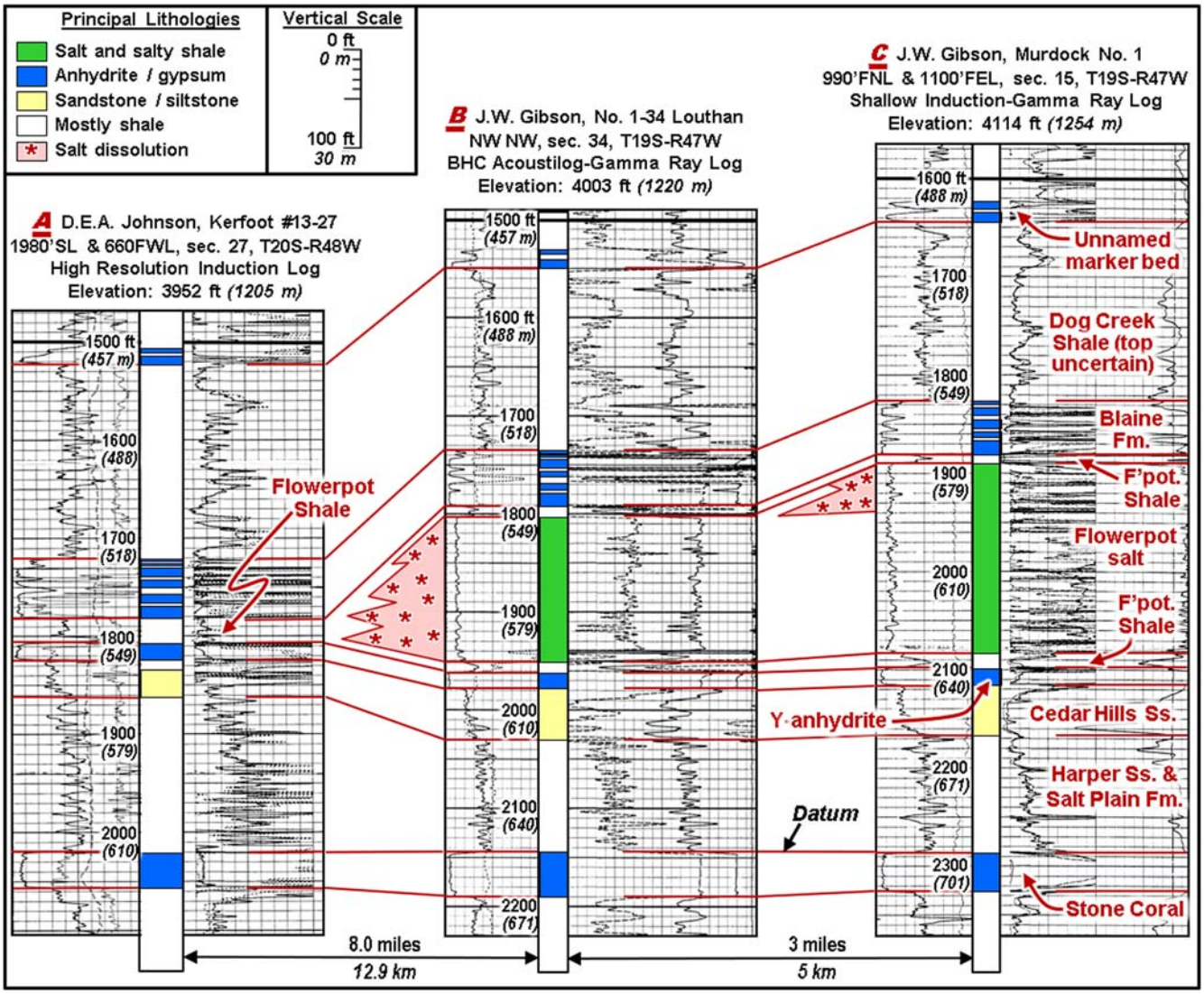

Figure 5. Stratigraphic cross section showing dissolution of Flowerpot salt across the main dissolution front. Between wells *C* and *B*, the upper part of the Flowerpot salt is dissolved; and between wells *B* and *A*, all the remaining Flowerpot salts are dissolved.

Texas: it is equivalent to part of the San Andres Formation in much of Texas and eastern New Mexico. The thickness of the Blaine Formation ranges from 40 to 100 ft in the northeast part of the study area and about 30–55 ft in the southwest. The two anhydrite beds in the lower part of the Blaine (Figs. 3, 5) are equivalent to the Medicine Lodge and Nescatunga Gypsum Beds of northwest Oklahoma, and the lowest of the upper Blaine anhydrite beds (Fig. 3) is equivalent to the Shimer Gypsum Bed of northwest Oklahoma. Between the lower- and upper-anhydrite parts of the Blaine Formation is the middle Blaine salt (Fig. 3): this salt is 15–40 ft thick at places in the eastern two-thirds of Ts. 19–21 S., R. 46 W., but is missing (because of dissolution) farther west, where that interval is represented only by shale (Fig. 5).

Overlying the Blaine Formation is the Dog Creek Shale, which consists predominantly of shale and mudstone. The top to the Dog Creek is not conspicuous in well logs of the study area, so the thickness of the formation here is unknown. About 180–200 ft above the Blaine/Dog Creek contact is a persistent pair of unnamed anhydrite beds, each typically 5–10 ft thick and separated by about 5 ft of shale. These anhydrite beds have been called "Day Creek" in Kansas (Zambito and others, 2012), but my studies from west Texas to the Texas Panhandle area suggest that they are the Alibates beds, and thus are equivalent to the Rustler Formation; perhaps, they are evaporites correlative with the Culebra and Magenta Dolomites in the Rustler of west Texas and southeast New Mexico; McGillis and Presley (1981) discuss the Alibates Formation as being two beds of

gypsum/anhydrite and dolomite in the Texas Panhandle that are in part equivalent to the Rustler Formation.

The youngest bedrock formations exposed in the area are sparse outcrops of the Upper Cretaceous Niobrara Formation, but these are extensively mantled by Pleistocene and Holocene loess, eolian sand, and slopewash throughout the GPR area (Dane and others, 1937; Voegeli and Hershey, 1965; Sharps, 1976). I am not familiar with the stratigraphy of strata between the unnamed anhydrite beds above the Dog Creek Shale and the outcropping Niobrara in this area, and, therefore, have not attempted to identify these strata on the geophysical logs.

FLOWERPOT SALT DISSOLUTION

The Flowerpot salt underlies essentially the northeast half of the study area (Fig. 4). The salt unit ranges from 105 to 245 ft thick in the area, and most commonly is 200–245 ft thick. The salt is but 105–176 ft thick at sites approaching the dissolution front, where some of the salt (most likely the upper-most salt) has been dissolved. In one well, located in sec. 36, T. 19 S., R. 46 W., about 8–10 mi east of the dissolution front, the Flowerpot salt is absent: this undoubtedly is a site where groundwater has descended to the salt and dissolved it. Such groundwater movement in an area surrounded by thick salt normally occurs where overlying strata are fractured and/or faulted, and the result commonly is a collapse breccia or breccia pipe that can lead to a sinkhole at the land surface—such as the Wallace Sinkhole that formed in 2013 in Wallace County, Kansas, nearly 70 mi to the northeast (Johnson, 2021). The east–west trend of wells with partial or total Flowerpot-salt removal, in the south part of T. 19 S., Rs. 46–47 W., suggests the possibility of a zone of faults and/or fractures that allowed groundwater to circulate down to, and dissolve, some or all of the salt: however, there is no direct evidence of such faults, fractures, or collapse breccia.

In the southwest half of the study area, all the Flowerpot salts have been dissolved, except for two residual patches of salt identified so far (Fig. 4); of course, there probably are additional outliers of salt that are not yet identified. One outlier of Flowerpot salt is 10–35 ft thick in T. 21 S., R. 47 W., and the second outlier has 30–176 ft of salt in secs. 19 and 30, T. 20 S., R. 47W. This outlier, with 176 ft of salt still present, is nearly the original thickness of the salt unit in the area, and it indicates that there may be additional pinnacles of thick salt elsewhere southwest of the dissolution front. The dissolution front, as shown in this report, is a refinement of the Flowerpot salt limits, as shown earlier by Ege (1985) (Fig. 6). Ege also noted an outlying, undissolved mass of salt (Flowerpot salt or middle Blaine salt?) farther west in Crowley County.

Dissolution of the Flowerpot salt across the dissolution front is clearly shown in Figure 5. Salt and salty

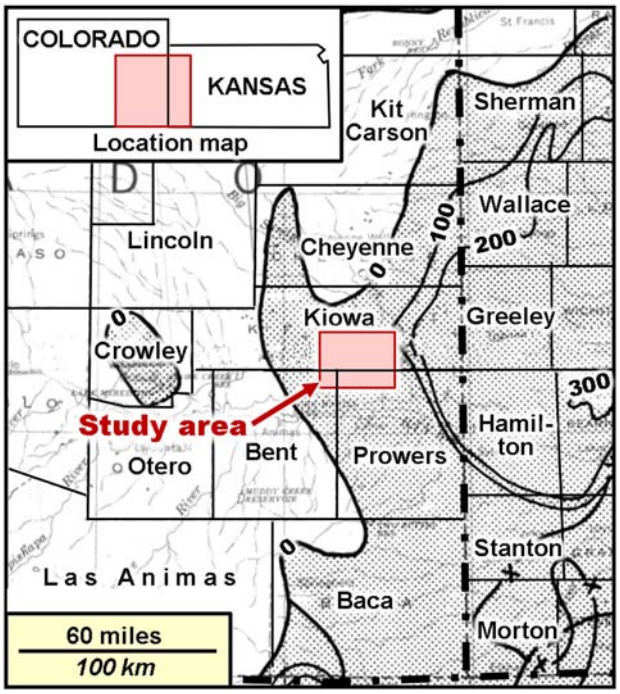

Figure 6. Map showing study area and distribution and thickness (in feet) of Flowerpot and middle Blaine salts in parts of parts of Colorado and Kansas; modified from Ege (1985). Area where the thickness is in excess of 100 ft is underlain by Flowerpot salt and maybe middle Blaine salt; areas of less than 100 ft are probably only (or mostly) middle Blaine salt.

shale in the Flowerpot is 195 ft thick in well C, and the salt unit is underlain and overlain, respectively, by 20 and 10 ft of Flowerpot Shale. Three miles to the south, well B penetrated 150 ft of salt and salty shale that is underlain and overlain by 10 ft of shale. Therefore, within that distance, 45 ft of the uppermost salt has been dissolved. In addition, in well A, another 8 mi farther southwest, all of the salt is dissolved, and the Flowerpot Shale here is about 27 ft thick. The Flowerpot salt appears to be of high purity in the study area, inasmuch as the great thickness of the salt unit to the north is represented by a relatively thin sequence of shale to the south where all salts have been dissolved.

The age or timing of salt dissolution here is not known: however, with comprehensive study of the thickness of strata that overlie the unnamed marker bed, it may be possible to determine something about the probable time of dissolution. Several studies in southeast Colorado and western Kansas provide information on the timing of salt dissolution in the region. For example, dissolution of the Flowerpot and middle Blaine salts about 20 mi north of the GPR area, in parts of Cheyenne and Kiowa Counties, was studied by Berry (2018). In this area, the Flowerpot salt is about 180–200 ft thick, and the middle Blaine salt is about 40 ft thick. Both salts,

generally 2,200–2,500 ft deep, are locally dissolved. Berry examined results of a seismic survey and concluded that dissolution of the middle Blaine salt (therein referred to as "upper Blaine halite") occurred mainly before Taloga deposition (Late Permian), and that dissolution of the Flowerpot salt (therein referred to as "lower Blaine halite") occurred in post-Taloga time, but before deposition of the early Late Cretaceous Dakota Formation.

Surface evidence of fossil sinkholes in Prowers County, about 20 mi southeast of GPR, was described by Dane and Pierce (1934). Three roughly circular sinks, 100–200 ft in diameter, contain brecciated blocks of the Late Cretaceous Niobrara Formation (Hayes Limestone and Smokey Hill Members) in sec. 6, T. 22 S., R. 44 W. My examination of geophysical well logs in the vicinity of those sinks shows the following: 1) Flowerpot salt is not present in this area, and 2) the middle Blaine salt is 50 ft thick, at a depth of 1,450 ft just 0.6 mi south of the sinks, and is thinner or absent in several other wells within several miles of the sinks. I assume that the Flowerpot salt was not deposited here, because if it had been, and is now dissolved, then the middle Blaine salt should also be gone in all the local wells: the middle Blaine salt would be above any Flowerpot salt, and it should have been dissolved first by descending waters. I conclude that local dissolution of the middle Blaine salt caused these sinkholes, and that the time of dissolution was at least during or after Late Cretaceous time.

Farther south, in Baca County, Colorado, Askew (2013) showed that a series of parallel zones of salt-thins in the middle Blaine salt are aligned along a northeast–southwest trend that overlies similarly oriented, deep-seated faults radiating from an Ancestral Apishapa High. The Flowerpot salt is absent in this area, as it is in the Prowers County area described above, so the only salt unit available for dissolution is the 60-ft-thick middle Blaine salt, present at depths of about 700–1,200 ft. Askew concluded that salt dissolution occurred in post-Triassic time, but he suggested that Tertiary tectonism in the area could have reactivated these deep-seated faults, and that this could have provided vertical pathways whereby near-surface fresh water in the Dakota and Ogallala aquifers could migrate down to the middle Blaine salt and cause its dissolution.

Studies in western Kansas have also provided some results on the timing of dissolution of salt—mainly the Flowerpot salt. General studies or summaries of sinkholes and collapse features in western Kansas were made by Johnson (1901), Schoewe, (1949), Merriam and Mann (1957), Merriam (1963, Appendix D), and Macfarlane and Wilson (2006). In general, the major dissolution and collapses occurred after deposition of early Late Cretaceous strata (after Dakota or Fort Hays/Niobrara deposition), and before or during deposition of the Tertiary Ogallala Formation (Macfarlane and Wilson, 2006). Their conclusions are based on the following studies: 1) study of the Coolidge and Devil's Hole Sinks and the Little Bear Fault in Hamilton County (McLaughlin, 1943) and 2) study of the Crooked Creek and Fowler

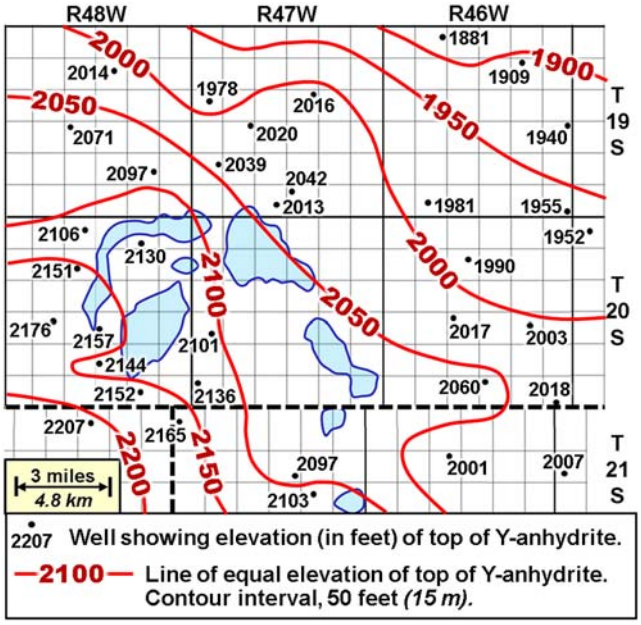

Figure 7. Structure-contour map showing elevation of top of the Y-anhydrite in the Great Plains Reservoirs area.

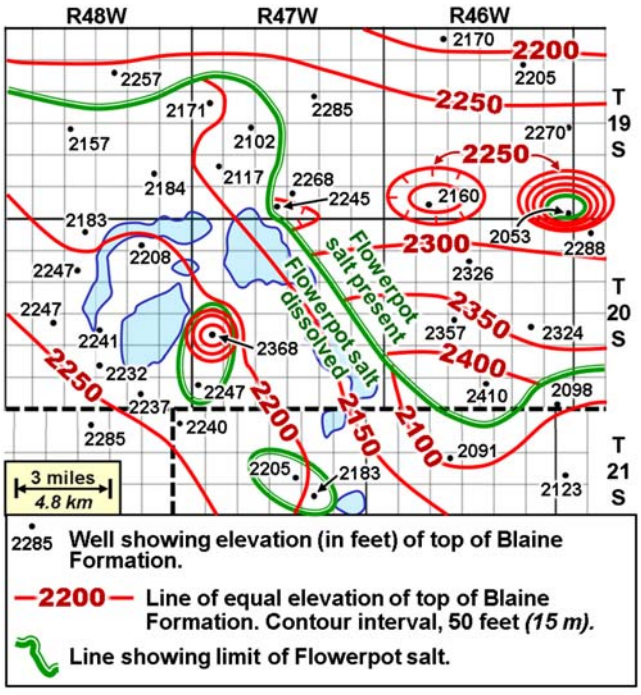

Figure 8. Structure-contour map showing elevation of top of the Blaine Formation in the Great Plains Reservoirs area.

Faults in Meade County (Gutentag and others, 1981). Similar results were observed in a study of salt dissolution and sinkholes in the Sharon Springs–Wallace area of Wallace County (Johnson, 2021).

It appears, therefore, that most of the salt dissolution in southeast Colorado and western Kansas began during or after Late Cretaceous time, and that certainly is possible in the GPR area. Regardless of when dissolution started in this area, it seems likely that it continued until at least the late Pleistocene, or perhaps even the Holocene Epoch. Such late-stage (late Pleistocene/Holocene) dissolution is indicated by the major depressions still being present: they would likely have been filled and covered by windblown or sheetwash sediment if the current depressions had formed at a much earlier time. In addition, it is even likely that salt is still being dissolved in the GPR area today.

STRUCTURAL GEOLOGY

The structural geology, based upon mapping of two excellent marker beds, shows the results of salt dissolution on local structure. A contour map on top of the Y-anhydrite (Fig. 7), just below the Flowerpot Formation, shows that the subsalt strata dip gently to the northeast at about 10–30 ft/mi (about one-ninth to one-third of one degree). There are no soluble salts beneath the Y-anhydrite, so this structure map should be fairly representative of underlying strata for the next several hundred to, perhaps, several thousand feet.

The structure-contour map on top of the Blaine Formation, however, presents a totally different, more complicated situation (Fig. 8). The Blaine Formation is directly above the Flowerpot Formation, and thus dissolution and removal of some 200–245 ft of salt have caused collapse and settlement of the Blaine Formation into the dissolution cavities. Northeast of the dissolution front, the Blaine dips gently to the north at 10–30 ft/mi (about one-ninth to one-third of 1°), except for the several places along the south side of T. 19 S., Rs. 46–47 W., were some or all of the Flowerpot salt is missing. However, to the southwest, the top of the Blaine Formation drops sharply across the northwest-trending dissolution front, and here the formation dips gently to the northeast at the same rate of about 10–30 ft/mi. If one were to look only at contours on top of the Blaine Formation, and not at the presence and absence of underlying Flowerpot salt, one would probably conclude that a significant fault, with a throw of 100 to more than 200 ft, separates the northeast and southwest parts of the study area. A notable exception to the gentle northeast dip in the southwest is the anomalous high of 2,368 ft for the top of the Blaine in sec. 19, T. 20 S., R. 47 W. This anomaly results from the 176-ft-thick mass of undissolved Flowerpot salt that underlies the Blaine at this site (Fig. 4).

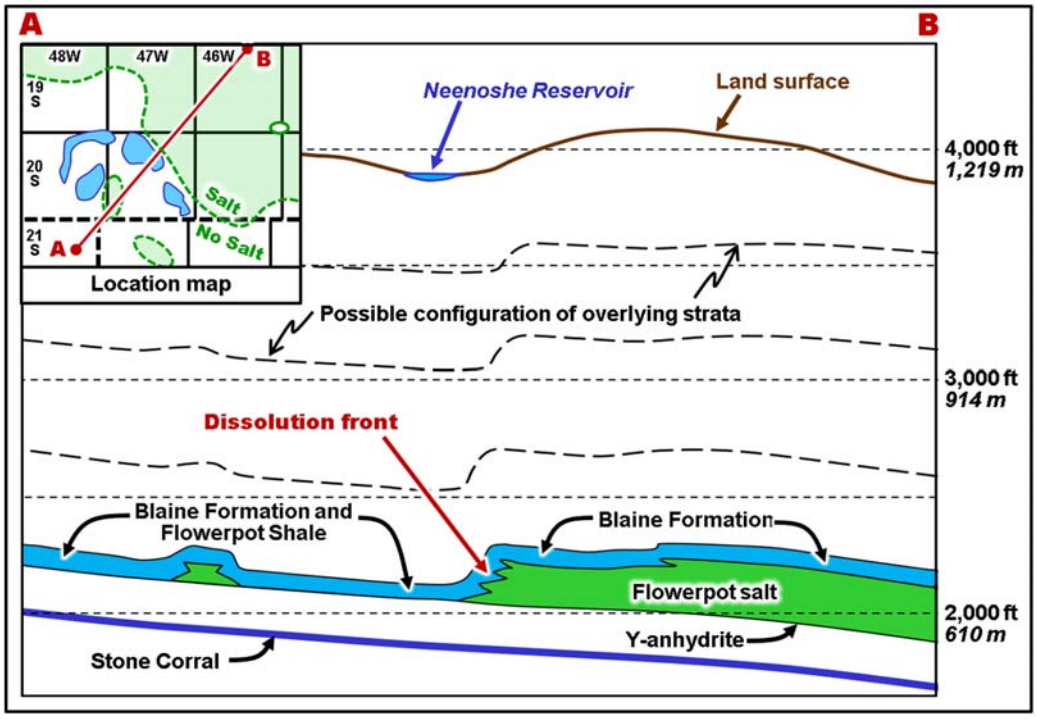

Figure 9. Schematic structural cross section showing: 1) Flowerpot salt dissolution front; 2) possible configuration of overlying strata; and 3) relationship of Neenoshe Reservoir and other major reservoirs to salt dissolution and collapse in the Great Plains Reservoirs area.

ORIGIN OF THE GREAT PLAINS RESERVOIRS

The main area of Flowerpot salt removal, just southwest of the dissolution front, is the location of the large, natural depressions that are now artificial reservoirs of the GPR. Clearly, these natural depressions were caused by dissolution of the Flowerpot salt southwest of the dissolution front (Fig. 9). Dissolution caused foundering and collapse of all overlying strata, until the collapse eventually reached the current land surface. The collapse probably was not uniform in timing and distribution across the area, and thus some areas have subsided more—and also more recently—than adjacent areas: this created the scattered natural depressions in the present landscape. It is possible, and even likely, that additional patches of residual Flowerpot salt remain in the immediate area of the reservoirs, but sparse drilling in T. 20 S., R. 47 W., makes it impossible to know. There are at least two known patches of residual salt southwest of the dissolution front. The timing of this collapse, as mentioned above, is uncertain, but it probably occurred between Late Cretaceous and late Pleistocene/Holocene time. It certainly was prior to settlement of the area in the late 1800s, as there are no historic reports of subsidence or collapse in the GPR area.

Most of the major reservoirs in the GPR have been developed by flooding of two or more adjacent natural depressions. Examination of aerial photos of the area, when the reservoirs were at low levels, reveals that three of the four major reservoirs occupy multiple depressions (Fig. 10). A photo taken in 1987 shows the reservoirs at near capacity, and does not indicate the number or shape of individual depressions. However, another photo, taken in 2001, shows four separate depressions in Neesopah Reservoir, three in Neenoshe Reservoir, and two in Neeskah Reservoir. A final photo in 2016 shows the same multiple depressions for those three reservoirs, and also shows that Neegronda Reservoir results from the filling of a single depression.

A total of 10 natural depressions are used to impound water in the four major reservoirs, and the perimeters of these depressions can be outlined from aerial photos (Fig. 11). Neegronda Reservoir occupies one immense depression, whereas the other three major reservoirs occupy two-to-four contiguous depressions. The approximate size of individual depressions ranges from 0.6 to 5.0 mi^2 (Table 1), making them some of the larger salt-dissolution/collapse features in the region. I could not find data on the true depth of the depressions, although water depths in the reservoirs, when full, reportedly range from 13 to 25 ft.

In addition to the four major reservoirs, there are some smaller reservoirs that are part of the GPR. Mud Lake, King Reservoir, and Thurston Reservoir are within the current study area, and several other small reservoirs are just to the south. All of these reservoirs appear also to be natural depressions that are fed by the extensive GPR canal system. Study of the 1:24,000-scale topographic maps of areas southwest of the Flowerpot salt dissolution front shows that there are many more natural depressions that most likely are collapse features resulting from salt dissolution: admittedly, some of them

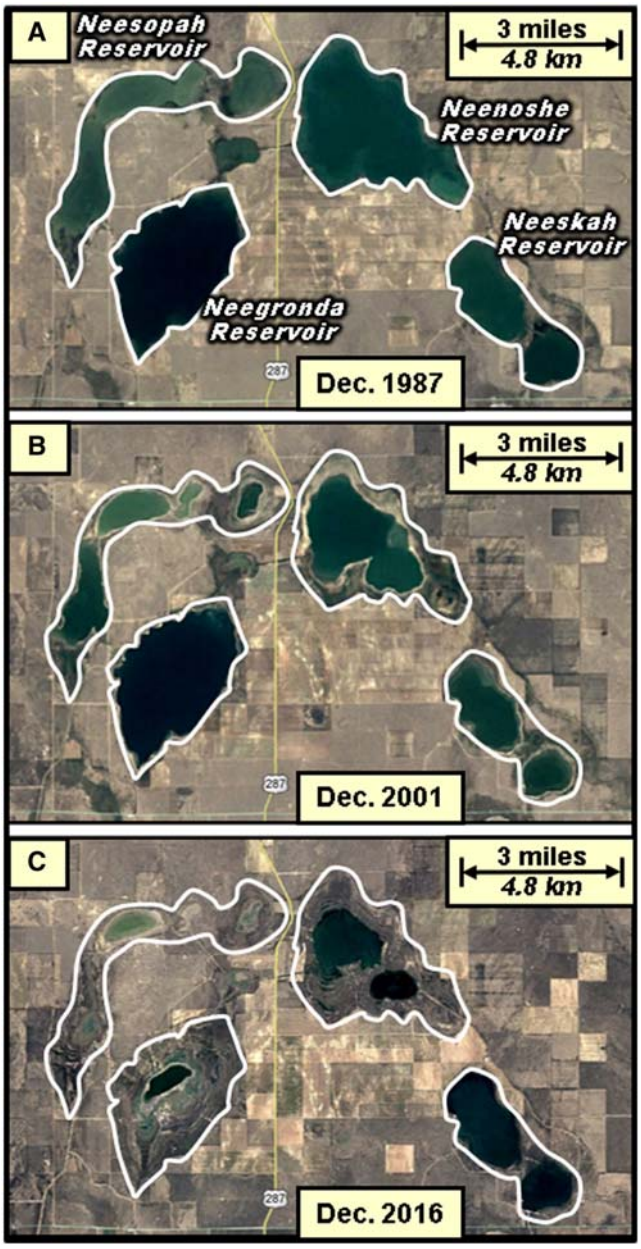

Figure 10. Aerial photographs of Great Plains Reservoirs showing outline of major reservoirs at near capacity (white lines), and actual reservoirs at various times of photography (photos from Google Earth). Photo A shows reservoirs at near-capacity; photo B shows smaller reservoirs, which occupy separate natural depressions; and photo C shows even smaller reservoirs occupying natural depressions.

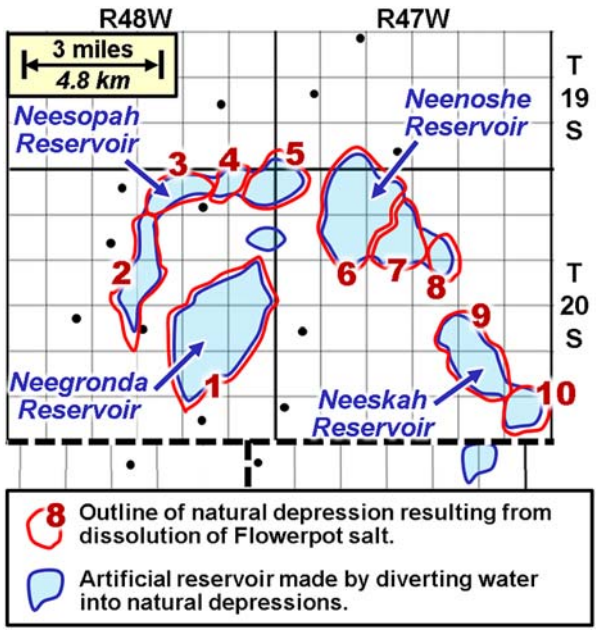

Figure 11. Map showing approximate perimeter of ten natural depressions (red) and four major reservoirs at near capacity (blue) in the Great Plains Reservoirs area. Data for numbered depressions given in Table 1.

TABLE 1.—Approximate dimensions of natural depressions filled by the four major reservoirs at Great Plains Reservoirs. Measurements made using the "polygon" and "line" options in the "ruler" tool on Google Earth Pro. See Figure 11 for location of the depressions.

	Area		Length		Width	
Depression	Miles²	Km²	Miles	Km	Miles	Km
1	5.0	13.0	3.5	5.6	1.9	3.1
2	1.8	4.7	3.0	4.8	0.8	1.3
3	0.9	2.3	1.5	2.4	0.7	1.1
4	0.6	1.6	1.0	1.6	0.6	1.0
5	1.3	3.4	1.4	2.3	1.0	1.6
6	3.6	9.3	2.7	4.3	1.6	2.6
7	1.1	2.8	1.7	2.7	1.0	1.6
8	0.6	1.6	0.9	1.4	0.6	1.0
9	2.0	5.2	2.1	3.4	1.1	1.8
10	1.0	2.6	1.1	1.8	1.0	1.6

may also be depressions associated with sand-dune morphology. Some of these depressions contain water (ephemeral lakes or ponds), and some of them are dry.

CONCLUSIONS

Dissolution of the Permian Flowerpot salt has created 10 natural depressions at the Earth's surface that are now being used to store water in four major reservoirs in the Great Plains Reservoirs area of southeast Colorado. The Flowerpot salt is 200–245 ft thick, and 1,800–2,000 ft deep, in the northeast part of the study area, but it thins to the southwest and is mostly absent southwest of a salt-dissolution front. Timing of salt dissolution is not known, but probably started during or after Late Cretaceous time, and persisted until the late Pleistocene or Holocene Epochs. Structure mapping in the area also shows the effect of salt dissolution; the Y-anhydrite, below the salt, dips gently across the site of the dissolution front without effect, whereas the Blaine Formation, above the salt, shows what appears to be a fault that is offset 100–200 ft across the dissolution front.

REFERENCES CITED

Askew, R.L., 2013, Distribution of the Permian Blaine Formation salt in the subsurface of the Hugoton Embayment area of Baca County, southeast Colorado: Rocky Mountain Association of Geologists, The Mountain Geologist, Vol. 50, No. 2, p. 65-75.

Berry, H.D., 2018, Dissolution of Permian salt, Las Animas Arch, Colorado: unpublished MS thesis, University of Louisiana at Lafayette, 96 p.

Dane, C.H., and Pierce, W.G., 1934, Fossil sink holes in Cretaceous beds of Prowers County, Colorado: American Association of Petroleum Geologists, Bulletin, p. 1493-1505.

Dane, C.H., Pierce, W.G., and Reeside, J.B, Jr., 1937, The stratigraphy of the Upper Cretaceous rocks north of the Arkansas River in eastern Colorado: U.S. Geological Survey, Professional Paper 186-K, p. 207–232. https://pubs.er.usgs.gov/publication/pp186K

Ege, J.R., 1985, Maps showing distribution, thickness and depth of salt deposits of the United States: U.S. Geological Survey, Open-File Report 85–28, 11 p., 4 plates. https://pubs.er.usgs.gov/publication/ofr8528

Gutentag, E.D., Lobmeyer, D.H., and Slagle, S.E., 1981, Geohydrology of southwestern Kansas: Kansas Geological Survey, Irrigation Series 7, 73 p. http://www.kgs.ku.edu/Publications/Bulletins/IRR7/index.html

Johnson, K.S., 2021, Salt dissolution and the Wallace Sinkhole in the Sharon Springs–Wallace area, Wallace County, Western Kansas, *in* Johnson, K.S., Land, L., and Decker, D.D., eds., Evaporite karst in the Greater Permian Evaporite Basin (GPEB) of Texas, New Mexico, Oklahoma, Kansas, and Colorado: Oklahoma Geological Survey, Circular 113.

Johnson, W.D., 1901, The High Plains and their utilization: US Geological Survey, 21st Ann. Report, Part 4, p. 9–488. https://pubs.usgs.gov/ar/21-4/report.pdf

Macfarlane, P.A., and Wilson, B.B., 2006, Enhancement of the bedrock-surface-elevation map beneath the Ogallala portion of the High Plains Aquifer, western Kansas: Kansas Geological Survey, Technical Series 20, 28 p. http://www.kgs.ku.edu/Publications/Bulletins/TS20/ts20.pdf

McGillis, K.A., and Presley, M.W., 1981, Tansill, Salado, and Alibates Formations: Upper Permian evaporate/carbonate strata of the Texas Panhandle: The University of Texas at Austin, Bureau of Economic Geology, Geological Circular 81–8, 31 p.

McLaughlin, T.G., 1943, Geology and ground-water resources of Hamilton and Kearny Counties, Kansas: Kansas Geological Survey, Bulletin 49, 220 p. http://www.kgs.ku.edu/General/Geology/Hamilton/index.html

Merriam, D.F., 1963, The geologic history of Kansas: Kansas Geological Survey, Bulletin 162, 317 p. http://www.kgs.ku.edu/Publications/Bulletins/162/index.html

Merriam D.F., and Mann, C.J., 1957, Sinkholes and related geologic features in Kansas: Kansas Academy of Science, Transactions, Vol. 60, No. 3, p. 207-243. https://digital.lib.usf.edu/SFS0054165/00001

Newell, F.H., 1901, Report of progress of stream measurements for the calendar year 1899: U.S. Geological Survey, 21st Ann. Report, Part 4, p. 601-741. https://pubs.usgs.gov/ar/21-4/report.pdf

Schoewe, W.H., 1949, The geography of Kansas, part 2, physical geography (geology): Kansas Academy of Sciences, Transactions, Vol. 52, No. 3, p. 261-333.

Sharps, J.A., 1976, Geologic map of the Lamar quadrangle, Colorado and Kansas: U.S. Geological Survey, Miscellaneous Investigations Series Map I–944, scale 1:250,000. https://ngmdb.usgs.gov/Prodesc/proddesc_9832.htm

Voegeli, P.T., and Hershey, L.A., 1965, Geology and ground-water resources of Prowers County, Colorado: U.S. Geological Survey, Water Supply Paper 1772, 101 p. https://pubs.er.usgs.gov/publication/wsp1772

Zambito, J.J., Benison, K.C., Foster, T.M., Soreghan, G.S., Soreghan, M.J., and Kane, M., 2012, Lithostratigraphy of Permian red beds and evaporites in the Rebecca K. Bounds core, Greeley County, Kansas: Kansas Geological Survey, Open-File Report 2012–15, 45 p. http://www.kgs.ku.edu/Publications/OFR/2012/OFR12_15/KGS_OF_2012-15.pdf